An investigation of the role of ADAM-like Decysin 1 in intestinal mucosal inflammation

Tomoko Kumagai

A thesis submitted to UCL for the degree of Doctor of Philosophy

2022

Eastman Dental Institute
Department of Microbial Disease

Supervisors:
Professor Andrew Smith
Dr Farooq Rahman

Declaration

I, Tomoko Kumagai, certify that the work presented in this thesis is my own. Where information has been derived from other sources or generated from collaboration with other researchers, I confirm that this has been indicated in the thesis.

Abstract

ADAM-like decysin 1 (ADAMDEC1) is a highly conserved metalloprotease which is exclusively expressed in the gastrointestinal (GI) tract, under healthy state, in various mammalian species including human. The physiological function and catalytical substrate of ADAMDEC1 remain unknown. However, a reduction in its normally high expression is seen within the tissue of GI inflammatory diseases and cancer, such as inflammatory bowel disease and colorectal cancer, which suggests that ADAMDEC1 is likely to play a vital role in physiology and potentially pathogenesis of GI diseases. Previous studies utilising dextran sodium sulfate (DSS) colitis model in *Adamdec1* knockout (*Adamdec1*$^{-/-}$) mice demonstrated an exaggerated mucosal inflammation during experimental colitis in these mice, thus the protective role of ADAMDEC1 in mucosal inflammation. However, the mechanism through which ADAMDEC1 mediates such a role in inflammation remains unknown. This project primarily aimed to characterise the role of ADAMDEC1 during intestinal mucosal inflammation.

By utilising DSS-colitis model, the components of mucosal defence and immune response in which ADAMDEC1 might potentially be involved to mediate its protective role were narrowed down to: antigen presenting cell - T cell interaction, monocyte to macrophage differentiation, phenotype of monocytes and macrophages, polarisation of Th17 and Treg cells, susceptibility of epithelial cells to DSS, and inhibitory effect of ADAMDEC1 on bacterial enzymes. Furthermore, analysis of the gut microbiome of the *Adamdec1*$^{-/-}$ and WT mice revealed that ADAMDEC1's role in mucosal inflammation was unlikely to be mediated via interaction with the microbiome. Finally, the marked impact of the environment on the gut microbiome and its impact on the expressivity of genotype were demonstrated. In conclusion, an advance was made in defining the potential role of ADAMDEC1 during mucosal inflammation. The project also demonstrated important challenges relating to environmental control when designing experiments to examine the phenotype of transgenic animals.

Impact statement

Induction pathways responsible for ADAMDEC1 was found to be mitogen-activated protein kinase pathway via activation of p38 and JNK in THP-1 cells. Reduced levels of ADAMDEC1 are observed in tissue of gastrointestinal (GI) diseases such as inflammatory bowel disease (IBD) and colorectal cancer (CRC), which are associated with high morbidity, mortality and significant burden on healthcare. If the reduced level of ADAMDEC1 is proven to play a mechanistic role in the pathogenesis of these GI diseases, p38 and JNK could potentially be therapeutic targets for the treatment and prevention of these diseases by augmenting the expression of ADAMDEC1. In addition, increased levels of ADAMDEC1 are observed in tissue of several diseases and cancers outside of the GI tract, such as non-small cell lung cancer, rosacea and glioblastoma. p38 and JNK could be potential therapeutic targets to inhibit the expression of ADAMDEC for the treatment and prevention of these diseases outside of the GI tract. Thus, this finding from the project has a potential impact on a broader population, not just limited to patients affected with GI diseases, as well as healthcare where the burden from these diseases is significant.

The phenotype of macrophages derived from murine Hoxb8-cells has been validated against murine bone marrow-derived macrophages (BMDM) and shown to be similar to that of BMDM. However, they have not been validated against any other type of macrophages. The phenotype of BMDM has been validated against peritoneal and splenic macrophages and has been shown to be distinct, possessing different functions.[1] BMDM have not been validated against intestinal macrophages. The findings from this project suggested that both Hoxb8-derived macrophages and BMDM did not express ADAMDEC1, thus indicating that these macrophages possess a different phenotype from the intestinal macrophages. The findings benefit the academics who intend to examine ADAMDEC1 in a murine model by providing the knowledge that Hoxb8-derived macrophages and BMDM are not suitable models to study ADAMDEC1 in vitro. The beneficiary can be extended to academics who intend to study the specific function of intestinal macrophages in general since the phenotype of the Hoxb8-derived macrophages and BMDM are likely to differ from that of the intestinal macrophages.

Recombinant human and mouse ADAMDEC1 and its mutant E353A were produced and purified using the Baculovirus expression system successfully. The recombinant ADAMDEC1 produced in insect cells and purified in this project retained its catalytical activity. The commercially available recombinant ADAMDEC1 is costly and most are sold as inactive immature form requiring removal of the prodomain before it can be used for functional analysis. The protocol optimised in this project provides a powerful tool for any academics who intend to produce recombinant ADAMDEC1 for functional analysis.

Finally, variable expressivity of ADAMDEC1 genotype was clearly demonstrated using *Adamdec1* knockout mice, which was dependent on the environment. This highlighted the influential power of the environment on genotype penetrance and expressivity, thus the importance of research into the interaction between the environment and genes. Such an interaction is involved in the development of complex diseases ranging from diabetes mellitus and coronary artery diseases affecting millions of people globally. However, the mechanism of this interaction is still poorly understood. Research into the environment and gene interaction, whose importance was emphasised by this project, would benefit not only people already suffering from complex diseases but a much broader population and healthcare globally from public health point of view by potentially preventing these diseases by modulation of environmental factors.

Acknowledgement

This project was supported by the United Kingdom Medical Research Council.

First and foremost, I would like to show my deepest gratitude to my supervisors, Professor Andrew Smith and Dr Farooq Rahman, for their guidance and support. I am truly grateful to Professor Smith for giving me the opportunity to take up this intriguing and exciting project and allowing me to take its ownership. I would also like to thank him sincerely for his endless patience, encouragement and tireless effort in providing constructive advice throughout the project, as well as for being extremely understanding at times when life threw unexpected events. I am grateful to Dr Farooq Rahman, who has shown me the art of connecting clinical medicine and science, for believing in my aspiration to embark on a PhD and for introducing myself to the exciting field of research and to Professor Smith. I could not have asked for better mentors and supervisors. I would also like to mention my gratitude to Professor Tony Segal for his critical opinion and contagious passion for science and research.

I would like to express my sincere appreciation to Juliet Foote, Julio Martinez-Torres, Francesca Semplici, Erni Marlina, Shuangqi Fan, David Sanders, Silke Rath and Paul Gill for their generous sharing of their invaluable knowledge and skills. Especially, I cannot thank Shuangxi enough, without whom I would not have been able to process as many mouse bowels as I managed. I am forever grateful for his generous support and those hours he spent tackling mice with me in the lab, as well as for our endless discussions and also priceless friendship. My huge special thanks also go to Juliet and David, who have spent a considerable amount of their precious time generously providing hands-on mentorship and incomparable guidance through many parts of this project. I would not have achieved many milestones during my PhD without their effort. Another special appreciation goes to Silke, who has helped enormously with the analysis of microbiome data and shared her expert knowledge on the microbiome and guided me through my final experiments in the lab. I would also like to thank Chris Batters, from Professor Buss's team at Cambridge Institute for Medical Research, who has kindly helped me with the Baculovirus protein expression system using insect cells with his invaluable knowledge, experience and enormous patience.

I would also like to thank colleagues from the Smith team: Aziz Ghannam, Mathena Vinayaga-Pavan, Gregory Sebepos-Rogers, Hajeena Saravanapavan, John Barragry and Saskia Innis for the scientific discussions, their companionship, and banters that lifted me up in the lab.

My heartfelt appreciation also goes to my husband, Simone, for his unbounded support towards my aspirations and for allowing me to selfishly become preoccupied with this project over the last few years. His presence right by my side through the ups and downs and his calmness and composure were the pillar of my strength which I am eternally grateful for. Furthermore, he has created some graphics for my publications during this PhD. I thank him for his time and patience in working with me. I also would like to thank my son, Takumi, who arrived during this PhD, for being such a happy easy-going baby/toddler allowing me to be a selfish mother to spend time in the lab away from him. I am truly grateful for his presence and would like to thank him for being the eternal source of my enthusiasm and positivity.

Finally, I would like to thank my parents for their unconditional love and support not only during this PhD but throughout my entire education and career. I would not have achieved what I have without them, whom I will always look up to as the most inspirational role models in the entire world.

Table of Contents

Declaration **2**

Abstract **3**

Impact statement **4**

Acknowledgement **6**

List of abbreviations **15**

List of figures **18**

List of tables **29**

Chapter 1 Introduction **32**

1.1 Molecular and genetic characteristics of ADAMDEC1 32

1.1.1 ADAMDEC1 and ADAM proteins 32

1.1.2 Conservation of ADAMDEC1 through evolution 36

1.2 Physiological expression of ADAMDEC1 in healthy status 37

1.2.1 Highly restricted expression of ADAMDEC1 in healthy status 37

1.3 Potential functions of metalloprotease and integrin-like domains 37

1.3.1 Catalytical activity and proteolytic target of ADAMDEC1 37

1.3.2 Potential function of Disintegrin-like domain of ADAMDEC1 39

1.4 Expression of ADAMDEC1 at the cellular level and its potential function in healthy intestine 39

1.4.1 ADAMDEC1 expression in the monocyte-derived macrophages of the intestine 39

1.4.2 ADAMDEC1 expression in non-monocyte derived macrophages of the intestine 42

1.4.3 ADAMDEC1 expression in non-macrophage cells of the intestine 43

1.5 Expression of ADAMDEC1 at a cellular level in extra-intestinal organs 45

1.6 Expression and potential involvement of ADAMDEC1 in human diseases 47

1.6.1 Gastrointestinal inflammatory disease 47

1.6.2 Gastrointestinal cancer 50

1.6.3 Extra-intestinal inflammatory diseases and cancers 56

1.7 ADAMDEC1 and gastrointestinal mucosal inflammation 60

1.7.1 Findings from previous studies using *Adamdec1*$^{-/-}$ mice and experimental colitis 60
1.7.2 ADAMDEC1 and intestinal microbiome in the context of intestinal inflammation 63
1.8 Outline of the thesis....64

Chapter 2 General materials and method 66
2.1 Ethics approval....66
2.2 General reagents and buffers....66
2.3 Heat-killed bacteria and fungi stock....68
2.4 Microscopy 69
2.5 Quantification of DNA and RNA 69
2.6 Cloning 69
2.6.1 DNA sequencing....69
2.6.2 Bacterial glycerol stocks 69
2.6.3 Plasmid DNA extraction 70
2.6.4 Analysis of plasmid and complementary DNA (cDNA) by gel electrophoresis....71
2.7 Gene expression 73
2.7.1 RNA extraction and purification....73
2.7.2 Conversion of RNA to cDNA 75
2.7.3 Quantitative PCR (qPCR) 76
2.8 Western blot 76
2.8.1 Cell lysate preparation 76
2.8.2 Supernatant preparation 77
2.8.3 Loading sample preparation 77
2.8.4 SDS-polyacrylamide gel electrophoresis (SDS-PAGE) gel electrophoresis....78
2.8.5 Transfer of protein from SDS-PAGE to membrane 78
2.8.6 Antibody staining....79
2.9 *Adamdec1*$^{-/-}$ and WT mice 80
2.9.1 Sources and generation of *Adamdec1*$^{-/-}$ and WT mice....80
2.9.2 Husbandry of mice 80
2.9.3 Euthanasia of mice 81
2.9.4 Genotyping of mice 81

Chapter 3 Identification of stimuli and signalling pathways responsible for the induction of ADAMDEC1 during monocyte to macrophage differentiation 84

3.1 Background and aims 84

3.2 Materials and method 86

3.2.1 Cells and cell culture media 86

3.2.2 Stimulation of THP1 cells 86

3.2.3 THP1 cell stimulation with inhibitors 87

3.2.4 qPCR and primers used for qPCR 88

3.2.5 qPCR data analysis method 88

3.2.6 Generation of MDMs and stimulation of MDMs 89

3.3 Results 91

3.3.1 *ADAMDEC1* is induced by bacteria-related ligands 91

3.3.2 ADAMDEC1 is induced by opsonised HkC but not by non-opsonised HkC 93

3.3.3 *ADAMDEC1* is induced by selected pro-inflammatory cytokines 94

3.3.4 *ADAMDEC1* induction occurs during monocyte to macrophage-like cell differentiation 95

3.3.5 TLR2/4-induced *ADAMDEC1* is mediated partially by activation of TNF receptor 100

3.3.6 *ADAMDEC1* induction is mediated by MAPK signalling pathway via phosphorylation of p38 and JNK 101

3.3.7 ADAMDEC1 is detected at protein level and the mature ADAMDEC1 is secreted from the THP-1 cells stimulated with HkEc 103

3.3.8 ADAMDEC1 is induced during the differentiation of blood peripheral monocyte into macrophages 105

3.4 Discussion 107

Chapter 4 Generation and characterisation of the Hoxb8 immortalised myeloid cell line 110

4.1 Background and aims 110

4.2 Materials and method 113

4.2.1 Cells and cell culture media 113

4.2.2 Macrophage differentiation protocol for the gifted WT Hoxb8 progenitor cells 115

4.2.3 Generation of WT and Adamdec1-/- Hoxb8 progenitor cells 115

4.2.4 Macrophage differentiation protocol for the newly generated Hoxb8 cells 120

4.2.5 Macrophage differentiation of the newly generated Hoxb8 cells with stimuli....120
4.2.6 Generation of mouse BMDM....121
4.2.7 FACS of Hoxb8 progenitor cells, Hoxb8-derived macrophages and MDMs....121
4.2.8 qPCR....122
4.3 Results....123
4.3.1 Expression of macrophage surface markers and ADAMDEC1 by the macrophages derived from the gifted WT ER-Hoxb8 progenitor cells....123
4.3.2 Generation of WT and *Adamdec1*$^{-/-}$ Hoxb8 progenitor cells....126
4.3.3 Characterisation of the newly generated WT and Adamdec1$^{-/-}$ GMCSF Hoxb8 progenitor cells....129
4.3.4 Differentiation of the newly generated WT and Adamdec1$^{-/-}$ GMCSF Hoxb8 progenitor cell into macrophages....132
4.3.5 Expression of ADAMDEC1 in the WT and *Adamdec1*$^{-/-}$ Hoxb8-derived macrophages....134
4.3.6 Characterisation of the WT macrophages derived from newly generated Hoxb8 cells....135
4.4 Discussion....143

Chapter 5 Production and purification of recombinant human and mouse ADAMDEC1 and its mutant E353A....145

5.1 Background and aims....145
5.2 Materials and method....152
5.2.1 ExpiSf9 cells....152
5.2.2 Baculovirus expression vector system....152
5.2.3 Transfection of ExpiSf9 cells to generate recombinant baculovirus encoding human and mouse ADAMDEC1-His and E353A-His....161
5.2.4 Infection of ExpiSf9 cells with P0 baculovirus for protein expression....161
5.2.5 Purification of the recombinant mature human and mouse ADAMDEC1 and E353A by immobilised metal affinity chromatography (IMAC)....162
5.2.6 Trichloacetic acid precipitation of protein samples....164
5.2.7 Purity analysis of the sample fractions collected at each step of purification process by SDS-PAGE Coomassie stain and Western blot....165
5.2.8 Quantification of the purified recombinant proteins by densitometry....165

5.2.9 Incubation of the recombinant human ADAMDEC1 and E353A with α2-macroglobulin 166
5.3 Results 168
5.3.1 Generation of a bacmid encoding human ADAMDEC1 with a C-terminal 6 x Histidine tag (hADAMDEC1-His) 168
5.3.2 Site-directed mutagenesis for the generation of hADAMDEC1-E353A-His bacmid 178
5.3.3 Generation of mADAMDEC1-His and mE353A-encoding bacmids 179
5.3.4 Generation of recombinant baculovirus encoding hADAMDEC1-His and hE353A-His 180
5.3.5 Optimisation of recombinant ADAMDEC1-His and hE353A protein expression in ExpiSf9 cells using the harvested P0 baculoviral stocks 181
5.3.6 Optimisation of immobilised metal affinity chromatography (IMAC) purification process using the recombinant mature hADAMDEC1 .191
5.3.7 Protein expression and purification of hE353A using the hE353A P0 baculovirus 196
5.3.8 Protein expression and purification of mADAMDEC1 and mE353A 198
5.3.10 Quantification of the purified mADAMDEC1 and mE353A 201
5.3.11 Confirmation of synthesis and purification of the recombinant human and mouse ADAMDEC1 and E353A 202
5.4 Discussion 206

Chapter 6 Characterisation of the immune response in *Adamdec1*$^{-/-}$ mice upon induction of DSS-induced colitis 208

6.1 Background and aims 208
6.2 Materials and method 211
6.2.1 DSS administration 211
6.2.2 Experimental timeline and output of DSS-induced acute colitis mouse model 211
6.2.2 Weight measurement of mice 213
6.2.3 Isolation of mouse colonic cells 213
6.2.4 FACS of isolated mouse colonic cells 215
6.2.5 FACS of murine splenocytes with or without enzymatic digestion step 217
6.2.6 qPCR of the murine colonic tissues and primers used for qPCR ...219
6.2.7 qPCR data analysis method 220
6.3 Results 221

6.3.1 The features of DSS-induced colitis in the WT and *Adamdec1*$^{-/-}$ mice 221
6.3.2 Cage-dependant variability in the expressivity of *Adamdec1*$^{-/-}$ genotype 223
6.3.3 Flow cytometry analysis of colonic intestinal cells.....225
6.3.4 Analysis of the gene expression in the colonic tissue of WT and *Adamdec1*$^{-/-}$ mice on day 9 of the DSS challenge by qPCR 254
6.4 Discussion 263

Chapter 7 Investigation of the effect of ADAMDEC1 on the murine intestinal microbiome 275
7.1 Background and aims.....275
7.2 Material and Method.....279
7.2.1 Experimental set-up 279
7.2.2 Faecal sample collection.....282
7.2.3 Microbial DNA extraction from faecal samples 282
7.2.4 Amplification of microbial DNAs by PCR and sequencing of the amplicons.....283
7.2.5 16S gene sequence analysis 283
7.2.6 ITS gene sequence analysis.....284
7.2.7 Downstream microbial community analysis 285
7.3 Results 287
7.3.1 Experiment 1 - Effect of ADAMDEC1 on the gut microbiome 287
7.3.2 Experiment 2 – Effect of ADAMDEC1 on gut microbiome after prolonged period of housing of the mice per genotype, after cohousing of WT and *Adamdec1*$^{-/-}$ mice and after DSS colitis 301
7.4 Discussion 338

Chapter 8 General discussion.....343
8.1 Summary of findings.....343
8.2 Overall discussion 346
8.3 Proposed future works.....352

Appendix 1.....354

Appendix 2.....355

Appendix 3.....356

Appendix 4.....357

Appendix 5 ..... **358**

Appendix 6 ..... **359**

Appendix 7 ..... **360**

Appendix 8 ..... **361**

Appendix 9 ..... **362**

Appendix 10 ..... **363**

Appendix 11 ..... **364**

Appendix 12 ..... **365**

Appendix 13 ..... **366**

References **367**

List of abbreviations

8p	Short arm of chromosome 8
AcMNPV	*Autographa Californica* multiple nucleopolyhedosis virus
ADAMDEC1	ADAM like decysin 1
ANOSIM	Analysis of similarities
ANOVA	Analysis of variance
APC	Allophycocyanin
BEVS	Baculovirus expression vector system
BMDM	Bone marrow-derived macrophages
BSA	Bovine serum albumin
BV	Brilliant Violet™
bp	Base pairs
CCL2	C-C Motif Chemokine Ligand type 2
CCR2	C-C Motif Chemokine receptor type 2
cDNA	complementary DNA
CH	Compound heterozygote
CRC	Colorectal adenocarcinoma
CXCL1	C-X-C Motif Chemokine Ligand 1
CX3CR1	C-X3-C Motif Chemokine Receptor 1
Cy7	Cyanine-7
DF	Degree of freedom
DMSO	Dimethyl sulfoxide
DNA	Deoxyribonucleic acid
DSS	Dextran sodium sulfate
ECM	Extracellular matrix
E. coli	*Escherichia coli*
EDAC	Epithelial defence against cancer
EGF	Epidermal growth factor
ER	Oestrogen-receptor
ERK	Extracellular signal-regulated kinase 1/2
FACS	Fluorescence-activated cell sorting
FcγR	Fc-gamma receptor
F/B	*Firmicutes* to *Bacteroides*
FBS	Fetal bovine serum
FGF2	Fibroblast growth factor-2
FGFR1	Fibroblast growth factor receptor-1
FITC	Fluorescein isothiocyanate
FOXP3	Forkhead box P3
GAC	Gastric adenocarcinoma
GBM	Glioblastoma
GCSF	Granulocyte stimulating factor
GMCSF	Granulocyte-macrophage colony-stimulating factor
GWAS	Genome-wide association study

HEPES	4-(2-hydroxyethyl)-1-piperazineethanesulfonic acid
HMOX-1	Heme oxygenase-1
HkC	Heat-killed *Candida albicans*
HkEc	Heat-killed *Escherichia coli*
Hoxb8	Homeobox protein Hox-B8
IBD	Inflammatory bowel disease
IFN-	Interferon-
IL-	Interleukin-
ILC3	Type 3 innate lymphoid cells
IPTG	Isopropyl ß-D-1-thiogalactopyranoside
ITS	Internal transcribed spacer
JNK	c-Jun N-terminal kinase
LB	Luria-Bertani
LB-Amp	Luria-Bertani containing ampicillin
LOH	Loss of heterogenicity
LPS	Lipopolysaccharide
Mac-1	Macrophage-1 antigen
MAPK	Mitogen-activated protein kinase
MCSF	Macrophage colony-stimulating factor
MDCK	Madin-Darby canine kidney
MDMs	Monocyte-derived macrophages
MDP	Muramyl dipeptide
MEK	MAPK/ERK kinase
MFI	Mean fluorescent intensity
MOI	Multiplicity of infection
MSCV	Murine stem cell provirus
MWCO	Molecular weight cut-off
nMDS	Non-metric multi-dimensional scaling
NOD2	Nucleotide-binding oligomerization domain 2
OD_{600}	Optical density at 600 nm
PBS	Phosphate buffered saline
PE	R-phycoerythrin
PD-1	Programmed cell death protein-1
PD-L1	Programmed-death ligand-1
PERMANOVA	Permutational analysis of variance
PKC	Protein kinase C
PMA	Phorbol 12-myristate 13-acetate
PPR	Pattern-recognition receptor
Poly(I:C)	Polyinosinic:polycytidylic acid
RBC	Red blood cell
RDP	Ribosomal Database Project
RNA	Ribonucleic acid
RORγt	Retinoic acid receptor-related orphan receptor γt
scRNA-seq	Single cell RNA sequencing

SD	Standard deviation
SDS	Sodium dodecyl sulfate
SDS-PAGE	Sodium dodecyl sulfate-polyacrylamide gel electrophoresis
SMAC	Supramolecular activation cluster
SSC	Side scatter
TCA	Trichloroacetic acid
Th1	T helper 1
Th2	T helper 2
Th17	T helper 17
TIMP	Tissue inhibitors of metalloprotease
TLR	Toll-like receptor
TNF-α	Tumour necrosis factor alpha
Treg	Regulatory T
UCL	University College London
WT	Wild type
YPD	Yeast Peptone Dextrose

List of figures

Figure 1.1 Schematic diagram of ADAMs structure 32

Figure 1.2 Simplified schematic diagram illustrating the differences between the structures of typical ADAMS and ADAMDEC1.....35

Figure 1.3 Amino acid sequence of the zinc-binding motif in various mammalian species. 36

Figure 1.4 Distribution of *ADAMDEC1* in human tissue 37

Figure 1.5 Schematic diagram of colonic tissue and *ADAMDEC1* expressing cells.....45

Figure 1.6 Expression of *ADAMDEC1* in various types of cell within extra-intestinal organs analysed by scRNA-seq 46

Figure 1.7 Expression of *ADAMDEC1* in normal and IBD tissues analysed using the data extracted from NCBI Gene Expression Omnibus (GEO) data repository 47

Figure 1.8 Possible mechanism through which the reduced expression of *ADAMDEC1* in the monocyte-derived macrophages in the lamina propria could lead to chronic mucosal inflammation of Crohn's disease.....49

Figure 1.9 Expression of genes in normal adenoma, CRC and IBD tissues analysed using data extracted from NCBI Gene Expression Omnibus (GEO) data repository. 51

Figure 1.10 A possible mechanism in which the loss of ADAMDEC1 in macrophages might facilitate the development of colorectal adenoma and adenocarcinoma by hindering EDAC. 54

Figure 1.11 Expression of *ADAMDEC1* in paired normal and gastric adenocarcinoma tissues analysed using data extracted from GEO data repository 55

Figure 2.1 Schematic diagram showing alignment location of the primers used for mouse genotyping.....82

Figure 2.2 Example of the DNA gel electrophoresis of the mouse genotyping.83

Figure 3.1 Expression of *ADAMDEC1* in THP-1 cells after incubation with various bacterial-related ligands for 24 hours 92

Figure 3.2 Expression of *ADAMDEC1* in the unstimulated MDMs from patients with Crohn's disease categorised into 3 different cohorts based on their NOD2 mutation status 92

Figure 3.3 Expression of *ADAMDEC1* in THP-1 cells after incubation with HkC or opsonised HkC for 24 hours 93

Figure 3.4 Expression of *ADAMDEC1* in THP-1 cells after incubation with various pro-inflammatory cytokines for 24 hours 94

Figure 3.5 Expression of *ADAMDEC1* in THP-1 cells after incubation with PMA over 24 hours and cytokines over 72 hours 96

Figure 3.6. Morphological changes in THP-cells observed after stimulation with LPS and HkEC over 24 hours 97

Figure 3.7 Expression of *CD14* and *CD80* in THP-1 cells after incubation with various stimuli for 24 hours 98

Figure 3.8 The correlation between the expression of *CD14* and ADAMDEC1, and *CD80* and *ADAMDEC1* in the THP-1 cells after incubation with various stimuli for 24 hours 99

Figure 3.9 Expression of *ADAMDEC1* in THP-1 cells after incubation with HkEc, Pam3CSK4, LPS or TNF-α with or without Adalimumab for 24 hours 100

Figure 3.10 Simplified schematic diagram showing the direct and indirect mechanism of *ADAMDEC1* induction by activation of TLR2 and TLR4 101

Figure 3.11 Effect of inhibition of NF-κB and MAPK cascades on the HkEc-mediated induction of *ADAMDEC1* in THP-1 cells 103

Figure 3.12 Western blot of THP-1 cell lysates and supernatants collected after THP-1 cells were incubated with HkEc for 24, 48 and 72 hours 104

Figure 3.13 Western blot of cell lysates and supernatants collected from MDMs 7 days after the monocytes were isolated from the blood (day 8), and after further 48 hours of incubation with or without stimulation with HkEc or LPS (day 10) 106

Figure 3.14 The signalling pathways responsible for the induction of *ADAMDEC1* in THP-1 cell is MAPK signalling pathway specifically via p38 and JNK 108

Figure 4.1 Schematic overview of generation, maintenance, and differentiation of Hoxb8 immortalised progenitor cells. 112

Figure 4.2 Western blot of Hoxb8 progenitor cells and Hoxb8-derived macrophages harvested at different timepoints during the macrophage differentiation protocol 124

Figure 4.3 Basic macrophage markers on Hoxb8-derived macrophages generated from the gifted GMCSF Hoxb8 cells and BMDMs 125

Figure 4.4 Scheme showing the position of the primers targeting Hoxb8 within ER-Hoxb8 insert.....127

Figure 4.5 DNA gel electrophoresis confirming the presence of *Hoxb8* expression in the transfected GP2-293 cells.....127

Figure 4.6 Morphological appearance of the WT and *Adamdec1*$^{-/-}$ GMCSF Hoxb8 progenitor cells.....129

Figure 4.7 Expansion and viability of Hoxb8 progenitor cells 130

Figure 4.8 Cell marker expression of the gifted Hoxb8 cells and newly generated WT and *Adamdec1*$^{-/-}$ GMCSF Hoxb8 cells 131

Figure 4.9 Anti-Hoxb8 Western blot demonstrating the presence of Hoxb8 in the newly generated WT and *Adamdec1*$^{-/-}$ Hoxb8 progenitor cells and disappearance of it in the WT and *Adamdec1*$^{-/-}$ GMCSF Hoxb8-derived macrophages 132

Figure 4.10 Morphology of the newly generated WT and *Adamdec1*$^{-/-}$ GMCSF Hoxb8-derived macrophages under a light microscope 133

Figure 4.11 Cell count and viability of the WT and *Adamdec1*$^{-/-}$ GMCSF Hoxb8-derived macrophages during the differentiation protocol.....134

Figure 4.12 Anti-ADAMDEC1 Western blot of ADAMDEC1 expression in the Hoxb8 progenitor cells and Hoxb8-derived macrophages.....135

Figure 4.13 Cell surface marker expression of the progenitors and macrophages derived from newly generated GMCSF and SCF WT Hoxb8 cells, and the WT and *Adamdec1*$^{-/-}$ BMDMs. 138

Figure 4.14 Anti-ADAMDEC1 Western blot of cells differentiated from the newly generated GMCSF and SCF WT Hoxb8 cells following the macrophage differentiation protocol augmented with HkEc, and WT BMDMs. 140

Figure 4.15 Morphology of the cells differentiated from WT GMCSF Hoxb8 cells in differentiation media supplemented with MCSF, HkEc and additionally mouse serum, WT mouse colonic tissue or CCL2. 141

Figure 5.1 Overview of the steps involved in the Bac-to-Bac system for production of recombinant protein.....148

Figure 5.2 A plasmid map of pCMV-hADAMDEC1 encoding hADAMDEC1-GFP 168

Figure 5.3 Agarose gel electrophoresis of the PCR products generated by gradient PCR to determine the optimal annealing temperature for generation of hADAMDEC1 insert.....169

Figure 5.4 Agarose gel electrophoresis of the PCR product for generation of hADAMDEC1 amplicon visualised under ultraviolet light 170

Figure 5.5 Cloning site of pFastBac/CT-TOPO plasmid.....171

Figure 5.6 A plasmid map of pFastBac/CT-TOPO with hADAMDEC1 construct inserted in the cloning site.....172

Figure 5.7 Agarose gel electrophoresis of the PCR products generated from the ligation products using various pFastBac vector to hADAMDEC1 insert ratios 173

Figure 5.8 Transformation and screening results of the MAX Efficiency® DH10Bac™ chemically competent *E. coli* transformed with pFastBac-hADAMDEC1-His plasmid.....175

Figure 5.9 Confirmation of the successful incorporation of hADAMDEC1-His in bacmid within *E. coli* colony selected in the first round of antibiotic selection and white-blue screening. 176

Figure 5.11 Agarose gel electrophoresis of the PCR products generated from the recombinant bacmid using pUC/M13 forward and reverse primers.....177

Figure 5.10 Position of the transposed hADAMDEC1-His sequence and binding sites for pUC/M13 forward and reverse primers within Bacmid-hADAMDEC1-His 177

Figure 5.12 The sequences and binding positions of the primers used for the mutagenesis PCR to generate pFastBac-E353A-His plasmid.....179

Figure 5.13 Morphological appearance of ExpiSf9 cells before and after (72 hours and 96 hours post-transfection) transfected with Bacmid-hADAMDEC1-His. 180

Figure 5.14 Small scale trial infections of ExpiSf9 cells with hADAMDEC1-His and hE353A-His P0 baculoviral stocks.....182

Figure 5.15 Total number of ExpiSf9 cells during infection with 250 μl or 500 μl of hADAMDEC1-His or hE353A-His P0 baculoviruses assessed over 96 hours 183

Figure 5.16 Cell viability of ExpiSf9 cells during infection with 250 μl or 500 μl of hADAMDEC1-His or hE353A-His P0 baculoviruses assessed over 96 hours 183

Figure 5.17 Number of live ExpiSf9 cells during infection with 250 µl or 500 µl of hADAMDEC1-His or hE353A-His P0 baculoviruses assessed over 96 hours. 184

Figure 5.18 Anti-His Western blot of cell lysate (A) and supernatant (B) of ExpiSf9 cells infected with 250 µl or 500 µl of hADAMDEC1-His P0 baculovirus collected at various timepoints over 96 hours. 187

Figure 5.19 Anti-His Western blot of cell lysate (A) and supernatant (B) of ExpiSf9 cells infected with 250 µl or 500 µl of hE353A-His P0 baculovirus collected at various timepoints over 96 hours. 188

Figure 5.20 Anti-ADAMDEC1 Western blot of cell lysate (A) and supernatant (B) of ExpiSf9 cells infected with 250 µl or 500 µl of hADAMDEC1-His P0 baculovirus collected at various timepoints over 96 hours. 189

Figure 5.21 Anti-ADAMDEC1 Western blot of cell lysate (A) and supernatant (B) of ExpiSf9 cells infected with 250 µl or 500 µl of hE353A-His P0 baculovirus collected at various timepoints over 96 hours. 190

Figure 5.22 SDS-PAGE (A) and Western blot (B) analyses of the fractions collected at each step of hADAMDEC1 purification process 194

Figure 5.23 Quantification analysis of the purified recombinant hADAMDEC1 by densitometry.....195

Figure 5.24 SDS-PAGE analysis of the fractions collected at each step of the hE353A purification process.....197

Figure 5.25 Quantification analysis of the purified recombinant hE353A by densitometry.....198

Figure 5.26 SDS-PAGE analysis of the fractions collected at each step of mADAMDEC1 (A) and mE353A (B) purification processes.....200

Figure 5.27 SDS-PAGE gels with various volumes of the purified recombinant mADAMDEC1 (A) and mE353A (B) and weights of BSA loaded in each well. 201

Figure 5.28 Western blot of the purified recombinant human and mouse ADAMDEC1 and E353A probed with anti-His and anti-ADAMDEC1 antibodies 203

Figure 5.29 Analysis of catalytical activity of the purified mature hADAMDEC1 and hE353A. 204

Figure 5.30 Growth curves of *E. coli* (A) and *Salmonella enterica* (B) incubated with various concentrations of hADAMDEC1 and hE353A.....205

Figure 6.1 Scheme demonstrating the experimental timeline and output of the analysis to characterise the effect of ADAMDEC1 during DSS-induced colitis. 211

Figure 6.2 Photograph of colons harvested from the WT and *Adamdec1*$^{-/-}$ mice after DSS challenge 221

Figure 6.3 Weight change in the WT and *Adamdec1*$^{-/-}$ mice during DSS challenge. 222

Figure 6.4 Weight change in the WT and *Adamdec1*$^{-/-}$ mice in Cage 1 (A) and Cage 2 (B) during DSS challenge 223

Figure 6.5 Weight change in the WT and *Adamdec1*$^{-/-}$ mice in Cage 1 and Cage 2 during DSS challenge.....224

Figure 6.6 Flow cytometry gating strategy for analysis of the murine colonic cells using the lymphoid panel antibodies 227

Figure 6.7 Flow cytometry gating strategy for analysis of the murine colonic cells using the myeloid panel antibodies 228

Figure 6.8 Changes in the proportion of CD45- cells (A) and CD45+ cells (B) in the colonic tissue of the WT and *Adamdec1*$^{-/-}$ mice during DSS challenge....230

Figure 6.9 The proportion of CD45+ cells in the colonic tissue of the WT and *Adamdec1*$^{-/-}$ mice in Cage 1 and Cage 2 on day 9 of the DSS challenge 231

Figure 6.10 Changes in the proportion of CD45+ CD3- cells (A) and CD45+ CD3+ cells (B) in the colonic tissue of the WT and *Adamdec1*$^{-/-}$ mice during DSS challenge.....232

Figure 6.11 Flow cytometry plots demonstrating the changes in CD4+ and CD8+ cell populations in the murine colonic tissue during DSS challenge.....234

Figure 6.12 The proportion of CD4+ (A) and CD8+ (B) cells in the murine colonic tissue in naïve state.....235

Figure 6.13 MFI of CD4 (A) and CD8 (B) within the CD45+ CD3+ cell population 235

Figure 6.14 Flow cytometry plots showing the CD4+ and CD8+ cell populations in spleens of the healthy WT and *Adamdec1*$^{-/-}$ mice treated with dispase or not treated with dispase 237

Figure 6.15 MFI of CD4 (A) and CD8 (B) in the splenocytes of the healthy WT and *Adamdec1*$^{-/-}$ mice treated with dispase or not treated with dispase.....238

Figure 6.16 The expression of *Cd4* (A) and *Cd8* (B) in the colonic tissues of the WT and *Adamdec1*$^{-/-}$ mice on day 9 of the DSS challenge 239

Figure 6.17 Changes in the proportion of Th17 cells (A) and Treg cells (B) in the colonic tissue of the WT and *Adamdec1*$^{-/-}$ mice during DSS challenge.....241

Figure 6.18 Changes in the proportion of RORγt+ FOXP3+ T cells in the colonic tissue of the WT and *Adamdec1*$^{-/-}$ mice during DSS challenge.....242

Figure 6.19 Changes in the proportion of ILC3 in the colonic tissue of the WT and *Adamdec1*$^{-/-}$ mice during DSS challenge.....244

Figure 6.20 Changes in the proportion of dendritic cells (A), neutrophils (B) and F4/80+ monocyte and macrophage population (C) in the colonic tissue of the WT and *Adamdec1*$^{-/-}$ mice during DSS challenge.....245

Figure 6.21 Changes in the proportion of SSC^{low} Ly6C^{high} monocytes (A) and SSC$^{mid/high}$ Ly6C$^{low/mid}$ macrophages (B) in the colonic tissue of the WT and *Adamdec1*$^{-/-}$ mice during DSS challenge.....247

Figure 6.22 Change in MFI of CX3CR1 in SSC^{low} Ly6C^{high} monocyte population of the WT and *Adamdec1*$^{-/-}$ mice during DSS challenge 248

Figure 6.23 Change in MFI of Ly6C in SSC$^{mid/high}$ Ly6C$^{low/mid}$ macrophage population of the WT and *Adamdec1*$^{-/-}$ mice during DSS challenge.....249

Figure 6.24 MFI of CX3CR1 in B cell, neutrophil, macrophage and dendritic cell populations of the WT and *Adamdec1*$^{-/-}$ mice during DSS challenge.....250

Figure 6.25 Effect of dispase on the surface expression of CX3CR1 in the murine splenocytes 251

Figure 6.26 Effect of dispase on the surface expression of Ly6C in the murine splenocytes 252

Figure 6.27 MFI of CD11b in neutrophil, dendritic cell, monocyte and macrophage cell populations of the WT and *Adamdec1*$^{-/-}$ mice during DSS challenge.....253

Figure 6.28 Expression of *Cd4* (A) and *Cd8* (B) in the colonic tissue of the WT and *Adamdec1*$^{-/-}$ mice in Cage 1 and Cage 2 during DSS challenge.....255

Figure 6.29 Expression of *Il-1β* (A) and *Tnf-α* (B) in the colonic tissue of the WT and *Adamdec1*$^{-/-}$ mice in Cage 1 and Cage 2 during DSS challenge.....256

Figure 6.30 Expression of *Cxcl1* in the colonic tissue of the WT and *Adamdec1*$^{-/-}$ mice in Cage 1 and Cage 2 during DSS challenge.....257

Figure 6.31 Expression of *Ccr2* (A) *and Ccl2* (B) in the colonic tissue of the WT and *Adamdec1*$^{-/-}$ mice in Cage 1 and Cage 2 during DSS challenge 258

Figure 6.32 Proportion of monocyte (A) and macrophage (B) population in the colonic tissue of the WT and *Adamdec1*$^{-/-}$ mice in Cage 1 and Cage 2 on day 9 of the DSS challenge.....259

Figure 6.33 Expression of *Lgr5* (A), *Ki67* (B) *and Cdx2* (C) in the colonic tissue of the WT and *Adamdec1*$^{-/-}$ mice in Cage 1 and Cage 2 during DSS challenge 261

Figure 6.34 Expression of *Fgf2* in the colonic tissue of the WT and *Adamdec1*$^{-/-}$ mice in Cage 1 and Cage 2 during DSS challenge 262

Figure 6.35 Weight change in the WT mice (Cage 1 and 2 combined) and *Adamdec1*$^{-/-}$ mice in Cage 1 and Cage 2 during DSS challenge……..271

Figure 7.1 Scheme demonstrating the number, sex and genotype of the mice in 4 cages used in Experiment 1 279

Figure 7.2 Scheme demonstrating the experimental set up of Experiment 2 .281

Figure 7.3 Global bacterial composition of the microbiome in faecal samples from WT, heterozygous and *Adamdec1*$^{-/-}$ mice assessed at 4 taxonomic levels: phylum (A), family (B), genus (C), species (D) in Experiment 1 290

Figure 7.4 Differentially abundant bacterial taxonomic groups in the microbiome of WT and *Adamdec1*$^{-/-}$ mice in Experiment 1. 291

Figure 7.5 Heatmap of the bacterial microbiome composition of WT, heterozygous and *Adamdec1*$^{-/-}$ mice assessed at phylum, genus, family and species levels in Experiment 1 292

Figure 7.6 F/B ratio of WT, heterozygous and *Adamdec1*$^{-/-}$ mice in Experiment 1 293

Figure 7.7 Alpha diversity of the bacterial microbiome of the mice according to their genotype (A), sex (B), sibling state (C) and cage (D) in Experiment 1 ...295

Figure 7.8 nMDS plot demonstrating the β diversity of the bacterial microbiome composition in WT, heterozygous and *Adamdec1*$^{-/-}$ mice in Experiment 1.....297

Figure 7.9 Global fungal composition of the microbiome in faecal samples from WT, heterozygous and *Adamdec1*$^{-/-}$ mice assessed at 6 taxonomic levels: phylum (A), class (B), order (C), family (D), genus (E) and species (F) in Experiment 1 299

Figure 7.10 nMDS plot demonstrating β diversity of the mycobiome composition in WT, heterozygous and *Adamdec1*$^{-/-}$ mice in Experiment 1.....301

Figure 7.11 Global bacterial composition of the microbiome in faecal samples from WT, heterozygous and *Adamdec1*$^{-/-}$ mice assessed at each timepoint, at 4 taxonomic levels: phylum (A), family (B), genus (C), species (D).....304

Figure 7.12 Differentially abundant taxonomic groups in the microbiome of the pre-pool samples collected from WT and *Adamdec1*$^{-/-}$ mice assessed at phylum (A), family (B and C), genus (D) and species (F and G) levels.....305

Figure 7.14 F/B ratio of WT and *Adamdec1*$^{-/-}$ mice assessed at pre-pool, pre-DSS and post-DSS timepoints 306

Figure 7.13 The relative abundances of *Duncaniella dubosii* and *Ligilactobacillus apodeme* in the microbiome of the pre-pool samples collected from WT and *Adamdec1*$^{-/-}$ mice 306

Figure 7.15 Alpha diversity of the bacterial microbiome in the pre-pool samples of WT and *Adamdec1*$^{-/-}$ mice.....307

Figure 7.16 nMDS plot demonstrating the β diversity of the bacterial microbiome composition in the pre-pool samples of WT and *Adamdec1*$^{-/-}$ mice 308

Figure 7.17 The relative abundance of *Paramuribaculum intestinale* in the microbiome of pre-DSS samples collected from WT and *Adamdec1*$^{-/-}$ mice ..309

Figure 7.18 Changes in the α diversity of WT and *Adamdec1*$^{-/-}$ mice bacterial microbiome over pre-pool, pre-DSS and post-DSS timepoints assessed by Chao1 (A and B) and Shannon (C and D) indices.....310

Figure 7.19 nMDS plot demonstrating the β diversity of the bacterial microbiome in pre-DSS samples of the WT and *Adamdec1*$^{-/-}$ mice 312

Figure 7.20 Heatmap of bacterial microbiome composition in the pre-pool, pre-DSS and post-DSS samples of WT and *Adamdec1*$^{-/-}$ mice assessed at phylum, genus, family and species levels.....314

Figure 7.21 Differentially abundant bacterial species in the microbiome of the post-DSS samples collected from WT and *Adamdec1*$^{-/-}$ mice.....315

Figure 7.22 nMDS plot demonstrating the β diversity of bacterial microbiome in the pre and post-DSS samples of WT and *Adamdec1*$^{-/-}$ mice 316

Figure 7.23 nMDS plot demonstrating the β diversity of bacterial microbiome composition in the post-DSS samples of WT and *Adamdec1*$^{-/-}$ mice 317

Figure 7.24 Global fungal composition of the microbiome in faecal samples from WT and *Adamdec1*$^{-/-}$ mice assessed at 6 taxonomic levels: phylum (A), class (B), order (C), family (D), genus (E) and species (F) 319

Figure 7.25 Differentially abundant fungal taxonomic groups in the microbiome of the pre-pool samples collected from WT and *Adamdec1*$^{-/-}$ mice assessed at phylum (A), order (B), genus (C) and species (D) levels 320

Figure 7.26 Alpha diversity of the fungal microbiome in the pre-pool samples of WT and *Adamdec1*$^{-/-}$ mice.....321

Figure 7.27 nMDS plot demonstrating the β diversity of the fungal microbiome composition in pre-pool samples of the WT and *Adamdec1*$^{-/-}$ mice 322

Figure 7.28 Change in the α diversity of WT and *Adamdec1*$^{-/-}$ mice fungal microbiome composition over pre-pool, pre-DSS and post-DSS timepoints assessed by Chao1 (A and B) and Shannon (C and D) indices. 323

Figure 7.29 nMDS plot demonstrating β diversity of mycobiota composition in the pre-DSS samples of WT and *Adamdec1*$^{-/-}$ mice.....325

Figure 7.30 nMDS plot demonstrating the β diversity of mycobiome composition in the pre and post-DSS samples of WT and *Adamdec1*$^{-/-}$ mice 327

Figure 7.31 nMDS plot demonstrating the β diversity of mycobiome composition in the post-DSS samples of WT and *Adamdec1*$^{-/-}$ mice 328

Figure 7.33 Correlation analysis between the DSS-induced severity of weight loss and relative abundance of *Duncaniella muricolitica* (A) and *Sangeribacter muris* (B).....330

Figure 7.32 The relative abundances of *Duncaniella muricolitica* (A) and *Sangeribacter muris* (B) according to the severity of weight loss induced by DSS-challenge.....330

Figure 7.34 Relative abundances of the differentially abundant bacterial taxonomic groups compared between the pre-DSS microbiome of *Adamdec1*$^{-/-}$ mice in Cage 1 and Cage 2 assessed at phylum (A, B and C), family (D and E), genus (F and G) and species (H) levels.....333

Figure 7.35 Relative abundances of *Duncaniella muricolitica* and *Sangerbacter muris* compared between the microbiome of *Adamdec1*$^{-/-}$ mice in Cage 1 and Cage 2.....334

Figure 7.36 Relative abundance of Basidiomycota compared between the microbiome of *Adamdec1*$^{-/-}$ mice in Cage 1 and Cage 2. 335

Figure 7.37 Bacterial (A) and fungal (B) α diversity by Chao1 index compared between the microbiome of *Adamdec1*$^{-/-}$ mice in Cage 1 and Cage 2.....336

Figure 7.38 nMDS plot demonstrating the β diversity of bacterial microbiome composition in the pre-DSS samples of WT and *Adamdec1*$^{-/-}$ mice in Cage 1 and Cage 2.....337

List of tables

Table 1.1 Summary of the domains of ADAMs and their main functions.....33

Table 1.2 Summary of the extra-intestinal inflammatory diseases in which differentially expressed levels of ADAMDEC1 have been identified by transcriptomic analyses.....57

Table 1.3 Summary of extra-intestinal cancers in which differentially expressed levels of ADAMDEC1 have been identified by transcriptomic analyses 59

Table 2.1 The working concentrations of antibiotics and reagents added to LB broth and LB agar.....67

Table 2.2 Components of PCR reaction for detection of construct by DNA gel electrophoresis.....72

Table 2.3 PCR condition for detection of construct by DNA gel electrophoresis. 72

Table 2.4 Components of reverse transcription reaction mixture to synthesise cDNA.....75

Table 2.5 Incubation times and temperatures used for reverse transcription to synthesise cDNA.....75

Table 2.6 Components of qPCR reaction mixture 76

Table 2.7 qPCR condition 76

Table 2.8 List of reagents and volumes used to make one SDS-PAGE gel. 78

Table 2.9 List of primary antibodies and working concentration used for Western blot. 79

Table 2.10 List of secondary antibodies and working concentration used for Western blot. 80

Table 2.11 Components of PCR reaction for mouse genotyping 81

Table 2.12 Primers used for mouse genotyping.....82

Table 2.13 PCR condition used for mouse genotyping 83

Table 3.1 List of stimulants and their working concentrations used for THP-1 stimulation experiments.....87

Table 3.2 List of inhibitors and their working concentrations used in THP-1 stimulation experiments.....88

Table 3.3 List of primers used to determine gene expressions in the THP-1 stimulation experiments.....88

Table 3.4 List of stimuli used to incubate THP-1 and their receptors, or target molecules, and downstream signalling pathways.....102

Table 4.1 Primers used to detect presence of *Hoxb8* in the transfected GP2-293 cells.....117

Table 4.2 List of antibodies used for flow cytometry analysis of the Hoxb8 cells, Hoxb8-derived macrophages and BMDMs.....122

Table 4.3 List of primers used to quantify expression of *Adamdec1* in Hoxb8 progenitor cells, Hoxb8-derived macrophages and BMDMs. 122

Table 5.1 Sequences of primers used to amplify human and mouse ADAMDEC1 from plasmid pCMV-hADAMDEC1-tGFP and pCMV-mADAMDEC1-Myc-DDK respectively. 153

Table 5.2 Components of the PCR reaction for amplification of human and mouse ADAMDEC1 coding sequences from pCMV-hADAMDEC1-tGFP and pCMV-mADAMDEC1-Myc-DDK plasmids respectively.....153

Table 5.3 PCR condition used for the amplification of human and mouse ADAMDEC1 coding sequences from pCMV-hADAMDEC1-tGFP and pCMV-mADAMDEC1-Myc-DDK plasmids respectively.....153

Table 5.4 Sequences of polyhedrin and SV40 primers. 155

Table 5.5 Sequences of pUC/M13 forward and reverse primers used to amplify the transposed sequence within the recombinant bacmid.....158

Table 5.6 Sequences of the mutagenic primers used to introduce single point mutations to generate pFastbac CT-TOPO transfer vector encoding human or mouse E353.....159

Table 5.7 Components of the mutagenesis PCR reaction to generate pFastbac CT-TOPO transfer vector encoding human and mouse E353.....159

Table 5.8 PCR condition for the mutagenesis PCR to generate pFastbac CT-TOPO transfer vector encoding human or mouse E353.....160

Table 5.9 Components of the ligation reaction mix for ligation of the mutagenesis PCR product.....160

Table 5.10 Steps of the purification process and main purpose of each step.192

Table 6.1 Number of the WT and *Adamdec1*$^{-/-}$ mice used in each experimental cohort and different end-point analyses. 212

Table 6.2 List of lymphoid panel antibodies used for flow cytometry analysis of the mouse colonic cells 216

Table 6.3 List of myeloid panel antibodies used for flow cytometry analysis of the mouse colonic cells 217

Table 6.4 List of lymphoid panel antibodies used for flow cytometry analysis of the murine splenocytes. Clone name of each antibody is specified in brackets. 219

Table 6.5 List of myeloid panel antibodies used for flow cytometry analysis of the murine splenocytes 219

Table 6.6 List of primers used for gene expression analysis of mouse colonic tissues by qPCR. 220

Table 6.7 List of cells and gating strategies to identify them by flow cytometry analysis. 226

Table 6.8 Summary of the change in gene expressions during the DSS-induced inflammation with respect to the genotype and cage difference. 271

Table 7.1 The demographics of mice used in Experiment 1 and the quantity and quality of microbial DNA extracted from the faecal samples. 287

Table 7.2 Demographics of the mice used in Experiment 2 and quantity of the microbial DNA extracted from the faecal samples collected from each mouse at 3 timepoint.....302

Table 7.33 Bacterial strains that have been reported to influence the severity of DSS-induced colitis and their relative abundances in the mice used in Experiment 2 329

Chapter 1

Introduction

1.1 Molecular and genetic characteristics of ADAMDEC1

1.1.1 ADAMDEC1 and ADAM proteins

ADAM like decysin 1 (ADAMDEC1) was first discovered through sequencing of messenger ribonucleic acid (RNA) extracted from dendritic cells of human tonsils in 1997.[2] Following its discovery, it was categorised to a family of A disintegrin and metalloproteases (ADAMs) due to its high sequence homology with ADAM proteins. ADAMs are highly conserved secreted or transmembrane metalloproteases that share a common structural composition consisting of N-terminal signalling sequence, prodomain, metalloprotease, disintegrin-like domain, cysteine-rich region, as well as transmembrane and cytoplasmic tail domains in a case of transmembrane ADAMs (Figure 1.1).

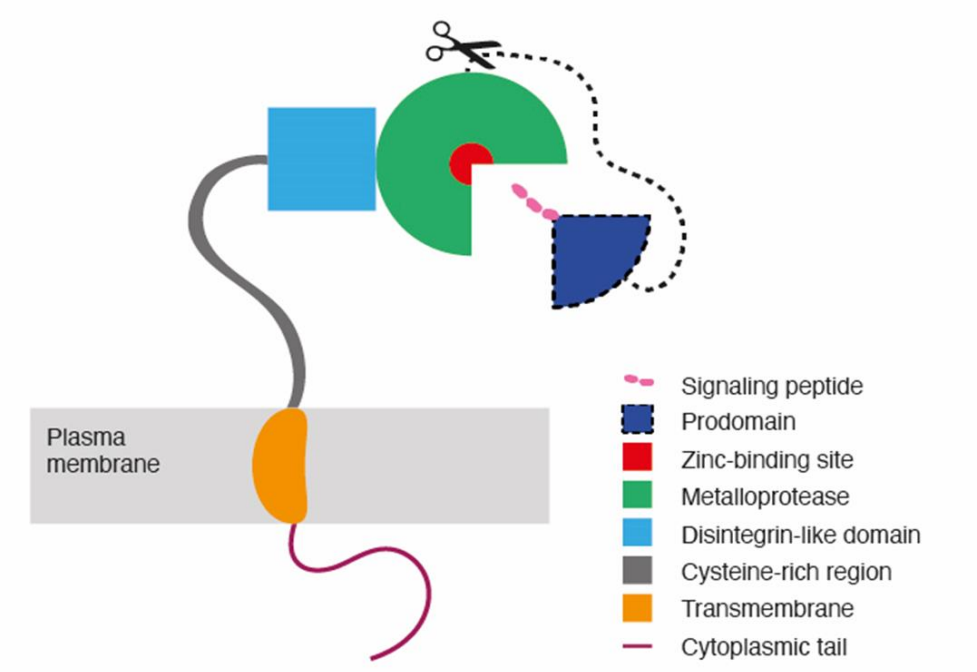

Figure 1.1 Schematic diagram of ADAMs structure. Each domain is represented by distinct colour. The scissors indicate the cleavage by proprotein convertases which results in a removal of the prodomain intracellularly.

The signalling peptide at the N-terminus facilitates the protein to move towards plasma membrane and is a characteristic feature of proteins destined to be

secreted or translocated across the plasma membrane.[3] The prodomain has an inhibitory function and interacts directly with the metalloprotease domain rendering it catalytically inactive.[4] The prodomain is usually removed intracellularly in the Golgi apparatus by proprotein convertases, such as furin, at one or more furin cleavage sites.[5] Disintegrin-like domain is believed to interact with cell surface integrins and play a role in cell to cell recognition and adhesions.[6,7] Cysteine-rich region is thought to regulate the metalloprotease activity and disintegrin-like domain's ability to interact with integrins.[8,9] Transmembrane domains anchor ADAMs to the plasma membrane, in the case of transmembrane ADAMs, and cytoplasmic tails are believed to be involved in intracellular signalling and trafficking.[3,5] The different domains of the ADAMs and their functions are listed in Table 1.1.

Domains	Function
N-terminal signalling sequence	Directs ADAMs to the plasma membrane[3]
Prodomain	Maintains catalytic latency of the metalloprotease and structural stability of ADAMs[4]
Metalloprotease	Catalysis[5]
Disintegrin-like domain	Integrin recognition[6,7]
Cysteine-rich region	Regulatory role of metalloprotease catalytic activity and disintegrin-like domain exposure[8,9]
Transmembrane	Anchoring ADAMS to the plasma membrane[3]
Cytoplasmic tail	Intracellular signalling and trafficking[5]

Table 1.1 Summary of the domains of ADAMs and their main functions.

ADAMs are found in a vast number of animals ranging from invertebrates such as nematodes and arthropods as well as chordate and its extensive family of vertebrates playing diverse roles in the physiology of a wide range of living organisms.[1] In humans, there are 21 ADAMs expressed at the protein level with various functions.

Thirteen of the 21 human ADAMs possess the characteristic catalytically active zinc-binding motif with 3 histidine (**H**) residues within their metalloprotease domain

(**H**EXX**H**XXGXX**H)**.[10] These ADAMs are believed to be active metalloproteases functioning as sheddases. One of the most well-known ADAMs with the sheddase activity is ADAM17, also known as tumour necrosis factor-α converting enzyme, TACE. ADAM17 cleaves membrane-bound tumour necrosis factor-α (TNF-α), releasing bioactive TNF-α, thereby playing a vital role in the immune system.[11] Each catalytically active ADAMs commonly has multiple ligands to their metalloprotease domains. For example, over 80 proteins have been reported to be processed by ADAM17, highlighting the versatility and importance of ADAMs' involvement in various biological processes.[12]

The remaining 8 ADAMs have altered zinc-binding motifs making them catalytically inactive, suggesting their primary roles in cell to cell recognition or adhesions through their disintegrin-like domain.[10] ADAM2, also known as fertilin-β, is one of such ADAMs and is believed to play a pivotal role in the fusion of sperm and oocyte during fertilisation by interacting with α6β1 integrin via its disintegrin-like domain.[13]

The exact roles of many ADAMs are still to be elucidated. However, overall, their conservation through evolution implies that they have vital functions in the physiology of living organism and dysregulation of ADAMs have been reported in the pathogenesis of numerous human diseases.[10]

ADAMDEC1, although belonging to the family of ADAMs, is considered to be a unique member of the family for a number of reasons. First of all, ADAMDEC1 is missing the cytoplasmic tail, transmembrane, cysteine-rich domains, thus consisting of only prodomain, metalloprotease and disintegrin-like domains. Additionally, its disintegrin-like domain is truncated, resulting in the protein structure comprised of 470 amino acids which is almost half the size of the typical ADAMs (Figure 1.2).[2] It is then believed to be cleaved at a furin recognition site releasing the prodomain intracellularly and secreted as a mature active form as indicated by the absence of transmembrane domain.[14–16] Furin has been, in fact, shown to process and cleave off the prodomain of ADAMDEC1 in vitro.[15] The immature uncleaved form of ADAMDEC1 has a molecular weight of ~52 kDa (referred to as immature ADAMDEC1 hereafter), whereas the mature cleaved form of ADAMDEC1 has a molecular weight of ~32 kDa (referred to as mature ADAMDEC1 hereafter).[14,15]

Furthermore, within the zinc-binding site of ADAMDEC1, the third histidine is replaced by aspartate (D) resulting in the motif sequence of **H**EXX**H**XXGXX**D** instead of the characteristic three histidine repeat, **H**EXX**H**XXGXX**H,** found in the rest of the catalytically active ADAMs (Figure 1.2).[2] The **H**EXX**H**XXGXX**D** motif within the zinc-binding site of ADAMDEC1 is extremely rare. It has only been found in three other proteins, immune inhibitor A and PrtV peptidases belonging to the M6, and snapalysin belonging to the M7 families of proteolytic enzymes, which are all bacterial proteases.[17–19] These bacterial proteases are known to be catalytically active. Thus, ADAMDEC1 is also expected to possess a metalloprotease function despite the critical alteration in the zinc-binding site. However, the replacement of the third histidine with aspartate has been shown to attenuate the catalytical activity and substrate specificity of ADAMDEC1 compared to typical ADAMs.[14,20] Moreover, the alteration in the zinc-binding motif seems to render a natural resistance to the usual regulation by tissue inhibitors of metalloproteases (TIMPs), which are naturally occurring inhibitors of ADAMs.[14] These findings suggest that ADAMDEC1 may have a physiological role that differs from the conventional ADAMs and is under an alternative regulatory system.

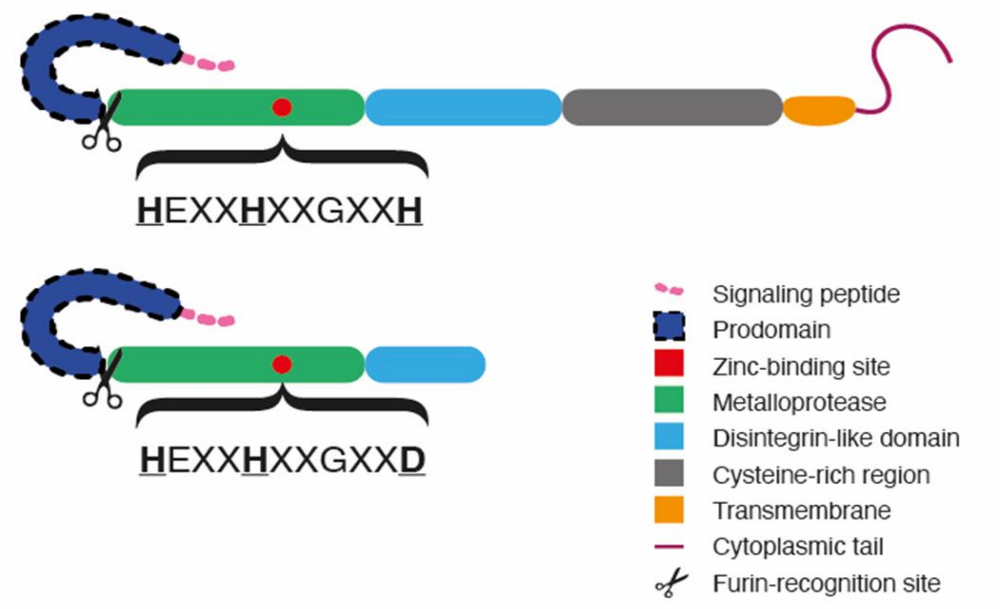

Figure 1.2 Simplified schematic diagram illustrating the differences between the structures of typical ADAMS and ADAMDEC1. The structural composition of ADAMDEC1 consists of a signalling peptide, prodomain, metalloprotease and disintegrin-like domain. The third histidine (H) of the characteristic histidine repeat motif in the zinc-binding site is replaced by aspartate (D) within the metalloprotease domain of ADAMDEC1.

1.1.2 Conservation of ADAMDEC1 through evolution

To date, *ADAMDEC1* has been identified in 130 mammalian species and no other classes of animals. ADAMDEC1 resembles ADAM7 and ADAM28 at both nucleotide and amino acid levels with a sequential amino acid homology of 36% and 47% respectively.[21] In humans, the genes of ADAMDEC1, ADAM7 and ADAM28 are all found clustering together on the short arm of chromosome 8 (8p). The clustering of these three ADAMs is similarly found in other mammalian species including marsupials and monotremes.[22] Whereas in the genomes of non-mammalian vertebrates such as fishes, amphibians, reptiles and birds, *ADAM7* and *ADAMDEC1* are absent with no existing orthologues for them.[22,23] Instead, in these animals *ADAM28* locus alone is present in this region. It is, therefore, suggested that *ADAMDEC1* is likely to have arisen by partial gene duplication from *ADAM28* at this locus, and acquired a novel function after the divergence of mammals from reptiles. Within the 130 species of mammals that possess *ADAMDEC1*, the zinc-binding site amino acid sequence of **H**ELG**H**XLGMX**D** has been either detected or predicted in 126 species so far. This amino acid sequence of the zinc-binding motif is highly conserved among these species, with variations seen at only two amino acid positions (Figure 1.3).

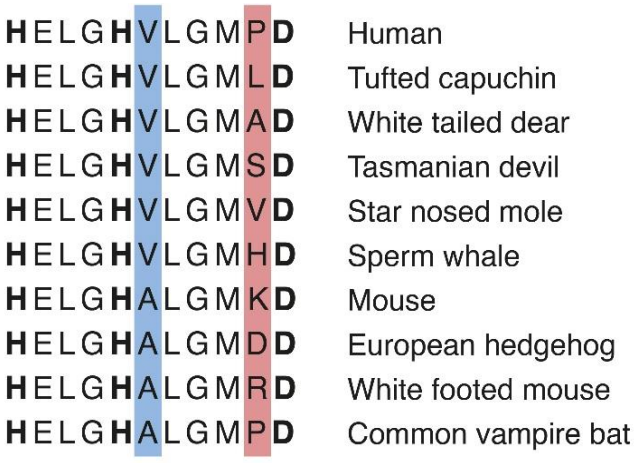

Figure 1.3 Amino acid sequence of the zinc-binding motif in various mammalian species. The zinc-binding motif in the metalloprotease catalytic site of ADAMDEC1 is highly conserved in mammals. The bold letters represent the amino acids positioned at the ADAMs' characteristic histidine repeat, in which the third histidine is replaced by aspartate (D) in ADAMDEC1. Only two and nine variations in amino acid exist at two positions, shaded blue and pink respectively, within the zinc-binding motif of ADAMDEC1 among the 130 mammalian species known to possess ADAMDEC1.

1.2 Physiological expression of ADAMDEC1 in healthy status

1.2.1 Highly restricted expression of ADAMDEC1 in healthy status

ADAMDEC1 is almost exclusively expressed in the gastrointestinal tract proximally from the duodenum to the rectum distally (Figure 1.4).[2,15,24–26] The highest expression is seen in the small intestine, followed by the rectum and the colon.[2,24] Outside of the gastrointestinal tract, *ADAMDEC1* is expressed in the lymph nodes, urinary bladder, tonsils, smooth muscles, placenta and spleen but to a much lesser extent.[2,24] This localised expression pattern seems to be conserved and has been reported in humans, pigs, and mice.[27]

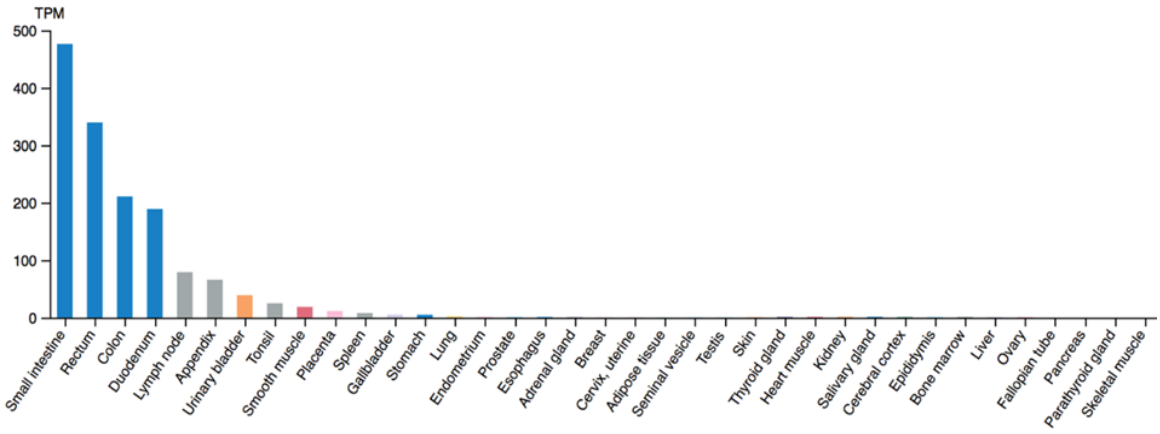

Figure 1.4 Distribution of *ADAMDEC1* in human tissue. *ADAMDEC1* is predominantly expressed in the gastrointestinal tract, proximally from the duodenum to the rectum distally.
Taken from The Human Protein Atlas https://www.proteinatlas.org[23]

These unique molecular, genetic and expression patterns of ADAMDEC1 suggest that it is likely to play a vital role in the physiology of mammals, particularly within the intestine. However, its definitive biological function remains to be unknown.

1.3 Potential functions of metalloprotease and integrin-like domains

1.3.1 Catalytical activity and proteolytic target of ADAMDEC1

Very little is known about the catalytical activity of ADAMDEC1 or its true biological targets. The mature recombinant human ADAMDEC1 has demonstrated a catalytic ability to process α2-macroglobulin, casein and carboxymethylated transferrin in vitro.[14,16,20,28,29] The ADAMDEC1's ability to bind to α2-macroglobulin was

unaffected by the removal of its disintegrin-like domain. However, its ability to cleave α2-macroglobulin and casein were lost when the glutamate following the first histidine in the zinc-binding motif was replaced by alanine (H**A**XXHXXGXXD), the catalytically inactive mutant ADAMDEC1 E353A (referred to as E353A hereafter).[14,16] These findings indicate that the catalytic function of ADAMDEC1 depends on the zinc-binding motif in the metalloprotease domain. Interestingly, however, the mature recombinant mouse ADAMDEC1 does not demonstrate any catalytical activity on casein or carboxymethylated transferrin. Moreover, the cleavage of α2-macroglobulin by ADAMDEC1 in vitro required 20 – 65 hours of incubation, which is much slower than expected if α2-macroglobulin was a true physiological substrate for ADAMDEC1.[14,16,20,28] These findings suggest that these compounds are unlikely to be the true biological substrates for ADAMDEC1.

One potential substrate for ADAMDEC1 with more physiological relevance is epidermal growth factor (EGF). The mature ADAMDEC1 was shown to cleave the membrane-bound pro-EGF on the surface of activated platelets functioning as a sheddase in accordance with the majority of the ADAMs family.[30] Chymostatin, a naturally occurring protease inhibitor which is known to inhibit the hydrolysis reaction of several ADAMs, was also able to inhibit the cleavage of pro-EGF by ADAMDEC1. However, in healthy intestinal lamina propria, where high expression of ADAMDEC1 is seen normally, the abundance of platelets is low. Additionally, within the intestine, EGF is believed to be secreted predominantly from Paneth cells of the intestinal epithelium, not requiring the involvement of a sheddase.[31] These findings suggest pro-EGF is unlikely to be the only or main biological proteolytic target of ADAMDEC1. Another potential physiological target of ADAMDEC1's catalytical activity is fibroblast growth factor-2 (FGF2). ADAMDEC1 was demonstrated to cleave complex-bound FGF2 within the extracellular matrix (ECM) surrounding glioblastoma (GBM) cancer stem cells.[29] FGF2 was detected in the media minutes after GBM cancer stem cells were incubated with recombinant ADAMDEC1. In tissue, FGF2 is secreted from cells and forms complex by binding to various proteins including immobilised molecules anchored within ECM. The bioavailability, stability and concentration of FGF2 are tightly regulated through the formation and breakage of these complexes within the microenvironment.[32] ADAMDEC1 was shown to increase the concentration of FGF2 by increasing the release of FGF2 from ECM rather than by stimulating the

secretion from the GMB cancer stem cells.[29] In the context of the healthy intestine, FGF2 is mainly expressed by mesenchymal cells at the basement membrane surrounding the crypts and is believed to play various roles, including the homeostasis of epithelium.[33] Further studies are, however, needed to provide the relevance of ADAMDEC1 on FGF2 within the intestine under physiological conditions.

Overall, there is evidence to support a potential catalytic ability of ADAMDEC1 that depends on its metalloprotease domain. However, the catalytic targets suggested to date do not reflect the physiological expression pattern of ADAMDEC1, which is confined almost exclusively to the intestine. Thus, it is anticipated that the true main physiological substrates of ADAMDEC1 are yet to be fully elucidated.

1.3.2 Potential function of Disintegrin-like domain of ADAMDEC1

It had been speculated that the disintegrin-like domain of ADAMDEC1 was unlikely to function as an integrin recognition adhesion molecule based on the fact that it is truncated. However, in a study where ADAMDEC1 was shown to promote the apical extrusion of oncogene, RasV12, expressing Madin-Darby Canine Kidney (MDCK) epithelial cells, the catalytically inactive mutant E353A maintained the ability to do so. This indicated a distinct role of the disintegrin-like domain of ADAMDEC1 independent of the metalloprotease activity.[28] The exact mechanistic function of ADAMDEC1 and its disintegrin-like domain in the apical extrusion process, which has been termed epithelial defence against cancer (EDAC), is still unclear. (Discussed in more detail later.)

1.4 Expression of ADAMDEC1 at the cellular level and its potential function in healthy intestine

1.4.1 ADAMDEC1 expression in the monocyte-derived macrophages of the intestine

Earlier studies involving in-situ hybridisation of mouse intestinal tissues and Northern blot of macrophages isolated from human intestinal tissues demonstrated that ADAMDEC1 was expressed in the macrophages within the lamina propria of the healthy intestine.[25,26] This is further supported by numerous in vitro studies where induction of ADAMDEC1 was detected during differentiation of peripheral

blood monocytes into macrophages by various differentiation stimuli such as macrophage colony-stimulating factor (MCSF), human AB serum and 1α-25-dihydroxyvitamin D3.[16,25,34] Additionally, induction of ADAMDEC1 was also detected upon differentiation of THP-1 cells, a human monocyte cell line, into macrophages-like cells by Phorbol 12-myristate 13-acetate (PMA) or 1α-25-dihydroxyvitamin D3.[25]

Under a normal physiological state, the majority of the macrophages of the gastrointestinal tract are believed to be continuously replenished by the migration and differentiation of circulating monocytes into the lamina propria.[35,36] On the other hand, resident macrophages of the organs, except for the gastrointestinal tract, are believed to be replenished predominantly by self-renewing yolk-sac and/or embryonic foetal liver precursors. In these organs, where ADAMDEC1 is not normally expressed under healthy status, recruitment of circulating monocytes and monocyte-derived macrophages (MDMs) are thought to play a role in pathological situations such as inflammation, during which upregulation of ADAMDEC1 has been reported (discussed in more detail below). Thus, based on these findings, it has been speculated that the strikingly high abundance of ADAMDEC1 in the healthy gastrointestinal tract is secondary to the continuous migration and differentiation of circulating monocytes into macrophages in the lamina propria.

This hypothesis is supported by in vitro studies comparing transcriptomes of the MCSF-differentiated MDM and granulocyte-macrophage colony-stimulating factor (GMCSF)-differentiated MDMs which are historically termed “M2”, or anti-inflammatory, and “M1”, or pro-inflammatory, respectively. A higher expression of ADAMDEC1 was seen in the MCSF-differentiated MDMs compared to the GMCSF-differentiated MDMs.[37,38] It has been widely accepted that, in general, the resident intestinal macrophages resemble the phenotype of the MCSF-differentiated “M2” MDMs than the GMCSF-differentiated “M1“ MDMs. This is based on the characteristics of the MCSF-differentiated “M2” MDMs including constitutive production of IL-10, greater phagocytic activity and hyporesponsiveness to toll-like receptor (TLR) stimulation, as well as promoting the expansion of Treg cells.[39] The upregulation of ADAMDEC1 seen during the differentiation of peripheral blood monocytes into macrophages by 1α-25-dihydroxyvitamin D3 in vitro is also supportive of this hypothesis as the 1α-25-

dihydroxyvitamin D3-differentiated macrophages exhibit similar phenotype to the MCSF-differentiated macrophages.[40,41]

However, a more recent study had found an opposite observation where a greater increase in *ADAMDEC1* expression was seen when the human AB serum-differentiated MDMs were further activated by a combination of lipopolysaccharide (LPS) and interferon-γ (IFN-γ), thereby activating them more towards "M1" phenotype. This was in comparison to when the MDMs were activated by IL-4, rendering them more towards the "M2" phenotype.[42] Furthermore, this LPS and IFN-γ-induced "M1" activation was disrupted by siRNA-mediated silencing of *ADAMDEC1,* suggesting that ADAMDEC1 played a functional role in the pro-inflammatory activation of the MDMs in vitro. Another study, by Western blot, also demonstrated that the amount of ADAMDEC1 secreted from the "inactivated", "M1-activated" and "M2-activated" MDMs did not differ significantly. However, the differentiation and activation method used to differentiate peripheral blood monocytes to MDMs in this study were not stated.[16] Several other studies comparing the transcriptomics of the MCSF-differentiated MDMs activated to more "M1" or "M2" phenotypes by a combination of LPS and IFN-γ, or IL-4 respectively also did not detect *ADAMDEC1* to be differentially expressed between the two activated MDMs.[43–45]

In summary, current evidence suggests that the expression and secretion of ADAMDEC1 are induced during early monocyte to macrophage differentiation irrespective of the final phenotype. However, consideration must be taken regarding the applicability of these in vitro studies, using various phenotypes of MDMs, to the in-situ *bona fide* monocyte to macrophage differentiation process in the intestine. Macrophages are considered to be highly heterogeneous cells with extremely high plasticity.[46] Their phenotypes are believed to be on a range of the spectrum that depends on the surrounding microenvironment.[47] Current models of in vitro monocyte to macrophage differentiation are unable to account for the complexity of the in-situ gut microenvironment. Hence they are unlikely to yield an exact replication of the resident intestinal macrophages. Furthermore, categorising MDMs into "M1" and "M2" and applying M2 macrophages to represent the resident intestinal macrophages has become myopic due to the ever-growing evidence of the extremely high heterogenicity of macrophages. This is highlighted by a single-cell RNA sequencing (scRNA-seq) study of human healthy intestine tissue that

identified 11 subtypes of intestinal monocyte/macrophage populations in which ADAMDEC1 was identified as one of the highly expressed genes in one subpopulation of the macrophages.[48] Nevertheless, overall, the currently available evidence supports the hypothesis that the exclusively high expression of ADAMDEC1 seen in the lamina propria of the gastrointestinal tract is likely to reflect the continuous recruitment and differentiation of circulating monocytes into intestinal macrophages.

1.4.2 ADAMDEC1 expression in non-monocyte derived macrophages of the intestine

More recently, there has been some evidence to suggest ADAMDEC1 is expressed in the non-monocytes derived macrophages of the intestine in healthy status. This is partially built on the findings from recent studies that challenged the long-believed concept of the resident intestinal macrophages being fully dependent on the replenishment by recruitment and differentiation of circulating monocytes.[49,50] By using a fate-mapping approach, a population of self-renewing resident macrophages was identified in the healthy intestine which were predominantly located in the submucosa and muscularis externa regions rather than lamina propria.[50] Within the self-renewing population of the resident intestinal macrophages, four further sub-types were identified which had distinct anatomical localisation. Interestingly, *ADAMDEC1* was identified as one of the top marker genes for the second most abundant self-renewing macrophages subpopulation of the lamina propria and submucosa, providing evidence that expression of *ADAMDEC1* is not limited to the macrophages of monocyte origin within the intestine. The gene expression profiling of these *ADAMDEC1*$^{+}$ self-renewing macrophages revealed that they were enriched for vascular and immune response associated genes. In-situ hybridisation further demonstrated a close proximity of these self-renewing *ADAMDEC1*$^{+}$ macrophages to the vasculature, whereas the self-renewing *ADAMDEC1*$^{-}$ macrophages were located within the muscularis externa. Moreover, the ablation of this self-renewing *ADAMDEC1*-expressing macrophage subpopulation resulted in disruption of the vasculature with increased vascular permeability, suggesting the *ADAMDEC1*$^{+}$ macrophages' role in supporting and maintaining the local vessels. A precise role of ADAMDEC1 in vascular regulation has not been described. However, *ADAMDEC1* expression has

been identified within the placenta at mid-pregnancy specifically at the foeto-maternal junction and around maternal vessels with an increase in expression that mirrored angiogenesis.[51] Another scRNA-seq study using cells from healthy human colonic tissues sorted for macrophages also identified a subpopulation of macrophages that expressed a high level of *ADAMDEC1* in association with a gene profile consistent with cells of the self-renewing origin.[52] In this study, the authors also analysed data from another scRNA-seq study using unsorted global cells of intestinal tissues collected from human foetuses, which showed a high expression of *ADAMDEC1* in one subpopulation of macrophages that expressed low levels of monocyte-related genes. In summary, as the concept of the presence of self-renewing macrophages within the intestine evolves, more evidence is emerging to suggest the expression of ADAMDEC1 within the intestine is not limited to the MDMs. Thus, the exclusive expression pattern of ADAMDEC1 confined in the gastrointestinal tract might not be solely secondary to the high abundance of MDMs.

1.4.3 ADAMDEC1 expression in non-macrophage cells of the intestine

With the advance in technology and use of scRNA-seq, more evidence is emerging to suggest that cells other than macrophages in the healthy intestine express *ADAMDEC1*. A scRNA-seq study using $CD45^+$ and $EpCAM^+$ cell-depleted mesenchymal cells of healthy human intestine identified a population of fibroblasts that expressed high levels of *ADAMDEC1,* which were found to be located throughout the lamina propria.[53] A similar finding was also reported by two other scRNA-seq studies, using unsorted global cells of adult and foetal human healthy intestinal tissues, where the size of fibroblast population expressing a high level of *ADAMDEC1* increased with the foetal age.[54,55] Another study using mouse colonic tissues also identified a subpopulation of fibroblasts that expressed a high level of *Adamdec1* by scRNA-seq of $CD45^+$ and $EpCAM^+$ cell-depleted mesenchymal cells.[56] The expression of *Adamdec1* also increased in the fibroblast subpopulation during multiple cycles of low-dose sodium dextran sulfate (DSS) challenge to induce chronic mucosal inflammation in mice. This increase in *Adamdec1* level was seen in association with the transition of fibroblasts into myofibroblasts. This study, more importantly, showed an exaggerated form of mucosal inflammation in *Adamdec1* knockout (*Adamdec1*$^{-/-}$) mice during DSS-induced colitis in association

with impaired ECM repair, indicating a potential mechanistic role of ADAMDEC1 in ECM remodelling (discussed in more detail later in 1.7.1).[56]

In summary, earlier studies have pointed towards the exclusive expression of ADAMDEC1 in the healthy intestine to be secondary to the physiologically high abundance of MDMs within the intestine. This is supported overwhelmingly by numerous in vitro studies demonstrating upregulation of ADAMDEC1 during monocyte to macrophage differentiation at the RNA messenger and protein levels. However, the function of ADAMDEC1 with respect to MDMs within lamina propria of the healthy intestine remains undetermined. More recent studies have revealed that other types of cells, such as self-renewing macrophages, fibroblasts and myofibroblasts express ADAMDEC1 in the healthy gastrointestinal tract and the potential involvement of ADAMDEC1 in vascular homeostasis and ECM remodelling (Figure 1.5). However, the vast majority of these studies identifying cells other than MDMs expressing *ADAMDEC1* within the intestine are sc-RNA-seq analyses, thus, further ex vivo or in vitro studies are required to validate these findings.

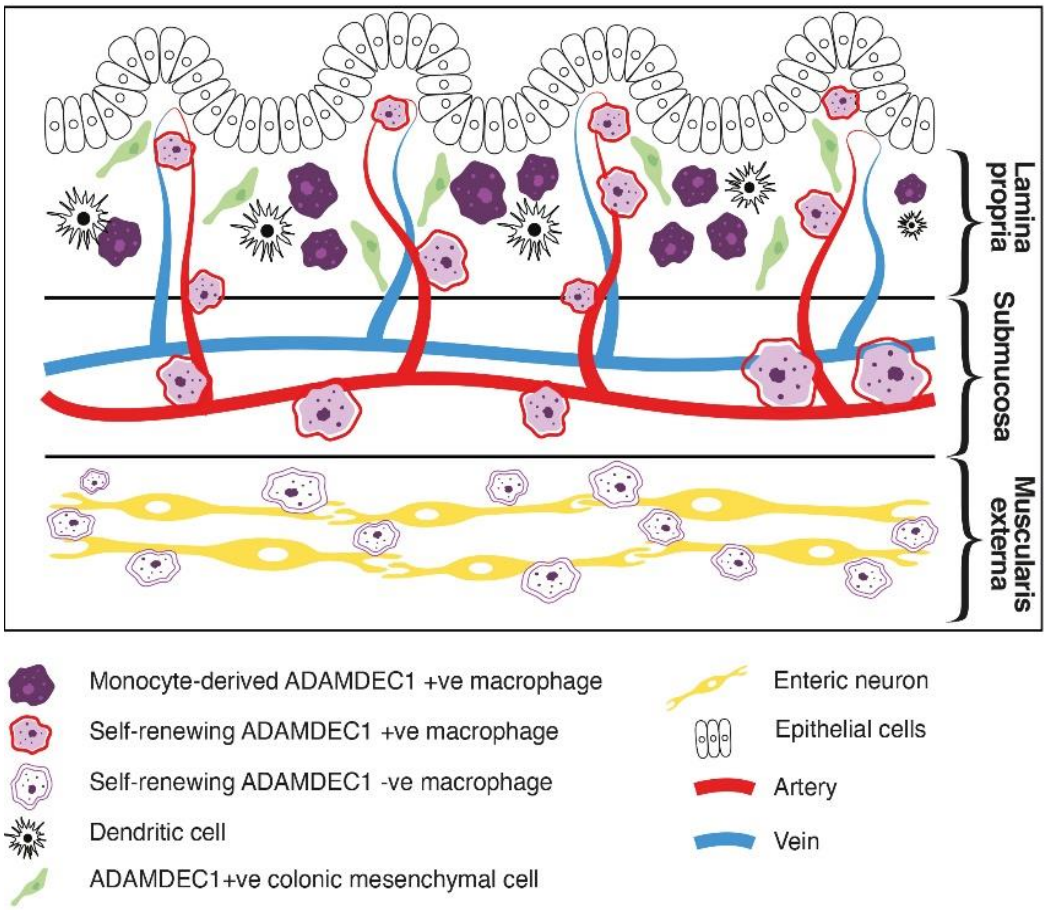

Figure 1.5 Schematic diagram of colonic tissue and *ADAMDEC1* expressing cells. Monocyte-derived macrophages and fibroblasts expressing *ADAMDEC1* are found through lamina propria. Self-renewing macrophages expressing *ADAMDEC1* are located in lamina propria and submucosa close to the vasculature. Self-renewing macrophages that do not express *ADAMDEC1* are located within muscularis externa.

1.5 Expression of ADAMDEC1 at a cellular level in extra-intestinal organs

The expression of ADAMDEC1 is much lower in the extra-intestinal organs in comparison to the intestine. However, similar to the intestine, scRNA-seq data suggests ADAMDEC1 to be expressed predominantly in macrophages within the organs outside of the intestine (Figure 1.6).

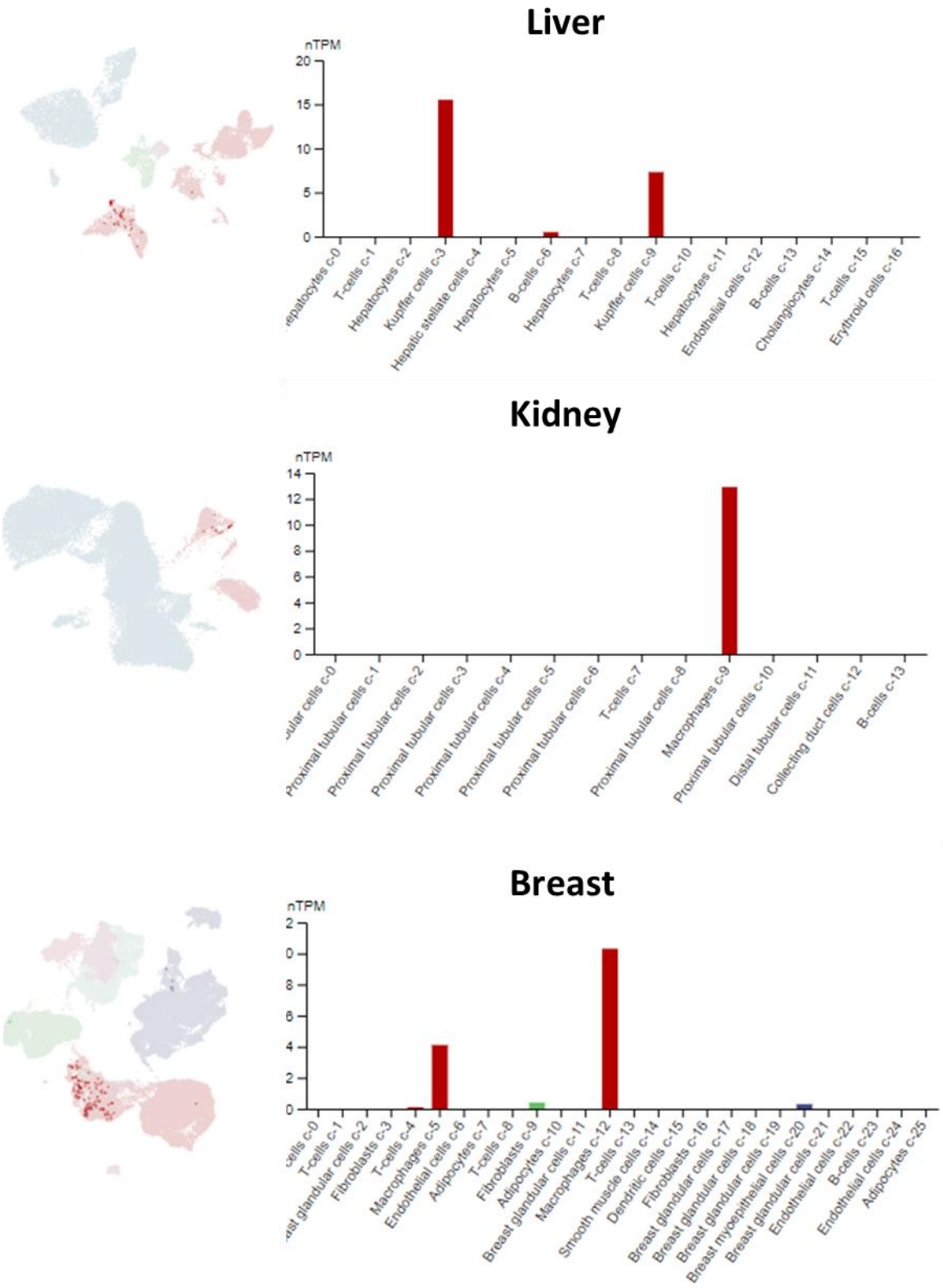

Figure 1.6 Expression of *ADAMDEC1* in various types of cell within extra-intestinal organs analysed by scRNA-seq. *ADAMDEC1* is predominantly expressed by macrophages in the extra-intestinal organs. Taken from The Human Protein Atlas https://www.proteinatlas.org/ENSG00000134028-ADAMDEC1/single+cell+type[322]

1.6 Expression and potential involvement of ADAMDEC1 in human diseases

1.6.1 Gastrointestinal inflammatory disease

The physiological highly expressed level of ADAMDEC1 within the intestine is significantly reduced in the tissues of inflammatory bowel disease (IBD) (Figure 1.7).[57] IBD is comprised of Crohn's disease and ulcerative colitis. The main manifestation of both of these diseases is a chronic inflammation affecting the bowel, although they have distinct pathogeneses. Except for the data from transcriptomic analysis, the available data regarding the association between ADAMDEC1 and ulcerative colitis is extremely sparse. However, there is more evidence regarding the connection between ADAMDEC1 and Crohn's disease.

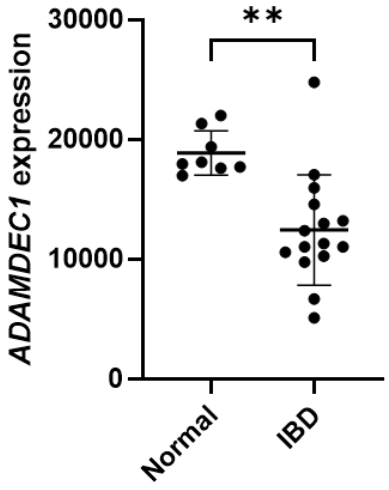

Figure 1.7 Expression of *ADAMDEC1* in normal and IBD tissues analysed using the data extracted from NCBI Gene Expression Omnibus (GEO) data repository. GEO GSE4183[57] The expression of *ADAMDEC1* is significantly lower in the tissue of IBD (including tissues from patients with Crohn's disease and ulcerative colitis) in comparison to the tissue of healthy controls. Unpaired student t-test was used. The graph shows mean with SD.

1.6.1.1 Crohn's disease

The association between ADAMDEC1 and gastrointestinal inflammatory disease was first reported in 2014 by a study involving a whole genome transcriptomic analysis of intestinal tissue taken from healthy controls and patients with Crohn's disease.[58] Crohn's disease is characterised by a patchy transmural chronic inflammation of the bowel, most commonly affecting the terminal ileum and proximal colon, with alternating periods of remission and relapse of various durations that last life-long. The study identified *ADAMDEC1* to be significantly downregulated in the inflamed ileal tissues taken from patients with Crohn's disease compared to healthy controls. Notably, the low expression of *ADAMDEC1* in the inflamed ileum from the Crohn's disease cohort was unaffected after the patients received Infliximab, anti-TNF-α antibody therapy. The lack of responsiveness of *ADAMDEC1* expression by Infliximab was in contrast to other matrix metalloproteinases, TIMPs and ADAMs as the dysregulated expression levels of these proteins pre-Infliximab therapy were restored in the patients who responded to the therapy, demonstrating a strong correlation with the resolution of inflammation. This suggests that the lower expression of *ADAMDEC1* in the ileum of Crohn's disease was independent of the degree of mucosal inflammation and, therefore, might have an underlying role in the pathogenesis of the disease. A further link between ADAMDEC1 and Crohn's disease was reported by another study in 2015 in which MDMs generated from circulating monocytes of patients with Crohn's disease displayed a lower *ADAMDEC1* expression compared to the MDMs of healthy controls.[59] Furthermore, when these MDMs were stimulated with heat-killed *Escherichia coli* (HkEc), the Crohn's disease MDMs secreted lower levels of TNF-α and IFN-γ compared to the healthy control MDMs.

Although the pathophysiology of Crohn's disease is yet to be fully elucidated, one of the hypotheses is an inability of the innate immune system to elicit an effective inflammatory response at a time of mucosal barrier breakdown.[60] In this hypothesis, this leads to defective initial clearance of invading bacteria and subsequent inappropriate activation of the adaptive immune response, involving T helper 1 (Th1) and T helper 17 (Th17) cells, leading to the development of chronic inflammation. In support of this hypothesis, an aberrant macrophage cytokine secretion leading to an impaired bacterial clearance by MDMs as well as an impaired acute immune response in the intestine following trauma to the mucosa

have been reported in Crohn's disease.[61,62] It is possible, therefore, that the reduced expression level of ADAMDEC1 in macrophages affects the phenotype of the macrophages that might alter the host's immune response and contribute to the disease pathogenesis of Crohn's disease (Figure 1.8).

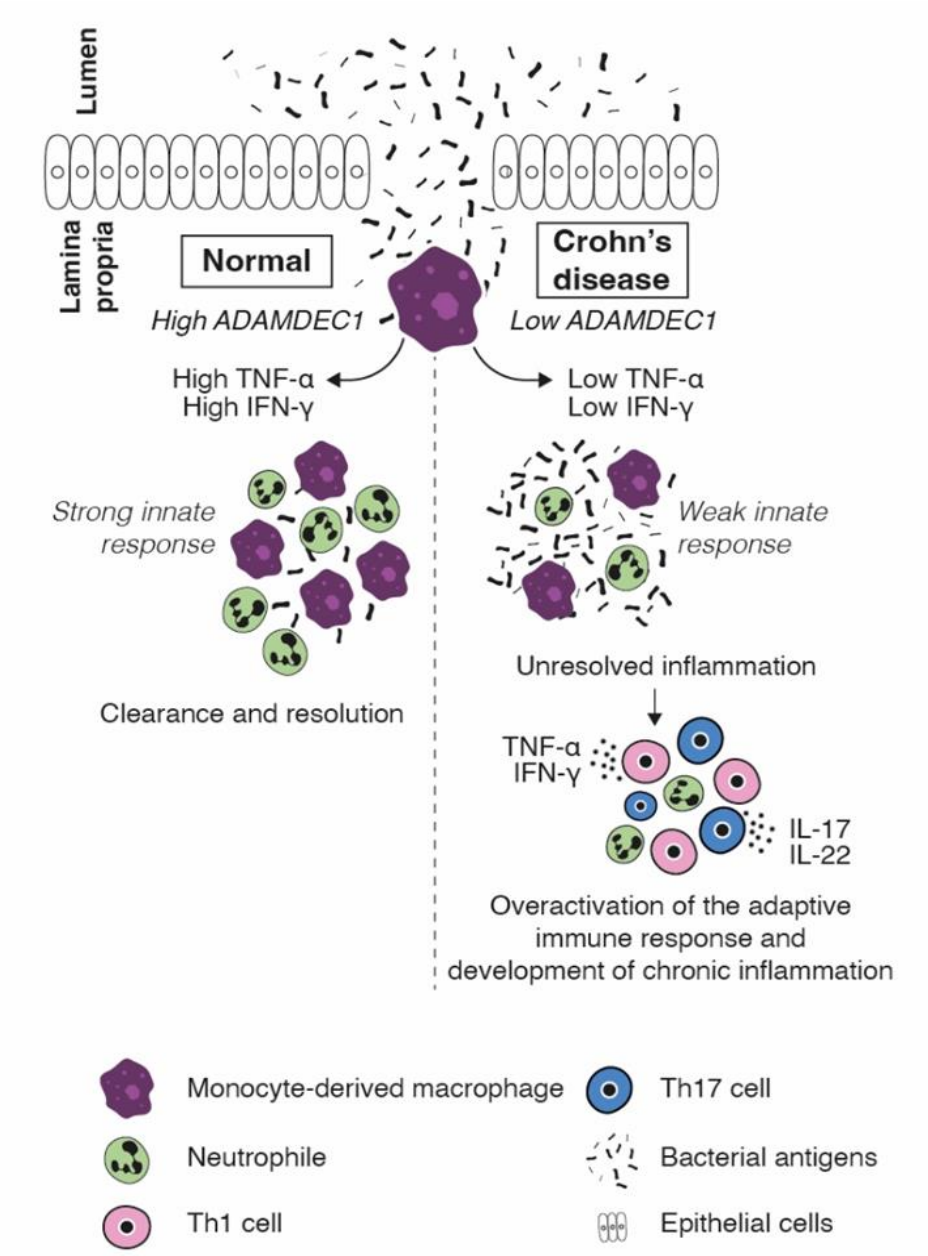

Figure 1.8 Possible mechanism through which the reduced expression of *ADAMDEC1* in the monocyte-derived macrophages in the lamina propria could lead to chronic mucosal inflammation of Crohn's disease. Monocytes-derived macrophages expressing reduced levels of *ADAMDEC1* secrete lower levels of TNF-α and IFN-γ leading to weak innate response against invading pathogens at the time of mucosal barrier breakdown. This leads to unresolved inflammation and subsequent activation of the adaptive immune response involving Th1 and Th17 cells resulting in the development of chronic inflammation.[60]

Th1: T helper 1, Th17: T helper 17

1.6.2 Gastrointestinal cancer

1.6.2.1 Colorectal adenocarcinoma

Similarly to the trend seen in Crohn's disease, the normally high expression of *ADAMDEC1* in the colon was shown to be drastically under-expressed in the tissues of various stages of colorectal adenocarcinoma (CRC) by several transcriptomic analyses (Figure 1.9 A, B and C).[57,63,64] The downregulated expression of *ADAMDEC1* has also been detected in the tissues of colorectal adenoma, a precursor lesion of CRC, in comparison to normal tissue by several studies (Figure 1.9 B and C),[57,64] including a study where a paired expression comparison was performed between the tissues of adenoma and normal mucosa from the same individuals (Figure 1.9 E).[65] The low expressions of *ADAMDEC1* in the tissue of CRC and adenoma do not seem to be rendered by a reduction in the abundance of macrophages as there were no differences in the macrophage marker, *CD68*, between the normal, adenoma and CRC tissues (Figure 1.9 D).[64] Another study showed that the expressions of *ADAMDEC1* were lower in the tissues of CRC and colorectal adenoma as well as the intestinal tissues taken from patients with IBD in comparison to normal tissues (Figure 1.9 B).[57] The IBD cohort in this transcriptomic analysis included patients with Crohn's disease and ulcerative colitis. Ulcerative colitis is characterised by a chronic continuous mucosal inflammation of remitting and relapsing nature affecting the colon. IBD, particularly ulcerative colitis, is a well-established risk factor for CRC. An increase in the epithelial cell turnover leading to dysplasia and aberrations in immune surveillance against tumour in the background of a chronic inflammatory environment, which itself is pro-neoplastic, are believed to play roles in the development of CRC in the presence of IBD.[66]

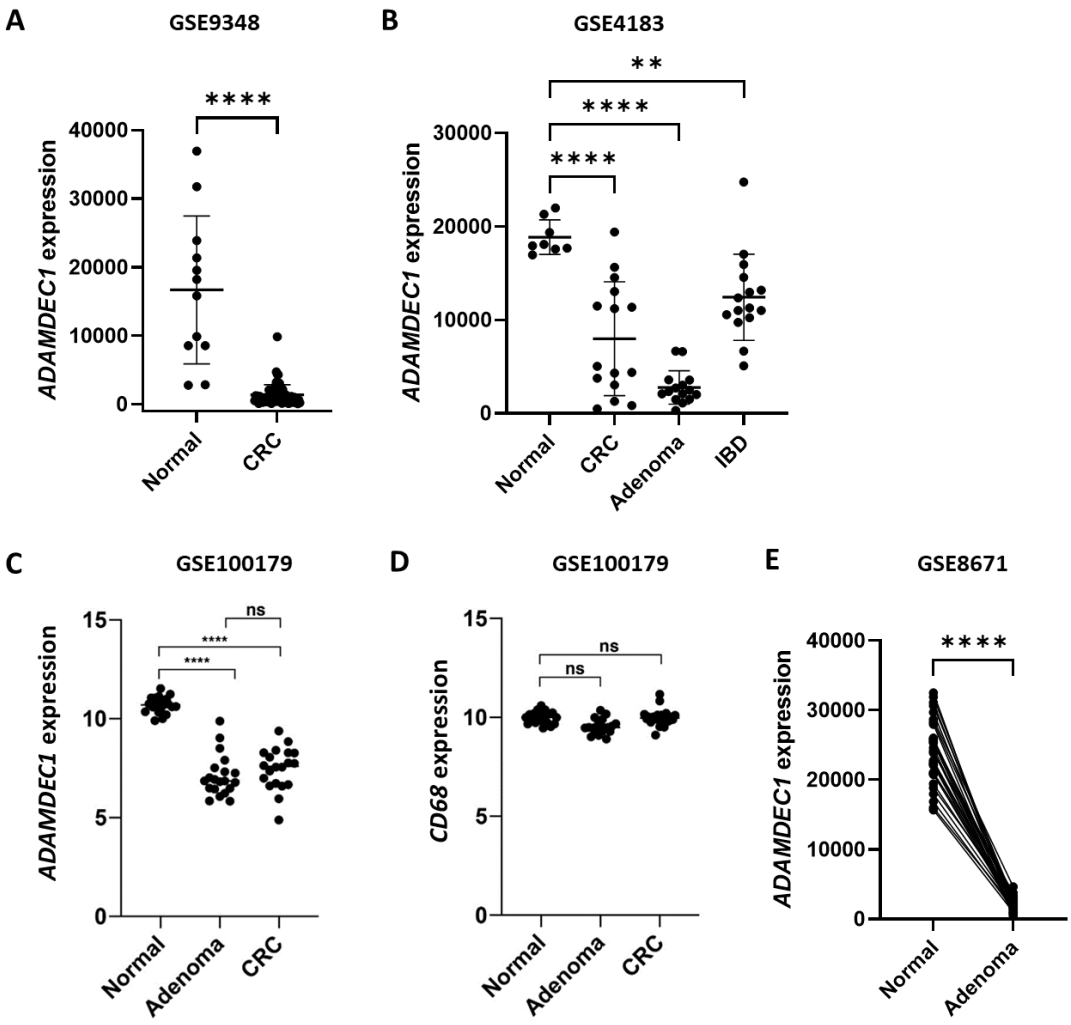

Figure 1.9 Expression of genes in normal adenoma, CRC and IBD tissues analysed using data extracted from NCBI Gene Expression Omnibus (GEO) data repository.

A. The expression of *ADAMDEC1* is significantly lower in the tissue of CRC in comparison to the normal tissue. GEO ID GSE9348[63]

B. The expression of *ADAMDEC1* is significantly lower in the tissues of CRC, adenoma and IBD in comparison to the normal tissue. GEO ID GSE4183[57]

C and D. The expression of *ADAMDEC1* in the tissues of adenoma and CRC are significantly lower in comparison to the normal tissue. However, there are no differences in the expressions of *CD68* between these tissues. GEO ID GSE100179[64]

E. The expression of *ADAMDEC1* is significantly lower in the adenoma tissue in comparison to the paired normal tissue taken from the same individuals. GEO ID GSE8671[65]

Data for Graph A -D were analysed by One-way NAOVA. Data for Graph E was analysed by paired student t-test.

CRC: Colorectal adenocarcinoma, IBD: Inflammatory bowel disease, ns: Non-significant, **: $p < 0.01$, ****: $p < 0.001$

Despite the growing evidence of the reduced level of *ADAMDEC1* in the CRC, discovered by numerous transcriptomic analyses, studies exploring the explanation behind the reduced ADAMDEC1 expression in CRC or the potential mechanistic role of the reduced ADAMDEC1 expression in the tumourigenesis of CRC are limited.

One possible explanation for the reduced level of *ADAMDEC1* found in the tissue of CRC is by loss of heterozygosity (LOH) of the gene. The LOH on chromosome 8p is well established in the pathogenesis of CRC, which is associated with more invasive and poor clinical outcome.[67,68] One study identified LOH in a region of 8p21-23, where the locus for *ADAMDEC1* is located, in the tissues of both primary and secondary CRC in association with a significantly reduced expression of *ADAMDEC1*.[69] Another study also identified a frequent LOH at 8p21-22 within the tissue of CRC, both primary and metastatic, again in association with a reduction in *ADAMDEC1* expression. These findings indicate the reduction in *ADAMDEC1* level occurs during the tumourigenesis of CRC from the pre-cancerous stage to the metastatic progression, and that the reduced *ADAMDEC1* expression might be secondary to p8 LOH. Neither the genomic deoxyribonucleic acid (DNA) analysis for identification of LOH nor transcriptomic studies exploring the expression of *ADAMDEC1* within the CRC tissues specify the type of cells in which the LOH or the reduction of *ADAMDEC1* occurs. The LOH, which is thought to be one of the fundamental pathogenetic events leading to CRC, is postulated to occur in the epithelial cells where *ADAMDEC1* has not been reported to be normally expressed. Thus, the relevance of the reported LOH in the region of 8p21-23 in association with the reduction of *ADAMDEC1*, that is normally believed to be expressed in the macrophages or mesenchymal cells of the intestine, within the CRC tissues, therefore, remains unknown.

With regards to a possible mechanism through which the low *ADAMDEC1* expression might contribute to the tumourigenesis of CRC is the *ADAMDEC1*'s reported role in EDAC. EDAC refers to an anti-cancer defence process in which the transformed epithelial cells are recognised by the surrounding normal epithelial cells and are actively eliminated from the epithelial monolayer.[70] The expulsion of the transformed cells during EDAC occurs through a series of modifications in cytoskeletal proteins, such as filamin and vimentin, within the surrounding normal epithelial cells.[71] Using MDCK cells, the expression of *ADAMDEC1* in the normal

epithelial cells was shown to increase when these cells were positioned adjacent to the oncogene-expressing transformed epithelial cells.[28] A subsequent knockdown of *ADAMDEC1* in the normal epithelial cells resulted in a failure of filamin accumulation at the interface of the normal and transformed cell, and the expulsion of the transformed epithelial cells was suppressed. However, the finding of the increased *ADAMDEC1* levels in the epithelial cells positioned adjacent to the transformed cells in this study is contradictory to the data from the transcriptomic studies showing reduced levels of *ADAMDEC1* in the tissues of adenoma and CRC. One potential explanation for this might be the possibility of EDAC occurring perpetually as a physiological process and a continual upregulation of *ADAMDEC1* in association with this, where macroscopically and microscopically apparently normal epithelia could be detecting and removing the mutated cells before they acquire morphological changes. This hypothesis would be consistent with the highly expressed level of *ADAMDEC1* in the intestinal tissues under normal physiological state and the reduction in *ADAMDEC1* to contribute to the development of colorectal adenoma and CRC. However, once again, as mentioned earlier, *ADAMDEC1* has not been reported to be expressed in the human colonic epithelial cells. Furthermore, while apical extrusion is a well-recognised physiological process, in which surplus live or dying cells are expelled from overcrowded regions of epithelium,[72] the concept of EDAC is still relatively new, and its role in the physiology and tumourigenesis of CRC is still to be shown. It might be possible that the loss of *ADAMDEC1* in the macrophages and/or mesenchymal cells within the lamina propria could lead to the same result of the impaired EDAC (Figure 1.10). However, overall, the relevance of EDAC within the gastrointestinal tract and the precise role of *ADAMDEC1* in the tumourigenesis of colorectal adenocarcinoma remain to be elucidated.

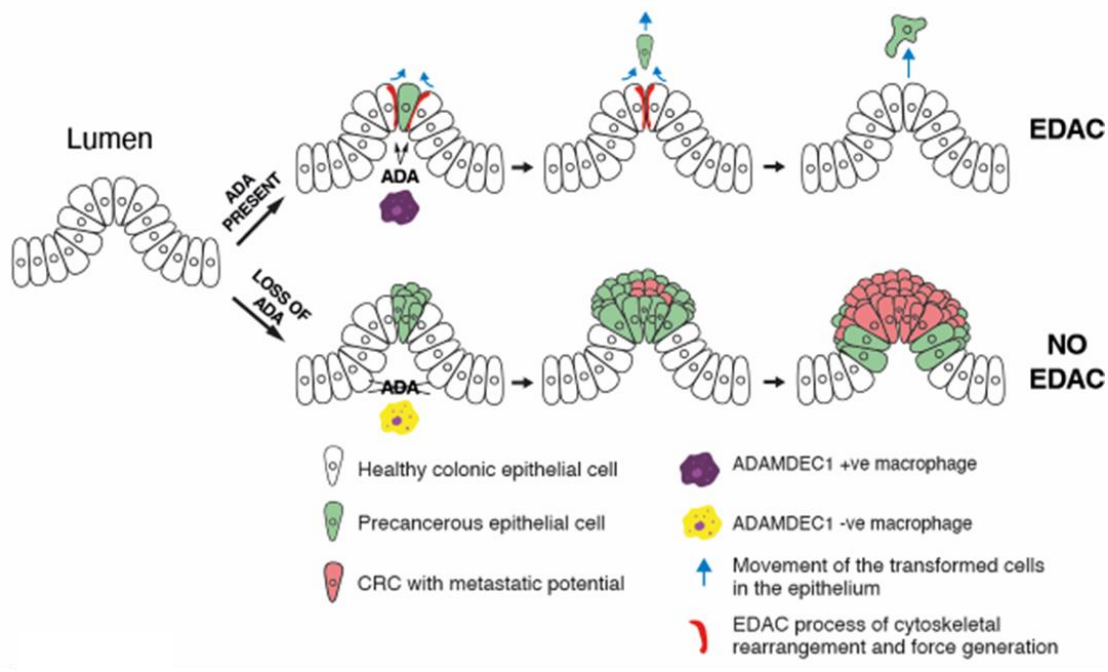

Figure 1.10 A possible mechanism in which the loss of ADAMDEC1 in macrophages might facilitate the development of colorectal adenoma and adenocarcinoma by hindering EDAC.
ADA: ADAMDEC1, CRC: Colorectal adenocarcinoma, EDAC: Epithelial defence against cancer

Additionally, a recent study has identified a subpopulation of fibroblasts expressing high levels of ADAMDEC1 in the healthy mouse intestine. The *ADAMDEC1*-expressing fibroblasts were located adjacent to the intestinal crypts and were enriched in genes that suppress Wnt signalling.[56] A tumour-driving effect of Wnt signalling in the carcinogenesis of CRC is well established.[73,74] The finding from this study provides a potential explanation for the reduced level of *ADAMDEC1* in association with the development of CRC.

Finally, the reduction of *ADAMDEC1* detected in the tissue of IBD, adenoma and CRC, and the ADAMDEC1's potential to modulate immune response suggests a possibility of altered immune surveillance against cancer that might contribute to the development of CRC by the loss of ADAMDEC1 (discussed in more detail later in 1.6.2.2).

1.6.2.2 Gastric cancer

Unlike within CRC, the expression of *ADAMDEC1* in the tissues of gastric adenocarcinoma (GAC) seems to be unaffected compared to the healthy gastric tissues, where the expression of *ADAMDEC1* is much lower than in the small and large intestine (Figure 1.11).[75]

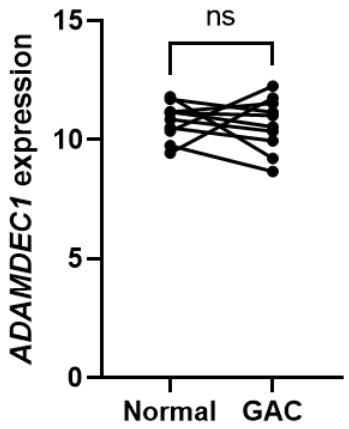

Figure 1.11 Expression of *ADAMDEC1* in paired normal and gastric adenocarcinoma tissues analysed using data extracted from GEO data repository. GEO ID GSE79973[75] There was no significant difference in the expression of *ADAMDEC1* between the normal and GAC tissues. Paired student t-test was used.
GAC: Gastric adenocarcinoma, ns: Non-significant

However, similar to the pattern seen in the CRC, low expressions of *ADAMDEC1* were found in the GAC tissues with a poor prognosis compared to the GAC tissues with a favourable prognosis.[76] This finding was associated with a reduction in the expression of genes related to the immune system and inflammation. The gene network analysis further revealed that the genes associated with the immune system in the GAC with a poor prognosis displayed a poorer correlation and connection to each other, suggesting that the immune system was less actively regulated in this cohort than in the GAC tissues with a better prognosis.

Another study which conducted a transcriptomic analysis of a large cohort of GAC also detected a higher expression of *ADAMDEC1* in the tissues of GAC with a favourable prognosis.[77] This high *ADAMDEC1*-expressing subgroup of GAC with a favourable prognosis was also found to have transcriptomic features indicative of the tumour tissues being highly infiltrated with immune cells, such as

upregulation in the genes related to inflammatory macrophages, activated $CD4^+$ T helper cells, $CD8^+$ T cells and γδ T cells. Furthermore, the same study went on to show that silencing *ADAMDEC1* in the GAC cell line, MGC-803, increased the expression of programmed-death ligand 1 (PD-L1), and the cancer cell proliferation and migration. Ligation of PD-L1 to its receptor, programmed cell death protein-1 (PD-1), on T cells has an inhibitory effect on the T cell's anti-tumour properties, thus promoting cancer development by escaping anti-tumour immune surveillance. PD-L1 is predominantly expressed on tumour cells and macrophages.[78] The same study further demonstrated that co-culturing of the *ADAMDEC1*-silenced MGC-803 cells with Jurkat cells, a primary T cell line, enhanced the apoptosis of the T cell. These findings suggest a potential protective mechanistic role of ADAMDEC1 in the tumourigenesis of GAC by suppressing PD-L1 thus promoting the anti-tumour immune response against GAC.

Additionally, macrophages in the tissues of mouse colonic tumours are also known to express high levels of PD-1. The ligation of PD-L1 and PD-1 on macrophages impaired the phagocytic property of the macrophages and the blockade of this ligation improved the macrophage phagocytosis, tumour progression and survival in the mouse.[79] Although the role of ADAMDEC1 with regards to PD-L1 expression in CRC has not been explored, these findings support a potential protective mechanistic role of ADAMDEC1 by modulating immune surveillance against gastrointestinal cancer development.

1.6.3 Extra-intestinal inflammatory diseases and cancers

Recent extensive usage of microarray technology and next generation sequence have allowed hypothesis-free genome-wide transcriptomic analysis of many human diseases. This approach led to the identification of *ADAMDEC1* as a differentially expressed transcriptomic in various extra-intestinal inflammatory diseases and cancers.

1.6.3.1 Extra-intestinal inflammatory diseases

As discussed earlier, the expressions of *ADAMDEC1* in extra-intestinal organs are low in normal healthy status. Interestingly, contrarily to the inflammatory disease

of the gastrointestinal tract, upregulations of *ADAMDEC1* have been detected in a number of inflammatory diseases affecting the extra-intestinal organs (Table 1.2).

Disease	Expression of *ADAMDEC1*	Tissues/cells	Extra details	Reference
Sarcoidosis	↑	Lung tissue of sarcoid vs HC, and cells collected in bronchoalveolar lavage of sarcoid vs HC	*ADA* upregulation correlated with disease severity. ADA not co-localised with CD68 within the disease tissues	80
Rheumatoid arthritis	↑	Fibroblast-like synovial cells of RA joints vs Post-trauma non-RA joints	*ADA* upregulation independent of disease severity	81
Sjogren's syndrome	↑	Minor salivary glands of Sjogren's syndrome vs HC	*ADA* upregulation in association with upregulation of macrophage-related genes in the disease tissues	82
Systemic Lupus Erythematosus	↑	Peripheral blood monocytes of SLE patients vs HC	N/A	83
Carotid artery sclerosis	↑ in unstable parts of atherosclerotic tissues	Stable vs unstable parts of atherosclerotic vessels	N/A	84
	↑	Peripheral blood monocytes from patients with carotid artery atherosclerosis vs HC	N/A	85
Rosacea	↑	Skin tissues of rosacea vs HC	ADA co-localised with CD68	42

Table 1.2 Summary of the extra-intestinal inflammatory diseases in which differentially expressed levels of ADAMDEC1 have been identified by transcriptomic analyses. In contrast to the reduced level of *ADAMDEC1* in the tissues of gastrointestinal inflammatory diseases, upregulations of *ADAMDEC1* are seen in all of the extra-intestinal diseases where differentially expressed levels of *ADAMDEC1* have been identified.
ADA: ADAMDEC1, HC: Healthy controls, N/A: Not applicable, RA: Rheumatoid arthritis, SLE: Systemic lupus erythematosus

A majority of these studies identifying *ADAMDEC1* as a differentially expressed gene in the diseased cells/tissues provide no more than the associations between

the increased level of *ADAMDEC1* and the diseases without an explanation behind it. However, one of the potential explanations is the increased level of *ADAMDEC1* being simply secondary to the increase in the recruitment of monocytes and their differentiation into macrophages during inflammation driving these diseases. However, the upregulation of *ADAMDEC1* is clearly not found in all extra-intestinal inflammatory diseases, which implies that there may be other reasons behind this trend. One study, which identified an upregulation of *ADAMDEC1* in the skin tissues collected from patients with rosacea, explored beyond the association and showed a potential mechanistic role of ADAMDEC1 in the disease pathogenesis.[42] Rosacea is a chronic inflammatory skin condition in which the ultraviolet light-mediated vitamin D synthesis and upregulation of TLR2 stimulate secretions of proteases and antimicrobial cathelicidin peptides. This leads to the subsequent secretion of pro-inflammatory cytokines and activation of Th1- and Th17-mediated adaptive immune responses, which are believed to play a role in the disease pathogenesis.[86] The study firstly showed that ADAMDEC1 had a mechanistic role in driving MDMs, derived from monocytes collected from healthy controls, to a more pro-inflammatory phenotype. The siRNA-mediated silencing of *ADAMDEC1* prior to the pro-inflammatory activation of the MDMs resulted in a failure to upregulate pro-inflammatory genes. The local injection of siRNA, to silence *ADAMDEC1,* subsequently demonstrated attenuation in the rosacea disease activity in the murine experimental rosacea model. This attenuation in the disease activity was in association with reductions in the expression of pro-inflammatory signature genes such as *Il-6*, *Tnf-α* and *Nos*. The findings from this study suggest ADAMDEC1's involvement in rendering the MDMs to more pro-inflammatory phenotype thus modulating the immune response which in turn may be responsible for the disease process.

1.6.3.2 Extra-intestinal cancers

Similarly to the trend seen with the extra-intestinal inflammatory diseases, upregulations of *ADAMDEC1* have been reported in several extra-intestinal cancers (Table 1.3). In contrast to the downregulated levels of *ADAMDEC1* in the tissues of gastrointestinal cancers such as CRC, an elevation was reported in these extra-intestinal cancers.

Disease	Expression of *ADAMDEC1*	Tissues/cells	Extra details	Reference
Non-small cell lung cancer	↑	Non-small cell lung cancer tissue vs paired adjacent non-cancerous lung tissue	*ADA* upregulation correlated with poor clinical outcome. Knockdown of ADA in non-small cell lung cancer cell line increased cancer cell apoptosis by activating PI3K/AKT signalling pathway and reduced cancer cell proliferation.	87
Glioblastoma	↑	Glioblastoma tissue vs non-cancerous brain tissue (unpaired)	*ADA* upregulation correlated with poor clinical outcome. ADA located and secreted exclusively from glioblastoma cancer stem cells. ADA released FGF2 from ECM within the cancer tissues. FGF2 induced *ADA* via FGFR1.	29
Glioma	↑	Glioma tissue vs paired non-cancerous brain tissue	Knockdown of *ADA* in glioma cancer cell line inhibited growth of glioma cells in association with upregulation of pro-apoptosis genes.	88

Table 1.3 Summary of extra-intestinal cancers in which differentially expressed levels of ADAMDEC1 have been identified by transcriptomic analyses. In contrast to the reduced level of *ADAMDEC1* in the tissues of gastrointestinal cancers, the upregulations of *ADAMDEC1* are seen in all of the extra-intestinal cancers where differentially expressed levels of *ADAMDEC1* have been identified.
ADA: *ADAMDEC1*, FGF2: Fibroblast growth factor-2, FGFR1: Fibroblast growth factor receptor-1

All of the studies that identified upregulation of *ADAMDEC1* in the tissues of extra-intestinal cancers gave evidence towards a potential pro-tumour mechanistic role of *ADAMDEC1* by demonstrating attenuated tumour cell proliferation or growth by knockdown of *ADAMDEC1*.[29,87,88] Two of these studies have identified a potential effect of ADAMDEC1 on cancer cell survival as the knockdown of *ADAMDEC1* resulted in an increased cancer cell apoptosis.[87,88] Another study, in which

upregulation of *ADAMDEC1* was detected in the tissue of GBM, revealed that ADAMDEC1 increased the concentration of soluble FGF2 by releasing the complex-bound inactive FGF2 within the cancer ECM, thereby indicating ADAMDEC1's role as a sheddase.[29] The cancer promoting role of FGF2 is well-established in GBM, although the exact mechanism underlying these effects had remained unknown.[89,90] In this study FGF2 was shown to stimulate GMB cancer stem cell proliferation and tumourigenesis.[29] The same study further demonstrated that FGF2 signalling via FGFR1 induced ADAMDEC1 thus creating a positive feedback loop in the GBM cancer stem cell. The findings from this study revealed a specific role of ADAMDEC1, as a sheddase, in cancer development.

In summary, within the gastrointestinal tract, where a high level of ADAMDEC1 is expressed in healthy status, downregulations of *ADAMDEC1* have been detected in the tissues of inflammatory diseases and cancer. The evidence suggests ADAMDEC1 might play a role in the homeostasis of the intestine and a protective role against these diseases. In contrast, upregulations of *ADAMDEC1* have been reported in numerous extra-intestinal inflammatory diseases and cancers. The pathogenic role of ADAMDEC1 has been suggested in these diseases. Further studies are required to reveal the explanation behind these opposite trends between the gastrointestinal and extra-intestinal organs.

1.7 ADAMDEC1 and gastrointestinal mucosal inflammation

1.7.1 Findings from previous studies using *Adamdec1*$^{-/-}$ mice and experimental colitis

The generation of a transgenic *Adamdec1*$^{-/-}$ mouse provided crucial evidence to support the role of ADAMDEC1 in gastrointestinal immune regulation upon induction of inflammation.[26] Interestingly, it is worth noticing that despite the high expression of ADAMDEC1 in the gastrointestinal tract, *Adamdec1*$^{-/-}$ mice did not exhibit any abnormality with regard to development, growth, reproductivity and intestinal mucosal permeability and did not exhibit any signs of gastrointestinal pathologies under specific-pathogen-free conditions. This suggests that the function of ADAMDEC1 is dispensable or substituted by an alternative mechanism under healthy normal status. However, when colonic inflammation was induced over 7 days by oral administration of DSS, *Adamdec1*$^{-/-}$ mice demonstrated more

severe systemic sequala of inflammation with a greater weight loss and a higher mortality rate compared to the wild type (WT) mice. The histological examination of the colonic tissue after the DSS administration also confirmed a greater degree of local mucosal inflammation in the *Adamdec1*$^{-/-}$ mice colonic tissue compared to WT, with increased cellular infiltration and crypt distortion and ulceration. Furthermore, *Adamdec1*$^{-/-}$ mice showed an even greater degree of weight loss and mortality compared to WT when challenged with live *Citrobacter rodentium*, which usually causes self-limiting bacterial colitis predominantly affecting the caecum in WT animals. A similar exaggerated inflammatory response was also seen when *Adamdec1*$^{-/-}$ mice were challenged *Salmonella enterica* serovar Typhimurium, a mouse pathogen that affects the distal ileum. These findings suggest that the exaggerated mucosal inflammation in the absence of ADAMDEC1 occurs irrespective of the mode of inflammation or location of inflammation along the small and large intestine, but bacteria-induced mucosal inflammation intensifies the degree of inflammation. With the case of *Citrobacter rodentium* infection, it was also noted that a greater number of the bacteria was found in the spleen of the *Adamdec1*$^{-/-}$ mice compared to the WT mice indicating a more severe breakdown of the host's mucosal defence mechanism and greater bacteraemia in the absence of ADAMDEC1. Importantly, this study also showed an upregulation of ADAMDEC1 in the colonic tissue of WT mice during the DSS challenge and a downregulation of ADAMDEC1 to the baseline on cessation of the DSS challenge mirroring the degree and resolution of the inflammation. This observation supports the hypothesis that ADAMDEC1 might be a marker of circulating monocyte recruitment and differentiation to macrophages in the intestinal tissue during inflammation. This study provided crucial evidence for the first time that the presence or absence of ADAMDEC1 has an effect on the degree of mucosal inflammation in vivo thus, ADAMDEC1 is involved in the regulation of mucosal inflammation. It does not, however, provide the underlying mechanism through which ADAMDEC1 regulates mucosal inflammation.

Recently another study has also demonstrated a protective role of ADAMDEC1 in intestinal mucosal inflammation using *Adamdec1*$^{-/-}$ mice.[56] This study, first of all, identified a subpopulation of fibroblasts that expressed high levels of *ADAMDEC1* in the CD45^{+} and EpCAM^{+} cell-depleted mesenchymal cells from WT mouse colonic lamina propria by scRNA-seq. These *ADAMDEC1*-expressing fibroblast

cells were located adjacent to the edge of crypts and were enriched in genes associated with negative regulation of Wnt signalling that, in turn, prevent epithelial proliferation while promoting differentiation. Furthermore, in the same study by using CRISPR-generated *Adamdec1*$^{-/-}$ mice and acute DSS colitis model, it was demonstrated that greater systemic and mucosal inflammation, increased susceptibility to epithelial injury, and abnormal ECM remodelling were observed in the *Adamdec1*$^{-/-}$ mice in comparison to the WT mice. The aberrant ECM remodelling was observed particularly in the area between the muscularis mucosa and muscularis which was characterised by the abnormal disorganised ECM accumulation. Based on these findings, the authors concluded that ADAMDEC1 was indispensable to the ECM remodelling and healing following epithelial injury. However, in this study, the WT and *Adamdec1*$^{-/-}$ mice were generated from Balb/c mice, which are known to be less susceptible to DSS-mediated colitis than other strains such as C57BL/6.[91] This was reflected by a complete lack of weight loss in the WT mice during the 7-day DSS challenge. This indicates that the histological differences observed between the colonic tissues of the WT and *Adamdec1*$^{-/-}$ mice would have been exaggerated since the WT tissues would likely have exhibited very little inflammation. Additionally, the process of epithelial and tissue healing and remodelling typically occur few days after the cessation of DSS. Therefore, the histological features captured by this study using the acute DSS model would likely have represented a phase of ongoing inflammation and tissue destruction rather than the tissue healing and remodelling.[92] In fact, some of the histological features that were seen in the colonic tissues of the *Adamdec1*$^{-/-}$ mice that were suggested to be secondary to the aberrant ECM remodelling, such as submucosal and muscularis thickening and disordered ECM collagen fibre alignment, are known expected features of DSS-mediated colitis in general in WT mice in comparison to the normal uninflamed colonic tissue.[93] Together with the observation of greater immune cell infiltrate seen within the colonic tissues of the *Adamdec1*$^{-/-}$ mice, overall, these findings could simply indicate that the mice lacking ADAMDEC1 demonstrated an exaggerated level of mucosal inflammation in general and might not imply that the abnormal mucosal healing and ECM remodelling occurred in the absence of ADAMDEC1. A further study using *Adamdec1*$^{-/-}$ mice generated from C57BL/6 mice and a chronic DSS model should allow more suitable evaluation of the potential role of ADAMDEC1 in the mucosal epithelial and tissue repair, and ECM remodelling.

In summary, two independent studies utilising *Adamdec1*$^{-/-}$ mice have demonstrated a greater mucosal inflammation in the absence of ADAMDEC1, thus ADAMDEC1's protective role within the gastrointestinal tract upon induction of inflammation. However, the mechanism through which ADAMDEC1 renders such an effect still remains to be elucidated. One potential explanation, however, comes from a study in which ADAMDEC1 was shown to release FGF2 from the FGF2-bound complexes within ECM of GBM stem cells.[29] FGF2 has been shown to promote epithelial proliferation, repair and healing of the mucosa in a synergic manner with IL-17.[94] FGF2 has been reported to enhance epithelial stem cell survival following radiation and improve the healing process of inflammatory duodenal ulcers. [95,96] FGF2 knockout mice have also displayed a greater susceptibility to DSS-induced colitis, suggesting its protective role in mucosal inflammation.[94] it is possible that the mechanism of the protective effect of ADAMDEC1 during the mucosal inflammation could be due to the catalytical activity of ADAMDEC1 in cleavage of the complex-bound FGF2 within ECM and the subsequent FGF2 signalling cascade promoting epithelial repair. However, further studies are required to validate the hypothesis.

1.7.2 ADAMDEC1 and intestinal microbiome in the context of intestinal inflammation

Extensive bidirectional interaction between the microbiome and immune system of intestine has become apparent over the past decades. There have not been, however, any studies specifically evaluating the potential relationship between the intestinal microbiome and ADAMDEC1 in the context of mucosal immune system or inflammation.

However, one study using obese Zucker, Zucker-*Lepra*$^{fa/fa}$, rats provided a potential link between the intestinal microbiome, ADAMDEC1 and intestinal inflammation.[97] The obese Zucker rats are known to have increased serum concentrations of TNF-α, IL-6 and LPS in accordance with obesity being associated with skewing of the intestinal and systemic immune system towards a pro-inflammatory state.[97–99] It was demonstrated that the obese phenotype in these rats occurred in association with increase in the expression of *ADAMDEC1* and markers of macrophages and dendritic cells, F4/80 and CD40, within the intestine.[97] Oral administration of probiotic strains of *Lactobacillus paracasei*,

Bifidobacterium breve and *Lactobacillus rhamnosus* individually reduced the expression of ADAMDEC1, F4/80 and CD40, as well as the serum LPS concentration in these obese rats indicating the attenuation of the inflammatory state within the intestine of the obese rats. These three strains of probiotics were previously shown to modify the faecal bacterial composition of healthy human.[98] The findings from this study suggest a modification to the microbiome, by probiotics, could, in turn, affect the intestinal immune system. It is not apparent from the study whether the reduction of ADAMDEC1 expression followed by the administration of probiotics was simply a reflection of the reduced abundance of ADAMDEC1-expressing macrophages in association with the attenuated inflammatory state within the intestine, or if the administration of probiotics led to the reduction of ADAMDEC1 which played a role in reducing the macrophages and dendritic cell abundances and the reversal of inflammatory state. Nevertheless, it provides the first insight into a possible interaction between the microbiome, ADAMDEC1 and intestinal immune system.

1.8 Outline of the thesis

This thesis primarily aimed to investigate the role of ADAMDEC1 in the immune response during intestinal inflammation. The evidence indicating that ADAMDEC1 is expressed in cells other than macrophages, such as mesenchymal cells, within the intestine emerged towards the end of this PhD. Thus the experiments to characterise the effect of ADAMDEC1 during mucosal inflammation were conducted with a focus on the innate immune response, particularly macrophages. The results and data generated during the project lead to an adjustment in project design and aims which will be discussed. The main individual aims of this thesis were:

- To investigate the mechanism responsible for the induction of ADAMDEC1 using human monocytic cell line, THP-1 cells (Chapter 3)
- To generate Hoxb8 immortalised progenitor cells from the WT and *Adamdec1*$^{-/-}$ mice and investigate the function of ADAMDEC1 in macrophages using the macrophages derived from these Hoxb8 progenitor cells (Chapter 4)

- To synthesise recombinant ADAMDEC1 and its catalytically inactive mutant E353A and investigate the potential antimicrobial role of ADAMDEC1 (Chapter 5)
- To characterise the effect of ADAMDEC1 on mucosal immune response in mice upon induction of DSS-induced colitis (Chapter 6)
- To investigate the effect of ADAMDEC1 on the intestinal microbiome and how this might affect the immune response to the DSS-induced inflammation (Chapter 7)

Chapter 2

General materials and method

2.1 Ethics approval

Experiments involving samples collected from healthy volunteers were carried out in accordance with the recommendations of the Joint University College London (UCL)/UCL Hospitals Committees on the Ethics of Human Research with written informed consent from all subjects (Project numbers 02/0324 and 10/H0806/115). In addition, all healthy volunteers gave written informed consent in accordance with the Declaration of Helsinki.

Studies using animals were performed in accordance with the United Kingdom Animals (Scientific Procedures) Act 1986 (Project licence 70/8452) and European Directive 2010/63/EU on the protection of animals used for scientific purposes.

2.2 General reagents and buffers

Luria-Bertani (LB) Broth

Lennox LB Broth was used as LB broth throughout this project. 10 g of LB Broth (Lennox) powder (Sigma L3022) were dissolved in 500 ml of distilled water in a Duran bottle and autoclaved at 121°C for 15 minutes.

LB Agar

8 g of Lennox LB agar power (Invitrogen) was dissolved in 250 ml of distilled water in a Duran bottle and autoclaved at 121°C for 15 minutes, and then stored at room temperature. The stored LB agar was heated in a microwave until it was liquefied completely, and approximately 20 ml of LB agar was poured into each 10 cm petri dish (Star Lab) inside a laminar flow cabinet and allowed to solidify for over 30 minutes.

Working concentrations of antibiotics and reagents added to LB Broth and LB agar

The concentrations of antibiotics and reagents added to LB Broth and LB agar are listed in Table 2.1. The heated LB broth and LB agar were allowed to cool approximately to 55°C before antibiotics or reagents were added.

Antibiotics and reagents	Working concentration (/ml)
Ampicillin	100 µg
Kanamycin	50 µg
Gentamicin	7 µg
Tetracycline	10 µg
Bluo-gal	100 µg
Isopropyl ß-D-1-thiogalactopyranoside (IPTG)	40 µg

Table 2.1 The working concentrations of antibiotics and reagents added to LB broth and LB agar.

Yeast Peptone Dextrose (YPD) broth

50 g of YPD broth powder (Sigma) was dissolved in 1 L of distilled water in a Duran bottle and autoclaved at 121°C for 15 minutes, and stored at room temperature.

YPD agar

65 g of YPD agar powder (Sigma) was dissolved in 1 litre of distilled water in a Duran bottle and autoclaved at 121°C for 15 minutes, and stored at room temperature. The stored LB agar was heated in a microwave until it was completely liquefied and approximately 20 ml of LB agar was poured into each 10 cm petri dish inside a laminar flow cabinet and allowed to solidify for over 30 minutes.

Western blot buffers

Tris-Glycine running buffer (x10): 144 g glycine (Sigma), 30.2 g Tris base and 10 g sodium dodecyl sulfate (SDS) (Sigma) were dissolved, using magnetic stir, in ~ 800 ml distilled water and finally made up to 1 litre and stored at room temperature.

Tris-Glycine transfer buffer (x10): 144g glycine (Sigma), 30.25g Tris-Base (VWR) and 3.74g SDS (Sigma) were dissolved, using a magnetic stirrer, in ~ 800 ml distilled water and finally made up to 1 litre and stored at room temperature.

Phosphate-buffered saline (PBS) – Tween (PBS-T): 5 tablets of PBS (Sigma P4417) were dissolved in 1 litre of distilled water to obtain a 137 mM NaCl, 2.7 mM KCl and 10 mM phosphate buffer solution (pH 7.4 at 25°C). 1 ml of Tween 20 (Sigma) was added.

Blocking solution: 1.25 g of non-fat dried milk bovine powder (Sigma) was added to 25 ml of PBS-T.

Fluorescence-activated cell sorting (FACS) Buffer

FACS buffer was made by mixing 500 ml PBS, 10 ml fetal bovine serum (FBS) (Sigma) and 50 mg sodium azide (Sigma) and stored at 4°C.

2.3 Heat-killed bacteria and fungi stock

Heat-killed *Escherichia coli* (HkEc) stock

Escherichia coli (*E. coli*) NCTC 10418 (TCS Biosciences), a fully antibiotic sensitive clinical isolate, was cultured by adding 1µl glycerol stock into 10ml LB broth and incubation at 37°C, at a constant agitation at 250 rpm in an InnovaTM 4000 incubator shaker (New Brunswick Scientific) overnight. *E. coli* was centrifuged at 3000 g for 20 minutes at room temperature in a Heraeus Multifuge X1R (Thermo Fisher Scientific) and was subsequently washed once in PBS, then resuspended in 1 ml of PBS. The killing of *E. coli* was carried out by incubating 1 ml of bacteria in PBS at 60°C for 1 hour in a Grant GD100 circulating immersion bath. Confirmation of killing was achieved by plating and culturing of 80 µl of HkEc onto a LB agar plate with no antibiotics overnight. HkEc solution was counted at 1:20 dilution using a Cecil BioQuest™ CE2502 spectrophotometer. The optical density at 600 nm (OD_{600}) of *E. coli*, at a density of 1×10^8 bacteria/ml in PBS, is 0.365 as previously established in our laboratory. The concentration of HkEc in PBS was adjusted to 1×10^{10} bacteria/ml and stored at -20°C.

Heat-killed *Candida albicans (HkC)* and opsonised *HkC* stock

One *Candida albicans* vitroid disc (Sigma) was grown on a YPD agar plate overnight at 37˚C in a non-CO_2 incubator. One colony was picked and cultured in 15 ml YPD broth at 37˚C in a non-CO_2 shaking incubator until the broth turned cloudy. The solution was washed twice in PBS by centrifuging at 3000 g for 10 min. The yeast particles were resuspended in 50 ml of PBS and heat-killed by completely submerging the whole tube in a pre-warmed 60˚C water bath for 1 hour. The killing was confirmed by streaking the HkC sample on a fresh YPD agar plate and culturing overnight. Heat-killed Candida was stored in 5 x 10^8 /ml samples at -20˚C.

100 µl of human pooled IgG serum (160 mg/ml), Vivaglobin, (ZLB Behring) was added to 100 µl aliquot of HkC (at a density of 5 x 10^7 /ml) and incubated at 37˚C

for 1.5 hours in a shaking incubator set at 1100 rpm. The suspension was washed three times in PBS by centrifuging at 14000 g for 1 minute, then resuspended in PBS and stored at -20˚C.

2.4 Microscopy

Zeiss Axiovert 200 microscopy was used to image cells. Zen software (Zeiss) was used to process the images captured.

2.5 Quantification of DNA and RNA

The quality and concentration of DNA and RNA were determined using a NanoDrop ND-1000 spectrophotometer (NanoDrop Technologies) measuring OD260/OD280 and OD260/OD230. A low ratio of OD260/OD280 indicated contamination of samples with protein, and a low ratio of OD260/OD230 indicated contamination of sample with salts, carbohydrates and phenol. The ratio of 1.7 – 2 and 1.8 – 2 were considered pure for DNA and RNA, respectively.

2.6 Cloning

2.6.1 DNA sequencing

Sequencing of DNA was outsourced to Eurofins Genomics (Germany) using their Mix2Seq service. 15 µl of purified DNA (10 – 100 ng/µl in a volume of 15 µl) were mixed with 2 µl of 10 µM primer in a tube pre-labelled with unique barcode provided by Eurofins Genomics following their instruction. The samples were couriered overnight, and DNA sequences were provided electronically the next day.

2.6.2 Bacterial glycerol stocks

Within a sterile field created by a Bunsen burner, a 500 µl aliquot of an overnight culture of transformed bacteria was added to 500 µl of autoclaved glycerol in 2 ml cryotube. The cryotube stocks were immediately stored at -80°C. Glycerol stocks were thawed on ice and streaked on appropriate selection plates for overnight incubation for further use.

2.6.3 Plasmid DNA extraction

2.6.3.1 Miniprep

To extract plasmid DNA of a small quantity and relatively inferior quality for DNA sequencing purpose, Monarch® Plasmid DNA Miniprep Kit (NEB) was used and the manufacturer's protocol was followed. All the buffers were provided in the kit. RNase was added to the buffer by the manufacturer, which removed RNA during the DNA extraction. 1.5 ml of the transformed bacterial cell culture, expanded in 3-6 ml of LB broth containing appropriate antibiotics, were pelleted by centrifugation at 16000 g for 30 seconds. The pellet was resuspended in 200 µl of Plasmid Resuspension Buffer and vortexed until the cells were completely resuspended with no visible clumps. Cells were then lysed by adding 200 µl of Plasmid Lysis Buffer. The tube was inverted immediately and gently 5 -6 times until the colour of the mixture changed to dark pink, and the solution was clear and viscous. Following an incubation at room temperature for 1 minute, the mixture was neutralised by adding 400 µl of Plasmid Lysate Buffer and inverted gently until the colour of the solution uniformly turned yellow with some precipitates. The neutralised lysate was then incubated at room temperature for 2 minutes and centrifuged at 16000 g for 2 minutes. Only supernatant was transferred to the spin column, provided in the kit, and centrifuged at 16000 g for 1 minute. The follow-through was discarded, and the spin column was re-inserted into the collection tube. The plasmid DNA trapped on the membrane within the spin column was washed with 200 µl of Plasmid Wash Buffer 1 to remove protein and endotoxin. The column was centrifuged at 16000 g for 1 minute. The follow-through was discarded, and the membrane was washed again with 400 µl of Plasmid Wash Buffer 2 and centrifuged at 16000 g for 1 minute. The column was then transferred to a clean 1.5 ml Eppendorf tube, and DNA was eluted by adding 30 µl of DNA Elution buffer to the centre of the membrane and centrifugation at 16000 g for 1 minute. The quality and quantity of the extracted plasmid DNA were determined using NanoDrop Spectrometer.

2.6.3.2 Maxiprep

To extract plasmid DNA of a large quantity and high quality for subsequent cloning, HiSpeed® Plasmid Maxi Kit (Qiagen) was used, and the manufacturer's protocol was followed. All the buffers were provided in the kit. RNase A, provided in the kit, was added to Buffer P1 to obtain a final concentration of 100 µg/ml to remove RNA during the DNA extraction as per the manufacturer's instruction.

The transformed bacteria were expanded in 300 ml of LB broth, containing appropriate antibiotics, overnight. The bacterial culture was centrifuged at 6000 g for 15 minutes. The supernatant was removed, and the bacterial cell pellet was resuspended in 10 ml of Buffer P1 and homogenised completely by vortexing. 10 ml of Buffer P2 was then added to lyse the cells, and the container was inverted 6 - 7 times immediately until the colour of the mixture changed to blue. The lysate was incubated at room temperature for 5 minutes. 10 ml of pre-chilled Buffer P3 was added to neutralise the lysate, and the container was inverted 6 - 7 times until the colour of the solution turned colourless with white precipitates. The mixture was incubated at room temperature for 5 minutes, then poured into QIAfilter Cartridge and incubated again at room temperature for 10 minutes. 10 ml of Buffer QBT was poured into the HiSpeed Tip column to equilibrate the column, and the sample was filtered out of the QIAfilter Cartridge into the equilibrated HiSpeed Tip column using a plunger. DNA trapped in the membrane of the HiSpeed Tip column was washed with 60 ml of Wash Buffer QC and eluted off the membrane into a 50 ml Falcon tube by adding 15 ml of Elution Buffer QF. 10.5 ml of 100% isopropanol was added to the eluate to precipitate DNA. The solution was then passed through QIAprecipitator to bound the DNA onto the precipitator membrane using a syringe. The membrane was washed with 2 ml of 70% ethanol using a syringe and dried by incubation at room temperature for 20 minutes. DNA was then eluted off the membrane by adding 0.5 – 1 ml of Buffer TE directly onto the membrane using a 5 ml syringe attached to the QIA precipitator. The concentration and quality of DNA were measured using NanoDrop Spectrometer.

2.6.4 Analysis of plasmid and complementary DNA (cDNA) by gel electrophoresis

2.6.4.1 PCR condition

To detect the presence of construct within plasmid or cDNA from the transfected cells by DNA gel electrophoresis, PCR of the extracted and purified plasmid DNA or the cDNA synthesised from total RNA of the transfected cells (Chapter 2.7.2) was performed using One *Taq* Hot Start polymerase (NEB). The plasmid DNA amplified by the transformation of *E. coli* and extracted either by Miniprep or Maxiprep were diluted in nuclease-free water (Qiagen) to achieve a concentration

of 1 ng/µl. Likewise, the RNA extracted from the transfected cells were converted to cDNA and diluted in nuclease-free water (Qiagen) to achieve a concentration of 1 ng/µl. The components of the PCR reaction mix are listed in Table 2.2. C1000 Touch™ Thermal Cycler (BioRad) was used to perform PCR with the cycling conditions shown in Table 2.3. Step 2 to 4 of the PCR thermal cycling were repeated 32 - 36 times. The individual sequence of the primers and annealing temperatures used are specified in the chapter specific materials and method.

Component	Volume (µl)
5x One *Taq* Standard Reaction Buffer (NEB)	10
10 mM dNTPs (Thermo Fisher Scientific)	1
Forward primer (10 µM)	1
Reverse primer (10 µM)	1
One *Taq* Hot Start Polymerase (NEB)	0.25
Purified plasmid DNA (1 ng/mg)	1
Nuclease-free water (Qiagen)	35.75
Total volume	**50**

Table 2.2 Components of PCR reaction for detection of construct by DNA gel electrophoresis

Step	Temperature	Time	Process
1	94°C	3 minutes	Initial denaturation
2	94°C	45 seconds	Denaturation
3	Variable	45 seconds	Annealing
4	68°C	5 minutes	Elongation
5	68°C	7 minutes	Final extension

Table 2.3 PCR condition for detection of construct by DNA gel electrophoresis. Step 2 to 4 were repeated 32 – 36 times.

2.6.4.2 Agarose gel

Agarose gels were made by suspending an appropriate amount of agarose powder, molecular biology grade, (BioLine) in Tris-acetate-EDTA buffer (Thermo Fisher Scientific) and heating the solution in a microwave until the agarose powder had completely dissolved. 1 in 10000th volume of SYBR™ Safe DNA Gel Stain was added, and the agarose solution was poured into a plastic gel tray with appropriate combs and allowed to solidify over 20 minutes at room temperature.

2.6.4.3 Agarose gel electrophoresis

Agarose gel was placed in Sub-Cell GT Cell Electrophoresis System (BioRad) and submerged in Tris-acetate-EDTA buffer (Thermo Fisher Scientific). 25 µl of the PCR product made (Chapter 2.6.4.1) was mixed with 5 µl of Gel Loading Dye, Purple (6X) (NEB) and loaded in a well of agarose gel. A molecular weight marker, dependent on the expected band size, was loaded in a well as well. The agarose gels were run at 80 - 100 Volts for 20 - 40 minutes, depending on the size of the PCR product. The gel was imaged on myECL™ Imager using its UV mode (Thermo Fisher Scientific).

2.7 Gene expression

2.7.1 RNA extraction and purification

Total RNA from cells/tissues were extracted using Qiagen RNeasy Mini Kit (Qiagen) following the manufacturer's protocol.

2.7.1.1 Cultured cells

To extract RNA from MDMs and macrophages derived from THP-1 cells, Hoxb8 cells and bone marrow-derived macrophages (BMDM), after a specific incubation period, the culture media in each well or 92 mm culture dish were collected into 5 ml Eppendorf tubes and centrifuged for 5 minutes at 1000 rpm. After centrifugation, supernatants were removed leaving cell pellets in the tube. 350 µl, if using 6-well plate, or 700 µl, if using 92 mm culture dish, of RLT buffer provided in the kit containing 1% of 2-mercaptoethanol (Sigma) were added into each well/dish and adhering cells were scraped with sterile 24 cm cell scrapers (Scientific Laboratory Supplies). The RLT buffer containing the scraped cells was then transferred into 5 ml Eppendorf tubes containing the cell pellets from the corresponding well/dish to ensure both adherent and non-adherent cells in each well/dish were collected. For RNA extraction from the transfected GP2-293 cells, the culture medium was removed and the adherent cells were simply scrapped in the RLT buffer containing 1% of 2-mercaptoethanol (Sigma). The cells were then homogenised by passing the lysate 10 times through 23G needle (BG) fitted to a sterile 1 ml syringe (Scientific Laboratory Supplies) to release all RNA contained within the organelles and cell membrane. 350 µl or 700 µl of 70% ethanol was added to each

homogenised sample and mixed by pipetting to precipitate RNA.

2.7.1.2 Tissue samples

To extract RNA from mouse colonic tissues, colonic tissues harvested from mice and stored in 1.5 ml Eppendorf tubes submerged in RNAlater at -80°C were thawed. The tubes were centrifuged at 500 g for 3 minutes, and RNAlater was discarded. The colonic tissues were washed in 1 ml of PBS and centrifuged at 500 g for 5 minutes. The PBS was discarded, and the samples were transferred into fresh 2 ml Eppendorf tubes. 900 µl of RLT buffer containing 1% 2-mercaptoethanol was added to each tube. Three 7 mm diameter stainless steel Tungsten Carbide Beads (Qiagen) were placed into each tube. The colonic tissues were homogenised using TissueLyzer LT (Qiagen) set at the maximum speed for 3 minutes. This was repeated 3 times with incubation of the samples on ice for 1 minute between each burst of the homogenisation. The beads were carefully removed from each tube, and the tubes were centrifuged at 1000 g for 3 minutes. 750 µl of the supernatants were carefully transferred into fresh 2 ml Eppendorf tubes, and 750 µl of 70% ethanol was added to each sample and mixed by pipetting to precipitate RNA.

2.7.1.3 Downstream RNA extraction and purification from cultured cells and tissue samples

The solutions prepared in Chapter 2.7.1.1 and 2.7.1.2 were then pipetted into the spin columns provided in the kit and centrifuged at 8000 g for 15 seconds at room temperature to bound RNA onto the column membrane. 80 µl of DNase, RNase-free DNase Set (Qiagen), were added to each spin column to remove genomic DNA. The spin columns were then washed with 700 µl Buffer RWT and subsequently with 700 µl Buffer RPE and centrifuged after each time at 8000 g for 3 minutes to discard any follow-through containing contaminants. Finally, the columns were placed in fresh 1.5 ml Eppendorf tubes, and 30 µl of RNase-free water was pipetted directly onto the column membranes and centrifuged at 8000 g for 1 minute at room temperature to elute the RNA. The concentration and the purity of total RNA extracted from each sample were measured using NanoDrop Spectrometer. The elution samples containing RNA were stored at -80°C immediately to prevent degradation of RNA.

2.7.2 Conversion of RNA to cDNA

Total RNA extracted from each sample (Chapter 2.7.1) were mixed with nuclease-free water (Qiagen) to achieve a final concentration of 1 µg in 30 µl. 2 µl of 100 µM Oligo (dT) (Thermo Fisher Scientific) was added to each reaction mix to increase the efficacy of primary reactioncatalysed by the reverse transcriptase. The reaction mixes were then incubated for 10 minutes at 70°C and then placed on ice for 5 minutes. The reverse transcription master mix consisting of 10 µl of M-MLV 5x reaction buffer (Promega), 5 µl of 20 mM dNTPs (Thermo Fisher Scientific), 2 µl of RNAsin Plus RNase inhibitor (Promega) and 2 µl of M-MLV reverse transcriptase (Promega) were added to each reaction mixture (Table 2.4). The reaction mixtures were then incubated at room temperature for 10 minutes, then at 40°C for 90 minutes, followed by at 70°C for 5 minutes. C1000 Touch™ Thermal Cycler (BioRad) was used to incubate reaction mixtures at specific temperatures (Table 2.5).

	Reaction mix component	**Volume per reaction (1µg RNA)**	
	RNA	Variable	30 µl
	Nuclease-free water	Variable	
	100 µM Oligo (dT)	2 µl	
Reverse transcription master mix	M-MLV 5x reaction buffer	10 µl	
	20 mM dNTPs	5 µl	
	RNAsin Plus RNase inhibitor	2 µl	
	M-MLV reverse transcriptase	2 µl	
	Total volume	51 µl	

Table 2.4 Components of reverse transcription reaction mixture to synthesise cDNA

Step	**Temperature**	**Time (min)**	**Process**
1	70°C	10	Denaturation of RNA
2	On ice	5	Cooling
3	Room temperature	10	Oligo (dT) annealing
4	40°C	90	cDNA synthesis
5	70°C	5	Heat inactivation

Table 2.5 Incubation times and temperatures used for reverse transcription to synthesise cDNA
min: Minutes

2.7.3 Quantitative PCR (qPCR)

qPCR was performed using the SYBR® Green Real-Time PCR kit (Qiagen), the cDNA produced from the reverse transcription (Chapter 2.7.2) and primers. The componentsof the final qPCR reaction mixtures are summarised in Table 2.6. The primers used are listed in the chapter-specific material and methods. qPCR reactions were run in triplicates using a Mastercycler® ep RealPlex (Eppendorf) with the cycling condition shown in Table 2.7. Step 2 to 4 of qPCR thermal cycling (Table 2.7) were repeated 40 times, and fluorescence was measured at each cycle during Step 4. Melting curve analysis was performed. The annealing temperature of 60°C was used for all primers as per the manufacturer's protocol.

Component	Volume (µl)
SYBR® Green Real-Time PCR master mix	12.5
Forwards primer (10 µM)	0.5
Reverse primer (10 µM)	0.5
cDNA	2
Nuclease-free water	9.5
Total volume	25

Table 2.6 Components of qPCR reaction mixture

Step	Temperature	Time	Process
1	95°C	5 minutes	Initial denaturation
2	95°C	10 seconds	Denaturation
3	60°C	30 seconds	Annealing
4	60°C	20 seconds	Elongation
5	60-95°C	20 minutes	Melting curve analysis

Table 2.7 qPCR condition. Step 2 to 4 were repeated 40 times.

2.8 Western blot

2.8.1 Cell lysate preparation

For experiments using MDMs and macrophages derived from THP-1 cells or Hoxb8 cells, after a specific incubation period, the culture media were transferred into 5 ml Eppendorf tube and centrifuged for 3 minutes at 1000 rpm. After centrifugation, supernatants were removed and stored at -80°C leaving cell pellets in the tube. 1.5 ml, if using 6-well plates, or 3 ml, if using culture dishes, of ice-cold

sterile PBS was then added to the well/dish and adherent cells were scraped using sterile 24 cm cell scrapers (Science laboratory supplies). The PBS containing the scraped cells in each well/dish was transferred into the 5 ml Eppendorf tube containing the cell pellets from the corresponding well/dish to ensure both non-adherent and adherent cells in each well/dish were collected. Cells were suspended and centrifuged at 1000 rpm for 3 minutes. PBS was removed and cells were washed again with 4 ml of ice-cold PBS and centrifuged at 1000 rpm for 3 minutes. For Western blot of ExpiSf 9 cells, the cells were simply collected from the culture media and washed twice in 50 ml of PBS by centrifugation at 300 g for 5 minutes before the cells were lysed.

Cells were lysed in 350 µl – 700 µl of RIPA lysis buffer (Sigma) containing protease inhibitor, cOmplete™ Protease Inhibitor Cocktail (Roche) and incubated on ice for 30 minutes. The cell lysate was then sonicated using a MSE Soniprep 150 (MSE) for 3 bursts of 10 seconds, at an amplitude of 7 microns, with a 10-seconds of cooling period on ice between each burst of sonication to disrupt cell membrane, organelles and shear DNA.

2.8.2 Supernatant preparation

Supernatants collected from the cell culture media and separated from cell pellets were filtered through Acrodisc® Syringe Filter 0.2µm Supor® Membrane (Pall) to remove any cells. For supernatants collected from the culture media of MDMs and macrophages derived from THP-1 cells or Hoxb8 cells, Albumin and immunoglobulin G were removed from the supernatant using Albumin & IgG Depletion SpinTrap (GE Healthcare) following the manufacturer's instruction.

2.8.3 Loading sample preparation

The total concentration of proteins within each cell lysate and supernatant, except for the supernatant collected from ExpiSf 9 cell culture media, were measured using Pierce™ BCA Protein Assay Kit (Thermo Fisher Scientific) according to the manufacturer's instructions and read on a CLARIOstar microplate reader (BMG Labtech) at 526nm. The protein concentrations of the samples were then standardised by diluting the samples with an appropriate volume of RIPA buffer, for the cell lysates, or PBS, for the supernatants. Loading samples were made by

adding the cell lysate, or the supernatant, to Laemmli sample buffer (4x) (BioRad) and 2-mercaptoethanol (Sigma M6250), making up 25% and 2.5% of the final sample volume respectively. The loading samples were then incubated at 75°C for 15 minutes.

2.8.4 SDS-polyacrylamide gel electrophoresis (SDS-PAGE) gel electrophoresis

SDS-PAGE gel (12%) with stacking gel was made by mixing the reagents listed in Table 2.8 using Mini-PROTEAN® Tetra Cell casting system (BioRad). The SDS-PAGE gel was left to set for at least 20 minutes at room temperature to ensure complete polymerisation of the gel before being placed in Mini-PROTEAN® Tetra Cell and submerged in ~700 ml of the running buffer (x1). The samples were then loaded in each well of the SDS-PAGE gel, and the apparatus was connected to run for ~ 60 minutes at a constant voltage of 120V.

Reagents	Volume	
	SDS-PAGE gel	Stacking gel
Acrylamide	2 ml	250 µl
1.5 M Tris-HCl pH 8.8	1.25 ml	Nil
1 M Tris-HCl pH 6.8	Nil	160 µl
Distilled water	1.65 ml	1.1ml
10% SDS	50 µl	20 µl
10% APS	50 µl	20 µl
TEMED	4 µl	4 µl

Table 2.8 List of reagents and volumes used to make one SDS-PAGE gel. Acrylamide: PhotoFLOWGel (Scientific Laboratory Supplies), SDS (Sigma), APS: Ammonium persulphate (Sigma), TEMES: Tetramethylethylenediamine (Sigma)

2.8.5 Transfer of protein from SDS-PAGE to membrane

Immobilon-P PVDF Membrane (Merck) was cut into a 6 cm x 9 cm rectangle and soaked in 100% methanol to be activated. A filter paper was cut into 6 cm x 9 cm rectangles and soaked in the transfer buffer (x1) containing 20% methanol together with sponges. SDS-PAGE gel was taken out of the Mini-PROTEAN® Tetra Cell system, and the stacking gel was removed carefully using a spatula. The activated

PVDF membrane and the SDS-PAGE gel were briefly soaked in the transfer buffer containing 20% methanol to be equilibrated. Novex™ Bolt™ Vertical Mini Blot Module cassette was opened. Sequentially the sponge, filter paper, SDS-PAGE gel and the PVDF membrane, followed by another filter paper and sponge were placed on top of the cathode half of the cassette. A mini-roller was used to expel any air bubbles between the membrane and the gel. The anode half of the cassette was placed on top of the sandwich to close the cassette. The cassette was mounted in the tank containing the transfer buffer containing 20% methanol and run at a constant voltage of 20V for 60 minutes.

2.8.6 Antibody staining

After transferring the protein from SDS-PAGE gel to the membrane, the membranes were removed from the transfer cassette and placed in the blocking solution on constant agitation for 1 hour. Membranes were then probed with primary antibody (Table 2.9), dissolved in the blocking solution, at 4°C overnight on constant gentle agitation, and then washed in PBS-T 3 times for 5 minutes per wash. The membranes were probed with secondary antibody (Table 2.10), except for the membrane probed with 6x-His-HRP primary antibody, dissolved in the blocking solution for 1 hour at room temperature on constant gentle agitation, then washed with TBS-T 3 times for 5 minutes per wash. The bound antibody was detected by applying Luminata Crescendo Western HRP substrate (Merck) directly onto the membrane. The membranes were then sandwiched between a clear layer of plastic and exposed onto Hyperfilm ECL (Amersham) in a dark room then scanned with an Epson Perfection V700 Photo, or visualised using Thermo Scientific MYECL Imager (Thermo Fisher Scientific).

Primary antibody	Manufacturer	Catalogue	Working concentration	Secondary antibody
ADAMDEC1	AVIVA	ARP55070_P050	1:1000	Rabbit
Vinculin	Milipore	MAB3574	1:1000	Mouse
Hoxb8	Santa Cruz Biotechnology	SC517156	1:1000	Mouse
6x-His (HRP)	Invitrogen	R731-25	1:10000	N/A

Table 2.9 List of primary antibodies and working concentration used for Western blot.

Secondary antibody	Manufacture	Catalogue	Working concentration
Polyclonal goat anti-mouse	Dako	P044701-2	1:10000 (Vinculin) 1:5000 (Hoxb8)
Polyclonal goat anti-rabbit	Dako	P044801-2	1:2000

Table 2.10 List of secondary antibodies and working concentration used for Western blot.

2.9 *Adamdec1*$^{-/-}$ and WT mice

2.9.1 Sources and generation of *Adamdec1*$^{-/-}$ and WT mice

Originally, *Adamdec1* heterozygous mice were generated by targeted mutagenesis of the *Adamdec1* gene 1227 on chromosome 8 and insertion of a neomycin resistant cassette. The line of *Adamdec1* heterozygous mice was reconstituted from frozen embryonic stem cells re-derived from 129/OlaHsd mice embryos at the Deltagen repository (Deltagen, Inc, USA). The chimeric mice were backcrossed onto C57BL/6 mice for at least 6 generations before three *Adamdec1* heterozygous mice were purchased by UCL. These heterozygous mice were then cross-matched to generate WT and *Adamdec1*$^{-/-}$ mice in 2016 for previous experiments in our laboratory, during which *Adamdec1* heterozygous embryos were preserved by in vitro fertilisation using the spermatozoa of the *Adamdec1*$^{-/-}$ mice and C57BL/6 mice oocytes. For this project, these *Adamdec1* heterozygous embryos previously preserved were re-derived and implanted into surrogate C57BL/6 female mice to first of all generate *Adamdec1* heterozygous litters. These heterozygous mice were then cross-matched to obtain colonies of WT and *Adamdec1*$^{-/-}$ mice.

One additional WT C57BL/6 mouse was purchased internally from the UCL Biological Sciences Unit, which was bred from C57BL/6 mice originally purchased from Charles River (UK).

2.9.2 Husbandry of mice

Mice were bred and maintained in specific-pathogen-free, individually ventilated cages in the animal facility of the UCL Biological Sciences Unit. The litters were weaned from their parents at the age of 4 - 5 weeks and moved into new cages separated by sex with a maximum of 5 mice per cage during the maintenance. The

environmental conditions such as temperature, humidity and hours of light (standard 12 hours light/12 hours dark cycle) were kept constant and monitored by the Named Animal Care and Welfare Officer (NACWO) in the animal facility. The cages and bedding were changed weekly. Mice were fed with sterilised Harlan 2018 Teklad Global 18% protein rodent diet, and breeders were fed with sterilised 19% protein rodent diet. Drinking water was sterilised. Routine health screens for infection were carried out for parasites and opportunistic infections.

2.9.3 Euthanasia of mice

All mice used in experiments were culled by carbon dioxide overdose. This was followed by cervical dislocation as the secondary method of euthanasia as per Schedule 1 to the Animals (Scientific Procedures) Act 1986.

2.9.4 Genotyping of mice

Ear clips were taken from each mouse at the time of weaning and stored in sterile individual 1.5 ml Eppendorf tubes. 75 µl of 25 mM NaOH / 0.2 mM EDTA were added to each sample and incubated for 1 hour at 95°C. The samples were then placed on ice for 5 minutes, and 75 µl of 40 mM Tris HCl (pH 5.5) were added and vortexed for 20 seconds to neutralise. The tubes were then centrifuged at 16000 g for 5 minutes to pellet the hair and debris, and 1 µl of the solution from each sample was used for subsequent genotyping by PCR using Hot Start Taq 2x Master Mix (Qiagen) and gel DNA electrophoresis. PCR reaction mixture was made up as shown in Table 2.11 and the primers used are listed in Table 2.12.

Component	Volume (µl)
Hot Start Taq 2x Master Mix	12.5
Forwards primer (5 µM)	2
Reverse primer (5 µM)	2
DNA extracted from ear clip	1
Nuclease-free water	7.5
Total volume	25

Table 2.11 Components of PCR reaction for mouse genotyping

Primer	Sequence
1 (Forward within the target region of *Adamdec1*)	AGCTTGAGCGCAAACCCAATGCTTC
2 (Forward within Neomycin cassette)	GACGAGTTCTTCTGAGGGGATCGATC
3 (Reverse within the endogenous region of gene)	CCTCAGGTACTGATTCATCACACAG

Table 2.12 Primers used for mouse genotyping

The presence of *Adamdec1* was detected by Primer 1 and Primer 3 (Table 2.12), generating a PCR product of 322 base pairs (bp) (Figure 2.1 and 2.2). The presence of neomycin cassette, indicating the absence of *Adamdec1*, was detected by Primer 2 and Primer 3 (Table 2.12), generating a PCR product of 600 bp (Figure 2.1 and 2.2). PCR was performed by C1000 Touch™ Thermal Cycler (BioRad) using the conditions shown in Table 2.13. Step 2 to 4 of the PCR thermal cycling (Table 2.13) were repeated 35 times. The size of the PCR products was determined by DNA gel electrophoresis using 2% agarose gel and imaged on myECL™Imager (Thermo Fisher Scientific).

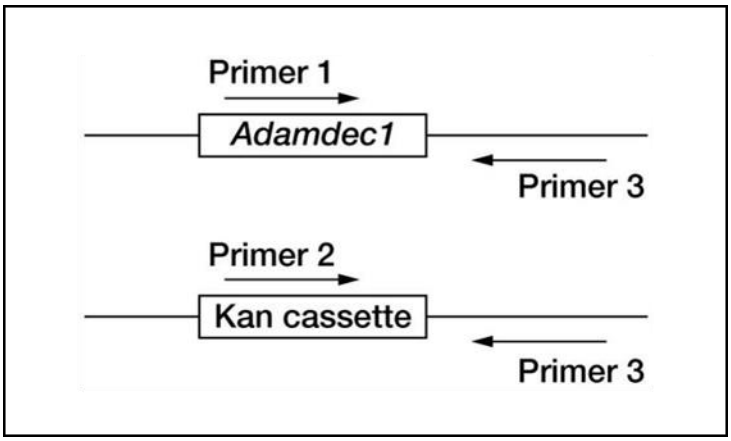

Figure 2.1 Schematic diagram showing alignment location of the primers used for mouse genotyping

Step	Temperature	Time	Process
1	95°C	15 minutes	Initial denaturisation
2	95°C	45 seconds	Denaturisation
3	60°C	45 seconds	Annealing
4	72°C	45 seconds	Extension
5	72°C	10 minutes	Final extension
6	4°C	∞	Cooling

Table 2.13 PCR condition used for mouse genotyping. Step 2 to 4 were repeated 35 times.

Following PCR, 5 µl of gel loading dye purple x6 (New England Bio) was added to each PCR product and loaded onto each well. An example of the gel electrophoresis of the genotyping PCR product is shown in Figure 2.2. The first well for each mouse was loaded with the PCR product using Primer 1 and 3 (Table 2.12), in which the presence of the band indicated the presence of *Adamdec1* allele. The second well for each mouse was loaded with the PCR product using Primer 2 and 3 (Table 2.12), in which the band indicated the presence of Kanamycin cassette, thereby the absence of *Adamdec1* allele.

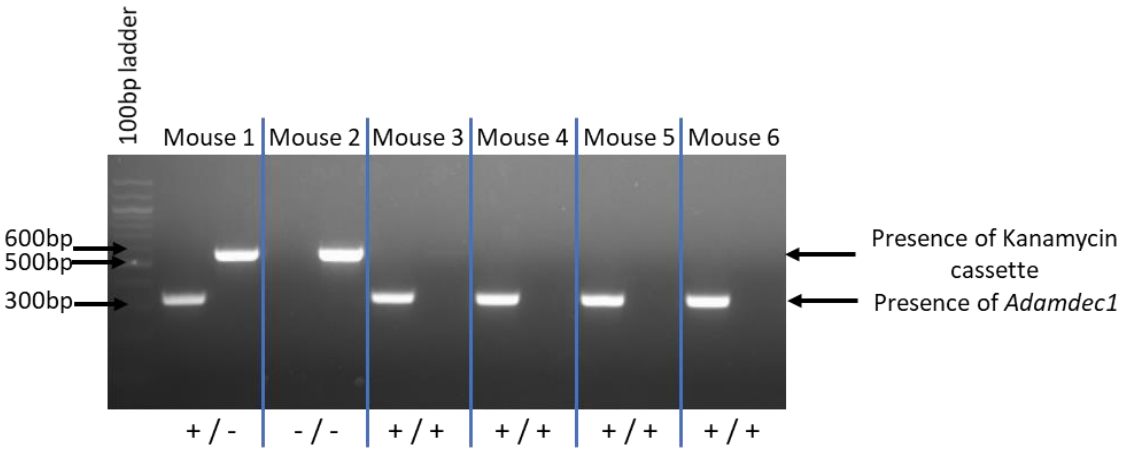

Figure 2.2 Example of the DNA gel electrophoresis of the mouse genotyping. The presence of a band in the first well of each mouse indicates the presence of *Adamdec1* allele. The presence of a band in the second well of each mouse indicates the presence of kanamycin cassette thereby the absence of *Adamdec1* allele. 2% agarose gel was used.

Chapter 3

Identification of stimuli and signalling pathways responsible for the induction of ADAMDEC1 during monocyte to macrophage differentiation

3.1 Background and aims

Currently available evidence suggests that ADAMDEC1 is induced during monocytes to macrophage differentiation and is predominantly expressed in the macrophages within the gastrointestinal tract. The normally high expression of ADAMDEC1 appears to be reduced in the tissues of some gastrointestinal diseases such as IBD and CRC.[57,63,64,100] This reduction in the expression of ADAMDEC1 does not seem to be dependent on the degree of inflammation or the abundance of macrophages within the tissue.[64,100] This leads to the hypothesis that the macrophages in the diseased tissue may express an attenuated level of ADAMDEC1, which might play a mechanical role in the pathogenesis of these diseases. Although there is modest evidence to support that the induction of ADAMDEC1 occurs during monocyte to macrophage differentiation, little is known about the exact mechanism responsible for this. A better understanding of the mechanism behind the induction of ADAMDEC1 would help to unfold the events responsible for the reduced level of ADAMDEC1 in the diseased gastrointestinal tissue and how this might be involved in the pathogenesis of these diseases.

Many of the previous studies examining the induction of ADAMDEC1 utilised THP-1 cells. THP-1 cells are spontaneously immortalised monocyte-like cell line originally isolated from the peripheral blood of a patient with acute monocytic leukaemia.[101] They can be differentiated into macrophage-like cells (referred to as macrophages for conciseness hereafter), thereby serving as a valuable in vitro tool to study the structure and function of monocytes and macrophages, and are extensively used for this purpose.[102,103] The use of THP-1 cells thus eliminates the need for collecting blood from volunteers and subsequent isolation of monocytes prior to each experiment which places a major restriction on the scale of experiments that can be conducted in a limited time.

In this chapter, THP-1 cells were incubated with various stimuli, and the induction of *ADAMDEC1* was determined by qPCR to identify stimuli, receptors and

signalling pathways responsible for the induction of ADAMDEC1. Previous studies reporting the upregulation of ADAMDEC1 during differentiation of THP-1 cells to macrophages utilised PMA or 1α-25-dihydroxyvitamin D3 to trigger the differentiation of THP-1 cells.[25,42] In this chapter, naïve THP-1 cells were stimulated with a broader selection of stimuli, including microbial ligands and various cytokines which are present in the intestinal tissue and thus are more relevant to the process of monocyte to macrophage differentiation in vivo intestinal environment. Additionally, since more recent studies have suggested cells other than MDMs to be the main ADAMDEC1-expressing cells within the healthy intestine, the stimuli-induced induction of ADAMDEC1 and the macrophage markers on the stimulated THP-1 cells were examined. This would verify that the induction of ADAMDEC1 occurs during monocytes macrophage differentiation, and thus MDMs to be the ADAMDEC1 expressing cells.[50,54] Finally, the experiments using THP-1 cells were repeated using peripheral blood monocytes to verify the findings in the primary monocytes ex vivo.

The main aims for Chapter 3 were:

- To identify stimuli that induce ADAMDEC1 expression in THP-1 cells
- To verify whether the stimuli-induced induction of ADAMDEC1 in THP-1 cells correlates with upregulation in the expression of macrophage surface marker
- To identify the signalling pathway responsible for the induction of ADAMDEC1 by using selective inhibitors for various signalling pathways
- To verify the findings of the experiments using THP-1 cells in peripheral blood monocytes collected from healthy volunteers

3.2 Materials and method

3.2.1 Cells and cell culture media

THP-1 cells

THP-1 cells were cultured and maintained in THP-1 complete medium at 37°C and 5% CO_2. The culture medium was changed every 2 to 3 days, and the cells were maintained at a density between 1.5 x 10^5 – 1 x 10^6 cells/ml. Fresh frozen aliquots of the cells were taken out of liquid nitrogen and thawed every 3 months. The viability of cells was checked every 2 to 3 days and the cells with a viability of ≥ 98% were used for experiments.

THP-1 complete medium

RPMI 1640 Medium GlutaMAX™ (Gibco)
10% FBS (Sigma)
Penicillin/Streptomycin (50 U/ml and 50 µg/ml) (Gibco)
20 mM HEPES solution (Sigma)
20 µM 2-mercaptoethanol (Sigma)

Serum-free culture medium

RPMI 1640 Medium GlutaMAX™ Supplement (Gibco)
Penicillin/Streptomycin (50 U/ml and 50 µg/ml) (Sigma)
20 mM HEPES solution (Sigma-Aldrich)

MDMs serum medium

RPMI 1640 Medium GlutaMAX™ Supplement (Gibco)
10% FBS (Sigma)
Penicillin/Streptomycin (50 U/ ml and 50 µg/ml) (Gibco)
20 mM HEPES solution (Sigma)

3.2.2 Stimulation of THP1 cells

THP-1 cells in 2 ml of complete media at a density of 5 x 10^5 /ml were plated in each well of a tissue-culture treated 6-well plate (Falcon). The stimulant was then added to each well and the cells were incubated at 37°C, 5% CO_2 for 24 hours or 72 hours. The stimulants were used at working concentrations listed in Table 3.1 unless otherwise stated.

Stimulants	Manufacturer	Working concentration (/ml)
HkEc	NTCT	5×10^6
Pam3Cys-Ser-(Lys)4, Trihydrochloride (Pam3CSK4)	Alexis Biochemicals	4µg
LPS from Salmonella abortus equi S-form	Alexis Biochemicals	200ng
Poly(I:C)	Invivogen	1µg
Muramyl dipeptide (MDP)	Invivogen	1µg
PMA	Sigma-Aldrich	50ng
HkC	N/A	5×10^6
Opsonised HkC	N/A	5×10^6
TNF-α	PeproTech	20ng
MCSF	PeproTech	20ng
Interleukin–1β (IL-1β)	PeproTech	10ng
Interleukin–6 (IL-6)	PeproTech	20ng
Interleukin–12 (IL-12)	PeproTech	20ng
Interleukin–23 (IL-23)	PeproTech	20ng
Interferon-β (IFN-β)	PeproTech	50ng
Interferon-γ (IFN-γ)	PeproTech	50ng

Table 3.1 List of stimulants and their working concentrations used for THP-1 stimulation experiments.

3.2.3 THP1 cell stimulation with inhibitors

Some of the above stimulation experiments using THP-1 cells were repeated with the addition of inhibitor(s) (Table 3.2). The inhibitors, except for Adalimumab, were reconstituted in dimethyl sulfoxide (DMSO) and stored as stocks at -20°C, and diluted in THP-1 complete media to achieve working concentration for the experiments. For the experiments using Adalimumab, THP-1 cells were stimulated with either HkEc, Pam3CSK4 or LPS with or without Adalimumab simultaneously and incubated for 24 hours. For the experiments using the signalling pathway inhibitors, THP-1 cells were incubated with a NF-κB inhibitor (JSH-23) or selective inhibitor of the individual components of mitogen-activated protein kinase (MAPK) cascade: MAPK/ERK kinase (MEK)1/MEK2 (PD98059), p38 (SB203580), c-Jun N-terminal kinase (JNK) (SP600125), or a combination of them for 30 minutes at 37°C prior to being stimulated with HkEc.

Inhibitors	Manufacture	Catalogue	Target	Working concentration
Adalimumab	AbbVie	N/A	TNF-α	10 μg/ml
JSH-23	Sigma	749886-87-1	NF-κB	20 μM
SB203580	Cambridge Biosciences	SM30-2	P38	20 μM
SP600125	Cambridge Biosciences	SM41-2	JNK	10 μM
PD98059	Invivogen	tlrl-pd98	MEK1 and MEK2	10 μM

Table 3.2 List of inhibitors and their working concentrations used in THP-1 stimulation experiments.

3.2.4 qPCR and primers used for qPCR

Total RNA from the cells was extracted using RNeasy Mini Kit (Qiagen) (Chapter 2.7.1.2 and 2.7.1.3). The extracted RNA was converted into cDNA (Chapter 2.7.2). qPCR was conducted using SYBR® Green Real-Time PCR kit as described (Chapter 2.7.3) using primers listed in Table 3.3.

Target gene	Forward primer (5' to 3')	Reverse primer (5' to 3')
PPIA	CCCACCGTGTTCTTCGACATT	GGACCCGTATGCTTTAGGATGA
β-actin	AACGAGCATCCCCCAAAGTT	GGGCACGAAGGCTCATCATT
ADAMDEC1	CAACACCAGTGTGTGGGAAC	TCCTGGCAAGGTAGCATCTC
CD14	GTGGCCTTGTCAGGAACTCT	ATCAGGGGTCAAGTTTGCTG
CD80	ATCTGACGAGGGCACATACG	GAGAGGTGAGGCTCTGGAAA

Table 3.3 List of primers used to determine gene expressions in the THP-1 stimulation experiments.

3.2.5 qPCR data analysis method

The expressions of the genes of interest were analysed and presented using the relative quantification method, in which the CT value of the gene of interest in each sample was, first of all, normalised to the CT value of the housekeeping gene in each sample to generate delta CT (dCT). The dCT of each sample was then normalised to the dCT of the control sample i.e. the THP-1 cells incubated for 24 hours without any stimuli, to generate delta delta CT value (ddCT). The

expressions of genes of interest were presented as fold change by taking 2 to the power of -ddCT so that more negative numbers corresponded to lower gene expression.

$$dCT = CT\ (\text{gene of interest in each sample}) - CT\ (\beta\text{-actin in each sample})$$

$$ddCT = dCT\ (\text{stimulated sample}) - dCT\ (\text{unstimulated sample})$$

$$\text{Fold change} = 2^{-(ddCT)}$$

Fold change is an estimate of the amount of cDNA present in each stimulated samples in comparison to the experimental control, i.e. unstimulated sample incubated for 24 hours or 72 hours, based on several experimental assumptions.[104] While it allows easily interpretable representation of the effect of each stimuli in inducing *ADAMDEC1*, fold change is not recommended to be subjected to statistical analysis unlike CT values, which are the observed raw experimental values generated by qPCR that should be the primary statistical metric of the qPCR data analysis.[105] The qPCR result of this chapter was robust and did not require statistical analysis to conclude the biological questions being asked. Thus the qPCR results were presented and concluded without statistical analysis in this chapter.

3.2.6 Generation of MDMs and stimulation of MDMs

Peripheral blood (50 ml) was collected from healthy volunteers by venopuncture into a sterile 50 ml syringe (Scientific Laboratory Supplies) containing 300 µl of 1000 IU/ml heparin (Wockhardt). Blood was then transferred and diluted 1:1 with endotoxin-free sterile PBS (Gibco). 15 ml of Lymphoprep™ (Alere Technologies) were poured into four 50 ml Falcon tubes. Slowly 25 ml of the diluted blood was pipetted on top of the Lymphoprep™. Falcon tubes were centrifuged at 900 g for 30 minutes at 20°C with centrifuge breaks off. Layers of different cell types, including an interphase layer containing peripheral blood mononuclear cells (T cells, monocytes, B cells and Natural killer cells), were formed by the centrifugation. The interphase layer was then carefully aspirated by a sterile serological pipette and transferred into two new 50 ml Falcon tubes. 35 ml of sterile PBS was added to each tube and centrifuged at 400 g for 4 minutes with brakes on to pellet the

cells. The supernatant was removed and cells were resuspended and washed in 50 ml of fresh sterile PBS. Tubes were centrifuged at 400 g for 4 minutes and the supernatant was removed. Cells were resuspended in 10 ml of the serum-free culture medium (Chapter 3.2.1) and plated onto 92mm Nunc™ surface coated tissue culture plate (Thermo Fisher Scientific). The cells were incubated for 2 hours at 37°C, 5% CO_2 to allow adherence of the activated monocyte induced by serum-starvation. After 2 hours, the serum-free medium was removed and 10 ml of fresh sterile PBS was added to the culture dish to remove any non-adherent cells. After PBS was removed, 10 ml of the MDMs serum medium (Chapter 3.2.1) was then added to the culture dish and the cells were incubated for 24 hours at 37°C, 5% CO_2. After 24 hours (day 2), the cells were fed with a further 10 ml of the fresh MDMs serum media. On day 5, the media was removed from the culture dish, and the adherent cells were washed with 10 ml of sterile PBS. The cells were then fed once again with 20 ml of the MDMs serum media for further 48 hours. On day 7, the media was removed from the culture dish and the adherent MDMs were washed with 10 ml of sterile PBS and scraped. Cell number and viability were assessed using BioRad Automated cell counter with trypan blue exclusion. MDMs were resuspended in the MDM serum media to make up cell density of 5 x 10^5 /ml and 2 ml of this cell culture per well were plated into 6-well plate (Falcon). On day 8, the supernatant was removed from one well and stored at -80°C. MDMs in this well were scraped and used as day 8 MDMs baseline lysate for Western blot. MDMs in the other wells were stimulated with either HkEc or LPS (Table 3.1), or without stimuli for further 48 hours. On day 10, the supernatant was removed from each well and stored at -80°C, and the cells were scraped to be processed for Western blot as described in Chapter 2.8.1. The supernatants stored were subsequently processed for Western blot as described in Chapter 2.8.2. Western blot was performed as described in Chapter 2.8.

3.3 Results

In order to evaluate the mechanism of induction of *ADAMDEC1* in monocytes, naïve THP-1 cells were incubated with various stimuli over 24 hours and expression of *ADAMDEC1* was measured at the messenger level by qPCR. The expression of housekeeping candidates, PPIA and β-actin, were measured in all samples. PPIA was selected as the housekeeping gene to be used in this chapter as its expression was more stable across the samples in comparison to β-actin.

3.3.1 *ADAMDEC1* is induced by bacteria-related ligands

Strong induction of *ADAMDEC1* was seen by the stimulation of naïve THP-1 cells with microbial-related ligands over 24 hours. The strongest *ADAMDEC1* inducer was HkEc followed by Pam3CSK4 and LPS, TLR2 and TLR4 ligands respectively. (Figure 3.1). Poly(I:C), a TLR3 ligand, did not induce *ADAMDEC1,* which was consistent with previous reports indicating that TLR3 is absent or expressed at a very low level in naïve THP1 cells as well as in human circulating monocytes.[106–108] Stimulation with MDP also resulted in induction of *ADAMDEC1* but to a lesser extent compared to the *ADAMDEC1* induction by the TLR2 and TLR4 ligands. MDP is an immunostimulatory fragment of the bacterial cell wall that activates an intracellular receptor NOD2 and is not recognised by TLRs.[109]

NOD2 mutation is a well-known risk factor for Crohn's disease.[110] Susceptibility for Crohn's disease is increased by 2- to 4- folds by possession of one of the three disease-associated alleles and by 15- to 40- folds with homozygosity or compound-heterozygosity for these alleles.[111] To assess if NOD2 genotype has an effect on the *ADAMDEC1* expression, the expression of *ADAMDEC1* in MDMs from patients with Crohn's disease was extracted and analysed according to their NOD2 genotypes using a transcriptomic microarray data from a previous study.[59] In this study, circulating monocytes from patients with Crohn's disease were differentiated into macrophages by serum starvation over 4 hours. The analysis showed that there was no significant difference in the expression of *ADAMDEC1* in the MDMs between the different genotypes of NOD2 amongst the patients with Crohn's disease (Figure 3.2). This indicated although the activation of NOD2 by MDP induced *ADAMDEC1* expression in THP-1 cells, the induction via this pathway is dispensable.

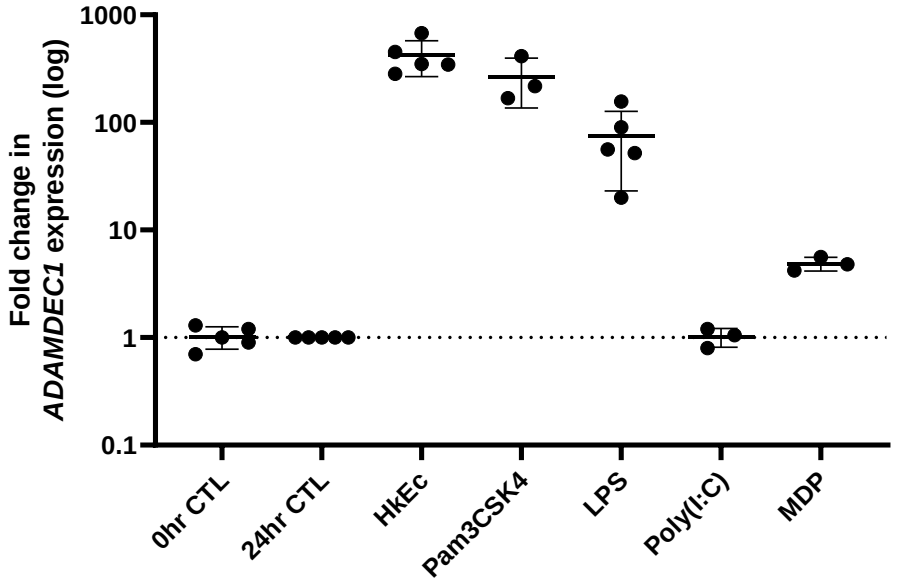

Figure 3.1 Expression of *ADAMDEC1* in THP-1 cells after incubation with various bacterial-related ligands for 24 hours (normalised to THP-1 cells incubated without any stimuli for 24 hours). The strongest expression of *ADAMDEC1* was induced by HkEC, followed by Pam3CSK4 and LPS. A weaker expression of *ADAMDEC1* was induced by MDP. The graph shows mean with SD.
CTL: Control

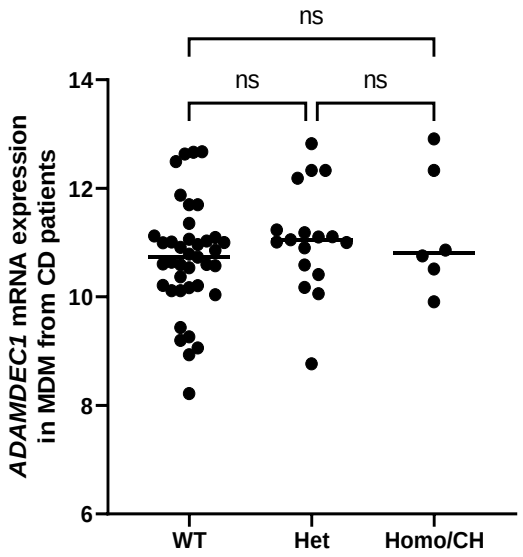

Figure 3.2 Expression of *ADAMDEC1* in the unstimulated MDMs from patients with Crohn's disease categorised into 3 different cohorts based on their NOD2 mutation status. The expression was analysed using the data extracted from GEO GSE60083.[59] There were no differences between the expression of *ADAMDEC1* between the 3 cohorts of Crohn's disease patients. Thus the expression of *ADAMDEC1* in MDMs of Crohn's disease patients does not depend on the NOD2 genotype. One-way ANOVA test was used.
CD: Crohn's disease, WT: Wild type, Het: Heterozygous, Home/CH: Homozygous or compound-heterozygous, ns: Non-significant

3.3.2 *ADAMDEC1* is induced by opsonised HkC but not by non-opsonised HkC

Since the bacteria-related ligands were found to be strong inducers of *ADAMDEC1* in THP-1 cells, the experiments were repeated using HkC to assess the effect of fungal ligands on *ADAMDEC1* induction. Stimulation of THP-1 cells with HkC did not induce *ADAMDEC1* (Figure 3.3).

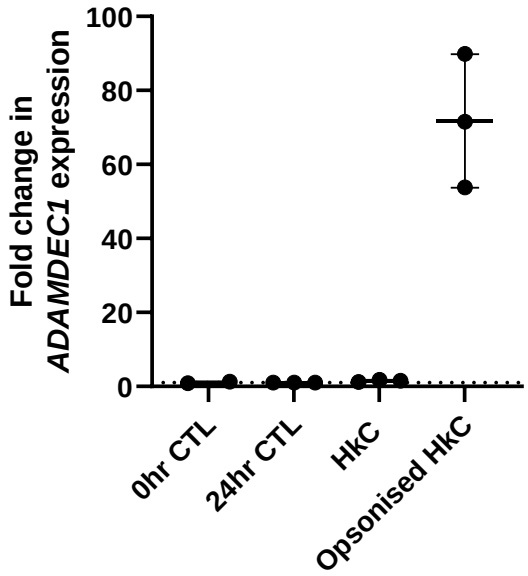

Figure 3.3 Expression of *ADAMDEC1* in THP-1 cells after incubation with HkC or opsonised HkC for 24 hours (normalised to THP-1 cells incubated without any stimuli for 24 hours). Induction of *ADAMDEC1* was not observed by HkC but a strong induction of *ADAMDEC1* was observed in the THP-1 cells stimulated with opsonised HkC indicating that activation of FcγR can induce *ADAMDEC1*. The graph shows mean with SD.
CTL: Control

The main fungal pattern-recognition receptors, Dectin-1 along with mannose receptor, which recognise β-glucan and mannose of fungal bacterial wall respectively, are however reported to be not expressed on naïve THP-1 cell.[112] The circulating monocytes, on the other hand, are reported to express moderately high levels of Dectin-1, which makes naïve THP-1 cells a poor model to evaluate the involvement of fungal ligands in *ADAMDEC1* induction in monocytes.[113] Subsequent stimulation of THP-1 cells with opsonised HkC, however, induced a relatively strong expression of *ADAMDEC1* indicating that activation of Fc-gamma receptor (FcγR) is also capable of *ADAMDEC1* induction.

3.3.3 *ADAMDEC1* is induced by selected pro-inflammatory cytokines

Following the findings that *ADAMDEC1* was induced in THP-1 cells by pro-inflammatory bacterial ligands and opsonised HkC, THP-1 cells were stimulated with various pro-inflammatory cytokines over 24 hours to assess the effect of individual pro-inflammatory cytokines (Figure 3.4). Stimulation with 20 ng/µl TNF-α resulted in the highest expression of *ADAMDEC1*. IL-1β, IL-6 and IFN-β, at concentrations of 10 ng/µl, 20 ng/µl and 50 ng/µl respectively, also induced *ADAMDEC1,* however, to a much lesser extent in comparison to the induction by TNF-α (Figure 3.4). The rest of the cytokines examined (MSCF, IL-12, IL-23 and IFN-γ) did not induce *ADAMDEC1* over a period of 24 hours. This was confirmed by repeating the experiment using a range of concentrations (10 – 100 ng/µl) of MSCF, IL-12, IL-23 and IFN-γ. Over a 24-hour incubation period, these cytokines were incapable of inducing *ADAMDEC1* (Data not shown).

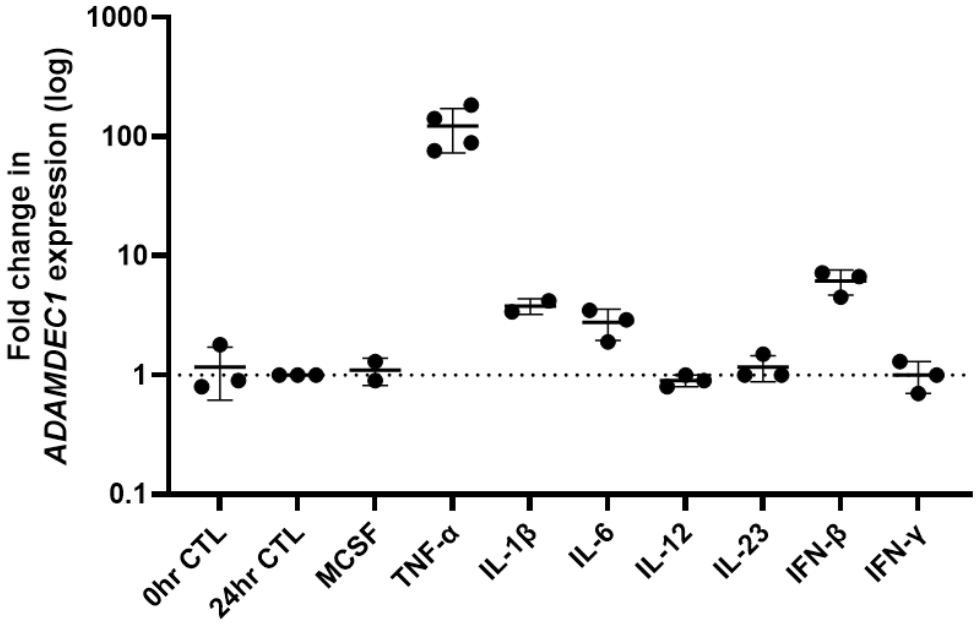

Figure 3.4 Expression of *ADAMDEC1* in THP-1 cells after incubation with various pro-inflammatory cytokines for 24 hours (normalised to THP-1 cells incubated without any stimuli for 24 hours). A strong expression of *ADAMDEC1* was induced by TNF-α (20 ng/µl). Much weaker expressions of *ADAMDEC1* were induced by IL-1β (10 ng/µl), IL-6 (20 ng/µl) and IFN-β (50 ng/µl). *ADAMDEC1* was not induced by stimulation with MCSF, IL-12, IL-23 or IFN-γ over 24 hours. Results are expressed as the mean with SD.
CTL: Control

3.3.4 *ADAMDEC1* induction occurs during monocyte to macrophage-like cell differentiation

To test the hypothesis that *ADAMDEC1* is induced during monocyte to macrophage differentiation, THP-1 cells were stimulated with PMA. PMA is not a microbial ligand but it is a diacylglycerol mimetic and an activator of protein Kinase-C (PKC). PKC activation drives THP-1 cell differentiation into macrophage phenotype similar to peripheral blood MDMs.[114–116] As expected, a relatively strong *ADAMDEC1* expression was induced by PMA (Figure 3.5 A). MCSF, another stimulator that is often used to differentiate THP-1 cells into macrophages, on the other hand, did not induce *ADAMDEC1* over a period of 24 hours contradictory to a previous in vitro study detecting an induction of *ADAMDEC1* in MCSF-differentiated MDMs (Figure 3.4).[34] However, THP-1 cells are usually incubated with MCSF for at least 4-5 days during the differentiation protocols using MCSF, unlike the protocols using PMA (over 1 or 2 days). Thus, to test the hypothesis that *ADAMDEC1* is induced during monocyte to macrophage differentiation, THP-1 cells were stimulated with MCSF, along with the other cytokines that failed to induce *ADAMDEC1* expression, over 72 hours. This revealed that *ADAMDEC1* was indeed induced by stimulation with MCSF over 72 hours supporting the hypothesis that *ADAMDEC1* is induced during monocyte to macrophage differentiation (Figure 3.5 B).

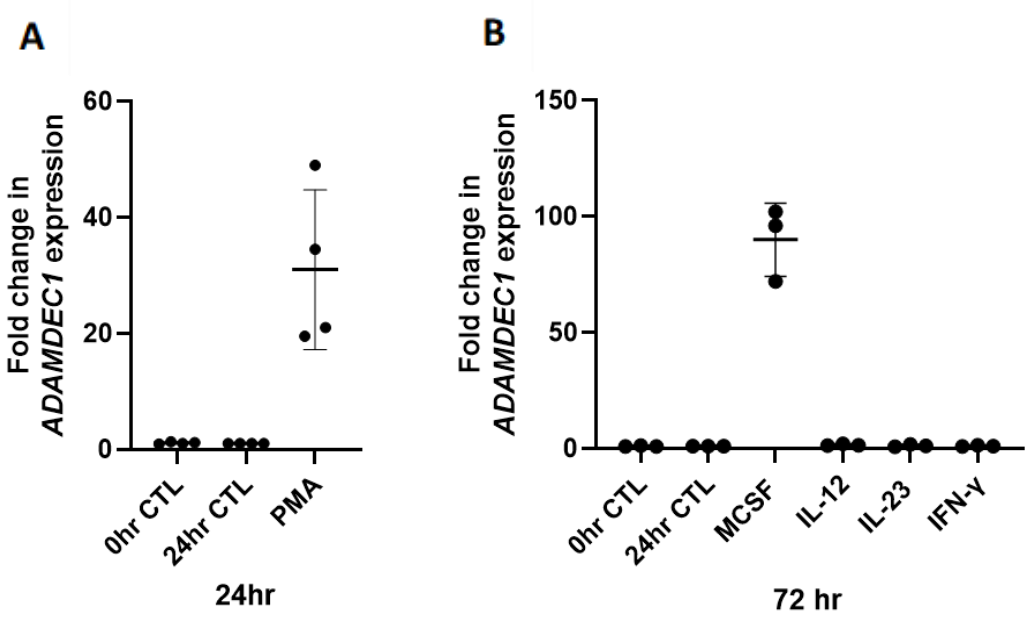

Figure 3.5 Expression of *ADAMDEC1* in THP-1 cells after incubation with PMA over 24 hours and cytokines over 72 hours (normalised to THP-1 cells incubated without any stimuli at each time point).

A: Expression of *ADAMDEC1* after incubation with PMA for 24 hours. A strong induction of *ADAMDEC1* was observed with stimulation with PMA over 24 hours.

B: Expression of *ADAMDEC1* after 72 hour-incubation with the cytokines that failed to induced *ADAMDEC1* expression over 24 hours. Stimulation with MCSF induced strong expression of *ADAMDEC1* after 72 hours corresponding to the time required for THP-1 cells to differentiate into macrophages using MCSF. Stimulation with IL-12, IL-23 and IFN-γ did not induced *ADAMDEC1* over 72 hours. The graphs show mean with SD.

CTL: Control

Furthermore, when THP-1 cells were incubated with stimuli that induced strong *ADAMDAC1* induction, such as HkEc, the initiation of morphological changes consistent with macrophage differentiation was evident over 24 hour period (Figure 3.6). The stimulated cells became adherent, and some of them displayed lamellipodial extensions and amoeboid morphology. These morphological changes were, however, more subtle in the cells stimulated with the weaker inducers of *ADAMDEC1* such as LPS (Figure 3.6).

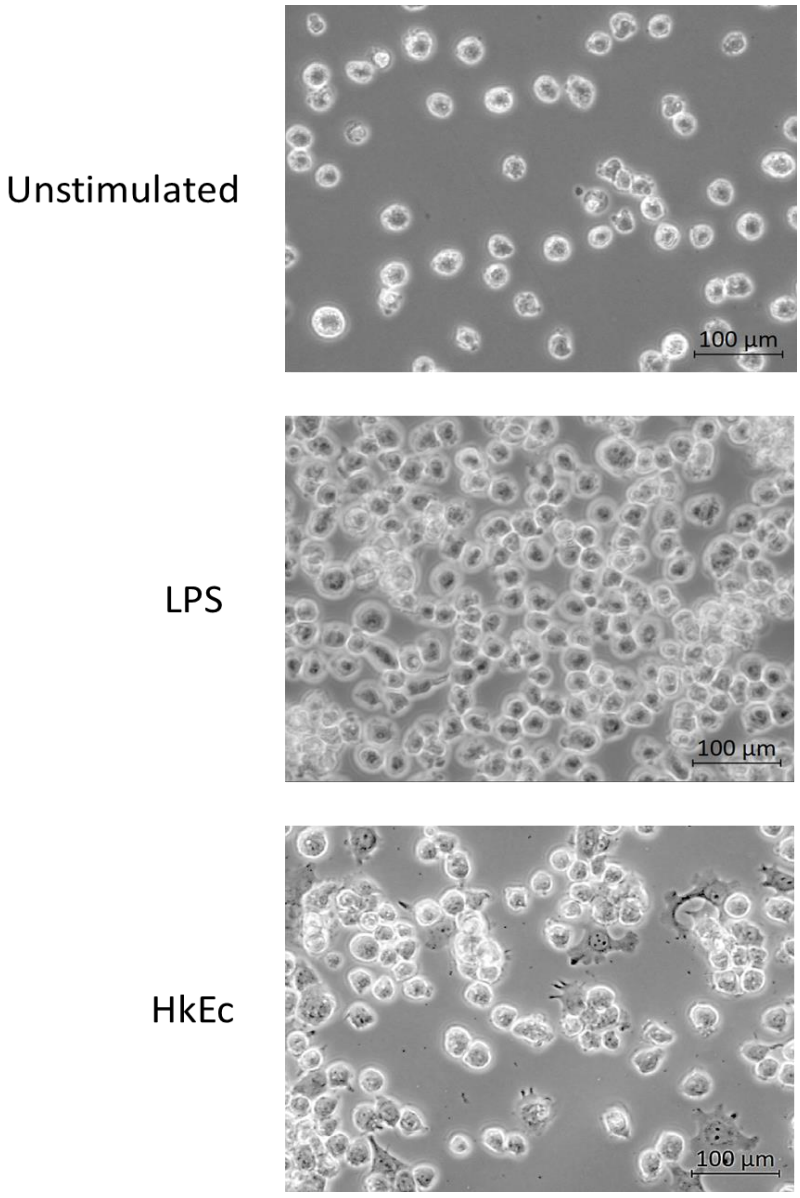

Figure 3.6. Morphological changes in THP-cells observed after stimulation with LPS and HkEC over 24 hours. Stimulation with HkEc resulted in the morphological changes consistent with macrophage differentiation over 24 hours. The HkEc-stimulated cells became adherent and displayed lamellipodial extensions and amoeboid morphology. These changes were more subtle with the THP-1 cells stimulated with LPS.

Thus, in order to assess whether the induction of *ADAMDEC1* in THP-1 cells was associated with their differentiation to a macrophage phenotype, the expression of two known THP-1 derived macrophage markers, *CD14* and *CD80*, were measured by qPCR. This showed that *CD14* and *CD80* were induced in the cells incubated with the stimuli that induced *ADAMDEC1* expression (Figure 3.7). Furthermore, the

degree of *CD14* and *CD80* expression levels correlated significantly with that of the *ADAMDEC1* expression. (Figure 3.8)

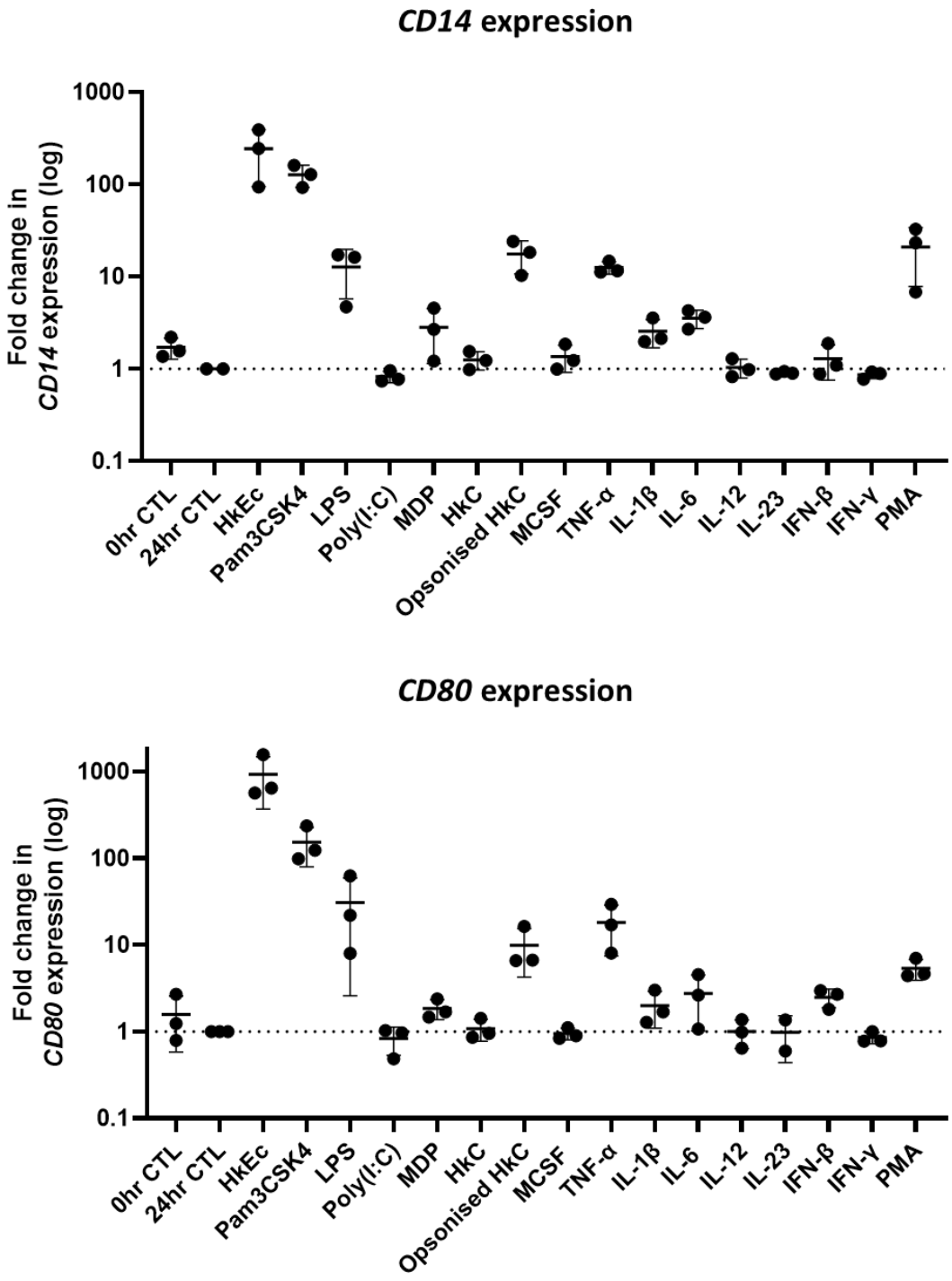

Figure 3.7 Expression of *CD14* and *CD80* in THP-1 cells after incubation with various stimuli for 24 hours (normalised to THP-1 cells incubated without any stimuli for 24 hours). Induction of *CD14* and *CD80* expressions were observed in the THP-1 cells incubated with stimuli that induced *ADAMDEC1* induction. Results are expressed as the mean with SD.
CTL: Control

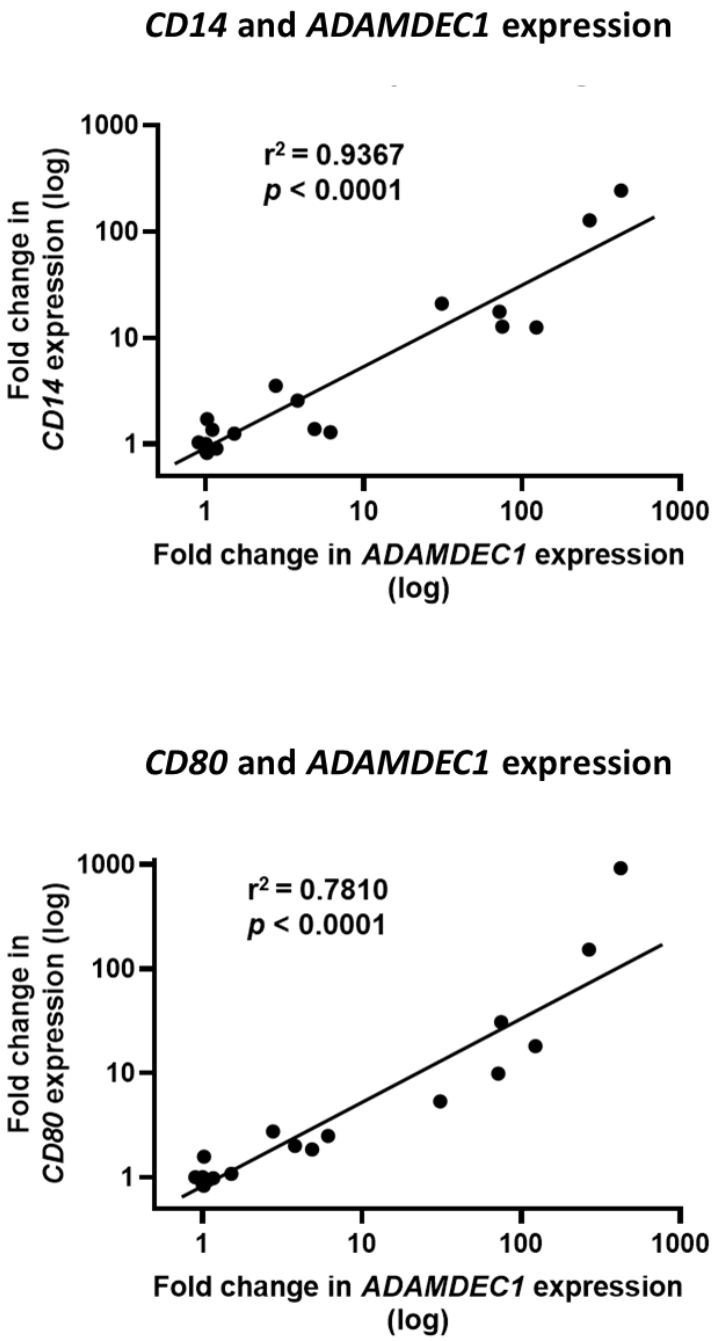

Figure 3.8 The correlation between the expression of *CD14* and ADAMDEC1, and *CD80* and *ADAMDEC1* in the THP-1 cells after incubation with various stimuli for 24 hours. The expression of *CD14* and *CD80* correlated significantly with the expression of *ADAMDEC1* in the stimulated THP-1cells. Results is presented using mean expression of *CD14*, *CD80* and *ADAMDEC1* per stimulus (n=3 per stimulus). Pearson's correlation coefficient was used to determine the linear correlation between expression of *CD14* and *ADAMDEC1*, and expression of *CD80* and *ADAMDEC1*.
r^2: Coefficient determination

3.3.5 TLR2/4-induced *ADAMDEC1* is mediated partially by activation of TNF receptor

Activation of TLR2 and TLR4 in THP-1 cells results in the secretion of multiple pro-inflammatory cytokines including TNF-α. To evaluate whether the *ADAMDEC1* induction by the bacterial ligands was mediated by a direct downstream signalling cascade of TLR2 and TLR4 or indirectly via the secreted TNF-α, THP-1 cells were incubated with the bacterial ligands with or without Adalimumab, a TNF-α neutralising antibody.

The inductions of *ADAMDEC1* by HkEc, Pam3CSK4 and LPS were suppressed, approximately by 50-60%, by the addition of Adalimumab (Figure 3.9). In contrast, the TNF-α-induced *ADAMDEC1* expression was completely abolished by Adalimumab. This indicated that a proportion of *ADAMDEC1* induction by TLR2 and TLR4 was mediated indirectly by TNF-α, secreted in response to TLR activation, and TNF receptor engagement (Figure 3.10).

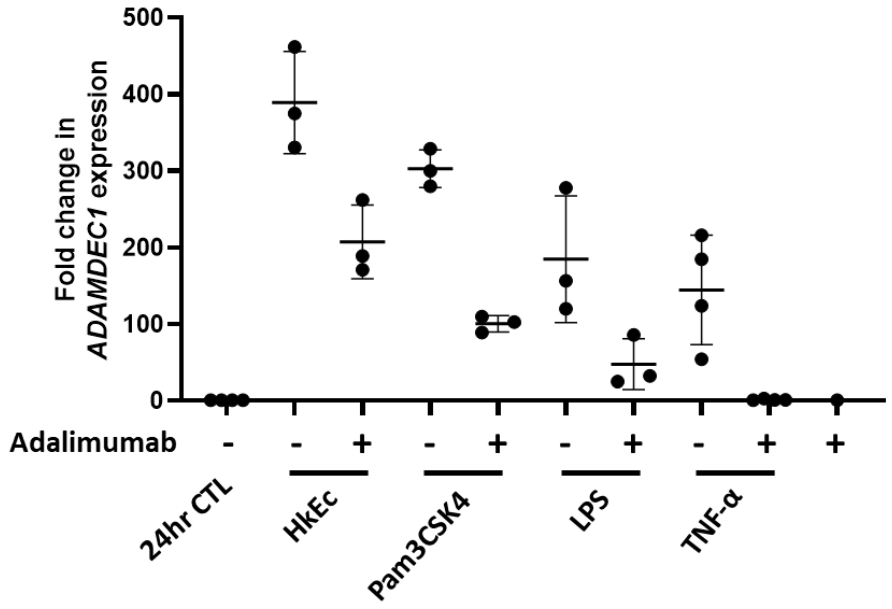

Figure 3.9 Expression of *ADAMDEC1* in THP-1 cells after incubation with HkEc, Pam3CSK4, LPS or TNF-α with or without Adalimumab for 24 hours (normalised to THP-1 cells incubated without any stimuli or Adalimumab for 24 hours). The induction of *ADAMDEC1* by stimulation with HkEc, Pam3CSK4 and LPS were partially suppressed by Adalimumab. The induction of *ADAMDEC1* by TNF-α was completely obliterated by Adalimumab. The graph shows mean with SD.
CTL: Control

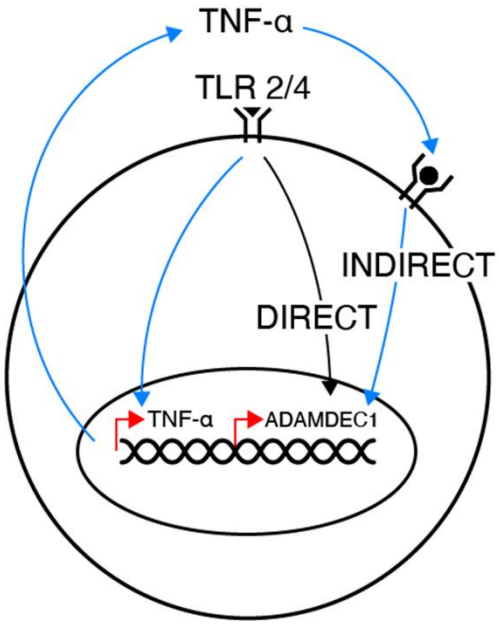

Figure 3.10 Simplified schematic diagram showing the direct and indirect mechanism of *ADAMDEC1* induction by activation of TLR2 and TLR4. A proportion of *ADAMDEC1* induction by TLR2 and TLR4 were mediated directly by the downstream signalling of these receptor independently, indicated by black arrow, and also indirectly by TNF-α, indicated by blue arrows, secreted in response to TLR activation.

3.3.6 *ADAMDEC1* induction is mediated by MAPK signalling pathway via phosphorylation of p38 and JNK

The stimuli that were used in this part of the project, their receptors or target molecules and their main downstream signalling pathways were reviewed (Table 3.4). The common downstream signalling pathways that were shared by the stimuli which induced *ADAMDEC1* were NF-κB and MAPK.

Stimulus	Receptor/Target	Downstream signalling pathway
HkEc	TLR2 & TLR4	NF-κB, MAPK, TBK1[117]
Pam3CSK4	TLR2	NF-κB, MAPK[117]
LPS	TLR4	NF-κB, MAPK, TBK1[117]
MDP	NOD2	NF-κB, MAPK, TBK1[118,119]
Opsonised HkC	FcγR	NF-κB, MAPK[120]
TNF-α	TNFR1 & TNFR2	NF-κB, MAPK, TBK1[121]
MCSF	CSF1R	PI3K/Akt, MAPK[122]
IL-1β	IL-1R1	NF-κB, MAPK[123]
IL-6	IL-6R	Jak/STAT, NF-κB[124]
IL-12	IL-12R	Jak/STAT[125]
IL-23	IL-23R	Jak/STAT[126]
IFN-β	IFNAR	Jak/STAT, MAPK[127]
IFN-γ	IFNGR	Jak/STAT[127]
PMA	PKC	MAPK, NF-κB,[128]

Table 3.4 List of stimuli used to incubate THP-1 and their receptors, or target molecules, and downstream signalling pathways. The common signalling pathways shared by the stimuli that induced *ADAMDEC1* in THP-1 cells were NF-κB and MAPK.

In order to evaluate which of these signalling pathways were responsible for the induction of *ADAMDEC1*, THP-1 cells were stimulated with HkEc and inhibitor of NF-κB (JSH-23) and selective inhibitors for the individual components of MAPK cascade, MEK1/MEK2 (PD98059), p38 (SB203580) and JNK (SP600125). The strongest inhibition of the HkEc-induced *ADAMDEC1* expression was seen with SB203580, p38 inhibitor, followed by SP600125, JNK inhibitor. In contrast, a MEK1/MEK2 inhibitor, PD98059, and an NF-κB inhibitor, JSH-23, had minimal inhibitory effects on the induction of *ADAMDEC1* (Figure 3.11). The HkEc-mediated *ADAMDEC1* induction was almost completely blocked by combining all of the individual MAPK inhibitors. The inhibitory effect of the combined MAPK inhibitors was not augmented by the addition of JSH-23, confirming that NF-κB was unlikely to be responsible for the induction of *ADAMDEC1*. These findings indicated that the dominant signalling pathway responsible for the induction of *ADAMDEC1* in THP-1 cells was the MAPK pathway, and importantly specifically via p38 and JNK components of the MAPK pathway. These findings for THP-1 cells were consistent with a previous study which demonstrated that the LPS-mediated *ADAMDEC1* induction in circulating blood monocytes was inhibited most effectively by SB203580, followed by SP600125.[34]

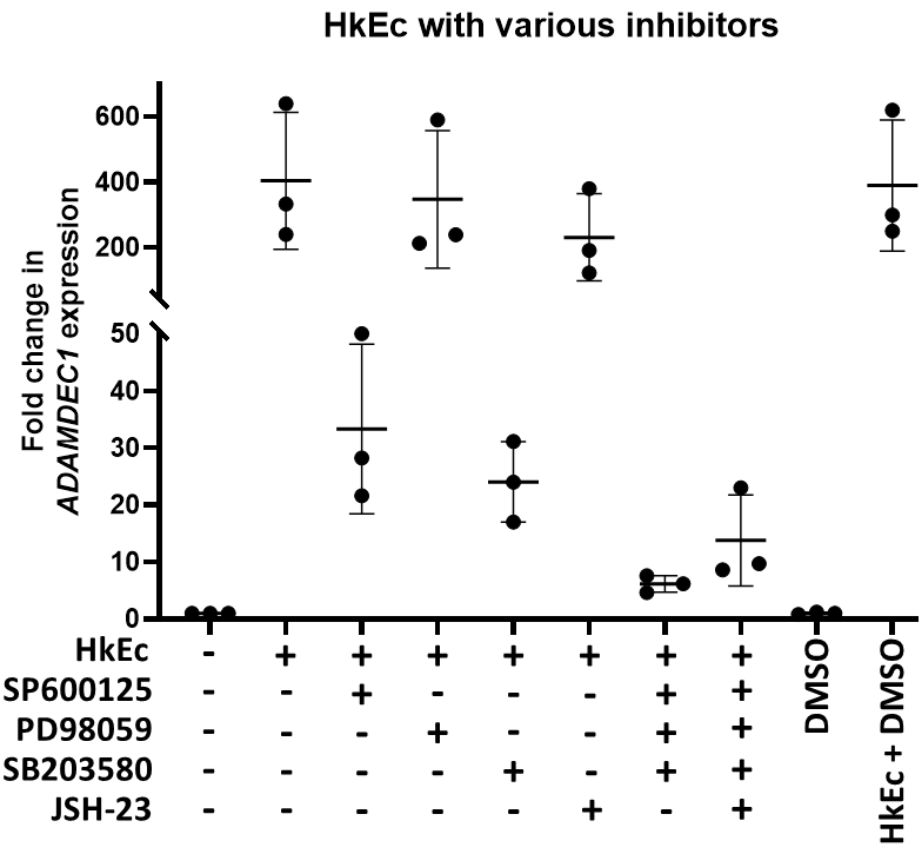

Figure 3.11 Effect of inhibition of NF-κB and MAPK cascades on the HkEc-mediated induction of *ADAMDEC1* in THP-1 cells. Inhibition of p38, by SB203580, and JNK by, SP600125, individually resulted in marked reduction in the HkEc-mediated *ADAMDEC1* induction. The HkEc-mediated induction of *ADAMDEC1* was almost completely abolished by addition of all of the individual MAPK inhibitors (SP600125, PD98059 and SB203580). The inhibitors were dissolved in DMSO which did not induce or inhibit expression of ADAMDEC1. The graph shows mean with SD.

3.3.7 ADAMDEC1 is detected at protein level and the mature ADAMDEC1 is secreted from the THP-1 cells stimulated with HkEc

In order to establish the induction of ADAMDEC1 at the protein level in THP-1 cells, Western blot was performed using the cell lysates and supernatants from the THP-1 cells stimulated with HkEc. HkEc was selected as a stimulator since it induced the strongest *ADAMDEC1* expression in THP-1 cells at the RNA messenger level detected by qPCR.

The Western blot of lysates from THP-1 cell stimulated with HkEc showed

expression of immature ADAMDEC1, at 52 kDa (Figure 3.12 Arrow A), from 24 hours after the stimulation and onwards. The immature ADAMDEC1 was not detected in the lysates of unstimulated cells. With regards to the cell lysate, non-specific bands were visible at around 35 kDa in all the samples, including the unstimulated cell lysates (Figure 3.12 Arrow B). These bands appeared just above where the band corresponding to the mature active ADAMDEC1 was expected at around 32 kDa (Figure 3.12 Arrow C1). The lack of any messenger RNA for *ADAMDEC1* in unstimulated THP1 cells (Figure 3.1) indicated that the upper bands (Figure 3.12 Arrow B) corresponded to a non-specific protein recognised by the anti-ADAMDEC1 antibody. Thus the lower bands at ~32 kDa (Figure 3.12 Arrow C1) were believed to correspond to the mature active ADAMDEC1, which were only detected in the cell lysates of HkEc stimulated cells in association with the presence of the immature ADAMDEC1.

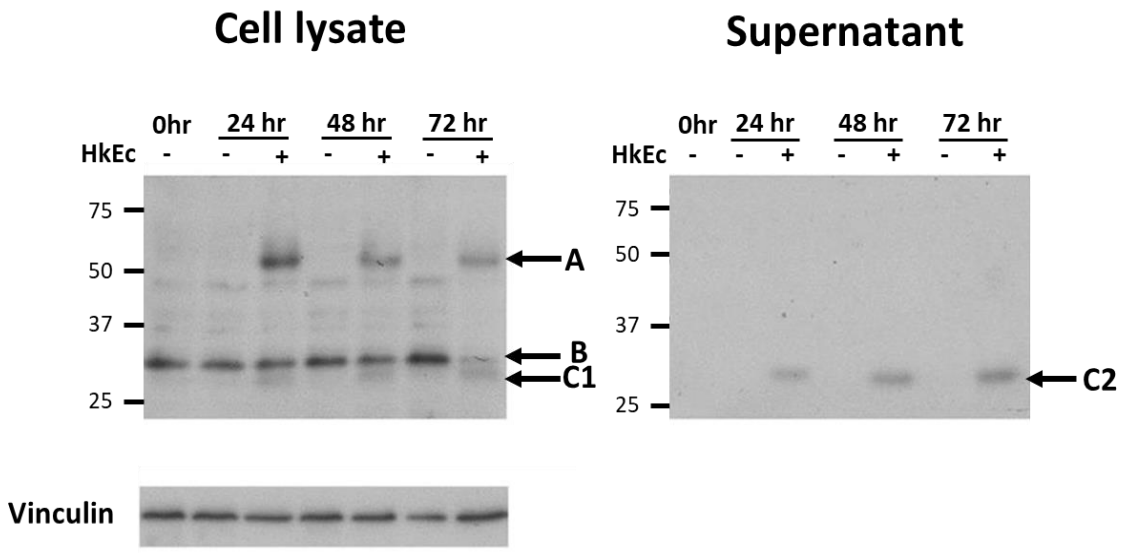

Figure 3.12 Western blot of THP-1 cell lysates and supernatants collected after THP-1 cells were incubated with HkEc for 24, 48 and 72 hours. **A**: Immature ADAMDEC1 at ~ 52kDa **B**: Non-specific binding bands at ~35kDa **C1 and C2**: Mature ADAMDEC1 at ~ 32kDa. Immature and mature ADAMDEC1 were detected in THP1 cell lysates stimulated with HkEc for 24, 48 and 72 hours but neither of them were present in the unstimulated cell lysates. Mature ADAMDEC1 were detected in the supernatants of THP-1 cells stimulated with HkEc but not in the supernatants collected from the unstimulated cells. The blot is representative of n=4.

In order to confirm that the mature ADAMDEC1 is secreted out of the cell, Western blots were performed using the supernatants collected from the THP-1 cells stimulated with HkEc. Only the mature ADAMDEC1 was detected, at ~32 kDa (Figure 3.12 Arrow C2), in the supernatants from the THP-1 cells stimulated with HkEc, at all the time points tested, but not in the supernatants from the unstimulated THP1 cells. Only the mature ADAMDEC1 was detected in the supernatants of the HkEc-stimulated THP-1 cells suggesting that the cleavage of the immature ADAMDEC1 occurred intracellularly during the secretion process and that the secretion of the mature ADAMDEC1 occurred constitutively once the immature ADAMDEC1 was synthesised without requiring any further stimuli.

3.3.8 ADAMDEC1 is induced during the differentiation of blood peripheral monocyte into macrophages

To validate the findings of the qPCR and Western blot results using THP-1 cells, which suggested that the induction of ADAMDEC1 occurred during monocyte to macrophage differentiation, the experiment was repeated using peripheral blood monocytes. Peripheral blood monocytes were collected from healthy volunteers and differentiated into macrophages using the serum starvation method. The serum starvation method is an inexpensive and effective method to differentiate monocyte to macrophages, by induction of autophagy, in vitro maximising the macrophage yield without additional cytokines such as MCSF or GMCSF.[129] Serum starvation has been reported to activate p38 and JNK, which in turn can contribute to the induction of autophagy.[130–133] Additionally, in order to determine whether the expression of ADAMDEC1 was affected by the further activation of MDMs by pro-inflammatory stimuli, as previously reported in some studies, the MDMs were cultured for further 2 days with or without bacterial ligands, either HkEc or LPS.[42] Western blot was performed to detect expression of ADAMDEC1 at the protein level in the cell lysate and supernatant collected on day 8 and day 10.

In cell lysate, the immature ADAMDEC1 was detected but the mature ADAMDEC1 was not detected in the MDMs on day 8 (Figure 3.13 Arrow A). On day 10, both the immature and mature ADAMDEC1 were detected in all the MDMs irrespective of whether they were stimulated with the bacterial ligands (Figure 3.13 Arrow A and B). With regards to the supernatant, neither of the mature or immature ADAMDEC1 was detected in the supernatant collected on day 8. In contrast, only

the mature ADAMDEC1 was detected in all the supernatants collected on day 10, irrespective of whether they were stimulated with the bacterial ligands (Figure 3.13 Arrow B2).

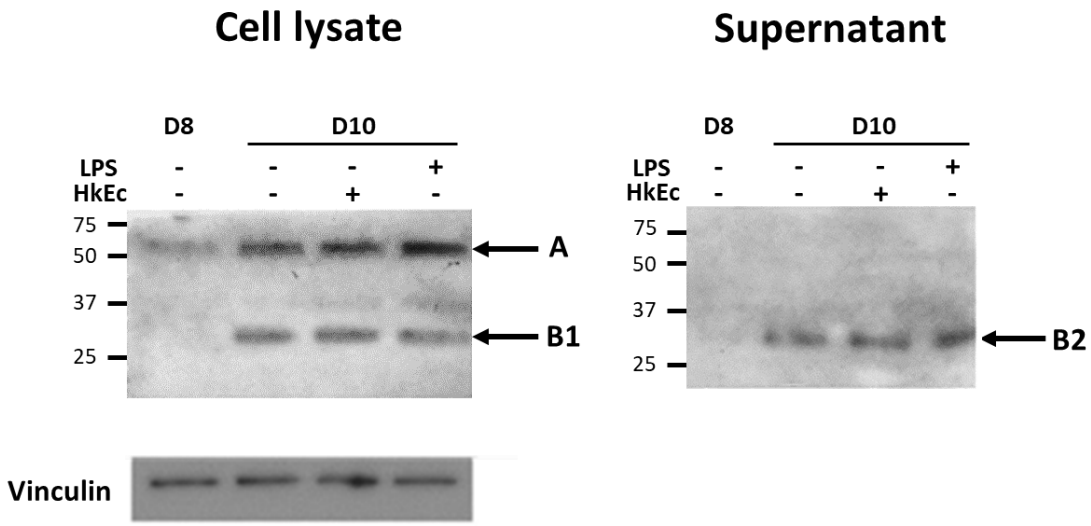

Figure 3.13 Western blot of cell lysates and supernatants collected from MDMs 7 days after the monocytes were isolated from the blood (day 8), and after further 48 hours of incubation with or without stimulation with HkEc or LPS (day 10). **A**: Immature ADAMDEC1 at ~52 kDa **B1 and B2**: Mature ADAMDEC1 at ~32 kDa. Only a weak expression of mature ADAMDEC1 was detected in the cell lysate on day 8. Both immature and mature ADAMDEC1 were detected in the cell lysates on day 10 regardless of whether they were stimulated with the bacterial ligands. Only the mature ADAMDEC1 was detected in all the supernatants on day 10 regardless of whether they were stimulated with the bacterial ligands. The blot is representative of n=4.
D8: Day 8, D10: Day 10

The previous experiment using THP-1 cells in this chapter showed that once immature ADAMDEC1 was synthesised intracellularly, it was cleaved and secreted constitutively (Figure 3.12). This was not observed in the lysate and supernatant from the MDMs collected on day 8. Given that the amount of the immature ADAMDEC1 in the unstimulated MDMs on day 8 appeared to be lower than that of the MDMs on day 10, it is possible that the mature ADAMDEC1 was secreted from the MDMs on day 8 but it was below the concentration detectable by the Western blot. Overall, these findings confirmed that ADAMDEC1 was induced during the monocyte to macrophage differentiation and an additional pro-inflammatory stimulation did not seem to increase, nor was required for the induction of ADAMDEC1 once the monocytes have differentiated into macrophages.

3.4 Discussion

In naïve THP-1 cells, *ADAMDEC1* was induced by bacterial ligands via TLR2, TLR4, HkEc, NOD2, and by opsonised HkC via FcγR. Pro-inflammatory cytokines TNF-α, IL-1β, IL-6 and IFN-β also induced *ADAMDEC1*. Furthermore, PMA, a widely used reagent to differentiate THP-1 cells to macrophages, induced *ADAMDEC1* over 24 hours, whereas MCSF induced *ADAMDEC1* over 72 hours corresponding to the time generally required by each reagent to render the differentiation. The increase in the expression of *ADAMDEC1* induced by these stimuli mirrored the increase in expression of *CD14* and *CD80*, widely used markers for THP-1-derived macrophages. Through antigen sampling by the intestinal epithelial cells, microbial ligands are present under normal circumstances within the lamina propria, and these ADAMDEC1-inducing cytokines are also secreted constitutively within the lamina propria.[134–136] The findings from this chapter, therefore, suggested that *ADAMDEC1* is induced in monocytes upon their migration into the lamina propria and exposure to the gut environment, which promotes their differentiation into macrophages giving rise to the exclusively high expression of ADAMDEC1 in the intestine.

By reviewing the stimuli that induced *ADAMDEC1* in THP-1 cells, NF-κB and MAPK were identified to be the candidate signalling pathways responsible for the induction of *ADAMDEC1* in THP-1 cells. By using the NF-κB inhibitor and selective inhibitors for the individual component of the MAPK cascade, the MAPK signalling pathway, specifically via p38 and JNK was revealed to be responsible for the induction of *ADAMDEC1* (Figure 3.14). This was consistent with a previous study demonstrating the attenuation of LPS-induced ADAMDEC1 expression by selective p38 and JNK inhibitors individually but not by a selective MEK1/MEK2 inhibitor in human peripheral blood monocytes.[34] However, another study reported ERK signalling to be specifically responsible for the FGF2-mediated induction of ADAMDEC1 using a different selective MEK1/MEK2 inhibitor in GBM stem cells.[29] The discrepancy might be secondary to the difference in the type of cells used in the studies.

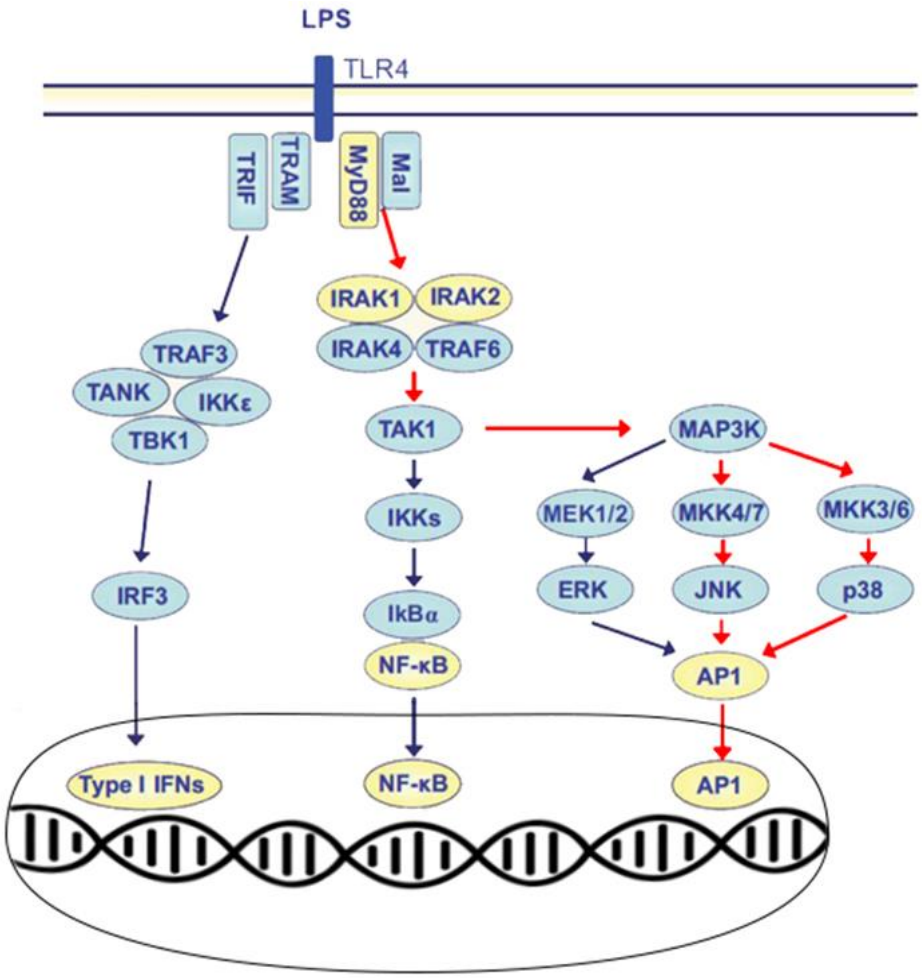

Figure 3.14 The signalling pathways responsible for the induction of *ADAMDEC1* in THP-1 cell is MAPK signalling pathway specifically via p38 and JNK. The candidate signalling pathways for the induction of *ADAMDEC1* in THP-1 cells are demonstrated using downstream signalling pathways of TLR4 as an example. The arrows in red are the pathways responsible, MAPK signalling via p38 and JNK, for the induction of ADAMDEC1 in THP-1 cells. The image was adopted from Klavier *et al* and modified.[323]

It is possible that the reduced levels of ADAMDEC1 seen in the tissue of some gastrointestinal diseases, such as IBD and CRC, are mediated through the suppression of p38 and/or JNK components of the MAPK signalling in monocytes by an unknown mechanism. Further studies are needed to elucidate the events resulting in the suppressed levels of ADAMDEC1 in the intestinal tissues affected by these diseases, and to confirm the mechanistic role of ADAMDEC1 in their pathogeneses. However, if the reduced level of ADAMDEC1 is proven to have a mechanistic role in the pathogeneses of these gastrointestinal diseases, the MAPK

signalling via p38 and JNK could potentially serve as therapeutic targets to boost the expression of ADAMDEC1, which may prevent or treat such diseases. Vice versa, selective MAPK inhibitors could potentially be used to suppress the expression of ADAMDEC1 in the extra-intestinal diseases where upregulation of ADAMDEC1 has been identified if its mechanistic role is to be proved. These diseases include non-small cell lung cancer, where upregulation of ADAMADEC1 has been shown to correlate with a poor prognosis, and glioma where knockdown of ADAMDEC1 inhibited the tumour progression in vitro.[87,88]

Finally, the induction of ADAMDEC1 in THP-1 cells determined at the RNA messenger level by qPCR was verified at the protein level by Western blot. The simultaneous presence of the immature ADAMDEC1 in the cell lysate and the mature ADAMDEC1 in the supernatant suggested that its cleavage and secretion occurred constitutively. Furthermore, the induction of ADAMDEC1 during monocyte to macrophage differentiation at the protein level was verified by using peripheral blood monocytes and serum-starvation as the differentiation stimulus, which involves activation of p38 and JNK.[130–133] The mature ADAMDEC1 was once again detected in the supernatant, confirming that ADAMDEC1 is induced upon monocyte to macrophage differentiation, and is secreted after cleavage intracellularly.

Chapter 4

Generation and characterisation of the Hoxb8 immortalised myeloid cell line

4.1 Background and aims

Currently available evidence suggests ADAMDEC1 is likely to play a role in the immune response during mucosal inflammation. Additionally, the findings from the previous chapter, as well as previous studies, indicate that ADAMDEC1 is induced and secreted during monocyte to macrophage differentiation. This was shown by using both THP-1 and human peripheral blood monocytes. It was, therefore, deemed necessary to examine the effect of ADAMDEC1 on the functions of macrophages and how this might affect immune response within the intestine. Conducting experiments for this purpose can be delivered by knockout or silencing of *ADAMDEC1* in macrophages derived from human peripheral blood monocytes by CRISPR/cas9 system or siRNA respectively.[137,138] However, these methodologies are known to cause off-target effects that could have an impact on the phenotype of cells.[139,140] Moreover, since macrophages are terminally differentiated cells, they have relatively a short life in vitro which makes the application of genetic modification in them difficult. Furthermore, isolation of monocytes from volunteers would be required for each experiment hindering conducting experiments on a large scale in a time-efficient manner. An alternative is to generate *ADAMDEC1*-knockout or silenced stable THP-1 cell lines, which can be expanded indefinitely in culture and differentiated into macrophages that are deficient in ADAMDEC1. However, THP-1 cells are a cancer cell line, having been isolated from a patient with acute monocytic leukaemia originally, and although they provide a useful simplified model to study certain aspects of biological processes of monocytes and macrophages, their behaviours in response to stimuli, such as LPS, do not entirely reproduce those of MDMs.[102,141] Thus use of macrophages generated from WT and *Adamdec1*$^{-/-}$ mice were considered and deemed suitable to overcome these obstacles. The expression pattern of ADAMDEC1 in mice is believed to be comparable to that in humans, and murine intestinal macrophages were shown to express ADAMDEC1 previously.[26] However, isolation of large numbers of murine intestinal macrophages, or peripheral blood monocytes or bone marrow progenitor cells which can be differentiated into

macrophages in vitro, is either difficult or time-consuming. Several mice would need to be sacrificed for each experiment, which would then need to be repeated multiple times, making this methodology ethically unfavourable and costly. Thus the generation of Homeobox protein Hox-B (Hoxb8) immortalised myeloid cell line from WT and *Adamdec1*$^{-/-}$ mice followed by differentiation of these cells into macrophages was, therefore, considered and deemed as an appropriate model to examine the phenotype of macrophages in the absence and presence of ADAMDEC1.

Hoxb8 is a transcription factor specific to myeloid progenitor cells. Its activation is known to promote self-renewal proliferation while inhibiting the differentiation of myeloid progenitor cells.[142] A conditionally immortalised myeloid progenitor cell line can be generated by retrovirus transduction of murine stem cell provirus (MSCV) containing *Hoxb8* fused to the C-terminus of the oestrogen-binding domain of oestrogen receptor (ER) in mouse bone marrow cells.[143] Upon successful transduction, this allows a continuous activation of Hoxb8 within the myeloid progenitor cells in the presence of oestrogen, which is added to the culture medium. The immortalised progenitor cells are expanded and maintained in the oestrogen containing medium supplemented with either GMSCF or stem cell factor (SCF), which pre-condition the progenitor cells towards terminal differentiation into macrophages or neutrophils respectively. The resulting cell populations are referred to as GMCSF ER-Hoxb8 and SCF ER-Hoxb8 progenitors, respectively.[143] Here, they will be referred to as GMCSF Hoxb8 and SCF Hoxb8 cells. These cells are maintained and serve as indefinitely expanding pools of myeloid progenitor cells that can be differentiated either into neutrophils or macrophages. The SCF Hoxb8 cells are positioned at an earlier stage of the myeloid differentiation pathway and express genes resembling granulocyte-macrophage progenitors.[143] Whereas GMCSF Hoxb8 cells are placed at a later stage of the differentiation pathway and express monocytic lineage gene profile.[143] An inactivation of Hoxb8 and thereby differentiation of GMCSF Hoxb8 cells into macrophages occur upon withdrawal of oestrogen and GMCSF followed by culturing the progenitor cells in the differentiation medium containing MCSF over 5-7 days. Whereas the removal of oestrogen and SCF in the medium followed by culturing the SCF Hoxb8 cells in differentiation media supplemented with GCSF generates neutrophils (Figure 4.1).

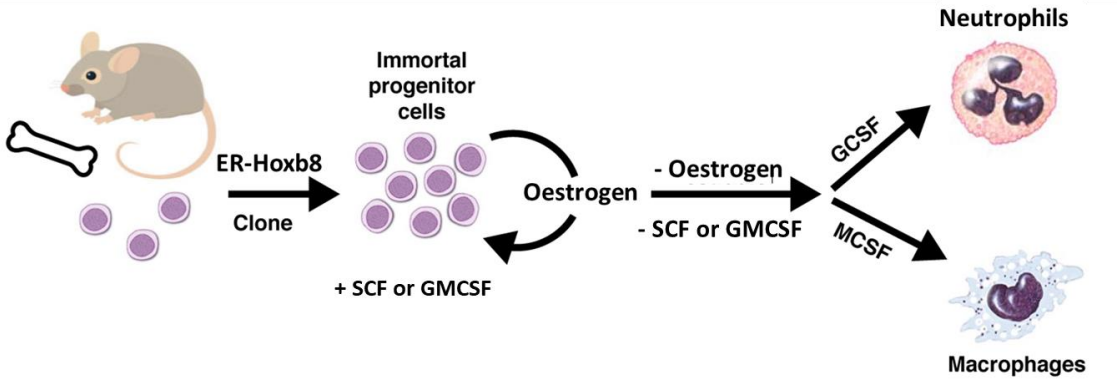

Figure 4.1 Schematic overview of generation, maintenance, and differentiation of Hoxb8 immortalised progenitor cells.

The phenotype of Hoxb8-derived macrophages and BMDM have previously been shown to be similar regarding cell surface markers and functions including cell adhesion, phagocytosis and generation of reactive oxygen species.[144] The Hoxb8-derived macrophages also demonstrated an ability to elicit a robust inflammatory response upon TLR2 and TLR4 stimulation.[143] Thus, the generation of WT and *Adamdec1*$^{-/-}$ Hoxb8 myeloid progenitor cells from bone marrow isolated from the WT and *Adamdec1*$^{-/-}$ mice and subsequent differentiation of these cells into macrophages were deemed as a suitable model to conduct experiments to interrogate the functional difference in the WT and *Adamdec1*$^{-/-}$ macrophages.

The main aims for Chapter 4 were:

- To differentiate WT GMCSF Hoxb8 progenitor cells gifted by Dr Annette Zehrer and confirm the expression of ADAMDEC1 in the WT Hoxb8-derived macrophages as a proof of concept
- To generate WT and *Adamdec1*$^{-/-}$ GMCSF Hoxb8 progenitor cells from bone marrow isolated from the WT and *Adamdec1*$^{-/-}$ mice
- To characterise the WT and *Adamdec1*$^{-/-}$ GMCSF Hoxb8 progenitor cells and their terminally differentiated macrophages
- To verify the expression and knockout of ADAMDEC1 in the WT and *Adamdec1*$^{-/-}$ Hoxb8-derived macrophages respectively

4.2 Materials and method

4.2.1 Cells and cell culture media

GP2-293 Packaging Cell Line

GP2-293 Packaging Cell Line (Takara Bio) were cultured and maintained in GP2-293 complete medium at 37 °C and 5% CO_2 and passaged every 2 – 3 days.

Gifted WT Hoxb8 progenitor cells

Previously, our lab had been gifted WT Hoxb8 progenitor cells by Dr Annette Zehrer, Ludwig-Maximillians-University, Munich, Germany. These Hoxb8 progenitor cells from WT C57BL/6 mice (WT Hoxb8) were generated by Dr Zehrer following the original immortalisation protocol.[143] These cells were cultured and maintained at 37 °C and 5% CO_2 in GMCSF myeloid medium and passaged every 2-3 days. The cell density was maintained between 0.3 – 2 x 10^6 /ml.

GP2-293 Complete medium

DMEM (Gibco)
10% FBS (Sigma)
Penicillin/Streptomycin (50 U/ml and 50 µg/ml) (Gibco)
1 mM sodium pyruvate (Thermo Fisher)

Stem cell medium

RPMI Glutamax (Gibco)
15% FBS (Sigma)
Penicillin/Streptomycin (50 U/ml and 50 µg/ml) (Gibco)
10 ng/ml Murine IL-3 (Peprotech)
20 ng/ml Murine IL-6 (Peprotech)
25 ng/ml Murine SCF (Peprotech)
30 µM 2-mercaptoethanol (Sigma)

Progenitor outgrowth media

OptiMEM Glutamax (Gibco)

10% FBS (Sigma)

Penicillin/Streptomycin (50 U/ml and 50 µg/ml) (Gibco)

10 ng/ml Murine SCF (Peprotech)

30 µM 2-mercaptoethanol (Sigma)

10 µM Oestradiol (Sigma)

GMCSF Myeloid medium

RPMI Glutamax (Gibco)

10% FBS (Sigma)

Penicillin/Streptomycin (50 U/ml and 50 µg/ml) (Gibco)

20 ng/ml Murine GMCSF (Peprotech)

30 µM 2-mercaptoethanol (Sigma)

10 µM Oestradiol (Sigma)

SCF Myeloid medium

RPMI Glutamax (Gibco)

10% FBS (Sigma)

Penicillin/Streptomycin (50 U/ml and 50 µg/ml) (Gibco)

20ng/ml Murine SCF (Peprotech)

30 µM 2-mercaptoethanol (Sigma)

10uM Oestradiol (Sigma)

Macrophage differentiation medium

RPMI Glutamax (Gibco)

10% FBS (Sigma)

Penicillin/Streptomycin (50 U/ml and 50 µg/ml) (Gibco)

20 ng/ml Murine MCSF (Peprotech)

30 µM 2-mercaptoethanol (Sigma)

BMDM medium

DMEM (Low glucose) (Gibco)

10% FBS (Sigma)

Penicillin/Streptomycin (50 U/ml and 50 µg/ml) (Gibco)

20 mM HEPES solution (Sigma)

20 ng/ml Murine MCSF (Peprotech)

4.2.2 Macrophage differentiation protocol for the gifted WT Hoxb8 progenitor cells

The gifted WT Hoxb8 progenitor cells were washed twice with PBS in a 50 ml Falcon tube to remove oestradiol and GMCSF by centrifugation at 500 g for 5 minutes. The cells were then resuspended in the macrophage differentiation medium at a cell density of 5 x 10^5 /ml, and 10 ml of this culture was added into four 92 mm Nunc^{TM} Delta surface coated culture dishes (Thermo Fisher Scientific). The cells were incubated at 37°C and 5% CO_2. On day 4 of the differentiation protocol, the cells were fed with a further 10 ml of the macrophage differentiation medium. On day 6 of the differentiation protocol, the supernatant was removed from one culture dish, and the adherent macrophages were scraped. The cells in this culture dish were processed for Western blot (Chapter 2.8). Either HkEc (5 x 10^6 / ml) or LPS (200 ng/ml) was added to two of the remaining three culture dishes and incubated for further 2 days. The cells in the third dish were incubated for 2 days without any stimuli. On day 8 of the differentiation protocol, supernatants were removed from all three culture dishes, and adherent cells were scraped. The cells were processed for Western blot (Chapter 2.8).

4.2.3 Generation of WT and *Adamdec1*$^{-/-}$ Hoxb8 progenitor cells

4.2.3.1 Transformation of competent *E. coli* to amplify MSCV ER-Hoxb8 plasmid DNA

MSCV plasmid containing ER-Hoxb8 construct was produced and generously gifted by Dr Hans Haecker, at St. Jude's Hospital, Boston, USA. The plasmid was the same as the original plasmid used to generate the incipient Hoxb8 progenitor cells as well as the plasmid used by Dr Zehrer.[143]

The Hoxb8 plasmid was delivered infused on a blotting paper. This was resuspended in 50 µl sterile nuclease-free water for 1 hour under a laminar flow tissue culture hood. The DNA concentration of the suspension was measured by NanoDrop, which was 6.9 ng/µl. Stellar competent *E. coli* cells (1 x 10^9 /ml) (CloneTech) were thawed on ice and 50 µl of it was gently transferred into a 1.5 ml Eppendorf tube. Approximately 70 ng of the plasmid DNA was mixed with the competent *E. coli* cells, and the bottom of the tube was gently tapped few times. The mixture was incubated on ice for 20 minutes, then heat shocked in a water bath set to 42°C for exactly 45 seconds. The tube was then placed immediately on ice and incubated for 2 minutes before 250 µl of pre-heated S.O.C medium (Sigma) was added. The tube was incubated once again at 37°C for 1 hour with constant agitation at 250 rpm in ThermoMixer® Comfort (Eppendorf). After 1 hour, 50 µl of the cell suspension was plated onto one agar plate of LB augmented with ampicillin (LB-Amp), while the remaining suspension was plated onto a separate agar plate. The plates were incubated overnight at 37°C. After overnight incubation, a single colony was picked using a sterile inoculating loop (VWR) and dropped in 10 ml of LB-Amp broth. The bacterial culture was incubated at 37°C for 6 hours at constant agitation at 250 rpm. This culture was then added to 300 ml of fresh LB-Amp broth, and incubated overnight. The next day, 10 ml of the growth suspension was used to create a glycerol stock of transformed bacteria (Chapter 2.6.2). The rest of the bacterial culture was used to extract and purify MSCV ER-Hoxb8 plasmid by Maxiprep (Chapter 2.6.3.2)

4.2.3.2 Generation of ER-Hoxb8 retrovirus by GP2-293 cells

4.2.3.2.1 Preparation of GP2-293 cells

GP2-293 cells were cultured in tissue culture-treated T175 flasks (Corning) in GP2-293 complete media (Chapter 4.2.1). The cells were grown to ~ 80% confluency, and then detached from the surface of the culture dish with 25 ml of trypsin/EDTA solution (Sigma). The cells were transferred to a 50 ml Falcon tube and centrifuged at 500 g for 5 minutes, then resuspended at a density of approximately 4 x 10^5 /ml in GP2-293 complete medium. 10 ml of the cell suspension was added to 92mm Nunc™ surface coated tissue culture plate (Thermo Fisher Scientific). The cells were incubated to adhere overnight at 37°C and 5% CO_2.

4.2.3.2.2 Transfection of GP2-293 cells with MSCV ER-Hoxb8 plasmid

Transfection of GP2-293 cells was conducted using Xfect Transfection Reagent (Takara Bio). 15 µg of the ER-Hoxb8 plasmid DNA and 15 µg of envelope plasmid, pEco vector (Takara Bio), were added to 600 µ of Xfect reaction buffer. For the negative control, 15 µg of the envelope plasmid was added to the Xfect reaction buffer without the ER-Hoxb8 plasmid DNA in a separate tube. The tubes were vortexed thoroughly for 5 minutes. Xfect polymer was vortexed thoroughly and 9 µl of it was added to each tube which was then vortexed at high speed for 10 seconds. The tube contents were left to incubate for 10 minutes at room temperature to allow nanoparticle complexes to form. The content of each tube was then added dropwise to a plate of prepared GP2-293 cells. The plates were rocked gently back and forth, and then incubated overnight at 37°C and 5% CO_2. The next day, the transfection medium was replaced with 10 ml of fresh complete GP2-293 cell medium, then returned to the incubator. 48 hours later, the supernatant containing the retrovirus was harvested and filtered through a sterile 0.2 µm PES syringe filter (Appleton Woods). 1 ml aliquots were stored in 1.5 ml Eppendorf tubes at -80°C. At the same time, 10 ml of PBS was added to the culture dish to wash the adherent cells. 6 ml of RLT buffer of RNeasy Mini Kit (Qiagen), containing 1% 2-mercaptoethanol, were added to each culture dish. Cells were scraped for RNA extraction and cDNA synthesis (Chapter 2.7.1 and 2.7.2). PCR and DNA electrophoresis were performed (Chapter 2.6.4) to confirm successful transfection of GP2-293 cells using the primers designed against Hoxb8 (Table 4.1). 1% agarose gel was used, and the gel was run for 25 minutes on a constant 100V. 3 µl of Quick-Load® Purple 100 bp DNA Ladder (NEB) was loaded in the first well of the agarose gel.

Target gene	Forward primer (5'-3')	Reverse primer (5'-3')	T_A
Hoxb8	AGCTCTTATTTCGTCAACTCAC	CTTCTTGTCACCCTTCTGCG	58°C

Table 4.1 Primers used to detect presence of *Hoxb8* in the transfected GP2-293 cells.
T_A: Annealing temperature

4.2.3.3 Infection of the WT and *Admadec1*$^{-/-}$ mice bone marrow progenitor cells with ER-Hoxb8 retrovirus

4.2.3.3.1 Harvesting of the mouse bone marrow cells

One 8 week-old female WT mouse and one age-matched *Adamdec1*$^{-/-}$ female mouse were sacrificed. Femurs and tibiae were carefully removed from each mouse so that the bones remained intact to prevent contamination of the bone marrow cells. The bones were submerged in 70% ethanol and taken into a laminar flow cabinet and then submerged in ice cold sterile PBS. The ends of the bones were cut with sterile surgical scissors over a 92 mm petri dish. Bone marrow within the bone marrow cavity was flushed out using a sterile 26G needle, 5 ml syringe and ice-cold sterile PBS. The PBS containing the bone marrow cells from individual mice were then filtered through a 70 µm nylon cell strainer (Thermo Fisher Scientific) into a separate 50 ml Falcon tube and centrifuged at 500 g for 5 minutes at 4°C. The PBS was discarded leaving the bone marrow cell pellets, which were resuspended in 1 ml of Red Blood Cell Lysing Buffer Hybri-Max (Sigma) and incubated at room temperature for 3 minutes. 30 ml of ice-cold sterile PBS were added to each tube and centrifuged at 500 g for 5 minutes at 4°C. The cells were resuspended in 4 ml of PBS.

4.2.3.3.2 Removal of red blood cells and granulocytes

3 ml of room temperature Ficoll-Paque Premium (GE Healthcare) were poured into two 15 ml Falcon tubes. Two lots of 4ml of PBS containing total bone marrow cells from either WT or *Adamdec1*$^{-/-}$ mouse prepared as described above were each gently layered on top of the Ficoll-Paque using a Pasteur pipette. The tubes were centrifuged at 500 g for 30 minutes at room temperature. The cell pellets at the bottom of the tubes contained red blood cells and granulocytes. The interface and all supernatants containing bone marrow stem cells were collected carefully into new 50 ml Falcon tubes without disturbing the pellet. The collected samples were diluted in PBS to make up 50 ml of the total volume and centrifuged at 300 g for 5 minutes at 4°C.

4.2.3.3.3 Culture of the stem cells to stimulate progenitor cell replication

The supernatants were removed leaving the stem cell pellets which were resuspended in 10 ml of the stem cell media (Chapter 4.2.1) and plated on 92mm

Nunc™ surface coated tissue culture plate (Thermo Fisher Scientific). The cells were incubated for 2 days at 37 °C and 5% CO_2.

4.2.3.3.4 Transfection of progenitor cells with Hoxb8

After 2 days, the WT and *Adamdec1*$^{-/-}$ progenitor cells were collected from the culture plates and transferred separately into a 50 ml Falcon tube and centrifuged at 500 g for 5 minutes at 4°C. The supernatants were discarded and the cells were resuspended in the progenitor outgrowth media (Chapter 4.2.1). The cells were centrifuged once again at 300 g for 5 minutes at 4°C and the supernatants were removed. The ER-Hoxb8 retroviral supernatants generated and stored at -80°C (Chapter 4.2.3.2.2) were thawed and 1 ml of it was mixed with 0.8 µl of Polybrene Infection / Transfection Reagent (Millipore). 1ml of this mixture was added to the pellets of the WT and *Adamdec1*$^{-/-}$ progenitor cells. 100 µl of the cells were transferred into each well of a 12-well culture plate and the cells were spin-infected in a centrifuge pre-heated to 30°C for 90 min at 300 g. The cells were collected and pooled per genotype and 3 ml of the progenitor outgrowth media (Chapter 4.2.1) were added to each of the pooled cells. The cells were then transferred into a 6-well plate and incubated for 2 days at 37 °C and 5% CO_2.

4.2.3.3.5 Initiation of pre-conditioning of the progenitor cells and antibiotic selection

After 2 days, cells were collected from the 6-well plates and pooled per genotype and then each divided in half. The cells were centrifuged at 500 g for 5 minutes and supernatants were removed. One-half of the cells per genotype was resuspended in the myeloid medium supplemented with GMSCF (Chapter 4.2.1) containing 1 µg/ml Neomycin (Sigma). The other half was resuspended in the myeloid medium supplemented with SCF (Chapter 4.2.1) containing 1 µl/ml Neomycin (Sigma). The cells were plated in a 12-well plate and cultured at 37°C and 5% CO_2 and passaged every 3 - 4 days to the cell density of 1 x 10^6 /ml in the neomycin supplemented GMCSF or SCF myeloid media accordingly. Over 4 weeks, the cells were expanded and cultured in 6-well plates. After 4 weeks, neomycin was removed from the culture media. The immortalised progenitor cells were cultured for a further week in the GMCSF or SCF myeloid media without neomycin to observe any potential changes in the cell viability and morphology

after the cessation of antibiotic selection. The WT and *Adamdec1*$^{-/-}$ SCF Hoxb8 progenitor cells were frozen down at this point and stored in liquid nitrogen for potential future use. The WT and *Adamdec1*$^{-/-}$ GMCSF Hoxb8 progenitor cells were maintained in the GMCSF myeloid medium hereafter and expanded in T25 followed by T75 surface coated culture flasks (Corning). The cells were passaged every 2-3 days to maintain cell density between 1 – 6 x 10^6/ ml until differentiation of the cells were required.

4.2.4 Macrophage differentiation protocol for the newly generated Hoxb8 cells

The newly generated Hoxb8 progenitor cells (Chapter 4.2.3) were washed twice in PBS to remove oestradiol and GMCSF (or SCF) by centrifugation at 300 g for 5 minutes. The cells were then resuspended in the macrophage differentiation medium (Chapter 4.2.1) at a cell density of 5 x 10^5 /ml and 2 ml, if using 6-well plate, or 10 ml, if using 92 m culture dish, of the cell culture was plated and incubated at 37°C and 5% CO_2. On day 4 of the differentiation protocol, a further 2 ml or 10 ml of the fresh macrophage differentiation medium was added to the cells in 6-well plate or 92 mm culture dish respectively. On day 8, the supernatants were removed and the adherent cells were scraped and processed either for Western blot or qPCR (Chapter 2.7 and 2.8).

4.2.5 Macrophage differentiation of the newly generated Hoxb8 cells with stimuli

The Hoxb8 progenitor cells were washed twice in PBS to remove oestradiol and GMCSF (or SCF) by centrifugation at 300 g for 5 minutes. In an attempt to generate WT Hoxb8-derived macrophages that expressed ADAMDEC1, the cells were then resuspended in the macrophage differentiation medium (Chapter 4.2.1) at a cell density of 5 x 10^5 /ml and 10 ml of the cell culture were plated in 92 mm Nunc^{TM} Delta surface coated culture dish (Thermos Fisher Scientific) with one of the stimuli listed below:

- HkEc (5 x 10^6 /ml)
- HkEc (5 x 10^6 /ml) + WT mouse colonic tissue
- HkEc (5 x 10^6 /ml) + 20% Inactivated mouse serum (R&D System)

- HkEc (5 x 10^6 /ml) + 50 ng/ml Murine C-C Motif Chemokine Ligand type 2 (CCL2) (Peprotech)

To prepare the WT mouse colonic tissue, the colon was harvested from a WT mouse and washed in PBS supplemented with Penicillin/Streptomycin (50 U/ml and 50 µg/ml) (Gibco) and 10% FBS (Sigma) on ice. The colonic tissue was dissected longitudinally with surgical scissors and washed twice in PBS supplemented with Penicillin/Streptomycin (50 U/ml and 50 µg/ml) (Gibco) and 10% FBS (Sigma) to remove intra-luminal faeces. The colonic tissue was cut into approximately 5 mm x 5 mm pieces and placed in the culture dish with Hoxb8 cells suspended in the macrophage differentiation media. On day 4 of the differentiation protocol, the cells in each dish were fed with the fresh macrophage differentiation media containing the same stimuli. The cells were harvested on day 8 and processed for Western blot and qPCR (Chapter 2.7 and 2.8).

4.2.6 Generation of mouse BMDM

The WT and *Adamdec1*$^{-/-}$ mice were sacrificed and bone marrow was harvested as described in Chapter 4.2.3.3. However, after the red blood cell lysis, the cell pellets from each mouse were resuspended in 4 ml of the BMDM medium (Chapter 4.2.1) pre-warmed to 37°C, instead of PBS. 1 ml of the resuspended cells were plated in 92 mm surface coated culture dish and 9 ml of the BMDM medium was added to each plate. The cells were incubated at 37°C and 5% CO_2. After 48 hours,10 ml of fresh BMDM media were added to each plate, and the cells were incubated for a further 5 days prior to being harvested and processed for Western blot, qPCR (Chapter 2.7 and 2.8) or flow cytometry analyses (Chapter 4.2.7).

4.2.7 FACS of Hoxb8 progenitor cells, Hoxb8-derived macrophages and MDMs

The cells harvested were centrifuged at 300 g for 5 minutes and resuspended at a density of roughly 1 x 10^6 /ml in FACS buffer (Chapter 2.2) and 1 µl of Fc block (BioLegend) per 100 µl. Appropriate antibodies (Table 4.2) for each panel were added and the cells were incubated in 96-well non-coated V-shaped bottom plate at 4˚C in the dark for 30 min to 1 hour. Unstained control cells were run for each experiment. Compensation beads (BioSciences) were run for each experiment

after incubation with 1 µl of each antibody. After incubation, the plate was centrifuged at 500 g for 5 minutes at 4˚C, and the supernatants were removed. The cells and beads were washed by resuspension in 100 µl of FACS buffer. This wash step was repeated three times. Each well was then resuspended in 150 µl of 1% paraformaldehyde in PBS, and transferred to FACS tubes with a further 150 µl oof FACS buffer added. Flow cytometry was performed immediately on LSR Fortessa (BD Biosciences) or stored at 4˚C in the dark for no more than 4 hours. Flow cytometry data were analysed using FlowJo software (BD Biosciences).

Target	Fluorescence	Manufacturer	Catalogue
CD117 (2B8)	FITC	BioLegend	105805
CD115 (AFS98)	APC	BioLegend	135509
CD11c (HL3)	BV786	BD Biosciences	563735
CD11b (M1/70)	APC/Cy7	BioLegend	101225
F4/80 (BM8)	PE/CF594	BioLegend	123145
Ly6C (HK1.4)	BV711	BioLegend	128037
Ly6G (1A8)	BV421	BioLegend	127628
CX3CR1 (SA011F11)	PE	BioLegend	149005

Table 4.2 List of antibodies used for flow cytometry analysis of the Hoxb8 cells, Hoxb8-derived macrophages and BMDMs. Clone name of each antibody is specified in brackets.
FITC: Fluorescein isothiocyanate, APC: Allophycocyanin, BV: Brilliant Violet™, Cy7: Cyanine-7, PE: R-phycoerythrin

4.2.8 qPCR

The cells were harvested and total RNA was extracted and converted to cDNA, and qPCR was performed (Chapter 2.7) to determine the expression of *Adamdec1* in the Hoxb8 progenitor cells, Hoxb8-derived macrophages and BMDMs (Table 4.3).

Target gene	Forward primer (5' to 3')	Reverse primer (5' to 3')
Ppia	GGGCCGCGTCTCCTTT	ATCCTTTCTCTCCAGTGCTCAGA
Adamdec1	TTTCACCTAAAGAGAACCAAGCATC	CCTTCATAGTAGCAGGGTTTCACA

Table 4.3 List of primers used to quantify expression of *Adamdec1* in Hoxb8 progenitor cells, Hoxb8-derived macrophages and BMDMs.

4.3 Results

4.3.1 Expression of macrophage surface markers and ADAMDEC1 by the macrophages derived from the gifted WT ER-Hoxb8 progenitor cells

Before committing to generate WT and *Adamdec1*$^{-/-}$ Hoxb8 progenitor cells using bone marrow progenitor cells isolated from WT and *Adamdec1*$^{-/-}$ mice, a proof of concept for this study model was tested using the WT Hoxb8 progenitor cells gifted by Dr Zehrer to ensure that the macrophages derived from WT Hoxb8 cells expressed ADAMDEC1. The gifted WT Hoxb8 cells were thawed and cultured in media containing oestradiol and GMCSF to pre-condition the WT Hoxb8 cells for the subsequent terminal differentiation to macrophages.

Macrophages were derived from the gifted WT Hoxb8 cells by removing oestradiol and GMCSF and culturing them in the differentiation medium containing MCSF. Six days after the initiation of the differentiation protocol, the cells were stimulated for a further 2 days in the absence or presence of bacterial ligand, either HkEc or LPS. The purpose of adding the bacterial ligand was to determine if the resulting activation of the macrophages would augment the ADAMDEC1 expression, as the previously performed experiment to determine the expression of ADAMDEC1 in MDMs described in Chapter 3. The Hoxb8-derived macrophages were harvested on day 6, before the bacterial ligands were added, and on day 8. The cell lysates were made and the expression of ADAMDEC1 was examined in each sample together with a cell lysate made from undifferentiated WT Hoxb8 cells harvested on day 0. Tissue lysate was also made from the small bowel of WT mice which was used as a positive control.

The undifferentiated WT Hoxb8 cells on day 0 and the Hoxb8-derived macrophages harvested on day 6 did not express ADAMDEC1 (Figure 4.2). Strong expression of ADAMDEC1 was, however, detected in all of the WT Hoxb8-derived macrophages harvested on day 8 irrespective of the presence or type of the bacterial ligands added. These findings indicated that ADAMDEC1 was not expressed in the WT Hoxb8 progenitor cells but was expressed in the WT Hoxb8-derived macrophages following the differentiation protocol using MCSF, consistent with the knowledge that the ADAMDEC1 is induced during cell differentiation to macrophages. The addition of bacterial ligands was not required for the induction of ADAMDEC1 in the WT Hoxb8-derived macrophages, and the optimum harvest

timepoint with regards to the expression of ADAMDEC1 appeared to be no earlier than day 8.

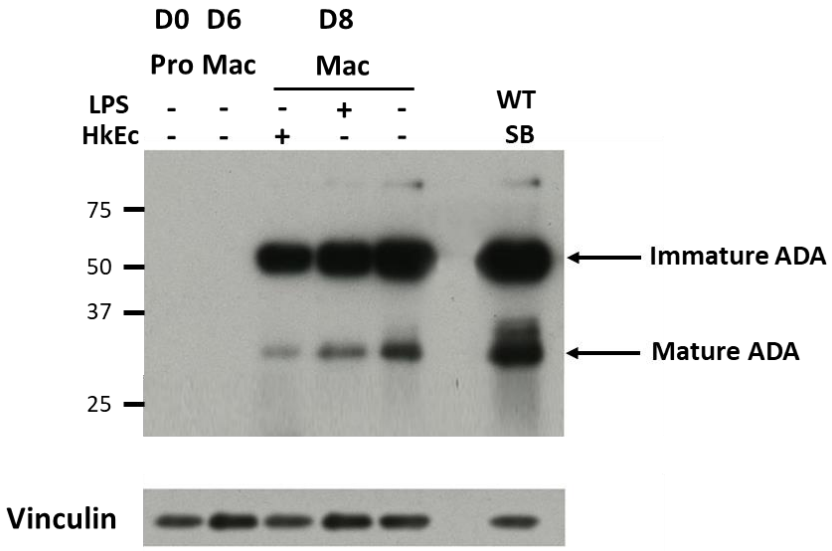

Figure 4.2 Western blot of Hoxb8 progenitor cells and Hoxb8-derived macrophages harvested at different timepoints during the macrophage differentiation protocol. ADAMDEC1 was not detected in undifferentiated Hoxb8 progenitor cells and Hoxb8-derived macrophages harvested on day 6. Both mature and immature ADAMDEC1 were detected in the Hoxb8-derived macrophages harvested on day 8 irrespective of whether they were stimulated with the bacterial ligands. Lysate made from small bowel of WT mouse was used as a positive control. The blot is representative of n=3.
Pro: Hoxb8 progenitor cells, Mac: Hoxb8-derived macrophages, SB: Small bowel, ADA: ADAMDEC1, WT: Wild type, D0: Day 0, D6: Day 6, D8: Day 8

To verify that these cells derived from the gifted WT Hoxb8 progenitor cells were macrophages, the differentiated cells harvested on day 8 without the bacterial ligand stimulation were stained with macrophage marker CD11b and F4/80. The harvested cells were also stained for a dendritic cell marker, CD11c, as the divergence to either macrophage or dendritic cells differentiation is positioned at a late stage of the myeloid cell differentiation pathway and it has been reported that it is possible to generate terminally differentiated cells that resemble phenotypes of dendritic cells from GMCSF Hoxb8 cells.[145] Additionally, macrophages were freshly derived from bone marrow progenitor cells isolated from WT mice and these WT BMDM were used as positive controls for the expression of these surface markers.

A slightly lower expression of F4/80 was observed in the gifted WT Hoxb8-derived macrophages in comparison to the BMDM (Figure 4.3). However, overall, the gifted WT Hoxb8-derived macrophages were positive for F4/80 and CD11b, and negative for CD11c, mirroring the surface expression of these markers in the WT BMDM. The absence of CD11c suggested that both BMDM and the WT Hoxb8-derived cells were terminally differentiated macrophages rather than dendritic cells. These findings indicated that by following the differentiation protocol using MCSF, the gifted WT GMCSF Hoxb8 progenitor cells differentiated into macrophages and expressed ADAMDEC1 upon terminal differentiation to macrophages.

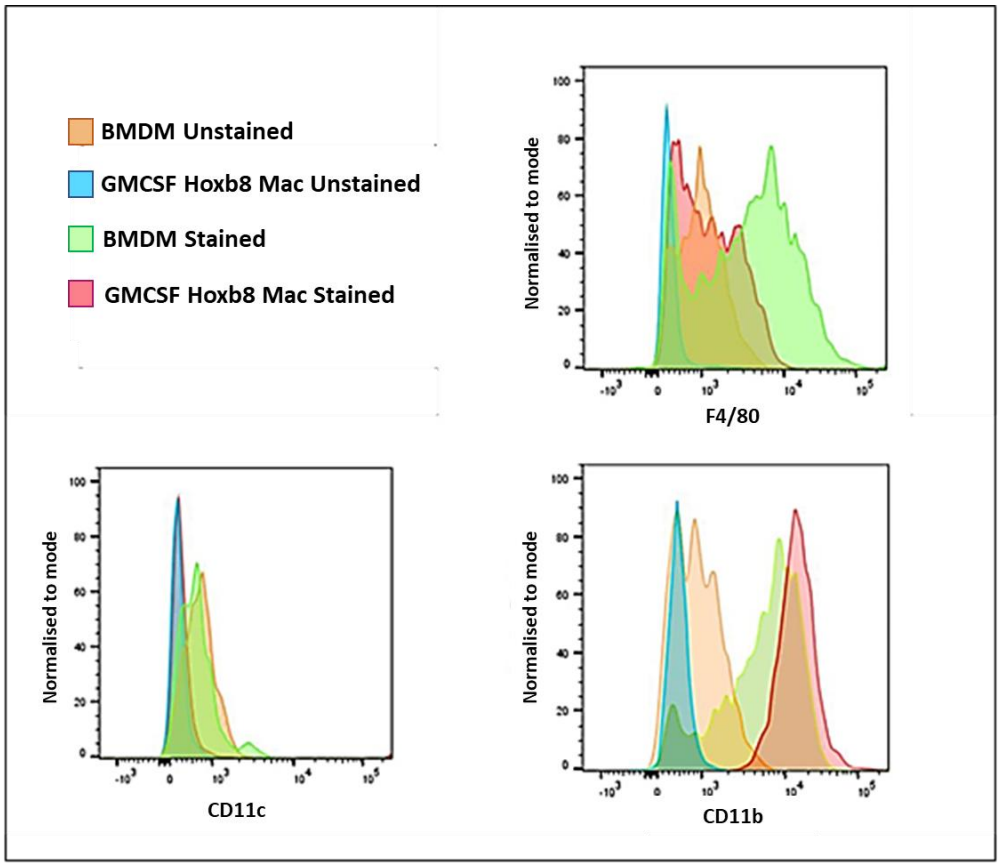

Figure 4.3 Basic macrophage markers on Hoxb8-derived macrophages generated from the gifted GMCSF Hoxb8 cells and BMDMs. Unstained cells were used as a negative control. Both Hoxb8-derived macrophages and BMDMs express macrophages markers F4/80 and CD11b but not dendritic cell marker CD11c. The result is representative of n=3.

Based on this, it was decided to generate both WT and *Adamdec1*$^{-/-}$ Hoxb8 progenitor cells using bone marrow isolated from the WT and *Adamdec1*$^{-/-}$ mice. A generation of a fresh batch of the WT Hoxb8 cells inhouse would minimise any

potential difference in the phenotype of the immortalised, or subsequently differentiated macrophages, that might arise from genetic and technical variation during the immortalisation process, since these WT and *Adamdec1*$^{-/-}$ mice were bred from the same heterozygous breeding pair and the bone marrow harvested from them would be immortalised simultaneously.

4.3.2 Generation of WT and *Adamdec1*$^{-/-}$ Hoxb8 progenitor cells

The WT and *Adamdec1*$^{-/-}$ Hoxb8 progenitor cells were generated following the protocol described in the original study by Wang.[143] This protocol was the same as the one Dr Zehrer followed to generate the WT Hoxb8 progenitor cells that she subsequently kindly gifted to our lab.

4.3.2.1 Amplification of MSCV ER-Hoxb8 plasmid

MSCV plasmid containing ER-Hoxb8 construct was amplified by heat shock transformation of Stellar competent *E.coli* cells followed by culturing of a single colony isolated from the transformed *E.coli* cells (Chapter 4.2.3.1). The plasmid was extracted and purified by Maxi-prep (Chapter 2.6.3.2). The final elution step of the plasmid in 0.5 ml of TE buffer resulted in the extraction of MSCV ER-Hoxb8 plasmid DNA at a concentration of 494 ng/µl. The presence and the correct sequence of the construct within the plasmid DNA were confirmed by DNA sequencing (Chapter 2.6.1) (Data not shown).

4.3.2.2 Generation of ER-Hoxb8 retrovirus by GP2-293 cells

HEK-293 cells are known for their reliable growth and ease of transfection, making them a preferred cell line for producing large quantities of viral particles. GP2-293 cell line is a commercially available HEK-293-based retroviral packaging cell line which contains the essential viral packaging genes, *gag* and *pol*.[146] Transfection of GP2-293 cells with a retroviral expression vector, such as MSCV, and a plasmid that expresses the viral envelope results in a high titre retrovirus production. In order to generate retrovirus containing ER-Hoxb8, which would be used to transduce mice bone marrow cells, GP2-293 cells were transfected with MSCV ER-Hoxb8 plasmid and an envelope plasmid, pEco vector, using Xfect Transfection Reagent (Chapter 4.2.3.2). 48 hours later, the supernatant containing

the retrovirus was harvested. To confirm a successful transfection of GP2-293 cells, RNA was extracted from the transfected GP2-293 cells 48 hours after the transfection. The RNA extracted was converted to cDNA and PCR was performed using primers targeting *Hoxb8* (Figure 4.4). Gel electrophoresis of the PCR product confirmed the expression of *Hoxb8* within the transformed GP2-293 cells by the presence of a band at 726 bp (Figure 4.5). The purified MSCV ER-Hoxb8 plasmid DNA was used as a positive control.

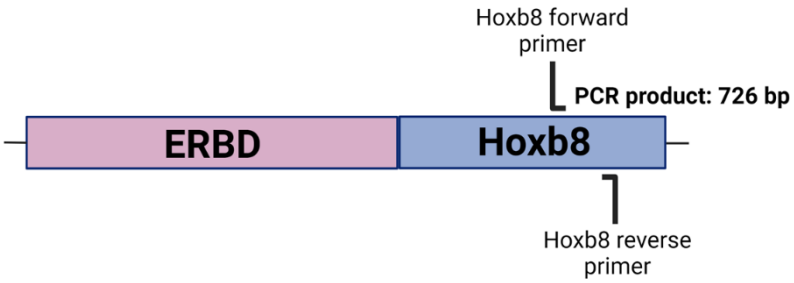

Figure 4.4 Scheme showing the position of the primers targeting Hoxb8 within ER-Hoxb8 insert. PCR was performed using these primers to detect the presence of Hoxb8 expression in the transfected GP2-293 cells.
ERBD: Oestrogen-receptor binding-domain

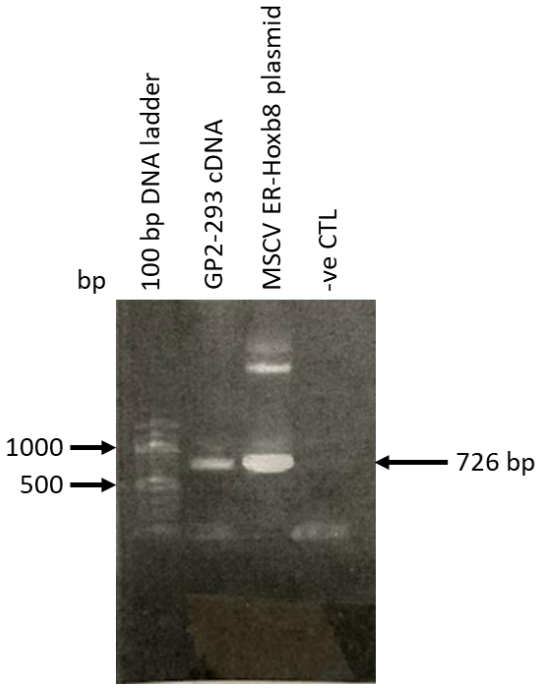

Figure 4.5 DNA gel electrophoresis confirming the presence of *Hoxb8* expression in the transfected GP2-293 cells. PCR was conducted using primers targeting Hoxb8 and MSCV ER-Hoxb8 plasmid as a positive control.
CTL: Control

4.3.2.3 Infection of the WT and *Adamdec1*$^{-/-}$ mice bone marrow progenitor cells with ER-Hoxb8 retrovirus

Having confirmed that the transfected GP2-293 cells expressed Hoxb8 indicating a successful transfection and production of retrovirus containing ER-Hoxb8, the retrovirus was used to transduce ER-Hoxb8 into mouse bone marrow progenitor cells. Bone marrow was harvested from the WT and *Adamdec1*$^{-/-}$ mice, during which RBC and granulocytes were removed to reduce contamination of the bone marrow stem cells. The harvested bone marrow cells were cultured in the stem cell medium supplemented with IL-3, IL-6 and SCF to stimulate the proliferation of progenitor cells over 2 days. Within few hours of culturing, an increase in the cell number was visible under a microscope. After 2 days of culturing, a large expansion in the number of rounded progenitor cells in suspension was clearly observed under a microscope. However, there were also numerous cells adhering to the bottom of the culture dish that seemed to have undergone some morphological changes. Only the cells in suspensions were transferred to a sterile container for the subsequent retrovirus transduction to reduce contamination of the progenitor cells with the cells that had undergone morphological differentiation. The progenitor cells were infected with the ER-Hoxb8 retrovirus by spin transfection method using polybrene for the transduction of ER-Hoxb8 (Chapter 4.2.3.3.4).

Following the transduction, the cells were suspended and cultured in the progenitor outgrowth medium supplemented with oestradiol and SCF over 2 days to activate Hoxb8 and to stimulate the proliferation of the progenitor cells. After 2 days, the progenitor cells were washed and divided into two batches. One batch was resuspended in the myeloid medium supplemented with oestradiol and GMCSF to initiate pre-conditioning of the progenitor cells towards macrophage differentiation. Another batch was resuspended in the myeloid medium supplemented with oestradiol and SCF to pre-condition the progenitor cells towards neutrophil differentiation, for future if this was ever needed. At the same time, the antibiotic selection with neomycin was initiated to eliminate the cells that did not successfully integrate the plasmid DNA. The initial cell viability was 60 - 64% for the WT and *Adamdec1*$^{-/-}$ progenitor cells in both GMCSF and SCF myeloid media. The antibiotic selection with neomycin was carried out over the next 4 weeks. The cell viability increased to greater than 70% for both WT and *Adamdec1*$^{-/-}$ progenitor cells within 1 week of commencing the antibiotic selection irrespective of the

difference in the growth factor in the media. This increased steadily over the next 4 weeks to above 95%.

After 4 weeks, neomycin was removed from the culture media. The immortalised progenitor cells were cultured for a further 1 week in the complete myeloid medium without neomycin to observe any potential changes in the cell viability and morphology after the cessation of antibiotic selection. The cessation of antibiotic selection resulted in no change in the cell viability and morphology over the seven days. The WT and *Adamdec1*$^{-/-}$ SCF Hoxb8 progenitor cells were frozen down at this point and stored for potential future use as Hoxb8-derived neutrophils were not intended to be used in this project. The WT and *Adamdec1*$^{-/-}$ GMCSF Hoxb8 progenitor cells were cultured and maintained in the myeloid medium supplemented with oestradiol and GMCSF.

4.3.3 Characterisation of the newly generated WT and *Adamdec1*$^{-/-}$ GMCSF Hoxb8 progenitor cells

Morphologically, the WT and *Adamdec1*$^{-/-}$ GMCSF Hoxb8 cells appeared the same under a light microscope (Figure 4.6). These progenitor cells also replicated and died in a similar manner when they were cultured in the myeloid medium for 7 days without passaging or feeding of fresh media (Figure 4.7). Since there was a reduction in the cell viability when the cell density exceeded approximately 1.2 x 10^6 cells/ml, both WT and *Adamdec1*$^{-/-}$ GMCSF Hoxb8 cells were maintained at a cell density of 2.5 - 10 x 10^5 cells/ml and passaged every 48-72 hours.

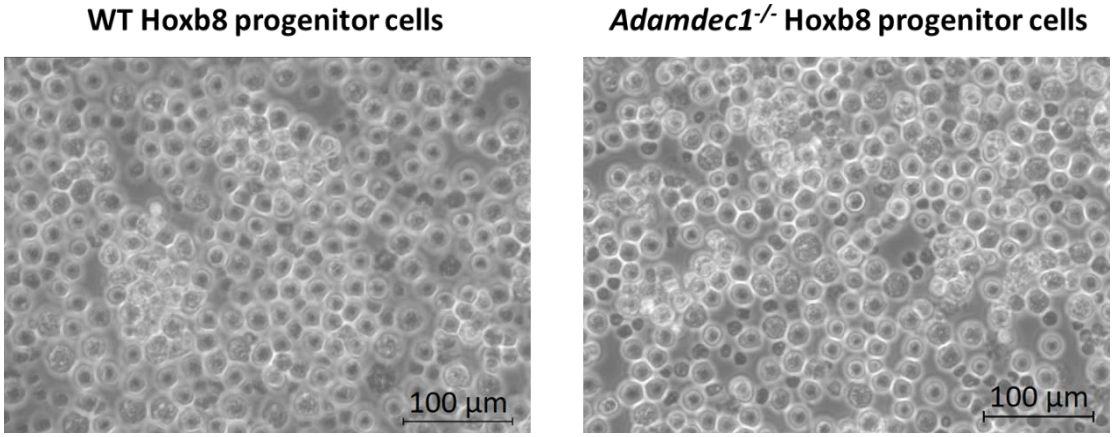

Figure 4.6 Morphological appearance of the WT and *Adamdec1*$^{-/-}$ GMCSF Hoxb8 progenitor cells. These cells appeared morphologically the same under a light microscope.

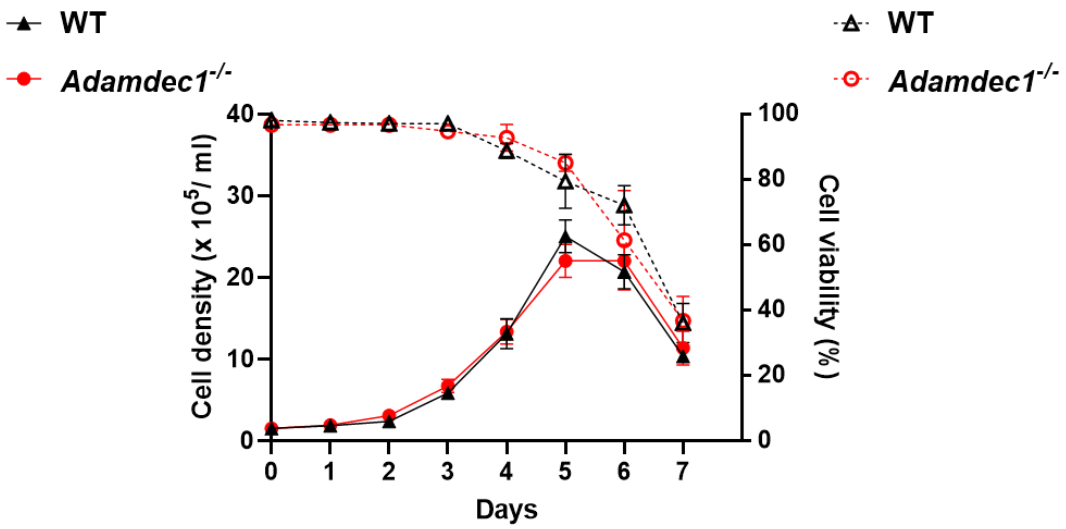

Figure 4.7 Expansion and viability of Hoxb8 progenitor cells. Cell count on the left y-axis is presented by solid lines, while cell viability on the right y-axis is presented by dashed lines. Cells were seeded at 2.5 x 10^5 cells/ml per plate and cell counts and viability were assessed daily over 7 days without passaging or feeding of additional media. Measurements for WT (black lines) and *Adamdec1*$^{-/-}$ (red lines) are shown as mean and SD, n = 5.
WT: Wild type

To verify the successful immortalisation of the newly generated WT and *Adamdec1*$^{-/-}$ GMCSF Hoxb8 cells comparative to the gifted WT Hoxb8 cells, the surface expression of CD117, CD11b, F4/80 and Ly6G on the newly generated WT and *Adamdec1*$^{-/-}$ GMCSF Hoxb8 cells were compared to the gifted WT GMCSF Hoxb8 cells by flow cytometry. These surface markers were used to characterise Hoxb8 progenitor cells in the study that originally described the generation of Hoxb8 progenitor cells, thus allowing validation of the immortalisation process against the original study.[143] CD117 is a SCF receptor that is also a haematopoietic stem cell marker. The expression of CD11b and F4/80 indicates successful pre-conditioning of the progenitor cells towards subsequent macrophage differentiation, and the absence of Ly6G indicates the absence of neutrophil differentiation.[143] The gifted WT, and newly generated WT and *Adamdec1*$^{-/-}$ GMCSF Hoxb8 cells all expressed CD117, CD11b and F4/80 but did not express Ly6G in a very similar pattern to each other (Figure 4.8). These expression patterns were also consistent with the previously reported finding of the surface marker expression of GMCSF Hoxb8 progenitor cells.[143] Cell lysates were also made from the newly generated WT and *Adamdec1*$^{-/-}$ Hoxb8 cells, which confirmed the expression of Hoxb8 in both cells (Figure 4.9). These observations confirmed a successful generation of WT

and *Adamdec1*$^{-/-}$ GMCSF Hoxb8 progenitor cells and suggested that the genotype of the progenitors did not seem to affect the phenotype of the Hoxb8 progenitor cells. This is consistent with the expectation that *Adamdec1* is not expressed in progenitor cells before differentiation into macrophages, thus unlikely to affect the phenotype of the progenitor cells.

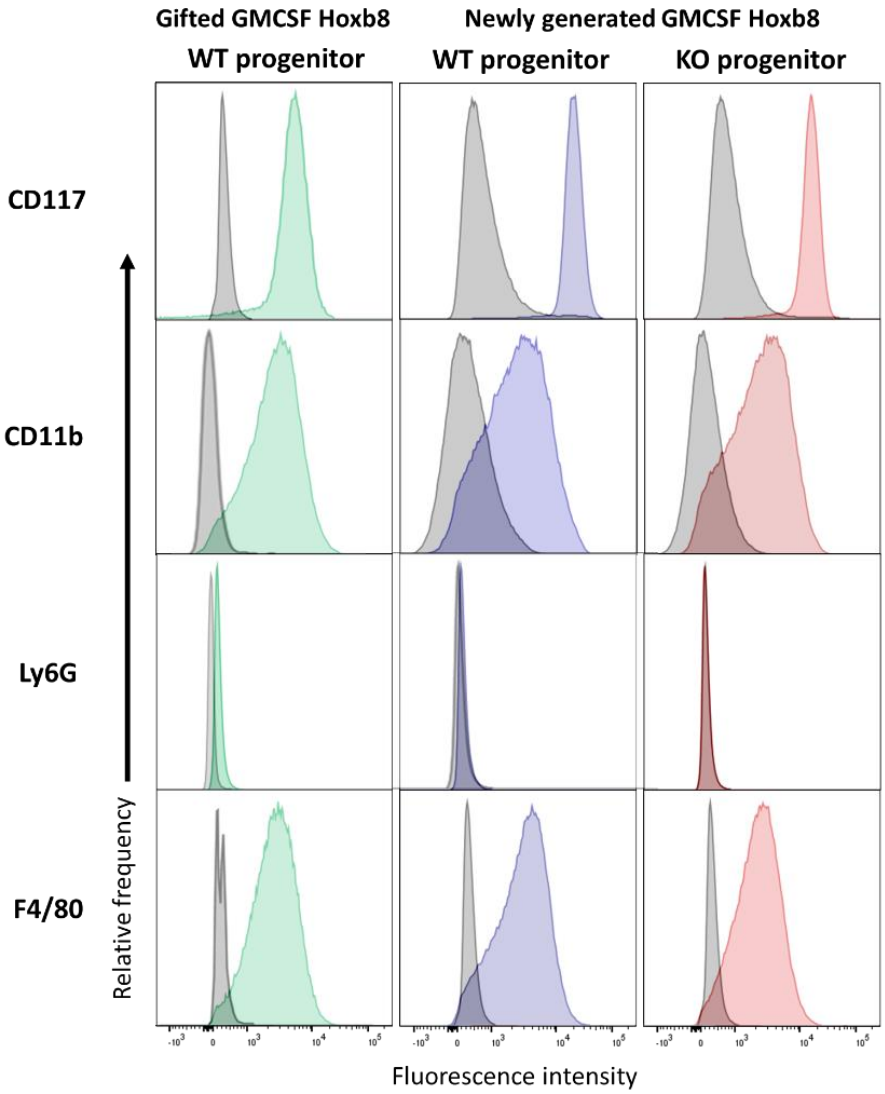

Figure 4.8 Cell marker expression of the gifted Hoxb8 cells and newly generated WT and *Adamdec1*$^{-/-}$ GMCSF Hoxb8 cells. Fluorescence intensity is presented on x-axis and the relative frequency of the cell normalised to mode is presented on y-axis. Stained cells are in blue for the gifted WT Hoxb8 progenitors, purple for the newly generated WT GMCSF Hoxb8 cells, and red for the newly generated *Adamdec1*$^{-/-}$ GMCSF Hoxb8 cells. The grey shades represent unstained controls. The expression patterns of CD117, CD11b, Ly6G and F4/80 were similar in the gifted Hoxb8 cells and new newly generated WT and *Adamdec1*$^{-/-}$ GMCSF Hoxb8 cells. The image was created in FlowJo software (BD Biosciences). The result is representative of n=3.
KO: *Adamdec1*$^{-/-}$, WT: Wild type

4.3.4 Differentiation of the newly generated WT and *Adamdec1*$^{-/-}$ GMCSF Hoxb8 progenitor cell into macrophages

The differentiation of GMCSF Hoxb8 progenitor cells into macrophages occurs upon removal of oestradiol and GMCSF from the culture media, the subsequent inactivation of Hoxb8 expression and the addition of the differentiation medium supplemented with MCSF in a coated culture dish over 5-7 days.[143] The inactivation of Hoxb8 gene induction and the loss in protein expression by removal of oestradiol was confirmed by the Western blot showing the disappearance of Hoxb8 protein in the WT and *Adamdec1*$^{-/-}$GMCSF Hoxb8-derived macrophages harvested on day 7 after initiation of the differentiation protocol (Figure 4.9).

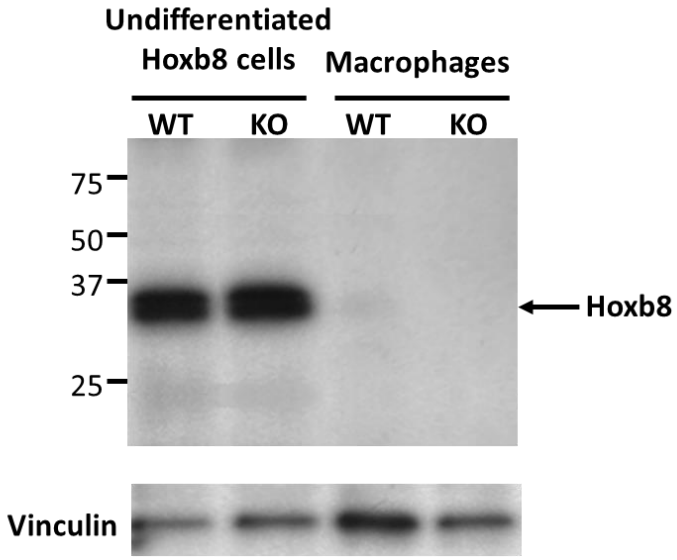

Figure 4.9 Anti-Hoxb8 Western blot demonstrating the presence of Hoxb8 in the newly generated WT and *Adamdec1*$^{-/-}$ Hoxb8 progenitor cells and disappearance of it in the WT and *Adamdec1*$^{-/-}$ GMCSF Hoxb8-derived macrophages. The WT and *Adamdec1*$^{-/-}$ Hoxb8 cells were differentiated into macrophages over 7 days and the macrophages were harvested on day 7 of the differentiation protocol. The blot is representative of n=4.
KO: *Adamdec1*$^{-/-}$, WT: Wild type, Macrophages: Hoxb8-derived macrophages

Upon initiation of the macrophage differentiation protocol, the morphology of both WT and *Adamdec1*$^{-/-}$ Hoxb8 progenitor cells changed from round-shaped suspension cells to adherent cells with lamellipodial extensions typical of macrophages. These changes were evident under a light microscope from day 3 onwards after the initiation of the differentiation protocol. There were no

morphological differences detectable between the WT and *Adamdec1*$^{-/-}$ GMCSF Hoxb8-derived macrophages (Figure 4.10).

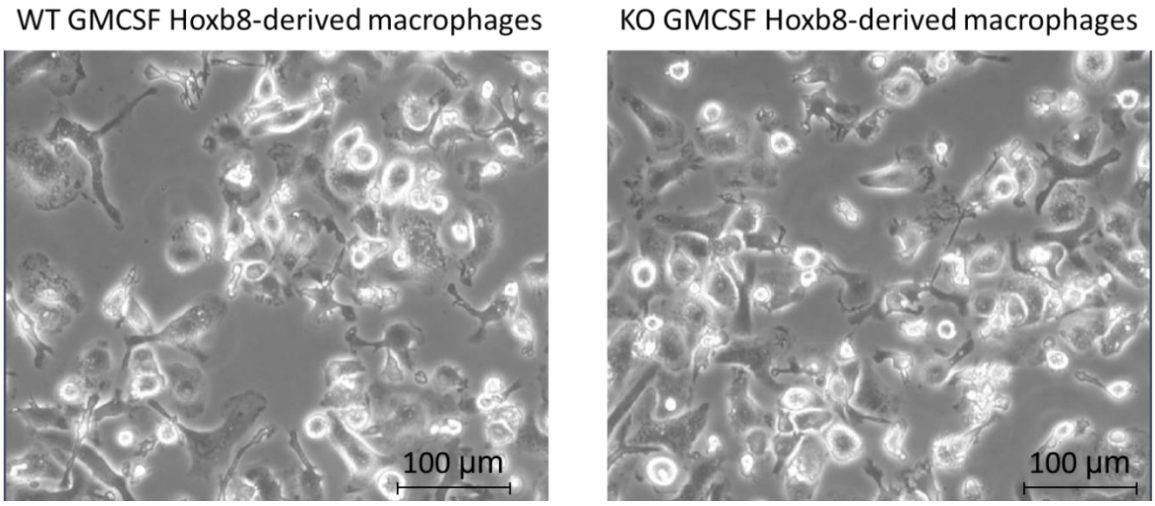

Figure 4.10 Morphology of the newly generated WT and *Adamdec1*$^{-/-}$ GMCSF Hoxb8-derived macrophages under a light microscope. Morphological features typical of macrophages were observed as early as day 3 of the macrophage differentiation protocol. The images were taken on day 7 of the differentiation protocol. KO: *Adamdec1*$^{-/-}$

To assess the course of macrophage differentiation of the newly generated Hoxb8 cells and to determine the optimal timepoint to harvest the macrophages for functional experiments, the WT and *Adamdec1*$^{-/-}$ GMCSF Hoxb8 cells were differentiated in coated culture dishes. After removal of the media containing suspension progenitor cells, PBS was added to the dish and the adherent Hoxb8-derived macrophages were scraped and their number and viability were examined daily over 9 days. The maximum number of Hoxb8-derived macrophages with the highest viability was observed on day 6 and day 7 after the initiation of the differentiation protocol (Figure 4.11). The number and viability of the macrophages started to decline thereafter. There were no differences in the cell number or viability between the WT and *Adamdec1*$^{-/-}$ Hoxb8-derived macrophages. Since the expression of ADAMDEC1 was detected in the macrophages derived from the gifted WT Hoxb8 cells on day 8 after the initiation of the differentiation protocol previously (Figure 4.2), it was decided to harvest the WT and *Adamdec1*$^{-/-}$ Hoxb8-derived macrophages on day 8 to be used for the subsequent functional experiments.

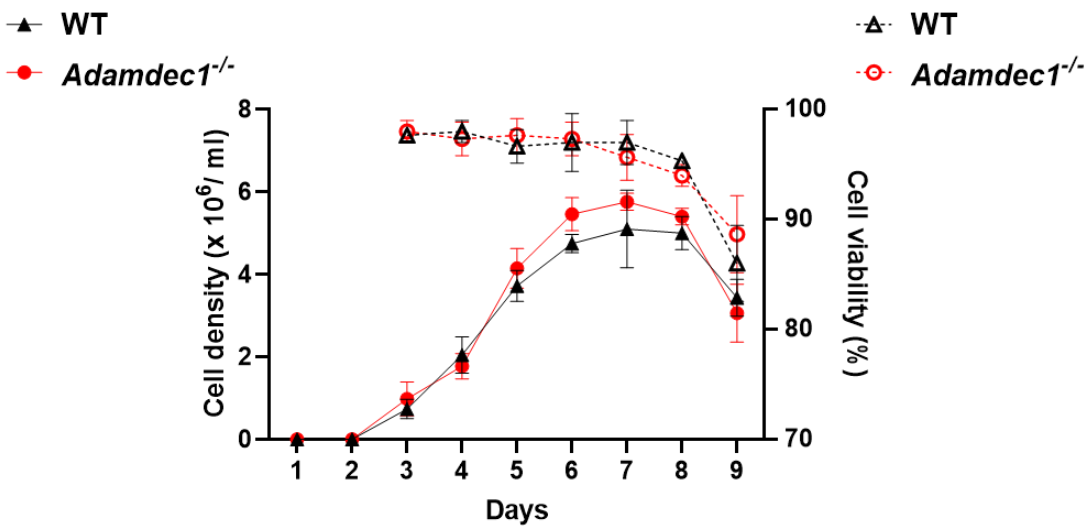

Figure 4.11 Cell count and viability of the WT and *Adamdec1*$^{-/-}$ GMCSF Hoxb8-derived macrophages during the differentiation protocol. Cell count on the left y-axis is represented by solid lines, while cell viability on the right y-axis is represented by dashed lines over 9 days. Cells were seeded at 2.5 x 10^5 cells/ml per plate after removal of oestrogen and GMCSF and differentiated in the macrophage differentiation media. Measurements for WT (black lines) and *Adamdec1*$^{-/-}$ (red lines) are shown as mean and SD, n = 5.
WT: Wild type

4.3.5 Expression of ADAMDEC1 in the WT and *Adamdec1*$^{-/-}$ Hoxb8-derived macrophages

The newly generated WT and *Adamdec1*$^{-/-}$ GMCSF Hoxb8 cells were differentiated into macrophages, and the differentiated cells were harvested on day 8. To verify the expression of ADAMDEC1 in these macrophages, lysates were made and the expression of ADAMDEC1 was determined by Western blot. Based on the expression of ADAMDEC1 previously detected in the macrophages derived from the gifted WT Hoxb8 cells, the macrophages derived from the newly generated WT GMCSF Hoxb8 cells were anticipated to express ADAMDEC1. However, unexpectedly, the expression of ADAMDEC1 was not detected in the macrophages derived from the newly generated WT GMCSF Hoxb8 cells. (Figure 4.12). The undifferentiated progenitor cells, irrespective of the genotype, and the *Adamdec1*$^{-/-}$ Hoxb8-derived macrophages did not show expression of ADAMDEC1 as expected.

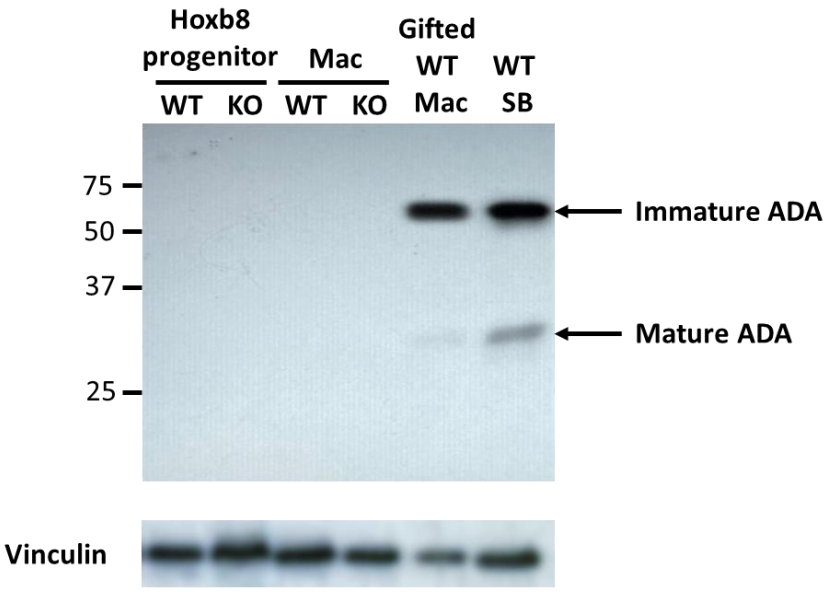

Figure 4.12 Anti-ADAMDEC1 Western blot of ADAMDEC1 expression in the Hoxb8 progenitor cells and Hoxb8-derived macrophages. The newly generated WT Hoxb8-derived macrophages were expected to express ADAMDEC1, which was not observed. Lysates made from the gifted WT Hoxb8-derived macrophages and small bowel of WT mouse were used as positive controls. The blot is representative of n=7.
ADA: ADAMDEC1, KO: *Adamdec1*$^{-/-}$, Mac: Hoxb8-derived macrophages SB: Small bowel

4.3.6 Characterisation of the WT macrophages derived from newly generated Hoxb8 cells

Given that the WT macrophages derived from the newly generated WT GMCSF Hoxb8 cells did not express ADAMDEC1, the surface marker profile on these differentiated cells was interrogated to determine whether they appropriately differentiated into macrophages.

At this point, the WT SCF Hoxb8 cells which were generated and frozen down earlier were thawed. The SCF Hoxb8 cells are positioned at an earlier stage of the myeloid differentiation pathway and retain the ability to differentiate into a wider range of alternative fates in response to lineage-specific cytokines than GMCSF Hoxb8 cells, which are committed to macrophage, or dendritic cell, differentiation.[143,145] Although SCF Hoxb8 cells are, by definition, pre-conditioned to differentiate into neutrophils, upon withdrawal of oestradiol and initiation of the macrophage differentiation protocol with MCSF, instead of GCSF, they can give rise to macrophages, even though a yield of macrophages is much lower than

using GMCSF Hoxb8 cells.[143] The thawed WT SCF Hoxb8 cells were thus differentiated to macrophages to see if macrophages generated from the progenitor cells more primitive on the differentiation pathway would express ADAMDEC1. The surface marker profile of the differentiated cells derived from WT SCF Hoxb8 cells was also interrogated to gain a more comprehensive idea on what these differentiated cells would resemble.

Furthermore, to determine whether the immortalisation process of the bone marrow cells altered the phenotype of the newly generated Hoxb8 cells, which may account for the non-expression of ADAMDEC1, bone marrow was freshly harvested from the WT mouse and differentiated into macrophages in vitro and their surface markers were analysed in comparison to the Hoxb8-derived macrophages. Additionally, bone marrow was also harvested from the *Adamdec1*$^{-/-}$ mouse and differentiated into macrophages to be compared to the WT BMDM to assess the effect of ADAMDEC1 on the differentiation of bone marrow cells to macrophages.

CD115 is a MCSF receptor and it is expressed on murine monocytes and macrophages. The expression of CD115 is known to increase during progenitor cell differentiation to macrophages.[147,148] CD11b is expressed abundantly on myeloid cells such as neutrophils and macrophages and its expression increases through the differentiation pathway of progenitor cells.[148,149] Ly6G and Ly6C make up the epitope, Gr-1, which are expressed on both macrophages and neutrophils. However, a higher Ly6G expression is found on neutrophils while a higher expression of Ly6C is found on macrophages, thus serving as markers for these terminally differentiated cells.[150,151] CD11c is a dendritic cell marker, and CD117 is a progenitor cell marker.[152,153] CX3CR1 and F4/80 are expressed on monocytes and macrophages. Their expressions are known to increase during monocytes to macrophage differentiation in vitro.[154]

First of all, the WT macrophages derived from the newly generated WT GMCSF Hoxb8 cells indeed expressed the surface markers consistent with terminally differentiated macrophages, even though these cells did not express ADAMDEC1 (Figure 4.13 A). This was evident by the increase in expression of CD115 from the progenitor state to macrophages, and high expressions of CD11b, Ly6C, CX3CR1 and F4/80 upon differentiation. These observations indicated that the newly generated WT GMCSF Hoxb8 cells appropriately responded to MCSF and differentiated into macrophages. In contrast, the surface markers of the

differentiated cells derived from the WT SCF Hoxb8 cells resembled that of neutrophils, although these progenitor cells were differentiated in the medium supplemented with MCSF promoting the terminal differentiation to macrophages (Figure 4.13 B). This was evident by the higher expression of Ly6G and lower expressions of CX3CR1 and F4/80 on the differentiated cells derived from the WT SCF Hoxb8 cells in comparison to the WT macrophages derived from the GMCSF Hoxb8 cells. Interestingly, the undifferentiated GMCSF Hoxb8 progenitor cells expressed a modest degree of CD11b, Ly6C, CX3CR1 and F4/80, which were consistent with surface marker expression resembling monocytes (Figure 4.13 A). In contrast, the undifferentiated SCF Hoxb8 progenitor cells exhibited very little surface markers other than the progenitor cell marker, CD117, confirming that these progenitor cells were more primitive than the GMCSF Hoxb8 cells, with regard to the differentiation pathway (Figure 4.13 B). Despite this, the pre-conditioning of the progenitor cells with SCF seemed to have had a potent effect on the fate commitment of these cells to differentiate into neutrophils, even when the macrophage differentiation protocol with MCSF was followed.

Having established that the WT macrophages derived from the newly generated GMCSF Hoxb8 cells expressed the surface markers consistent with macrophages, their surface expression profile was compared to that of the WT BMDM (Figure 4.13 C) to determine if the immortalisation process had potentially altered the phenotype of the WT macrophages derived from the newly generated GMCSF Hoxb8 cells. Limited in regards to the surface expression markers examined, overall, the surface marker profile of the WT macrophages derived from the newly generated GMCSF Hoxb8 cells and the WT BMDM were similar and in accordance with the macrophage expression profile. However, a higher CD117, and lower F4/80 and CX3CR1 expressions were observed in the WT Hoxb8-derived macrophages in comparison to the WT BMDM. This indicated that the WT BMDM were more mature in terms of the differentiation pathway to macrophages.

Additionally, the surface marker expressions were largely similar in the WT and *Adamdec1*$^{-/-}$ BMDM (Figure 4.13 C). Although a small cell subpopulation expressing lower levels of F4/80 and CX3CR1 was present in the *Adamdec1*$^{-/-}$ BMDM, the majority of the WT and *Adamdec1*$^{-/-}$ BMDM mirrored each other in the expression of the surface markers examined. This suggested, limited to the surface marker analysis by these selected markers, that the absence of ADAMDEC1 did

not seem to affect the differentiation process of bone marrow stem cells to macrophages.

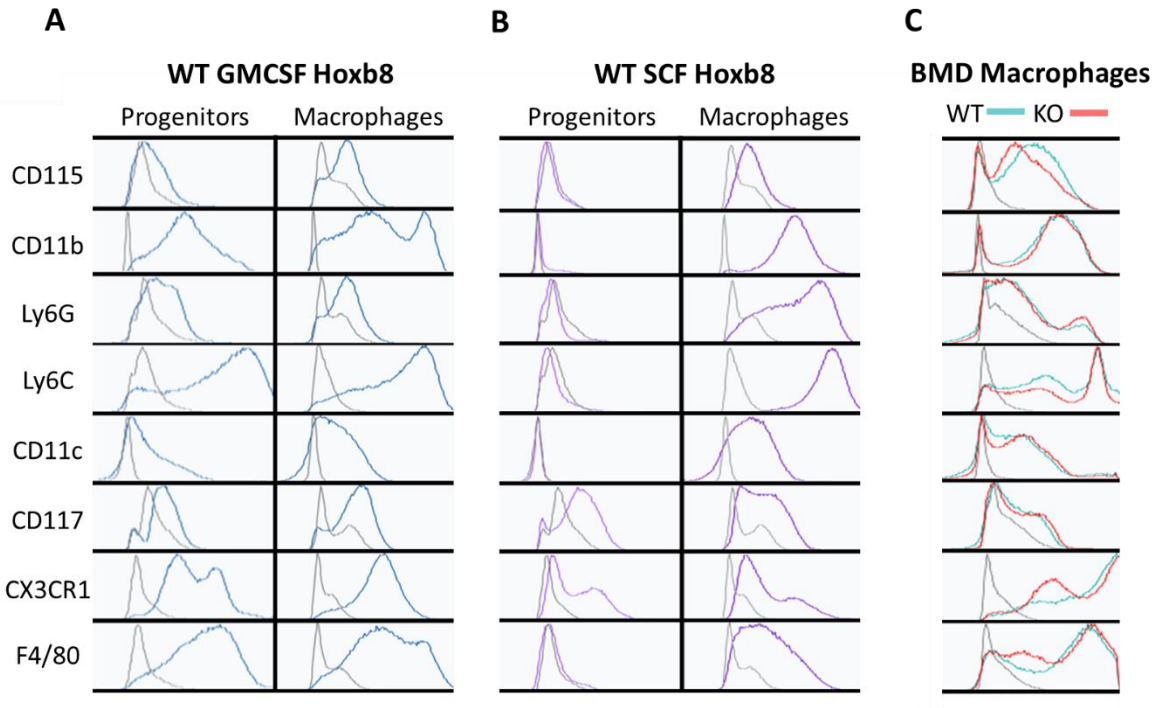

Figure 4.13 Cell surface marker expression of the progenitors and macrophages derived from newly generated GMCSF and SCF WT Hoxb8 cells, and the WT and *Adamdec1*$^{-/-}$ BMDMs.
A: Cell surface marker expression of WT GMCSF progenitor cells and macrophages derived from the WT GMCSF Hoxb8 cells.
B: Cell surface marker expression of WT SCF Hoxb8 progenitor cells and cells differentiated from the WT SCF Hoxb8 cells using the macrophage differentiation protocol.
C: Cell surface marker expression of the WT and *Adamdec1*$^{-/-}$ BMDMs.
Fluorescence intensity is presented on x-axis normalised and the relative frequency of the cell normalised to mode is presented on y-axis. Stained cells are in blue for the WT GMCSF Hoxb8 progenitors, purple for the WT SCF, green for the WT BMDMs and red for the *Adamdec1*$^{-/-}$ BMDMs. The grey lines represent unstained controls. The result is representative of n=3.
WT: Wild type, BMD: Bone marrow-derived

Having established that the WT macrophages derived from the newly generated GMCSF Hoxb8 cells appropriately expressed the surface markers consistent with macrophages and that their surface marker expression was similar to that of the WT BMDM, the WT GMCSF Hoxb8 cells were once again differentiated into macrophages. However, this time the differentiation media were supplemented

with HkEc in addition to MCSF to determine if the addition of HkEc could facilitate induction of ADAMDEC1 in the differentiated cells. This was based on the previous finding that identified HkEc as being the strongest ADAMDEC1 inducer in THP-1 cells (Chapter 3.3). Although the surface marker profile of the WT macrophages derived from the SCF Hoxb8 cells was more consistent with neutrophil phenotype, these cells were also differentiated once again with MCSF and HkEc to determine if they expressed ADAMDEC1 upon terminal differentiation. Freshly isolated bone marrow from the WT mice was also differentiated into macrophages once again. The expressions of ADAMDEC1 in these three differentiated cell populations were assessed by Western blot. Upon harvesting the cells differentiated from the WT GMCSF and SCF Hoxb8 cells, their surface marker profiles were examined by flow cytometry using the same markers as previously used to determine the effect of adding HkEc during the differentiation. The surface markers were largely unchanged except for an increase in the expressions of F4/80 and CX3CR1 (Data no shown). Despite this, these differentiated cells derived from the newly generated WT GMCSF and SCF Hoxb8 cells did not express ADAMDEC1 (Figure 4.14). Surprisingly, the expression of ADAMDEC1 was not detected in the WT BMDM either (Figure 4.14).

The expression of *Adamdec1* in the differentiated cells derived from the newly generated WT GMCSF and SCF Hoxb8 cells and the WT BMDM was also examined at the RNA messenger level by qPCR. This resulted in CT values of greater than 37, thus implying *Adamedc1* as a non-detected gene in the cDNAs made from all of the three differentiated cell populations (data not shown), confirming the Western blot result.

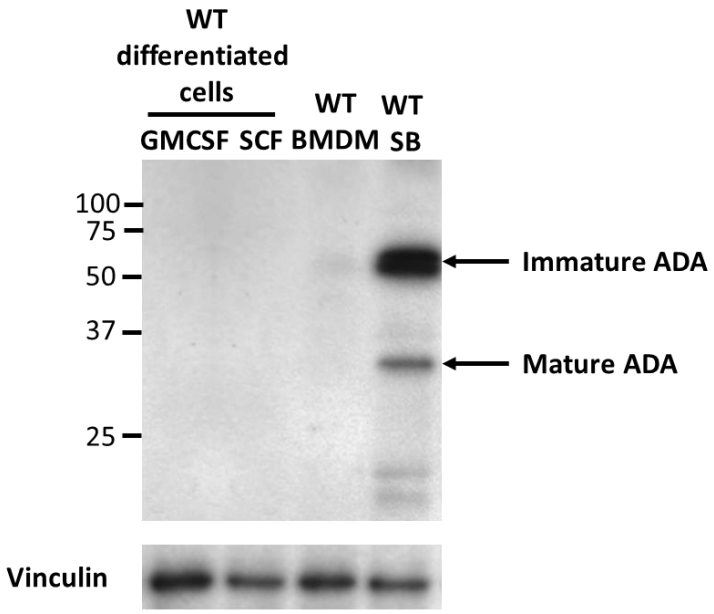

Figure 4.14 Anti-ADAMDEC1 Western blot of cells differentiated from the newly generated GMCSF and SCF WT Hoxb8 cells following the macrophage differentiation protocol augmented with HkEc, and WT BMDMs. The GMCSF and SCF WT Hoxb8 cells were differentiated following the macrophage differentiation protocol with additional HkEC. The differentiated cells were harvested on day 8. Lysates made from small bowel of WT mouse were used as positive controls. The blot is representative of n=5.
ADA: ADAMDEC1, WT: Wild type, BMDM: Bone marrow derived macrophages, SB: Small bowel

Although these findings indicated that the WT macrophages derived from the newly generated GMCSF Hoxb8 cells and WT BMDM did not express ADAMDEC1, there is well-established evidence (see Chapter 3), that the macrophages generated from peripheral blood monocytes and THP-1 cells in vitro express ADAMDEC1. Macrophages are extremely plastic cells and their phenotypes are on a spectrum depending on the surrounding environment. Based on these accounts, it was deliberated whether the *bona fide* pre-conditioning of the macrophage precursor cells within circulating blood was indispensable for these cells to differentiate into macrophages that expressed ADAMDEC1, as for the intestinal macrophages. It was also considered whether the intestinal environment was playing a vital role in modulating the phenotype of macrophages to express ADAMDEC1. Thus, the newly generated WT GMCSF Hoxb8 cells were differentiated into macrophages in the differentiation media supplemented with various stimuli to mimic the circulating blood and intestinal environment, such as heat-inactivated mouse serum, colonic

tissues freshly isolated from the WT mice and CCL2, a chemokine responsible for the recruitment of monocyte to macrophages, in addition to MCSF and HkEc. Although morphological changes suggestive of differentiation to macrophages were observed (Figure 4.15), none of these stimuli, or combination of them, resulted in the expression of ADAMDEC1 in the differentiated cells, which was determined by qPCR (data not shown).

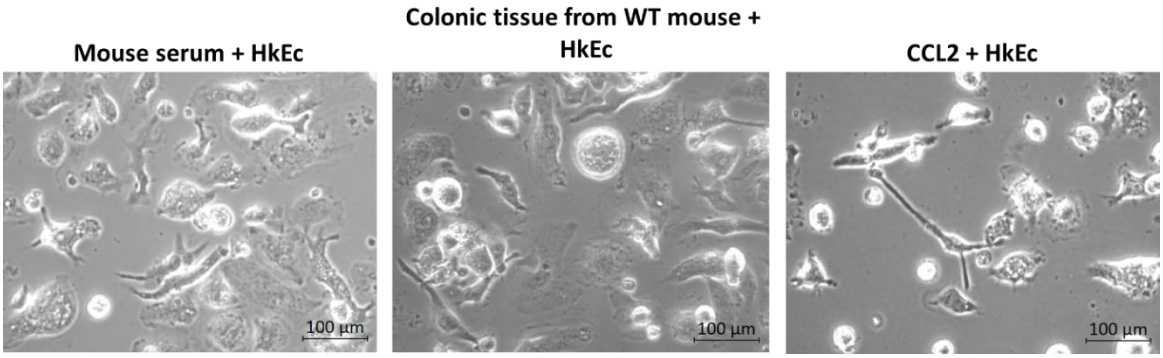

Figure 4.15 Morphology of the cells differentiated from WT GMCSF Hoxb8 cells in differentiation media supplemented with MCSF, HkEc and additionally mouse serum, WT mouse colonic tissue or CCL2. The morphological features resembling macrophages were observed. The pictures are representative of n=5.

Since the macrophages derived from the newly generated WT Hoxb8 cells did not express ADAMDEC1, it was not possible to use this WT and *Adamdec1*$^{-/-}$ Hoxb8-derived macrophage model to study the potential difference in the phenotype of macrophages in the absence and presence of ADAMDEC1. As the macrophages derived from the gifted WT Hoxb8 cell did express ADAMDEC1, using the WT macrophages derived from the gifted Hoxb8 cells to conduct functional experiments in conjunction with the *Adamdec1*$^{-/-}$ macrophages derived from the newly generated *Adamdec1*$^{-/-}$ Hoxb8 cells was considered. However, clearly the gifted WT GMCSF Hoxb8 cells and the newly generated WT GMCSF Hoxb8 cells give rise to macrophages that differ in phenotype, at least with regards to the expression of ADAMDEC1. Although the same immortalisation protocol was followed, a small variation in the process as well as the difference in the environment such as previous culture conditions may have caused the difference in the phenotypes of the macrophages derived from these immortalised progenitor cells. The culture-condition dependant alteration in phenotypes of cells has been reported in numerous studies.[155,156] Thus, the differences in the functional

phenotype between the WT macrophages derived from the gifted Hoxb8 cells and the *Adamdec1*$^{-/-}$ macrophages derived from the newly generated *Adamdec1*$^{-/-}$ Hoxb8 cells could not be reliably attributed to the genotype. Therefore, this part of the project was abandoned at this stage and an alternative way to study the functional role of ADAMDEC1 was explored.

4.4 Discussion

The results of this chapter highlighted the high plasticity of macrophages which appears to be remarkably sensitive to the environment and the difficulty associated with the applicability of in vitro macrophage models to study specific macrophages in *bona fide* tissue.

The surface marker profile and some aspects of the functional characteristics of Hoxb8-derived macrophages have been validated against those of BMDM previously and were shown to be similar, which was also supported by the findings from this chapter.[144] However, phenotypic comparison of Hoxb8-derived macrophages against any other types of macrophages has not been conducted. Isolating intestinal macrophages or generating substantial numbers of MDMs from mouse is limited by the small volume of intestinal tissue or blood that can be collected. Thus, BMDM and peritoneal macrophages are two typically used mouse macrophage models for in vitro studies. The phenotypic differences with regards to respiratory burst, phagocytosis, cytokine secretion and gene expression have been reported in these two different macrophage populations.[157] Furthermore, three distinct functional characteristics have been reported in mouse peritoneal macrophages, splenic macrophages and BMDM.[1] Thus, it is likely that Hoxb8-derived macrophages and BMDMs do not resemble the phenotype of the intestinal macrophages that express ADAMDEC1, accounting for the absence of ADAMDEC1 expression in these macrophages. Furthermore, the WT macrophages derived from the newly generated WT Hoxb8 cells and WT BMDM did not express ADAMDEC1, but the THP-1-derived macrophages and MDMs did (Chapter 3). These findings suggest that pre-conditioning of macrophage precursor cells in circulating blood might be one of the indispensable factors for the precursor cells to differentiate into macrophages that express ADAMDEC1 such as intestinal macrophages. There are no previous studies that have demonstrated induction of ADAMDEC1 during monocyte to macrophage differentiation in vitro using murine cells.

Interestingly, the macrophages derived from the gifted WT Hoxb8 cells, however, expressed ADAMDEC1. This was despite the same immortalisation protocol being followed to generate the Hoxb8 cells, and the gifted and newly generated WT Hoxb8 cells expressing a similar surface marker profile. It is possible that the difference in the environment has caused the phenotypic alteration between these

two WT Hoxb8 cells to give rise to macrophages with distinct characteristics. This is consistent with numerous studies demonstrating cell culture condition-dependent alterations in functional and gene expression profiles of cells, including THP-1 cells and BMDMs, in vitro.[155,156,158–160] The environmental factors tested in these studies included cell density, number and frequency of passaging during day-to-day maintenance of the cells, cell density at the initiation of the cell differentiation, and coating type of the culture dish used during cell differentiation. These findings and the results of this chapter support the highly sensitive nature of the environment-dependant plasticity in the macrophage phenotype which is consistent with the extremely high heterogeneity of a *bona fide* macrophage phenotype.

The outcome of the chapter was unexpected and the subsequent experiments to examine the phenotype of macrophages in the presence and absence of ADAMDEC1 using the Hoxb8 cell model had to be abandoned. However, it provided valuable knowledge that not all macrophages express ADAMDEC1 in vitro and thus appropriate experimental model must be carefully considered and selected to study the role of ADAMDEC1 in function of macrophages.

Chapter 5

Production and purification of recombinant human and mouse ADAMDEC1 and its mutant E353A

5.1 Background and aims

Conducting functional assays using WT and *Adamdec1*$^{-/-}$ Hoxb8-derived macrophages to study the biological function of ADAMDEC1 was not feasible since ADAMDEC1 was not expressed in the newly generated WT Hoxb8-derived macrophages as discussed in Chapter 4. Thus, an alternative pathway was explored in order to perform functional studies on ADAMDEC1. The production of recombinant ADAMDEC1 and its catalytically inactive mutant E353A using HEK 293 cells, immortalised human embryonic kidney cells, have been used previously to perform functional analyses of ADAMDEC1.[14,20,28] E353A is produced by replacement of glutamate, following the first histidine, in the zinc-binding motif of the metalloprotease domain by alanine (H**A**XXHXXGXXD), and is used as a control in functional studies of ADAMDEC1.[14,16] As well as conducting functional assays, successful production and purification of recombinant ADAMDEC1 and E353A could also lead to the evaluation of the potential catalytic substrate(s) of ADAMDEC1 by protease degradomic analysis. In our laboratory, the production of recombinant ADAMDEC1 using *E. coli* as a host expression system was attempted previously. However, this was not successful. Additionally, at the time of initiation of this part of the project, there was no commercially available recombinant ADAMDEC1. Having reviewed options of the available protein expression systems, the insect cell protein expression system, interchangeably called baculovirus expression vector system (BEVS), was chosen to produce recombinant ADAMDEC1 and its catalytically inactive mutant E353A in this project. The production of ADAMDEC1 using BEVS has never been described previously.

BEVS utilises insect cells, most commonly derived from *Spodoptera frugiperda* (Sf cells such as Sf9 and Sf21 cells) or *Trichoplusia ni* (Tn cells), and a viral vector derived from *Autographa Californica* multiple nucleopolyhedosis virus (AcMNPV). AcMNPV is a member of *Baculoviridae* virus with a large double-stranded circular DNA genome whose natural host is insect cells.[161–163] AcMNPV infection in insect

cells is characterised by the production of numerous vesicles called polyhedra within nuclei during the late stage of infection. Polyhedra are constituted by a matrix protein called polyhedrin, which accumulates to a high level and becomes over 25% of the total cell protein mass by the late stage of the viral infection.[164] Since polyhedrin is not required for the replication or infectivity of the virus in tissue culture cells, the BEVS exploits this unique characteristic of AcMNPV infection by replacing the polyhedrin coding sequence with a foreign DNA sequence while conserving the polyhedrin promoter to produce a recombinant protein with high yield.[165]

The advantages of the BEVS over the prokaryotic cell expression system, that are relevant to this project, include its ability to produce secreted protein by recognising and processing the signalling peptide, as well as to provide a majority of the post-translational modifications found in mammalian cells including core N-glycosylation, O-glycosylation, acylation and phosphorylation.[165,166] Human ADAMDEC1 is known to have 4 glycosylated sites in its structure.[167] In comparison to the mammalian expression system, BEVS allows more rapid expression of recombinant protein with a much higher yield. Additionally, insect cells are grown in serum-free culture media. This makes the subsequent purification of ADAMDEC1 and E353A less complicated since the mature active forms of these proteins are expected to be secreted in the culture media. Furthermore, BEVS has the best safety profile since AcMNPV is essentially non-infectious to mammals.[164,168] There are, however, limitations associated with the BEVS. The post-translational modifications in the insect cells are not identical to that of the mammalian cells which might affect the structure, therefore, the function of the expressed protein. This includes, particularly, the terminal glycosylation involving sialic acid complex-structure in mammalian cells which is typically substituted by paucimannose structure in insect cells.[169] Nevertheless, the use of BEVS was deemed suitable and worth attempting to produce and purify ADAMDEC1 in a large quantity over a relatively short frame of time.

Since BEVS was first developed in 1983,[165] the quality and yield of protein production by BEVS have improved dramatically through a series of optimisation in its methodology and advances in cloning technology. It is one of the most widely used, robust and versatile protein expression systems available at present. Commercially manufactured products utilising BEVS include multiple vaccines and

therapies approved for human use.[168] The most common and efficient method of BEVS currently used is *Tn*-7 mediated “bacmid” system, commercially available as Bac-to-Bac system.[170] Bacmid is a bacterial artificial chromosome (BAC), ~140k bp large plasmid of modified AcMNPV genome, which was developed to be maintained and generated in *E. coli*.[170]

The overview of the steps involved in the Bac-to-Bac system is summarised in Figure 5.1. The first step involves generating a DNA construct of the desired protein. This construct is then inserted into a transfer vector containing an expression cassette, incorporating a polyhedrin promotor, which is flanked by the right and left arm of *Tn*-7 forming a mini-*Tn*7. The use of a transfer vector is necessary for accurate and efficient generation of baculovirus in BEVS because a direct insertion of a construct into bacmid is not feasible due to the large size of bacmid. Additionally, various desirable features to the end product protein can be engineered, such as adding purification tag and signalling peptide, in the transfer vector which can be manipulated easily, unlike bacmid. After amplification and purification of the recombinant transfer vector containing the gene of interest, *E. coli* carrying a bacmid containing a mini-*attTn*7 attachment site and a helper plasmid is transformed with the recombinant transfer vector. A site-specific transposition of the expression cassette occurs between the mini-*Tn*7 on the transfer vector and the mini-*attTn*7 on the bacmid in the presence of transposition proteins provided by the helper plasmid. This mechanism results in highly efficient and accurate incorporation of the gene of interest into the bacmid plasmid.[170] The amplified and purified recombinant bacmid containing the gene of interest is then used to transfect insect cells to generate recombinant baculovirus. The isolated baculovirus stock after the transfection (P0) is then used to infect a fresh culture of insect cells to amplify the baculovirus (P1). Further amplifications of baculovirus are usually performed to achieve a higher viral titre through harvesting of P2 and P3 which is then used to infect a fresh culture of insect cells for protein expression.

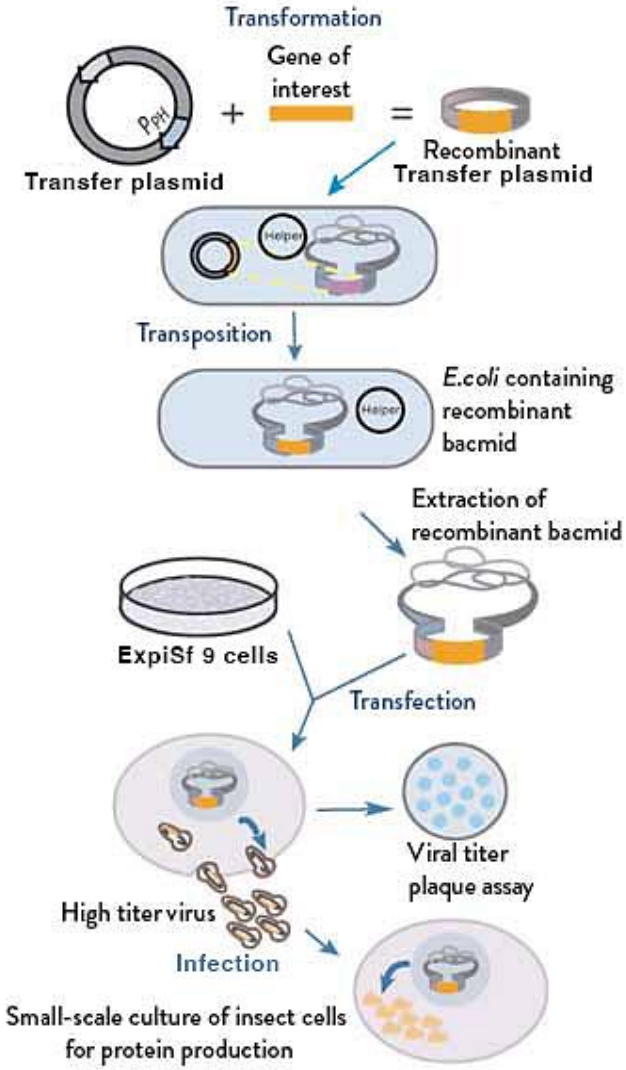

Figure 5.1 Overview of the steps involved in the Bac-to-Bac system for production of recombinant protein. The image was adapted from https://www.promab.com/baculovirus-expression and modified.[324]

In this project, commercially available Bac-to-Bac™ C-His TOPO™ Expression System (Gibco) was chosen for the production of recombinant ADAMDEC1 and E353A. A transfer vector provided in Bac-to-Bac™ C-His TOPO™ Expression System, pFastBac™ TOPO® vector, contained a C-terminal polyhistidine-tag (6xHis-tag) which was ideal for the subsequent purification of the cleaved mature form of ADAMDEC1 and E353A.

ExpiSf9™ cells (Thermo Fisher Scientific) were used to produce recombinant ADAMDEC1 and E353A in this project. These insect cells are commercially

developed, non-engineered derivative of Sf9 insect cells and are adopted to grow in suspension at a much higher density of 2.0 x 10^7 /ml.[171] ExpiSf9 cells have a broader range of log growth-phase, during which the optimal baculovirus infection for protein expression occurs, than the conventional insect cell lines used in the BEVS. These characteristics of ExpiSf9 result in the isolation of significantly higher viral tire in P0 viral stock and a much greater yield of expressed protein per volume of cell culture than the conventional cell lines.[172] The achievement of the higher viral titre in P0 allows elimination of further viral amplification, which typically takes 2-3 weeks prior to the infection of ExpiSf9 cells for protein expression.

The recombinant mature ADAMDEC1 and E353A were expected to be secreted into the culture media of ExpiSf9 cells infected with the recombinant baculovirus, which needed to be purified before they could be used for functional assays. A combination of diafiltration, immobilised metal affinity chromatography (IMAC) and dialysis was deemed appropriate for the subsequent purification of ADAMDEC1 and E353A.

Diafiltration involves passing a feed solution through a permeable filter membrane, with various molecular weight cut off (MWCO), under pressure. This removes micromolecules below the molecular weight cut off and concentrates the retained macromolecules in a smaller volume. By replenishing the volume lost by fresh solution, diafiltration also allows buffer exchange. This prepares the target protein to be in an optimum binding buffer for the subsequent downstream purification method of choice such as IMAC.

IMAC separates proteins using the affinity of certain peptides towards particular metal ions that are chelated onto resin. The most commonly used IMAC is a combination of nickel and histidine. Histidine is expressed on recombinant proteins as a polyhistidine tag, typically comprising 6 to 10 histidine repeat (6xHis and 10xHis respectively) with an increase in its affinity towards metal ion with its length.[173] Binding buffer of choice for IMAC include HEPES, tris-acetate, tris-HCL and sodium phosphate.[174] In this project, HEPES buffer was selected to be used as a binding buffer since it has a higher stability in maintaining the pH at 7.5.[175] Natural to slightly alkaline pH, pH 7-8, encourages the binding of histidine to the resin, whereas reduction in pH causes protonation of histidine thus breakage of the bonds between histidine and metal ion. Hence achieving accurate pH during the constitution of binding buffer and maintenance of pH during the purification process

are vital.[173] Non-specific binding of proteins to the resin can be reduced by adding a small amount of imidazole (up to 20 mM) to the binding buffer, which competes with histidine for nickel. Non-specific binding proteins can further be removed by multiple washes with a wash buffer containing a higher concentration of imidazole. The target protein with a polyhistidine tag is then finally eluted and collected, most commonly, by a buffer containing a high concentration of imidazole e.g. 500 mM. This elution method using imidazole provides a native condition, thereby likely preserving the biological nature of the protein product.[173] In this project, the imidazole concentration of 500 mM was used for the final elution of the recombinant ADAMDEC1 and E353A off the nickel resin.

Before ADAMDEC1 and E353A can be used for functional assay and protease degradomic analysis, it is desirable to remove imidazole in the elute following IMAC and change the solvent suitable for the downstream assays. Dialysis involves placing protein solution inside a semi-permeable membrane which is suspended in a large volume of dialysate. Small solutes move across the membrane by concentration gradient until the equilibrium is achieved, thereby removing small solutes from protein solution and allowing buffer exchange. In this project, ADAMDEC1 and E353A were dialysed after IMAC, and the buffer was exchanged to PBS.

The main objective of this chapter was to establish and optimise the synthesis and purification of human and mouse ADAMDEC1 and E353A using BEVS, and the purification process described above. Additionally, the catalytical activity of the recombinant human ADAMDEC1 was determined by incubation of the purified recombinant human ADAMDEC1 with α2-macroglobulin and subsequent detection of ADAMDEC1-α2-macroglobulin complex by Western blot. Finally, a potential anti-bacterial property of ADAMDEC1 was tested as a small pilot functional study using recombinant human ADAMDEC1 and E353A and *E. coli* and *Salmonella enterica*.

The main aims for Chapter 5 were:

- To produce bacmid and baculoviruses containing the coding sequence of:
    1. Human ADAMDEC1
    2. Human E353A

3. Mouse ADAMDEC1
4. Mouse E353A

- To infect ExpiSf9 insect cells with the baculoviruses containing the above coding gene to express the recombinant proteins
- To purify the human and mouse ADAMDEC1 and E353A
- To confirm the catalytic activity of human ADAMDEC1 compared to human E353A
- To determine the anti-microbial property of ADAMDEC1 on *E. coli* and *Salmonella enterica* using the recombinant human ADAMDEC1 and E353A

5.2 Materials and method

5.2.1 ExpiSf9 cells

ExpiSf 9 insect cells were kindly gifted by Dr Chris Batters, University of Cambridge. ExpiSf9 cells were cultured and maintained in ExpiSf9 complete medium in T75 vented flask (Greiner) at 27°C in a non-humidified, non-CO_2 atmosphere shaking incubator set at 65 rpm. The cells were passaged every 2- 3 days and maintained at a cell density between 2.5 – 12 x 10^6 /ml.

ExpiSf 9 complete medium

ExpiSf CD media (Thermo Fisher)

1 mg/ml Normocin (Invivogen)

5.2.2 Baculovirus expression vector system

5.2.2.1 Generation of human and mouse ADAMDEC1 coding insert

Untagged human and mouse ADAMDEC1 coding insert with blunt-ends was made from plasmid pCMV-hADAMDEC1-tGFP (Origene RG210181) and pCMV-mADAMDEC1-Myc-DDK (Origene MR223445) respectively by PCR amplification using Q5® Hot Start High-Fidelity DNA Polymerase (NEB) and primers (Table 5.1). Each plasmid was diluted in nuclease-free water (Qiagen) to achieve a concentration of 1 ng/µl. The primers were designed so that the constructs composed a coding sequence for human or mouse ADAMDEC1 without the coding sequence of GFP or Myc-DDK. The primers were made without 5' phosphates as they would inhibit subsequent ligation of the constructs into the vector by Topoisomerase. The components of the PCR reaction mix are summarised in Table 5.2. Triplicates of 50 µl PCR reaction mix were made and run simultaneously on C1000 Touch™ Thermal Cycler (BioRad) with the cycling conditions shown in Table 5.3. An annealing temperature of 62°C was selected for human ADAMDEC1 following gradient PCR using annealing temperatures between 52°C and 64°C. An annealing temperature of 70°C was selected for mouse ADAMDEC1 following gradient PCR using annealing temperature between 66°C and 73°C. Step 2 to 4 of PCR thermal cycling (Table 5.3) were repeated 32 times.

	Forward 5'-3'	Reverse 5'-3'
Human	GCGATCGCCATGCTGCGTGGG	CGTACGCGTCTCTGTGGTATGGTTTGGA
Mouse	GCGATCGCCATGCTGCCTGGG	CGTACGCGTTTCTGTGATGTGGTTGGAT

Table 5.1 Sequences of primers used to amplify human and mouse ADAMDEC1 from plasmid pCMV-hADAMDEC1-tGFP and pCMV-mADAMDEC1-Myc-DDK respectively.

Component	Volume (µl)
5X Q5 Reaction Buffer (NEB)	10
10 mM dNTPs (Thermo Fisher Scientific)	1
10 µM Forward Primer	2.5
10 µM Reverse Primer	2.5
Template DNA plasmid (1 ng/µl)	1
Q5 Hot Start High-Fidelity DNA Polymerase (NEB)	0.5
Nuclease-Free Water (Qiagen)	32.5
Total	**50**

Table 5.2 Components of the PCR reaction for amplification of human and mouse ADAMDEC1 coding sequences from pCMV-hADAMDEC1-tGFP and pCMV-mADAMDEC1-Myc-DDK plasmids respectively.

Step	Temperature	Time	Process
1	98°C	30 seconds	Initial denaturation
2	98°C	10 seconds	Denaturation
3	Human 62°C Mouse 70°C	30 seconds	Annealing
4	72°C	90 seconds	Elongation
5	72°C	30 minutes	Final extension

Table 5.3 PCR condition used for the amplification of human and mouse ADAMDEC1 coding sequences from pCMV-hADAMDEC1-tGFP and pCMV-mADAMDEC1-Myc-DDK plasmids respectively. Step 2 to 4 were repeated 32 times.

5.2.2.2 DNA construct clean-up

Triplicates of 50 µl PCR reaction were pooled together and the amplified DNA constructs were purified using NucleoSpin® Gel and PCR Clean-up kit (Macherey-Nagel) following the manufacture's protocol. All the buffers were provided in the kit. 300 µl of Buffer NTI were added to 150 µl of PCR reaction mix and loaded onto a NucleoSpin® Gel and PCR Clean-up Column in a 2 ml Collection Tube. The

column was centrifuged for 30 seconds at 11000 g and the flow-through was discarded. The column was then placed back in the 2ml collection tube and 700 µl of Buffer NT3 was loaded and tubes were centrifuged for 30 seconds at 11000 g. The flow-through was discarded and the column was placed back in the 2 ml collection tube. A further 700 µl of Buffer NT3 was loaded onto the column and tubes were centrifuged for 30 seconds at 11000 g. The follow-through was discarded and the column was placed in the 2 ml collection tube. The column was centrifuged for 1 minute at 11000 g to remove Butter NT3 completely. The column was then placed into a new 1.5 ml Eppendorf tube and 50 µl of Buffer NE was added to the column. The column was incubated at room temperature for 5 minutes then centrifuged for 1 minute at 11000 g to elute the DNA.

5.2.2.3 Ligation of human and mouse ADAMDEC1 constructs into pFastbac CT-TOPO vector plasmid

Human and mouse ADAMDEC1 constructs were each ligated into linearised pFastBac™/CT-TOPO® Plasmid supplied in Bac-to-Bac™ C-His TOPO™ Cloning Kit (Thermo Fisher Scientific) following the manufacturer's protocol. The vector to insert molar ratio of 1:2 was chosen after optimisation. The mass of the construct required for the ligation reaction was calculated using NEBBioCalculator Ligation Calculator https://nebiocalculator.neb.com/#!/ligation. Based on this 6 ng of human and mouse ADAMDEC1 construct was mixed with 1 ng of pFastBac™/CT-TOPO® vector plasmid and 1 µl of Salt Solution (provided in the kit) in a 0.2 ml non-flex PCR tube (StarLab). Sterile water (provided in the kit) was added to achieve the final reaction volume of 6 µl. The ligation reaction mixtures were mixed gently then incubated at room temperature for 1 hour.

5.2.2.4 Transformation of One Shot™ Mach1™ T1R Chemically Competent *E. coli* with pFastBac-ADAMDEC1-His

Immediately after 1 hour of the ligation incubation period, One Shot™ Mach1™ T1R Chemically Competent *E. coli* (provided in the kit) were transformed with the ligated product (referred to as pFastBac-ADAMDEC1-His hereafter). One vial of One Shot™ Mach1™ T1R Chemically Competent *E. coli* was thawed on ice. 2 µl of the ligation mix was then pipetted onto the competent *E. coli* cells and mixed by gentle tapping of the tube and incubated on ice for 30 minutes. The cells were then

heat shocked by incubation in a water bath set to 42°C for exactly 30 seconds. The vial was then placed immediately on ice for 2 minutes before 250 µl of pre-heated S.O.C. media (Sigma-Aldrich) was added. The transformation mix was then incubated at 37°C for exactly 1 hour on constant agitation at 250 rpm in ThermoMixer® Comfort (Eppendorf). After 1 hour, a two-fold serial dilution of transformed *E. coli* was plated on LB-Amp agar plates. Plates were inverted and incubated at 37°C overnight. After overnight incubation, 16 bacterial colonies were picked individually using sterile inoculating loop (VWR) and dropped into 6 ml of LB-Amp broth. The LB broth containing the bacterial colonies was then incubated at 37°C for 8 hours on constant agitation at 250rpm. After the incubation period, half of each bacterial culture was used to create a glycerol stock of the transformed bacteria as described in Chapter 2.6.2. The other halves were used to isolate DNA to analyse the presence and exact sequence of human and mouse ADAMDEC1 in these bacterial cultures.

5.2.2.5 Extraction, purification and analysis of recombinant pFastbac CT-TOPO plasmid

The plasmid DNA was extracted from each bacterial culture produced in Chapter 5.2.2.4 by Miniprep (Chapter 2.6.3.1). The concentration and quality of the extracted DNA were measured using NanoDrop Spectrometer. The isolated plasmid DNA from each bacterial culture was sequenced by Eurofin Genomics Custom DNA sequencing service and their Mix2Seq kits (Chapter 2.6.1) using polyhedrin and SV40 primers (Table 4.5). These primers were provided in Bac-to-Bac™ C-His TOPO™ Cloning Kit.

Polyhedrin forward primer 5'-3'	AAATGATAACCATCTCGC
SV40 reverse primer 5'-3'	GTGGTATGGCTGATTATGATC

Table 5.4 Sequences of polyhedrin and SV40 primers.

Upon receival of the sequence results, the presence, correct orientation and exact sequence of human and mouse ADAMDEC1 within the pFastBac-ADAMDEC1-His extracted from each bacterial culture were checked. A bacterial culture with the ADAMDEC1 construct in the correct orientation, with the N-terminus coding sequence placed adjacent to the polyhedrin end of the vector, and sequence was selected for the next step.

5.2.2.6 Transformation of MAX Efficiency® DH10Bac™ chemically competent *E. coli* with the plasmid DNA

The bacterial culture containing the ADAMDEC1 construct of correct sequence in the correct orientation within the pFastBac-ADAMDEC1-His was selected. Its frozen stock was thawed and restreaked on LB-Amp agar plate and incubated at 37°C overnight. Following this, one colony was picked using a sterile inoculating loop (VWR) and dropped into 300 ml of LB-Amp broth. The bacterial culture was then incubated at 37°C with constant agitation at 250 rpm overnight. The DNA in this bacterial stock was isolated and purified using HiSpeed Plasmid Maxi Kit (Qiagen) (Chapter 2.6.3.2). The concentration and quality of the extracted DNA were measured using NanoDrop Spectrometer (Chapter 2.5).

The purified DNA of pFastBac-ADAMDEC1-His was diluted to 0.2 ng/µl with nuclease-Free water (Qiagen). One vial of MAX Efficiency® DH10Bac™ chemically competent *E coli* (provided in Bac-to-Bac® TOPO® Expression System Kit) was thawed on ice, and 100 µl of it was transferred gently into a pre-chilled 1.5 ml Eppendorf tube. 5 µl of the purified pFastBac-ADAMDEC1-His was then pipetted in the MAX Efficiency® DH10Bac™ chemically competent *E. coli* and mixed gently. The mixture was incubated on ice for 30 minutes and heat shocked at 42°C for exactly 45 seconds in a pre-heated water bath. Following this, the tube was immediately transferred onto ice and incubated for 2 minutes. 900 µl of pre-warmed S.O.C. medium (Sigma) was added and incubated at 37°C on constant agitation at 225 rpm for 4 hours. After 4 hours, a 10-fold serial dilution of transformation bacterial culture was made using pre-warmed S.O.C. medium (Sigma). 100 µl of each dilution of the bacterial culture was plated on LB agar plate augmented with kanamycin (50 µl/ml), gentamicin (7 µl/ml), tetracycline (10 µl/ml), Bluo-gal (100 µl/ml) and IPTG (40 µl/ml). The plates were then incubated at 37°C for 48 hours. After 48 hours, 4 white colonies were picked using sterile inoculating loops (VWR) and restreaked once again onto fresh agar plates augmented with kanamycin, gentamicin, tetracycline, Bluo-gal and IPTG of the same concentrations as previously used. The plates were incubated overnight at 37°C. After the overnight incubation, two single white colonies were isolated from the plate with only white colonies grown on the agar. These bacterial colonies were inoculated separately into 300 ml of LB broth containing 50 µg/ml kanamycin, 7

µg/ml gentamicin, and 10 µg/ml tetracycline and incubated overnight at 37°C on constant agitation at 225 rpm.

5.2.2.7 Extraction and purification of recombinant bacmid DNA

Following the overnight incubation of the bacterial culture, the bacmid DNA was extracted and purified using PureLink™ HiPure Plasmid Maxiprep Kit (Thermo Fisher) following the manufacturer's protocol. The large size of bacmid required this special Maxiprep DNA extraction kit instead of the ordinary Maxiprep (Chapter 2.6.3.2). All the buffers were provided in the kit. Firstly, 30 ml of Equilibration Buffer was added to PureLink HiPure Maxi Column and the buffer was allowed to drain out of the column by gravity. The bacterial cultures (300ml) produced in Chapter 5.2.2.6 were centrifuged for 10 minutes at 4000 g to pellet the bacterial cells, and the supernatant was discarded. 20 ml of Resuspension Buffer with RNase A was added to the bacterial cell pellets and vortexed to resuspend the cells completely. 20 ml of Lysis Buffer was added to the cells and mixed gently by inverting the tube until the mixture was homogenous. The lysate was then incubated at room temperature for 5 minutes. 10 ml of Precipitation Buffer was added to the lysate and mixed by inverting the tube until the mixture was homogenous. The mixture was centrifuged at 12000 g for 10 minutes. The supernatant from the lysate mixture was carefully removed without disrupting the precipitants, containing cell debris, at the bottom of the tube and loaded onto the equilibrated PureLink HiPure Maxi Columns. 60 ml of Wash Buffer was then added to the column and allowed to drain from the column by gravity. The column was then placed over 50 ml Falcon tube and 15 ml of Elution Buffer was added to the column to elute the DNA into the Falcon tube. 10.5 ml of 100% isopropanol (VWR) was added to the elution solution and mixed well by inverting the tube 20 times to precipitate DNA. The tube was then centrifuged at 12000 g for 30 minutes at 4°C. The supernatant was carefully removed and discarded. 5 ml of 70 % ethanol was added into the tube to resuspend the DNA at bottom of the tube before the tube was centrifuged at 12000 g for 5 minutes at 4°C. The supernatant was carefully removed and discarded. The DNA at the bottom of the tubes was then air-dried inside a vertical laminar flow sterile cabinet for 30 minutes to ensure complete evaporation of the ethanol. The DNA pellet was resuspended in 500 µl TE Buffer. The concentration and quality of DNA were measured using NanoDrop Spectrometer (Chapter 2.5). The purified DNA

was transferred to 0.2 ml non-flex PCR tubes (StarLab) in aliquots of 50 µl to avoid repeated freezing and thawing in the future and stored at -80°C.

5.2.2.8 Analysis of the Bacmid DNA plasmid by PCR

PCR was performed on the purified recombinant bacmid using Q5® Hot Start High-Fidelity DNA Polymerase (NEB) as described in Chapter 5.2.2.1, and pUC/M13 forward primer and pUC/M13 reverse primer (Table 5.5). The sequences for these primers were provided in Bac-to-Bac™ C-His TOPO™ Cloning Kit (Thermo Fisher Scientific) and the primers were custom ordered from Sigma. An annealing temperature of 66°C was used as per manufacturer's protocol. The presence of ADAMDEC1-His in the bacmid plasmid was then confirmed by subsequent gel electrophoresis of the PCR products as described in Chapter 2.6.4.3. Additionally, PCR clean-up was then performed on the PCR product using NucleoSpin® Gel and PCR Clean-up kit (Macherey-Nagel) as described in Chapter 5.2.2.2. The exact nucleotide sequence of the ADAMDEC1-His within the bacmid was then confirmed by sequencing of the cleaned PCR product with polyhedrin and SV40 primers (Table 5.4) by Eurofin Genomics Custom DNA sequencing service as described in Chapter 2.6.1.

pUC/M13 Forward primer 5'-3'	CCCAGTCACGACGTTGTAAAACG
pUC/M13 Reverse primer 5'-3'	AGCGGATAACAATTTCACACAGG

Table 5.5 Sequences of pUC/M13 forward and reverse primers used to amplify the transposed sequence within the recombinant bacmid.

5.2.2.9 Site-directed mutagenesis for the generation of E353-His bacmid

A point mutation was introduced to the ADAMDEC1 coding sequence within pFastBac-ADAMDEC1-His created in Chapter 5.2.2.1 – 5.2.2.5 to generate pFastbac CT-TOPO transfer vector encoding E353A by PCR. Phusion™ Site-Directed Mutagenesis Kit (Thermo Fisher Scientific) was used following the manufacturer's protocol. Human and mouse pFastBac-ADAMDEC1-His created and purified in Chapter 5.2.2.1 – 5.2.2.5 were used as the template plasmids. The primers used to introduce the single point mutations in the human and mouse ADAMDEC1 coding sequence were designed manually and custom ordered from

Sigma (Table 5.6). The primers were designed to be phosphorylated at the 5' end to facilitate the circularisation of the PCR product. The annealing temperatures of 68.4°C and 70.3°C were calculated for human E353A and mouse E353A respectively for the mutagenesis PCR. These temperatures were calculated by the annealing temperature calculator on https://thermofisher.com/tmcalcultor as per protocol. The components and condition of the PCR for site-directed mutagenesis are summarised in Table 5.7 and Table 5.8 respectively. Step 2 to 4 of the PCR thermal cycling (Table 5.8) were repeated 25 times.

hE353A forward 5'-3'	[Phos]TGATGTCACATG**C**GCTGGGCCATGTC
hE353A reverse 5'-3'	[Phos]CTCCTACAAGAGCCACATTATTCTTTTTTTTAGCCTCA
mE353A forward 5'-3'	[Phos]TGATGTCACATG**C**GTTGGGCCACGCC
mE353A reverse 5'-3'	[Phos]GTGCAACAAGAGCCACATTATTCTTTTTTTTAGCCTCA

Table 5.6 Sequences of the mutagenic primers used to introduce single point mutations to generate pFastbac CT-TOPO transfer vector encoding human or mouse E353. The letters in red are the single point mutations incorporated into the primer.
hE353A: Human E353A, mE353A: Mouse E353A

Component	Volume (µl)
5x Phusion HF Buffer	10
10 mM dNTPs	1
10 µM Forward primer	2.5
10 µM Reverse primer	2.5
Template plasmid (50 ng/µl)	2
Phusion Hot Strat DNA Polymerase	0.5
Nuclease-free water	31.5
Total	**50**

Table 5.7 Components of the mutagenesis PCR reaction to generate pFastbac CT-TOPO transfer vector encoding human and mouse E353

Step	Temperature	Time	Process
1	98°C	30 seconds	Initial denaturation
2	98°C	10 seconds	Denaturation
3	Human 68.4°C Mouse 70.3°C	30 seconds	Annealing
4	72°C	3 minutes 50 seconds	Elongation
5	72°C	7 minutes	Final extension

Table 5.8 PCR condition for the mutagenesis PCR to generate pFastbac CT-TOPO transfer vector encoding human or mouse E353. Step 2 to 4 were repeated 25 times.

DpnI digestion was performed on the PCR products to destroy the template plasmids in the PCR reaction mix. For this, 1 µl of FastDigest DpnI enzyme was directly added to each mutagenesis PCR products and incubated at 37°C overnight. After this, ligation of the PCR products was performed using T4 DNA Ligase kit (provided in Phusion™ Site-Directed Mutagenesis Kit). The components of the reaction mix (Table 5.9) were added together in a 0.2 ml non-flex PCR tube (StarLab) and incubated at room temperature for 15 minutes.

Component	Volume (µl)
PCR product	1
5x Ligation buffer	2
T4 DNA Ligase	6.5
Nuclease-free water	0.5
Total	**10**

Table 5.9 Components of the ligation reaction mix for ligation of the mutagenesis PCR product.

5.2.2.10 Generation of hE353A-His and mE353A-His encoding bacmids

Chapter 5.2.2.4 - 5.2.2.8 were repeated using pFastbac CT-TOPO transfer vector encoding human and mouse E353 to generate bacmids encoding human and mouse E353A.

5.2.3 Transfection of ExpiSf9 cells to generate recombinant baculovirus encoding human and mouse ADAMDEC1-His and E353A-His

ExpiSf 9 cells were transfected with the recombinant bacmid using ExpiFectamine Sf Transfection Reagent (Gibco) following the manufacturer's protocol. 62.5 x 10^6 viable ExpiSf 9 cells were transferred into 50 ml Falcon tube and centrifuged at 300 g for 5 minutes. The supernatant was discarded and the cells were resuspended in 25 ml of fresh ExpiSF CD medium without Normocin to make 25 ml of ExpiSf 9 cell culture at a cell density of 2.5 x 10^6 /ml. The cells were then transferred into T75 flask. 30 µl of the ExpiFectamin Sf Transfection Reagent was added to 1 ml of Opti-MEM Reduced Serum Medium (Thermo Fisher Scientific) in 1.5 ml Eppendorf tube. The tube was inverted 10 times gently to mix the solution. The solution was incubated at room temperature for 5 minutes after which 12.5 µg of the recombinant bacmid DNA generated and purified were added and gently mixed by inverting the tube 10 time. The mixture was incubated at room temperature for 5 minutes. The transfection mixture was added dropwise to the ExpiSf9 cells prepared in T75 flask. The flask was swirled during the addition of the transfection mixture to ensure uniform delivery of the transfection mixture. ExpiSf9 cells were then incubated at 27°C in a non-humidified, non-CO_2 atmosphere shaking incubator set at 65 rpm. Based on the viability and appearance of the transfected cells under a light microscope, 96 hours was deemed the optimum timepoint at which the P0 baculovirus should be harvested. Thus, 96 hours after the transfection, the cell culture was transferred into a 50 ml Falcon tube and centrifuged at 300 g for 5 minutes. The supernatant containing P0 baculovirus was harvested and filtered through PES 0.22 µm Syringe filter (Appleton Woods). The harvested P0 baculovirus stocks were aliquoted into autoclaved 5 ml Eppendorf tubes and stored at -80°C.

5.2.4 Infection of ExpiSf9 cells with P0 baculovirus for protein expression

To optimise the protein expression protocol, infection of ExpiSf9 cells for protein expression was carried out using either 250 µl or 500 µl of the harvested P0 baculovirus encoding human ADAMDEC1 or E353A per 25 ml of ExpiSf9 cell culture, at a cell density of 5 x 10^6 /ml. The P0 baculovirus stocks were thawed and

either 250 µl or 500 µl of them were added to ExpiSf9 cells in T75 flask and incubated at 27°C in a non-humidified, non-CO_2 atmosphere shaking incubator set at 65 rpm. To determine the optimum timepoint to harvest the cells or supernatants for subsequent protein purification, 100 µl of the infected cell culture were collected at 24, 48, 72 and 96 hours post-infection into 1.5 ml Eppendorf tubes and centrifuged at 300 g for 5 minutes at 4°C. The supernatants were transferred into a fresh 1.5 ml Eppendorf tubes and stored at -80°C for the subsequent Western blot as described in Chapter 2.8. 100 µl of RIPA buffer (Thermo Fisher Scientific), 2 µl of Halt Protease and Phosphatase Inhibitor Cocktail x 100 (Thermo Fisher Scientific), 0.4 µl of Benzonase (Merk) and 0.2 µl of 2 mM Pepstatin A (Merk) were added to each cell pellet collected at each timepoint and pipetted up and down and incubated on ice for 10 minutes before they were stored at -80°C for subsequent Western blot as described in Chapter 2.8. This optimisation experiment revealed that the mature human ADAMDEC1 and E353A were present in the culture supernatant of the infected ExpiSf9 cells and that 250 µl of P0 baculovirus was efficient to infect 25 ml of ExpiSf9 cell culture, at a cell density of 5 x 10^6 /ml. The optimum time to harvest the culture supernatant of the infected ExpiSf9 was deemed to be 72 hours. Thus the subsequent rounds of infection of ExpiSF9 cells with P0 baculovirus for protein expression were performed using these conditions.

5.2.5 Purification of the recombinant mature human and mouse ADAMDEC1 and E353A by immobilised metal affinity chromatography (IMAC)

Binding buffer

50 mM HEPES

300 mM NaCl

10 mM Imidazole

Adjusted to pH 7.5 at 4°C

Elution buffer

50 mM HEPES

300 mM NaCl

500 mM Imidazole

Adjusted to pH 7.5 at 4°C

Both binding buffer and elution buffer were made and filtered through 0.22 µm PES Vacuum filter system using vacuum aspiration system (SciPette) and stored at 4°C.

5.2.5.1 Diafiltration of the harvested supernatants containing the recombinant protein

ExpiSf9 culture media were collected 72 hours after the cells were infected with P0 baculovirus. The cells were removed from the media by 2 rounds of centrifugation at 300 g for 5 minutes followed by 800 g for 5 minutes. The supernatant was filtered through Acrodisc® Syringe Filter 0.2 µm Supor® Membrane (Pall) to ensure complete removal of the cells. The supernatant was then passed through Vivaflow 200 diafiltration membrane (Sartorius), with MWCO of 10 kDa. The diafiltration and buffer exchange were performed over 40 minutes, as per manufacturer's protocol, to concentrate the supernatant harvested in the binding buffer containing 10 mM of imidazole.

5.2.5.2 IMAC to purify the recombinant proteins

0.01 volumes of Halt Protease and Phosphatase Inhibitor Cocktail x 100 (Thermo Fisher) were added to the concentrated sample following the diafiltration, which was then loaded onto 1 ml of nickel-IMAC resin (HisPur™ Ni-NTA Resin, Thermo Fisher) in a 50ml Falcon tube and incubated overnight at 4°C on a roller mixer. After the overnight incubation, the tube containing the nickel resin and the sample was centrifuged at 700 g for 3 minutes at 4°C and the flow-through containing proteins unbound to the nickel resin was removed carefully without disturbing the resin. The nickel resin was then washed several times with 10 ml of wash buffer containing various concentrations of imidazole. During the protocol optimisation, the imidazole concentrations of 20 to 120 mM, in an increment of 20 mM, were used in the wash buffer to determine the concentration of imidazole at which the maximum amount of non-specific binding proteins would be eluted off the nickel resin without disturbing the interaction between the His-tag and nickel significantly. Following the protocol optimisation, imidazole concentration of 60 mM was deemed optimum to remove the non-specific binding proteins most effectively thus the nickel resin was washed 5 times with wash buffer containing 60 mM imidazole. After each wash, the sample was centrifuged at 700 g for 3 minutes at 4°C and supernatants were removed carefully without disturbing the nickel resin. The

recombinant proteins were then eluted by adding 2 - 3 ml of elution buffer, with imidazole concentration of 500 mM, which was repeated 3 times.

5.2.5.3 Dialysis of the purified recombinant proteins

A dialysis cassette (Slide-A-Lyzer™ Dialysis Cassettes MWCO 10 kDa 12ml, Thermo Fisher Scientific) was used to dialyse the purified recombinant proteins after IMAC following the manufacturer's protocol. The cassette was submerged in PBS for 2 minutes to hydrate the dialysis membrane. The three lots of elutes from IMAC described above were pooled together and pipetted carefully into the dialysis cassette. The dialysis cassette was then placed in a beaker containing 2 litre of pre-chilled PBS and dialysed at 4°C with gentle swirling for 2 hours. After this, the PBS was changed and the sample was dialysed for further 2 hours in the fresh PBS. After this, PBS was changed once again and the sample was dialysed overnight in the fresh PBS at 4°C. After the overnight dialysis in PBS, the final purified sample was transferred out of the cassette and aliquoted and stored at -80°C as purified recombinant protein stock.

5.2.6 Trichloacetic acid precipitation of protein samples

Resuspension buffer

4% SDS

0.2 M Tris-HCl

0.15 M NaOH

At each step of the purification process, a small volume (30-300 µl) of the solution was collected from the sample and stored at -80°C. 1 in 10 volumes of 0.15% Sodium deoxycholate was added to each solution collected at each step of the purification process. The mixtures were mixed by pipetting and incubated at room temperature for 5 minutes. Following this, 1 in 10 volumes of 72% TCA was added to each sample and mixed by pipetting and incubated at room temperature for 10 minutes. The precipitated proteins were pelleted by centrifugation at 17000 g for 10 minutes. The supernatants were removed and discarded carefully using 0.5 mm gel-loading pipet tip (BioRad) and vacuum aspiration system (SciPette). The proteins were resuspended in 14 µl of the resuspension buffer.

5.2.7 Purity analysis of the sample fractions collected at each step of purification process by SDS-PAGE Coomassie stain and Western blot

12 µl of each protein sample resuspended at the end of TCA precipitation was mixed with Laemmli sample buffer (4x) (BioRad) and 2-mercaptoethanol (Sigma M6250), making up 25% and 2.5% of the final sample volume respectively. The mixtures were incubated at 75°C for 15 minutes and loaded onto 12% SDS-PAGE gel made as described in Chapter 2.8.4. The gel was placed in Mini-PROTEAN® Tetra Cell (BioRad) and submerged in ~700 ml of the running buffer (x1) as described in chapter 2.8.4. Electrophoresis was run for ~ 75 minutes at a constant voltage of 120V. Following this, the SDS-PAGE gel was washed in distilled water and staining of proteins was performed by incubating the gel in 10 ml of QC Colloidal Coomassie Stain (BioRad) overnight. After this, the SDS-PAGE gel was washed 3 times with distilled water. The destained SDS-PAGE gel was placed over a lightbox and the image was captured.

The remaining 2 µl of each protein concentrated and resuspended in the resuspension buffer at the end of TCA precipitation was diluted in 18 µl of PBS. This was mixed with Laemmli sample buffer (4x) (BioRad) and 2-mercaptoethanol (Sigma M6250), making up 25% and 2.5% of the final sample volume respectively. The mixture was incubated at 75°C for 15 minutes. These were used for Western blot as described in Chapter 2.8

5.2.8 Quantification of the purified recombinant proteins by densitometry

The concentration of the purified recombinant ADAMDEC1 and E353A were determined by SDS-PAGE gel and densitometry using Image-J. 2.5 µl, 5 µl and 10 µl of each purified recombinant protein were diluted and made up to 20 µl in PBS. These diluted purified recombinant proteins and 20 µl of the undiluted purified recombinant proteins were each mixed with Laemmli sample buffer (4x) (BioRad) and 2-mercaptoethanol (Sigma M6250), making up 25% and 2.5% of the final sample volume respectively. Bovine serum albumin (BSA) of various masses (0.125 µg – 2 µg) were diluted in 20 µl of PBS and loading samples were made by adding Laemmli sample buffer (4x) (BioRad) and 2-mercaptoethanol (Sigma M6250), with Laemmli sample buffer (4x) and 2-mercaptoethanol making

up 25% and 2.5% of the final sample volume respectively. The mixtures were incubated at 75°C for 15 minutes. The loading samples of the each recombinant protein and BSA were loaded onto a single 12% SDS-PAGE gel and electrophoresis was run for 95 minutes at a constant voltage of 100V. The gel was stained with 10 ml of QC Colloidal Coomassie Stain (BioRad) overnight. After this, the SDS-PAGE gel was washed 3 times with distilled water. The destained SDS-PAGE gel was placed over a lightbox and the image was captured and analysed using Image J (NIH). The densities of the BSA bands on the SDS-PAGE were used to generate a linear standard curve. The concentrations of the recombinant proteins were calculated using the equation generated by the standard curve.

5.2.9 Incubation of the recombinant human ADAMDEC1 and E353A with α2-macroglobulin

The recombinant human ADAMDEC1 and E353A were incubated with human α2-macroglobulin (Sigma) to determine their catalytic activities. Based on concentrations of the recombinant proteins determined by densitometry described in Chapter 5.2.8, the recombinant human ADAMDEC1 or E353A were mixed with human α2-macroglobulin and ZnCl in PBS to achieve final concentrations of 50 ng/µl, 900 ng/µl and 10 µM respectively in volume of 50 µl. The reaction mixtures were incubated at 37°C for 48 hours. Following this, 15 µl of 4x Laemmli sample buffer (BioRad) and 1.67 µl of 2-mercaptoethanol were added to each reaction mixture which were then incubated at 75°C for 15 minutes. The samples were analysed by Western blot using anti-His primary antibody as described in Chapter 2.8.

5.2.10 Bacterial growth curve assay with the recombinant ADAMDEC1 and E353A

Salmonella enterica subsp. enterica serovar Typhimurium (strain JT11), a clinical isolate kindly provided by Dr Elizabeth de Pinna, Public Health England, and *E. coli* NCTC 10418 (TCS Biosciences) were used to examine the potential anti-bacterial property of ADAMDEC1. The bacteria were plated on LB agar plates separately and incubated over night at 37°C. A single colony was picked from each plate and placed in 10 ml of LB broth and incubated at 37°C for 7 hours. The optical

densities of the bacterial cultures were determined at OD_{600} using a Cecil BioQuest™ CE2502 spectrophotometer and the bacterial cultures were diluted with LB broth as necessary to achieve OD_{600} of approximately 0.16. 190 µl of each bacteria culture were pipetted in each well of a 96-well flat-bottomed culture plate (Thermo Fisher Scientific). The purified recombinant human ADAMDEC1 was diluted in sterile PBS to achieve concentrations of 125 ng/µl, 37.5 ng/µl and 12.5 ng/µl. 10 µl of these diluted recombinant human ADAMDEC1 were added to each well containing the bacterial culture to achieve the final concentrations of 6.25 ng/µl, 1.875 ng/µl and 0.625 ng/µl of ADAMDEC1 in each well. 3 replicates were made for each incubation condition. This was repeated using the recombinant human E353A. The control wells containing either no recombinant proteins or bacteria were also made. The plate was sealed with a gas-permeable sealing film (Thermo Fisher Scientific) and set in a shaking microplate reader, CLARIOstar Plus (BMG Labtech) set at 37°C, 5% CO_2. The OD_{600} of each well was read every 20 minutes until the reading became static.

5.3 Results

5.3.1 Generation of a bacmid encoding human ADAMDEC1 with a C-terminal 6 x Histidine tag (hADAMDEC1-His)

5.3.1.1 Generation of hADAMDEC1 coding insert

5.3.1.1.1 Primer design and optimisation of PCR

Human ADAMDEC1 (hADAMDEC1) coding region was amplified from the plasmid pCMV-hADMDEC1-tGFP (Origene, RG210181) which encoded hADAMDEC1 with a C-terminal GFP-tag. PCR primers were designed manually to amplify the hADAMDEC1 coding region without the GFP-tag (Figure 5.2). Q5 High-Fidelity Polymerase was used, which has extremely low error rate, 5.3 x 10^{-7}, to ensure accurate replication of the template.[176]

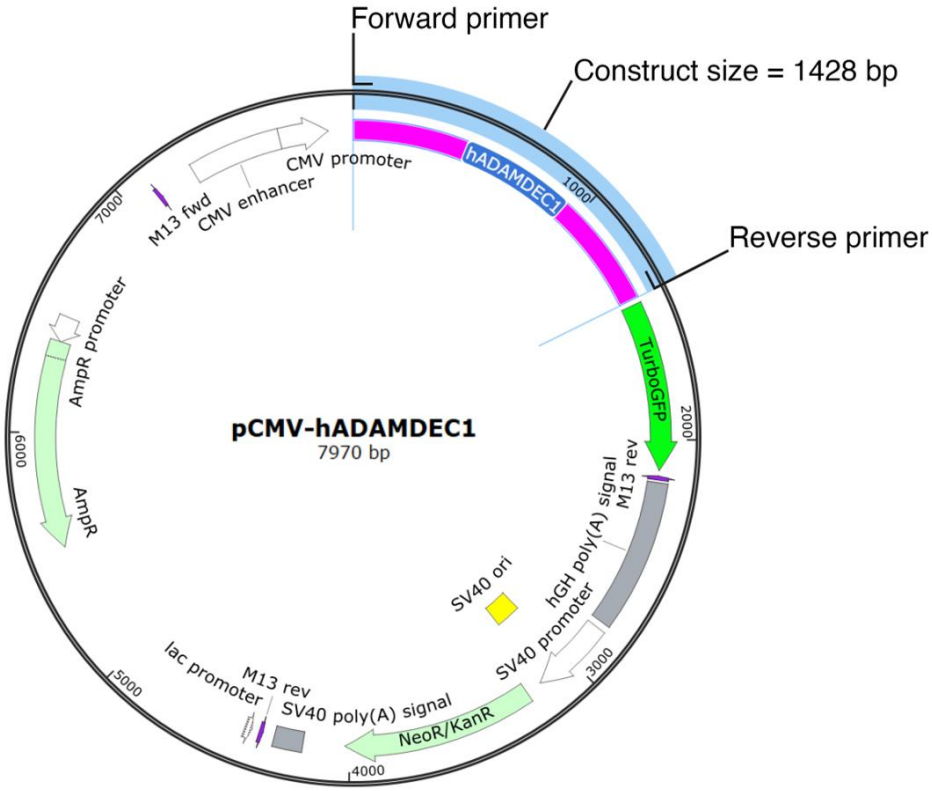

Figure 5.2 A plasmid map of pCMV-hADAMDEC1 encoding hADAMDEC1-GFP. Primers were designed to amplify hADAMDEC1 from the pCMV-hADAMDEC1 plasmid (Origene RG210181) without the GFP-tag (1428 bp in size). The image was generated in SnapGene viewer.

Gradient PCR was performed to determine the optimal primer annealing temperature to generate the hADAMDEC1 amplicon (1428 bp). To help narrow down the range of annealing temperature to be tested by gradient PCR, primer sequences were entered into the NEB TM Calculator online tool (https://tmcalculator.neb.com/#!/main; accessed on 10th May 2019). An annealing temperature of 59°C was recommended thus, a gradient PCR was performed with annealing temperatures ranging from 52 – 64°C. The PCR products separated by electrophoresis on an agarose gel revealed that an annealing temperature between 61.2°C and 63.1°C would produce the most product around the expected size of the hADAMDEC1 amplicon with minimal additional products, e.g. primer dimers (Figure 5.3). An annealing temperature of 62°C was therefore chosen for subsequent PCR to generate hADAMDEC1 insert.

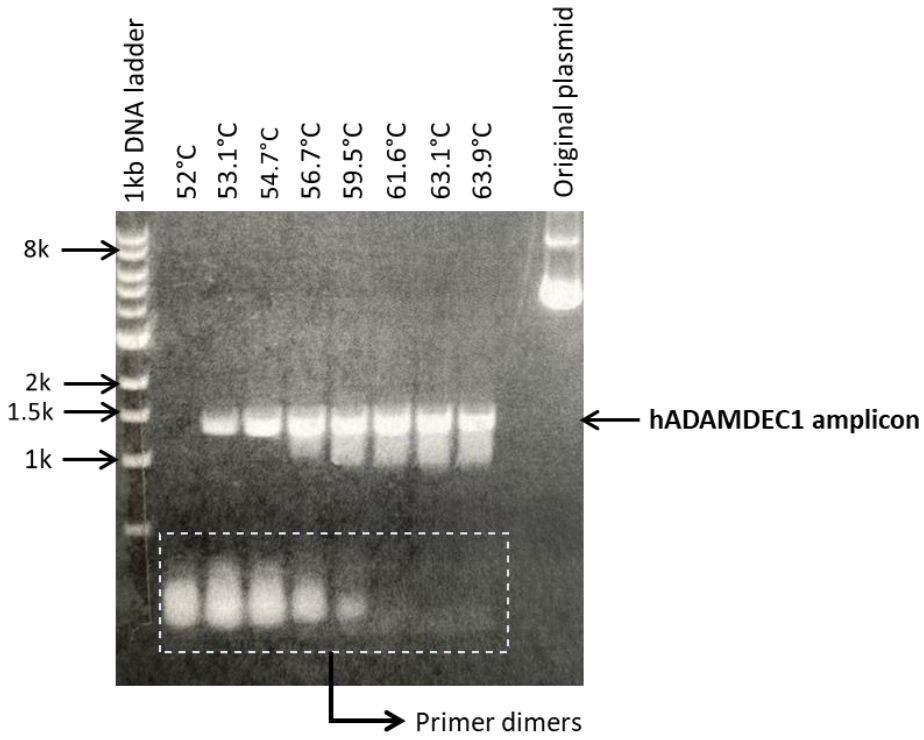

Figure 5.3 Agarose gel electrophoresis of the PCR products generated by gradient PCR to determine the optimal annealing temperature for generation of hADAMDEC1 insert. 2% agarose gel was used.

5.3.1.1.2 Generation of hADAMDEC1 insert by PCR

High fidelity PCR was repeated with an annealing temperature of 62°C in a triplicate of 50 µl reaction volume, and DNA purification was followed to remove primers, enzymes and nucleotides. Since the gel electrophoresis consistently demonstrated that the PCR was producing only a single construct with the correct size i.e. 1428 bp (Figure 5.4), the DNA purification was performed simply using the NucleoSpin PCR clean-up columns (Chapter 5.2.2.2) without gel extraction method.

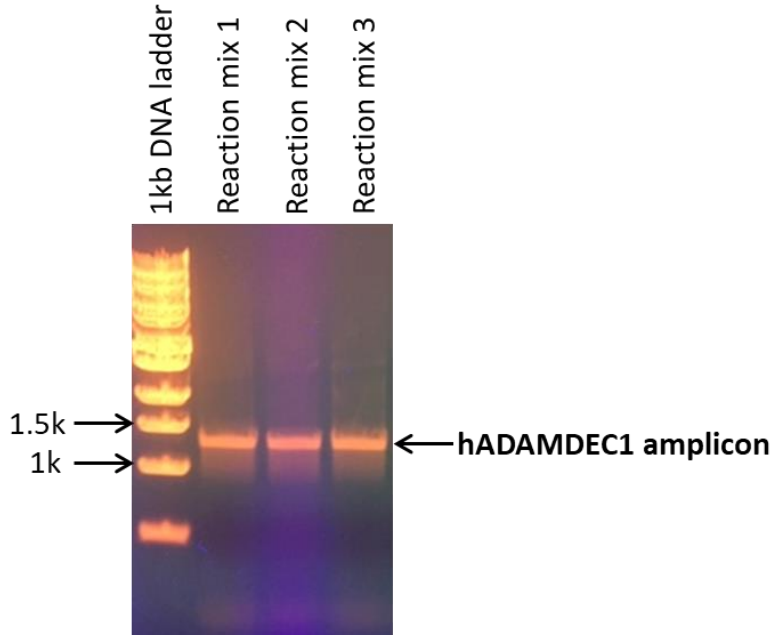

Figure 5.4 Agarose gel electrophoresis of the PCR product for generation of hADAMDEC1 amplicon visualised under ultraviolet light. Only a single construct with the correct size i.e. 1428 bp was seen in each reaction mix.

5.3.1.2 Ligation of hADAMDEC1 construct into pFastBac™/CT-TOPO® transfer vector plasmid

Direct insertion of a construct into bacmid is not feasible due to the large size of bacmid. Thus the construct is required to be inserted initially into a transfer vector. pFastBac™/CT-TOPO® plasmid (referred to as pFastBac plasmid hereafter) is a linearised transfer vector that accepts a blunt-end construct by TOPO cloning method. Introduction of hADAMDEC1 insert at the linearised cloning site within this plasmid results in a coding region that includes hADAMDEC1 with a 3' TEV (*Tobacco etch virus*) cleavage site followed by a region encoding a 6x histidine tag (referred to as His-tag hereafter) (Figure 5.5). Following the protein expression, the

C-terminal His-tag would allow for the subsequent purification of hADAMDEC1 using IMAC.

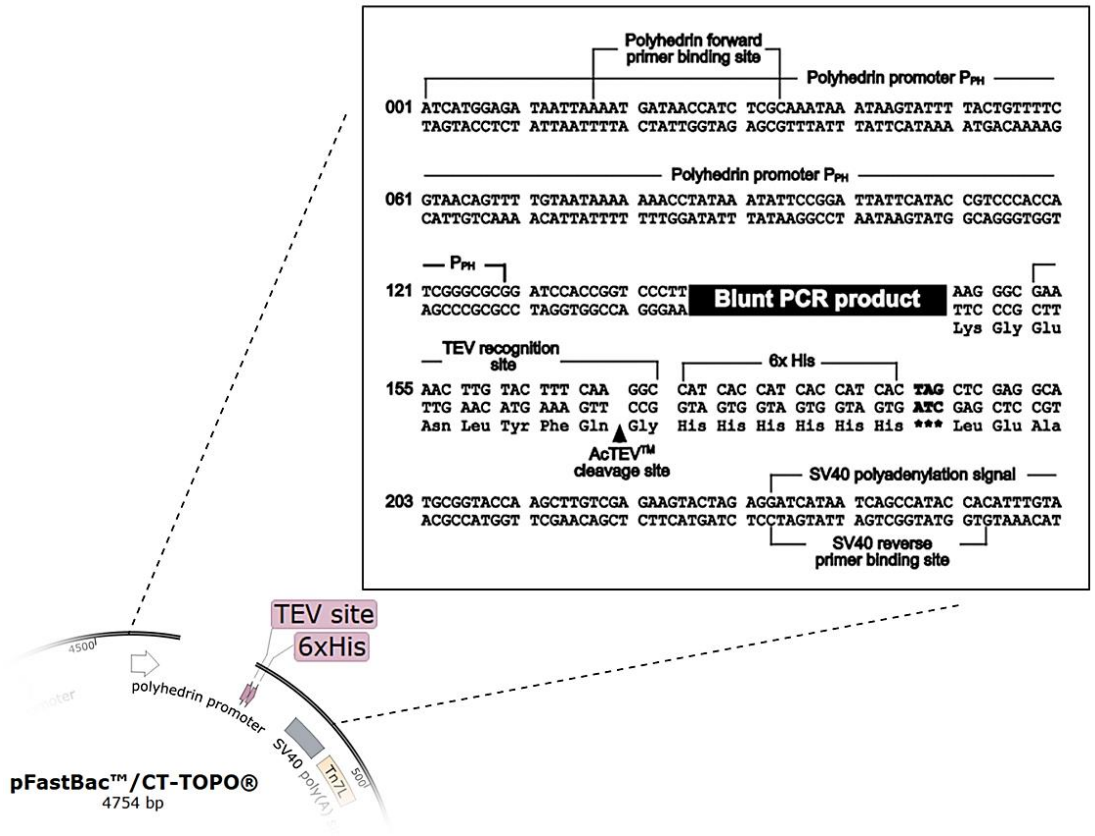

Figure 5.5 Cloning site of pFastBac/CT-TOPO plasmid. The positions of PCR product to be inserted, 6x histidine-tag and the binding sites for polyhedrin forward primer and SV40 reverse primer within are shown. A part of the figure was adapted from Bac-to-Bac™ TOPO™ Cloning Kit user guide.[325]
TEV: *Tobacco etch virus*, 6x His: 6x Histidine

For successful ligation of an insert into a vector, an optimal vector to insert ratio needs to be considered. To determine the optimum ligation molar ratio, ligation of the purified hADAMDEC1 insert and the linearised pFastBac plasmid was performed using vector to insert molar ratios of 1:1, 1:2 and 1:3. To confirm ligation success, PCR was then performed using the ligation products and the primers that recognise polyhedrin and SV40 coding regions 5’ and 3’ of the insertion site, respectively (Figure 5.6). If successful, a PCR product of around 1668 bp would be generated (Figure 5.6). All three vector to insert ratios tested were found to yield products around 1668 bp suggesting the formation of the pFastBac plasmid

containing hADAMDEC1 insert (referred to as pFastBac-hADAMDEC1-His hereafter) (Figure 5.7). However, the ligation product generated from using a vector to molar ratio of 1:2 appeared to produce slightly more PCR product. Therefore, the ligation reaction was repeated/scaled-up using a molar ratio of 1:2 with the resulting ligation product used in the transformation of competent bacteria.

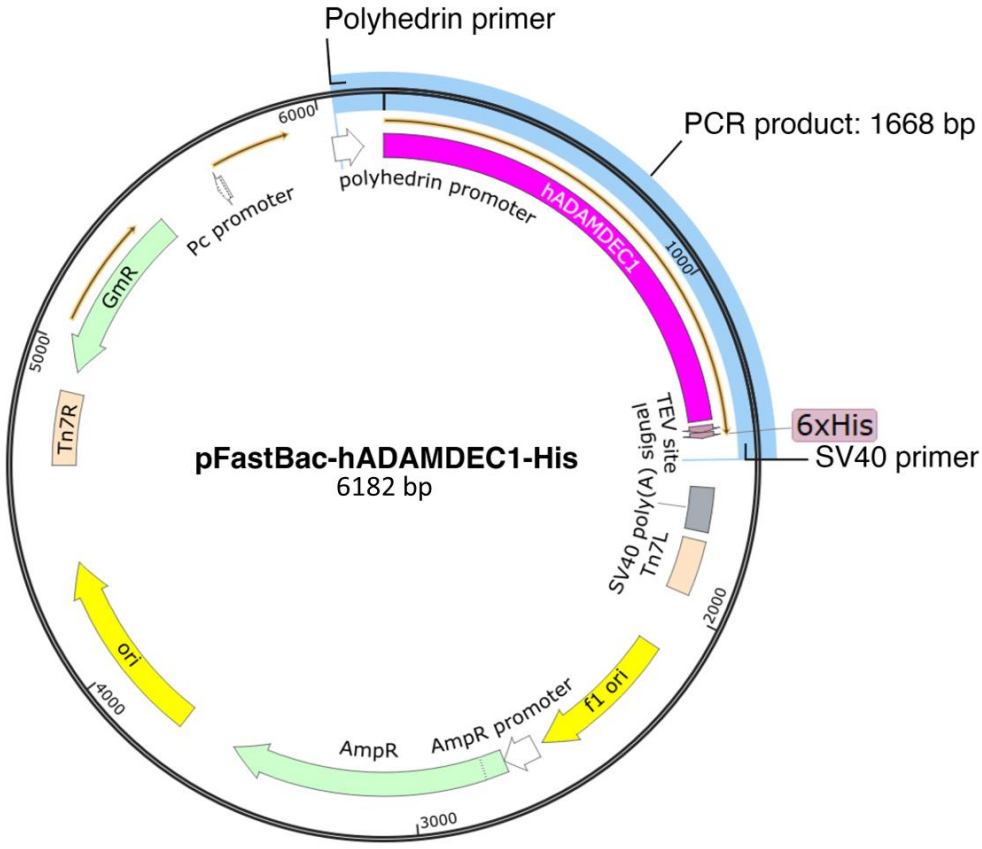

Figure 5.6 A plasmid map of pFastBac/CT-TOPO with hADAMDEC1 construct inserted in the cloning site. The positions of polyhedrin and SV40 primers' binding sites are shown. PCR using these primers after a successful ligation would generate a PCR product of 1668 bp in size. The image was generated in SnapGene viewer.

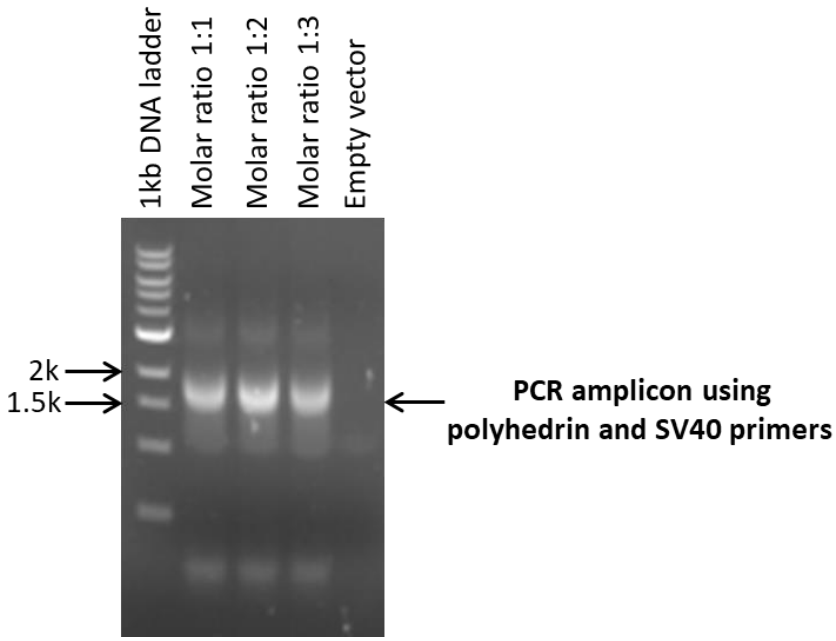

Figure 5.7 Agarose gel electrophoresis of the PCR products generated from the ligation products using various pFastBac vector to hADAMDEC1 insert ratios. PCR was conducted using polyhedrin and SV40 primers. All three vector to insert ratios were found to yield products around 1668 bp consistent with the presence of hADAMDEC1 insert within pFastBac plasmid. The ligation product generated from using a molar ratio of 1:2 appeared to produce slightly more PCR product.

5.3.1.3 Transformation of One Shot™ Mach1™ T1R Chemically Competent *E. coli* with pFastBac-hADAMDEC1-His

One Shot™ Mach1™ T1R Chemically Competent *E. coli* were transformed with pFastBac-hADAMDEC1-His ligation product (Chapter 5.2.2.4). The transformed *E. coli* cells were plated on agar plates. After overnight incubation at 37 °C, multiple colonies were seen on all of the agar plates (Data not shown). 16 colonies were picked and expanded in culture broth overnight. A relatively high number of colonies were isolated since there was only a 50% chance of hADAMDEC1 being inserted into the pFastBac plasmid with the correct orientation, reading 5' to 3' after the polyhedrin promoter. This is an expected consequence of the "blunt-end" TOPO cloning which does not dictate insert orientation. Overnight bacterial cultures were used to generate glycerol stocks for long-term plasmid storage, and to isolate the plasmid DNA by Miniprep (Chapter 2.6.3.1). The purified plasmid DNA was sequenced to screen for the presence, orientation and correct sequence of hADAMDEC1 (Chapter 2.6.1) within the plasmid using polyhedrin and SV40 primers. Sequencing of the purified plasmids revealed that 7 colonies out of the 16

contained plasmids with hADAMDEC1 of the correct sequence positioned with its N-terminal coding sequence adjacent to the polyhedrin promoter. One of these 7 colonies was re-streaked onto a fresh agar plate and grown overnight prior to a single colony from this plate being used to inoculate a 300 ml of culture broth to allow generation of a greater quantity of pFastBac-hADAMDEC1-His plasmid. Plasmid DNA was extracted and purified using the HiSpeed Plasmid Maxi Kit (Chapter 2.6.3.2).

5.3.1.4 Transformation of MAX Efficiency® DH10Bac™ chemically competent *E. coli* with the plasmid DNA

MAX Efficiency® DH10Bac™ chemically competent *E. coli* is a competent *E. coli* that carries a bacmid containing a mini-*attTn*7 attachment site and a helper plasmid. Transformation of the DH10Bac™ chemically competent *E. coli* with a transfer vector incorporating a polyhedrin promoter, such as pFastBac plasmid, and coding sequence of a gene of interest flanked by a mini-Tn7 results in transposition of the gene of interest, such as hADAMDEC1, from the mini-*Tn7* site of the transfer vector to mini-*attTn7* site within the bacmid. This results in highly efficient and accurate incorporation of the gene of interest into bacmid plasmid.

MAX Efficiency® DH10Bac™ chemically competent *E. coli* were transformed with the purified pFastBac-hADAMDEC1-His plasmid (Chapter 5.2.2.6). A 10-fold serial dilution of transformation culture was plated on agar plates containing kanamycin, tetracycline, gentamycin, Bluo-gal and IPTG for antibiotic selection and white-blue screening simultaneously. This allowed a rapid and convenient way to screen for the colonies containing the hADAMDEC1-His insert. After incubation for 48 hours at 37°C, numerous white and blue colonies were visible on all agar plates (Figure 5.8). Four white colonies were isolated from the agar plate inoculated with the bacterial culture diluted at 1:10. These 4 white colonies were re-streaked onto fresh agar plates containing the same combination of antibiotics, Bluo-gal and IPTG for another round of screening.

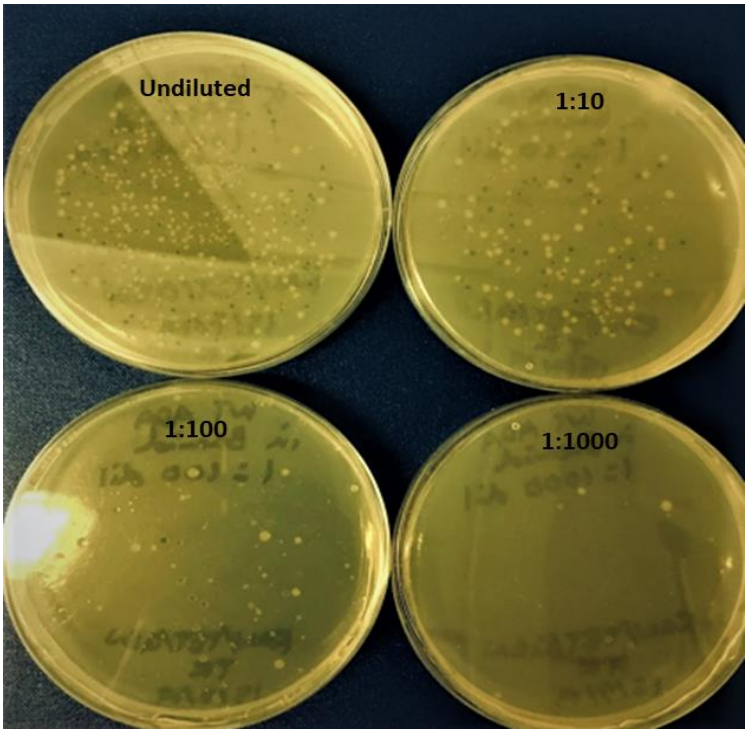

Figure 5.8 Transformation and screening results of the MAX Efficiency® DH10Bac™ chemically competent *E. coli* transformed with pFastBac-hADAMDEC1-His plasmid. A 10-fold serial dilution of transformation culture was plated on agar plates containing kanamycin, tetracycline, gentamycin, Bluo-gal and IPTG. The white colonies indicated successful incorporation of hADAMDEC1-His in bacmid within *E. coli*.

After overnight incubation, only white colonies were visible on all plates (Figure 5.9). Two colonies from one of the agar plates were isolated and expanded in 300 ml LB broth containing kanamycin, tetracycline and gentamicin. The resultant bacmid DNA (referred to as Bacmid-hADAMDEC1-His hereafter) was isolated and purified from bacterial cultures using PureLink™ HiPure Plasmid Maxiprep Kit (Chapter 5.2.2.7), which is a Maxiprep kit specifically designed to extract large plasmid such as bacmid.

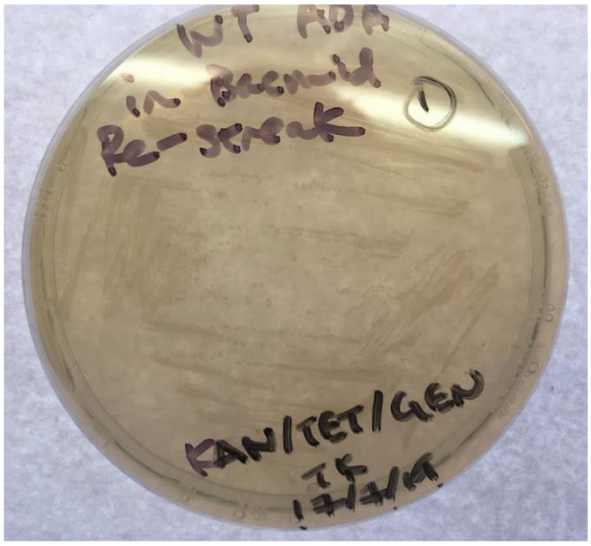

Figure 5.9 Confirmation of the successful incorporation of hADAMDEC1-His in bacmid within *E. coli* colony selected in the first round of antibiotic selection and white-blue screening. A white colony selected in the 1st round of screening was restreaked on an agar plate containing kanamycin, tetracycline, gentamycin, Bluo-gal and IPTG. Only white colonies were visible confirming the successful incorporation of hADAMDEC1-His in bacmid within the single *E. coli* colony selected.

5.3.1.5 Analysis of the recombinant bacmid containing hADAMDEC1-His

Confirmation of the presence and exact sequence of hADAMDEC1-His within the purified recombinant bacmid was not possible by direct sequencing of the bacmid due to its large size (>135 kb). The presence of hADAMDEC1-His in the recombinant bacmid was therefore first confirmed by PCR, using pUC/M13 forward and pUC/M13 reverse primers, which would generate a PCR product of 3832 bp in size if hADAMDEC1-His was present within the bacmid. The size of the PCR product would be 325 bp if hADAMDEC1-His had not been successfully transposed into the bacmid plasmid (Figure 5.10). Visualisation of PCR product following gel electrophoresis confirmed the presence of a PCR product of approximately 3800 bp, consistent with the presence of hADAMDEC1-His in the bacmid extracted from both colonies (Figure 5.11). PCR clean-up was performed on the PCR product (Chapter 5.2.2.2) and the exact nucleotide sequence of hADAMDEC1-His within the bacmid was confirmed by sequencing of the PCR products using polyhedrin and SV40 primers. (Results not shown.)

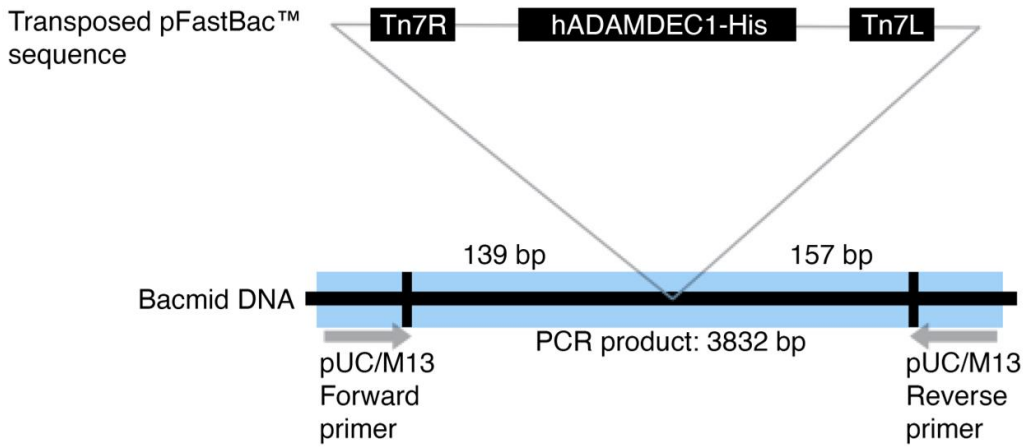

Figure 5.10 Position of the transposed hADAMDEC1-His sequence and binding sites for pUC/M13 forward and reverse primers within Bacmid-hADAMDEC1-His. PCR of Bacmid-hADAMDEC1-His with pUC/M13 forward and reverse primers would generate PCR product of 3832 bp in size if transposition of hADAMDEC1-His was successful and 325 bp in size if transposition was unsuccessful. The image was adapted from Bac-to-Bac™ TOPO™ Expression System user guide and modified.[326]

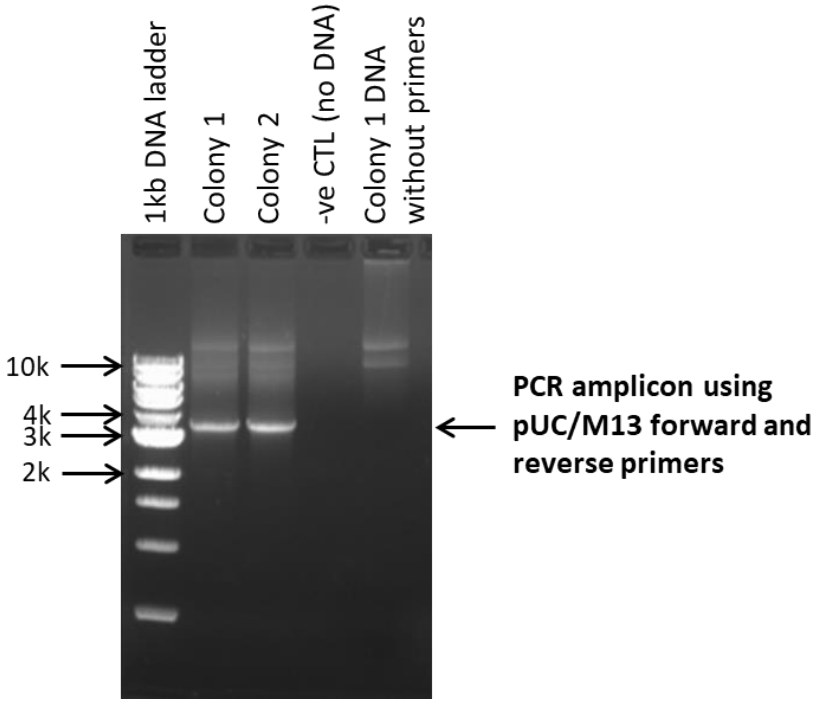

Figure 5.11 Agarose gel electrophoresis of the PCR products generated from the recombinant bacmid using pUC/M13 forward and reverse primers. PCR of the bacmid extracted and purified from both selected colonies produced PCR amplicons consistent with the presence of hADAMDEC1-His within the bacmid assessed by their size (3832 bp).

5.3.2 Site-directed mutagenesis for the generation of hADAMDEC1-E353A-His bacmid

Following the generation of pFastBac-hADAMDEC1 plasmid (Chapter 5.3.1.3), pFastBac plasmid containing human E353A (referred to as pFastBac-hE353A-His hereafter) was made by site-directed mutagenesis using the Phusion Site-Directed Mutageneis Kit (Chapter 5.2.2.9). An introduction of a point mutation to substitute glutamic acid to alanine at amino acid position 353 within the zinc-binding motif of the metalloprotease domain makes E353A catalytically inactive.[14,20]

Site-directed mutagenesis was performed using the pFastBac-hADAMDEC1-His plasmid previously made as a template. A mutagenic primer encoding a single point mutation resulting in E353A within ADAMDEC1 was designed. The reverse primer was designed to be complementary to the target strand without any mismatch (Figure 5.12). Both primers were synthesised with phosphorylated 5' ends to facilitate the ligation and circularisation of the PCR products. PCR was performed to amplify the pFastBac-hADAMDEC1-His plasmid to generate a PCR product which contained the point mutation encoding E353A. This was followed by DpnI digestion to remove any template plasmid, and ligation of the PCR product (Chapter 5.2.2.9). The ligated PCR product was used to transform One Shot Mach1 competent *E.coli* as previously described (Chapter 5.3.1.3). The transformed *E.coli* were plated on agar plates and grown overnight. 8 colonies were picked and grown in 6 ml of culture broth over 8 hours. The plasmid DNA from each culture was extracted and purified by Miniprep (Chapter 2.6.3.1) and sequenced using polyhedrin and SV40 primers as before. Two out of the 8 colonies were found to contain the correct E353A mutation within the newly formed pFastBac-hE353A-His plasmid. One of the two positive colonies was re-streaked onto a fresh agar plate and grown overnight prior to a single colony being used to start a 300 ml overnight culture to generate more pFastBac -E353A-His plasmid. The extracted and purified plasmid was used to transform MAX Efficiency® DH10Bac™ chemically competent *E. coli* to generate recombinant bacmid encoding hE353A-His in the same way as previously described for Bacmid-hADAMDEC1-His (Chapter 5.3.1.4). The presence and exact sequence of E353A-His within the recombinant bacmid were confirmed in the same way as previously described for Bacmid-hADAMDEC1-His (Chapter 5.3.1.5).

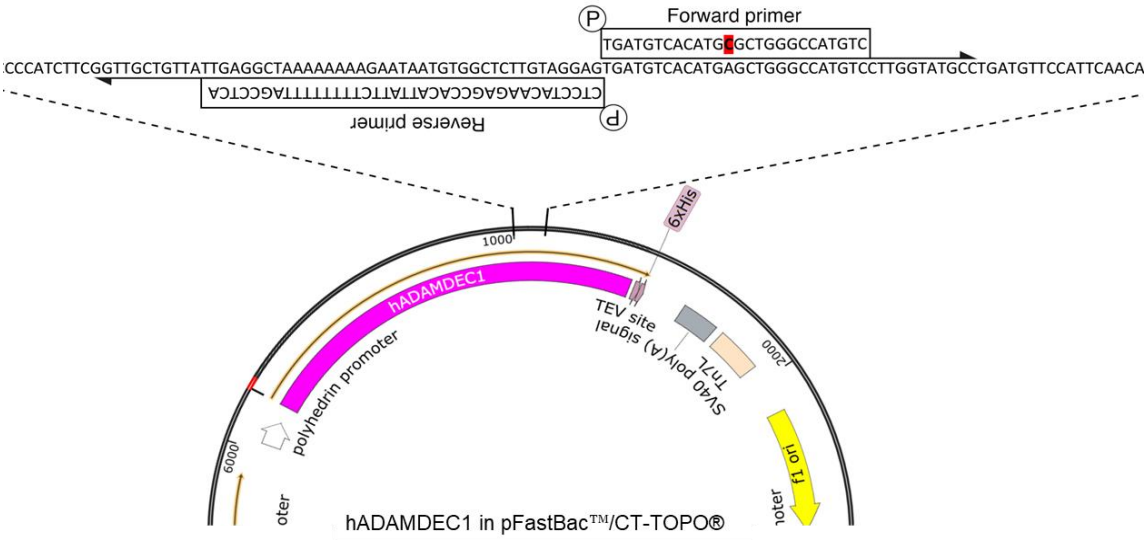

Figure 5.12 The sequences and binding positions of the primers used for the mutagenesis PCR to generate pFastBac-E353A-His plasmid. pFastBac-hADAMDEC1-His plasmid previously made was used as a template. The letter highlighted in red indicates the single point mutation incorporated into the primer.

5.3.3 Generation of mADAMDEC1-His and mE353A-encoding bacmids

A similar process to the one already described in this chapter for making hADAMDEC1-His and hE353A-His-encoding bacmids was followed to generate bacmids containing mouse ADAMDEC1-His (referred to as mADAMDEC1-His hereafter) and mouse E353A-His (referred to as mE353A-His hereafter). Initially, the plasmid pCMV-mADAMDEC1-Myc-DDK (Origene, MR223445) was used as a template to amplify mADAMDEC1 construct by PCR to allow subsequent insertion into the pFastBac plasmid. PCR was optimised as before by gradient PCR, testing annealing temperatures between 68 - 74°C. An annealing temperature of 70°C was selected as the optimum annealing temperature to generate mADAMDEC1 insert. The purified mADAMDEC1 insert was subsequently ligated into pFastBac, with the resultant plasmid (referred to as pFastBac-mADAMDEC1-His hereafter) amplified and purified before being used as a template for site-directed mutagenesis to generate pFastBac-mE353A-His. Both mADAMDEC1-His and mE353A-His were successfully transposed into bacmids following the same process described to make the human ADAMDEC1 and E353A-ecnoding bacmids. The presence and correct orientation of both mADAMDEC1-His and mE353A-His

within the bacmids were confirmed by PCR followed by sequencing of the PCR products using the same primer pair as for the human bacmids.

5.3.4 Generation of recombinant baculovirus encoding hADAMDEC1-His and hE353A-His

ExpiSf9 insect cells were transfected with each recombinant bacmid to produce baculovirus in the cell culture supernatant (Chapter 5.2.3). The harvested baculovirus would subsequently be used to infect ExpiSf9 cells to express ADAMDEC1-His and E353A-His. The cells transfected with the bacmid encoding hADAMDEC1-His or hE353A-His were examined microscopically and cell viability was determined 72 and 96 hours post-transfection. The optimum time for harvesting insect cell culture medium containing budded recombinant baculovirus is when cell viability has decreased to around 60-80 %.[177] At 72 hours, the cells were larger, more spherical, and had increased intracellular granularity consistent with baculovirus production (Figure 5.13). At this time point, there were few, if any cells, which appeared to have lysed, corresponding with relatively high cell viability of 86 - 89%. At 96 hours, in addition to the increased cellular granularity, numerous dead/lysed cells were observed, shown by the increased intracellular trypan blue staining and a high abundance of cellular debris (Figure 5.13). The cell viability at 96 hours was found to be between 63-78%. There were no differences in the cell morphology or viability between the cells transfected with bacmid encoding hADAMDEC1-His or h353A-His. Based on these observations, the spent culture medium containing the baculovirus was collected at 96 hours to form a P0 baculovirus stock.

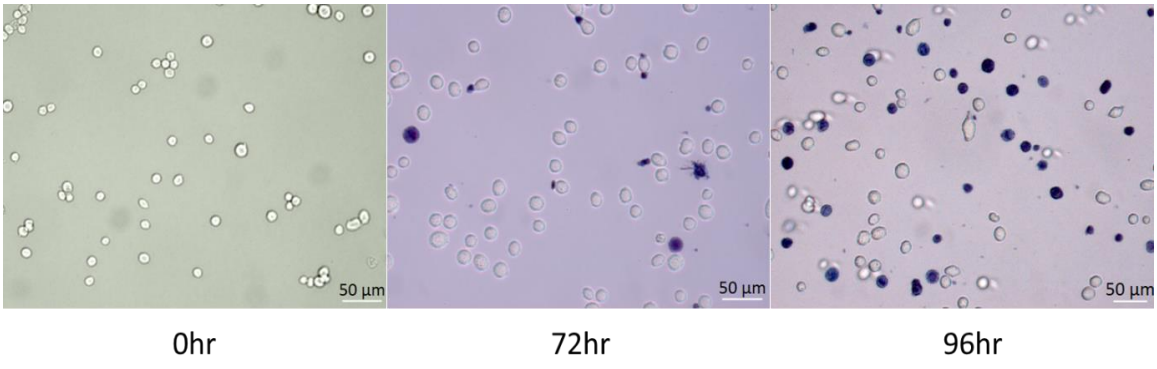

Figure 5.13 Morphological appearance of ExpiSf9 cells before and after (72 hours and 96 hours post-transfection) transfected with Bacmid-hADAMDEC1-His.

5.3.5 Optimisation of recombinant hADAMDEC1-His and hE353A protein expression in ExpiSf9 cells using the harvested P0 baculoviral stocks

ExpiSf9 cells have advantages over other available insect cell lines for both baculovirus and recombinant protein production, due primarily to their ability to grow at higher cell densities without loss of cell viability. Higher recombinant baculoviral titres can therefore be generated in these cells as well as, on average, a greater yield of recombinant protein.[172] Additionally, depending on the characteristics of individual bacmids, higher baculoviral titres remove the need for further amplification of baculovirus stocks prior to infection of insect cells for recombinant protein production.[172] Ideally, the viral titre of P0 baculoviral stocks should be quantified to help determine a suitable multiplicity of infection, the number of infectious viral particles per insect cell. However, quantification is in general time-consuming, labour-intensive and expensive to carry out. The appearances and viabilities of the ExpiSf9 cells transfected with bacmid encoding recombinant hADAMDEC1-His and hE353A-His at 96 hours (Chapter 5.3.4) were consistent with successful baculovirus production. Thus small scale trial infections of ExpiSf9 cells with P0 viral stocks were carried out, without quantifying the viral titres in them, to determine if viable baculoviruses were indeed generated and furthermore how much P0 stocks were required to generate intracellular and secreted recombinant hADAMDEC1-His and hE353A-His.

Small scale trial infections were conducted by infecting 25 ml of ExpiSf9 cells with two different volumes (250 μl or 500 μl) of P0 baculoviral stocks. Insect cell culture was collected at 0, 24, 48, and 96 hours post-infection with P0 baculoviruses to determine insect cell number and cell viability. A sample of the infected insect cell culture was also collected at these timepoints and separated into cell pellets and supernatants for subsequent assessment of intracellular and secreted protein, respectively by Western blot (Figure 5.14).

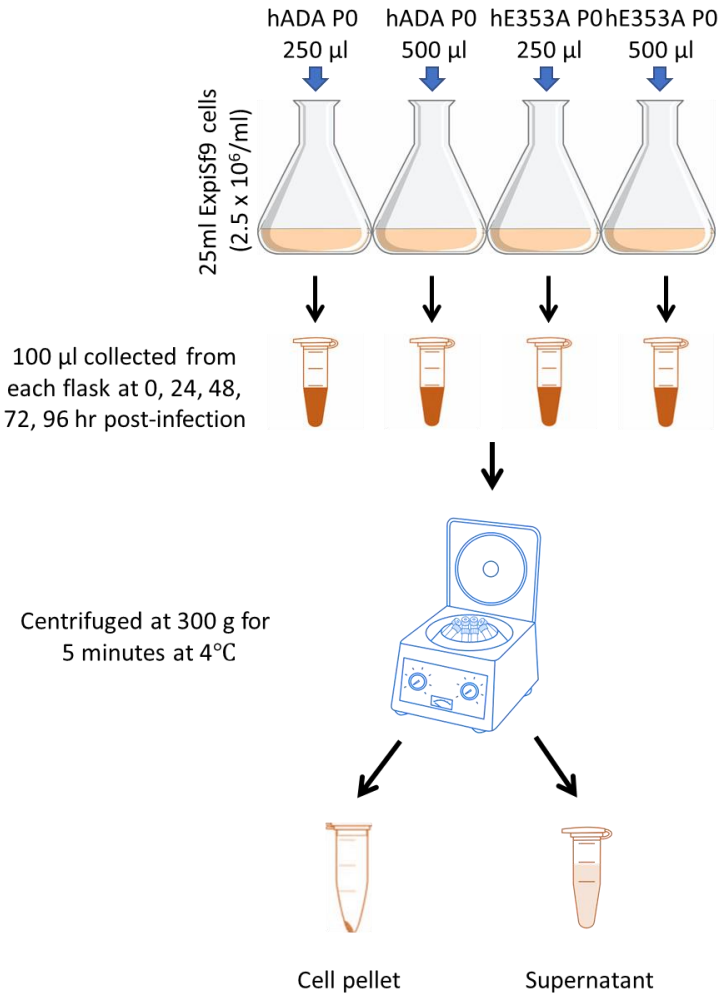

Figure 5.14 Small scale trial infections of ExpiSf9 cells with hADAMDEC1-His and hE353A-His P0 baculoviral stocks. 250 µl or 500 µl of the P0 baculovirus stocks were used to infect 25 ml of ExpiSf 9 cells. Each cell culture was collected and separated into lysates and supernatants at 5 different timepoints. Expression of the recombinant proteins in lysates and supernatants collected at each timepoint were assessed by Western blot.
hADA: hADAMDEC1, hr: hours

5.3.5.1 Cell number and viability during the baculovirus infection

The total number of insect cells increased significantly between 0 and 48 hours post-infection irrespective of whether the cells were infected with hADAMDEC1-His P0 baculovirus or E353A-His P0 baculovirus (Figure 5.15). Between 48 and 96 hours post-infection, the total number of insect cells reached a plateau, or decreased in the case of insect cells infected with 500 µl of hE353A-His baculovirus. Between 72 and 96 hours post-infection, the total number of insect cells was similar between cell cultures irrespective of the baculovirus and the volume of P0 viral stock used.

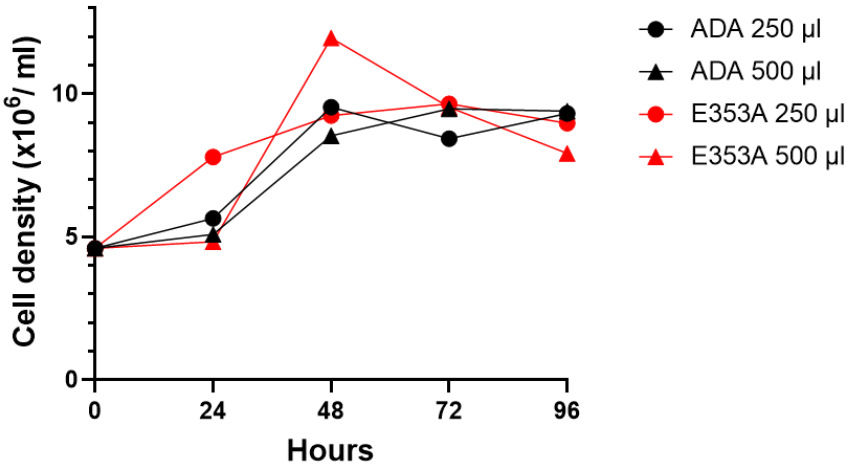

Figure 5.15 Total number of ExpiSf9 cells during infection with 250 µl or 500 µl of hADAMDEC1-His or hE353A-His P0 baculoviruses assessed over 96 hours.
ADA: hADAMDEC1

Despite an increase in the total number of insect cells during the first 48 hours post-infection, cell viability began to decrease after 24 hours and declined rapidly between 48 and 96 hours post-infection irrespective of the baculovirus and baculovirus volume used to infect the cells (Figure 5.16). It has been shown that optimal recombinant protein yields from baculovirus-infected ExpiSf9 cells can be achieved when the cell viability is between 50 - 70%.[172] The experiments conducted here showed that this level of cell viability was achieved approximately between 72 hours and 84 hours post-infection (Figure 5.16).

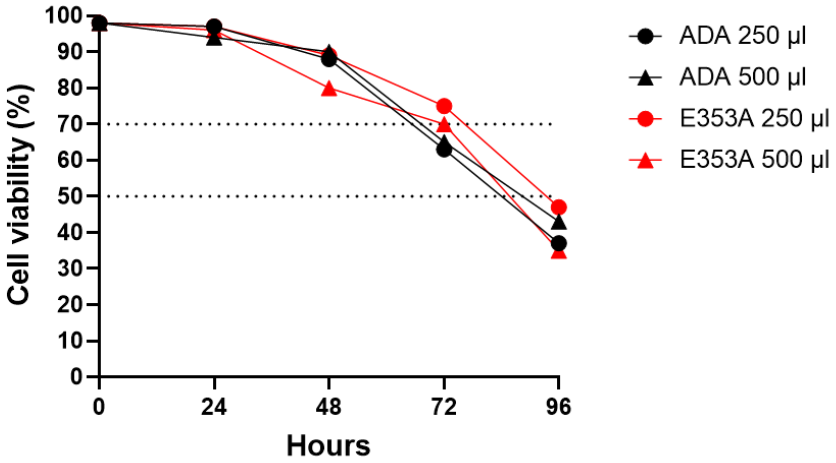

Figure 5.16 Cell viability of ExpiSf9 cells during infection with 250 µl or 500 µl of hADAMDEC1-His or hE353A-His P0 baculoviruses assessed over 96 hours. Generally an optimum protein expression occurs when the cell viability is between 50 – 70%.
ADA: hADAMDEC1

The number of live insect cells was reflective of the change in the total cell number and viability (Figure 5.17). The number of live cells increased between 0 and 48 hours post-infection, indicating cell proliferation and high cell viability. The number of live cells started to decrease rapidly from 48 to 96 hours post-infection, mirroring the change seen in the cell viability. This was irrespective of the baculovirus and the volume of the P0 viral stock used.

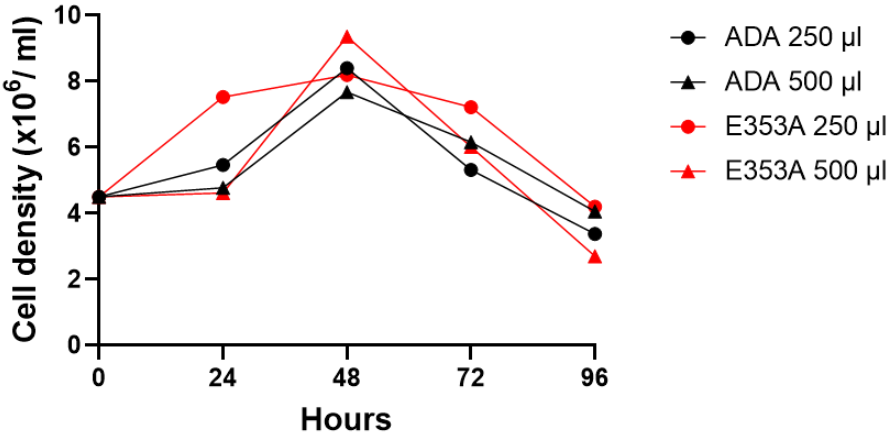

Figure 5.17 Number of live ExpiSf9 cells during infection with 250 µl or 500 µl of hADAMDEC1-His or hE353A-His P0 baculoviruses assessed over 96 hours.
ADA: hADAMDEC1

Overall, the total insect cell number, live insect cell number and cell viability, determined over 96 hours, suggested successful infection of ExpiSf9 cells with the hADAMDEC1-His and hE252A-His P0 baculoviruses generated. The trends in these variables were generally the same irrespective of the difference in baculovirus or the volume of P0 baculoviral stock used. This indicated that hADAMDEC1-His and hE353A-His-encoding baculoviruses infected ExpiSf9 cells with similar effectiveness, and a conserved P0 volume of 250 µl was sufficient to infect 25 ml of ExpiSf9 cells at a density of 5 x 10^6 /ml.

5.3.5.2 Western blot of cell lysates and supernatants harvested at different timepoints during infection of ExpiSf9 cells with P0 baculoviruses

To confirm the expression of hADAMDEC1 and hE353A following the infection of ExpiSf9 cells with the P0 baculoviral stocks, and to determine the optimum timepoint to harvest the culture for the greatest recombinant protein yield, Western

blots were performed using the the cell pellets and supernatants collected at 0, 24, 48, 72 and 96 hours post-infection (Figure 5.14).

The predicted molecular weight of the immature ADAMDEC1 was expected to be 52 kDa. The mature cleaved form was predicted to have a molecular weight of around 32 kDa. Post-translational modifications such as glycosylation were also believe to take place during protein synthesis intracellularly. Mature ADAMDEC1 after a removal of N-linked glycosylation by PNGase has been shown to have a molecular weight of around 30 kDa.[14]

Western blots were initially probed with anti-His antibody to confirm the production of recombinant hADAMDEC1 and hE353A protein with its C-terminal 6xHis tag in both cell lysates and supernatants.

Western blots probed with anti-His antibody showed detectable immature hADAMDEC1 (around 52 kDa) in the cell lysate samples generated from the ExpiSf 9 cells infected with hADAMDEC1 baculovirus 24 hours post-infection (Figure 5.18 A). The level of this immature protein increased further up until 96 hours post-infection, where protein abundance was the greatest (Figure 5.18 A). The mature ADAMDEC1 (at 32 kDa) was also detected in the cell lysate samples from 48 hours post-infection onwards. This data would indicate the presence of either intracellular mature hADAMDEC1 prior to secretion or sample contamination brought about by incomplete removal of the culture medium during the cell pellet isolation. Nevertheless, the dominant form of hADAMDEC1 in the cell lysate appeared to be the immature form. This Western blot also revealed that both the immature and mature form of hADAMDEC1 were detected as at least two distinct bands, most likely due to variable post-translational modification such as N-linked glycosylation.

The Western blot generated using the supernatant collected from ExpiSf 9 cells infected with hADAMDEC1 P0 baculovirus and probed with anti-His antibody showed prominent bands around 32 kDa, expected to be mature hADAMDEC1 (Figure 5.18 B). This dominant form of hADAMDEC1 was most prevalent 48 hours post-infection for the duration of the remaining time course. The immature form of hADAMDEC1 was also present at far lower levels in the samples collected from 48 hours onwards, however, its abundance seemed to decrease after 48 hours post-infection. The presence of the immature ADAMDEC1 in the supernatant was likely to be due to either contamination of the culture medium with cells or release of

immature hADAMDEC1 by cell lysis during the sample separation. The pattern of recombinant protein expression was the same irrespective of the volume of the baculoviruses used to infect the cells.

A similar pattern of protein expression was seen with the cell lysates and supernatants prepared from ExpiSf9 cells infected with hE353A P0 baculovirus compared with the cell lysates and supernatants prepared from the insect cells infected with hADAMDEC1 P0 baculovirus (Figure 5.19 A and B). An exception to this was that maximal protein expression of hE353A seemed to occur 72 hours post-infection, rather than 96 hours.

These Western blots proved with anti-His primary antibody demonstrated that the pattern of recombinant protein expression was the same for hADAMDEC1 and hE353A, and the two volumes of the baculovirus used to infect the cells, either 250 µl or 500 µl, did not affect the protein expression for both hADAMDEC1 and hE353A. This indicated that the viral titre of the baculoviral P0 stocks harvested at 96 hours post-transfection was sufficiently high so that insect cells were infected effectively in these experiments when using between 250 µl to 500 µl of the P0 baculoviruses.

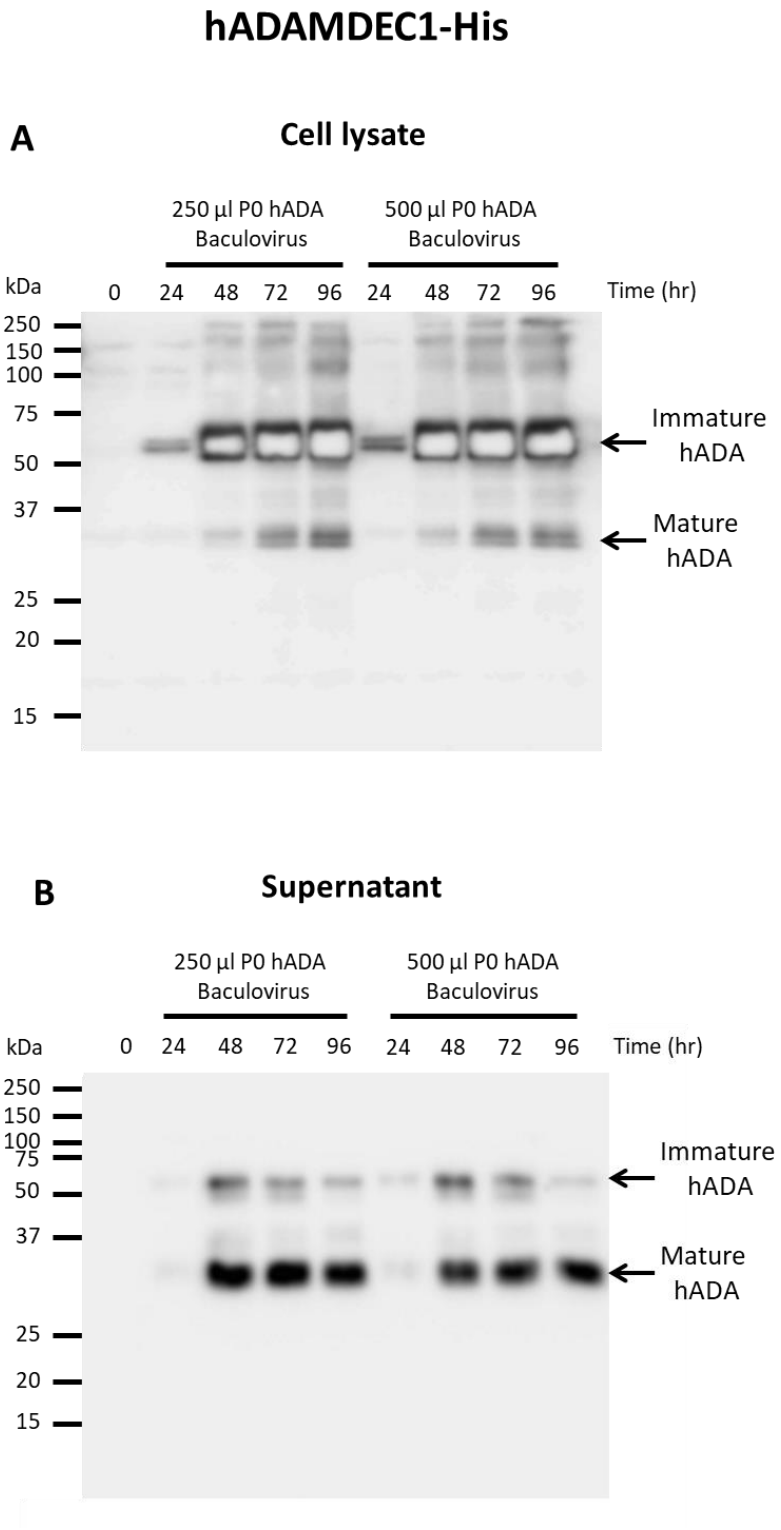

Figure 5.18 Anti-His Western blot of cell lysate (A) and supernatant (B) of ExpiSf9 cells infected with 250 µl or 500 µl of hADAMDEC1-His P0 baculovirus collected at various timepoints over 96 hours. The blots are representative of n=2.
hADA: hADAMDEC1, hr: hours

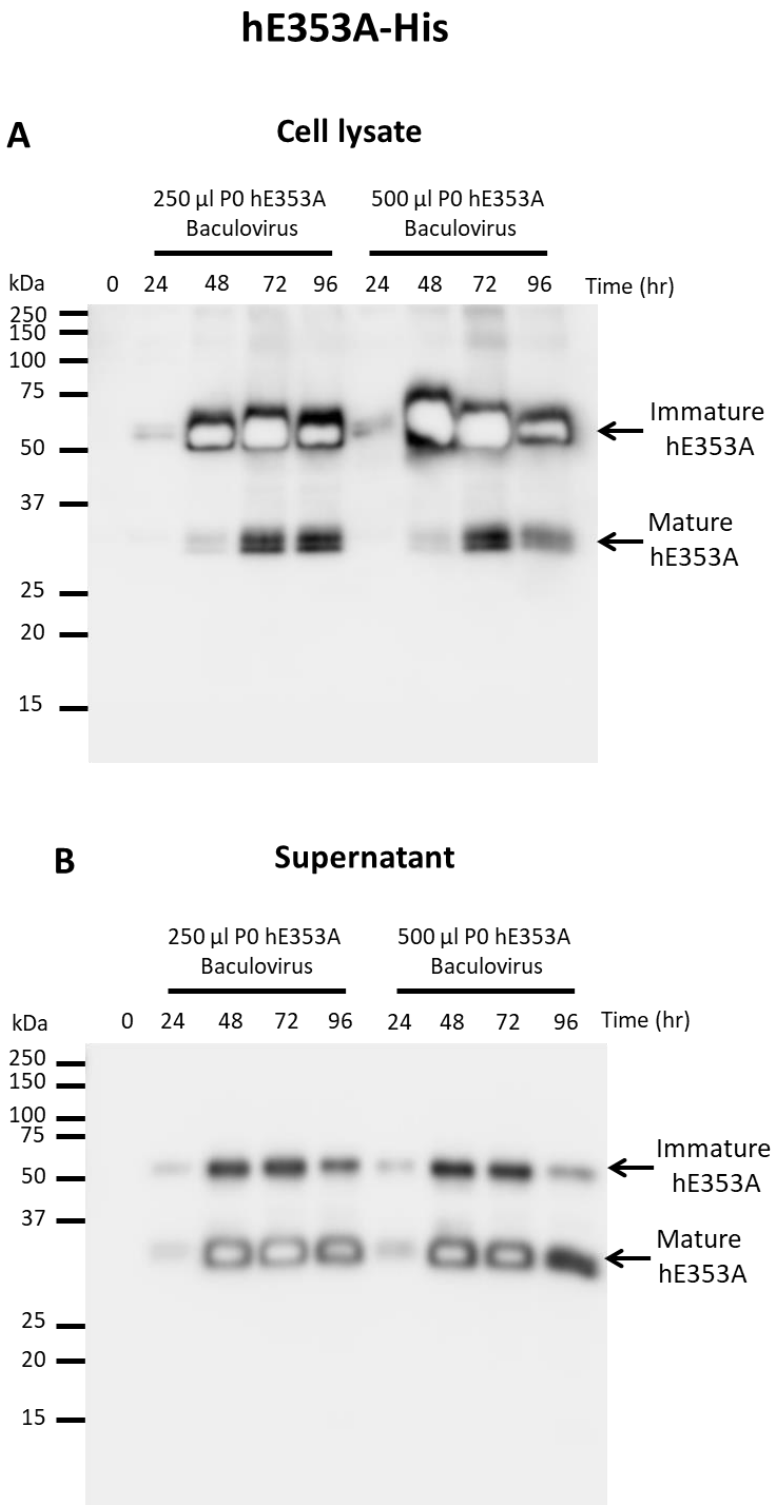

Figure 5.19 Anti-His Western blot of cell lysate (A) and supernatant (B) of ExpiSf9 cells infected with 250 µl or 500 µl of hE353A-His P0 baculovirus collected at various timepoints over 96 hours. The blots are representative of n=2.
hr: hours

To validate and confirm the result generated from the Western blots probed with anti-His antibody, Western blots were repeated and instead probed with anti-ADAMDEC1 antibody (Figure 5.20 and 5.21). Similar Western blots were produced when using anti-His or anti-ADAMDEC1 antibodies, which further increased confidence that the bands detected were recombinant ADAMDEC1 and E353A.

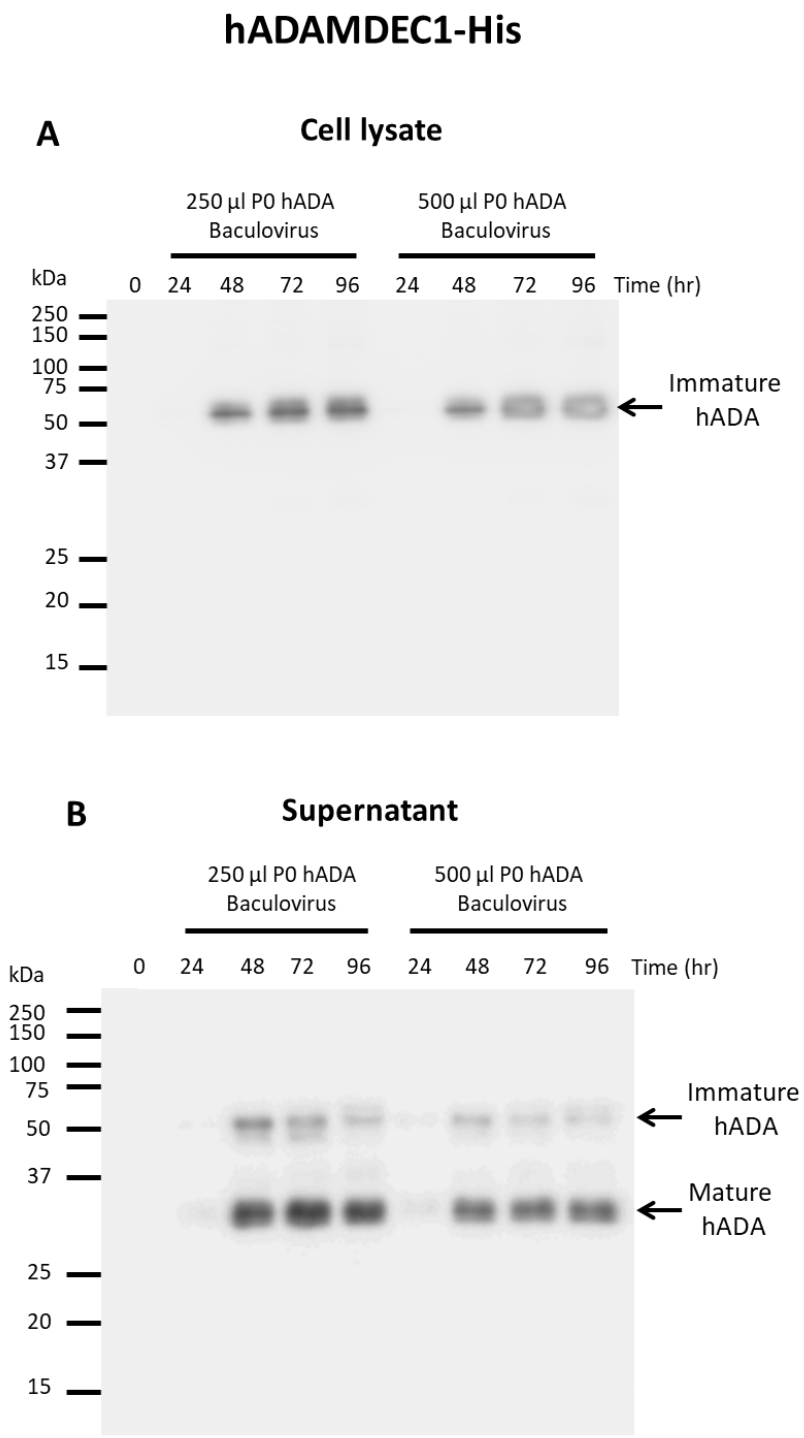

Figure 5.20 Anti-ADAMDEC1 Western blot of cell lysate (A) and supernatant (B) of ExpiSf9 cells infected with 250 µl or 500 µl of hADAMDEC1-His P0 baculovirus collected at various timepoints over 96 hours. The blots are representative of n=2. hADA: hADAMDEC1, hr: hours

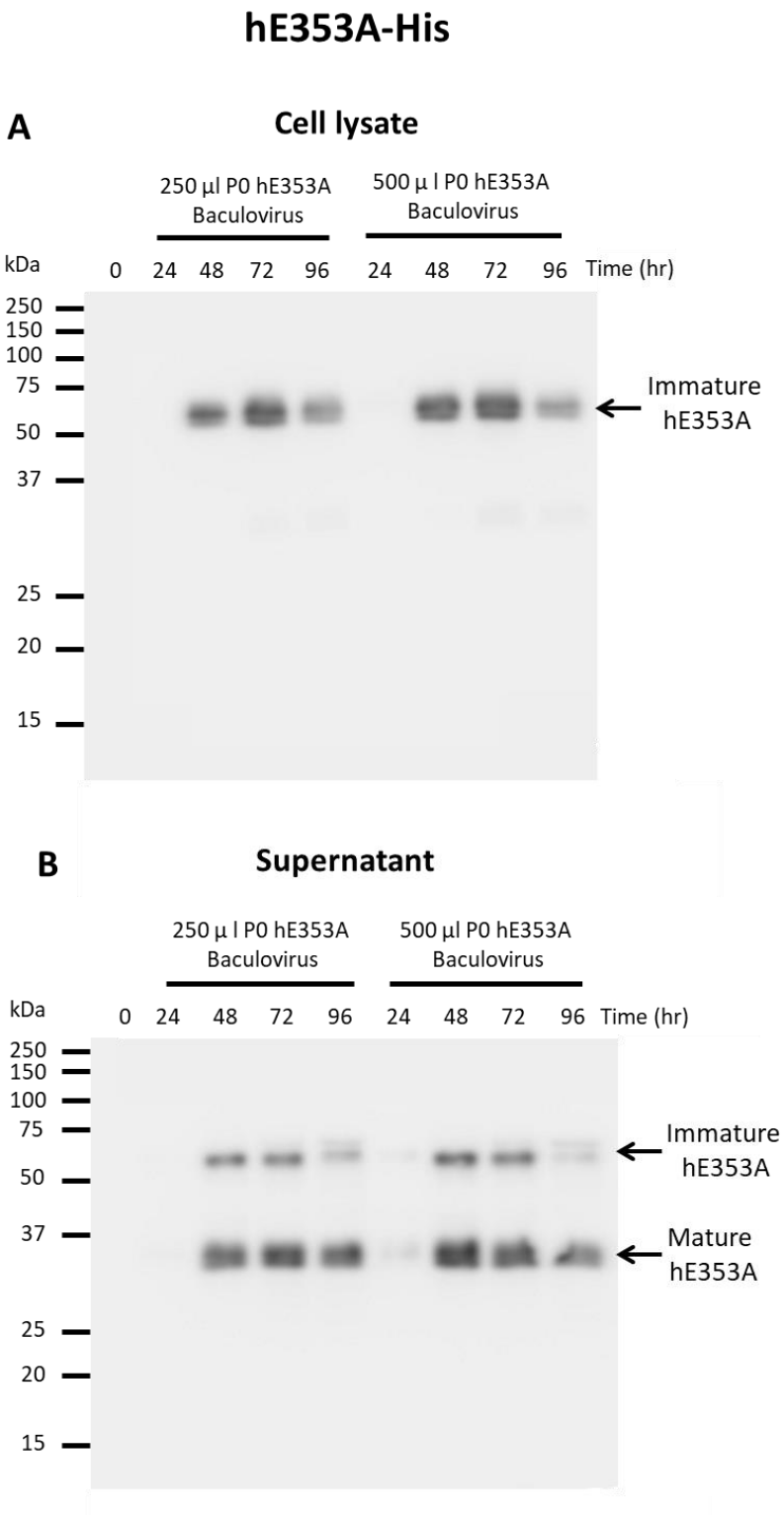

Figure 5.21 Anti-ADAMDEC1 Western blot of cell lysate (A) and supernatant (B) of ExpiSf9 cells infected with 250 µl or 500 µl of hE353A-His P0 baculovirus collected at various timepoints over 96 hours. The blots are representative of n=2. hr: hours

In summary, the small-scale infection of insect cells confirmed that hADAMDEC1 and hE353A P0 baculovirus stocks, harvested at 96 hours post-transfection, were both effective in infecting ExpiSf9 insect cells and subsequently driving the production of recombinant protein, peaking at 72 to 96 hours post-infection. This process excluded the need to quantify the baculoviral titre or amplify the baculovirus stocks prior to the insect cell infection. The evidence of easily detectable immature and mature recombinant hADAMDEC1 and hE353A protein by Western blot after using 250 μl P0 baculoviral stock to infect 25 ml of ExpiSf9 insect cells indicated that the viral titres were sufficiently high enough. Additionally, it was shown that the dominant form of hADAMDEC1 or hE353A found intracellularly following the infection with either baculovirus was the uncleaved immature form. However, in the supernatants, the dominant form of the recombinant proteins was found to be the cleaved mature form, with levels remaining constant between 48 and 96 hours post-infection for both hADAMDEC1 and hE353A. Lastly, at least two bands on Western blots were shown for both mature and immature forms of hADAMDEC1 and hE353A, which was most likely due to variable post-translational glycosylation.

Based on the results generated from these trial infections, the recombinant protein production was scaled up using the basis that 250 μl of the P0 baculovirus stock was needed per 25 ml of ExpiSf9 cells, at a density of 5 x 10^6 /ml. To maximise protein yield and limit protein degradation, the supernatant would be harvested 72 hours post-infection to allow purification of the active mature form of ADAMDEC1 and E353A.

5.3.6 Optimisation of immobilised metal affinity chromatography (IMAC) purification process using the recombinant mature hADAMDEC1

The recombinant proteins were purified from the harvested supernatant following a sequential process of diafiltration, batch IMAC, and finally dialysis. The steps of the purification process and the main purpose of each step are summarised in Table 5.10.

Purification step	Purpose
Diafiltration	Desalting/buffer exchange and concentration of mature ADAMDEC1/E353A harvested from the insect cell culture supernatant
IMAC	Binding of His-tag to nickel-NTA and washes in low concentration of imidazole to remove non-specific binding proteins. Elution of ADAMDEC1/E353A using high concentration imidazole.
Dialysis	Desalting, buffer exchange and removal of imidazole

Table 5.10 Steps of the purification process and main purpose of each step.

To test and optimise the purification workflows, a trial purification was carried out using 100 ml of ExpiSf9 cells, at a density of 5 x 10^6 /ml, infected with 1 ml of hADAMDEC1 P0 baculovirus stock. The culture media was collected 72 hours after the infection. 95 ml of supernatant was harvested after the removal of the cell pellets. The diafiltration and buffer exchange were performed, which produced 28.5 ml of the concentrated sample in the HEPES-based binding buffer containing 10 mM of Imidazole (Chapter 5.2.5.1). The sample was loaded onto nickel-NTA to allow the binding of His-tag to nickel-resin (Chapter 5.2.5.2). During this optimisation trial, the imidazole concentration of 20 to 120 mM, in an increment of 20 mM, was used in the wash buffer to determine the concentration of imidazole at which the maximum amount of non-specific binding proteins would be eluted off the nickel resin without disturbing the interaction between the His-tag and nickel significantly. hADAMDEC1 was then eluted by elution buffer, with imidazole concentration of 500 mM, which was then dialysed in PBS to remove imidazole (Chapter 5.2.5.3). At each step of the purification process, a small volume of the solution was collected from the sample and stored at -80°C. Once the entire purification process was completed, TCA precipitation was performed on these collected fractions to concentrate the protein and remove contaminants which were then used for subsequent purity analysis of the fractions using SDS-PAGE and Western blot (Chapter 5.2.6, 5.2.7 and 2.8)

5.3.6.1 Purity analysis of the fractions collected during the purification of mature hADAMDEC1

The SDS-PAGE of the fractions collected at each step of the purification process showed non-specific binding proteins being removed effectively by the increasing concentration of imidazole, from 20 mM to 120 mM, in the wash buffer (Figure 5.22 A Lane W20 to W120). The maximum amount of non-specific binding proteins was appeared to be removed by the wash buffer with imidazole concentration of 60 mM. The SDS-PAGE, however, showed that the imidazole concentration of 60 mM and above appeared to break the interaction between the His-tag and nickel, resulting in the loss of mature ADAMDEC1 (Figure 5.22 A Lane W60 to W120). The final elution with the elution buffer containing 500 mM of imidazole successfully eluted ADAMDEC1, which was repeated 3 times, with minimal impurities. The post-dialysis fraction in the SGS-PAGE (Figure 5.22 A Lane P) showed ADAMDEC1 was not lost during the dialysis. Despite losing ADAMDEC1 by the wash buffer with imidazole concentration of 60 mM and above in this optimisation trial, the final solution contained a significant amount of mature ADAMDEC1. Additionally, the Western blot of the fractions collected at each step of the purification process probed with anti-His antibody showed successful binding of the His-tag, thus ADAMDEC1, to the nickel-resin with no detectable ADAMDEC1 in the flow-through (Figure 5.22 B Lane 3). The Western blot also confirmed the loss of hADAMDEC1 during the wash step, particularly with an imidazole concentration higher than 40 mM. Despite this, the Western blot indicated a successful purification process, without protein degradation, with a significant amount of hADAMDEC1 in the post-dialysis sample. Having considered the balance between achieving the most effective removal of the non-specific binding proteins whilst minimising the loss of mature ADAMDEC1 during the wash step, the wash step for the subsequent purification was decided to be performed with 5 lots of washes with a constant imidazole concentration of 60mM.

Figure 5.22 SDS-PAGE (A) and Western blot (B) analyses of the fractions collected at each step of hADAMDEC1 purification process. A small fraction of solution was collected at each step of the purification process and proteins were concentrated by TCA precipitation. 12% SDS-PAGE was used. Western blot was proved with anti-His antibody.
hADA: hADAMDEC1

Well	Sample loaded
1	Culture supernatant
2	Post-diafiltration and concentration
3	Flow-through
W20	Wash with 20 mM Imidazole
W40	Wash with 40 mM Imidazole
W60	Wash with 60 mM Imidazole
W80	Wash with 80 mM Imidazole
W100	Wash with 100 mM Imidazole
W120	Wash with 120 mM Imidazole
W10	Wash with 10 mM Imidazole
E1	Elution 1 with 500 mM Imidazole
E2	Elution 2 with 500 mM Imidazole
E3	Elution 3 with 500 mM Imidazole
P	Post-dialysis

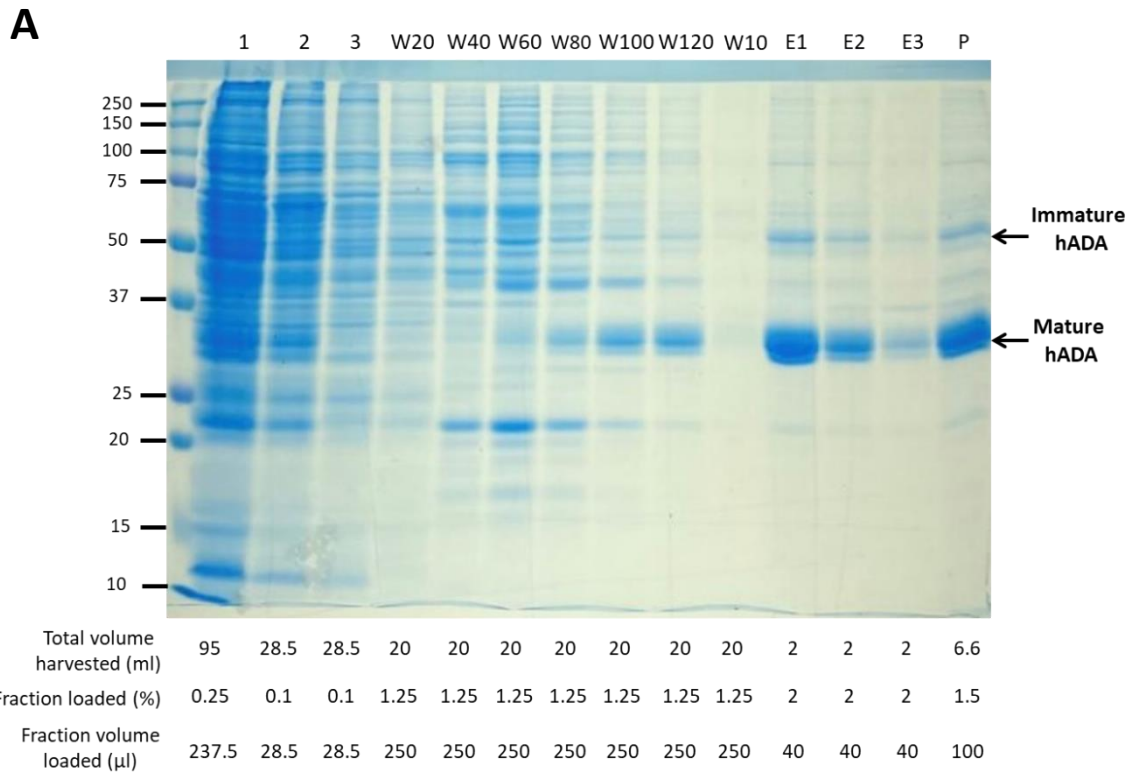

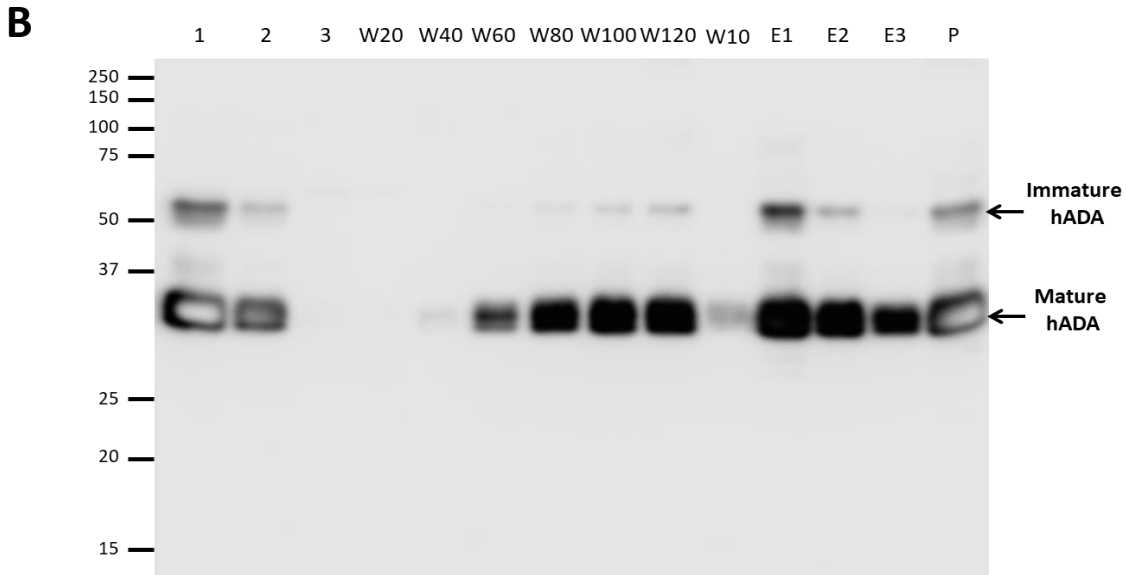

5.3.6.2 Quantification of the purified hADAMDEC1

The recombinant hADAMDEC1 purified in the trial purification described above was quantified by SDS-PAGE and densitometry (Chapter 5.2.8). BSA was used as a standard protein to calculate a standard curve (Figure 5.22 A and B). The concentration of the purified hADAMDEC1 was 125 ng/µl, which indicated that a total of 825 µg, in a volume of 6.6ml, was harvested and purified from 95 ml of the starting culture medium in this batch of purification.

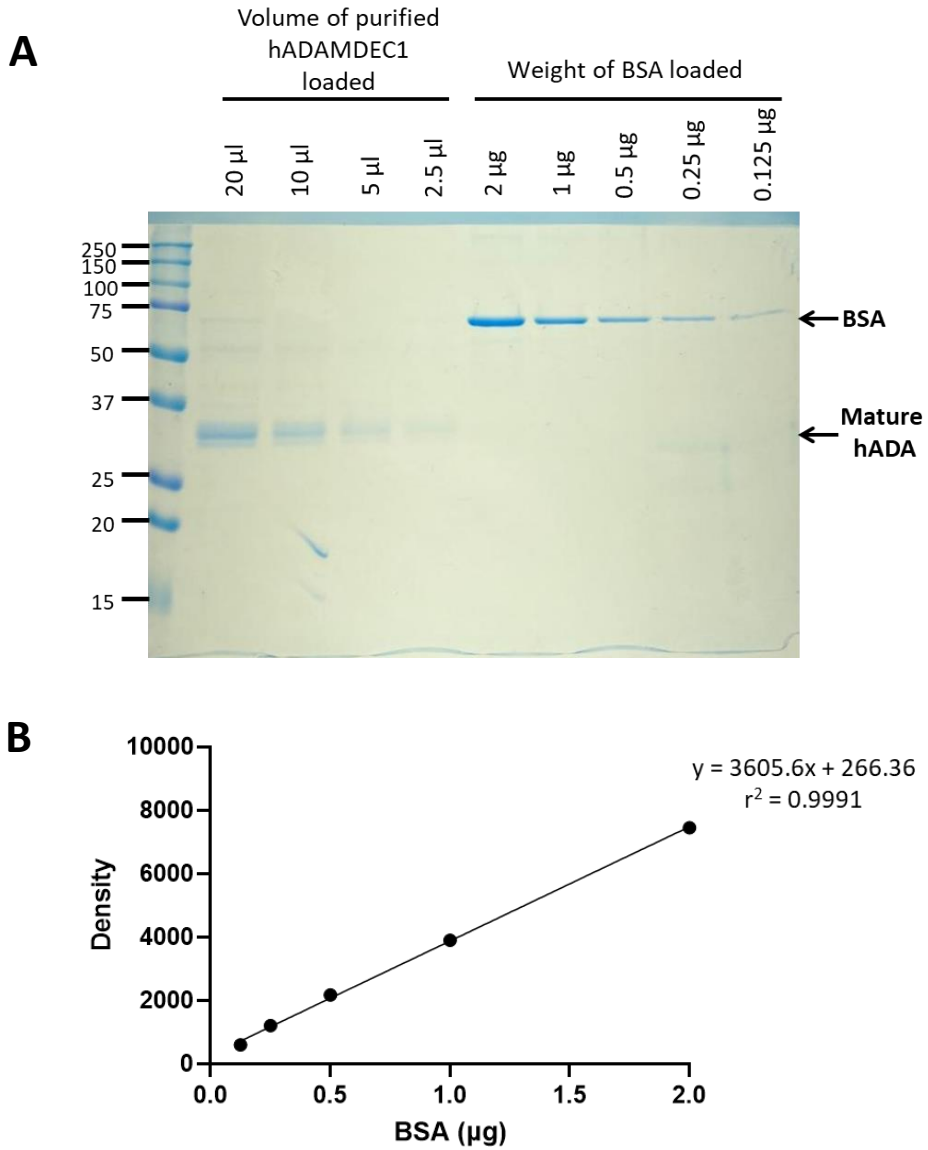

Figure 5.23 Quantification analysis of the purified recombinant hADAMDEC1 by densitometry.

A: SDS-PAGE gel used for densitometry. Various volumes of the purified recombinant hADAMDEC1 and masses of BSA were loaded in each well. 12% SDS-PAGE was used.

B: A standard curve generated by the densitometry of BSA used as a control.

The concentration of recombinant hADAMDEC1 was calculated using the equation generated by the standard curve.

hADA: hADAMDEC1, r^2: coefficient of determination

5.3.7 Protein expression and purification of hE353A using the hE353A P0 baculovirus

Following the optimisation of recombinant hADAMDEC1 expression and purification, 105 ml of ExpiSf9 insect cells were infected with 1 ml of hE353A P0 baculovirus. 103 ml of the culture supernatant was harvested 72 hours after the cells were infected, and the purification process optimised in Chapter 5.3.6 were followed. The wash step was performed with 5 lots of washes with a constant imidazole concentration of 60 mM in the wash buffer. Additionally, in an attempt to increase the concentration of the recombinant protein in the final elute, E353A was eluted in a reduced total volume of the elution buffer (4.5 ml). The SDS-PAGE of the fractions collected at each step of the purification process showed a successful removal of the impurities with a minimal loss of mature hE353A during the wash step (Figure 5.24). However, since the concentration of imidazole in the wash buffer was maintained at 60 mM, the final sample appeared to contain more impurities than the previously purified hADAMDEC1 (Figure 5.22 A). Also, the volume of the pooled elutes increased from 4.5 ml to 6.6 ml during the dialysis by osmosis, which was not observed during the previous purification of hADAMDEC1. This resulted in dilution of the E353A in the post-dialysis final sample. Nevertheless, with the minimal loss of hE353A during the wash step and a 25% reduction in the final elution volume compared to the final elution volume used in the purification of the hADAMDEC1, the amount of hE353A in the post-dialysis sample appeared greater than that of the purified hADAMDEC1 on the SDS-PAGE gel (Figure 5.22 A and Figure 5.24). This was confirmed by densitometry (Figure 5.25). The concentration of hE353A in the post-dialysis sample was 245 ng/μl, which indicated that a total of 1.617 mg of recombinant hE353A, in a volume of 6.6 ml, was purified from the 103 ml of the culture supernatant harvested from the ExpiSf 9 cells infected with hE353A P0 baculovirus.

Well	Sample loaded
1	Culture supernatant
2	Post-diafiltration and concentration
3	Flow-through
W60	Wash with 60 mM Imidazole
W60	Wash with 60 mM Imidazole
W60	Wash with 60 mM Imidazole
W60	Wash with 60 mM Imidazole
W60	Wash with 60 mM Imidazole
E1	Elution 1 with 500 mM Imidazole
E2	Elution 2 with 500 mM Imidazole
E3	Elution 3 with 500 mM Imidazole
P	Post-dialysis

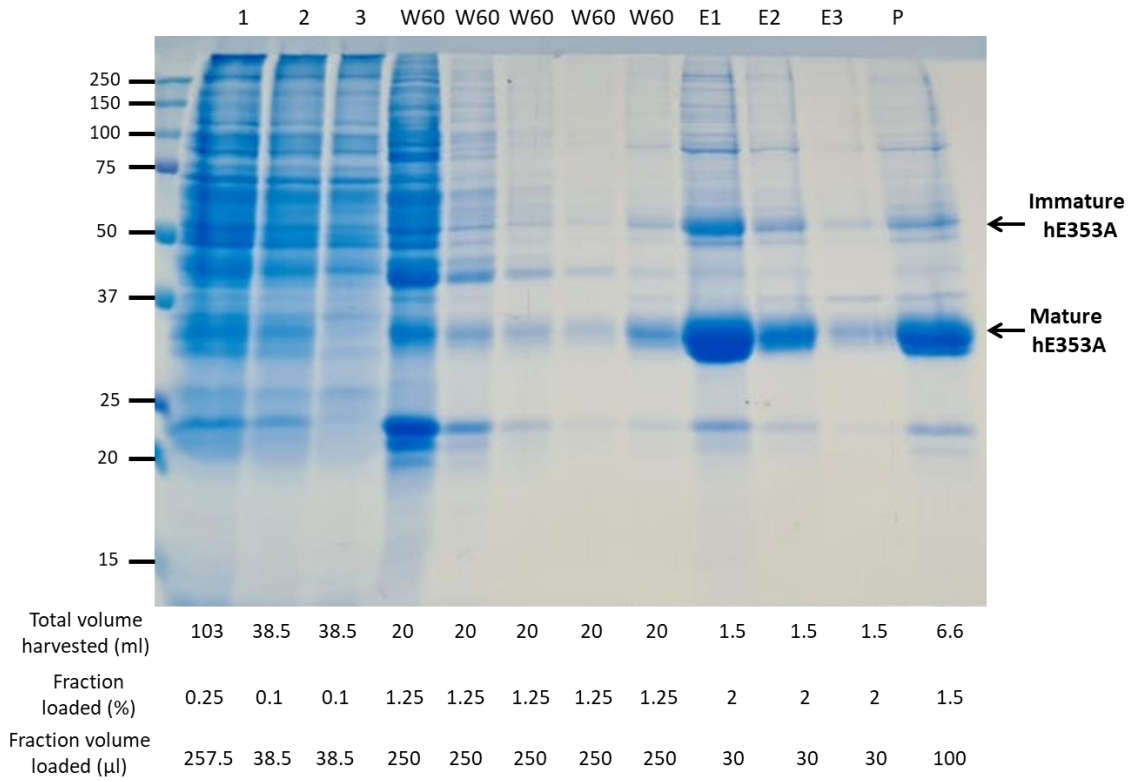

Figure 5.24 SDS-PAGE analysis of the fractions collected at each step of the hE353A purification process. A small fraction of solution was collected at each step of the optimised purification process and proteins were concentrated by TCA precipitation. 12% SDS-PAGE was used.

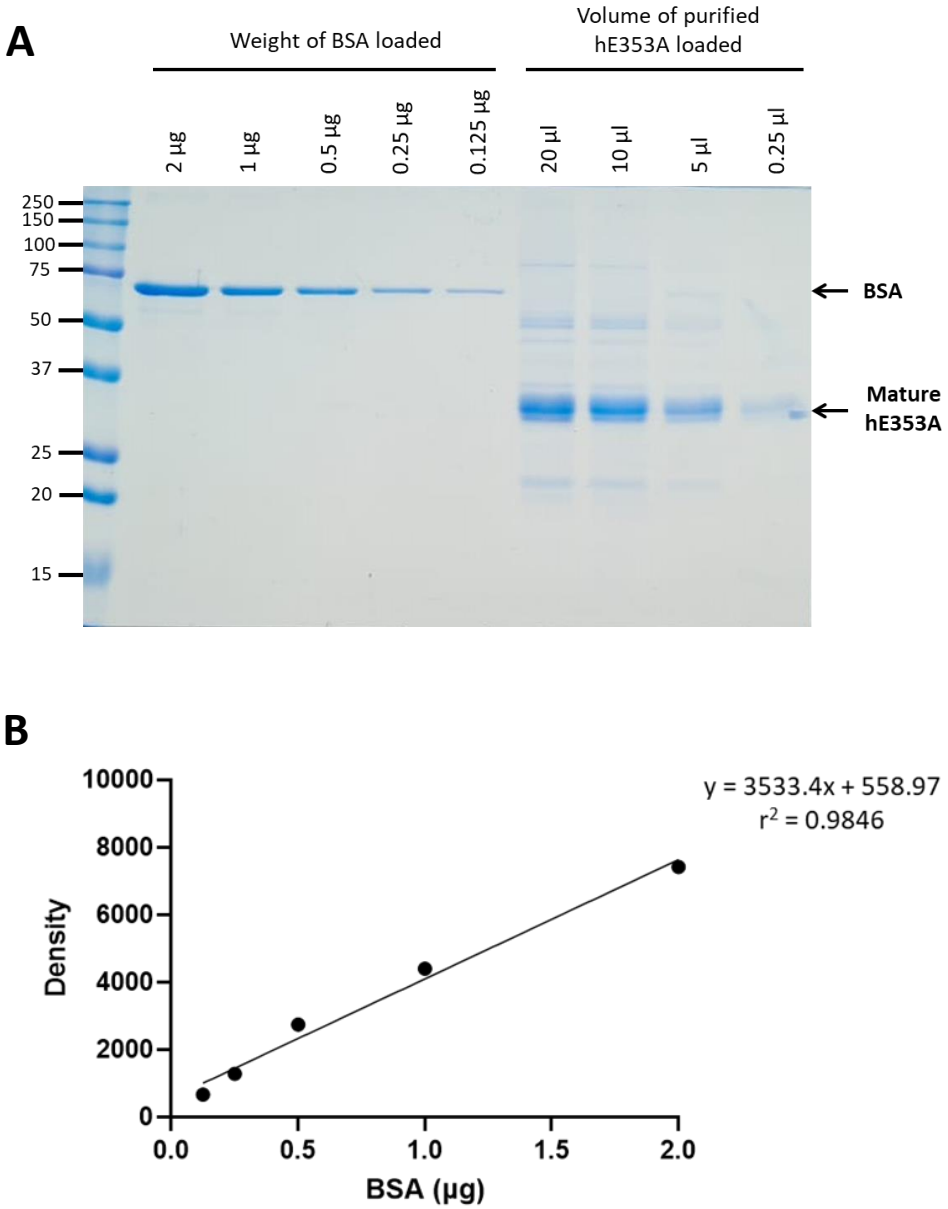

Figure 5.25 Quantification analysis of the purified recombinant hE353A by densitometry.

A: SDS-PAGE gel used for densitometry. Various volumes of the purified recombinant hE353A and weights of BSA were loaded in each well. 12% SDS-PAGE was used.

B: A standard curve generated by the densitometry of BSA used as a control.

The concentration of recombinant hE353A was calculated using the equation generated by the standard curve.

r^2: coefficient of determination

5.3.8 Protein expression and purification of mADAMDEC1 and mE353A

Following successful expression and purification of human ADAMDEC1 and E353A, mouse ADAMDEC1 and E353A P0 baculoviruses were produced following the same method used for the baculoviruses encoding the human ADAMDEC1 and

E353A. ExpiSf9 cells were transfected with the bacmids encoding mADAMDEC1 and mE353A, and the cell culture media containing budded recombinant baculoviruses were harvested at 96 hours after the transfection. However, the cell viability at 96 hours post-transfection was 82% and 83% for the cells transfected with mADAMDEC1 and mE353A bacmids respectively, which were higher than that of the cells transfected with hADAMDEC1 and hE353A bacmids (63%-79%). Based on this, it was anticipated that the viral titre in the P0 of mADAMDEC1 and mE353A were likely to have been lower than that of the hADAMDEC1 and hE353A P0 baculoviruses. Thus, double the volume of mADAMDEC1 and mE353A P0 baculoviruses were used to infect ExpiSf9 cells to express the recombinant mouse proteins.

105 ml of ExpiSf 9 cells were infected either with 2.1 ml of mADAMDEC1 or mE353A P0 baculovirus. At 72 hours post-infection, 103 ml of culture supernatants were harvested from the infected ExpiSf9 cells. The cell viabilities at 72 hours post-infection were 83% and 80% for the cells infected with mADAMDEC1 P0 baculovirus and mE353A P0 baculovirus respectively, which were notably higher than the cells previously infected with the hADAMDEC1 or hE353A P0 baculoviruses. This suggested that the infectivity, thus most likely the viral titres, of the mADAMDEC1 and mE353A baculoviruses was likely to have been inferior to that of the hADAMDEC1 or hE353A P0 baculoviruses, even though double the volume of P0 baculovirus encoding the mouse proteins were used to infect the cells. The supernatants were then processed and purified following the optimised protocol used to purify the recombinant hE353A (Chapter 5.3.7). During the dialysis, the volume of the solution containing the recombinant mE353A increased from 4.5 ml to 8.5 ml by osmosis. Overall, the protein expressions of the recombinant mouse ADAMDEC1 and E353A were much lower than that of the human recombinant proteins (Figure 5.26 A and B). This was likely to have been due to the lower viral titre in the P0 baculoviruses encoding the mouse proteins. Since the concentrations of the purified mature mADAMDEC1 and mE353A were much lower in comparison to the human counterparts, the mature mADAMDEC1 and mE353A were clearly seen as double lines which were likely to be due to the difference in glycosylation state (Figure 5.26 A and B). This was obscured in the SDS-PAGE and western blots of the purified human recombinant proteins (Figure 5.22 A and 5.24).

Figure 5.26 SDS-PAGE analysis of the fractions collected at each step of mADAMDEC1 (A) and mE353A (B) purification processes. A small fraction of solution was collected at each step of the optimised purification process and proteins were concentrated by TCA precipitation. 12% SDS-PAGE was used.

Well	Sample loaded
1	Culture supernatant
2	Post-diafiltration and concentration
3	Flow-through
W60	Wash with 60 mM Imidazole
W60	Wash with 60 mM Imidazole
W60	Wash with 60 mM Imidazole
W60	Wash with 60 mM Imidazole
W60	Wash with 60 mM Imidazole
E1	Elution 1 with 500 mM Imidazole
E2	Elution 2 with 500 mM Imidazole
E3	Elution 3 with 500 mM Imidazole
P	Post-dialysis

A

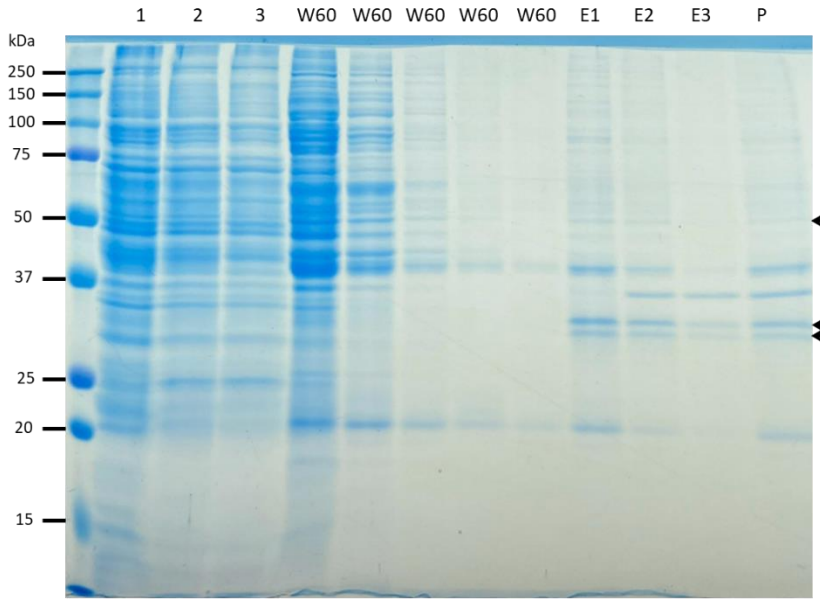

Total volume harvested (ml)	103	30	30	20	20	20	20	20	1.5	1.5	1.5	4.3
Fraction loaded (%)	0.25	0.1	0.1	1.25	1.25	1.25	1.25	1.25	2	2	2	1.5
Fraction volume loaded (µl)	257.5	30	30	250	250	250	250	250	30	30	30	64.5

B

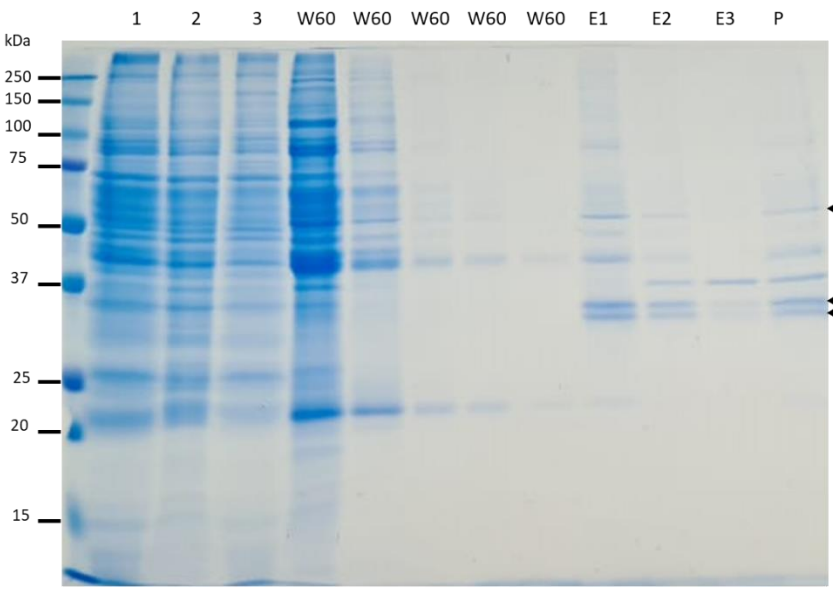

Total volume harvested (ml)	103	28	28	20	20	20	20	20	1.5	1.5	1.5	8.5
Fraction loaded (%)	0.25	0.1	0.1	1.25	1.25	1.25	1.25	1.25	2	2	2	1.5
Fraction volume loaded (µl)	257.5	28	28	250	250	250	250	250	30	30	30	127.5

5.3.10 Quantification of the purified mADAMDEC1 and mE353A

Densitometry was attempted to quantify the concentration of purified recombinant mADAMDEC1 and mE353A following the same protocol used for the recombinant human proteins. However, the concentrations of purified recombinant mouse proteins were not high enough to be visible on SGS-PAGE gels followed by Coomassie staining (Figure 5.27 A and B). This prevented densitometry analysis and quantification of the purified recombinant mouse proteins

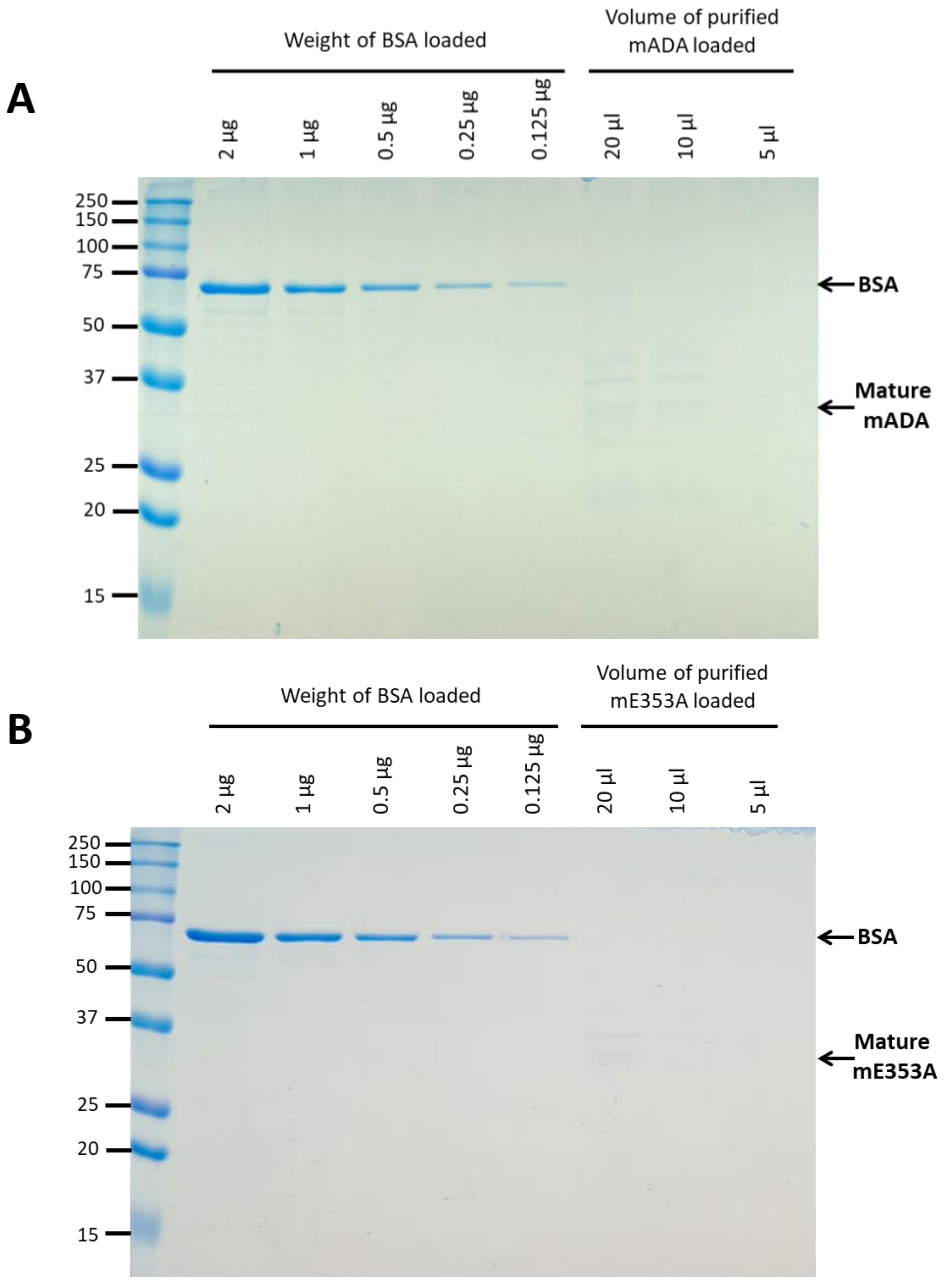

Figure 5.27 SDS-PAGE gels with various volumes of the purified recombinant mADAMDEC1 (A) and mE353A (B) and weights of BSA loaded in each well. The yields of purified mouse recombinant proteins were too low to be visualised by Coomassie staining of the SDS-PAGE gels to allow subsequent quantification analysis by densitometry. 12% SDS-PAGE gels were used.

5.3.11 Confirmation of synthesis and purification of the recombinant human and mouse ADAMDEC1 and E353A

In order to verify the synthesis and purification of the recombinant human and mouse ADAMDEC1 and E353A against each other, the purified recombinant proteins were examined by Western blot probed with anti-His and anti-ADAMDEC1 antibodies following TCA precipitation. Since the sensitivity of anti-ADAMDEC1 antibody was inferiror to that of the anti-His antibody, a greater volume of samples were loaded onto the wells to be exposed to the anti-ADAMDEC1 antibody. Similarly, since the concentrations of the purified mouse recombinant proteins were unknown but much lower than that of the human recombinant proteins, greater volumes of the purified mouse recombinant proteins were used to make the mouse recombinant protein loading samples in comparison to the human recombinant proteins.

The immature mouse ADAMDEC1 and E353A were not detectable by both anti-His or anti-ADAMDEC1 primary antibodies (Figure 5.27). This was likely to be secondary to the low concentrations of the immature mouse recombinant proteins in the purified solutions. However, the Western blots probed with anti-His and anti-ADAMDEC1 primary antibodies indicated that both human and mouse mature ADAMDEC1 and E353A were synthesised and purified successfully, which was demonstrated by bands at a molecular weight around 32 kDa uniformly across all the samples (Figure 5.28).

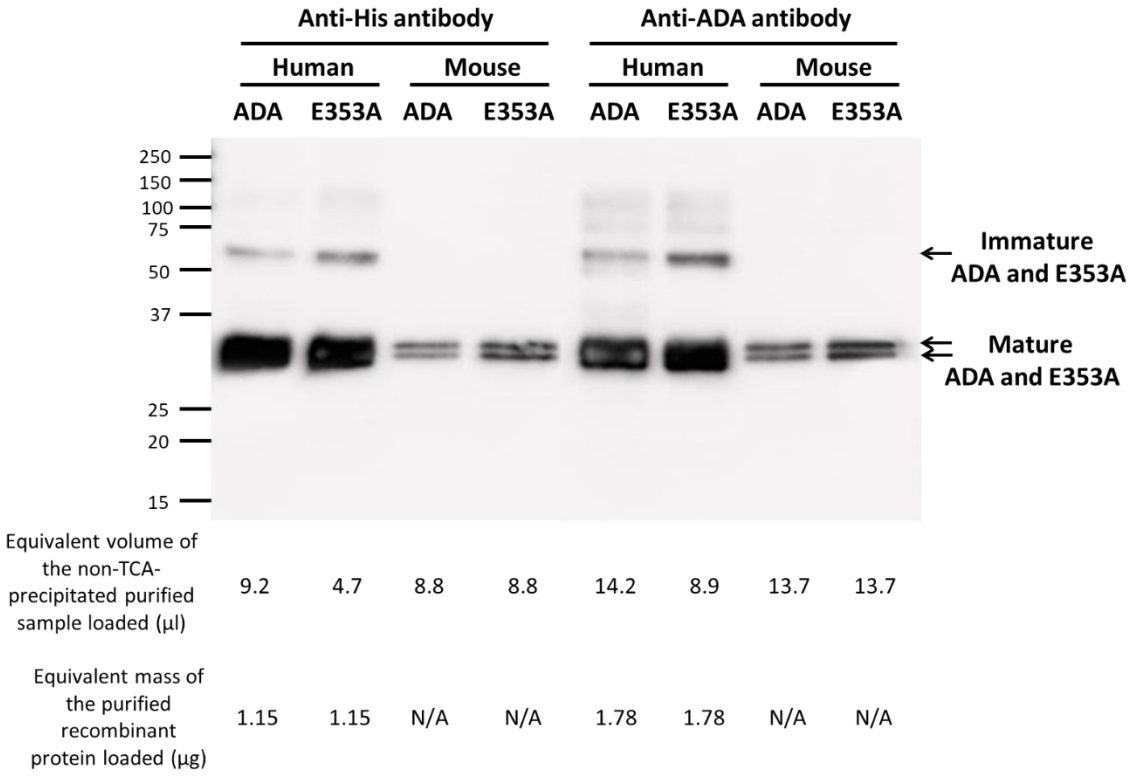

Figure 5.28 Western blot of the purified recombinant human and mouse ADAMDEC1 and E353A probed with anti-His and anti-ADAMDEC1 antibodies. The purified recombinant proteins were concentrated by TCA precipitation. The presence of mature ADAMDEC1 or E353A were observed in all the samples by bands at around 32 kDa detected by both anti-His ad anti-ADAMDEC1 antibodies. The blot is representative of n=2.
ADA: ADAMDEC1

5.3.11 Confirmation of the catalytical activity of purified recombinant hADAMDEC1

Recombinant hADAMDEC1 has previously been shown to cleave human α2-macroglobulin, during which a cross-linked molecule comprising ADAMDEC1 and α2-macroglobulin, weighing ~ 225 kDa, is formed and can be detected by Western blot.[14,28] In order to verify the catalytical activity of the purified recombinant hADAMDEC1, the purified hADAMDEC1 was incubated with human α2-macroglobulin, and its catalytical activity was examined against that of the purified recombinant hE353A by Western blot probed with anti-His primary antibody.

The cross-linked hADAMDEC1 and α2-macroglobulin complex molecule was detected after incubating α2-macroglobulin with the purified hADAMDEC1 but not with the purified hE353A (Figure 5.29). This indicated that the purified recombinant hADAMDEC1 possessed a catalytical activity, whereas the purified recombinant

hE353A did not. Additionally, the presence of the His-tag did not hinder the catalytic ability of the recombinant mature hADAMDEC1. These findings indicated that the purified recombinant hADAMDEC1 could be used in functional studies in future, and the purified recombinant hE353A could be used as a counterpart control.

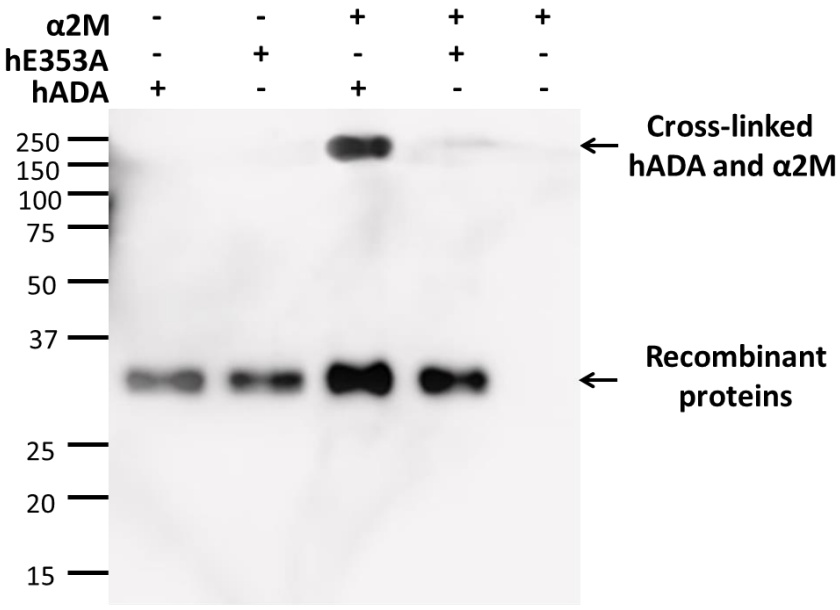

Figure 5.29 Analysis of catalytical activity of the purified mature hADAMDEC1 and hE353A. The purified recombinant human ADAMDEC1 and E353A were incubated with human α2-macroglobulin. The catalytical activities of the recombinant proteins were assessed by the presence of ADAMDEC1-α2-macroglobulin complex by Western blot proved with anti-His antibody. The formation of ADAMDEC1-α2-macroglobulin complex was detected by a band approximately 225 kDa in the hADAMDEC1 sample but not in hE353A sample. The blot is representative of n=2. hADA: Human ADAMDEC1, α2M: α2-macroglobulin

5.3.12. The potential anti-bacterial property of ADAMDEC1

Having established the catalytical activity of the purified recombinant human ADAMDEC1, a potential anti-bacterial property of ADAMDEC1 was examined using *E.coli* and *Salmonella. enterica* and 3 different concentrations (6.25 ng/μl, 1.875 ng/μl, 0.625 ng/μl) of hADAMDEC1 as a small pilot functional assay. The purified recombinant hE353A was used as a control. *E coli* is a commensal bacteria and is one of the most-studied bacterial species. *Salmonella enterica*, in contrast, is an opportunistic pathogen which can cause mucosal inflammation in the intestine. The bacterial growth curve analyses demonstrated that there were no inhibitory

effects of hADAMDEC1 on the growth of both *E.coli* and *Salmonella enterica* tested with these 3 different concentrations of hADAMDEC1 (Figure 5.30 A and B).

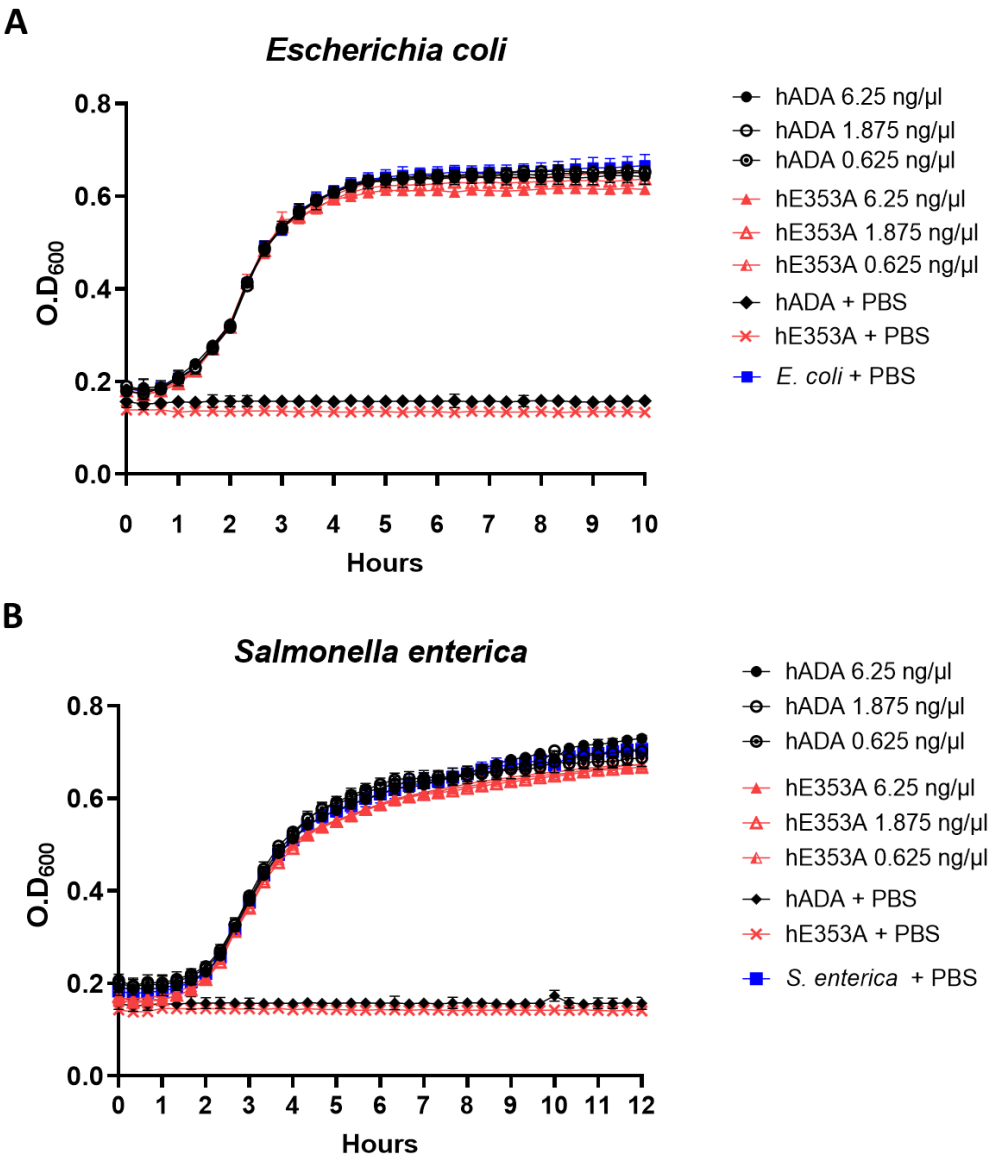

Figure 5.30 Growth curves of *E. coli* (A) and *Salmonella enterica* (B) incubated with various concentrations of hADAMDEC1 and hE353A. Both hADAMDEC1 and E353A did not demonstrate inhibit effect on the growth of these bacteria. The results are representative of n=3.
hADA: Human ADAMDEC1, *S. enterica*: *Salmonella enterica*

5.4 Discussion

In this chapter, the methodology to synthesise recombinant human and mouse ADAMDEC1 and the protease dead mutant E353A using the BEVS was verified. Bacmids encoding the human and mouse ADAMDEC1 and E353A were generated. This was followed by successful transfection and transduction of ExpiSf9 insect cells to produce baculoviruses and subsequently recombinant human and mouse ADAMDEC1 and E353A proteins. Although the production of the mouse ADAMDEC1 and E353A still requires some further optimisation to increase the yield of the recombinant protein, the proof of concept was met. This was followed by successful purification of the recombinant proteins using diafiltration, nickel-histidine IMAC and dialysis.

The catalytical activity and inactivity of the recombinant human ADAMDEC1 and E353A respectively were confirmed using human α2-macroglobulin, a known substrate for ADAMDEC1 in vitro.[14,16,20,28] Importantly, this, first of all, proved that the recombinant mature ADAMDEC1 produced by insect cells possessed the catalytical function comparable to that of the recombinant ADAMDEC1 produced in human cells such as HEK293 cells.[14,16,20] Secondly, ADAMDEC1 and E353A were synthesised as full immature forms and cleaved intracellularly to produce mature forms similar to the protein synthesis and processing in human cells. Furthermore, the processing did not require auto-cleavage as the recombinant E353A was also secreted as a mature processed form. Thirdly, it indicated that recombinant ADAMDEC1 from the insect cells remained stable and its catalytic function was preserved in the insect cell culture media and during the purification process. This implied that the recombinant ADAMDEC1 produced and purified by the methodology used in this chapter could be used for various future experiments to examine the biological and chemical characteristics of ADAMDEC1. The up-scaling of production of these 4 recombinant proteins is now possible using the same methodology.

Using the recombinant human ADAMDEC1 and its mutant counterpart E353A, the anti-microbial property of ADAMDEC1 was examined using *E.coli* and *Salmonella enterica* as a small pilot functional study of ADAMDEC1. This revealed that recombinant human mature ADAMDEC1 did not have anti-microbial properties against either of the bacteria. However, it is still possible for ADAMDEC1 to

possess anti-microbial properties on other bacterial species that were not tested in this chapter.

Chapter 6

Characterisation of the immune response in *Adamdec1*$^{-/-}$ mice upon induction of DSS-induced colitis

6.1 Background and aims

The potential mechanistic role of ADAMDEC1 during mucosal inflammation in the gastrointestinal tract has been demonstrated by two previous studies using *Adamdec1*$^{-/-}$ mice.[26,56] Both of these studies demonstrated exaggerated systemic and colonic inflammation in *Adamdec1*$^{-/-}$ mice by DSS-induced colitis. One of these studies also demonstrated that the exaggeration in systemic inflammation exhibited by the *Adamdec1*$^{-/-}$ mice compared to the WT mice was even greater using bacteria-induced colitis affecting both small and large intestines.[26] These findings suggested a protective role of ADAMDEC1 in mucosal inflammation irrespective of the specific mode of the inflammatory trigger or location within the lower gastrointestinal tract. In the same study, a significantly larger size of the neutrophil population was observed in the tissue of *Adamdec1*$^{-/-}$ mice compared to the WT on day 3 of the DSS challenge. There was no difference in the size of macrophage populations between the WT and *Adamdec1*$^{-/-}$ mice. However, this macrophage population was defined simply by cells expressing CD11b but negative for the Gr-1 expression. Many cells other than the macrophages within the intestine, such as monocytes, dendritic cells and eosinophils, are known to express CD11b but not Gr-1, thus the macrophage population identified in this study was likely to have been unprecise. The intestinal macrophages are notoriously difficult to be identified accurately, requiring a combination of multiple cell surface markers.[178–181] Additionally, in the same study, the expressions of *Il-17* and *Il-22* at the RNA messenger level were also shown to be increased in the colonic tissues of the *Adamdec1*$^{-/-}$ mice in comparison to the WT, with statistical significance achieved 8 days after the cessation of the DSS-administration. However, the population of Th17 cells, the main cells that secrete both IL-17 and IL-22 within lamina propria, was not examined. Another study using *Adamdec1*$^{-/-}$ in the BALB/c genetic background, on the other hand, suggested possible aberrant ECM remodelling as the responsible mechanism for the exacerbated mucosal

inflammation in the absence of ADAMDEC1.[56] This study was published at the time of writing this thesis thus this aspect of ADAMDEC1's potential role to ECM remodelling was not examined during this project. Overall, despite the findings from these two studies, the mechanism through which ADAMDEC1 may affect the intestinal mucosal inflammation and immune response remained largely unknown. This chapter primarily aimed to interrogate the role of ADAMDEC1 during intestinal mucosal inflammation using *Adamdec1*$^{-/-}$ mice and DSS-colitis model.

In this chapter, colonic mucosal inflammation was induced by oral administration of 2% DSS in the WT and *Adamdec1*$^{-/-}$ mice. DSS is a synthetic sulphated polysaccharide composed of dextran and sulphated anhydroglucose. It has a highly variable molecular weight ranging between 5 – 1400 kDa. Murine colitis is most effectively induced by the oral administration of DSS with molecular weight between 40 - 50 kDa added to the drinking water, at a concentration varying between 1 – 5%.[182] The exact mechanism through which DSS induces inflammation along colonic tissue in mouse is not fully elucidated. However, in the most accepted mechanism proposed, DSS does not act directly to cause mucosal inflammation, but rather acts as a chemical toxin that causes epithelial injury. This leads to an influx of luminal antigens including microbes that results in mucosal inflammation via activation of the immune response.[183–185] The simplicity, rapidity and reproducibility of the DSS-induced colitis as well as the non-immunogenic nature of DSS itself have made this model the most widely used murine experimental colitis model to study the intestinal immune system and pathogenesis of IBD. Although the highest expression of ADAMDEC1 is seen in the small bowel under healthy status, there are no such reliable and well-established models as DSS-colitis to induce inflammation in the small intestine in mouse. Additionally, the exacerbated degree of inflammation in *Adamdec1*$^{-/-}$ mice compared to the WT was previously observed in both small and large intestine using *Salmonella enterica* serovar Typhimurium and DSS respectively, indicating that ADAMDEC1 has a mechanistic role in mucosal immune response affecting the large intestine despite its lower expression compared to the small intestine.[26] Furthermore, the use of DSS-induced colitis would generate results that are comparative to the previous studies using DSS-colitis model in *Adamdec1*$^{-/-}$ mice.[26,56] Taking these to account, DSS-colitis model was deemed the optimum experimental colitis model to study the role of ADAMDEC1 in mucosal immune response in this project.

The DSS concentration of 2 % was chosen to be orally administered to the mice to induce colitis in this project. This was based on the dose-response study performed previously in our laboratory using the same strain of WT and *Adamdec1*$^{-/-}$ mice. The concentration of 2% was deemed optimum to produce a sufficient degree of colitis without exceeding the moderate severity limit imposed on the Home Office project licence.

In this project, both WT and *Adamdec1*$^{-/-}$ mice were pooled and cohoused for 8 weeks prior to the commencement of DSS-challenge in an attempt to minimise the cage-effect on the intestinal microbiome, which may influence their immune response to DSS-induced epithelial injury. (Discussed in more detail in Chapter 7.) The colonic tissues were harvested and the gene expression and immune cell populations were examined by qPCR and flow cytometry respectively. qPCR was used to capture the overall global effect of ADAMDEC1 on the host's immune response within the colonic tissue at the RNA messenger level. Flow cytometry analysis was conducted using 2 panels of antibodies designed to examine the populations of selected lymphoid immune cells, including Th17 cells, and selected myeloid immune cells, including monocytes and macrophages. This allowed more comprehensive interrogation of the cell population profiles during DSS-induced colitis in the presence and absence of ADAMDEC1 and helped to address some unanswered questions from the previous study.[26]

The main aims for Chapter 6 were:

- To confirm the exaggerated degree of inflammation in *Adamdec1*$^{-/-}$ mice in comparison to the WT mice upon induction of DSS-induced colitis
- To examine the difference in the populations of lymphoid and myeloid immune cells between the *Adamdec1*$^{-/-}$ and WT mice upon induction of DSS-induced colitis
- To examine the difference in the expression of selected genes in the colonic tissues of the *Adamdec1*$^{-/-}$ and WT mice upon induction of DSS-induced colitis

6.2 Materials and method

6.2.1 DSS administration

DSS Salt - Colitis Grade (36,000-50,000 MW) (MP) was dissolved in sterile water to achieve a concentration of 2%. This was provided as drinking water to the mice and was replaced every other day for 7 days. For the Day 9 experiment, DSS was changed to sterile water on day 7 and administered to the mice for a further 2 days.

6.2.2 Experimental timeline and output of DSS-induced acute colitis mouse model

Three cohorts of mice: naïve, Day 7 Experiment, Day 9 Experiment, were used in this chapter to examine the effect of ADAMDEC1 during DSS-induced colitis by flow cytometry and qPCR analyses of the colonic tissue of the mice. Figure 6.1 and Table 6.1 summarise the experimental timeline, end-point analyses and the number of mice used in the experiment.

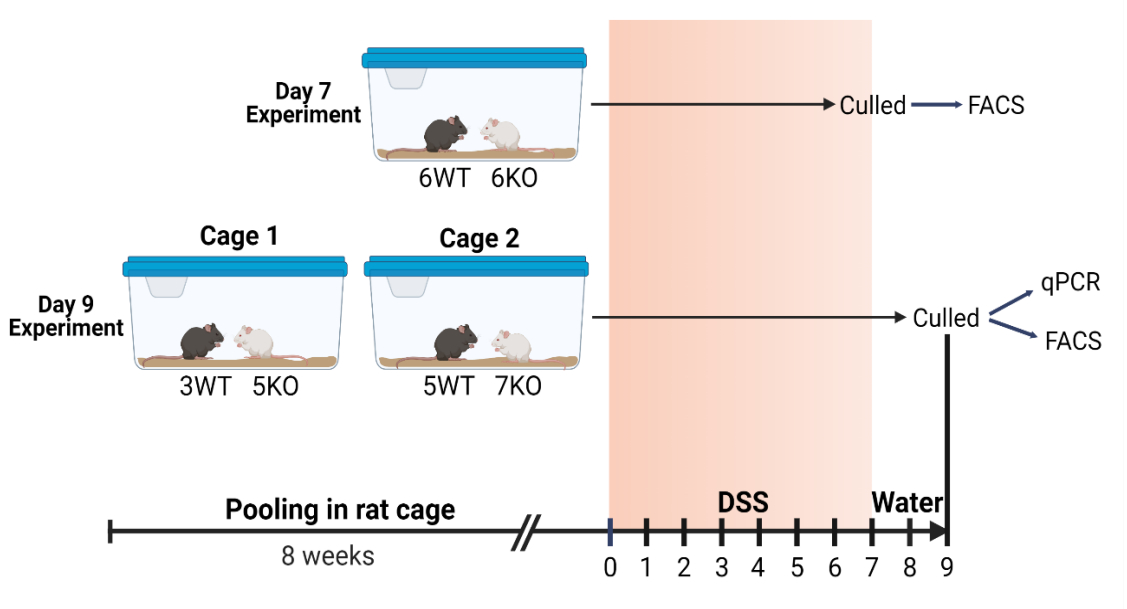

Figure 6.1 Scheme demonstrating the experimental timeline and output of the analysis to characterise the effect of ADAMDEC1 during DSS-induced colitis.
KO: *Adamdec1*$^{-/-}$, WT: Wild type

		Number of mouse			
		WT	**KO**	**TOTAL**	**End-point analysis**
Naïve		4	4	8	qPCR and FACS
Day 7 Experiment		6	6	12	FACS
Day 9 Experiment	**Cage 1**	3	5	8	qPCR and FACS
	Cage 2	5	7	12	

Table 6.1 Number of the WT and *Adamdec1*$^{-/-}$ mice used in each experimental cohort and different end-point analyses.
KO: *Adamdec1*$^{-/-}$, WT: Wild type

The mice in Day 7 Experiment cohort (6 WT and 6 *Adamdec1*$^{-/-}$ mice) were challenged with DSS for 7 days and were culled on day 7 of the experiment (Figure 6.1). The mice in Day 9 Experiment cohort (8 WT and 12 *Adamdec1*$^{-/-}$ mice) were challenged with DSS for 7 days and their drinking water was changed to sterilised water for further 2 days and were culled on day 9 (Figure 6.1). The mice in Day 9 Experiment cohort were caged in 2 separate cages and the experiment was conducted one week apart to reduce the number of samples being handled at one time to minimise the time-associated tissue degradation during the sample harvest and preparation. Day 9 Experiment Cage 1 was comprised of 3 WT and 5 *Adamdec1*$^{-/-}$ mice, and Cage 2 was comprised of 5 WT and 7 *Adamdec1*$^{-/-}$ mice. Another cohort of mice comprising age-matched 4 WT and 4 *Adamdec1*$^{-/-}$ mice, which had been consuming sterilised water, were culled to provide naïve colonic tissues as the baseline samples to be compared with the DSS-challenged tissues of the WT and *Adamdec1*$^{-/-}$ mice.

The mice that underwent DSS challenge had been housed in multiple smaller mouse cages (1 to 4 mice per cage) from the time they were weaned from their parents. As described in Chapter 7, the microbiome of the mice was significantly affected by the individual cages that they were housed. Thus in an attempt to minimise the cage-dependent variability in the microbiome of the mice, which might influence the immune response, the mice in multiple individual cages were pooled into large rat cages per experimental subgroup: Day 7 Experiment, Day 9 Experiment Cage 1 and Day 9 Experiment Cage 2, for 8 weeks prior to being challenged with DSS (Figure 6.1).

The colonic tissues harvested from the mice in the naïve and Day 9 Experiment cohorts were processed for both gene expression analysis by qPCR and flow cytometry analysis by FACS (Figure 6.1 and Table 6.1). The colonic tissues harvested from the mice in Day 7 Experiment cohort were processed only for FACS. The primary end timepoint of day 9, counting from the initiation of the DSS challenge, was chosen for both qPCR and FACS analysis. This was based on the previous DSS-induced colitis experiment using the same strain of WT and *Adamdec1*$^{-/-}$ mice which exhibited the greatest difference in the weight loss on day 9 after the initiation of the DSS challenge.[26] Also a maximum intensity of colitis, based on inflammatory score, epithelial permeability and weight loss, has been previously reported to occur 2 days after the cessation of DSS.[92] However, in this project, the WT mice started to demonstrate signs of recovery from day 8. Thus Day 7 Experiment cohort was created to provide an extra time point for the FACS analysis to ensure that the colonic cell populations at the height of mucosal inflammation were examined, thereby allowing more precise evaluation of the dynamic change in cell populations during the acute phase of inflammation.

6.2.2 Weight measurement of mice

The weights of the mice were measured prior to the commencement of the DSS challenge (day 0) and during the DSS challenge using calibrated Compass CX Series Portable Scale (Ohaus). The change in weight during the DSS challenge was analysed relative to the weight on day 0 for each mouse. Mice that recorded a weight loss > 20% were culled in accordance with the project licence guidelines.

6.2.3 Isolation of mouse colonic cells

Colon wash solution

PBS(Gibco)

10% FBS (Sigma)

Penicillin/Streptomycin (50 U/ml and 50 µg/ml) (Gibco)

Pre-digestion solution

HBSS (Ca^{2+} and Mg^{2+} free) (Gibco)

10% FBS (Sigma)

Penicillin/Streptomycin (50 U/ml and 50 µg/ml) (Gibco)

2mM EDTA (Sigma)

Digestion solution

HBSS (Ca^{2+} and Mg^{2+} free) (Gibco)

10% FBS (Sigma)

Penicillin/Streptomycin (50 U/ml and 50 µg/ml) (Gibco)

1.5 mg/ml Collagenase (Sigma)

0.75 mg/ml Dispase II (Sigma)

0.04 mg/ml DNase I (Sigma)

Mice were culled and colons were harvested. Caecum from each sample was removed and discarded. For the mice used in Day 9 Experiment, faeces in the lumen of the colon were expelled by gentle pressure applied on the colon and placed in 1.5 ml Eppendorf tubes and stored at -80°C to be processed subsequently for microbiome analysis (Chapter 7). The distal 1cm of each colonic sample was removed and placed in 1.5 ml Eppendorf tube containing 500 µl of RNAlater (Qiagen) and stored at -80°C for subsequent qPCR analysis (Chapter 6.2.6). The rest of the colons were washed in the ice cold colon wash solution in 92 mm petri dish. The colons were then cut open longitudinally with surgical scissors and washed twice in the fresh ice cold colon wash solution to remove luminal faecal matter. Each colon was then placed in a 50 ml Falcon tube containing 20 ml of the pre-digestion solution and incubated at 37°C with constant agitation at 250 rpm for 1 hour to remove epithelial cells. After 1 hour, colons were removed from the pre-digestion solution and washed in PBS to remove EDTA. Each colonic tissue was placed in a 5 ml Eppendorf tube containing 2 ml of PBS and cut into small pieces (approximately 2 mm x 2 mm) using surgical scissors. The PBS containing the cut colonic tissues was then added to 50 ml Falcon tubes containing 20 ml of the digestion solution. The digestion solutions containing cut colonic tissue were then incubated at 37°C on constant agitation at 250 rpm for 30 minutes. At the beginning, halfway and end of the incubation, the solutions were vigorously vortexed for 20 seconds. The solutions were then filtered through 70 µm nylon cell strainer (Fisher Scientific) into fresh 50 ml Falcon tubes to remove debris and centrifuged at 500 g for 10 minutes at 4°C. The supernatants were removed and the cells were resuspended in 20 ml of ice cold PBS. The cells were filtered

again through 40 µm nylon cell strainer (Fisher Scientific) into fresh 50 ml Falcon tubes and centrifuged at 500 g for 10 minutes at 4°C. The cells were then washed twice more in ice cold PBS and centrifuged at 500 g for 10 minutes at 4°C.

6.2.4 FACS of isolated mouse colonic cells

The cells isolated as above were resuspended in 2.1 ml of PBS. 50 µl from each sample was collected and pooled into a FACS tube (Thermo Fisher Scientific) to make unstained control. 2 µl of Live/Dead stain (Thermo Fisher SCientific) was added to the remaining of each sample and incubated for 30 minutes in the dark. The cells were centrifuged and the supernatants were removed. The cells were washed in 5 ml of PBS and centrifuged at 500 g for 10 minutes at 4°C. The cells were resuspended in 200 µl of FACS buffer and 2 µl of Fc block (BioLegend) was added to each sample and incubated for 15 minutes at room temperature. Each sample was divided in half which were stained with either Lymphoid panel or myeloid panel antibodies.

6.2.4.1 Lymphoid panel antibody staining

The antibodies for cell surface marker (CD3, CD45, CD8a, CD127) and intracellular marker (RORγt, FOXP3) were pooled separately in tubes and mixed gently by pipetting (Table 6.2). The intracellular antibody mix was placed in the dark. The mix of the surface marker antibodies were added to the cells prepared (Chapter 6.2.4.0) and vortexed briefly. The cells were incubated for 30 minutes at 4°C in the dark. After 30 minutes, the cells were washed with 1 ml of FACS buffer 3 times by centrifugation at 500 g for 5 minutes at 4°C. After the last wash, FACS buffer was discarded. Foxp3/Transcription Factor Staining Buffer Set (eBioscience) was used for staining of intracellular markers with antibodies. Working concentration of Fixation/Permeabilisation solution and Permeabilistaion buffer were prepared following the manufacturer's protocol. 1 ml of 1x Fixation/Permealisation solution was added to each sample. The cells were vortexed briefly and incubated at 4°C in the dark for 30 minutes. After 30 minutes, 2 ml of 1x Permealisation buffer was added to each tube and centrifuged at 500 g for 5 minutes at room temperature. The supernatants were discarded and the cells were resuspended in 100 µl of Permealisation buffer. The mix of the intracellular marker antibodies were then added to each tube

and the cells were incubated at room temperature in the dark for 30 minutes at 4°C. 2 ml of Permealisation buffer was added to each tube and the cells were centrifuged at 500 g for 5 minutes at room temperature. The supernatants were discarded. The cells were then washed 3 times with 1 ml of FACS buffer using centrifugation at 500 g for 5 minutes at 4°C. After the last wash, the supernatants were discarded and the cells were resuspended in 500 µl of FACS buffer. The stained cells were kept in the dark at 4°C until flow cytometry on a LSR Fortessa (BD Biosciences). Compensation beads were stained with 1 µl of each antibody by following the same protocols as the colonic cells and run for each experiment. Flow cytometry data were analysed using FlowJo software (BD Biosciences).

Target	Fluorescence	Manufacturer	Catalogue
CD45 (30-F11)	PE-Cy7	BioLegend	103113
CD3 (17A2)	FITC	BioLegend	100203
CD4 (RM4-5)	APC-Cy7	BioLegend	100525
CD8 (53-6.7)	BV786	BD Biosciences	563332
CD127 (A7R34)	BV421	BioLegend	135027
RORγt (q31-378)	PE	BD Biosciences	562607
FOXP3 (FJK-16s)	APC	eBioscience	17-5773-80
Dead cells	AmCyan	Thermo Fisher	L34967

Table 6.2 List of lymphoid panel antibodies used for flow cytometry analysis of the mouse colonic cells. Clone name of each antibody is specified in brackets.
PE: R-phycoerythrin Cy7: Cyanine-7, FITC: Fluorescein isothiocyanate, APC: Allophycocyanin, BV: Brilliant Violet™

6.2.4.2 Myeloid panel antibody staining

All the antibodies of the myeloid panel were pooled in a tube and mixed gently by pipetting (Table 6.3). The mix of the antibodies was added to the cells prepared (Chapter 6.2.4.0) and vortexed briefly. The cells were incubated at 4°C in the dark for 30 minutes. After 30 minutes, the cells were vortexed and washed 3 times with 1 ml of FACS buffer by centrifugation at 500 g for 5 minutes at 4°C. After the last wash, the cells were resuspended in 150 µl of FACS buffer. 150 µl of 4% paraformaldehyde was added to each sample and the cells were incubated at 4°C in the dark for 15 minutes. The cells were centrifuged at 500

g for 5 minutes at 4°C and the supernatants were discarded. The cells were then washed 3 times with 1 ml of FACS buffer by centrifugation at 500 g for 5 minutes at 4°C. After the last wash the cells were resuspended in 500 µl of FACS buffer and stored at 4°C in the dark until flow cytometry on a LSR Fortessa (BD Biosciences). Compensation beads were stained with 1 µl of each antibody by following the same protocols as the colonic cells and run for each experiment. Flow cytometry data were analysed using FlowJo software (BD BioSciences)

Target	Fluorescence	Manufacturer	Catalogue
CD45 (30-F11)	PE-Cy7	BioLegend	103113
CD3 (17A2)	FITC	BioLegend	100203
CD11b (SA011F11)	PE	BioLegend	149005
CD11c (N418)	BV786	BD Biosciences	565587
MHCII (M5/114.15.2)	Alexa Fuor 647	BD Biosciences	562367
Ly6G (1A8)	BV421	BioLegend	127628
F4/80 (BM8)	PE/CF594	BioLegend	123145
Ly6C (HK1.4)	BV711	BioLegend	128037
CX3CR1 (SA011F11)	PE	BioLegend	149005
Dead cells	AmCyan	Thermo Fisher	L34967

Table 6.3 List of myeloid panel antibodies used for flow cytometry analysis of the mouse colonic cells. Clone name of each antibody is specified in brackets. PE: R-phycoerythrin Cy7: Cyanine-7, FITC: Fluorescein isothiocyanate, APC: Allophycocyanin, BV: Brilliant Violet™

6.2.5 FACS of murine splenocytes with or without enzymatic digestion step

6.2.5.1 Isolation of murine splenocytes

Spleen wash solution

HBSS (Ca^{2+} and Mg^{2+} free) (Gibco)

10% FBS (Sigma)

Penicillin/Streptomycin (50 U/ml and 50 µg/ml) (Gibco)

Mice were culled and spleens were harvested. The intact spleens were washed in the spleen wash solution. Each spleen was transferred to 35 mm petri dish with 1 ml of fresh spleen wash solution. The spleens were sieved through 70 µm nylon cell strainer (Thermo Fisher Scientific) using plungers of 2.5 ml syringe. The cells

were collected and transferred into 50 ml Falcon tubes and centrifuged at 500 g for 5 minutes. The supernatants were discarded and the cells were resuspended in 1 ml of Red Blood Cell Lysing Buffer Hybri-Max (Sigma) and incubated for 3 minutes at room temperature. 30 ml of ice cold PBS was added to each sample and the cells were centrifuged at 500 g for 5 minutes at 4°C. The supernatants were discarded and the cells were resuspended in 1.5 ml of FACS buffer. Each sample was then divided in half. One half of each sample was mixed with 20 ml of digestion solution in 50 ml Falcon tube and incubated at 37°C with constant agitation at 250 rpm for 30 minutes. The other half of each sample was stored at 4°C. After 30 minutes, the digested splenocytes were centrifuged at 500 g for 10 minutes and supernatants were discarded. The digested cells were then washed 3 times with 25 ml of ice cold PBS and with centrifugation at 500 g for 5 minutes at 4°C. After the last wash, the digested splenocytes were resuspended in 750 µl of FACS buffer.

6.2.5.2 Antibody staining of digested and undigested splenocytes

7.5 µl of Fc block (BioLegend) was added to each sample of undigested and digested splenocytes and incubated for 15 minutes at room temperature. An appropriate antibody panel was added to both digested and undigested splenocytes and incubated at 4°C for 30 minutes in the dark (Table 6.4 and 6.5). The cells were then centrifuged at 500 g for 5 minutes at 4°C. The supernatants were discarded and the cells were washed 3 times with 1 ml of FACS buffer with centrifugation at 500 g for 5 minutes at 4°C. After the last wash, the supernatants were discarded and the cells were resuspended in 150 µl of FACS buffer. 150 µl of 4% paraformaldehyde was added to each sample and incubated at 4°C for 15 minutes in the dark. The cells were then centrifuged at 500 g for 5 minutes at 4°C. The supernatants were discarded and the cells were washed twice with 1 ml of FCAS buffer. The supernatants were discarded and the cells were then resuspended in 500 µl of FACS buffer and stored at 4°C in the dark until dark until flow cytometry on a LSR Fortessa (BD Biosciences). Compensation beads were stained with 1 µl of each antibody by following the same protocols as the colonic cells and run for each experiment. Flow cytometry data were analysed using FlowJo software (BD Biosciences).

Splenocytes lymphoid panel			
Target	**Fluorescence**	**Manufacturer**	**Catalogue**
CD45 (30-F11)	PE-Cy7	BioLegend	103113
CD3 (17A2)	FITC	BioLegend	100203
CD4 (RM4-5)	APC-Cy7	BioLegend	100525
CD8 (53-6.7)	BV786	BD Biosciences	563332

Table 6.4 List of lymphoid panel antibodies used for flow cytometry analysis of the murine splenocytes. Clone name of each antibody is specified in brackets. PE: R-phycoerythrin Cy7: Cyanine-7, FITC: Fluorescein isothiocyanate, APC: Allophycocyanin, BV: Brilliant Violet™

Splenocytes myeloid panel			
Target	**Fluorescence**	**Manufacturer**	**Catalogue**
CD45 (30-F11)	PE-Cy7	BioLegend	103113
CD3 (17A2)	FITC	BioLegend	100203
Ly6C (HK1.4)	BV711	BioLegend	128037
CX3CR1 (SA011F11)	PE	BioLegend	149005

Table 6.5 List of myeloid panel antibodies used for flow cytometry analysis of the murine splenocytes. Clone name of each antibody is specified in brackets.
PE: R-phycoerythrin Cy7: Cyanine-7, FITC: Fluorescein isothiocyanate, APC: Allophycocyanin, BV: Brilliant Violet™

6.2.6 qPCR of the murine colonic tissues and primers used for qPCR

Total RNA were extracted from the colonic tissues harvested and stored in RNAlater (Chapter 6.2.3) using RNeasy Mini Kit (Qiagen) (Chapter 2.7.1.2 and 2.7.1.3). The extracted RNAs were converted into cDNA (Chapter 2.7.2). qPCR was conducted using SYBR® Green Real-Time PCR kit as described (Chapter 2.7.3) using primers listed in Table 6.6.

Target gene	Forward primer (5' to 3')	Reverse primer (5' to 3')
B-actin	GGGCCGCGTCTCCTTT	ATCCTTTCTCTCCAGTGCTCAGA
Gapdh	AAGGTCATCCCAGAGCTGAA	CTGCTTCACCACCTTCTTGA
Ppia	GGGCCGCGTCTCCTTT	ATCCTTTCTCTCCAGTGCTCAGA
Cd4	TCAAGTGGTGGCCCCTGAGA	CTGCCTGGCGCTGTTGGTG
Cd8	CGTGGCTCAGTGAAGGGGAC	GCAAACACGCTTTCGGCTCC
Il-1β	TCAACAAGATAGAAGTCAAGAGCAA	ATGGTGAAGTCAATTATGTCCTGA
Tnf-α	CCACCACGCTCTTCTGTCTA	AGGGTCTGGGCCATAGAACT
Cxcl1	TCCAGAGCTTGAAGGTGTTGCC	AACCAAGGGAGCTTCAGGGTCA
Ccr2	CCTTGGGAATGAGTAACTGTGTGAT	ATGGAGAGATACCTTCGGAACTTCT
Ccl2	GCTACAAGAGGATCACCAGCAG	GTCTGGACCCATTCCTTCTTGG
Ki67	AGAGCCTTAGCAATAGCAACG	GTCTCCCGCGATTCCTCTG
Lgr5	TCTTCACCTCCTACCTGGACCT	GGCGTAGTCTGCTATGTGGTGT
Cdx2	GCCACCATGTACGTGAGCTAC	ACATGGTATCCGCCGTAGTC
Fgf2	GGCTGCTGGCTTCTAAGTGTGT	GCCCAGTTCGTTTCAGTGCC

Table 6.6 List of primers used for gene expression analysis of mouse colonic tissues by qPCR.

6.2.7 qPCR data analysis method

The expression of housekeeping gene candidates, *β-actin*, *Gapdh* and *Ppia* were measured in all samples and *Ppia* was excluded from the housekeeping gene panel as its expression was not stable across the samples. The CT values of genes of interest were normalised to the mean CT value of *β-actin* and *Gapdh* within each sample to generate delta CT (dCT) values. Since CT value is negatively proportional to the concentration of cDNA of gene of interest in each sample, the data was plotted as -dCT values so that a more negative number corresponds to lower gene expression.

$$-\text{delta CT} = -\{[\text{CT of gene of interest}] - [\text{CT of } (\beta\text{-actin} + \text{Gapdh})/2]\}$$

The expressions of genes of interest were compared between the naive tissues of the WT mice and *Adamdec1*$^{-/-}$ mice as well as the naïve tissues and DSS tissues of the WT and *Adamdec1*$^{-/-}$ mice. The one-way analysis of variance (ANOVA) was performed to determine whether the differences observed were statistically significant.

6.3 Results

6.3.1 The features of DSS-induced colitis in the WT and *Adamdec1*$^{-/-}$ mice

Upon initiation of DSS administration, generally the mice started exhibiting signs of colitis such as diarrhoea and blood per rectum as early as day 3 of the experiment. The length of colon was shorter in the *Adamdec1*$^{-/-}$ mice compared to the WT consistent with the previous finding and exaggerated colonic inflammation in these knockout mice (Figure 6.2).[26,56]

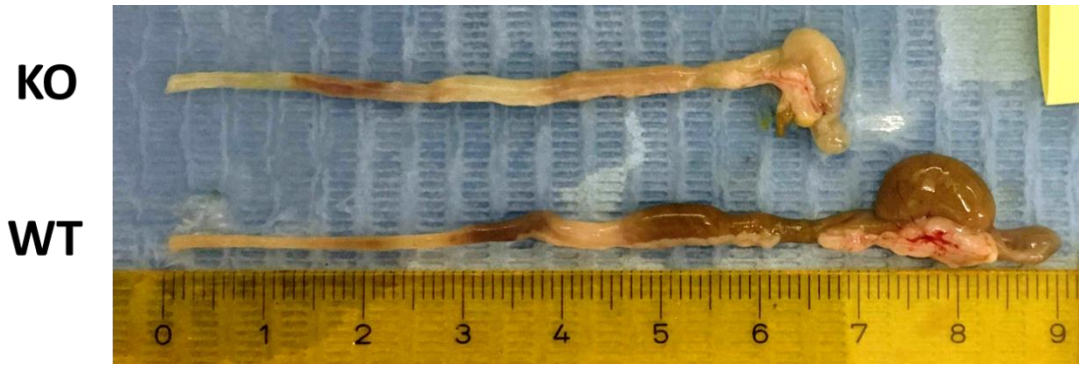

Figure 6.2 Photograph of colons harvested from the WT and *Adamdec1*$^{-/-}$ mice after DSS challenge. The colons harvested from the *Adamdec1*$^{-/-}$ mice were shorter than the colons harvested from the WT mice. The colons pictured were harvested from the mice in Day 9 Experimental cohort.
KO: *Adamdec1*$^{-/-}$, WT: Wild type

The histological features of the acute DSS-mediated colitis in *Adamdec1*$^{-/-}$ mice demonstrating a greater degree of mucosal inflammation had previously been established using the same strain of the mice.[26] Thus, only change in weight by the DSS challenge was measured in this project to verify the same effect. The correlation between the degree of weight loss and mucosal inflammation in this project was proved by the flow cytometry analysis of the colonic tissues of the *Adamdec1*$^{-/-}$ mice demonstrating a greater infiltration of the CD45+ CD3- immune cells. (Discussed in detail later.)

Overall, combining all the WT and *Adamdec1*$^{-/-}$ mice challenged with DSS, both WT and knockout mice started to lose weight on day 3 of the experiment onwards

and significant differences in the weight change were observed between the WT and *Adamdec1*$^{-/-}$ mice on day 8 and day 9 (Figure 6.3).

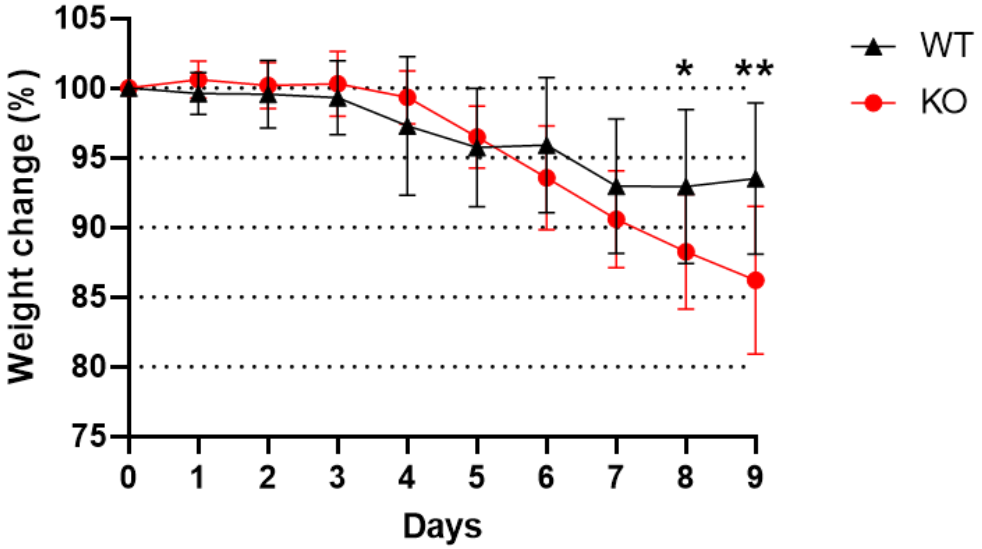

Figure 6.3 Weight change in the WT and *Adamdec1*$^{-/-}$ mice during DSS challenge. The *Adamdec1*$^{-/-}$ mice demonstrated significantly greater weight reduction in comparison to the WT mice on day 8 and 9 of the DSS challenge. WT n=14, *Adamdec1*$^{-/-}$ n=18 from day 0 to day 7. WT n=8, *Adamdec1*$^{-/-}$ n=12 on day 8 and 9. The graph shows mean with SD. One-way ANOVA test was used.
KO: *Adamdec1*$^{-/-}$, WT: Wild type, *: $p < 0.05$, **: $p < 0.01$

The peak weight loss in the WT mice occurred on day 7 to 8 after which the WT mice started to gain weight reflecting a resolution of inflammation and initiation of the recovery phase following the cessation of DSS administration. In the *Adamdec1*$^{-/-}$ mice, however, despite their drinking water being changed to sterile water, they continued to lose weight reflecting a continuation of inflammation. These findings confirmed the increased susceptibility to DSS-induced colitis in the absence of ADAMDEC1 as previously reported.[26,56] However, the weight loss demonstrated previously by the same strain of mice was more dramatic even though the experiments were carried out within the same facility.[26] This could be secondary to a number of factors including the age and weight of mice at the initiation of DSS challenge and environmental factors such as different rooms the mice were housed within the facility and the number of mice per experimental cage. (See Appendix 1 for the demographics and weight loss of the individual mouse)

6.3.2 Cage-dependant variability in the expressivity of *Adamdec1*$^{-/-}$ genotype

The analysis of weight changes of the mice in Cage 1 and Cage 2 of Day 9 Experiment cohort separately revealed that the *Adamdec1*$^{-/-}$ mice in Cage 2 exhibited less weight loss in comparison to the *Adamdec1*$^{-/-}$ mice in Cage 1 (Figure 6.4 A and B). Thus, a statistical difference in the weight change between the WT and knockout mice was achieved in Cage 1 on day 8 and day 9, however, these were not achieved in Cage 2.

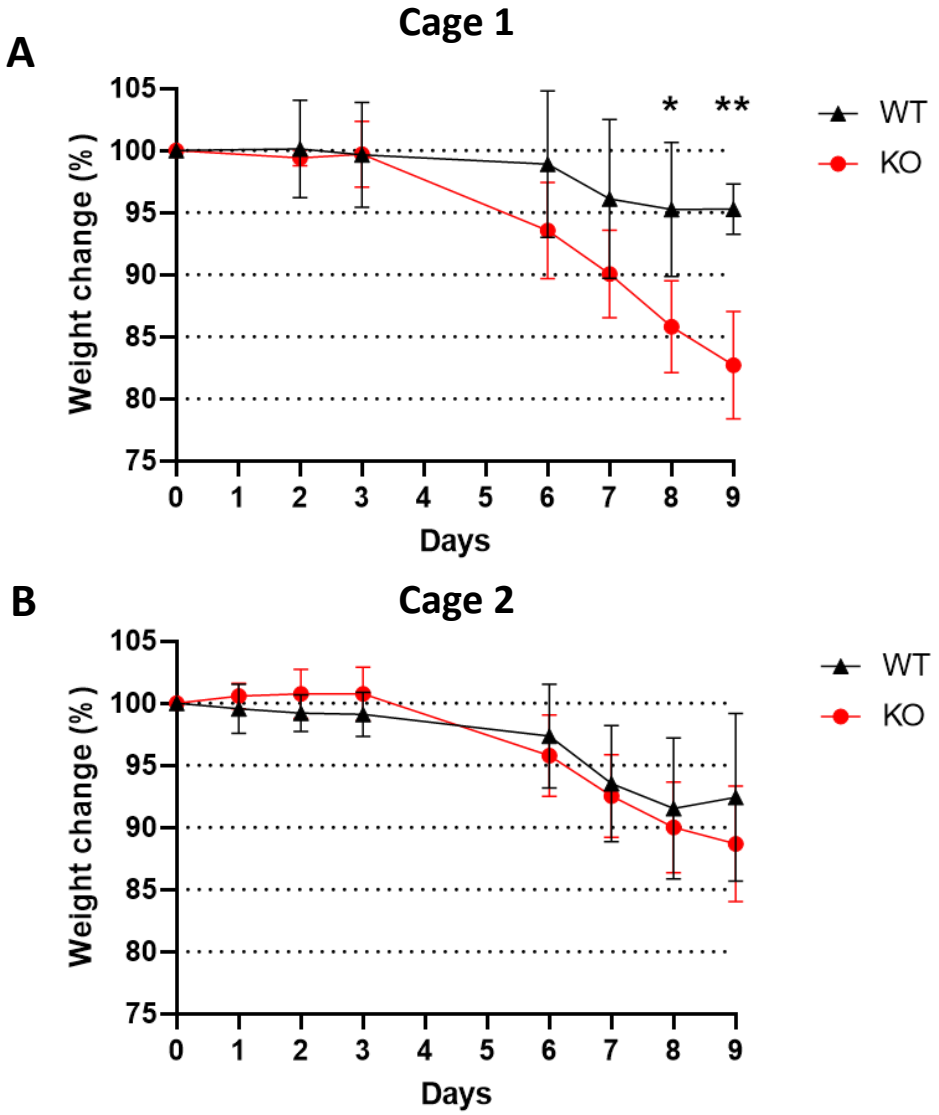

Figure 6.4 Weight change in the WT and *Adamdec1*$^{-/-}$ mice in Cage 1 (A) and Cage 2 (B) during DSS challenge. A statistical difference in the weight change between the WT and *Adamdec1*$^{-/-}$ mice was achieved on day 8 and 9 of the DSS challenge in Cage 1. This was not achieved in Cage 2. Cage 1 WT n=3, *Adamdec1*$^{-/-}$ n=5. Cage 2 WT n=5 *Adamdec1*$^{-/-}$ n=7. The graph shows mean with SD. One-way ANOVA test was used.
KO: *Adamdec1*$^{-/-}$, WT: Wild type, *: $p < 0.05$, **: $p < 0.01$

Furthermore, a comparison of the weight reductions exhibited by the *Adamdec1*$^{-/-}$ mice in Cage 1 and Cage 2 revealed that the *Adamdec1*$^{-/-}$ mice in Cage 1 lost significantly more weight than the *Adamdec1*$^{-/-}$ mice in Cage 2 (Figure 6.5). The knockout mice in Cage 2, however, did not demonstrate regaining of their weight after the cessation of DSS administration as seen with the WT mice on day 9. Therefore, their pattern of weight loss matched that of the knockout mice in Cage 1. Nevertheless, these findings indicated a cage-dependant variability in the degree of weight loss in *Adamdec1*$^{-/-}$ mice, thereby a cage-dependant variability in the degree of expressivity of genotype. It is unlikely that the greater weight loss seen in the knockout mice in Cage 1 was due to a technical error since the WT mice in Cage 1, which drunk exactly the same 2% DSS as the knockout mice in Cage 1, exhibited the least amount of weight loss over all.

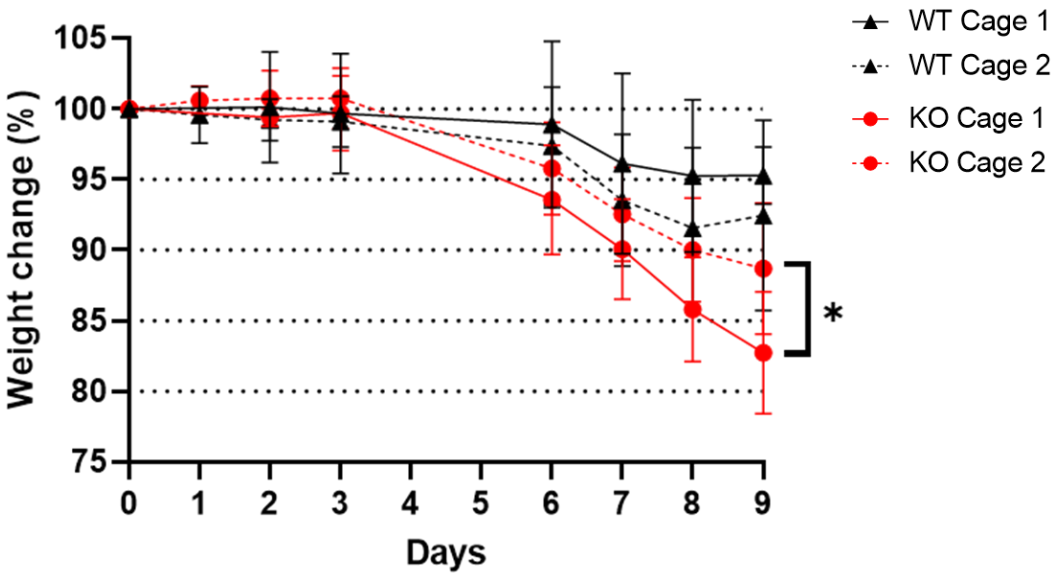

Figure 6.5 Weight change in the WT and *Adamdec1*$^{-/-}$ mice in Cage 1 and Cage 2 during DSS challenge. The *Adamdec1*$^{-/-}$ mice in Cage 1 lost significantly more weight than the *Adamdec1*$^{-/-}$ mice in Cage 2. Cage 1 WT n=3, *Adamdec1*$^{-/-}$ n=5. Cage 2 WT n=5 *Adamdec1*$^{-/-}$ n=7. The graph shows mean with SD. One-way ANOVA test was used.
KO: *Adamdec1*$^{-/-}$, WT: Wild type, *: $p < 0.05$

6.3.3 Flow cytometry analysis of colonic intestinal cells

To examine the effect of ADAMDEC1 on the colonic cell populations during mucosal inflammation, the colons were harvested from the WT and *Adamdec1*$^{-/-}$ mice in the naive state, and on day 7 and day 9 of the DSS experiment. Two timepoints (day 7 and day 9) for the flow cytometry analysis were created to capture the dynamic change in the cell populations during acute inflammation since the WT started exhibiting signs of recovery from day 8 in one cage, Cage 2. The colonic tissues were treated with EDTA to remove epithelial cells and digested with collagenase, dispase and DNase to generate single cell suspension. The single cell suspension from each mouse was divided in two and stained with either a panel of antibodies designed to capture selected lymphoid cells or a panel of antibodies designed to capture selected myeloid cells (Table 6.7). The panels were designed to catch a relatively broad range of different types of cells since flow cytometry analysis on the colonic tissue of *Adamdec1*$^{-/-}$ mice has never been performed previously and very little was known about the potential involvement of ADAMDEC1 in the immune system. Thus, focusing narrowly on particular types of cells was deemed to be counterintuitive. Nevertheless, previous works in our laboratory have found an increase in the level of IL-17 in the colonic tissues of *Adamdec1*$^{-/-}$ mice during DSS-induced colitis.[26] Additionally, with the evidence of ADAMDEC1 being predominantly expressed by the macrophages in the intestine and the previously demonstrated protective role of ADAMDEC1 in the mouse colitis model, the cells identified by the antibody panels included Th17 cells and Type 3 innate lymphoid cells (ILC3) cells as well as cells with anti-inflammatory properties such as Treg cells. The maturation and phenotype markers of monocytes and macrophages, Ly6C and C-X3-C Motif Chemokine Receptor 1 (CX3CR1), were also included to distinguish monocyte and macrophage populations. These markers were also used to determine any phenotypic differences during the monocyte to macrophage differentiation upon induction of colitis since there was some evidence suggesting that the expression of ADAMDEC1 may have an effect on the phenotype of macrophages.[59] Although, not initially intended, a T cell population expressing both FOXP3 and RORγt was identified by the lymphoid panel of antibodies during the FACS data analysis. Thus, proportions of these FOXP3+ RORγt+ T cells were also compared between the WT and *Adamdec1*$^{-/-}$ mice at each timepoint.

Panel	Gating strategy
Lymphoid panel	T helper cell: CD3+ CD4+
	Th17 cells: CD3+ CD4+ RORγt+
	Treg cells: CD3+ CD4+ FOXP3+
	Cytotoxic T cells: CD3+ CD8+
	Natural killer cells: CD3-, CD8+, CD127+
	ILC3: CD3- RORγt+ CD127+
	FOXP3+ RORγt+ T cells: CD3+ CD4+ FOXP3+ RORγt+
Myeloid panel	Dendritic cells: CD3- Ly6G- F4/80- $CD11c^{high}$ $MHCII^{high}$
	Neutrophils: CD3- CD11b+ Ly6G+
	Monocytes: CD3- F4/80+ SSC^{low} $Ly6C^{high}$
	Macrophages: CD3- F4/80+ $SSC^{mid/high}$ $Ly6C^{low/mid}$

Table 6.7 List of cells and gating strategies to identify them by flow cytometry analysis.

Initial data analysis revealed that there were no significant differences in the cellular compositions between the *Adamdec1*$^{-/-}$ mice in Cage 1 and Cage 2, even though these knockout mice demonstrated a cage-dependant variability in the degree of weight loss (Figure 6.5). Thus, FACS analysis was conducted by simply comparing the data of the WT and *Adamdec1*$^{-/-}$ mice (Cage 1 and Cage 2 combined) at each timepoint.

In order to eliminate the intra-batch variation in the fluorescent intensity and allow comparison of mean fluorescent intensity (MFI) between the WT and knockout samples in the naïve state, day 7 and day 9 of the DSS challenge, the MFI of the knockout samples were normalised to the mean MFI of the WT samples per timepoint and shown as percentage change relative to the mean MFI of the WT at each timepoint.

6.3.3.1 Gating strategy

Figure 6.6 and 6.7 show the gating strategies used to identify populations of cells by the lymphoid panel and myeloid panel of antibodies respectively.

Figure 6.6 Flow cytometry gating strategy for analysis of the murine colonic cells using the lymphoid panel antibodies. The image was created using FlowJo software (BD Biosciences).

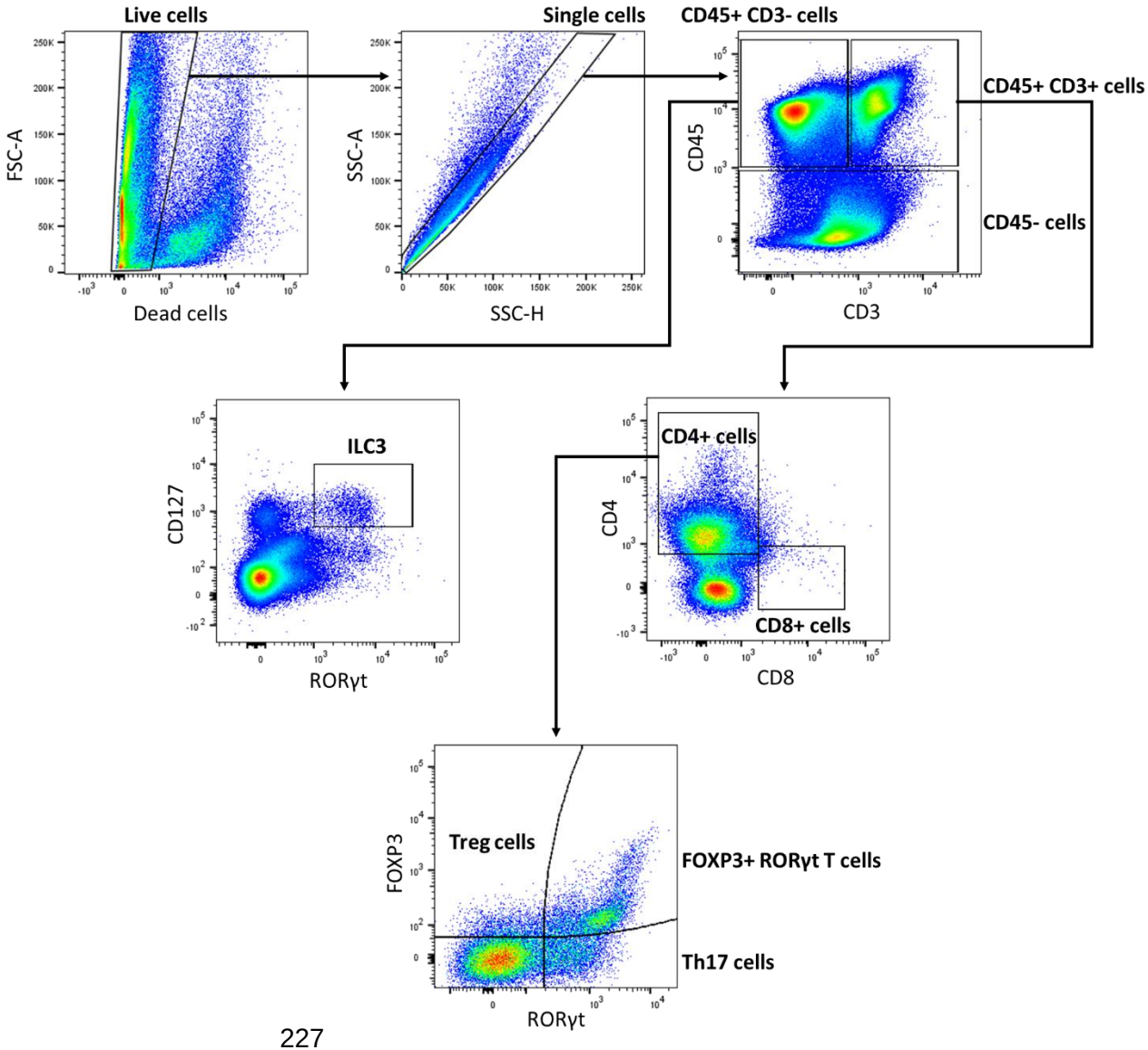

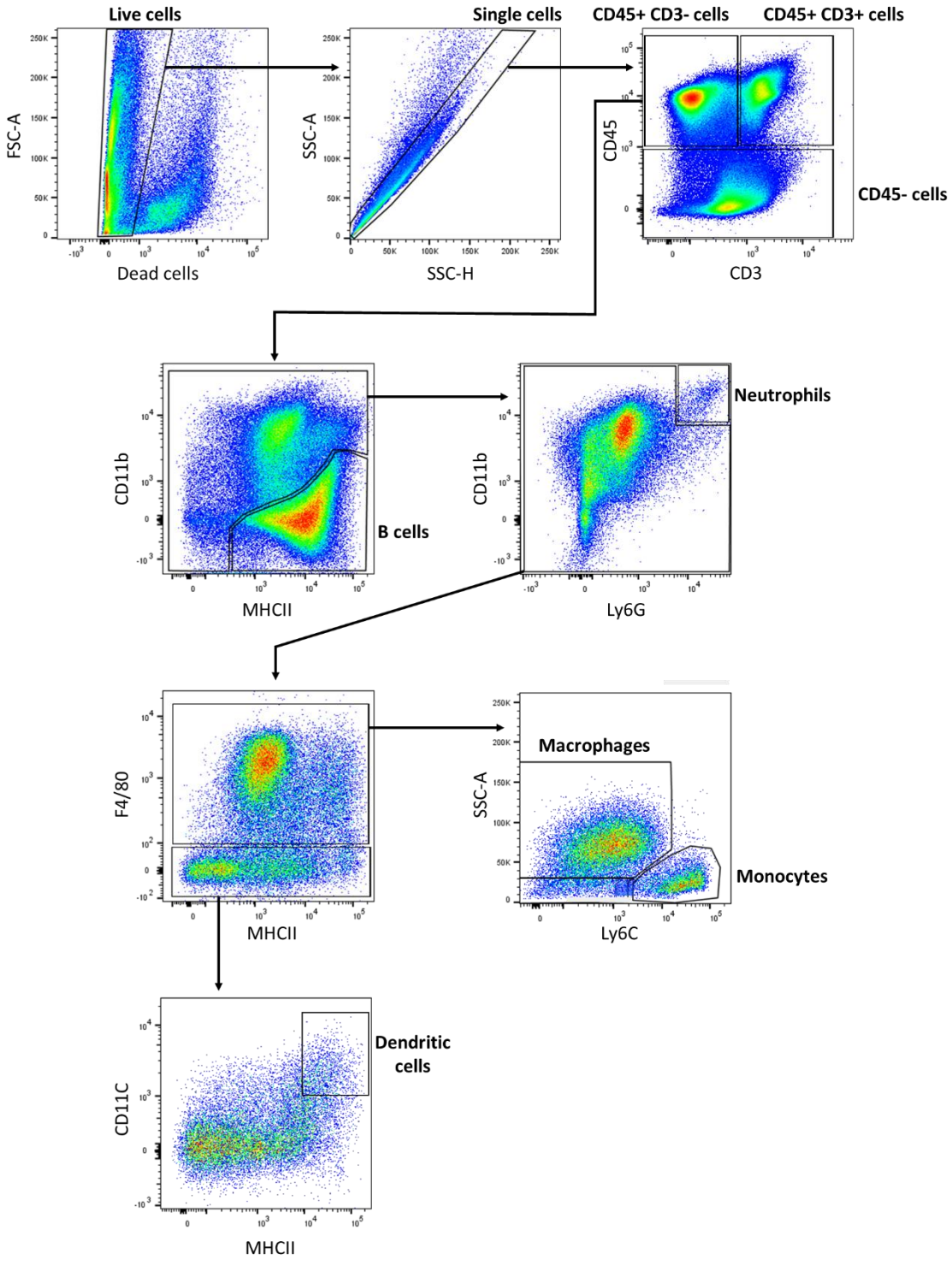

Figure 6.7 Flow cytometry gating strategy for analysis of the murine colonic cells using the myeloid panel antibodies. The image was created using FlowJo software (BD Biosciences).

6.3.3.2 The changes in haemopoietic immune cell population and non-haemopoietic cell population during DSS challenge

In order to appreciate the fundamental change in the cell population upon induction of mucosal inflammation, first of all, the proportions of CD45+, CD45-, CD45+ CD3- and CD45+ CD3+ cells were analysed. CD45+ cells are haemopoietic immune cells. CD45- cells are largely non-haemopoietic cells such as mesenchymal cells. CD45+ CD3- cells are largely the myeloid cells that elicit innate immune response and B cells. CD45+ CD3+ cells are mainly T cells that play a major role in the adaptive immune response. In the healthy state, approximately 60% of the cells of colonic tissue were CD45- cells in both WT and *Adamdec1*$^{-/-}$ mice (Figure 6.8 A). A rapid reduction in the proportion of CD45- cells was observed from the naïve state to day 7, and a further reduction from day 7 to day 9 upon induction of colitis in both WT and *Adamdec1*$^{-/-}$ mice. The degree of reductions in the proportion of CD45- cells was greater in the *Adamdec1*$^{-/-}$ mice compared to the WT mice on both day 7 and day 9, with a statistical difference achieved on day 9 (Figure 6.8 A) . This indicated a greater infiltration of hematopoietic CD45+ immune cells in the colon of the *Adamdec1*$^{-/-}$ mice in comparison to the WT mice upon induction of inflammation. This was verified by the proportion of CD45+ cells increasing upon induction of colitis in both WT and *Adamdec1*$^{-/-}$ mice (Figure 6.8 B). In accordance with the trend of the CD45- cell population, the degree of increase in the CD45+ cell population was greater in the *Adamdec1*$^{-/-}$ mice compared to the WT with a statistical difference achieved on day 9 (Figure 6.8 B). This indicated greater recruitment and proliferation of immune cells consistent with the previously reported histological finding of greater immune cell infiltration in the colonic tissues of the *Adamdec1*$^{-/-}$ mice and more severe mucosal inflammation in the these knockout mice.[26,56] Importantly, the findings also indicated that the immune response of the WT and *Adamdec1*$^{-/-}$ mice differed in intensity during the acute phase of inflammation.

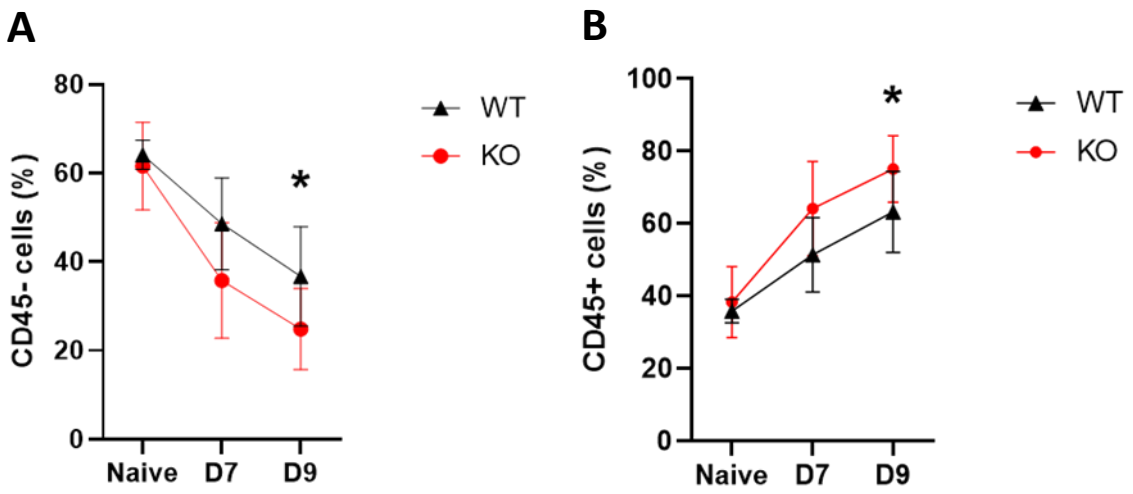

Figure 6.8 Changes in the proportion of CD45- cells (A) and CD45+ cells (B) in the colonic tissue of the WT and *Adamdec1*$^{-/-}$ mice during DSS challenge. The proportion of CD45- and CD45+ cell populations decreased and increased respectively upon induction of colitis. The proportion of CD45- cell population and CD45+ cell population were significantly higher in the *Adamdec1*$^{-/-}$ mice in comparison to the WT mice on day 9. The cell proportions are represented as percentage of the total live single cells. The graphs show mean with SD. One-way ANOVA test was used. For WT: naïve n=4, day 7 n=6, day 9 n=8. For *Adamdec1*$^{-/-}$: naïve n=4, day 7 n= 6, day 9 n=12.
KO: *Adamdec1*$^{-/-}$, WT: Wild type, *: $p < 0.05$

A greater degree of increase in the CD45+ cell population was observed in the *Adamdec1*$^{-/-}$ mice in comparison to the WT mice which coincided with the increased weight loss observed in these knockout mice. Furthermore, when the proportion of CD45+ cells was compared between the WT mice and *Adamdec1*$^{-/-}$ mice in Cage 1 and Cage 2 separately, the difference in the proportion of CD45+ cells was significant between the WT mice and *Adamdec1*$^{-/-}$ mice in Cage 1 but not significant between the WT mice and *Adamdec1*$^{-/-}$ mice in Cage 2 (Figure 6.9). This mirrored the greater weight loss exhibited by the *Adamdec1*$^{-/-}$ mice in Cage 1 (Figure 6.5). Thus, the CD45+ cell proportion correlated closely with the degree of weight loss, indicating that the reduction in weight loss upon induction of inflammation is an appropriate measure for the degree of mucosal inflammation in the DSS colitis model.

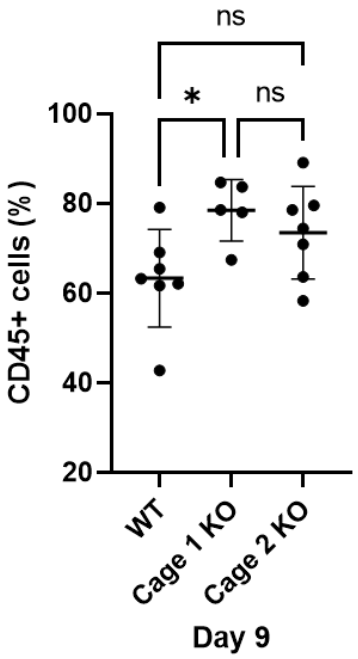

Figure 6.9 The proportion of CD45+ cells in the colonic tissue of the WT and *Adamdec1*$^{-/-}$ mice in Cage 1 and Cage 2 on day 9 of the DSS challenge. The proportion of CD45+ cell population was significantly higher in the *Adamdec1*$^{-/-}$ mice in Cage 1 in comparison to the WT, but not in the *Adamdec1*$^{-/-}$ mice in Cage 2 in comparison to the WT mice. The cell proportions are represented as percentage of the total live single cells. The graph shows mean with SD. One-way ANOVA test was used.
KO: *Adamdec1*$^{-/-}$, WT: Wild type, *: $p < 0.05$

6.3.3.3 The changes in the CD45+ CD3- and CD45+ CD3- cell populations during the DSS challenge

Mirroring the increase in CD45+ cells upon induction of inflammation, there was an increase in the proportions of CD45+ CD3- cells from the naïve state to day 7 and day 9 of the DSS challenge in both WT and *Adamdec1*$^{-/-}$ mice (Figure 6.10 A). The proportion of CD45+ CD3- cells doubled from approximately 20% to above 40-50% from the naïve state to day 7 and further increases were observed, though to a lesser extent, from day 7 to day 9. Consistent with the observation of the greater increase in the CD45+ cell proportion in the *Adamdec1*$^{-/-}$ mice, the increase in the proportion of CD45+ CD3- cells was greater in the knockout mice compared to the WT mice on both day 7 and day 9, with a statistical difference achieved on day 9 (Figure 6.10 A). As for the total CD45+ cell proportion, this trend mirrored the greater weight loss exhibited by the *Adamdec1*$^{-/-}$ mice thus indicting a greater degree of inflammation in these mice upon DSS challenge. Contrarily to the CD45+

CD3- cells, the changes in the proportion of CD45+ CD3+ cells were relatively small during 9 days of the experiment in both the WT and *Adamdec1*$^{-/-}$ mice (Figure 6.10 B). In the naïve state, only approximately 10% of the cells in the colonic tissues were CD45+ CD3+ cells and their proportion decreased to approximately 5% on day 7 followed by an increase to approximately 15% on day 9 during the inflammation. There were no statistical differences between the proportions of CD45+ CD3+ cells between the WT and *Adamdec1*$^{-/-}$ mice at all timepoints. This indicated that the increases in the proportion of CD45+ cells upon induction of inflammation were predominantly due to the infiltration of CD45+ CD3- cells rather than CD45+ CD3+ T cells in both WT and *Adamdec1*$^{-/-}$ mice. However, the significantly greater proportion of the CD45+ CD3- cell population in the *Adamdec1*$^{-/-}$ mice compared to the WT mice, on day 9, suggested that the innate immune system was likely to play a more major role than T lymphocytes in the aberrant inflammatory response seen in the absence of ADAMDEC1.

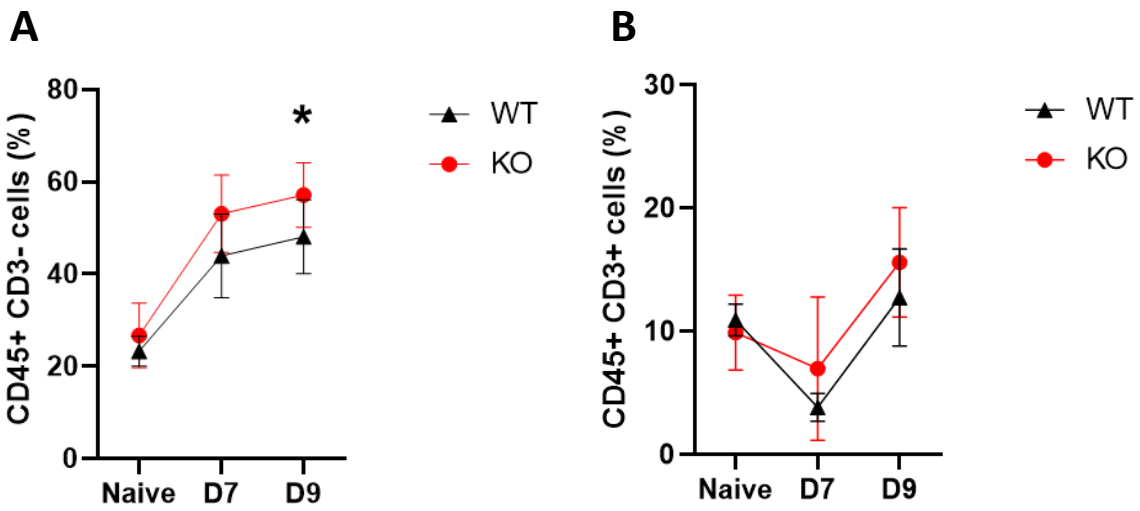

Figure 6.10 Changes in the proportion of CD45+ CD3- cells (A) and CD45+ CD3+ cells (B) in the colonic tissue of the WT and *Adamdec1*$^{-/-}$ mice during DSS challenge. The proportion of CD45+ CD3- cell population was significantly higher in the *Adamdec1*$^{-/-}$ mice in comparison to the WT mice on day 9 of the DSS challenge. The cell proportions are represented as percentage of the total live single cells. The graphs show mean with SD. One-way ANOVA test was used. For WT: naïve n=4, day 7 n=6, day 9 n=8. For *Adamdec1*$^{-/-}$: naïve n=4, day 7 n= 6, day 9 n=12.
KO: *Adamdec1*$^{-/-}$, WT: Wild type, D7: Day 7, D9: Day 9, *: $p < 0.05$

6.3.3.4 Analysis using the lymphoid panel antibodies

6.3.3.4.1 Analysis of the CD4+ and CD8+ expressing cell populations

Following the gating strategy described in Figure 6.6, the cells expressing CD4 and CD8 were identified in the CD45+ CD3+ cell population. There were very few cells expressing CD4+ within the CD45+ CD3+ cell population in the naïve state with no significant difference between the colonic cells of the WT and *Adamdec1*$^{-/-}$ mice (Figure 6.11 and 6.12 A). Upon DSS challenge, there appeared to be an increase in the number of cells expressing CD4+ overall. However, more importantly, this was accompanied by the convergence of CD4+ and CD4- cell populations hindering the identification of two distinct populations of CD4+ and CD4- cells that are normally present and easily identified (Figure 6.11). This indicated that upon induction of inflammation, the CD4+ cells shifted more negatively on the fluorescent intensity. This was more prominent in the *Adamdec1*$^{-/-}$ mice compared to the WT mice which was evident by the significantly low MFI of CD4 in the knockout samples on day 9 (Figure 6.13 A). The mergence of the distinct two populations of CD4+ and CD4- cells prevented an accurate quantification of the CD4+ cells upon induction of the inflammation, particularly in the *Adamdec1*$^{-/-}$ mice samples.

Similarly, the same trend was observed for CD8. The abundance of cells expressing CD8 was negligible in the naïve state in both WT and knockout samples indicating that the number of CD8+ cytotoxic T cells was extremely low in the healthy colon (Figure 6.11 and 6.12 B). Upon induction of inflammation, a distinct population of CD8+ cells, which is usually expected to be seen in the acute phase of DSS-induced colitis, could not be identified definitively.[186,187] Furthermore, the overall fluorescent intensity for CD8 appeared to have shifted more negatively in the knockout mice in comparison to the WT mice (Figure 6.11), resulting in a significantly lower MFI in the knockout mice on day 9 (Figure 6.13 B). As with the CD4 expression, this prevented accurate quantification of the CD8+ cells in the day 7 and day 9 samples.

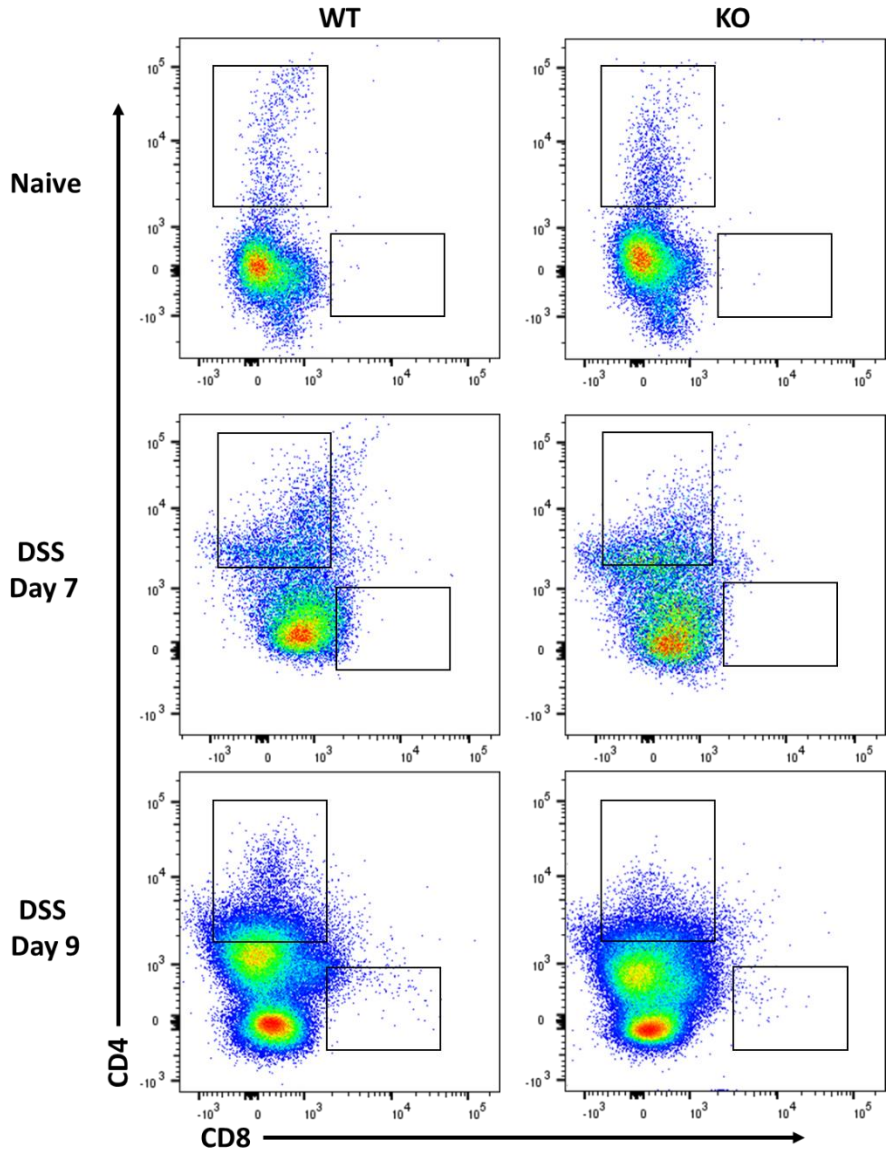

Figure 6.11 Flow cytometry plots demonstrating the changes in CD4+ and CD8+ cell populations in the murine colonic tissue during DSS challenge. Mergence of CD4+ and CD8+ cell populations into CD4- CD8- cell population was observed upon induction of colitis. This observation was more enhanced in the colonic cells of the *Adamdec1*$^{-/-}$ mice in comparison to the WT mice. The figure was created using the result of one WT and one *Adamdec1*$^{-/-}$ mice as examples. The image was created using FlowJo software (BD Biosciences).
KO: *Adamdec1*$^{-/-}$, WT: Wild type

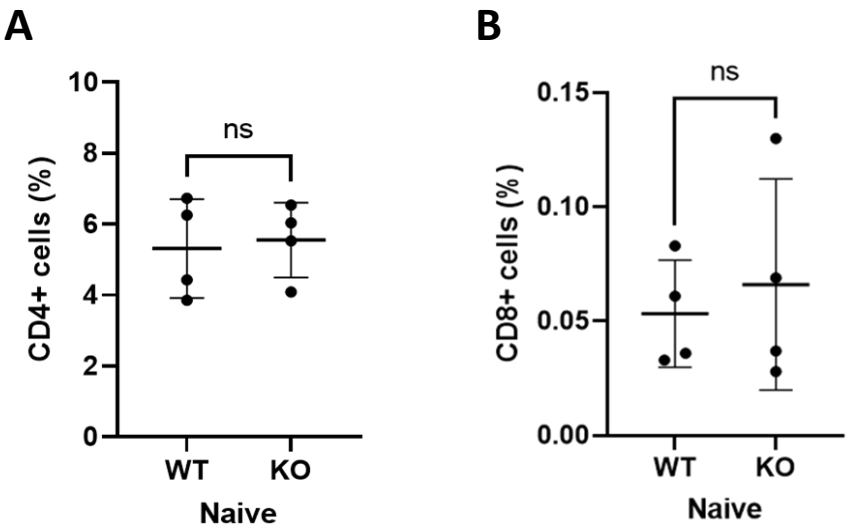

Figure 6.12 The proportion of CD4+ (A) and CD8+ (B) cells in the murine colonic tissue in naïve state. There were no significant differences in the proportion of CD4+ and CD8+ cell populations between the WT and *Adamdec1*$^{-/-}$ mice in the naïve state. The CD4+ and CD8+ cells are represented as percentage of CD45+ CD3+ cells. The graphs show mean with SD. Unpaired student t-test was used.
KO: *Adamdec1*$^{-/-}$, WT: Wild type, ns: Non-significant

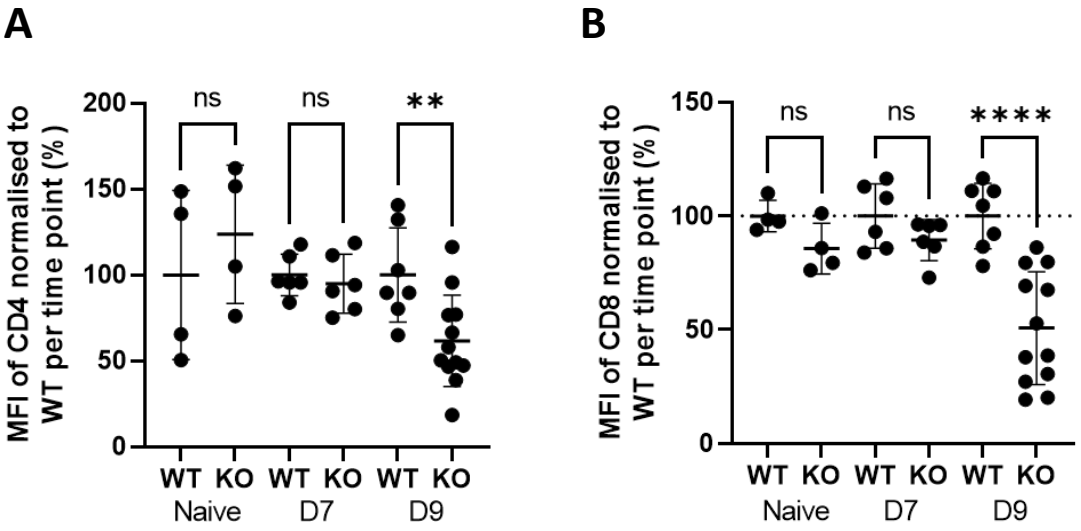

Figure 6.13 MFI of CD4 (A) and CD8 (B) within the CD45+ CD3+ cell population. MFI of CD4 and CD8 were significantly lower in the samples of the *Adamdec1*$^{-/-}$ mice in comparison to the WT mice on day 9 of the DSS challenge. MFI of the *Adamdec1*$^{-/-}$ samples were normalised to the mean MFI of the WT samples per timepoint and shown as percentage change relative to the mean MFI of the WT at each timepoint. The graphs show mean with SD. One-way ANOVA test was used.
KO: *Adamdec1*$^{-/-}$, WT: Wild type, D7: Day 7, D9: Day 9, **: $p < 0.01$, ****: $p < 0.0001$, ns: Non-significant

6.3.3.4.2 Digestion of CD4 and CD8 molecules by dispase

Given the findings described above (Chapter 6.3.3.4.1), a number of experiments were performed to establish if the cell preparation methodology using the proteases dispase and collagenase influenced the CD4 and CD8 staining. Single cell suspensions were prepared from spleens taken from healthy WT and *Adamdec1*$^{-/-}$ mice. Splenocytes are rich in CD4+ and CD8+ expressing T lymphocytes and do not require extensive sample preparation including enzyme digestion.[188,189] In order to see if tissue digestion by dispase during the colonic tissue preparation also resulted in the digestion of CD4 and CD8, splenocytes were stained with antibodies for CD45, CD3, CD4 and CD8 with or without a digestion step with dispase during the sample preparation.

After gating for CD45+ CD3+ cells, three distinct populations of cells were seen in the splenocytes stained without a digestion step with dispase (Figure 6.14). These were the cells negative for both CD4 and CD8, cells positive for CD4, and cells positive for CD8 expression (Figure 6.14). The addition of a dispase digestion step in the cell preparation, however, resulted in the loss of the CD4+ cell population and CD8+ cell population and thus mergences of the CD4+ and CD8+ cell populations with the CD4- CD8- cell population (Figure 6.14). The degree of digestion of CD4 and CD8 on the splenocytes did not differ between the WT and knockout mice (Figure 6.15 A and B). These findings indicated that the surface expressions of CD4 and CD8 on T cells were destroyed by dispase which explained the indistinguishable cell populations discriminated by the expression of CD4 and CD8 in the colonic cells of the mice. The capability of collagenase to destroy CD4 and CD8 on T cells was also examined using the same protocol. The reductions in MFI of CD4 and CD8 on splenocytes as a result of the addition of the digestion step with collagenase were minimal in both WT and *Adamdec1*$^{-/-}$ mice in accordance with the previously reported finding (Appendix 2).[190]

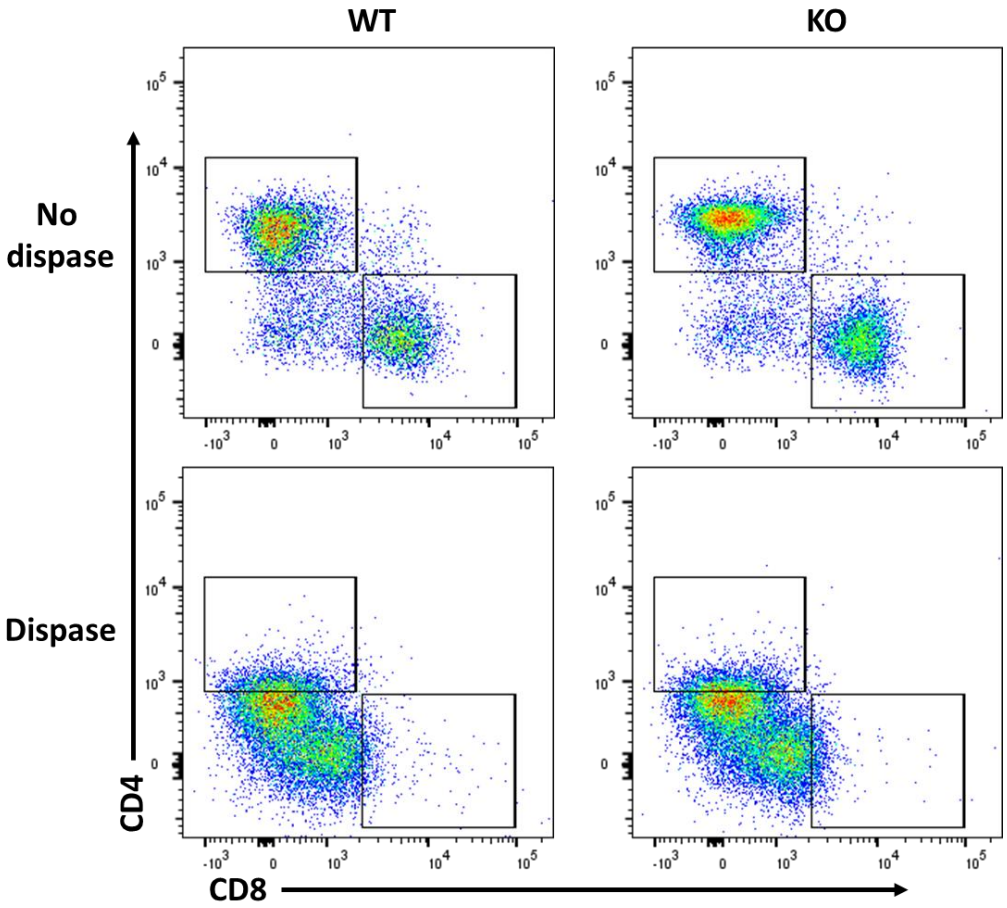

Figure 6.14 Flow cytometry plots showing the CD4+ and CD8+ cell populations in spleens of the healthy WT and *Adamdec1*$^{-/-}$ mice treated with dispase or not treated with dispase. Disappearance of the distinct CD4+ cell population and CD8+ cell population were observed by the digestion step using dispase during the sample preparation. The figure was created using the result of one WT and one *Adamdec1*$^{-/-}$ mice as examples. The image was created using FlowJo software (BD Biosciences).
KO: *Adamdec1*$^{-/-}$, WT: Wild type

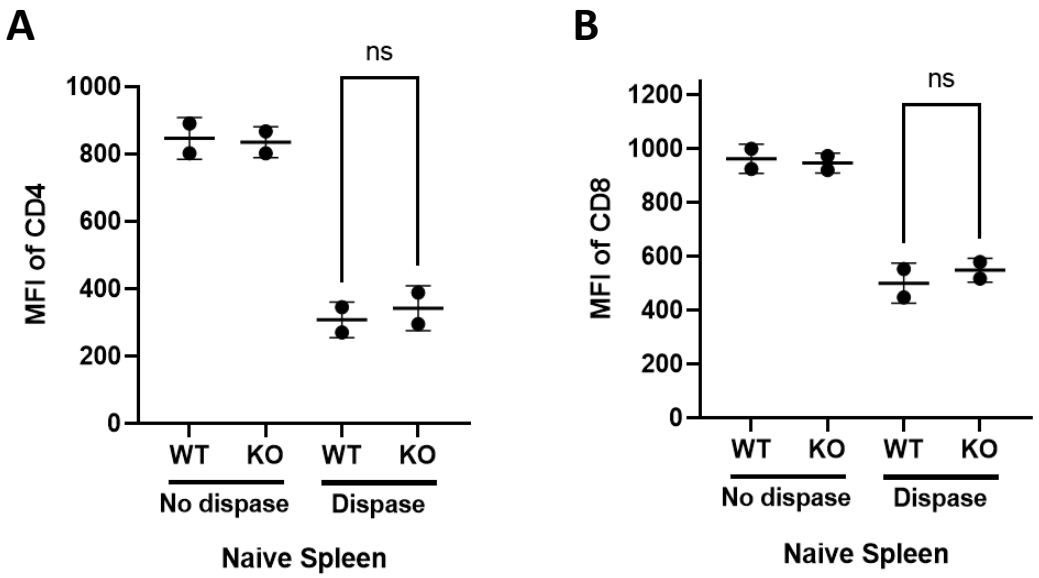

Figure 6.15 MFI of CD4 (A) and CD8 (B) in the splenocytes of the healthy WT and *Adamdec1*$^{-/-}$ mice treated with dispase or not treated with dispase. Marked reductions in the MFI of CD4 and CD8 were observed by treatment with dispase equally in the splenocytes of the *Adamdec1*$^{-/-}$ mice and WT mice. The graphs show mean with SD. Unpaired student t-test was used.
KO: *Adamdec1*$^{-/-}$, WT: Wild type, ns: Non-significant

A potent enzymatic disruption of the cell surface expression of CD4 and CD8 by dispase has indeed been reported previously.[190,191] However, during this project, a greater degree of the CD4 and CD8 digestion by dispase was seen in the colonic cells of the *Adamdec1*$^{-/-}$ mice in comparison to the WT mice during inflammation. These findings suggested that there were possibly lower abundances of CD4 and CD8 expressing cells in the inflamed lamina propria of the *Adamdec1*$^{-/-}$ mice compared to the WT mice. This would lead to less CD4 and CD8 for dispase to destroy during inflammation resulting in the significantly lower CD4 and CD8 MFIs in the *Adamdec1*$^{-/-}$ mice samples on day 9 of the DSS challenge. However, the qPCR results suggested otherwise as there were no differences between the absolute gene expression of CD4 and CD8 within the intestinal tissues of the WT and *Adamdec1*$^{-/-}$ mice on day 9. This indicated that the abundance of the CD4+ and CD8+ cells did not differ significantly between the WT and *Adamdec1*$^{-/-}$ mice on day 9 (Figure 6.16 A and B).

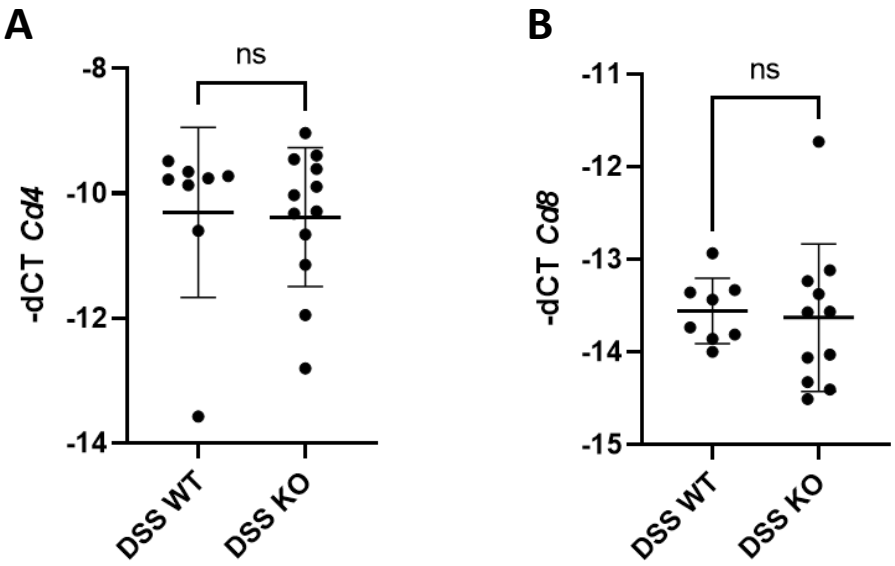

Figure 6.16 The expression of *Cd4* (A) and *Cd8* (B) in the colonic tissues of the WT and *Adamdec1*$^{-/-}$ mice on day 9 of the DSS challenge. There were no statistical differences in the gene expression of *Cd4* and *Cd8* between the colonic tissue of the WT and *Adamdec1*$^{-/-}$ mice. The graphs show mean with SD. Unpaired student t-test was used.
KO: *Adamdec1*$^{-/-}$, WT: Wild type, ns: Non-significant

More likely, the significant differences in the MFI of CD4 and CD8 between the colonic cells of WT and *Adamdec1*$^{-/-}$ mice on day 9 suggested that dispase digested CD4 and CD8 more effectively in the absence of ADAMDEC1. This could potentially be secondary to ADAMDEC1 possessing an inhibitory role against dispase directly and the abundance of CD4 and CD8 molecules were not high enough in the naïve state in both WT and knockout mice for dispase to render a significant effect. It could also potentially be secondary to ADAMDEC1 being involved in a release of another as yet unknown substance in the inflamed tissue that could inhibit the activity of dispase. Alternatively, the increased efficacy of dispase's capacity to destroy CD4 and CD8 in the inflamed tissue of the knockout mice might be due to the CD4 and CD8 molecules on CD3+ cells being more readily accessible for dispase to execute its catalytical activity in the absence of ADAMDEC1. Upon contact between T cells and antigens, presented by antigen presenting cells, immunological synapse, also known as supramolecular activation cluster (SMAC), forms at the interface of T cells and antigen presenting cells as a result of protein aggregation. SMAC is a multi-molecular complex consisting of T cell receptor and other co-receptors such as CD4 and CD8 centrally and multiple

rings of adhesion molecules peripherally. It is possible that ADAMDEC1 is involved in preserving the structural function of SMAC.

A loss of two distinct populations of CD4+ and CD4- cells secondary to the dispase digestion prevented an accurate identification of the CD4+ cell population. Nevertheless, the cells expressing relatively high fluorescent intensity for CD4 staining were selected in order to identify the cells downstream of the gating strategy (Figure 6.6).

6.3.3.4.3 Analysis of the Th17 and Treg cell populations

Th17 cells are a major source of IL-17 within the tissue. IL-17 was found to be elevated in the colonic tissues of *Adamdec1*$^{-/-}$ mice in comparison to the WT mice upon induction of DSS-mediated colitis during previous works in our laboratory.[26] Th17 cells secrete various pro-inflammatory and anti-inflammatory cytokines thus exhibit both pro- and anti-inflammatory effects in the immune response. Treg cells, on the other hand, secrete anti-inflammatory cytokines such as IL-10 and TGF-β and exhibit potent anti-inflammatory capabilities such as suppression of proliferation and activation of helper T cells and induction of cytotoxic T cells and natural killer cells.[192] Differentiation of naïve T cell to effector T cell occurs within the intestinal tissue. A small subset of T naïve cells that express CD116 differentiate into Th17 and Treg cells, thus the differentiation and development of these two subtypes of T cells are closely related.[193] The differentiation polarisation is largely dependent on the cytokine profile of the microenvironment. An equilibrium between Th17 and Treg cells has been implicated in the appropriate balancing of pro- and anti-inflammatory responses during inflammation.[194]

Upon induction of DSS challenge, the proportion of Th17 cells increased from the naïve state to day 7 in both WT and *Adamdec1*$^{-/-}$ mice (Figure 6.17 A). A degree of the increase was, however, greater in the WT mice thus there was a statistical difference in the proportion of Th17 cells between the WT and *Adamdec1*$^{-/-}$ mice on day 7 (Figure 6.17 A). In the WT mice, the proportion of the Th17 cells then decreased from day 7 to day 9, thereby initiating the restoration of the original state, whereas in the *Adamdec1*$^{-/-}$ mice it continued to increase. On the other hand, the proportion of Treg cells decreased from the naive state to day 7 in both WT and *Adamdec1*$^{-/-}$ mice (Figure 6.17 B). Mirroring the trend of the change in Th17 cell proportion, a greater reduction was seen in the WT mice thus there was a statistical

difference in the proportion of Treg cells between the WT and *Adamdec1*$^{-/-}$ mice on day 7. Again similarly to the trend in Th17 cells, in the WT mice the proportion of Treg cells increased from day 7 to day 9, thereby initiating the restoration of the original state, whereas in the *Adamdec1*$^{-/-}$ mice it continued to decrease (Figure 6.17 B). These findings showed, firstly, that the proportion of Th17 and Treg cells negatively correlated with each other irrespective of the genotype of the mice. Secondly, the Th17 polarisation was impaired in the *Adamdec1*$^{-/-}$ mice at an early stage of the acute inflammation which was associated with the continuation and prolongation of the Th17 polarisation induced by the DSS challenge. These findings thus suggested that the inflammatory response at the earlier stage of acute inflammation was less robust with regards to the Th17 polarisation in the *Adamdec1*$^{-/-}$ mice. This was followed by a subsequent prolongation of the inflammatory state in the colonic tissues of the *Adamdec1*$^{-/-}$ mice which correlated with the continuation of weight loss exhibited by these knockout mice on day 9 of the experiment.

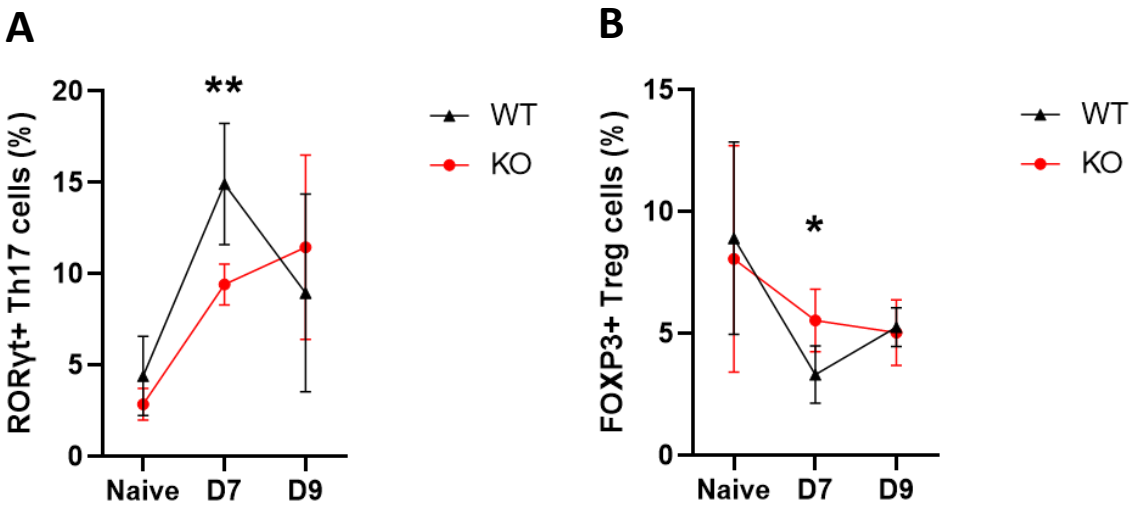

Figure 6.17 Changes in the proportion of Th17 cells (A) and Treg cells (B) in the colonic tissue of the WT and *Adamdec1*$^{-/-}$ mice during DSS challenge. The proportion of Th17 cell population was significantly higher in the WT in comparison to the *Adamdec1*$^{-/-}$ mice on day 7. The proportion of Treg cell population was significantly higher in the *Adamdec1*$^{-/-}$ mice in comparison to the WT mice on day 7. The cell proportions are represented as percentage of the CD3+ CD4^{high} cells. The graph shows mean with SD. One-way ANOVA test was used. For WT: naïve n=4, day 7 n=6, day 9 n=8. For *Adamdec1*$^{-/-}$: naïve n=4, day 7 n= 6, day 9 n=12.
KO: *Adamdec1*$^{-/-}$, WT: Wild type, D7: Day 7, D9: Day 9, *: $p < 0.05$, **: $p < 0.01$

6.3.3.4.4 Analysis of the RORγt+ FOXP3 + T cell population

During the FACS analysis, a relatively modest sized population of cells expressing both RORγt+ and FOXP3+ in the CD3+ CD4^{high} cells were identified. These cells were present in the naïve, day 7 and day 9 samples of both WT and *Adamdec1*$^{-/-}$ mice. RORγt+ FOXP3+ T cells are relatively newly identified cells.[195] One study has shown these cells to be a transitional state of T cells as upregulation of both RORγt and FOXP3 were observed during differentiation of T naïve cells, under Th17-inducing conditions, before T cells were committed to becoming either Th17 or Treg cells.[195] However, they have also been reported to be a stable lineage of T cells with a potent suppressive effect on Th1 cell-mediated inflammatory response.[196] Thus, the effect of ADAMDEC1 on these RORγt+ FOXP3+ cells was determined by examining the proportion of these cells in the WT and *Adamdec1*$^{-/-}$ mice during colonic inflammation. The proportions of RORγt+ FOXP3+ T cells increased from the naïve state to day 7 of the DSS challenge and then reduced from day 7 to day 9 in both WT and knockout mice (Figure 6.18). There were no significant differences in the proportion of the RORγt+ FOXP3+ T cells between the WT and *Adamdec1*$^{-/-}$ mice during the DSS challenge.

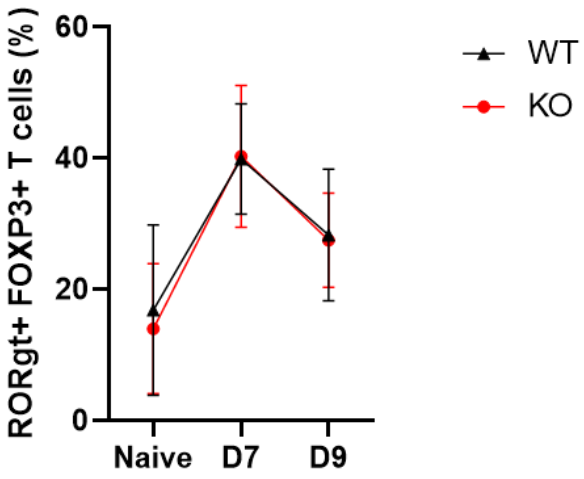

Figure 6.18 Changes in the proportion of RORγt+ FOXP3+ T cells in the colonic tissue of the WT and *Adamdec1*$^{-/-}$ mice during DSS challenge. The proportion of RORγt+ FOXP3+ cell population increased from day 0 to day 7 and decreased from day 7 to day 9 equally in the WT and Adamdec1-/- mice. The cell proportion is represented as percentage of the CD3+ CD4^{high} cells. The graph shows mean with SD. One-way ANOVA test was used. For WT: naïve n=4, day 7 n=6, day 9 n=8. For *Adamdec1*$^{-/-}$: naïve n=4, day 7 n= 6, day 9 n=12.
KO: *Adamdec1*$^{-/-}$, WT: Wild type, D7: Day 7, D9: Day 9

6.3.3.4.5 Analysis of the ILC3 population

Although identified by using the lymphoid panel of antibodies, ILC3 are CD3- innate immune cells. Since they are another type of cells that are known to secrete IL-17 ILC3 cells were included in the cells to be examined in this chapter. As well as IL-17, ILC3 are known to secret IL-22 which is believed to play a role in epithelial homeostasis and repair by stimulating the production of tight-junction proteins, mucin and anti-microbial substances by epithelial cells.[197] Mice deficient in ILC3 and IL-22 have been shown to exhibit more severe form of mucosal inflammation during DSS-induced colitis previously.[198]

Overall, a reduction in the proportions of ILC3 was observed from the naive state to day 9 irrespective of the genotype (Figure 6.19). The proportions of ILC3 were higher in the WT mice in comparison to the *Adamdec1*$^{-/-}$ mice in the naïve state and on day 7 with a statistical difference achieved on day 7. There was a sharp decrease in the proportion of ILC3 cells in the WT mice from day 7 to day 9, resulting in the similar proportions of ILC3 in the WT and *Adamdec1*$^{-/-}$ mice on day 9. The general trend of reduction in the ILC3 proportion during the inflammation in both WT and *Adamdec1*$^{-/-}$ mice might be explained by the increase in proportions of other CD3- cells, such as F4/80+ monocytes and macrophages, during inflammation since the proportions of these cells were represented as a percentage of CD45+ CD3- cells (Figure 6.20 B and C) (discussed in more detail below in 6.3.3.5.1). The lower proportion of ILC3 in the *Adamdec1*$^{-/-}$ mice in comparison to WT mice on day 7 might be explained by the greater proportion of other CD3- cell populations, such as dendritic cells and neutrophils (Figure 6.20 A and B), infiltrating in the colonic tissues of the *Adamdec1*$^{-/-}$ mice in comparison to the WT on day 7 of the inflammation (discussed in more detail below in 6.3.3.5.1).

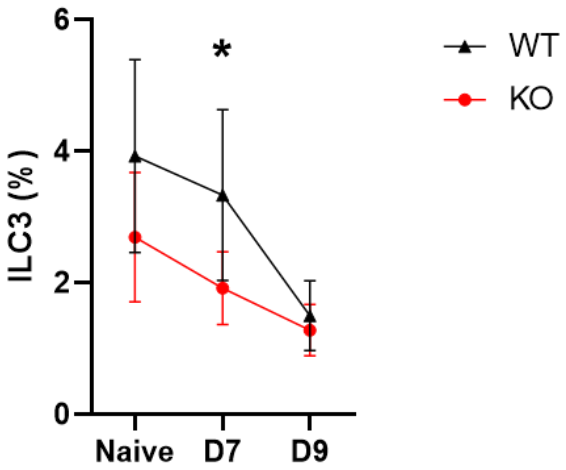

Figure 6.19 Changes in the proportion of ILC3 in the colonic tissue of the WT and *Adamdec1*$^{-/-}$ mice during DSS challenge. The proportion of ILC3 population decreased upon induction of inflammation in both WT and *Adamdec1*$^{-/-}$ mice. The proportion of ILC3 was significantly higher in the WT mice in comparison to the and *Adamdec1*$^{-/-}$ mice on day 7. The cell proportion is represented as percentage of the CD45+ CD3- cells. The graph shows mean with SD. One-way ANOVA test was used. For WT: naïve n=4, day 7 n=6, day 9 n=8. For *Adamdec1*$^{-/-}$: naïve n=4, day 7 n= 6, day 9 n=12.
KO: *Adamdec1*$^{-/-}$, WT: Wild type, D7: Day 7, D9: Day 9

6.3.3.5 Analysis using the myeloid panel antibodies

Following the gating strategy described in Figure 6.7, CD11b- MHCII^{high} B cells were excluded from the CD45+ CD3- cell population. The population of neutrophils, dendritic cells, and F4/80+ monocytes and macrophages were identified and their proportions within the CD45+ CD3- minus B cells population were compared between the WT and *Adamdec1*$^{-/-}$ mice at each timepoint. There were no significant differences in the proportions of B cells in the WT and *Adamdec1*$^{-/-}$ mice on any timepoints (Data not shown).

6.3.3.5.1 Analysis of dendritic cells, neutrophils, and combined monocytes and macrophages populations

The proportion of dendritic cells decreased from the naïve state to day 7 and then to day 9 with no major differences between the WT and *Adamdec1*$^{-/-}$ mice (Figure 6.20 A). In contrast, the proportion of neutrophils increased from the naïve state to day 7 then decreased slightly from day 7 to day 9 in both WT and knockout mice (Figure 6.20 B). A greater degree of the increase in the neutrophil proportion from the naïve state to day 7 was observed in the *Adamdec1*$^{-/-}$ mice in comparison to

the WT though no statistical difference was achieved. The proportion of F4/80+ monocyte and macrophage population drastically increased from the naïve state to day 7 with a further increase from day 7 to day 9 in both WT and *Adamdec1*$^{-/-}$ mice with very little difference observed between the WT and *Adamdec1*$^{-/-}$ mice (Figure 6.20 C). These findings indicated that the significantly higher proportion of the total CD45+ CD3- cells that was observed in the knockout mice in comparison to the WT mice during inflammation (Figure 6.10 A) was likely to be secondary to greater overall infiltration of myeloid cells rather than by a greater increase in a particular subtype of CD45+ CD3- cells.

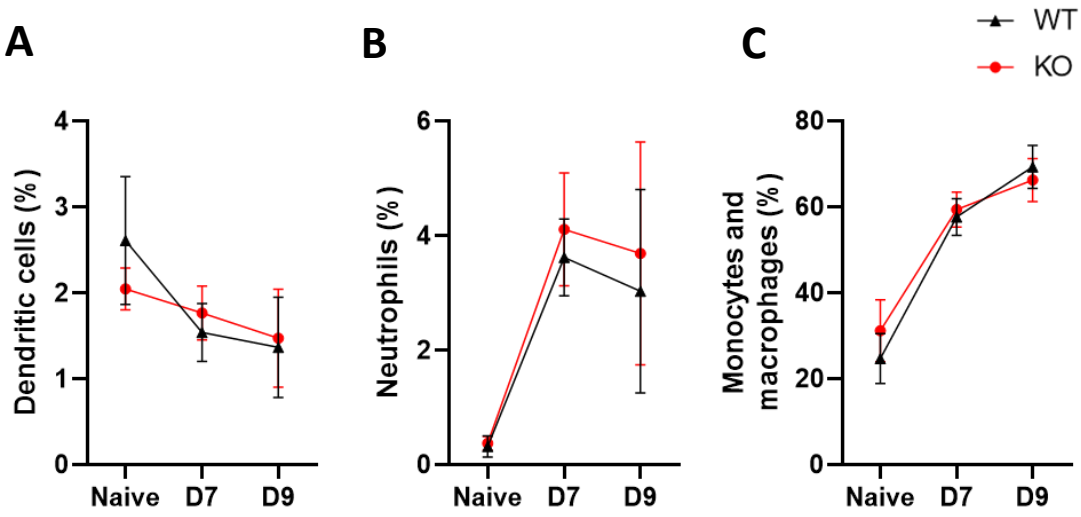

Figure 6.20 Changes in the proportion of dendritic cells (A), neutrophils (B) and F4/80+ monocyte and macrophage population (C) in the colonic tissue of the WT and *Adamdec1*$^{-/-}$ mice during DSS challenge. There were no statistical differences in the proportion of these cell populations between the WT and *Adamdec1*$^{-/-}$ mice. The cell proportions are represented as percentage of the CD45+ CD3- cells. The graph shows mean with SD. One-way ANOVA test was used. For WT: naïve n=4, day 7 n=6, day 9 n=8. For *Adamdec1*$^{-/-}$: naïve n=4, day 7 n= 6, day 9 n=12.
KO: *Adamdec1*$^{-/-}$, WT: Wild type, D7: Day 7, D9: Day 9

6.3.3.5.2 A ratio of SSC^{low} $Ly6C^{high}$ monocytes to $SSC^{mid/high}$ $Ly6C^{low/mid}$ macrophages

The F4/80+ monocytes and macrophage population was further divided into monocytes and macrophages according to their side scatter (SSC) and Ly6C expression. Monocytes were identified as cells with low SSC and high Ly6C expression.[178,180,199] Macrophages were identified as medium to high SSC and low to medium Ly6C expression.[178,180,199] The proportion of the SSC^{low} $Ly6C^{high}$ monocytes and $SSC^{mid/high}$ $Ly6C^{low/mid}$ macrophages were determined within the F4/80+ monocytes and macrophage cell population. An increase in $Ly6C^{high}$ monocytes to $Ly6C^{low/mid}$ macrophages ratio has been reported during DSS-induced colitis previously.[200] Additionally, $Ly6C^{high}$ monocytes were previously shown to be pro-inflammatory and subsequent ablation of $Ly6C^{high}$ monocytes ameliorated DSS-induced colitis.[201,202]

In the naïve state, the ratio of SSC^{low} $Ly6C^{high}$ monocytes to $SSC^{mid/high}$ $Ly6C^{low/mid}$ macrophages was extremely low and almost all F4/80+ expressing cells were macrophages in both WT and *Adamdec1*$^{-/-}$ mice (Figure 6.21 A and B). From the naïve state to day 7 of the DSS challenge, the ratio of monocytes to macrophages increased in both WT and *Adamdec1*$^{-/-}$ mice (Figure 6.21 A and B). There were no significant differences in the proportion of monocytes and macrophages within the F4/80+ cell population between the WT and knockout mice in the naïve state or on day 7. On day 9, however, the ratio of monocytes to macrophages decreased in the WT thus the initiation to restore the original state of the monocytes to macrophage ratio was evident. In contrast, there was a further increase in the proportion of monocytes, thus a further increase in the monocytes to macrophage ratio was observed in the *Adamdec1*$^{-/-}$ mice on day 9. The continuation of the increase in $Ly6C^{high}$ monocytes to macrophage ratio within the lamina propria beyond day 7 in the *Adamdec1*$^{-/-}$ mice may contribute to the ongoing inflammatory response and the continued weight loss observed in these knockout mice.

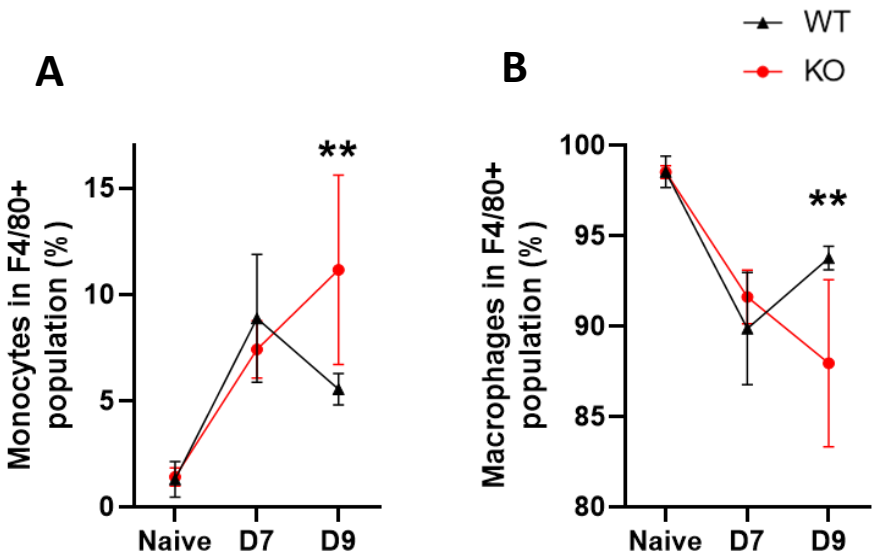

Figure 6.21 Changes in the proportion of SSC^{low} Ly6C^{high} monocytes (A) and SSC$^{mid/high}$ Ly6C$^{low/mid}$ macrophages (B) in the colonic tissue of the WT and *Adamdec1*$^{-/-}$ mice during DSS challenge. The ratio of monocyte to macrophage increased in both WT and *Adamdec1*$^{-/-}$ mice from day 0 to day 7. The ratio of monocytes to macrophages decreased in the WT but increased further in the *Adamdec1*$^{-/-}$ mice from day 7 to day 9. The cell proportions are represented as percentage of the CD11b+ F4/80+ cells. The graph shows mean with SD. One-way ANOVA test was used. For WT: naïve n=4, day 7 n=6, day 9 n=8. For *Adamdec1*$^{-/-}$: naïve n=4, day 7 n= 6, day 9 n=12.
KO: *Adamdec1*$^{-/-}$, WT: Wild type, D7: Day 7, D9: Day 9 **: $p < 0.01$

6.3.3.5.3 The expressions of CX3CR1 and Ly6C in the SSC^{low} Ly6C^{high} monocytes and SSC$^{mid/high}$ Ly6C$^{low/mid}$ macrophages

In order to evaluate whether the phenotype of monocytes and macrophages differed in the absence of ADAMDEC1, the expression levels of surface markers CX3CR1 and Ly6C were determined. In the naïve colonic mouse tissues, a higher expression of CX3CR1 on monocytes is seen as opposed to lower CX3CR1 expression during inflammation.[203] The high-CX3CR1 expressing monocytes have been shown to possess an anti-inflammatory signature.[201,203,204] Whereas a higher expression of Ly6C is seen on macrophages during inflammation, and macrophages with high Ly6C expression are believed to be pro-inflammatory.[201,205]

Significantly lower surface expressions of CX3CR1 were seen in the SSC^{low} Ly6C^{high} monocytes of the *Adamdec1*$^{-/-}$ mice upon induction of inflammation in comparison to the WT mice (Figure 6.22). The difference between the WT and

Adamdec1$^{-/-}$ mice is more evident on day 9 compared to day 7. Also, significantly lower surface expressions of Ly6C were detected in the SSC$^{mid/high}$ Ly6C$^{low/mid}$ macrophages upon induction of inflammation (Figure 6.23). These findings suggested that the proportion of monocytes and macrophages as well as the phenotype of these cells seemed to be affected by ADAMDEC1 thus a potential role of ADAMDEC1 in the modulation of innate inflammatory response. Together with the difference in the proportion of monocytes and macrophages observed between the WT and knockout mice on day 9 (Figure 6.21 A and B), these findings suggested there were a greater proportion of monocytes with potentially more pro-inflammatory phenotype and a smaller proportion of macrophages with potentially more anti-inflammatory phenotype in the colonic tissues of the *Adamdec1*$^{-/-}$ mice on day 9 compared to the WT mice.

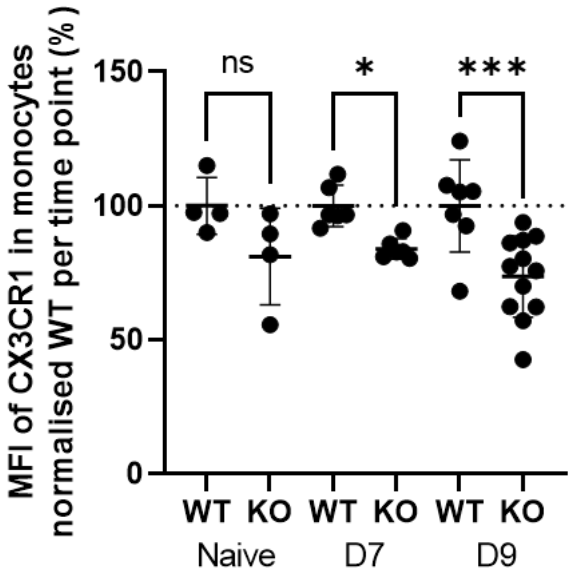

Figure 6.22 Change in MFI of CX3CR1 in SSC^{low} Ly6C^{high} monocyte population of the WT and *Adamdec1*$^{-/-}$ mice during DSS challenge. MFI of CX3CR1 was significantly lower in the samples of the *Adamdec1*$^{-/-}$ mice in comparison to the WT mice on day 7 and day 9 of the DSS challenge. MFI of the *Adamdec1*$^{-/-}$ samples were normalised to the mean MFI of the WT samples per timepoint and shown as percentage change relative to the mean MFI of the WT at each timepoint. The graph shows mean with SD. One-way ANOVA test was used.
KO: *Adamdec1*$^{-/-}$, WT: Wild type, D7: Day 7, D9: Day 9, **: $p < 0.01$, ***: $p < 0.001$, ns: Non-significant

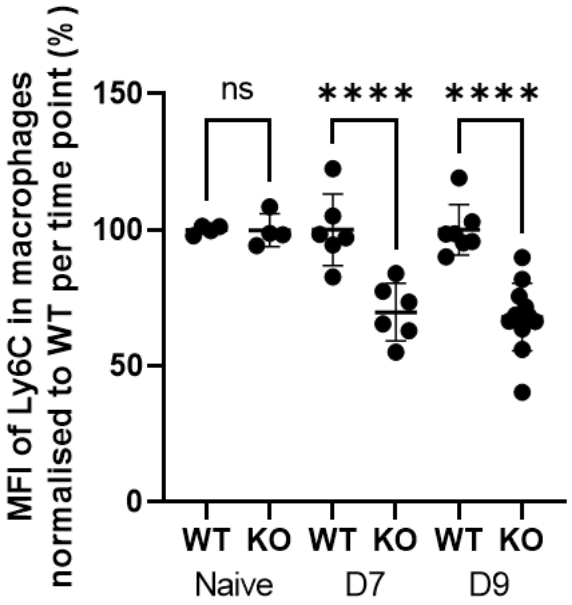

Figure 6.23 Change in MFI of Ly6C in SSC$^{mid/high}$ Ly6C$^{low/mid}$ macrophage population of the WT and *Adamdec1*$^{-/-}$ mice during DSS challenge. MFI of Ly6C was significantly lower in the samples of the *Adamdec1*$^{-/-}$ mice in comparison to the WT mice on day 7 and day 9 of the DSS challenge. MFI of the *Adamdec1*$^{-/-}$ samples were normalised to the mean MFI of the WT samples per timepoint and shown as percentage change relative to the mean MFI of the WT at each timepoint. The graph shows mean with SD. One-way ANOVA test was used.
KO: *Adamdec1*$^{-/-}$, WT: Wild type, D7: Day 7, D9: Day 9, ****: $p < 0.0001$, ns: Non-significant

6.3.3.5.4 The expression of CX3CR1 in different subtypes of CD45+ CD3- cells

Interestingly, when the expression of CX3CR1 on various subtypes of CD45+ CD3- cells were compared between the WT and *Adamdec1*$^{-/-}$ mice, an overall trend of lower levels of CX3CR1 in the cells of *Adamdec1*$^{-/-}$ mice in comparison to the WT mice were observed (Figure 6.24). Largely, this trend was seen at all timepoints including the naïve state although statistical differences were not achieved in all the cell subtypes or timepoints. In contrast, there was no uniform trend of a reduction in the expression of Ly6C across all the subtypes of CD45+ CD3- cells. (Data not shown.) These findings suggested a potential involvement of ADAMDEC1 in the regulation of surface expression of CX3CR1 on the colonic CD45+ CD3- cells.

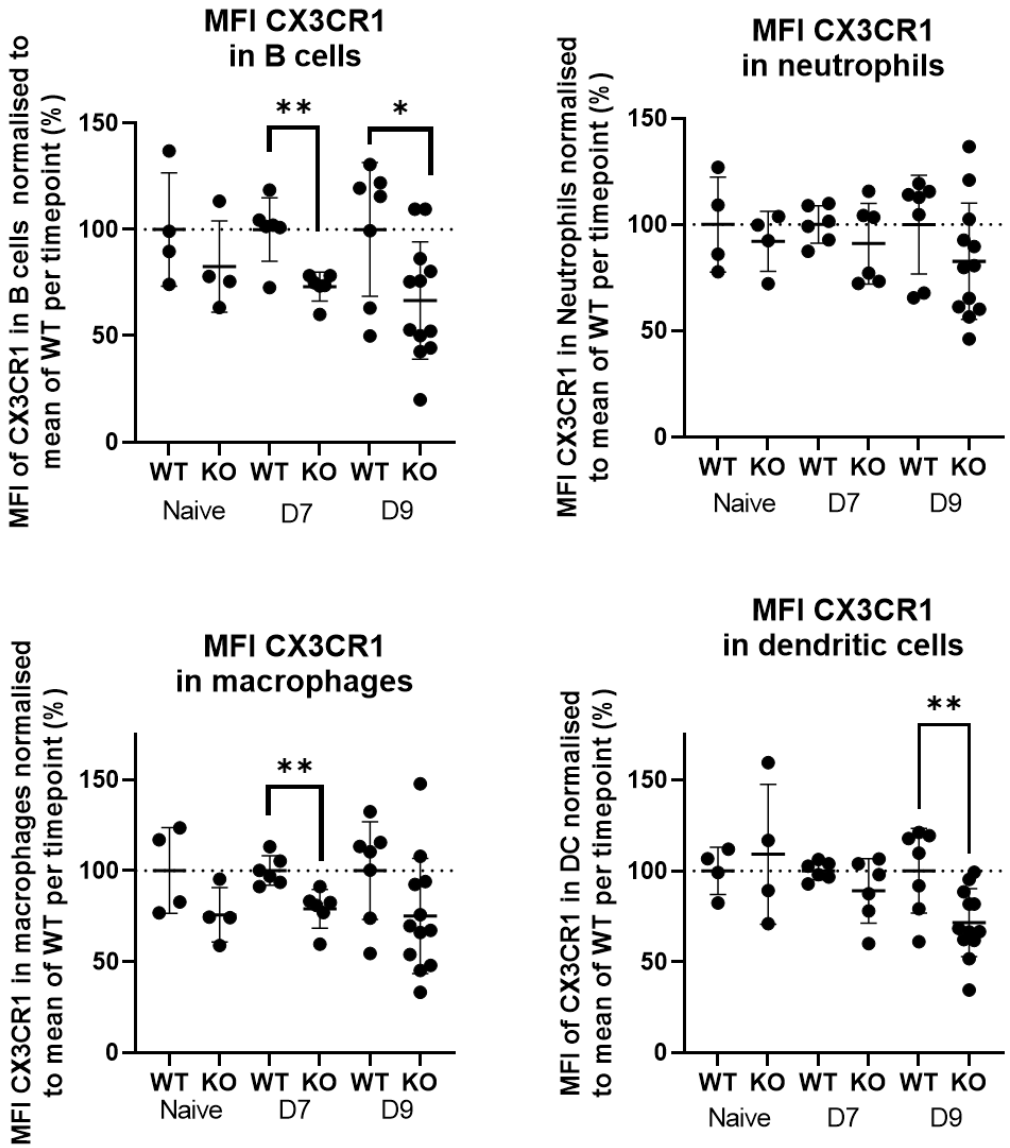

Figure 6.24 MFI of CX3CR1 in B cell, neutrophil, macrophage and dendritic cell populations of the WT and *Adamdec1*$^{-/-}$ mice during DSS challenge. An overall trend of lower CX3CR1 MFI was observed in the cells of *Adamdec1*$^{-/-}$ mice in comparison to the WT mice. MFI of CX3CR1 of the *Adamdec1*$^{-/-}$ samples were normalised to the mean MFI of CX3CR1 of the WT samples per timepoint and shown as percentage change relative to the mean MFI of the WT samples at each timepoint. One-way ANOVA test was used.
KO: *Adamdec1*$^{-/-}$, WT: Wild type, DC: Dendritic cells, D7: Day 7, D9: Day 9, *: $p < 0.05$, **: $p < 0.001$

Since the cell surface expressions of CD4 and CD8 were shown to be destroyed by dispase, the experiment using murine splenocytes was repeated to determine whether the reduction in CX3CR1 and Ly6C expression on the cells of the knockout mice involved the enzymatic activity of dispase. Single cell suspensions were prepared from spleens taken from healthy WT and *Adamdec1*$^{-/-}$ mice and were stained for the surface expression of CD45, CD3, CX3CR1 and Ly6C with or without the digestion step with dispase.

The disruption of CX3CR1 expression on CD45+ CD3- splenocytes by dispase was negligible in both the WT and *Adamdec1*$^{-/-}$ mice (Figure 6.25). The surface expression of Ly6C on these splenocytes was not affected by the by dispase (Figure 6.26). These indicated that the reduced surface expressions of CX3CR1 and Ly6C on the cell types described above in the absence of ADAMDEC1 was a genuine representation of surface expression levels within the colonic tissues.

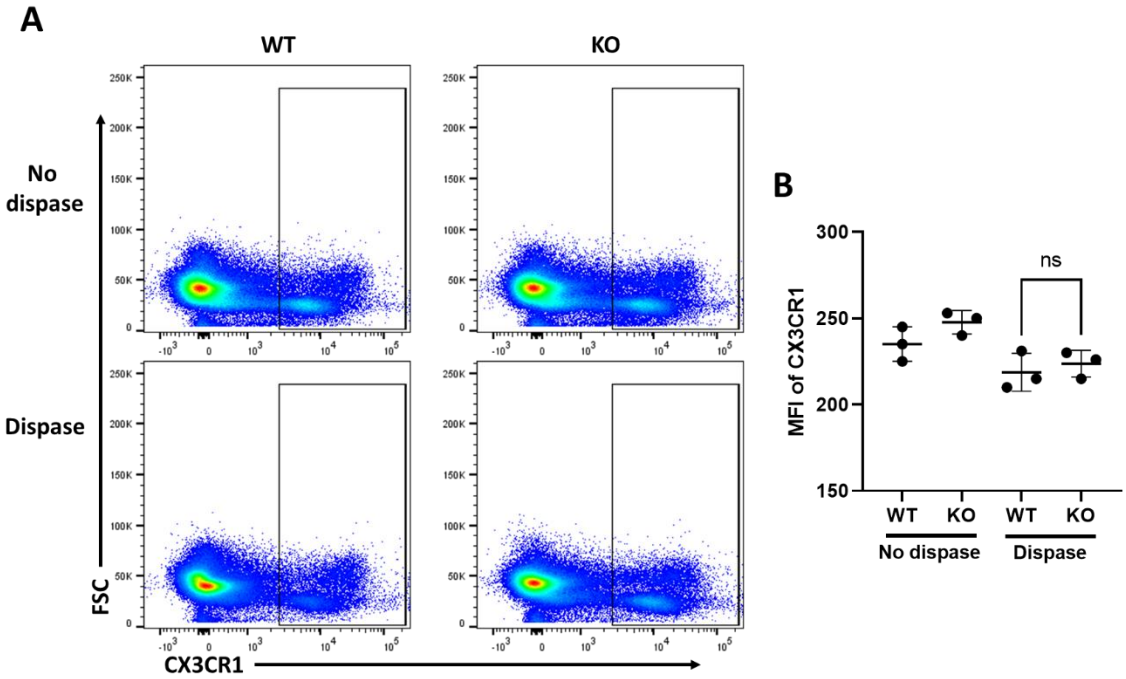

Figure 6.25 Effect of dispase on the surface expression of CX3CR1 in the murine splenocytes. The digestion step with dispase did not destroy Ly6C on murine splenocytes.
A: Flow cytometry plots showing the CX3CR1+ cell populations in the splenocytes of the healthy WT and *Adamdec1*$^{-/-}$ mice treated with dispase or not treated with dispase. The image was created using FlowJo software (BD Biosciences). The figure was created using the result of one WT and one *Adamdec1*$^{-/-}$ mice as examples.
B: MFI of CX3CR1 on the splenocytes of the healthy WT and *Adamdec1*$^{-/-}$ mice treated with dispase or not treated with dispase. The graph shows mean with SD. Unpaired student t-test was used.
KO: *Adamdec1*$^{-/-}$, WT: Wild type, ns: Non-significant

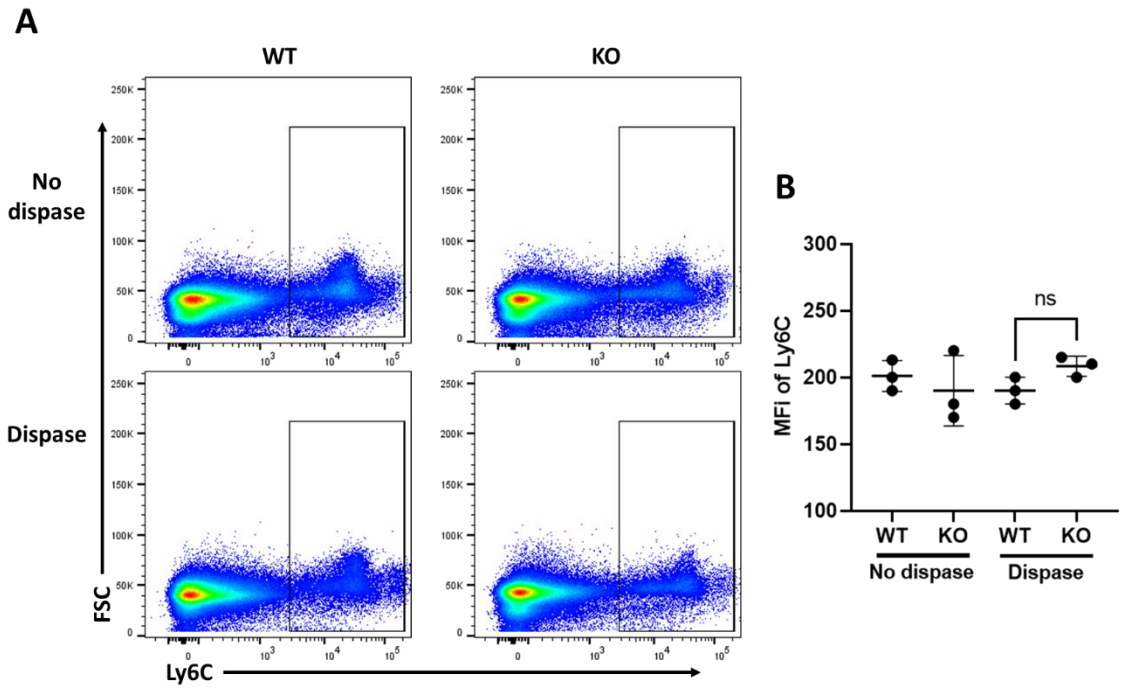

Figure 6.26 Effect of dispase on the surface expression of Ly6C in the murine splenocytes. The digestion step with dispase did not destroy Ly6C on murine splenocytes.
A: Flow cytometry plots showing the Ly6C+ cell populations in the splenocytes of the healthy WT and *Adamdec1*$^{-/-}$ mice treated with dispase or not treated with dispase. The image was created using FlowJo software (BD Biosciences). The figure was created using the result of one WT and one *Adamdec1*$^{-/-}$ mice as examples.
B: MFI of Ly6C on the splenocytes of the healthy WT and *Adamdec1*$^{-/-}$ mice treated with dispase or not treated with dispase. The graph shows mean with SD. Unpaired student t-test was used.
KO: *Adamdec1*$^{-/-}$, WT: Wild type, ns: Non-significant

6.3.3.5.5 The expression of CD11b on the subtypes of CD3- CD11b+ cells

CD11b is one of the heterodimers that comprises integrin, macrophage-1 antigen (Mac-1), which is found on leukocytes of the innate immune system. Mac-1-mediated signalling is believed to be involved in various immune response mechanisms such as cell adhesion, phagocytosis and intracellular killing of pathogens.[206,207] Upregulations of CD11b surface expression are seen on phagocytes during inflammation and its upregulation has been reported to indicate inflammatory activation of these cells.[208] It was noted during the FACS data analysis that an overall trend of higher expressions of CD11b on the subtype of CD3- CD11b+ cells was observed upon induction of inflammation in the *Adamdec1*$^{-/-}$ mice compared to the WT mice (Figure 6.27). The role of CD11b in DSS-medicated colitis is controversial since studies utilised CD11b knockout mice

have shown both suppressed and exaggerated forms of DSS-mediated colonic inflammation.[209,210] The finding of the higher expression of CD11b in the subtypes of the CD3- CD11b+ cell population of the *Adamdec1*$^{-/-}$ mice in comparison to the WT in this project likely indicated the more exaggerated form of inflammation in the colonic tissues of the knockout mice.

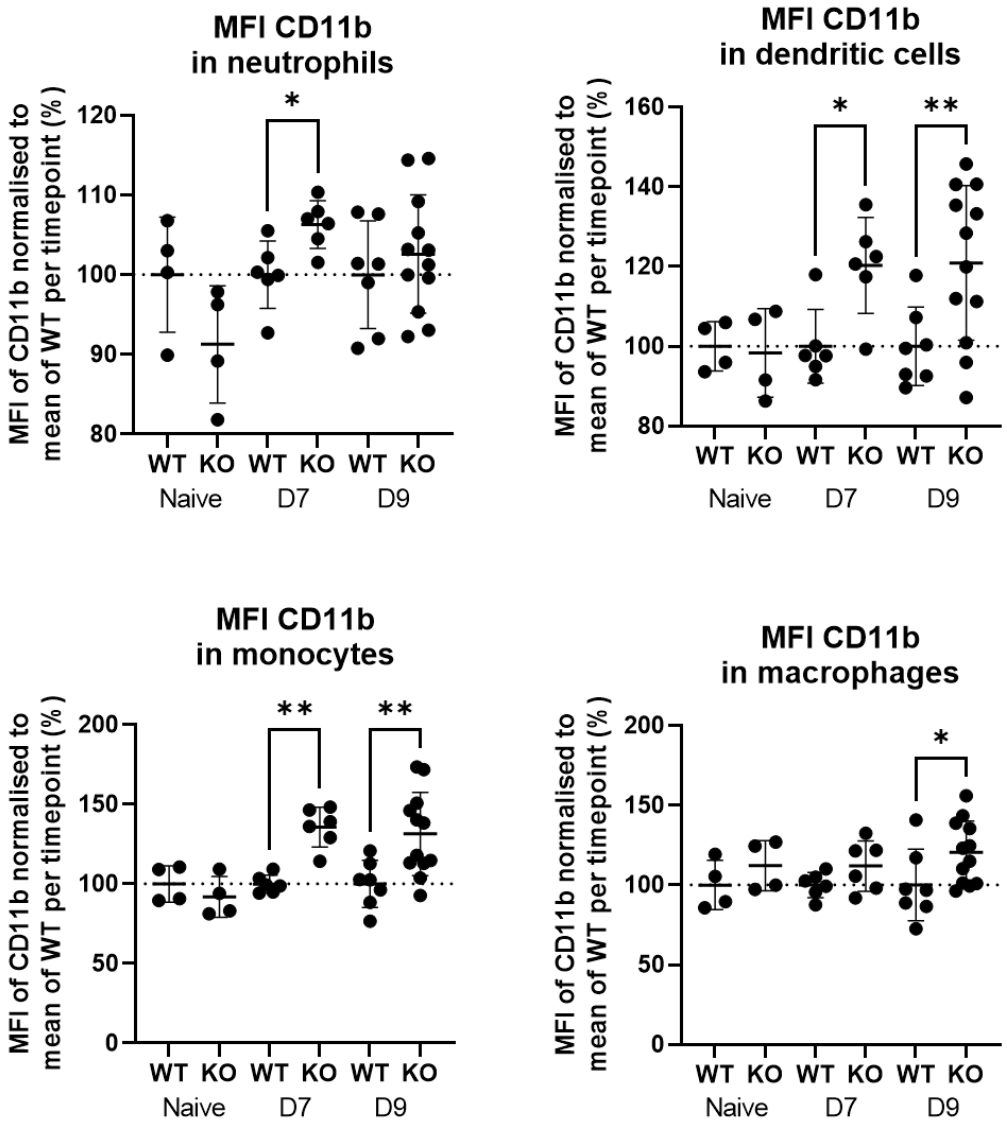

Figure 6.27 MFI of CD11b in neutrophil, dendritic cell, monocyte and macrophage cell populations of the WT and *Adamdec1*$^{-/-}$ mice during DSS challenge. An overall trend of higher CD11b MFI was observed in the cells of *Adamdec1*$^{-/-}$ mice in comparison to the WT mice. MFI of CD11b of the *Adamdec1*$^{-/-}$ samples were normalised to the mean MFI of CD11b of the WT samples per timepoint and shown as percentage change relative to the mean MFI of the WT samples at each timepoint. The graphs show mean with SD. One-way ANAOVA test was used.
KO: *Adamdec1*$^{-/-}$, WT: Wild type, DC: Dendritic cells, D7: Day 7, D9: Day 9, *: $p < 0.05$, **: $p < 0.001$

6.3.4 Analysis of the gene expression in the colonic tissue of WT and *Adamdec1*$^{-/-}$ mice on day 9 of the DSS challenge by qPCR

During the data analysis, it became apparent that there was a significant difference in the pattern of expression of some of the genes between Cage 1 and Cage 2 of the knockout mice consistent with the significant difference in their weight reduction during the DSS challenge. Thus, the data were analysed separately for the knockout mice in Cage 1 and Cage 2.

6.3.4.1 Recruitment and proliferation of CD4+ and CD8+ lymphocytes

In order to determine the effect of ADAMDEC1 on the recruitment and proliferation of T helper cells and cytotoxic T cells, the expression of *Cd4* and *Cd8* were examined respectively. qPCR was used in place of the more routine FACS analysis to determine the numbers of CD4+ and CD8+ cells in this experiment due to the digestive effect of dispase on these surface molecules as discussed earlier (Chapter 6.3.3.4.2). There were significant increases in the expression of *Cd4* from the naïve state to day 9 in the WT as well as *Adamdec1*$^{-/-}$ mice in both Cage 1 and Cage 2 (Figure 6.28 A). The same trend was seen for the *Cd8* expressions which increased from the naïve state to day 9 in the WT and *Adamdeci1*$^{-/-}$ mice in Cage 1 and Cage 2 (Figure 6.28 B). These observations indicated that the recruitment and proliferation of CD4+ T cells and the recruitment of CD8+ cytotoxic cells to the colonic tissues occurred in the same manner in both WT and knockout mice.

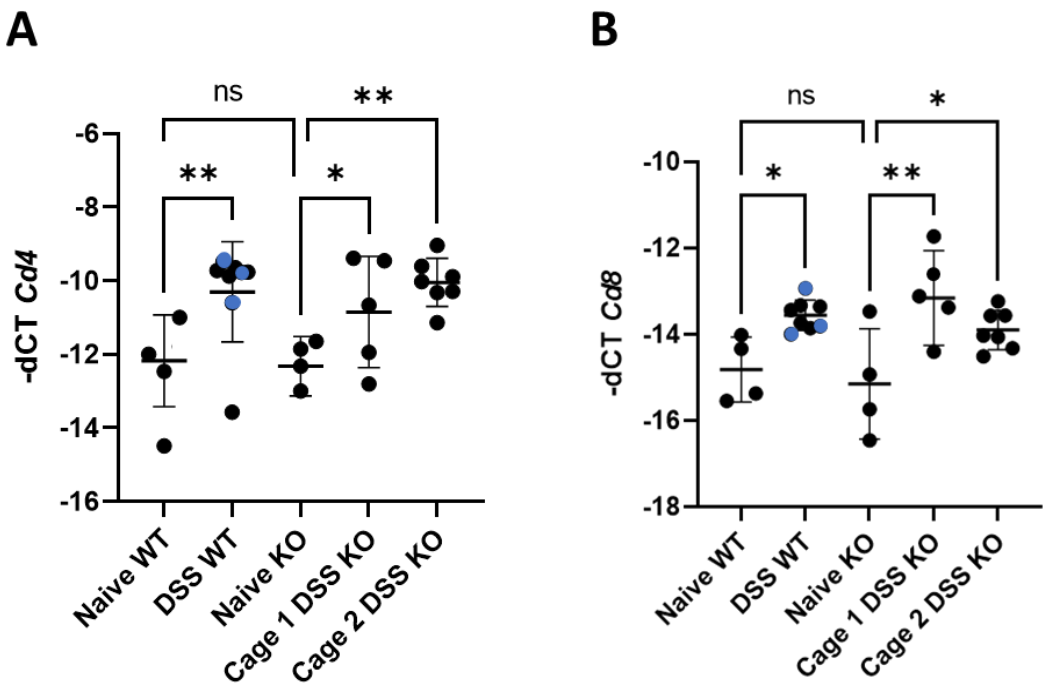

Figure 6.28 Expression of *Cd4* (A) and *Cd8* (B) in the colonic tissue of the WT and *Adamdec1*$^{-/-}$ mice in Cage 1 and Cage 2 during DSS challenge. The blue dots represent the WT DSS samples in Cage 1. The graphs show mean with SD. One-way ANAOVA test was used.
KO: *Adamdec1*$^{-/-}$, WT: Wild type, *: $p < 0.05$, **: $p < 0.01$, ns: Non-significant

6.3.4.2 Expression of pro-inflammatory cytokines

IL-1β and TNF-α are two of the main pro-inflammatory cytokines of the innate immune response and are secreted predominantly by monocytes and macrophages during inflammation. Both are known to be secreted during DSS-induced colitis, as well as being elevated in inflamed intestinal tissue from IBD patients and correlate with the degree of inflammation.[211–216]

As expected, on day 9, significant increases in the expression of *Il-1β* were detected in the DSS tissues of WT and *Adamdec1*$^{-/-}$ mice, both in Cage 1 and Cage 2, in comparison to the tissues from untreated mice reflecting the innate immune system response during the acute phase of inflammation (Figure 6.29 A). The expression of *Tnf-α* in the DSS tissues of the WT and *Adamdec1*$^{-/-}$ mice in Cage 2 also increased significantly in comparison to their naïve tissues (Figure 6.29 B). However, interestingly, this was not observed in the *Adamdec1*$^{-/-}$ mice in Cage 1 (Figure 6.29 B) despite these knockout mice exhibiting a greater ongoing inflammation on day 9 (Figure 6.5).

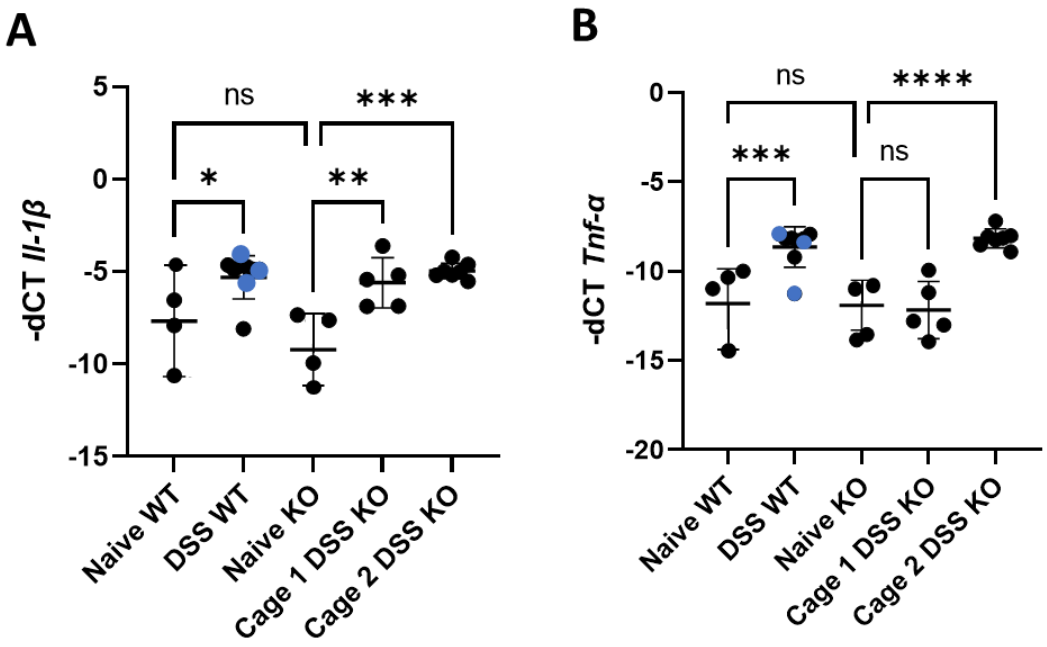

Figure 6.29 Expression of *Il-1β* (A) and *Tnf-α* (B) in the colonic tissue of the WT and *Adamdec1*$^{-/-}$ mice in Cage 1 and Cage 2 during DSS challenge. The blue dots represent the WT DSS samples in Cage 1. The graphs show mean with SD. One-way ANAOVA test was used.
KO: *Adamdec1*$^{-/-}$, WT: Wild type, *: $p < 0.05$, **: $p < 0.01$, ***: $p < 0.001$, ****: $p < 0.0001$ ns: Non-significant

6.3.4.3 Expression of neutrophile and monocyte chemokines and chemokine receptor

CXCL1 is a potent neutrophil chemokine which is known to increase during inflammation including in the inflamed intestinal tissues of patients with IBD.[217] CXCL1 is secreted by cells including macrophages and it is also known to stimulate secretion of IL-1β from macrophages during inflammation.[218,219] *Cxcl1* knockout mice have previously shown an inability to evoke neutrophil recruitment and demonstrated more severe inflammation during DSS-induced colitis.[220] The expression of *Cxcl1* was significantly increased in the DSS tissues of the WT and *Adamdec1*$^{-/-}$ mice, both in Cage 1 and Cage 2, in comparison to their naïve tissues (Figure 6.30). These findings suggested that *Cxcl1* was induced appropriately in response to mucosal injury in the *Adamdec1*$^{-/-}$ mice despite the absence of ADAMDEC1. The expression of *Cxcl1* was significantly higher in the DSS tissues of the *Adamdec1*$^{-/-}$ mice compared to the WT mice. The highest expression was seen in the DSS tissue of *Adamdec1*$^{-/-}$ mice in Cage 1 and the second highest

expression was seen in the DSS tissue of *Adamdec1*$^{-/-}$ mice in Cage 2 (Figure 6.30). These observations correlated with the greatest weight loss exhibited by the *Adamdec1*$^{-/-}$ mice in Cage 1 followed by the *Adamdec1*$^{-/-}$ mice in Cage 2 and then the WT mice.

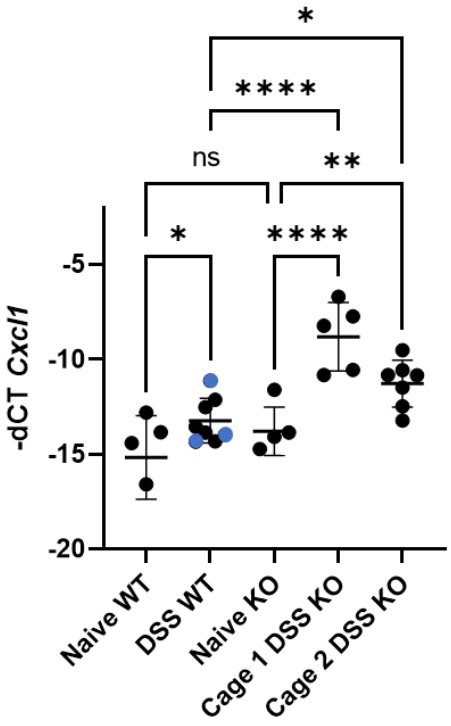

Figure 6.30 Expression of *Cxcl1* in the colonic tissue of the WT and *Adamdec1*$^{-/-}$ mice in Cage 1 and Cage 2 during DSS challenge. The blue dots represent the WT DSS samples in Cage 1. The graph shows mean with SD. One-way ANAOVA test was used.
KO: *Adamdec1*$^{-/-}$, WT: Wild type, *: $p < 0.05$, **: $p < 0.01$, ****: $p < 0.0001$ ns: Non-significant

The ratio of monocytes to macrophages was shown to be increased in the *Adamdec1*$^{-/-}$ mice in comparison to the WT on day 9 by FACS analysis (Figure 6.21 A and B). Thus, expressions of C-C Motif Chemokine receptor type 2 (CCR2) and CCL2, also known as monocyte-chemoattractant protein-1, were measured. CCR2 is predominantly expressed on monocytes and CCL2 is secreted mainly by macrophages.[221] Their expressions increase during inflammation and recruitment of monocytes to the inflamed colonic tissue during DSS colitis is believed to occur in CCL2-CCR2 dependent manner.[201,203,205] Upon induction of the DSS-induced inflammation, significant increases in the expression of *Ccr2* and *Ccl2* were observed in the WT mice and *Adamdec1*$^{-/-}$ mice in Cage 2 (Figure 6.31 A and B).

In contrast, this was not detected in the *Adamdec1*$^{-/-}$ mice in Cage 1 (Figure 6.31 A and B). Thus, once again the cage-dependant difference was observed in the *Adamdec1*$^{-/-}$ mice where the gene expressions of the *Adamdec1*$^{-/-}$ mice in Cage 2 were behaving similar to those of the WT mice. Additionally, the unchanged levels of *Ccr2* and *Ccl2* expression from the naive state to day 9 in the tissues of the *Adamdec1*$^{-/-}$ mice in Cage 1 did not correlate with the more severe inflammatory state of these mice. This suggested either aberrant *Ccr2* and *Ccl2* expressions by monocytes and macrophages or reduced number of these cells within the inflamed tissue of the *Adamdec1*$^{-/-}$ mice in the Cage 1.

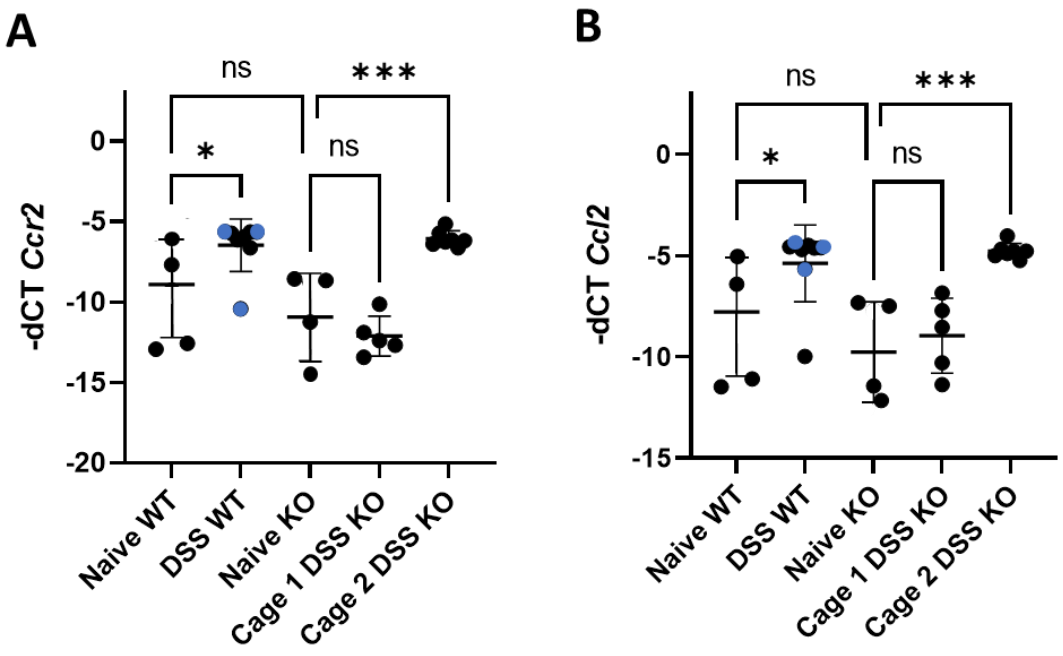

Figure 6.31 Expression of *Ccr2* (A) *and Ccl2* (B) in the colonic tissue of the WT and *Adamdec1*$^{-/-}$ mice in Cage 1 and Cage 2 during DSS challenge. The blue dots represent the WT DSS samples in Cage 1. The graphs show mean with SD. One-way ANAOVA test was used.
KO: *Adamdec1*$^{-/-}$, WT: Wild type, *: $p < 0.05$, ***: $p < 0.001$, ns: Non-significant

Based on these findings, the proportion of monocytes and macrophages on day 9 of the DSS challenge analysed by flow cytometry were examined separately for the *Adamdec1*$^{-/-}$ mice in Cage 1 and Cage 2. Despite the absence of the *Ccr2* upregulation in the *Adamdec1*$^{-/-}$ mice in Cage 1, the highest proportion of monocytes was seen in these mice on day 9 in comparison to the WT and

Adamdec1$^{-/-}$ mice in Cage 2, although statistical significance was not achieved between the knockout mice in Cage 1 and Cage 2. (Figure 6.32 A). In contrast, the macrophage proportions detected by the flow cytometry corresponded with the expression of *Ccl2*. The lowest proportion of macrophages was seen in the *Adamdec1*$^{-/-}$ mice in Cage 1 on day 9, although statistical significance was not achieved between the knockout mice in Cage 1 and Cage 2 (Figure 6.32 B), which was consistent with the absence of upregulation of *Ccl2* in the knockout mice in Cage 1 on day 9 (Figure 6.31 B). These findings indicated that the increase in the monocytes proportion seen in the *Adamdec1*$^{-/-}$ mice, in both Cage 1 and Cage 2, on day 9 was not rendered by an increase in CCR2-CCL2 axis.

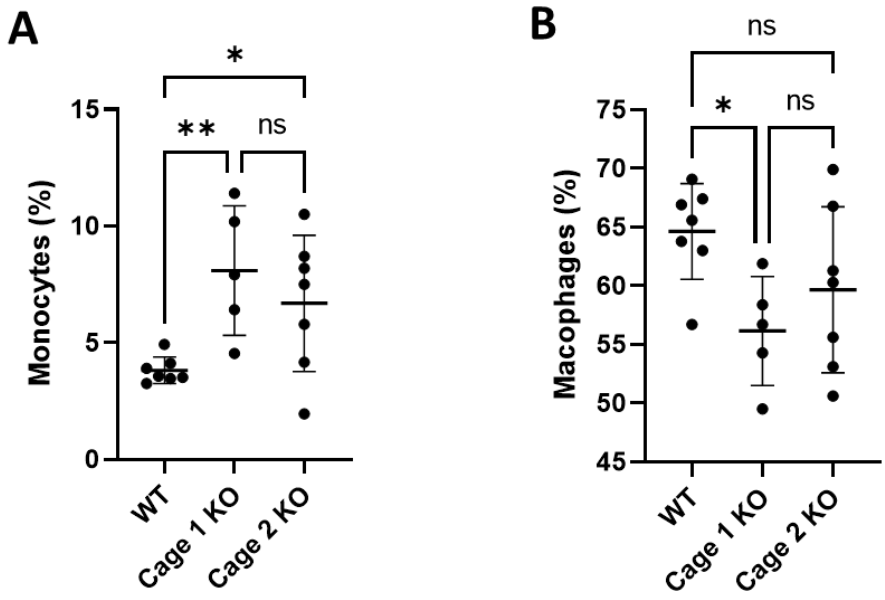

Figure 6.32 Proportion of monocyte (A) and macrophage (B) population in the colonic tissue of the WT and *Adamdec1*$^{-/-}$ mice in Cage 1 and Cage 2 on day 9 of the DSS challenge. The cell proportions are represented as percentage of the CD3- CD11b+ cells after B cells were excluded. The graphs show mean with SD. One-way ANAOVA test was used.
KO: *Adamdec1*$^{-/-}$, *: $p < 0.05$, **: $p < 0.01$, ns: Non-significant

6.3.4.4 Expression of genes associated with epithelial cells

In order to assess the effect of ADAMDEC1 on epithelial cells during the mucosal inflammation, the expression of *Lgr5*, *Ki67* and *Cdx2* were measured. The Lgr5-expressing intestinal stem cells, located at the base of crypts, proliferate to generate transit amplifying cells of the epithelium, located above the stem cells,

and eventually develop into fully differentiated intestinal epithelial cells. Thus, *Lgr5* serves as a marker for the intestinal stem cells. *Ki67* is a proliferative marker that largely conveys the proliferative state of the intestinal epithelial cells, particularly the transit amplifying cells of the epithelium which possess the highest mitotic activity in the intestine. Thus, the expression of *Ki67* is indicative of the epithelial turnover/repair. *Cdx2* is an established epithelial cell differentiation marker.[222]

The expression of *Lgr5* was reduced significantly in the *Adamdec1*$^{-/-}$ mice in both Cage 1 and Cage 2 from the naïve state to day 9. However, no significant change in the expression of *Lgr5* was observed between the naïve and inflamed tissues of the WT mice (Figure 6.33 A). This indicated a significant loss of intestinal stem cells in the *Adamdec1*$^{-/-}$ mice, independent of the cage.

The expression of *Ki67* increased significantly in the WT and *Adamdec1*$^{-/-}$ mice in Cage 2 from the naïve state to day 9 suggesting that the epithelia were in a phase of repair and healing following the cessation of oral administration of DSS in these mice (Figure 6.33 B). However, interestingly, the expression of *Ki67* was significantly reduced in the DSS tissues of the *Adamdec1*$^{-/-}$ mice in Cage1 compared to their naïve tissues which suggested that the epithelial repair had not been initiated in these knockout mice.

A significant reduction in the expression of *Cdx2* was observed only in the *Adamdec1*$^{-/-}$ mice in Cage 1 (Figure 6.33 C). Combining the findings of *Ki67* and *Cdx2* expressions of the *Adamdec1*$^{-/-}$ mice in Cage 1 suggested a greater loss of epithelial cells in these knockout mice which was likely to be secondary to the ongoing inflammation.

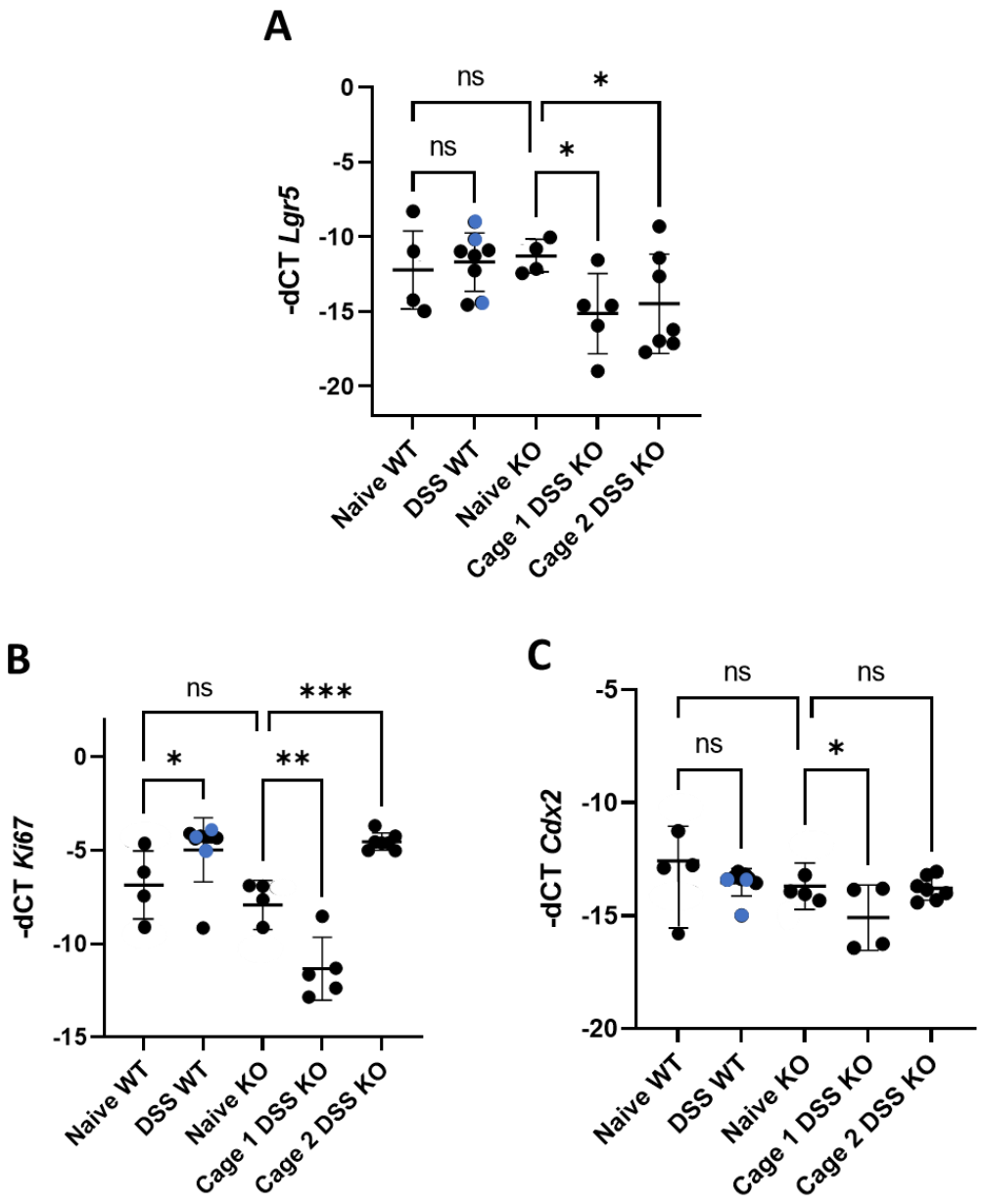

Figure 6.33 Expression of *Lgr5* (A), *Ki67* (B) *and Cdx2* (C) in the colonic tissue of the WT and *Adamdec1*$^{-/-}$ mice in Cage 1 and Cage 2 during DSS challenge. The blue dots represent the WT DSS samples in Cage 1. The graphs show mean with SD. One-way ANAOVA test was used.
KO: *Adamdec1*$^{-/-}$, WT: Wild type, *: $p < 0.05$, **: $p < 0.01$, ***: $p < 0.001$, ns: Non-significant

FGF2 is reported to play a role in epithelial homeostasis and repair.[33] It has been shown to promote intestinal stem cell survival following injury and an increase in its level has been detected during DSS-induced colitis.[33,223,224] Since *Lgr5* expression was found to be significantly reduced in the *Adamdec1*$^{-/-}$ mice indicating an increased susceptibility of the stem cells in these mice, the expression of *Fgf2*

was measured to determine if the absence of ADAMDEC1 resulted in a reduced FGF2 expression, which might influence the stem cell susceptibility to the DSS challenge and mucosal repair. FGF2 has also previously been shown to induce ADAMDEC1, which in turn released ECM-bound FGF2 and increased the level of active FGF2 creating a positive feedback loop in a study using GBM cancer cells.[29]

A significant increase in the expression of *Fgf2* was observed from the naïve state to day 9 in the knockout mice in Cage 1 which was not observed in the WT or *Adamdec1*$^{-/-}$ mice in Cage 2. This suggested that, at least at the RNA messenger level, the reduced expressions of *Lgr5*, *Ki67* and *Cdx2* in the *Adamdec1*$^{-/-}$ mice of Cage 1 upon the induction of inflammation (Figure 6.33 A, B and C) occurred in spite of the upregulation of *Fgf2*. Also the discrepancy between the change in *Fgf2* expression in the *Adamdec1*$^{-/-}$ mice in Cage 1 and the *Adamdec1*$^{-/-}$ mice in Cage 2 during the inflammation suggested that the *Fgf2* expression was likely to be inflammatory driven and not dependent on ADAMDEC1 at the RNA messenger level.

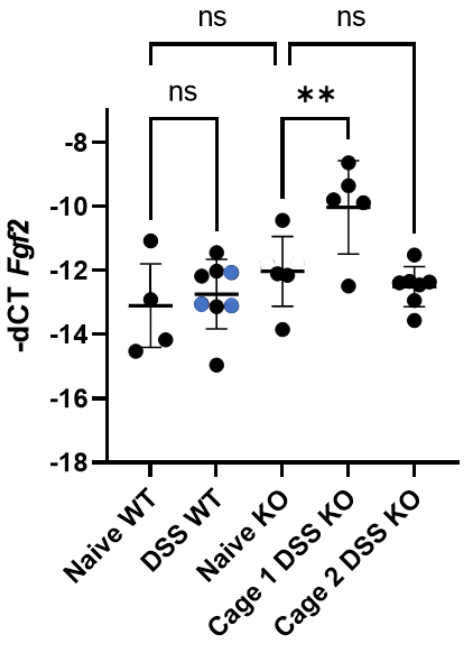

Figure 6.34 Expression of *Fgf2* in the colonic tissue of the WT and *Adamdec1*$^{-/-}$ mice in Cage 1 and Cage 2 during DSS challenge. The blue dots represent the WT DSS samples in Cage 1. The graph shows mean with SD. One-way ANAOVA test was used.
KO: *Adamdec1*$^{-/-}$, WT: Wild type, **: $p < 0.01$, ns: Non-significant

6.4 Discussion

In this chapter, through the combination of the DSS colitis model and use of *Adamdec1*$^{-/-}$ mice, the complexity of how genotype translates to phenotype, as well as, potential mechanisms through which the absence of ADAMDEC1 affects the hosts' defence against mucosal injury and inflammation have been revealed.

The most striking finding was the cage-dependant variability with respect to the inflammatory response following the exposure to DSS observed in the *Adamdec1*$^{-/-}$ mice. Variation in phenotype of any given genotype is not uncommon in experiments using mice, even when mice are standardised for factors such as age, sex, diet and husbandry condition.[225,226] Cage has been shown to be a significant factor resulting in variability of phenotype.[227] Inter-cage variation can be attributed by factors such as technical variability, poor experimental design as well as variability in the expressivity of genotype due to complex interplay between the genotype and environment.[228–230] In this project, the inter-cage variability was attempted to be reduced as much as possible through modifications to the normal DSS colitis protocol. The number of cage was reduced by pooling the mice into 2 larger cages. Additionally, the WT and *Adamdec1*$^{-/-}$ mice were cohoused in these larger cages for 8 weeks prior to being challenged with DSS in the same cage. Thus, the WT mice in each cage served as per cage controls. The *Adamdec1*$^{-/-}$ mice and WT mice per cage were culled and the tissues of the mice from each cage were processed as a single batch on the same day. The WT mice in Cage 1 Day 9 Experiment cohort did not exhibit a greater weight loss in comparison to the WT in cage 2. Additionally, there were no major differences in the gene expression data of the WT mice in Cage 1 and Cage 2 analysed by qPCR. These observations suggested that, firstly, the WT C56BL/6 mice in our facility responded to the DSS challenge in a similar manner irrespective of the cage environment. Secondly, the variability in the degree of weight loss and inflammation observed between the *Adamdec1*$^{-/-}$ mice in Cage 1 and Cage 2 were unlikely to be secondary to technical variability. Therefore, it was likely to represent a true variability in DSS sensitivity of *Adamdec1*$^{-/-}$ mice, which was probably profoundly influenced by the environment. The responsible environmental factor is unknown, but the colonic microbiome may play a role and is investigated in Chapter 7.

Literature on variability in expressivity of genotype in experimental mice is extremely sparse. However, the mechanisms behind variable expression of

genotype are of high importance and merits evaluation. Variation in penetrance and expressivity of genotype are reported in a vast number of human diseases. In Crohn's disease, for example, NOD2 genotype exhibits incomplete penetrance as well as variable expressivity. Individuals homozygous for the NOD2 mutation could be free from developing Crohn's disease or develop Crohn's disease with a range of disease severities and phenotypes.[231] The mechanism behind variable expression of genotype is still poorly understood. However, the complex interplay between the genotype and environment is likely to play a major role and studies examining the interaction between gene and environment in genetically modified mice have started to emerge.[232] Further research into mechanisms behind variable expressivity of genotype would help us to understand the pathogenesis of many complex human diseases and potentially lead to disease prevention, as well as improvement in management.

The findings from flow cytometry and qPCR analysis of the colonic tissue of the WT and *Adamdec1*$^{-/-}$ mice have generated valuable insight into the potential role of ADAMDEC1 during DSS-medicated mucosal injury. Recruitment and proliferation of CD4+ helper T cells, CD8 cytotoxic T cells, dendritic cells and neutrophils as well as the polarisation of naïve T cells to RORγt+ FOXP3+ T cells are unlikely to be involved in the aberrant immune response seen in the absence of ADAMDEC1.

First of all, flow cytometry analysis of the colonic tissues taken from the WT and *Adamdec1*$^{-/-}$ mice during DSS-induced colitis revealed that there was a higher abundance of CD45+ CD3- cells in the tissue of the *Adamdec1*$^{-/-}$ mice following the DSS challenge. This was consistent with the previous histological findings of the colonic tissues of *Adamdec1*$^{-/-}$ mice exhibiting more severe mucosal inflammation and a greater infiltration of immune cells.[26,56] The abundance of CD4+ and CD8+ cells could not be accurately identified by FACS upon induction of inflammation due to their degradation by dispase during the tissue preparation. The issues associated with dispase and CD4 and CD8 surface expression, however, revealed a potential inhibitory effect of ADAMDEC1, directly or indirectly, on dispase. Dispase is a neutral zinc-metalloendopeptidase that is produced by *Bacillus Polymyxa* and is a powerful fibronectinase and type IV collagenase.[233] It is also clearly able to target other proteins and is especially effective at cleaving both CD4

and CD8, co-receptors that play a vital role in the activation of T cells and cytotoxic T cells.[190,191] It is possible that ADAMDEC1's natural function in the intestine is to, directly or indirectly, suppress dispase-like molecules released by invading pathogens that might have degenerative effects on the intestinal tissue. Thus, ADAMDEC1 may play a tissue protective role in the event of epithelial damage, bacterial ingression and subsequent mucosal inflammation. Previously, it was demonstrated that *Adamdec1*$^{-/-}$ mice were highly susceptible to *Citrobacter rodentium* infection resulting in very high mortality and evidence of systemic bacterial infection (bacteraemia) in three-quarters of the infected mice.[26] WT C57BL/6 mice demonstrate considerable resistance to *Citrobacter rodentium* infection. Therefore, the increase in sensitivity of *Adamdec1*$^{-/-}$ mice may result from an inability to suppress the invasive properties of the bacteria. It is still unclear but, *Citrobacter rodentium* may possess a dispase-like neutral zinc-metalloendopeptidase which facilitates its invasive behaviour and if this is inhibited by ADAMDEC1, it would provide an explanation for the increased sensitivity of *Adamdec1*$^{-/-}$ mice. Alternatively, ADAMDEC1 could be playing a role in the formation and functional stability of SMAC. SMAC plays a vital role in the activation of CD4+ T cells and as well as CD8+ cytotoxic T cells thus ADAMDEC1 could be involved in host's ability to activate these cells during inflammation and bacterial infection.

The difference in Th17 and Treg polarisation was also observed in the WT and *Adamdec1*$^{-/-}$ mice on day 7 of the DSS challenge. Th17 polarisation was impaired in the *Adamdec1*$^{-/-}$ mice at an early stage of the acute inflammation which was associated with the continuation and prolongation of the Th17 polarisation induced by the DSS challenge in these knockout mice. A previous study using DSS-colitis model and *Adamdec1*$^{-/-}$ mice found a significantly increased level of IL-17, the main cytokine released by Th17, in the tissue of *Adamdec1*$^{-/-}$ mice 8 days after the cessation of the DSS challenge. In this project, FACS analysis was performed using colonic tissues collected at two timepoints (day 7 and day 9) during the DSS-induced inflammation. This demonstrated a dynamic change in the proportion of various cells including Th17 cells. The proportion of Th17 cells was lower in the *Adamdec1*$^{-/-}$ mice on day 7 but higher on day 9 in comparison to the WT. This raised the possibility that the previously reported higher level for IL-17 in the knockout mice compared to the WT mice might also have been a transient

observation. Therefore, its implication in the causative mechanism for the aberrant immune response in the absence of ADAMDEC1 must be considered taking this dynamic time-dependent nature of changes in cell population into account.

IL-17 stimulates recruitment and activation of neutrophils as well as secretion of pro-inflammatory cytokines such as IL-1β, IL-6, TNF-α, CXCL1 and CCL2 by cells including macrophages, fibroblasts, endothelial cells and epithelial cells.[194] However, an exaggerated DSS-induced mucosal inflammation has been demonstrated in the absence of IL-17 signalling by several studies utilising either IL-17 knockout mice or IL-17A neutralising antibodies.[234,235] The enhanced degree of inflammation was typically associated with more profound epithelial barrier dysfunction.[236] Thus, IL-17 seems to have a protective role in DSS-medicated colitis. Additionally, Th17 cells mediates pro-inflammatory attributes by secretion of IL-21, which promotes Th1 cell response and secretions of IL-8 and TNF-α. However, Th17 cells also exhibit anti-inflammatory attributes by secretion of cytokines such as IL-10 and IL-22. IL-22 is known to promote proliferation and cell survival of epithelial cells including intestinal stem cells.[237] Several studies have demonstrated a protective role of IL-22 in DSS-mediated colitis through promoting epithelial proliferation as well as enhancing the host's epithelial barrier function by stimulation of mucus and antimicrobial substance, defensin, secretions from epithelial cells.[238–240] Based on these, the greater inflammation seen in the *Adamdec1*$^{-/-}$ mice might be related to the failure to elicit adequate Th17 polarisation at the early stage of acute inflammation, leading to failure to execute a robust enough pro-inflammatory response against invading pathogens, and epithelial cell dysfunction mediated by lack of appropriate IL-17 and IL-22 secretion. However, since CD4 was digested by dispase, an accurate identification of the $CD4^+$ cells was not possible. This could have affected the quantification of the downstream cell populations dependant on CD4 gating thus the results regarding these cell populations would need to be validated in future without use of dispase during the tissue preparation.

FACS analysis of the mice bowel using the myeloid panel of antibodies revealed a higher ratio of SSC^{low} $Ly6C^{high}$ monocytes to $SSC^{mid/high}$ $Ly6C^{low/mid}$ macrophages in the *Adamdec1*$^{-/-}$ mice in comparison to the WT on day 9. An expansion of the $Ly6C^{high}$ monocytes and thus an increase in monocytes to macrophage ratio is a

known characteristic of DSS-induced colitis which is believe to be dependent on CCL2-CCR2 axis.[200,201,205] These high-Ly6C expressing monocytes possess pro-inflammatory characteristics and express high levels of IL-1β and TNF-α.[200] Ablation of these high-Ly6C expressing monocytes has been shown to ameliorate DSS-induced colitis suggesting their inflammation-inducing property in the DSS-mediated colitis.[201,202] Additionally to the increased ratio of monocytes to macrophages, the expression of CX3CR1 in these Ly6C^{high} monocytes was significantly reduced during inflammation in the *Adamdec1*$^{-/-}$ mice. Low expression of CX3CR1 is associated with pro-inflammatory and high expression is associated with anti-inflammatory properties. These findings indicated that there were a higher proportion of monocytes with a greater pro-inflammatory phenotype in the *Adamdec1*$^{-/-}$ mice in comparison to the WT mice on day 9 of the DSS challenge which may have attributed to the greater inflammation seen in these knockout mice.

How ADAMDEC1 may affect the monocytes' proportion within the inflamed colonic tissue cannot be inferred from the results of this chapter. In a healthy intestine, monocytes that express a high level of CX3CR1 dominate, where recruitment of monocytes to the intestine is believed to occur under CX3CL1-CXC3CR1 axis. During inflammation, there is an increase in monocytes with low expression of CX3CR1 in the intestine. Earlier studies have supported the hypothesis that these two monocytes with low and high expressions of CX3CR1 being two distinct populations of monocytes entering the intestine that would give rise to pro- and anti-inflammatory macrophages respectively.[203–205] In this hypothesis, an upregulation of CCR2 on monocytes during inflammation leads to a preferential recruitment of the low-CX3CR1 high-Ly6C expressing monocytes via CCR2-CCL2 axis, which leads to an expansion of the CX3CR1^{low} Ly6C^{high} monocytes in the inflamed intestine. However, the current consensus built on more recent studies suggests that a homogenous population of pro-inflammatory Ly6C^{high} CX3CR1^{low} monocytes enter the intestine, irrespective of the tissues' inflammatory state. In the presence of inflammation, their normal differentiation pathway, during which an upregulation of CX3CR1 occurs, to Ly6C^{low} CX3CR1^{high} resident macrophages with characteristic anti-inflammatory phenotype such as hyperresponsiveness to TLR stimulation and secretion of IL-10, is disrupted.[180,241,242] This disruption of the normal monocyte to macrophage differentiation in the inflammatory microenvironment, in turn, leads to an accumulation of Ly6C^{high} CX3CR1^{low} pro-

inflammatory monocytes during colitis.[242,243] One explanation for the higher monocyte to macrophage ratio seen in the *Adamdec1*$^{-/-}$ mice in comparison to the WT mice on day 9 may be secondary to an increase in monocyte recruitment. However, the increase in the monocytes to macrophage ratio observed in the knockout mice was not accompanied by an expansion of the overall F4/80+ monocytes/macrophage population which was expected if the monocyte recruitment was greater in the *Adamdec1*$^{-/-}$ mice and the rate of monocytes to macrophage differentiation was the same in the knockout and WT mice. Another alternative explanation might be that there was an increase in the monocyte recruitment in the knockout mice accompanied by a decrease in the macrophage survival in the knockout mice. Another possible explanation might be, in accordance with the hypothesis of disrupted monocytes to macrophage differentiation in the presence of inflammation, there was a more pronounced disruption of the monocyte to macrophage differentiation in the knockout mice leading to an accumulation of the pro-inflammatory monocytes. Which of these mechanisms led to the increased monocytes to macrophage ratio in the absence of ADAMDEC1 or how ADAMDEC1 may be involved in these mechanisms cannot be inferred from the result of this chapter. However, the findings suggest a possibility of ADAMDEC1's involvement in monocyte to macrophage differentiation during inflammation.

With regards to the functional significance of the lower level of CX3CR1 expression seen in the monocytes of the *Adamdec1*$^{-/-}$ mice, the potential involvement of CX3CR1 in modulating mucosal inflammation has been shown by several studies. These studies utilising CX3CR1 knockout mice demonstrated more severe form of mucosal inflammation during experimental colitis in the absence of CX3CR1 signalling.[244,245] In one of these studies, involvement of heme oxygenase-1 (HMOX-1) was suggested to be the pathway in which CX3CR1 regulated inflammation.[245] HMOX-1 is an enzyme that catalyses oxidative degradation of heme group and appears to have anti-inflammatory properties.[246,247] An increase in HMOX-1 expression ameliorated DSS-induced colitis which was associated with a reduction in apoptosis of epithelial cells, an increase in Treg cells number, and a decrease in Th17 cell number.[246,247] By using CX3CR1 knockout mice, the induction of HMOX-1 was shown to be dependent on CX3CR1-CX3CL1 signalling within F4/80+ monocytes/macrophages.[245] Furthermore, this study also showed

CX3CR1 knockout mice had an increased susceptibility to inflammation-related tumour development, thereby potentially providing a link between the known downregulation of ADAMDEC1 in tissues of CRC, CX3CR1 and tumour development.[245] Furthermore, the WT and CX3CR1 knockout mice were shown to possess significantly different microbiomes and co-hosing of these mice altered the microbiome of the knockout mice. This was associated with a reduction in the degree of mucosal inflammation and tumour development, thereby revealing an interaction between genotype, microbiome, environment, mucosal inflammation and tumorigenesis. Other findings from these studies using CX3CR1 knockout mice include reduced phagocytic ability of F4/80+ phagocytes, lack of expansion of Treg cell population, and a greater translocation of commensal bacterial which could be attributing mechanisms for the exaggerated mucosal inflammation in the deficiency of CX3CR1.[244,245,248] Additionally, CX3CR1 expressed on monocytes and macrophages was shown to be essential for vascular smooth muscle cell differentiation and revascularisation following mucosal injury. This provides a connection between the CX3CR1 deficiency and the reported disruption of vasculature following ablation of *Adamdec1*-expressing self-renewing macrophages within murine intestine.[50,249,250]

In addition to SSC^{low} $Ly6C^{high}$ monocytes, the expressions of CX3CR1 on other cells were also found to be reduced in the *Adamdec1*$^{-/-}$ mice. The expression of CX3CR1 within the intestine is reported to be predominantly on monocytes and macrophages. However, other cells including dendritic cells, endothelial cells, B-cells and CD4+ T cells are known to express CX3CR1 to varying degrees.[251] The formation of transepithelial dendrites of dendritic cells was shown to be dependent on CX3CR1-CX3CR1 signalling, and CX3CR1 knockout mice demonstrated inferior antigen sampling function thus impaired clearance of enteroinvasive pathogens by dendritic cells.[252] Additionally, CX3CR1 signalling has been shown to induce EGF expression in endothelial cells and promote vascularisation.[253] All of these previous findings supports potential detrimental effect on the immune system and inflammation in deficiency of CX3CR1.

How ADAMDEC1 may impact the cell surface expression of CX3CR1 cannot be elucidated from the results of this chapter. The reduced expression of CX3CR1 in the monocytes, taking into account the physiological change in CX3CR1 expression during monocyte to macrophage differentiation within the intestine,

suggests ADAMDEC1 might be involved in monocytes to macrophage differentiation. However, the globally low expression of CX3CR1 on other subtypes of CD3- cells suggests ADAMDEC1 might be involved in the regulation of surface expression of CX3CR1 on multiple types of cells. To date, the regulation of CX3CR1 expression has not been researched in great detail, however, internalisation of cell surface CX3CR1 by specific proteins in the surrounding environment has been reported.[254,255] It is possible that ADAMDEC1 might be involved in regulating yet unknown substances that might promote the internalisation of CX3CR1 on cells. However, the possibility of lower expression of CX3CR1 as a result of a greater degree of inflammation in the absence of ADAMDEC1 cannot be excluded. An auto-upregulation of CX3CR1 by CX3CL1-CX3CR1 signalling has been reported. CX3CL1 is known to be expressed by epithelial cells.[256,257] Thus, the under-expression of cell surface CX3CR1 in the *Adamdec1*$^{-/-}$ mice could be attributed by the more destructive state of the epithelia rather than the direct effect of the absence of ADAMDEC1.

Lastly, a smaller proportion of SSC$^{mid/high}$ Ly6C$^{low/mid}$ macrophages was detected in the *Adamdec1*$^{-/-}$ mice in comparison to the WT mice on day 9 of the DSS-induced colitis. Additionally, the surface expression of Ly6C was lower in these macrophages in the knockout mice than in the WT mice during the inflammation. Ly6C is a known marker for intestinal inflammatory macrophages. These macrophages have been shown to possess pro-inflammatory features such as increased secretion of TNF-α.[203,205] However, the studies addressing the precise functional role of Ly6C in macrophages are extremely sparse. One study has shown no effect of Ly6C on the severity of DSS-induced colitis, in terms of weight loss and survival rate using Ly6C knockout mice.[258] Nevertheless, the findings from this chapter suggest that a smaller proportion of macrophages with potentially more anti-inflammatory phenotype was present in the colonic tissues of the *Adamdec1*$^{-/-}$ mice on day 9 compared to the WT mice. Therefore, the findings once again highlighted the potential involvement of ADAMDEC1 in monocyte to macrophage differentiation and its influence on their phenotypes.

The analysis of the change in gene expression during DSS-induced colitis by qPCR generated some intriguing findings. By separating the *Adamdec1*$^{-/-}$ mice into Cage 1 and Cage 2, given their difference in response to inflammation (Figure 6.35), three categories of genes were identified based on their patterns of change in expression (Table 6.7).

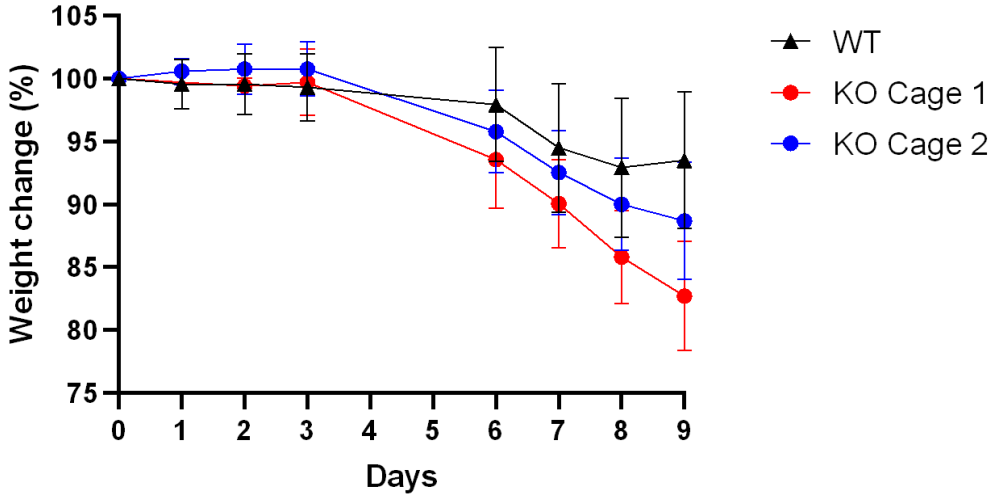

Figure 6.35 Weight change in the WT mice (Cage 1 and 2 combined) and *Adamdec1*$^{-/-}$ mice in Cage 1 and Cage 2 during DSS challenge.
KO: *Adamdec1*$^{-/-}$, WT: Wild type

<table>
<tr><th>Same trend observed
WT vs KO</th><th>Different trend observed
WT and Cage 2 KO vs Cage 1 KO</th><th>Different trend observed WT vs KO</th></tr>
<tr><td rowspan="11">Cd4 ↑
Cd8 ↑
Il-1β ↑
Cxcl1 ↑</td><td>Tnf-α ↑ in WT and Cage 2 KO,</td><td rowspan="11">Lgr5 ↓ in KO</td></tr>
<tr><td>no change in Cage 1 KO</td></tr>
<tr><td>Ccl2 ↑ in WT and Cage 2,</td></tr>
<tr><td>no change in Cage 1 KO</td></tr>
<tr><td>Ccr2 ↑ in WT and Cage 2,</td></tr>
<tr><td>no change in Cage 1 KO</td></tr>
<tr><td>Ki67 ↑ in WT and Cage 2,</td></tr>
<tr><td>↓ in Cage 1 KO</td></tr>
<tr><td>Cdx2 no change in WT and Cage 2,
↓ in Cage 1 KO</td></tr>
<tr><td>Fgf2 no change in WT and Cage 2,
↑ in Cage 1 KO,</td></tr>
</table>

Table 6.8 Summary of the change in gene expressions during the DSS-induced inflammation with respect to the genotype and cage difference.
KO: *Adamdec1*$^{-/-}$, WT: Wild type

The expressions of *Cd4*, *Cd8*, *Cxcl1* and *Il-1β* were all upregulated in the mice by the induction of inflammation irrespective of their genotype or the cage-dependant severity of inflammation observed in the *Adamdec1*$^{-/-}$ mice. However, the degree of increase in the expression of *Cxcl1* correlated closely with the degree of weight loss exhibited by the mice in this project. Thus, the difference on the expression of *Cxcl1* was likely to be due to the difference in the degree of the inflammation suggesting *Cxcl1* to be a suitable surrogate marker for the degree of inflammation in the DSS-colitis model using the *Adamdec1*$^{-/-}$ mice. Nevertheless, the potential mechanistic involvement of the higher levels of *Cxcl1* expression in driving a greater inflammation in the knockout mice in comparison to the WT mice cannot be excluded. The rest of the genes (*Cd4*, *Cd8* and *Il-1β*) are unlikely to be playing major roles in the aberrant immune response exhibited by the absence of ADAMDEC1. The changes in expression of *Tnf-α*, *Ccl2*, *Ccr2*, *Ki67*, *Cdx2* and *Fgf2* before and after induction of inflammation were the same for the WT and knockout mice in Cage 2 but differed in the knockout mice in Cage 1. These are the genes whose expressions are likely to be affected as a result of the absence of

ADAMDEC1 in combination with some environmental factors, or alternatively simply as a result of mucosal inflammation. The absence of upregulations of *Tnf-α*, *Ccl2* and *Ccr2* in the knockout mice in Cage 1 was observed despite the greatest weight loss exhibited by these mice. Upregulations of these 3 genes, especially, *Tnf-α*, are often used as a marker of exaggerated inflammation. However, the upregulations of these three genes did not correlate with an increase in the degree of inflammation in this project. This indicates that upregulations of these 3 genes are a poor surrogate marker for the increase in inflammation in DSS-mediated colitis model using *Adamdec1*$^{-/-}$ mice. Surprisingly, the upregulations of *Tnf-α*, *Ccl2* and *Ccr2*, in fact, correlated with the amelioration of weight loss and mucosal inflammation in this project. Although TNF-α is widely considered as a pro-inflammatory cytokine, its protective role in inflammation is recognised. An ablation of TNF-signalling, by means of TNF knockout mice or TNF neutralising antibodies, in several studies has demonstrated worsening of DSS-induced colitis.[259–261] The finding from this chapter supports the protective role of TNF-α during inflammation.

The downregulations of *Ki67* and *Cdx2*, and upregulation of *Fgf2* in Cage 1 knockout mice might simply reflect the greater degree of inflammation and epithelial cell loss, and delayed initiation of the recovery phase in Cage 1 knockout mice rather than the direct effect of *Adamdec1*'s absence with or without the influence of environmental factors. One of the protective effects of TNF-α during experimental colitis was shown to be mediated via enhancement of epithelial cell proliferation, thus epithelial barrier repair. This mechanism could be one of many other reasons for the reduced level of *Ki67* and *Cdx2* in the *Adamdec1*$^{-/-}$ mice in Cage 1 and the highest severity of inflammation seen in these mice.

Lgr5 was the only gene where downregulation was seen upon induction of inflammation in the *Adamdec1*$^{-/-}$ mice irrespective of their cage difference that was not observed in the WT mice. This suggested that the *Lgr5* expression was reduced in the knockout mouse from the naive state to day 9 in association with the absence of ADAMDEC1 and exposure to DSS, which was not affected by the environmental factors and was not directly proportional to the degree of weight loss. This potentially indicated that intestinal stem cells were more vulnerable to DSS-induced epithelial injury in the absence of ADAMDEC1. The role of ADAMDEC1 in intestinal stem cell survival was not via regulation of *Fgf2* expression as this was not reduced by the absence of ADAMDEC1. The potential effect of ADAMDEC1 in

the regulation of intestinal stem cells has been highlighted by a study where *Adamdec1*-expressing fibroblast in mice was found to be located close to the edges of crypts.[56] These cells were enriched in genes involved in the regulation of Wnt, which plays a vital role in stem cell proliferation, differentiation and homeostasis.[56] Although it is possible that ADAMDEC1 might affect the intestinal stem cell susceptibility to DSS-induced epithelial injury, the reduction in the *Lgr5* expression as a result of the greater intestinal stem cell destruction caused by the greater inflammation in the absence of ADAMDEC1 cannot be excluded.

Overall, the qPCR and FACS analysis of the colonic tissues of the WT and *Adamdec1*$^{-/-}$ mice have highlighted the areas of host's defensive mechanism against DSS-induced mucosal injury that are potentially affected by ADAMDEC1. These are areas of immune response mechanisms involving potential activation of helper T cells and cytotoxic T cells, Th17 and Treg cell polarisation, monocyte to macrophage differentiation and phenotypes of monocytes and macrophages. Additionally, the potential inhibitory effect of ADAMDEC1 on dispase, thus possibly on dispase-like molecules within the gastrointestinal environment. Finally, a potential effect of ADAMDEC1 on intestinal stem cell survival and epithelial repair during DSS-mediated mucosal injury was identified.

Whether these observations were due to the lack of ADAMDEC1 that led to the exacerbation of inflammation or whether these observations were the result of the exacerbated inflammation that occurred in the absence of ADAMDEC1 cannot be inferred. Further experiments focusing on these areas highlighted by the result of this chapter are clearly required to evaluate the role of ADAMDEC1 in mucosal inflammation.

Chapter 7

Investigation of the effect of ADAMDEC1 on the murine intestinal microbiome

7.1 Background and aims

Human intestine contains more than 10^{14} microorganism which play a vital role in host's physiology and function. The beneficial properties provided by the gut microbiota to host include digestion, the absorption of nutrients, epithelial defence barrier and the regulation of immune, endocrine and neurological systems.[262,263] The composition of microbiota is unique to an individual, but it is not fixed and can alter in response to a number of factors such as changes in the environment, diet, medication, and health. These factors are reported to account for 22 - 36% of the variability of the microbiome.[264] In contrast, the host genetics are reported to account for only 1.9 - 8.1% of the inter-person microbiota variability.[264]

Dysbiosis, the disturbance and imbalance of a harmonious composition of the microbiota, has been reported in numerous human diseases including IBD.[265] In general, a common dysbiosis theme observed in human diseases is a reduction in the diversity of the microbiota compared to healthy status. In addition to the reduced diversity of the gut microbiota, in IBD, multiple studies have reported reductions in the abundance of *Firmicutes*, *Bacteroidetes*, *Lachnospiraceae*, *Bifidobacteria* and *Lactobacillus*, and increases in the abundance of *Enterobacteria* and *Proteobacteria*.[266–273] Additionally, a reduction in the abundance of *Faecalibacterium prausnitzii* specific to Crohn's disease has been reported by several studies.[271,274,275] However, a considerable amount of discrepancies exist between these studies regarding the specifics of the differentially abundant microorganisms in IBD-associated dysbiosis. As for mycobiota, the fungal component of the microbiota, although relatively limited in number, several studies have also reported mycobiota dysbiosis in association with IBD. Similar to the bacterial microbiota, a reduction in the mycobiota diversity was found in patients with IBD, as well as an increased abundance of *Basidiomycota* and a reduced abundance of *Ascomycota* in association with IBD.[276,277] Importantly these association studies, however, do not provide an answer to whether the dysbiosis is a cause or an effect of the disease.

The evidence to support the notion that the microbiota can directly influence the host immune system and thus play a causative role in the pathogenesis of intestinal mucosal inflammation comes from mouse models. Germ-free mice exhibit aberrant local and systemic innate and adaptive immune systems, as well as, impaired intestinal epithelial barrier function.[278] Additionally, an amelioration in the degree of DSS-induced colitis has been demonstrated by oral administration of probiotics, either individually by *Lactobacillus brevis* or a combination of *Lactobacillus reuteri*, *Bacillus coagulans*, *Bifidobacterium longum*, and *Clostridium butyricum*.[279,280] Furthermore, more specifically, a targeted depletion of *Enterobacteriaceae*, an expansion of whose abundance was observed in new-onset Crohn's disease, as well as an oral administration of *Lachnospiraceae* ameliorated DSS-induced colitis.[281,282] The loss of *Faecalibacterium prausnitzii* reported in Crohn's disease by several studies has also been shown to have a potential mechanistic role in the pathogenesis of Crohn's disease. A supplementation of this bacteria ameliorated chemically-induced colitis in mice.[283] Subsequently, furthermore, a peptide was identified in the culture supernatant of *Faecalibacterium prausnitzii*, which inhibited the NF-κB signalling pathway in the intestinal epithelial cells in vitro and ameliorated experimental colitis in mouse.[283,284] Additionally, studies have also identified bacterial species, that are not known to possess virulence, which influence susceptibility to DSS-induced colitis.[285,286] One of these studies have recently identified *Duncaniella muricolitica* and *Alistipes Okayasuensis* to have an exacerbating effect, and *Anaerostipes faecis* and *Sangeribacter muris* to have an ameliorating effect on the severity of DSS-induced colitis in WT mice.[286] These findings indicate the ability of the microbiota to influence host's immune response during mucosal inflammation and support the notion that dysbiosis can contribute to mucosal inflammation and potentially the development and severity of IBD.

To explore whether the disease-associated mutation leading to the development of mucosal inflammation in IBD is mediated by dysbiosis, several studies have examined the microbiome in relation to NOD2 genotype status in human. The findings from some studies have found no impact of *NOD2* variants on the gut microbiome, which is anticipated given that the host genetics play a minor role in determining gut microbiome.[287] However, other studies have identified distinct NOD2 genotype-dependent microbiomes including a study which found increases in abundance of *Enterobacteriaceae* and *Proteobacteria* in association with mutant

variants of *NOD2*.[288,289] Furthermore, using *Nod2* knockout mice, which exhibit increased susceptibility to experimental colitis without the development of spontaneous colitis, several studies have reported a difference between the gut microbiota of WT and NOD2 deficient mice. An increase in abundance of *Bacteroidetes* and a decrease in abundance of *Firmicutes* were observed in the NOD2 deficient mice.[290–293] Some of these studies have additionally shown mechanistic role of the NOD2-associated dysbiosis in the exaggerated mucosal inflammation seen in the NOD2 deficient mice.[290,291] However, other studies, importantly in which WT and NOD2 deficient mice were cohoused, failed to identify any significant differences in the microbiome composition of WT and NOD2 deficient mice. In these studies, factors other than genotype such as cage and littermates determined the microbiome composition.[294,295] Thus, overall, whether the increased susceptibility to mucosal inflammation on a background of a particular genotype is mediated through the genotype-driven alteration in microbiota is still to be elucidated.

To date, the potential effect of ADAMDEC1 on the host's microbiota has never been explored. There is a possibility that the effect of ADAMDEC1 on immune response during mucosal inflammation might be mediated through its ability to alter the gut microbiota either in the naïve state or during an inflammatory episode. In this chapter, two experiments were conducted to explore the potential effect of ADAMDEC1 on mouse gut bacterial and fungal microbiota. Experiment 1 examined the microbiome of young WT, heterozygous and *Adamdec1*$^{-/-}$ mice (4-5 weeks age) where littermates from heterozygous breeding pairs were cohoused in mixed-sex groups to determine the presence of genotype-specific differences in their microbiome. Experiment 2, first of all, examined the microbiome of older female WT and *Adamdec1*$^{-/-}$ mice where littermates of the same genotype have been cohoused for more than 10 weeks to validate some of the findings from Experiment 1. The effect of pooling of cage to cohouse the WT and *Adamdec1*$^{-/-}$ mice as well as the effect of DSS challenge on the microbiome of the WT and *Adamdec1*$^{-/-}$ mice were determined. Other factors that may potentially influence the microbiome of mice were also explored. Finally, a potential difference in the microbiome of the *Adamdec1*$^{-/-}$ mice in cage 1 and Cage 2 which exhibited significant cage-dependant variability in the degree of DSS-induced inflammation (Chapter 6) was examined.

The microbiome analysis was conducted by gene amplicon sequencing method by targeting 16S rRNA and ITS genes. The 16s rRNA site of prokaryotes, and internal transcribed spacer (ITS) 1 and ITS2 sites of fungi within their nuclear DNAs are highly conserved.[296] However, these sites contain regions that are variable and specific to individual microbial species, thereby allowing detection of these individual species.[296]

The main aims for Chapter 7 were:

- To establish whether microbiome differs between the WT and *Adamdec1*$^{-/-}$ mice
- To establish the effect of pooling of cage on the microbiome of WT and *Adamdec1*$^{-/-}$ mice
- To establish the effect of DSS challenge on the microbiome of WT and *Adamdec1*$^{-/-}$ mice
- To explore other factors that might influence the microbiome of WT and *Adamdec1*$^{-/-}$ mice
- To determine any difference in the microbiome of the *Adamdec1*$^{-/-}$ mice in Cage 1 and Cage 2 which might explain the cage-dependant significant variability in the degree of DSS-induced inflammation (Chapter 6)

7.2 Material and Method

7.2.1 Experimental set-up

7.2.1.1 Experiment 1

Faecal samples were collected from 16 mice, of 4 - 5 weeks of age, from 4 different cages. In each cage, the mice cohoused were littermates from heterozygous breeding pairs and differed in sex and genotype but had remained in the same individual cages since birth with their parents (Figure 7.1). The faecal samples were collected from each mouse at the time of weaning from their parents.

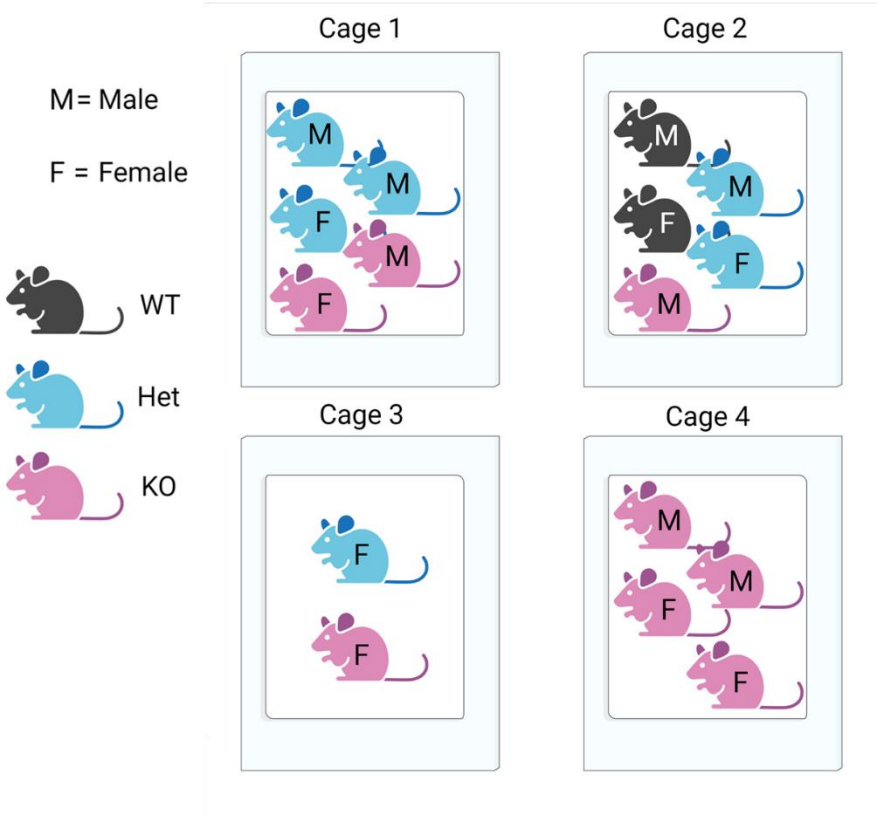

Figure 7.1 Scheme demonstrating the number, sex and genotype of the mice in 4 cages used in Experiment 1. Mice in each cage were littermates and remained in the same cage since birth. All mice were between age 4-5 weeks at the time of faecal sample collection.
Het: Heterozygous, KO: *Adamdec1*$^{-/-}$, WT: Wild type

7.2.1.2 Experiment 2

In Experiment 2, 20 female mice in total (8 WT and 12 *Adamdec1*$^{-/-}$ mice) were used. These mice were older than the mice used in Experiment 1 (mean age=16.0 weeks, SD=3.45) and they had been housed in 6 different cages for more than 10 weeks. They all originated from a common original heterozygous breeding pair and were siblings from one pair of WT and one pair of *Adamdec1*$^{-/-}$ breeders, with the exception of one WT mouse which was purchased (Figure 7.2 Cage D). The mice in each cage were littermates and were the same in their genotype, except for the WT mouse in Cage D. The mice in Cage A, B and C (3 WT and 5 *Adamdec1*$^{-/-}$ mice, n=8 in total) and Cage D, E and F (5 WT and 7 *Adamdec1*$^{-/-}$ mice, n=12 in total) were pooled into Cage 1 and Cage 2 respectively to make 2 cages of mice mixed in genotype (Figure 7.2). The mice were then housed in these 2 cages for 8 weeks after which they were challenged with 2% DSS in the drinking water to induce colitis for 7 days (Chapter 6.2). After 7 days, the DSS was switched to sterile drinking water for 2 days and the mice were culled. Faecal samples from the mice were collected at 3 timepoints: pre-pool, pre-DSS, post-DSS. The pre-pool samples were used verify some of the findings from Experiment 1. The effect of pooling of mice, to cohouse the WT and *Adamdec1*$^{-/-}$ mice, as well as the effect of DSS challenge on the gut microbiome of the WT and *Adamdec1*$^{-/-}$ mice were also examined using the pre-DSS and post-DSS samples. These mice provided the colonic tissue for the flow cytometry and qPCR experiments conducted in Chapter 6.

Due to the colitis and subsequent diarrhoea caused by the DSS challenge, the lumen of the colon was empty in 3 mice (2 *Adamdec1*$^{-/-}$ mice in Cage 1 and 1 *Adamdec1*$^{-/-}$ mouse in Cage 2) at the time of harvesting the post-DSS samples. Thus post-DSS sample could not be collected from these 3 mice (Figure 7.2). Furthermore, 1 pre-pool DNA sample, from *Adamdec1*$^{-/-}$ mouse in Cage D, and 2 post-DSS DNA samples, from 2 *Adamdec1*$^{-/-}$ mice in Cage 1, resulted in low reads from 16S rRNA gene and ITS gene sequencing, thus these samples were excluded from analysis (Figure 7.2).

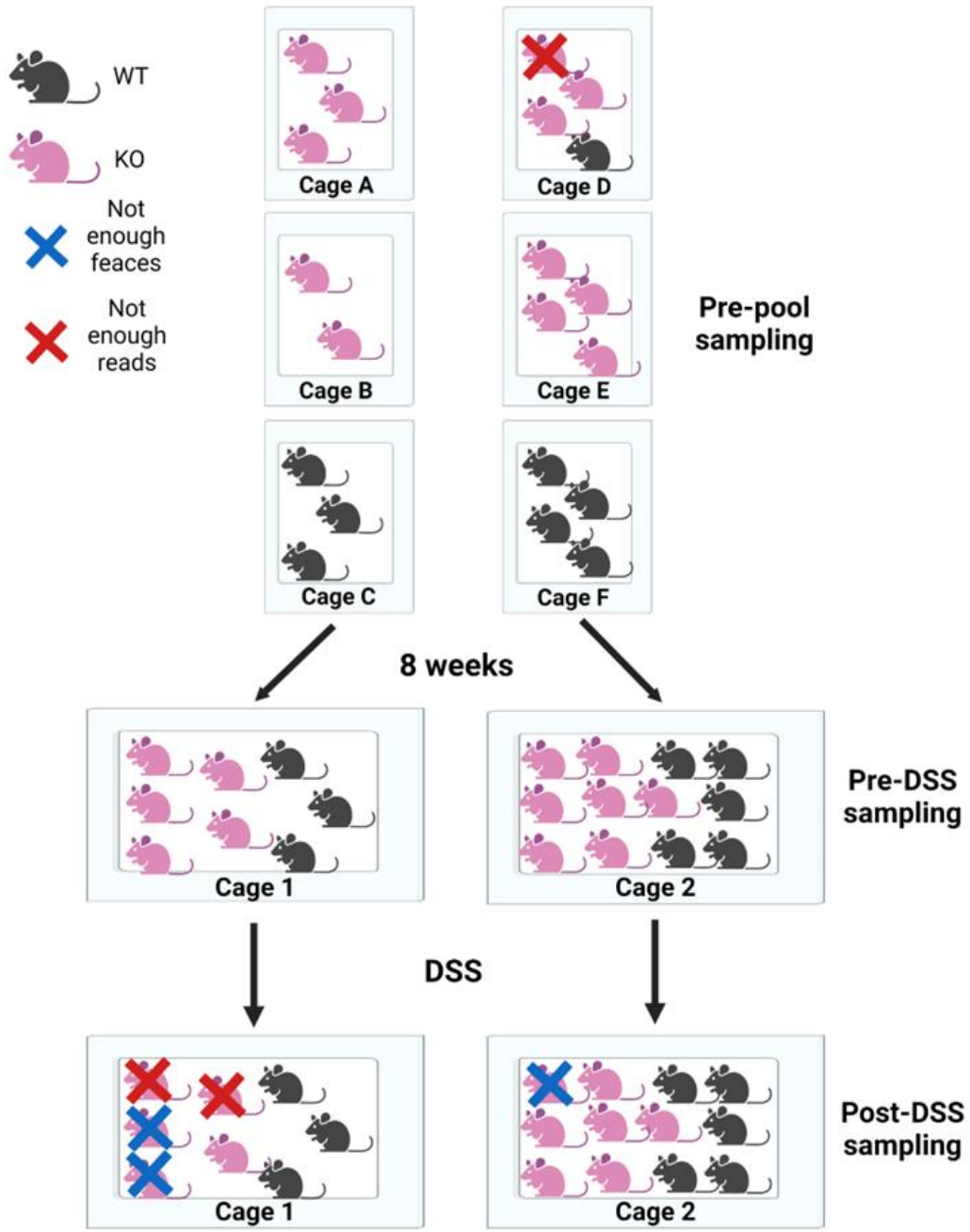

Figure 7.2 Scheme demonstrating the experimental set up of Experiment 2. Twenty mice in total which were originally housed in 6 different cages based on their genotype, except for Cage D, were used. The mice in Cage A, B and C were pooled into Cage 1, and the mice in Cage D, E and F were pooled into Cage 2. The WT and *Adamdec1*$^{-/-}$ mice were then cohoused in these 2 cages for 8 weeks prior to being challenged with DSS. Faecal samples were collected at pre-pool, pre-DSS and post-DSS timepoints. The mice marked with a blue cross did not produce enough faeces to extract microbial DNA from. The microbial DNA samples from the mice marked with red cross did not provide enough reads from the microbiome sequencing.
KO: *Adamdec1*$^{-/-}$, WT: Wild type

7.2.2 Faecal sample collection

Faecal samples harvested in Experiment 1 and harvested at pre-pool and pre-DSS timepoints in Experiment 2 were collected from live mice. Each mouse was placed in a glass beaker and 3 - 4 pellets of faeces per mouse were collected into 1.5 ml Eppendorf tubes and stored at -80°C. The faecal samples collected at the post-DSS time point in Experiment 2 were harvested after mice were sacrificed and their colons were dissected. The faecal materials were expelled out of the colonic lumen by application of gentle pressure along the intact colons, and collected into 1.5 ml Eppendorf tubes and stored at -80°C.

7.2.3 Microbial DNA extraction from faecal samples

Microbial DNA from the faecal samples was extracted using QIAamp PowerFecal Pro DNA Kit (Qiagen) following the manufacturer's protocol. All the reagents used were supplied in the kit. PowerBead Pro Tubes were centrifuged briefly to settle the beads at the bottom of the tubes. Faecal samples from each mouse, collected from each timepoint, and 800 µl of Solution CD1 were added to each tube to lyse the faeces. Solution CD1 disperses faecal particles, dissolves inhibitors and protects nucleic acids from degradation. The samples were homogenised and cells were lysed using TissueLyser II (Qiagen) set at 25 Hz for 10 minutes. The tubes were centrifuged at 15000 g for 1 minute, after which supernatants were carefully transferred into clean 2 ml Eppendorf tubes. 200 µl of Solution CD2 were added to each tube and vortexed for 5 seconds. Solution CD2 precipitates non-DNA organics and inorganic compounds such as polysaccharides, proteins and cell debris. The tubes were centrifuged at 15000 g for 1 minute and up to 700 µl of supernatants from each tube were carefully transferred to clean 2 ml Eppendorf tubes. 600 µl of Solution CD3, which adjusts the DNA salt concentration to optimise the subsequent binding of DNA to the column membrane, were added to each tube and the tubes were vortexed for 5 seconds. 650 µl of each lysate were loaded onto MB Spin Column and centrifuged at 15000 g for 1 minute, allowing the DNA to bound to the column membrane. The follow-throughs were discarded and the process was repeated using the remaining 650 µl of each sample. The MB Spin Columns were carefully transferred into 2 ml Eppendorf tubes. 500 µl of Solution EA were added to each column, to remove any proteins and other non-aqueous contaminants from the column membrane, and the tubes were centrifuged at

15000 g for 1 minute. The follow-throughs were discarded and the MB Spin Columns were placed back into the same 2 ml Eppendorf tubes. 500 µl of Solution C5, an ethanol-based wash solution, were added to each MB Spin Columns and the tubes were centrifuged at 15000 g for 1 minute to remove residual salts. The columns were carefully placed into clean 2 ml Eppendorf tubes and centrifuged at 16000 g for 2 minutes to allow complete evaporation of the ethanol from the column membrane. The columns were transferred to clean 1.5 ml Eppendorf tubes and 50 µl of elution solution C6 was added to the centre of each column membrane. The tubes were centrifuged at 15000 g for 1 minute to elute the DNA. The quality and quantity of the DNA extracted were determined using a NanoDrop ND-1000 spectrophotometer (NanoDrop Technologies).

7.2.4 Amplification of microbial DNAs by PCR and sequencing of the amplicons

Amplification of the microbial DNA by PCR and sequencing of the amplicons were performed by UCL Genomic department. Microbial DNA was amplified by PCR using 16S rRNA gene and ITS gene specific primers, Swift Amplicon 16S+ITS panel (Swift Biosciences). This panel provided a single primer pool covering all the variable regions of the16s rRNA site and ITS1 and ITS2. Sequencing of the PCR amplicons was performed using the Illumina Miseq (Illumina) with a v2 500 cycle run. The raw sequencing data were uploaded in the form of FASTQ files in Illumina Base Space by UCL Genomic department.

7.2.5 16S gene sequence analysis

Bioinformatic analysis of 16S gene sequences was kindly performed by Dr Silke Rath, a research fellow in our laboratory. The 16S rRNA gene sequencing data of PCR amplicons from the microbial DNAs were analysed using an open-source pipeline, Swift 16S SNAPP-AA, which associates sequence reads from all variable regions within the 16s gene to the templates sequence (https://github.com/swiftbiosciences/16S-SNAPP-py3). The number of sequences generated from the 3 samples of faecal DNAs were extremely low as described in Chapter 7.2.1.2 (Figure 7.2) thus they were not able to be analysed through the

process described below. These 3 samples were, therefore, omitted from the analysis.

During the analysis, first of all, short and low-quality reads, as well as the primers, were removed using Cutadapt (Version 3.5) and amplicon sequence variants (ASVs) were identified using DADA2 pipeline (Version 1.16). Duplicate reads and chimeras within the ASVs were identified and removed using VSEARCH (Version 2.16.0) leaving only unique sequences. Chimeras are sequence artifacts created when two dissimilar sequences join to form a hybrid sequence during PCR. The ASVs were then searched and mapped to reference 16S rRNA nucleotide sequence database, Ribosomal Database Project (RDP), (Version 11.5), using an alignment searching tool, BLAST (Version 2.2.30). Since these sequences were fragmented sequences within the 16S gene, the mapped sequences were then computed through Python 3 (Version 3.8.6) to generate a consensus sequence of the amplified 16S rRNA gene regions for each bacterium. These sequences were then classified using the RDP classifier (Trained classifier version 2.13) at the species level in order to generate an abundance lineage table.

7.2.6 ITS gene sequence analysis

Similar to the 16S rRNA gene sequence analysis, bioinformatic analysis of ITS gene sequences was kindly performed by Dr Silke Rath, a research fellow in our laboratory. For processing of the ITS gene sequencing data, the Swift's ITS analysis workflow, using Quantitative Insights Into Microbial Ecology (Qiime 2 Version 2021.8) and Python, was followed. In brief, fastq files were imported into Qiime 2. Subsequently, short and low-quality sequences, as well as primers and chimeras were removed and ASVs were identified similarly to the process used for the 16S rRNA gene sequencing data analysis. The sequences were classified using sklearn Naive Bayesian classifier of UNITE ITS reference set (Version 8, updated in April 2021).

7.2.7 Downstream microbial community analysis

7.2.7.1 Relative abundances

Statistical differences in the relative abundances of bacteria and fungi between different groups e.g. WT vs *Adamdec1*$^{-/-}$ mice were determined at multiple taxonomic levels using one-way ANOVA or Mann-Whitney tests by Prism 9.3.0.

7.2.7.2 Alpha diversity

Alpha-diversity refers to the diversity of bacteria in a single sample which is assessed in terms of richness, i.e. number of species observed, and evenness, i.e. equity in species abundance. Chao1 and Shannon indices were applied to the ASVs, rather than the classified species since a large proportion of the ASVs were unclassified at the species level, to determine the α diversity using the R package vegan (Version 2.5-7). Chao1 index primarily measures the richness whereas Shannon index takes account of both richness and evenness components of α diversity. The statistical differences between samples were determined by ANOVA or Mann-Whitney using Prism 9.3.0. Change in the α diversity over the pre-pool pre-DSS and post-DSS timepoints were calculated using Kruskal-Wallis test by Prism 9.3.0.

7.2.7.3 Beta diversity

Beta-diversity assesses similarity or dissimilarity between individual samples thus estimating the diversity within a given group of samples. β diversity was analysed in the PRIMER-e (Plymouth Routines in Multivariate Ecological Research) software (Version 7.0.13). For this, the Bray-Curtis distance was used to measure the difference in ASV composition between samples. Non-metric multi-dimensional scaling (nMDS) plots were created based on Bray-Curtis similarity of the square root-transformed relative abundance data.

Two statistical analyses were used to determine if the observations in the β diversity were statistically significant. Permutational analysis of variance (PERMANOVA) determines whether the centroids of samples grouped based on a particular factor differ from the centroid of other groups. Analysis of similarities (ANOSIM) determines the similarities among the samples clustered together by a particular factor. PERMANOVA and ANOSIM were conducted using the R package

vegan (Version 2.5-7). The R^2 value of PERMANOVA and the R-statistic value of ANOSIM indicated the degree of influence by a particular factor being examined, where values closer to 1 indicated strong influence and values closer to 0 indicated weak influence. “Added sequentially” option of PERMANOVA statistical tests determined how much variation in the centroids of the samples was left to explain by the second variable adjusted for the first variable.

Index of multivariate dispersion (MVDISP) in beta diversity, which estimates the relative dispersion of the microbiome composition of samples within each factor, was calculated using the R package vegan (Version 2.5-7).

7.2.7.4 Screening for the presence and abundance of specific species

The sequences derived from *Duncaniella muricolitica* strain A60, *Anaerostipes faecis* strain A14, *Alistipes okayasuensis* strain A61 and *Sangeribacter muris* strain A43 have not been verified nor added to the RDP database yet. Thus the sequences corresponding to these bacteria were manually searched for in the samples. For that, a new nucleotide BLAST database was built using the FASTA files of 16S rRNA gene sequences from isolated strains within the families *Muribaculaceae* and *Rikenellaceae* downloaded from the RDP database, and the FASTA files of the 16S rRNA gene sequences from the four new species downloaded from NCBI. The sequences from each sample were BLASTed against the created database and manually extracted from the output files. Only sequences that showed 100% identity to the sequence of interest were considered.

7.2.7.5 Severity of weight loss by DSS challenge

The severity of weight loss was defined as no/mild weight loss = weight reduction <10%, and severe weight loss = weight loss ≥10% using weight assessed on day 9 of the DSS challenge relative to the pre-DSS weight for each mouse.

7.3 Results

7.3.1 Experiment 1 - Effect of ADAMDEC1 on the gut microbiome

To investigate the effect of ADAMDEC1 on the microbiome and mycobiota of young mouse (4 - 5 weeks) in the naïve state, faecal samples were collected from 16 mice housed in 4 different cages. In each cage, the mice cohoused were littermates and differed in sex and genotype but had remained in the same individual cages since birth with their parents (Figure 7.1). The demographics and quality and quantity of the DNA extracted from the faecal sample from each mouse are summarised in Table 7.1.

Animal Number	Cage	Genotype	Sibling	Sex	DNA Conc. (ng/µl)	DNA 260/280	DNA 260/230
1	1	Het	S1	M	20.9	2	1.66
2		KO		M	22.1	1.78	1.69
3		Het		M	15.6	3.21	1.52
4		Het		F	26.5	2.32	2.31
5		KO		F	89.4	2.15	2.15
6	2	Het	S1	M	38	1.99	1.99
7		WT		M	39.5	2.04	2.07
8		KO		M	67.3	1.7	1.87
9		WT		F	59.2	1.83	2.14
10		Het		F	42.1	1.6	1.72
11	3	Het	S2	F	38	1.57	1.79
12		KO		F	47.9	1.52	2.05
13	4	KO	S3	M	81.4	1.64	2.23
14		KO		M	58.7	1.57	1.94
15		KO		F	33.4	1.36	1.74
16		KO		F	54	1.54	1.76

Table 7.1 The demographics of mice used in Experiment 1 and the quantity and quality of microbial DNA extracted from the faecal samples.
Het: Heterozygous, KO: *Adamdec1*$^{-/-}$, WT: Wild type, F: Female, M: Male, Conc.: Concentration

7.3.1.1 16S rRNA gene analysis

7.3.1.1.1 Relative abundances of bacteria

The relative abundances of bacteria at phylum, family, genus and species level were compared between the three genotypes (Figure 7.3).

At phylum level, across all 3 genotypes, the sequences were classified to 8 phyla: *Actinobacteria*, *Bacteroidetes*, *Campilobacterota*, *Deferribacteres*, *Firmicutes*, *Fusobacteria*, *Proteobacteria* and *Tenericute*. Out of these 8, the abundance of *Bacteroidetes* dominated (mean=84.69%, SD=1.68) followed by *Firmicutes* (mean=13.98%, SD=1.66) (Figure 7.3 A). The remaining 6 phyla were found on average in less than 1% of the sequences. There were no significant differences in the relative abundances of bacteria classified at phylum level between the 3 genotypes.

At family level, *Muribaculaceae* had the highest abundance in all 3 genotypes (mean=73.54%, SD=2.60) (Figure 7.3 B). *Lactobacillaceae* was the second most abundant family in the WT mice, whereas *Lachnospiraceae* was the second most abundant family in the *Adamdec1*$^{-/-}$ mice (Figure 7.3 B). The mean relative abundance of *Lactobacillaceae* was 8.08% and 4.12% in the WT and *Adamdec1*$^{-/-}$ mice respectively. The mean relative abundance of *Lachnospiraceae* was 2.76% and 7.12% in the WT and *Adamdec1*$^{-/-}$ mice respectively. A statistical difference was achieved for the difference in the abundance of *Lachnospiraceae* between the WT and *Adamdec1*$^{-/-}$ mice. (Figure 7.4 B).

The majority of the *Muribaculaceae* classified at the family level could not be classified to genus level as there were no isolated and described reference sequences in the database as yet. Thus the mean relative abundance of the unclassified bacteria accounted for approximately 50% in all 3 genotypes. However, the abundance of *Duncaniella* dominated in all 3 genotypes at the genus level (Figure 7.3 C). There were no statistical differences in the relative abundances of bacteria classified at genus level between the WT and *Adamdec1*$^{-/-}$ mice.

At species level, there was a greater number of the sequences which could not be classified resulting in 70 – 80% of the sequences being unclassified. However, *Duncaniella muris*, *Muribaculum intestinale* and *Paramuribaculum intestinale* were the 3 classified bacteria with the highest abundances in all 3 genotypes (Figure 7.3 D). The abundances of *Duncaniella dubosii* (WT mean=4.34%, SD 0.72,

Adamdec1$^{-/-}$ mean=2.00, SD 0.88) and *Ligilactobicillus apodemi* (WT mean=2.58%, SD=0.12, *Adamdec1*$^{-/-}$ mean=0.004%, SD 0.003) were significantly lower in the *Adamdec1*$^{-/-}$ mice compared to the WT mice (Figure 7.4 B and C).

Although statistically significant differences were observed in the relative abundances of these 3 bacteria: *Lachnospiraceae*, *Duncaniella dubosii*, *Ligilactobicillus apodemi*, between the WT and *Adamdec1*$^{-/-}$ mice (Figure 7.4), the heatmap of relative abundance of bacteria of individual mice at each taxonomic level demonstrated no obvious clustering per genotype overall (Figure 7.5).

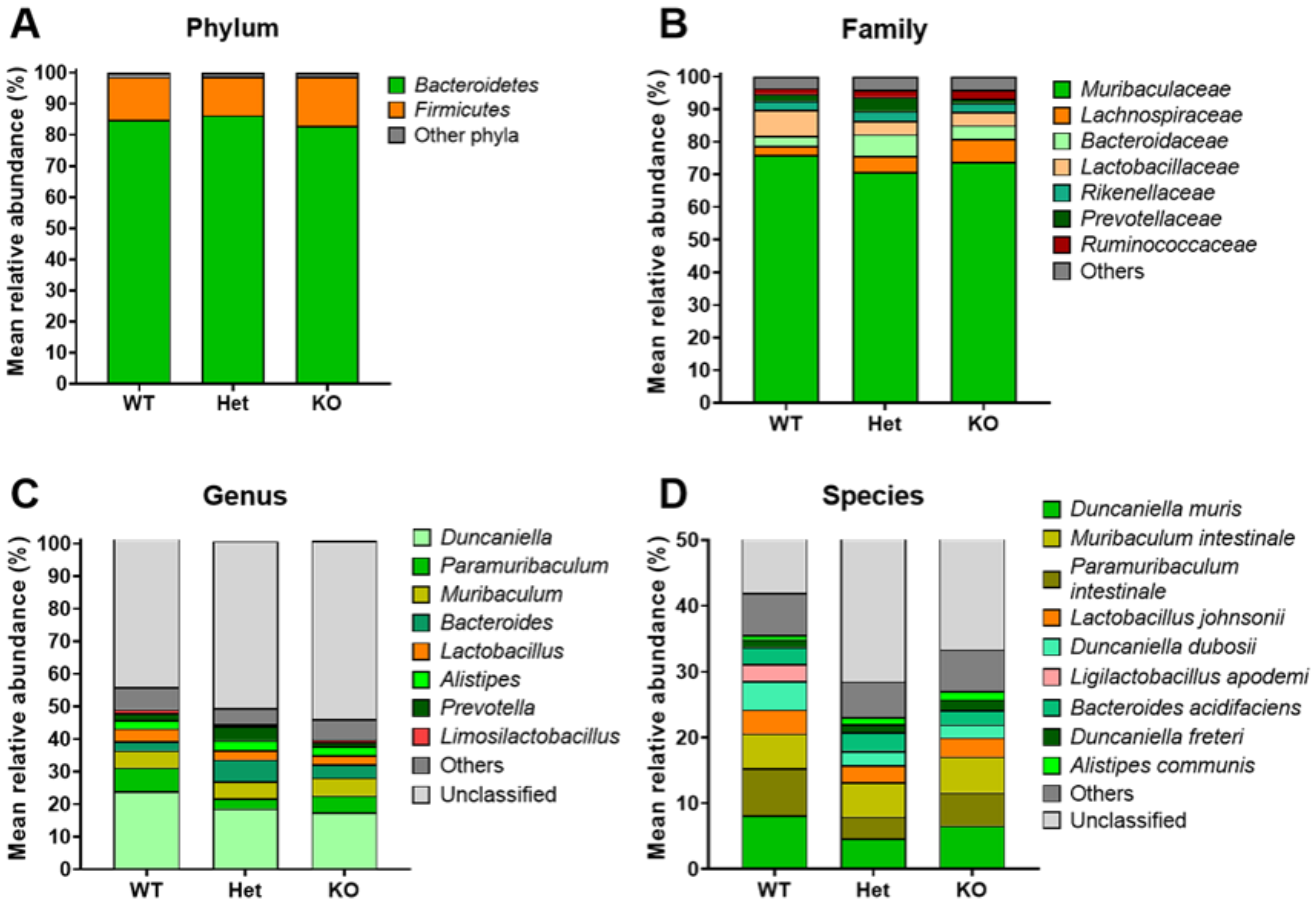

Figure 7.3 Global bacterial composition of the microbiome in faecal samples from WT, heterozygous and *Adamdec1*$^{-/-}$ mice assessed at 4 taxonomic levels: phylum (A), family (B), genus (C), species (D) in Experiment 1. Mean relative abundances according to genotype are shown in stacked bar graphs. Classified bacteria with relative abundances of less than 1% were pooled and categorised as “others”.
Het: Heterozygous, KO: *Adamdec1*$^{-/-}$, WT: Wild type

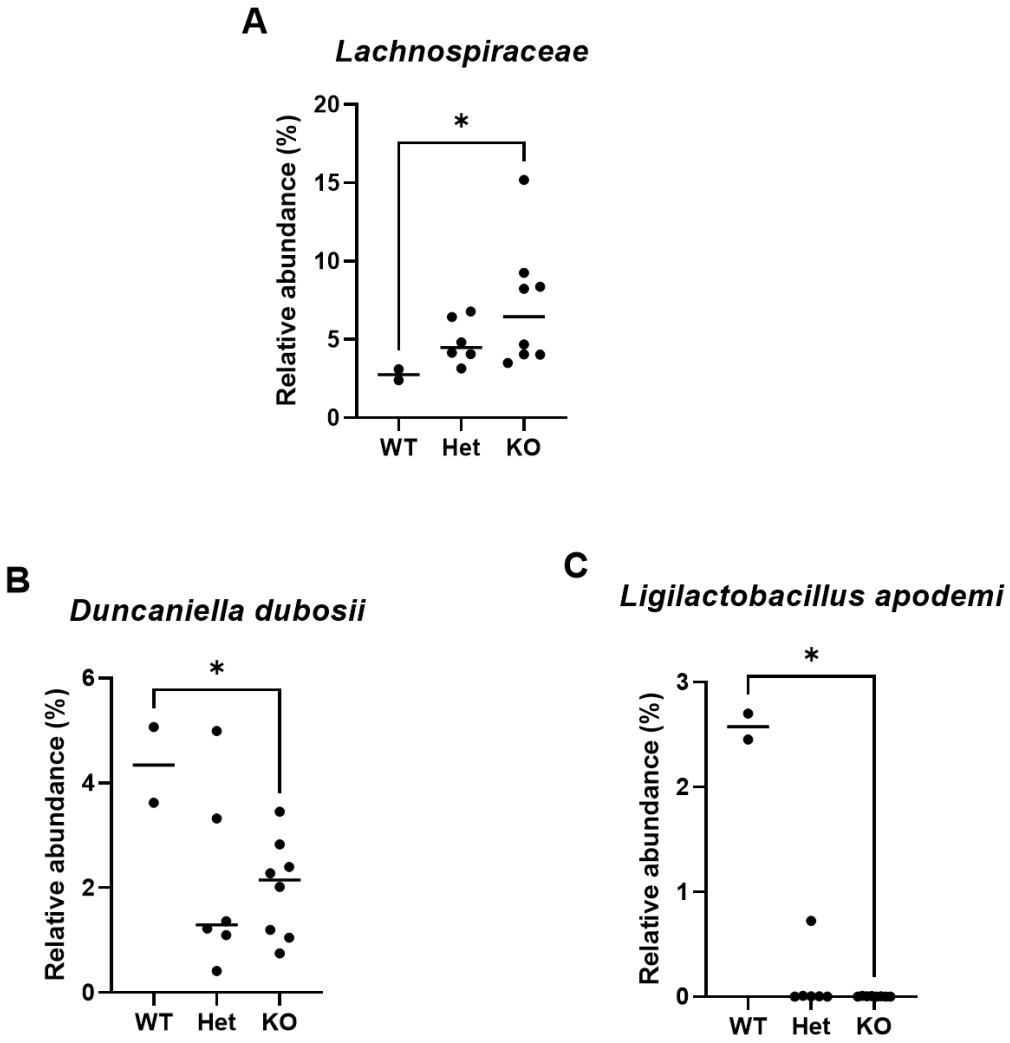

Figure 7.4 Differentially abundant bacterial taxonomic groups in the microbiome of WT and *Adamdec1*$^{-/-}$ mice in Experiment 1.

A: Relative abundance of *Lachnospiraceae* assessed at family level. The relative abundance of *Lachnospiraceae* was significantly higher in the *Adamdec1*$^{-/-}$ mice in comparison to the WT mice.

B and C: Relative abundance of *Duncaniella dubosii* and *Ligilactobacillus apodeme* assessed at species level. The relative abundance of *Duncaniella dubossi* and *Ligilactobacillus apodemi* were significantly lower in the *Adamdec1*$^{-/-}$ mice in comparison to the WT mice.

One-way ANOVA test was used.

Het: Heterozygous, KO: *Adamdec1*$^{-/-}$, WT: Wild type, *: $p < 0.05$

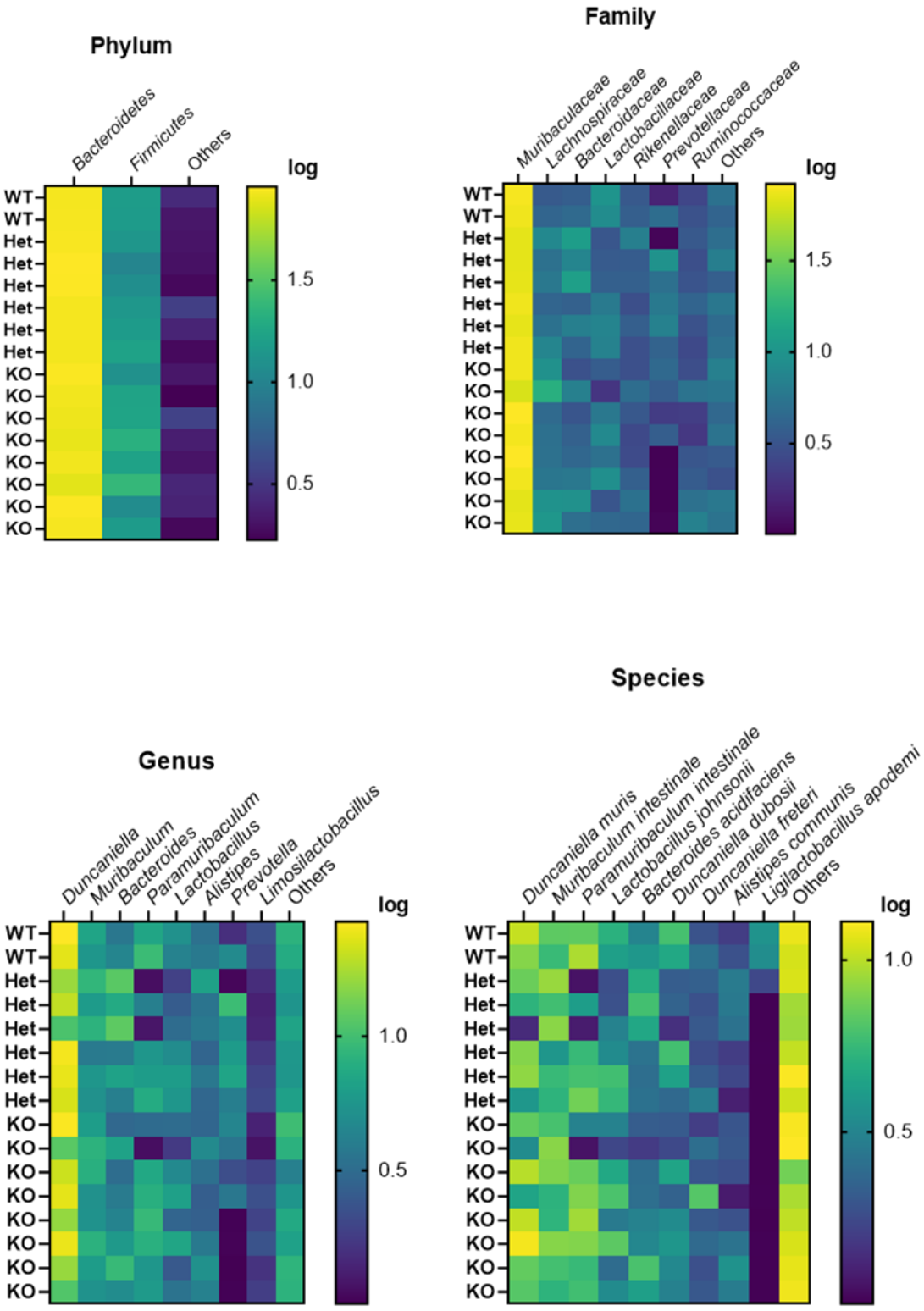

Figure 7.5 Heatmap of the bacterial microbiome composition of WT, heterozygous and *Adamdec1*$^{-/-}$ mice assessed at phylum, genus, family and species levels in Experiment 1. There were no obvious genotype-specific patterns in the bacterial microbiome composition. The heatmap was created using relative abundances of the classified bacteria. The classified bacteria with relative abundances of less than 1% were pooled and categorised as "others". The relative abundances were log-transformed.
Het: Heterozygous, KO: *Adamdec1*$^{-/-}$, WT: Wild type

7.3.1.1.2 *Firmicutes* to *Bacteroides* ratio

The ratio of Firmicutes to Bacteroides (F/B ratio) has been studied extensively in the microbiome of human and mouse and is believed to have an important influence on the homeostasis of the intestine. A higher F/B ratio is associated with obesity and metabolic syndrome, whereas a low F/B ratio has been reported in IBD, although discrepancies exist between studies.[297] There were no significant differences in the F/B ratio of WT, heterozygous and *Adamdec1*$^{-/-}$ mice (Figure 7.6). This was expected given that there were no significant differences in the relative abundances of *Bacteroidetes* and *Firmicutes* according to the genotype (Figure 7.3 A).

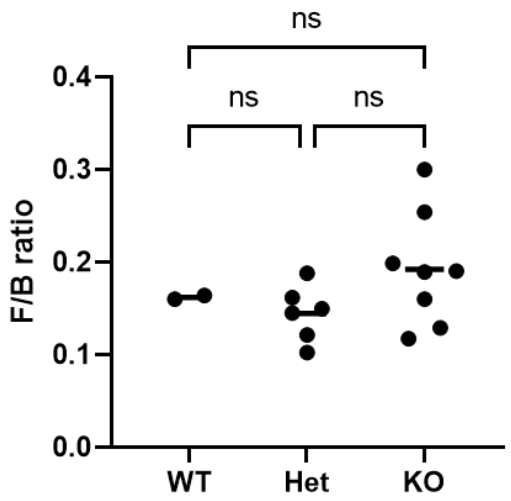

Figure 7.6 F/B ratio of WT, heterozygous and *Adamdec1*$^{-/-}$ mice in Experiment 1.
There were no significant differences in the F/B ratio of WT, heterozygous and *Adamdec1*$^{-/-}$ mice. One-way ANOVA test was used.
Het: Heterozygous, KO: *Adamdec1*$^{-/-}$, WT : Wild type, ns: Non-significant

7.3.1.1.3 Alpha diversity

Alpha diversity is studied extensively and is of importance as a high diversity of intestinal microbiome is generally accepted to be associated with health. Reduction in α diversity of intestinal microbiome has been reported in numerous diseases including IBD.[298–300] Alpha diversity was compared between the mice of different genotype as well as sex, sibling state and cage to determine if these factors other than the genotype influenced the α diversity of mice.

By applying Chao1 index, which accounts for the richness of bacterial composition, overall, there was no convincing effect of genotype and sex on the α diversity of the mice (Figure 7.7 A and B). However, the mice of Sibling 3 and Cage 4 appeared to have higher α diversities than their counterparts (Figure 7.7 C and D). The mice of Sibling 3 and Cage 4 were in fact the same mice (Table 7.1) thus it was unable to infer which of these variables might have been responsible for the high α diversities observed in these mice.

By applying Shannon index, which accounts for both richness and evenness of bacterial compositions, a lower α diversity was observed in the *Adamdec1*$^{-/-}$ mice compared to the WT mice, with the heterozygous mice exhibiting α diversity between that of the WT and *Adamdec1*$^{-/-}$ mice. With regards to sex, using Shannon index, higher alpha diversity was also observed in the females compared to male mice. The same trend has been reported previously.[301] As demonstrated by Chao1 index, a higher α diversity was observed in the mice of Sibling 3 and the mice from Cage 4.

Despite these observations, none of these differences was statistically significant.

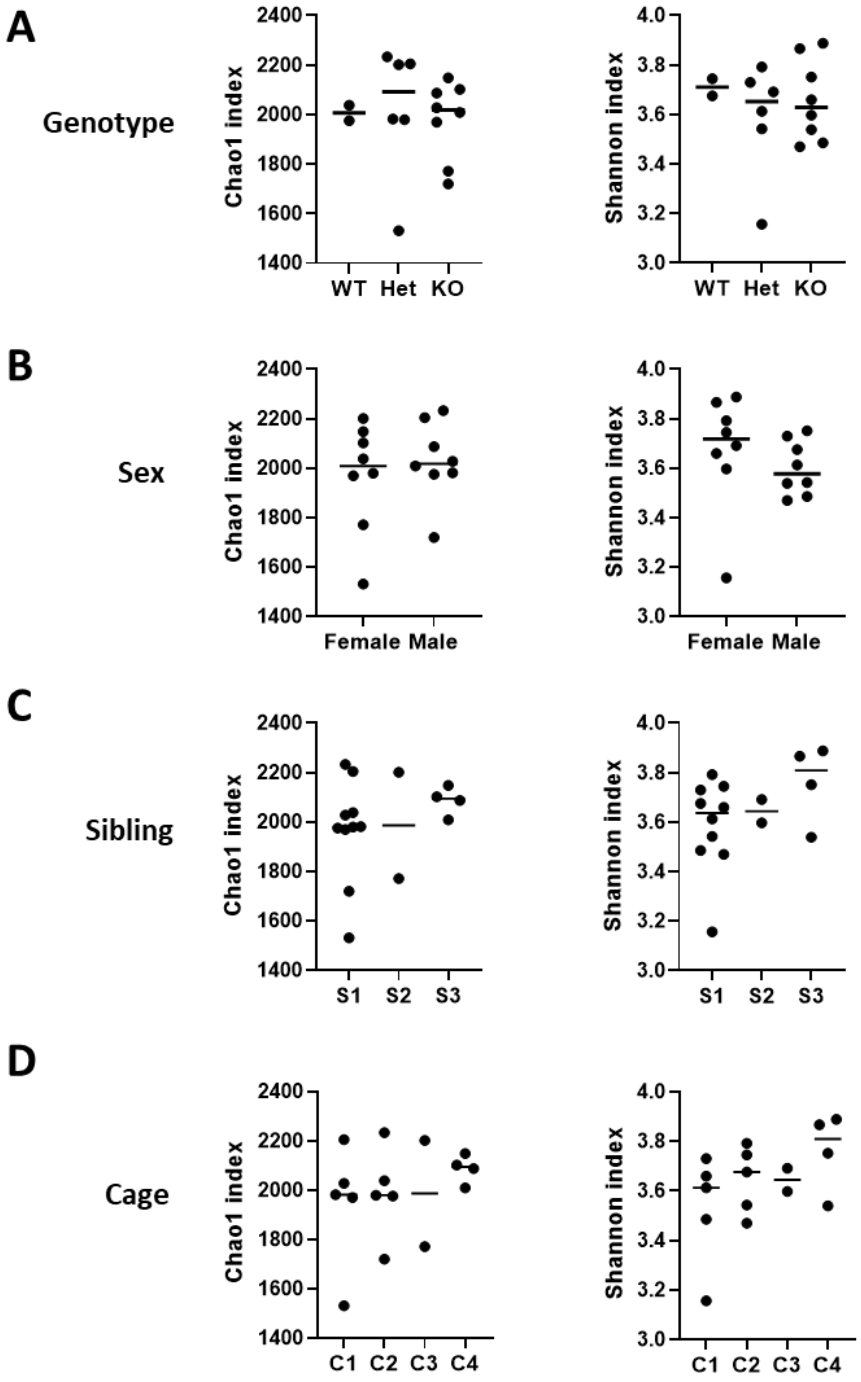

Figure 7.7 Alpha diversity of the bacterial microbiome of the mice according to their genotype (A), sex (B), sibling state (C) and cage (D) in Experiment 1. Both Chao1 (shown by graphs on the left) and Shannon (shown by graphs on the right) indices were applied. There were no statistical differences in α diversity of the mice compared according to the factors examined. One-way ANOVA test was used.
Het: Heterozygous, KO: *Adamdec1*$^{-/-}$, WT: Wild type, S: Sibling, C: Cage

7.3.1.1.4 Beta diversity

The β diversity of the 16 mice showed that the samples did not cluster according to the genotype indicating that the samples did not exhibit genotype-specific bacterial compositions (Figure 7.8). However, a clear clustering of the samples was seen based on their cage they were housed indicating that the bacterial composition of the mice was shaped by the individual cage environment and was distinct in each cage.

The results of PERMANOVA and ANOSIM were not significant for genotype confirming that the bacterial microbiome composition of the mice did not differ based on their genotype (PERMANOVA p=0.162, ANOSIM p=0.366). In contrast, the results of PERMINOVA and ANOSIM were both significant for cage and also sibling state (PERMANOVA and ANOSIM p=0.001 for both the cage and sibling state). Since there was an overlap of the cage and sibling states, the effects of the cage and sibling state were adjusted for each other. This showed that the effect of cage and sibling state on the bacterial microbiome composition both remained significant (p=0.001) which indicated that both factors independently had a significant effect on the bacterial microbiome composition of the mice. However, the higher R^2 and R-statistic value for the cage factor in comparison to the sibling state indicated that the effect of the cage was greater than the sibling state on the bacterial microbiome composition of the mice. (See Appendix 3 for the detailed PERMANOVA and ANOSIM values.)

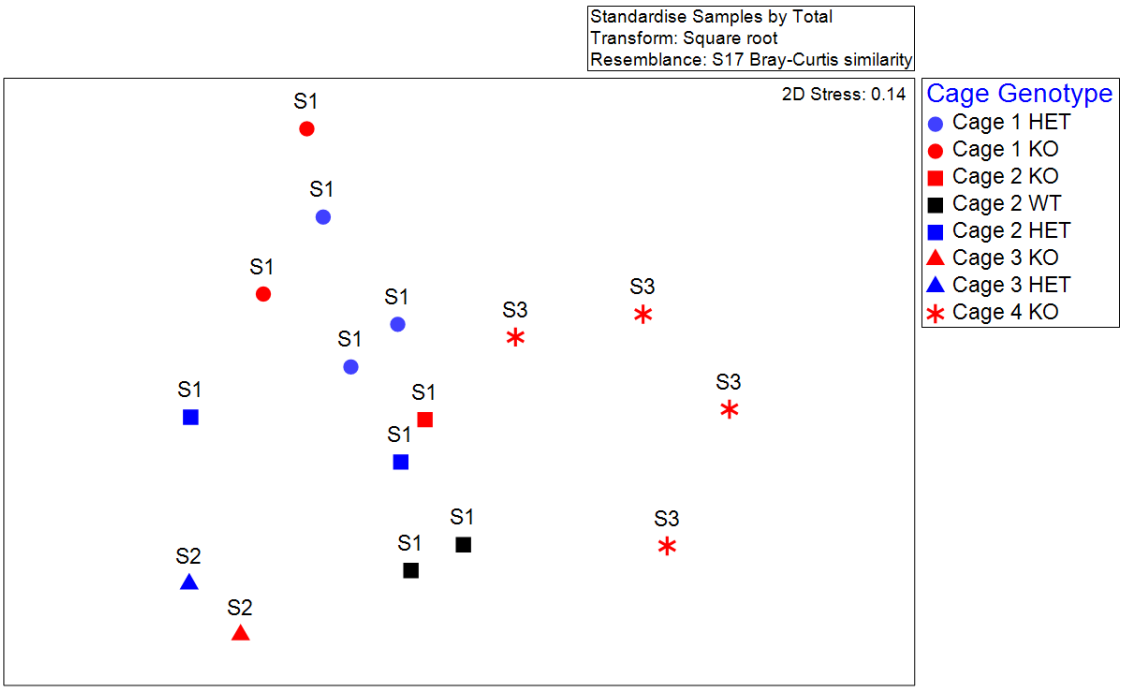

Figure 7.8 nMDS plot demonstrating the β diversity of the bacterial microbiome composition in WT, heterozygous and *Adamdec1*$^{-/-}$ mice in Experiment 1. Individual cages are indicated by the shape of mark representing the microbiome of each mouse (circle=Cage 1, square=Cage 2, triangle=Cage 3, asterisk=Cage 4). Genotypes are indicated by colour (black=WT, blue=heterozygous, red=*Adamdec1*$^{-/-}$). Sibling state (S) is indicated above each mark. Clustering of the samples were observed according to the cage and sibling state but not according to the genotype. HET: Heterozygous, KO: *Adamdec1*$^{-/-}$, WT: Wild type

7.3.1.2 ITS gene analysis

7.3.1.2.1 Relative abundances of fungi

The relative abundances of fungi at phylum, class, order, family, genus and species level were compared between the three genotypes (Figure 7.9).

At phylum level, only 2 phyla could be identified (Figure 7.9 A). These were *Ascomycota* and *Basidiomycota* with a mean relative abundance of 55.3% (SD=1.76) and 6.23% (SD=0.80) respectively across all 16 samples. More than a third (mean=38.44%, SD=1.44) of the sequences could not be classified.

At class level, the vast majority of the sequences (mean=92.6%, SD=0.89) could not be classified and only 2 classes of fungi were identified (Figure 7.9 B). These were *Agaricomycetes* and *Xylonomycetes* with a mean relative abundance of 4.72% (SD=0.85) and 2.64% (SD=0.42) respectively across all 16 samples.

All the fungi identified and classified at the level below class had abundances of less than 0.01% except for *Symbiotaphrina* which was classifiable down to the genus level with a mean relative abundance of 2.64% (SD=0.42) across all 16 samples (Figure 7.9 C, D and D).

At species level only 2 fungi were identified which were *Symbiotaphrina buchneri* and *Galerina triscopa* with mean relative abundances of less than 0.05% across all 16 samples (Figure 7.9 F).

There were no significant differences in the mean relative abundances of the classified fungal taxonomic groups assessed at 6 taxonomic levels between the WT and *Adamdec1*$^{-/-}$ mice. However, the assessment of potential difference in the abundance of fungal taxonomic groups between the WT and *Adamdec1*$^{-/-}$ mice below the level of phylum was largely not possible since the vast majority of the sequences could not be classified.

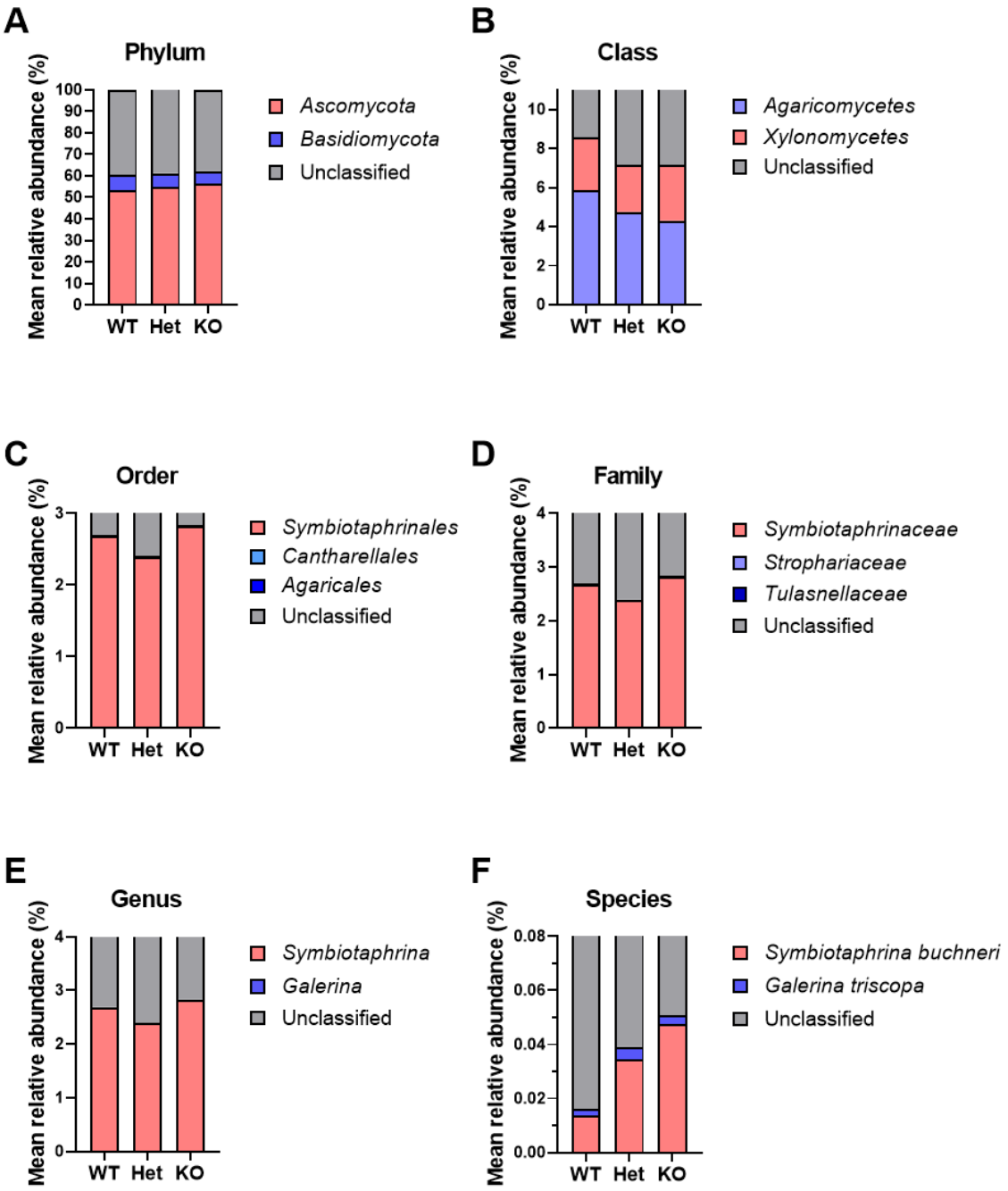

Figure 7.9 Global fungal composition of the microbiome in faecal samples from WT, heterozygous and *Adamdec1*$^{-/-}$ mice assessed at 6 taxonomic levels: phylum (A), class (B), order (C), family (D), genus (E) and species (F) in Experiment 1. Mean relative abundances according to genotype are shown in stacked bar graphs.
Het: Heterozygous, KO: *Adamdec1*$^{-/-}$, WT: Wild type

7.3.1.2.2 Alpha diversity

Chao1 and Shannon indices were applied to analyse the α diversity of the fungal features observed. There were no significant differences in the α diversities between the WT, heterozygous and *Adamdec1*$^{-/-}$ mice. Similar to the bacterial alpha diversity, there were no statistically significant differences observed in the alpha diversity according to other factors such as sex, sibling state and cage (data not shown).

7.3.1.2.3 Beta diversity

Similarly to the β diversity of the bacterial composition, β diversity of gut mycobiome composition of the 16 mice showed that the samples did not cluster according to the genotype (Figure 7.10). The results of PERMANOVA and ANOSIM confirmed that there was no statistical difference observed in the mycobiome composition of the mice based on the genotype (PERMANOVA p=0.194, ANOSIM p=0.404). However, once again clear clustering of the samples was seen based on their cage and sibling state. The results of PERMINOVA and ANOSIM were both significant for cage (PERMANOVA p=0.001, ANOSIM p=0.001) and sibling state (PERMANOVA p=0.002, ANOSIM p=0.019). The effect of cage and sibling state on the mycobiome composition remained significant (cage p=0.001, sibling state p=0.004) even the analysis was adjusted for each factor which indicated that both factors independently had a significant effect on the mycobiota composition of the mice. However, similar to the bacterial microbiome composition, the higher R^2 and R-statistic value for cage factor in comparison to the sibling state indicated that the effect of the cage was greater than the sibling state on the mycobiome composition of the mice. (See Appendix 4 for the detailed PERMANOVA and ANOSIM values.)

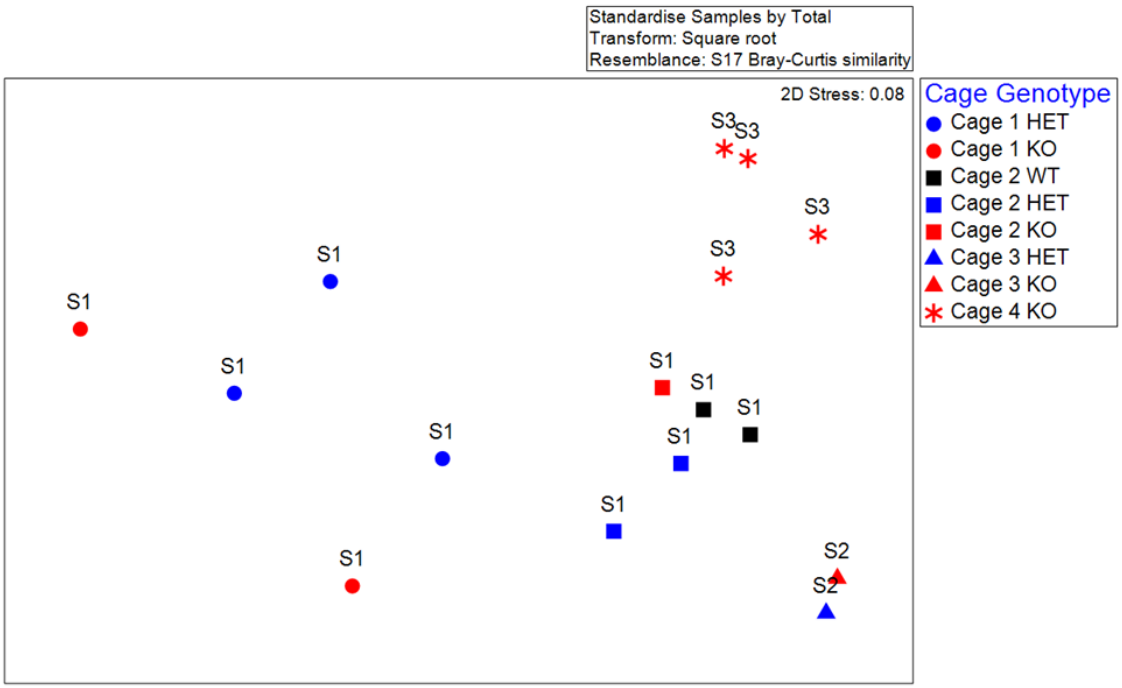

Figure 7.10 nMDS plot demonstrating β diversity of the mycobiome composition in WT, heterozygous and *Adamdec1*$^{-/-}$ mice in Experiment 1. Individual cages are indicated by the shape of mark representing the microbiome of each mouse (circle=Cage 1, square=Cage 2, triangle=Cage 3, asterisk=Cage 4). Genotypes are indicated by the colour (black=WT, blue=heterozygous, red=*Adamdec1*$^{-/-}$). Sibling state (S) is indicated above each mark. Clustering of the samples was observed according to the cage and sibling state but not according to the genotype.
Het: Heterozygous, KO: *Adamdec1*$^{-/-}$, WT: Wild type

7.3.2 Experiment 2 – Effect of ADAMDEC1 on gut microbiome after prolonged period of housing of the mice per genotype, after cohousing of WT and *Adamdec1*$^{-/-}$ mice and after DSS colitis

Experiment 2 was conducted to examine the microbiota of 20 same-sexed (female) WT (n=8) and *Adamdec1*$^{-/-}$ (n=12) mice, which were older and had been caged per litter and genotype, except for one cage (Cage D), for a much longer period of time compared to Experiment 1, to first of all validate the findings of Experiment 1. Following this, the effect of pooling animals from 6 small cages into 2 large cages cohousing the WT and *Adamdec1*$^{-/-}$ mice over 8 weeks and the effect of DSS on the microbiome of these mice were examined. Due to the colitis and subsequent diarrhoea caused by DSS, the lumen of the colon was empty in 3 mice (2 *Adamdec1*$^{-/-}$ mice in Cage 1 and 1 *Adamdec1*$^{-/-}$ mouse in Cage 2) at the time of harvesting the post-DSS samples. As described in Chapter 6, the effect of DSS

was more severe in *Adamdec1*$^{-/-}$ mice in comparison to WT, hence the inability to collect post-DSS samples from 3 of the 12 *Adamdec1*$^{-/-}$ mice (Figure 7.2 and Table 7.2). Furthermore, 1 pre-pool DNA sample (from *Adamdec1*$^{-/-}$ mouse in Cage D) and 2 post-DSS DNA samples (from 2 *Adamdec1*$^{-/-}$ mice in Cage 2) resulted in low reads from the 16S rRNA gene and ITS gene sequencing, thus these samples were excluded from the analysis (Figure 7.2 and Table 7.2).

Animal No.	Original cage	Pooled cage	Genotype	Sibling	Pre-pool DNA conc. (ng/µl)	Pre-DSS DNA conc. (ng/µl)	Post-DSS DNA conc. (ng/µl)
1	A	Cage 1	KO	S1	70.1	81.2	~~74.1~~
2			KO		86.4	57.6	No sample
3			KO		93.4	190.5	40
4	B		KO	S1	55.2	79.6	~~47.8~~
5			KO		123.4	85.8	No sample
6	C		WT	S2	87	115.2	13.1
7			WT		41.2	117.7	6.6
8			WT		64.1	132.7	29.7
9	D	Cage 2	KO	S1	~~121.2~~	29.7	No sample
10			KO		45.3	43	13.2
11			KO		53.7	26.6	26.2
12			WT	Purchased	44.2	59.2	56.6
13	E		KO	S1	100.8	66	57.5
14			KO		109.7	26.9	91.5
15			KO		103.5	40.2	121.4
16			KO		81.5	47.3	47.1
17	F		WT	S2	86.4	41.5	20
18			WT		93.4	63.4	61.3
19			WT		78.3	63.3	38.9
20			WT		103.7	107.9	82.7

Table 7.2 Demographics of the mice used in Experiment 2 and quantity of the microbial DNA extracted from the faecal samples collected from each mouse at 3 timepoint. The samples with struckthrough DNA concentration resulted in low sequencing reads. Faecal samples could not be obtained from 3 *Adamdec1*$^{-/-}$ mice at the time of post-DSS sample collection (indicated as 'no sample').
Het: Heterozygous, KO: *Adamdec1*$^{-/-}$, WT: Wild type, F: female, M: Male, Conc.: Concentration

7.3.2.1 16S rRNA gene analysis

7.3.2.1.1 Verification of findings from Experiment 1 using the pre-pool samples

Relative abundances of bacteria

The findings of the bacterial microbiome analysis of Experiment 1 were verified using the pre-pool samples. The finding from Experiment 1 suggested that the relative abundances of bacteria were largely similar between the WT and *Adamdec1*$^{-/-}$ mice, although subtle but statistically significant differences were observed in the relative abundances of *Lachnospiraceae, Duncaniella dubosii* and *Ligilactobacillus apodeme* between the WT and *Adamdec1*$^{-/-}$ mice. However, in Experiment 2 where the mice had been housed per genotype, except for cage D, in general, more noticeable differences in the abundance of some of the bacteria taxonomic groups were seen between the WT and *Adamdec1*$^{-/-}$ mice (Figure 7.11). Specifically, the abundances of 6 taxonomic groups, assessed at 4 taxonomic levels, were found to be statistically different between the WT and *Adamdec1*$^{-/-}$ mice (Figure 7.12).

At phylum level, the relative abundance of *Firmicutes* was significantly higher in the *Adamdec1*$^{-/-}$ mice in comparison to the WT mice (Figure 7.12 A). At family level, as seen in Experiment 1, the relative abundance of *Lachnospiraceae* was significantly higher in the *Adamdec1*$^{-/-}$ mice in comparison to the WT mice (Figure 7.12 B). Additionally, at family level, the relative abundance of *Erysupelotrichaceae* was also significantly lower in the *Adamdec1*$^{-/-}$ mice compared to the WT (Figure 7.12 C). Furthermore, the relative abundances of *Bacteroides* at genus level, and *Bacteroides acidifaciens* and *Turicibacter sanguinis* at species level were significantly lower in the *Adamdec1*$^{-/-}$ mice in comparison to the WT mice (Figure 7.12 D, E and F). The significantly lower relative abundances of *Duncaniella dubosii* and *Ligilactobacillus apodemi* in the *Adamdec1*$^{-/-}$ mice in comparison to the WT mice observed in Experiment 1, however, were not observed in the pre-pool samples of Experiment 2 (Figure 7.13).

F/B ratio

Although a higher F/B ratio was observed in the *Adamdec1*$^{-/-}$ mice compared to WT (WT mean=0.285 SD=0.10, *Adamdec1*$^{-/-}$ mean=0.534 SD=0.31) this was not statistically significant (Figure 7.14).

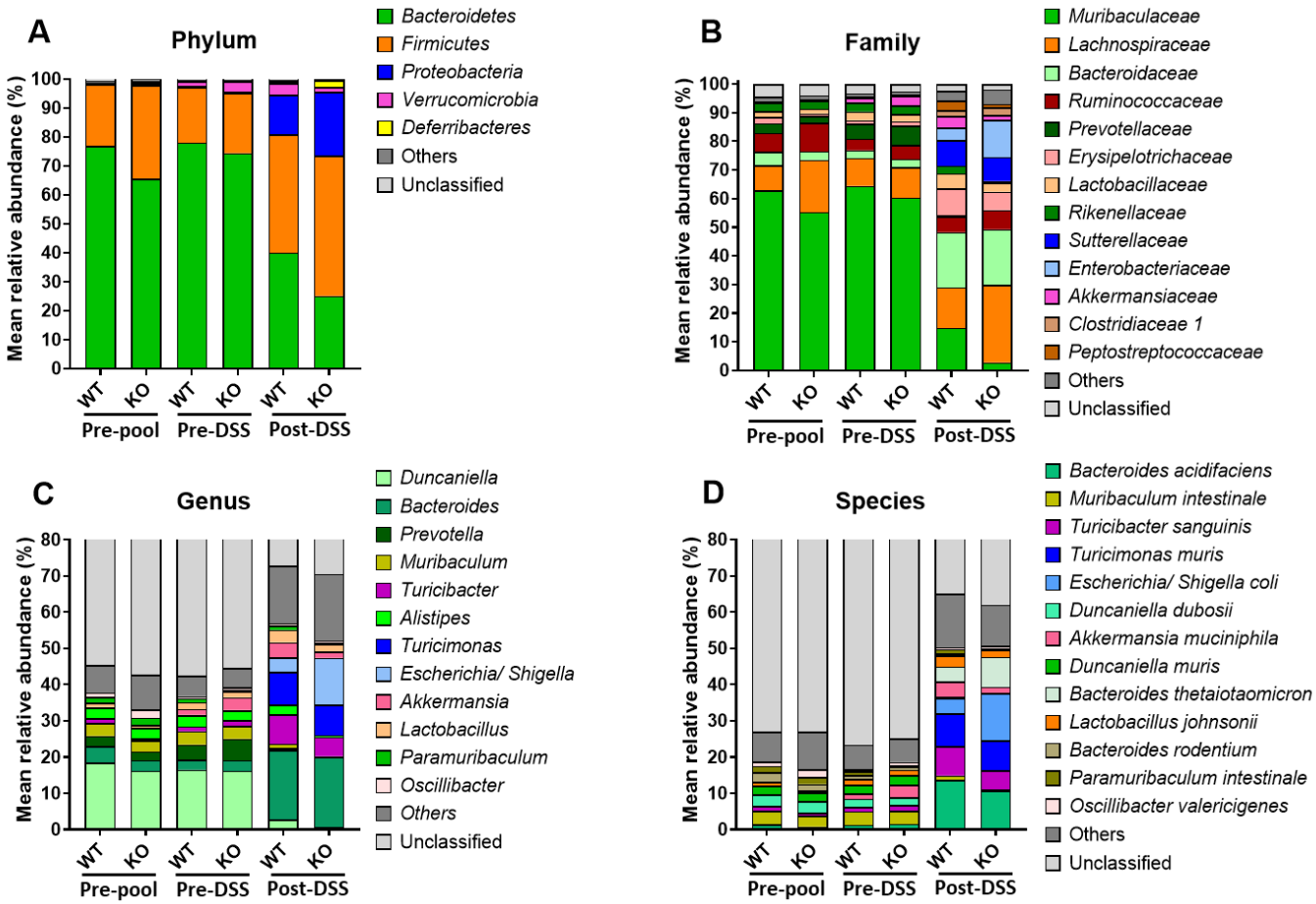

Figure 7.11 Global bacterial composition of the microbiome in faecal samples from WT, heterozygous and *Adamdec1*$^{-/-}$ mice assessed at each timepoint, at 4 taxonomic levels: phylum (A), family (B), genus (C), species (D). Mean relative abundances according to the genotype are shown in stacked bar graphs. Classified bacteria with relative abundances of less than 1% were pooled and categorised as "others".
KO: *Adamdec1*$^{-/-}$, WT: Wild type

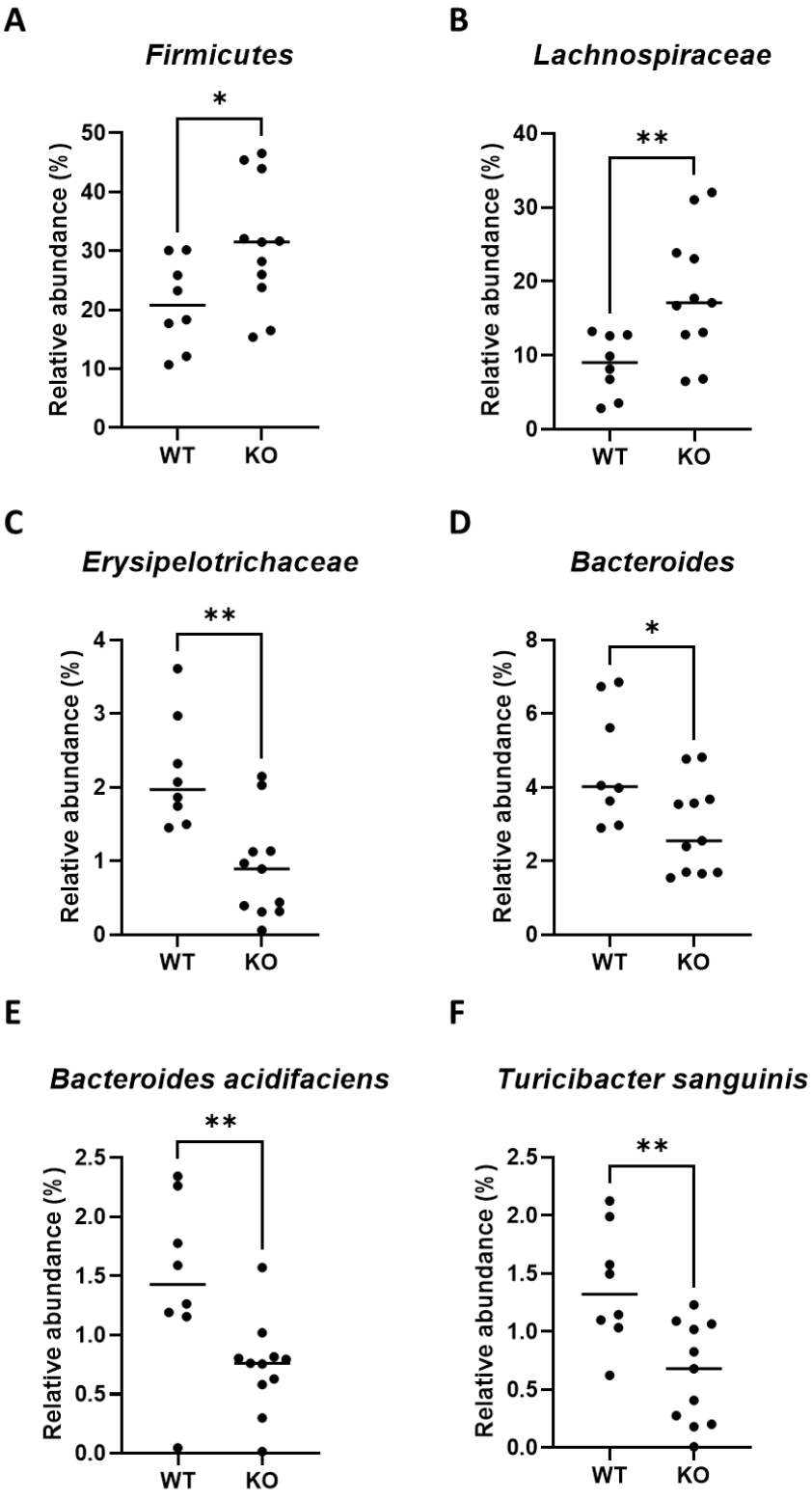

Figure 7.12 Differentially abundant taxonomic groups in the microbiome of the pre-pool samples collected from WT and *Adamdec1*$^{-/-}$ mice assessed at phylum (A), family (B and C), genus (D) and species (F and G) levels. The relative abundances of *Firmicutes* and *Lachnospiraceae* were significantly higher in the *Adamdec1*$^{-/-}$ mice in comparison to WT mice. The relative abundances of *Erysipelotrichaceae*, *Bacteroides*, *Bacteroides acidifaciens* and *Turicibacter sanguinis* were significantly lower in the *Adamdec1*$^{-/-}$ mice in comparison to WT mice. Mann-Whitney test was used.
KO: *Adamdec1*$^{-/-}$, WT: Wild type, *: $p < 0.05$, **: $p < 0.01$

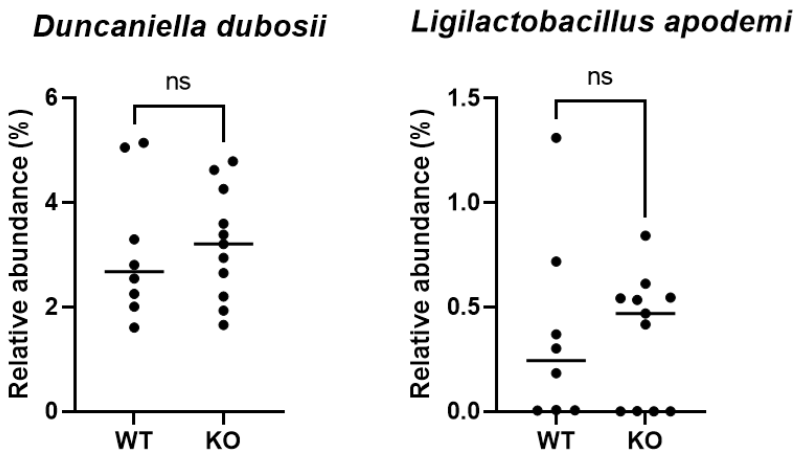

Figure 7.13 The relative abundances of *Duncaniella dubosii* and *Ligilactobacillus apodeme* in the microbiome of the pre-pool samples collected from WT and *Adamdec1*$^{-/-}$ mice. In contrast to Experiment 1, there were no significant differences in the relative abundances of these two bacterial species in the microbiome of the pre-pool samples. Mann-Whitney test was used.
KO: *Adamdec1*$^{-/-}$, WT: Wild type, ns: Non-significant

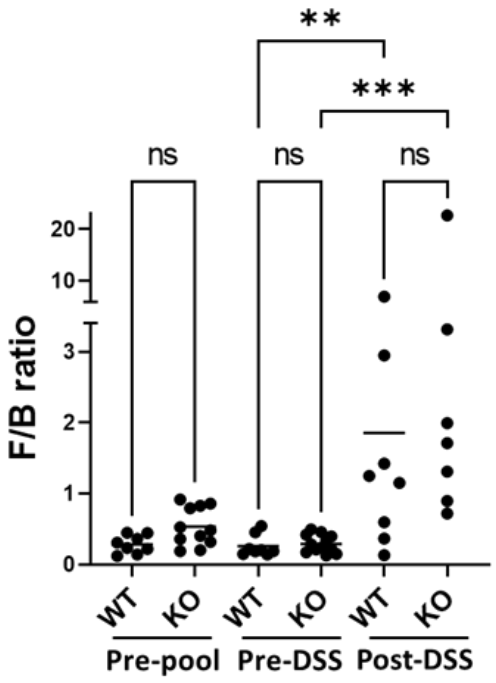

Figure 7.14 F/B ratio of WT and *Adamdec1*$^{-/-}$ mice assessed at pre-pool, pre-DSS and post-DSS timepoints. There were no statistically significant differences in the F/B ratio between the WT and *Adamdec1*$^{-/-}$ mice at all timepoints. The F/B ratio of both WT and *Adamdec1*$^{-/-}$ increased significantly by DSS-challenge. Mann-Whitney test was used.
KO: *Adamdec1*$^{-/-}$, WT: Wild type, **: $p < 0.01$, ***: $p < 0.001$, ns: Non-significant

Alpha diversity

With regards to α diversity, there were no differences between the WT and KO mice by both Chao1 and Shannon indices, verifying the finding from Experiment 1 that alpha diversity was not affected by ADAMDEC1 (Figure 7.15).

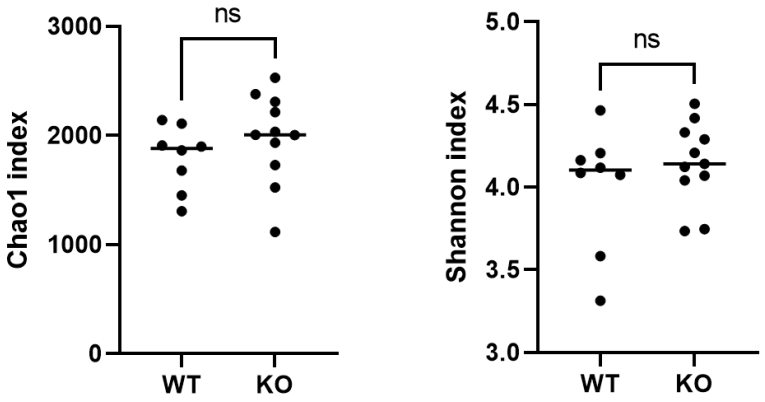

Figure 7.15 Alpha diversity of the bacterial microbiome in the pre-pool samples of WT and *Adamdec1*$^{-/-}$ mice. There were no significant differences in the α diversity of the pre-pool bacterial microbiome between the WT and *Adamdec1*$^{-/-}$ mice assessed by both Chao1 and Shannon indices. One-way ANOVA test was used
KO: *Adamdec1*$^{-/-}$, WT: Wild type, ns: Non-significant

Beta diversity

Similar to Experiment 1, the clustering of samples according to the individual cages was observed (Figure 7.16) which was statistically significant by both PERMANOVA and ANOSIM (PERMANOVA p=0.001, ANOSIM p=0.001). However, the effect of sibling state on the microbiome composition in the pre-pool samples became less compared to Experiment 1, with assessment by ANOSIM not reaching statical significance (PERMANOVA p=0.013, ANOSIM p=0.090). Consistent with more differences observed between the WT and *Adamdec1*$^{-/-}$ mice with regards to the relative abundances of bacterial taxonomic groups in the pre-pool samples compared to Experiment 1, clustering of the samples according to the genotype was observed to some degree in the pre-pool samples (Figure 7.16). However, this observation did not reach statistical significance by both PERMANOVA (p=0.057) and ANOSIM (p=0.090). Since the mice in each cage were of the same genotype and were from the same parents, except for the WT

mice in Cage D, the effect of sibling state and genotype on the bacterial microbiome composition were analysed adjusted for the cage effect. Once adjusted for the cage effect, the sibling state was no longer a statistically significant factor in affecting the clustering of the samples (p=0.215). The PERMANOVA p-value for the genotype also increased from 0.057 to 0.315 when the analysis was adjusted for the cage effect. These findings indicated that the bacterial compositions of the samples from the WT and *Adamdec1*$^{-/-}$ mice in the naïve state in Experiment 2 were driven predominantly by the individual cage environment. (See Appendix 5 for the detailed PERMANOVA and ANOSIM values.)

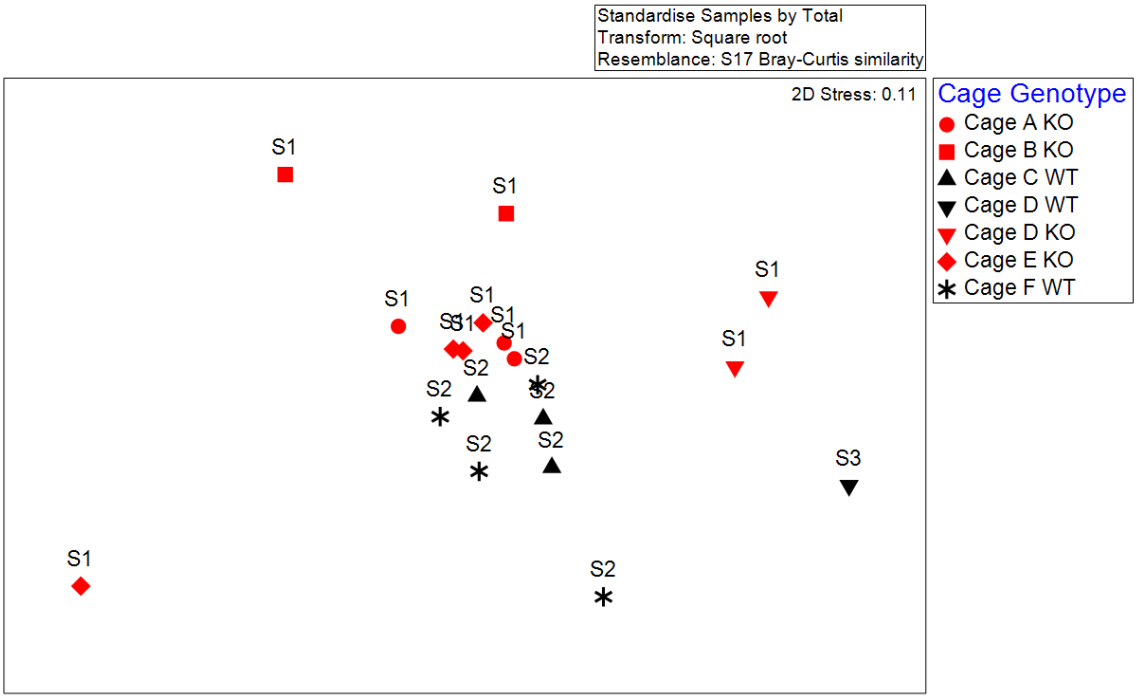

Figure 7.16 nMDS plot demonstrating the β diversity of the bacterial microbiome composition in the pre-pool samples of WT and *Adamdec1*$^{-/-}$ mice. Individual cages are indicated by the shape of mark representing the microbiome of each mouse. Genotypes are indicated by the colour (black=WT, red=*Adamdec1*$^{-/-}$). Sibling state (S) is indicated above each mark. Similar to Experiment 1, clustering of the samples according to the individual cages were observed. In contrast to Experiment1, clustering of the samples according to genotype was also observed to some degree.
KO: *Adamdec1*$^{-/-}$, WT: Wild type

7.3.2.1.2 Effect of pooling of mice on the intestinal bacterial composition

Relative abundances of bacteria

The effect of cage pooling on the intestinal bacterial composition of WT and *Adamdec1*$^{-/-}$ mice was assessed using the pre-DSS samples. By pooling the mice into 2 cages that contained both WT and *Adamdec1*$^{-/-}$ mice of a mixed sibling state, overall, the differences that were observed in the pre-pool samples between the WT and *Adamdec1*$^{-/-}$ mice were homogenised (Figure 7. 12). More specifically, the differences in the relative abundance of the 6 bacteria taxonomic groups, assessed at 4 taxonomic levels, detected between the pre-pool samples of the WT and *Adamdec1*$^{-/-}$ mice (Figure 7.12) diminished by the pooling of mice into 2 cages (data not shown). Instead, only a significantly lower relative abundance of *Paramuribaculum intestinale*, at species level, was detected in the pre-DSS samples of the *Adamdec1*$^{-/-}$ in comparison to the WT (Figure 7.17).

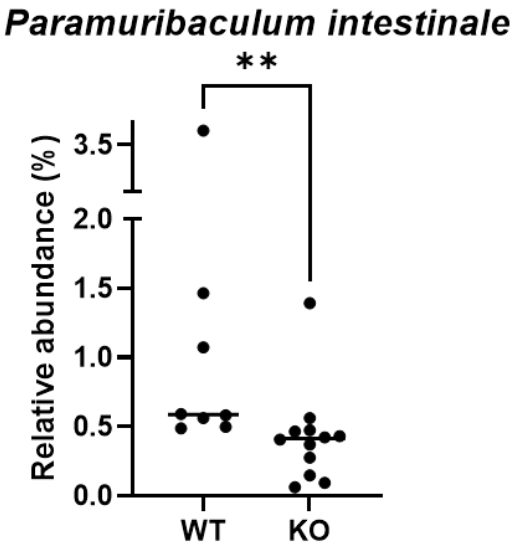

Figure 7.17 The relative abundance of *Paramuribaculum intestinale* in the microbiome of pre-DSS samples collected from WT and *Adamdec1*$^{-/-}$ mice.
The relative abundance was significantly lower in the *Adamdec1*$^{-/-}$ mice in comparison to WT mice. Mann-Whitney test was used.
KO: *Adamdec1*$^{-/-}$, WT: Wild type, **: $p < 0.01$

F/B ratio

The mean F/B ratio of the WT and *Adamdec1*$^{-/-}$ mice became more similar to each other by pooling in comparison to the pre-pool samples. (WT mean=0.26 SD=0.31, *Adamdec1*$^{-/-}$ mean=0.292 SD=0.22) (Figure 7.14).

Alpha diversity

Alpha diversity of the WT mice, assessed by Chao1 and Shannon indices, was not affected by the pooling of mice (Figure 7.18). However, in contrast, both Chao1 and Shannon indices indicated that the alpha diversity of the *Adamdec1*$^{-/-}$ mice decreased significantly by the pooling of mice.

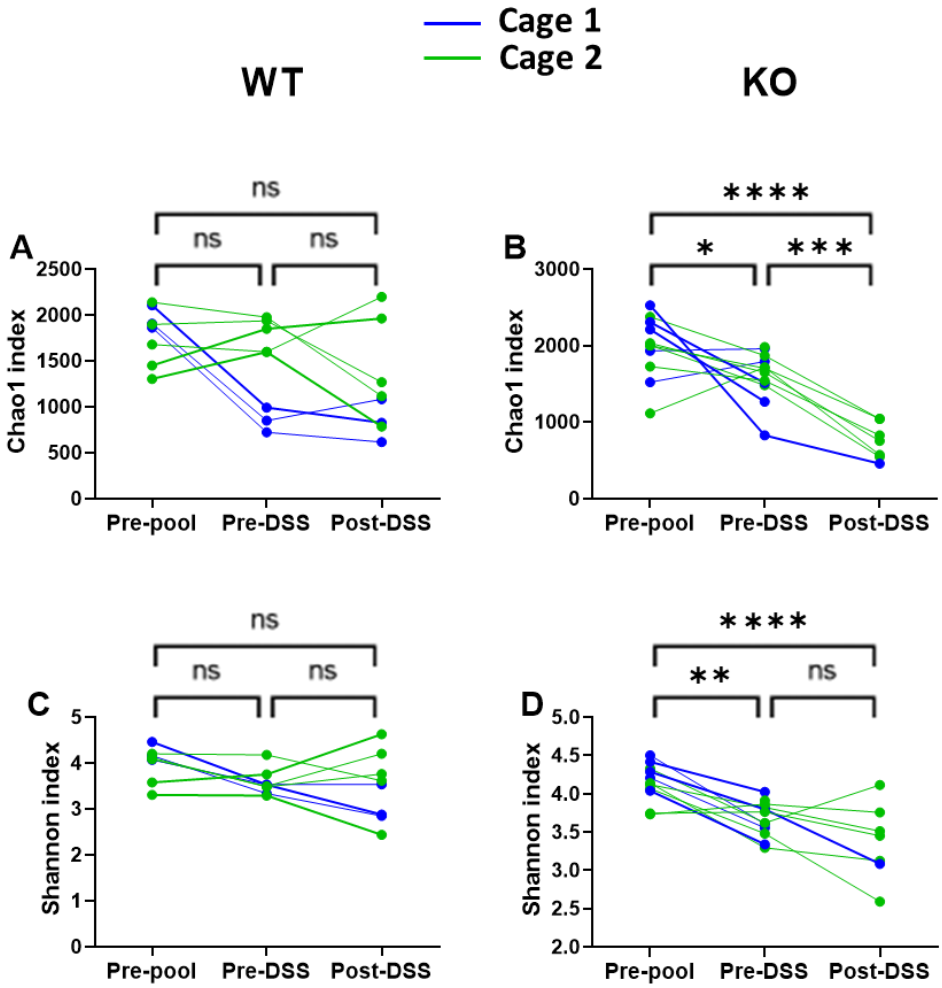

Figure 7.18 Changes in the α diversity of WT and *Adamdec1*$^{-/-}$ mice bacterial microbiome over pre-pool, pre-DSS and post-DSS timepoints assessed by Chao1 (A and B) and Shannon (C and D) indices. The mice in Cage 1 are indicated by blue dots and lines, and the mice in Cage 2 are indicated by green dots and lines. Alpha diversity of the WT mice, assessed by both Chao1 and Shannon indices, were not affected by the pooling of mice or by the DSS-challenge. Alpha diversity of the *Adamdec1*$^{-/-}$ mice reduced significantly by the pooling of mice, assessed by Chao1 and Shannon indices, and by the DSS-challenge, assessed by Chao1 index. Kruskal-Wallis test was used.
KO: *Adamdec1*$^{-/-}$, WT: Wild type, *: $p < 0.05$, **: $p < 0.01$, ***: $p < 0.001$, ****: $p < 0.0001$, ns: Non-significant

Beta diversity

Beta diversity of the pre-DSS samples showed clustering of the samples based on the new pooling cage (Figure 7.19) which was confirmed to be statistically significant by both PERMANOVA (p=0.003) and ANOSIM (p=0.002). The original cage effect analysed by unadjusted PERMANOVA as well as by ANOSIM was also significant (PERMANOVA p=0.004, ANOSIM p=0.006). However, when PERMANOVA was performed adjusted for the pooling cage effect, the original cage was no longer a statistically significant factor that affected the clustering of the samples (p=0.139). Once again the genotype did not influence the β diversity of the bacterial composition (PERMANOVA p=0.205, ANOSIM p=0.211). The sibling state also no longer affected the β diversity of the samples after the pooling of mice. Together with the findings from the β diversity of the pre-pool samples, these findings suggest that the intestinal bacterial composition was shaped by the individual cages that the mice were housed. This cage-specific composition appeared to be plastic and 8 weeks was long enough for the murine bacterial composition to lose the signature associated with the previous cage and acquired a new specific signature that was unique to the new cage. This observation was independent of the age of the mice (PERMANOVA for age p=0.295). (See Appendix 6 for the detailed PERMANOVA and ANOSIM values.)

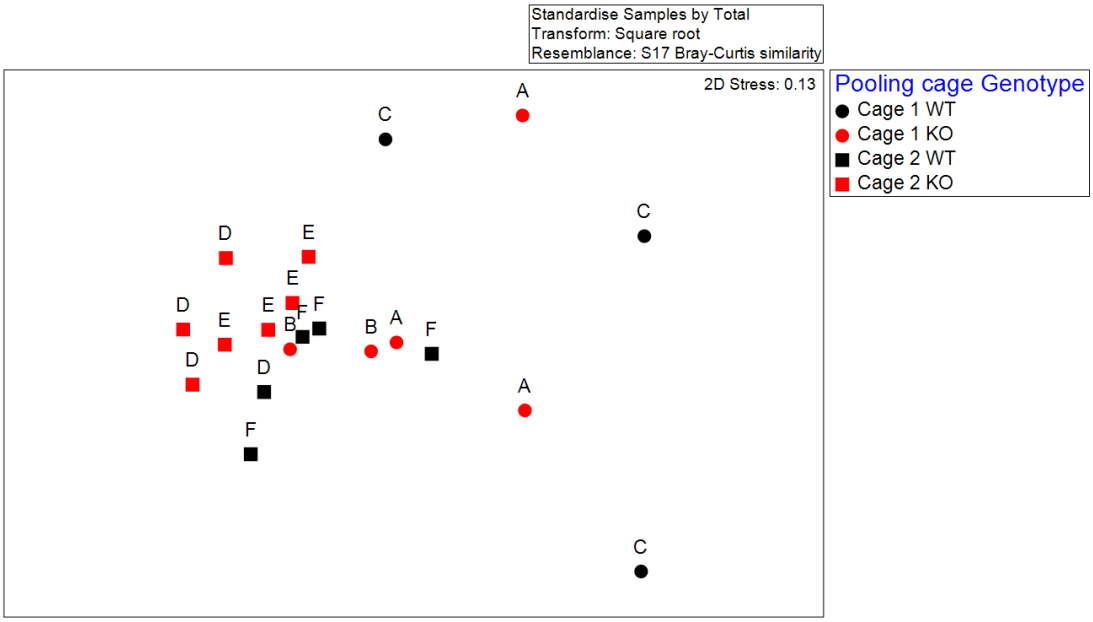

Figure 7.19 nMDS plot demonstrating the β diversity of the bacterial microbiome in pre-DSS samples of the WT and *Adamdec1*$^{-/-}$ mice. Pooling cages are indicated by the shape of mark representing the microbiome of each mouse (circle=Cage 1 and square=Cage 2). Genotypes are indicated by the colour (black=WT, red=*Adamdec1*$^{-/-}$). The original cages are indicated above each mark. Clustering of the samples according to the new cage i.e. Cage 1 and Cage 2 were observed. The samples did not cluster according to the genotype.
KO: *Adamdec1*$^{-/-}$, WT: Wild type

7.3.2.1.3 Effect of DSS challenge on the intestinal bacterial composition

Relative abundances of bacteria

The effect of the DSS challenge on the intestinal bacterial composition of the WT and *Adamdec1*$^{-/-}$ mice was analysed using the post-DSS samples. Alterations in the relative abundances of bacteria by the DSS-challenge were clearly observed overall in both WT and *Adamdec1*$^{-/-}$ mice (Figure 7.11 and 7.20).

At phylum level, overall, the abundance of *Bacteroides* decreased and the abundances of *Firmicutes*, *Proteobacteria* and *Deferribacteres* increased by the DSS challenge irrespective of the genotype (Figure 7.11 A). The relative abundance of *Verrucomicrobia* increased in the WT and decreased in the *Adamdec1*$^{-/-}$ by the DSS challenge. However, there were no statistical differences in the relative abundances of any of the bacterial phyla between the WT and *Adamdec1*$^{-/-}$ mice.

At family level, overall, the DSS challenge resulted in a marked reduction in the abundance of *Muribaculaceae* from the mean abundance of approximately 50 - 60% in the pre-pool and pre-DSS samples to the mean abundance of 14.8% (SD=15.3) and 2.8% (SD=4.0) in the post-DSS samples of the WT and *Adamdec1*$^{-/-}$ mice respectively. Additionally, increase in the abundances of *Lachnospiraceae*, *Bacteroidaceae*, *Erysipelotrichaceae*, *Sutterellaceae* and *Enterobacteriaceae* were also observed (Figure 7.11 B). However, there were no statistical differences in the relative abundances of these bacteria between the WT and *Adamdec1*$^{-/-}$ mice.

At genus level, overall, the DSS challenge resulted in reductions in the relative abundances of *Duncaniella*, *Prevotella* and *Muribaculum*, and increases in the relative abundance of *Bacteroides*, *Turicibacter*, *Turicimonas* and *Escherichia/Shigella* (Figure 7.11 C). The relative abundance of *Muribaculum*, which was classified down to the species level as *Muribaculum intestinale*, was statistically lower in the *Adamdec1*$^{-/-}$ compared to the WT mice (Figure 7.21 A).

At the specie level, overall, the DSS challenge resulted in a reduction in the relative abundance of *Muribaculum intestinale* (Figure 7.11 D). The relative abundances of the rest of the classified bacterial species increased by the DSS challenge. The relative abundance of *Muribaculum intestinale* and *Duncaniella dubosii* were statistically lower in the *Adamdec1*$^{-/-}$ mice compared to the WT mice (Figure 7.21 A and B).

Overall, the post-DSS samples demonstrated greater variability in the bacterial composition, assessed by relative abundances, among the mice irrespective of the genotype (Figure 7.14, Figure 7.20). Thus even though the mean relative abundances of some of the bacteria appeared markedly different between the WT and *Adamdec1*$^{-/-}$ mice, statistical differences were achieved in only 2 bacterial taxonomic groups examined at 4 taxonomic levels.

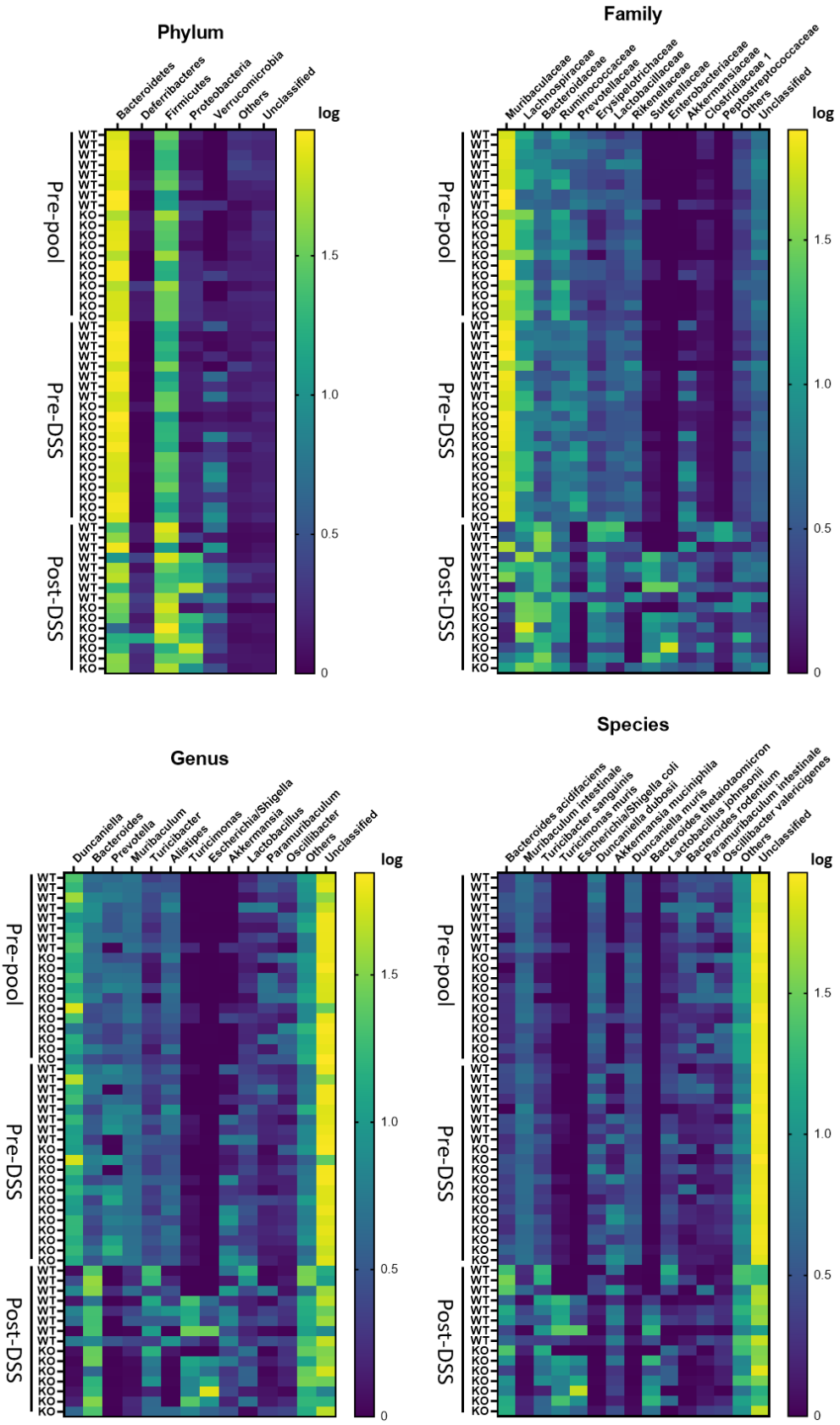

Figure 7.20 Heatmap of bacterial microbiome composition in the pre-pool, pre-DSS and post-DSS samples of WT and *Adamdec1*$^{-/-}$ mice assessed at phylum, genus, family and species levels. Overall, alteration in the bacterial microbiome composition was observed before and after the DSS challenge. There were no obvious genotype-specific patterns. The heatmap was created using the relative abundances of the classified bacteria which were log-transformed. The classified bacteria with relative abundances of less than 1% were pooled and categorised as “others”.
KO: *Adamdec1*$^{-/-}$, WT: Wild type

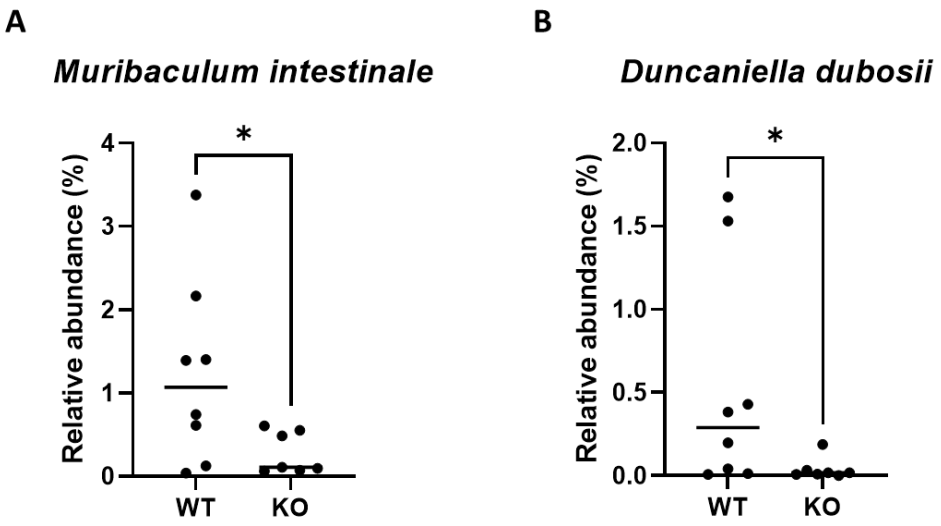

Figure 7.21 Differentially abundant bacterial species in the microbiome of the post-DSS samples collected from WT and *Adamdec1*$^{-/-}$ mice. The relative abundances of *Muribaculum intestinale* (A) and *Duncaniella dubosii* (B) at species level were significantly lower in the post-DSS samples collected from the *Adamdec1*$^{-/-}$ mice in comparison to the WT mice. Mann-Whitney test was used. KO: *Adamdec1*$^{-/-}$, WT: Wild type, *: $p < 0.05$

F/B ratio

Overall, the DSS challenge caused a significant increase in F/B ratio in both WT and *Adamdec1*$^{-/-}$ mice (Figure 7.14) However, there was no significant difference between the F/B ratio of the post-DSS samples between the WT and *Adamdec1*$^{-/-}$ mice.

Alpha diversity

Similar to the trends seen in the pre-DSS samples after the pooling of mice, the α diversity of the WT mice did not change by DSS challenge but the α diversity of the *Adamdec1*$^{-/-}$ mice decreased significantly by DSS challenge assessed by Chao1 index (Figure 7.18).

Beta diversity

Consistent with the overall marked changes in the relative abundances of bacteria as a result of DSS challenge, β diversity of the pre- and post-DSS samples showed a clear clustering of samples according to the DSS treatment state (Figure 7.22). This was confirmed to be statistically significant by both PERMANOVA (p=0.001)

and ANOSIM (p=0.001) indicating that the DSS challenge caused significant change in the bacterial microbiome composition of the mice. Additionally, similar to the β diversity of the pre-DSS samples, clustering of the pre- and post-DSS samples according to the pooling cage was also observed (Figure 7.22). This was confirmed to be statistically significant by both PERMANOVA (p=0.005) and ANOSIM (p=0.016). Even after adjusting PERMANOVA for the effect of the DSS challenge, the pooling cage remained statistically significant (p=0.007). This indicated that the DSS treatment state and pooling cage independently shaped the bacterial composition of the pre- and post-DSS samples, and that the change in the bacterial composition by the DSS challenge was unique in each pooled cage. Once again, clustering of the samples based on genotype was not observed which was confirmed by both PERMANOVA (p=0.208) and ANOSIM (p=0.637). (See Appendix 7 for the detailed PERMANOVA and ANOSIM values.)

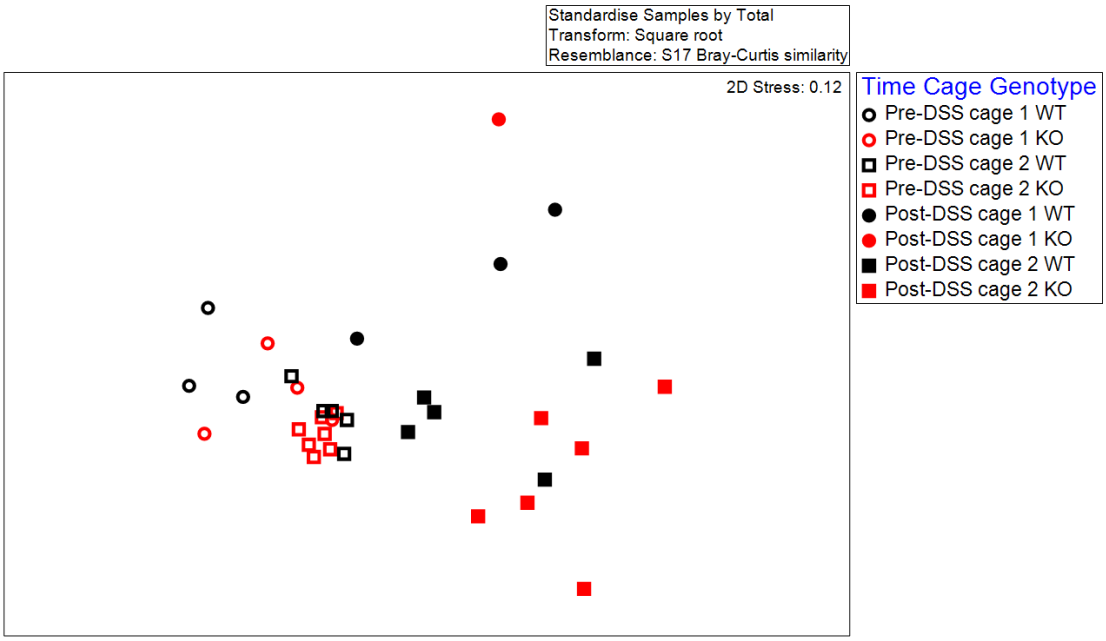

Figure 7.22 nMDS plot demonstrating the β diversity of bacterial microbiome in the pre and post-DSS samples of WT and *Adamdec1*$^{-/-}$ mice. DSS challenge state is indicated by the open or close feature of the mark representing the microbiome of each mouse (open=pre-DSS, close=post-DSS). Pooling cages are indicated by the shape of mark (circle=Cage 1 and square=Cage 2). Genotypes are indicated by the colour (black=WT, red=*Adamdec1*$^{-/-}$). Clustering of the samples according to the DSS challenge state and pooling cage were observed.
KO: *Adamdec1*$^{-/-}$, WT: Wild type

Beta diversity of the post-DSS samples alone once again showed clear clustering of the samples according to the pooling cage which was statistically significant (PERMANOVA *p*=0.004, ANOSIM *p*=0.002) (Figure 7.23). Additionally, clustering of the samples according to original cage and genotype were also observed (original cage; PERMANOVA *p*=0.001 ANOSIM *p*=0.001, genotype; PERMANOVA *p*=0.019, ANOSIM *p*=0.025). When PERMANOVA was adjusted for the effect of pooling cage the effect of original cage remained statistically significant (p=0.018) indicating that these two factors independently shaped the bacterial compositions of the post-DSS samples. In contrast, when PERMANOVA was adjusted for the original cage effect, the effect of genotype was no longer statistically significant (*p*=0.858). These findings indicate that the genotype did not shape the bacterial composition of the post-DSS samples in a similar manner to the pre-pool and pre-DSS samples. (See Appendix 8 for the detailed PERMANOVA and ANOSIM values.)

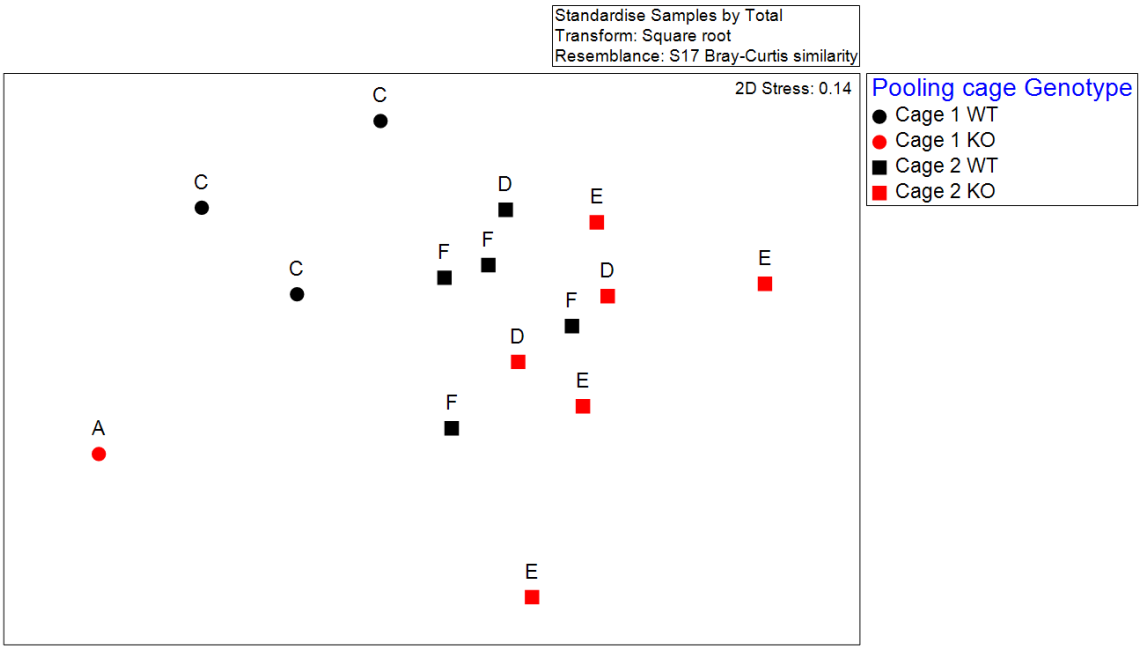

Figure 7.23 nMDS plot demonstrating the β diversity of bacterial microbiome composition in the post-DSS samples of WT and *Adamdec1*$^{-/-}$ mice. The pooling cages are indicated by the shape of mark representing the bacterial microbiome of each mouse (circle=Cage 1 and square=Cage 2). Genotypes are indicated by the colour (black=WT, red=*Adamdec1*$^{-/-}$). The original cage is indicated by the letters above each mark. Clustering of the samples according to the pooling cage and also original cage were observed.
KO: *Adamdec1*$^{-/-}$, WT: Wild type

7.3.2.2 ITS gene analysis

7.3.2.2.1 Verification of findings from Experiment 1 using the pre-pool samples

Relative abundances of fungi

The findings of the fugal microbiome analysis of Experiment 1 were verified using the pre-pool samples. The relative abundances of the classified fungi, examined at 6 taxonomic levels, were overall similar to that of Experiment 1. However, consistent with the bacterial microbiome analysis of Experiment 2, the differences in the relative abundance of some fungal taxonomic groups appeared greater between the pre-pool samples of the WT and *Adamdec1*$^{-/-}$ mice in comparison to Experiment 1 (Figure 7.24). In fact, in contrast to Experiment1, statistically significant differences in the relative abundances of 4 fungal taxonomic groups, examined at 6 taxonomic levels, were observed between the WT and *Adamdec1*$^{-/-}$ mice samples. These were *Ascomycota* at phylum level, *Catharellales* at order level, *Symbiotaphrina*| at genus level, and *Symbiotaphrina buchneri* at species level (Figure 7.25). The relative abundances of all of these taxonomic groups were significantly higher in the samples of *Adamdec1*$^{-/-}$ mice in comparison to the WT mice.

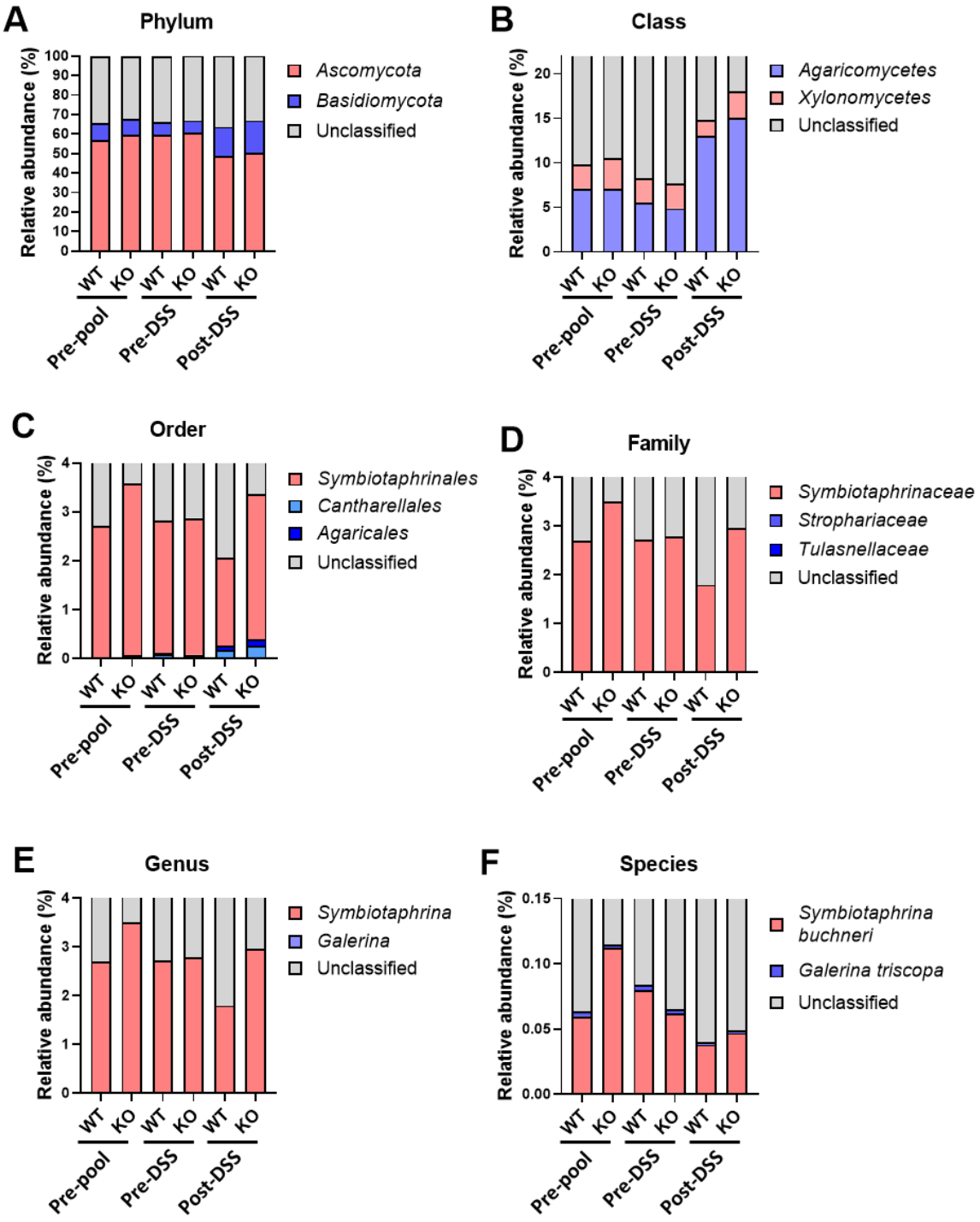

Figure 7.24 Global fungal composition of the microbiome in faecal samples from WT and *Adamdec1*$^{-/-}$ mice assessed at 6 taxonomic levels: phylum (A), class (B), order (C), family (D), genus (E) and species (F). Mean relative abundances according to genotype are shown in stacked bar graphs.
KO: *Adamdec1*$^{-/-}$, WT: Wild type

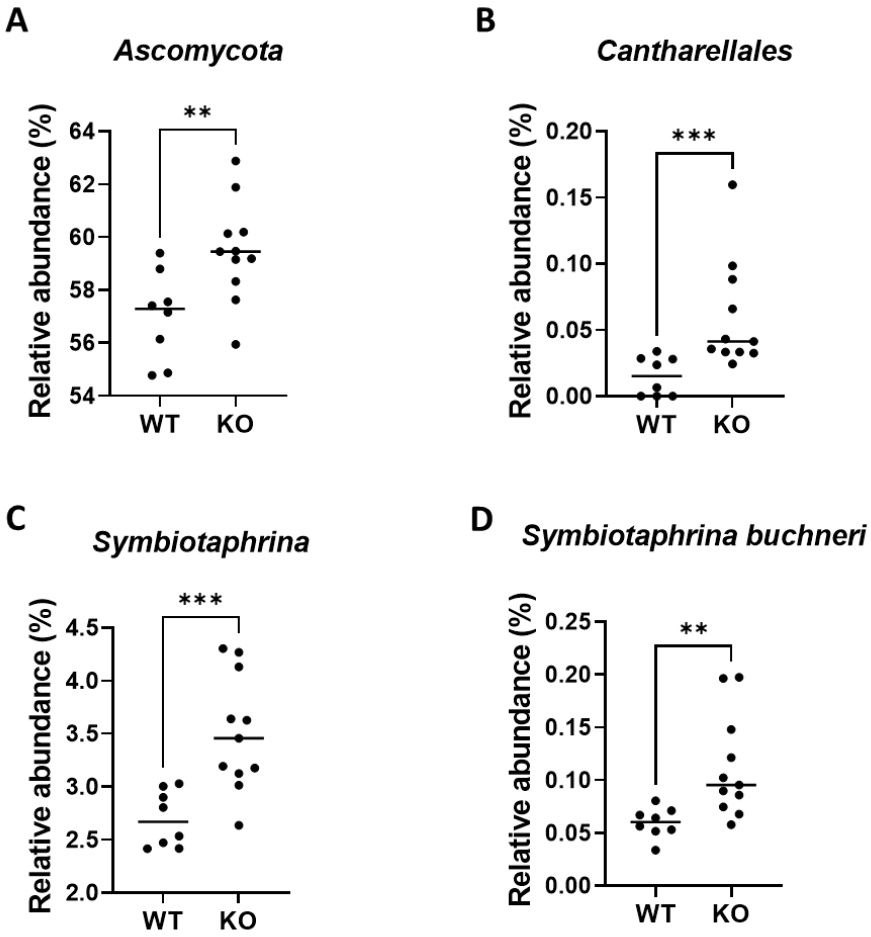

Figure 7.25 Differentially abundant fungal taxonomic groups in the microbiome of the pre-pool samples collected from WT and *Adamdec1*$^{-/-}$ mice assessed at phylum (A), order (B), genus (C) and species (D) levels. The relative abundances of these fungal taxonomic groups were all significantly higher in the *Adamdec1*$^{-/-}$ mice in comparison to WT mice. Mann-Whitney test was used. KO: *Adamdec1*$^{-/-}$, WT: Wild type, **: $p < 0.01$, ***: $p < 0.001$

Alpha diversity

In contrast to the ITS gene analysis in Experiment 1 and the 16S rRNA gene analysis of Experiment 2, there were differences in the alpha diversity of the fungal composition in the pre-pool samples of WT and *Adamdec1*$^{-/-}$ mice assessed by both Chao1 and Shannon indices (Figure 7.26). The alpha diversity of fungal microbiome composition was significantly higher in the *Adamdec1*$^{-/-}$ mice in comparison to the WT mice.

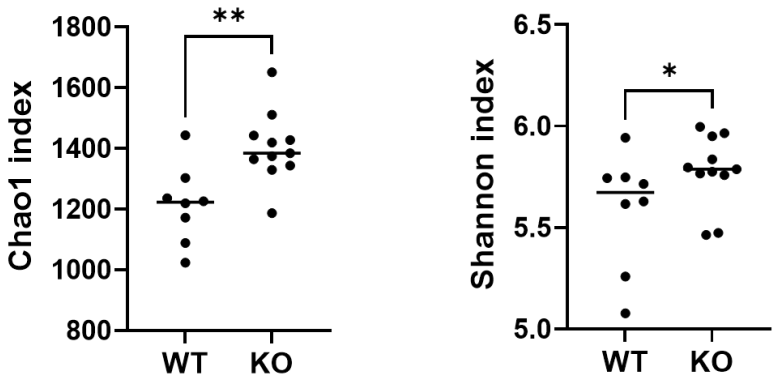

Figure 7.26 Alpha diversity of the fungal microbiome in the pre-pool samples of WT and *Adamdec1*$^{-/-}$ mice. Alpha diversity of the fungal microbiome in the pre-pool samples was significantly higher in the *Adamdec1*$^{-/-}$ mice in comparison to the WT mice by both Chao1 and Shannon indices. Mann-Whitney test was used.
KO: *Adamdec1*$^{-/-}$, WT: Wild type, *: $p < 0.05$, **: $p < 0.01$

Beta diversity

Beta diversity of the fungal compositions of pre-pool samples showed statistically significant clustering of the samples according to the individual cages, genotype and sibling state (Figure 7.27) (cage; PERMANOVA p=0.001 ANOSIM p=0.001, genotype; PERMANOVA p=0.025 ANOSIM p=0.004, sibling; p=0.003, ANOSIM p=0.002). However, when PERMANOVA was adjusted for the cage effect, both genotype and sibling state lost statistical significance in shaping the fungal composition of the samples. Similar to the bacterial composition, this indicated that the cage environment was the predominant driving factor in shaping the fungal microbiome composition of the WT and *Adamdec1*$^{-/-}$ mice. (See Appendix 9 for the detailed PERMANOVA and ANOSIM values.)

Figure 7.27 nMDS plot demonstrating the β diversity of the fungal microbiome composition in pre-pool samples of the WT and *Adamdec1*$^{-/-}$ mice. The individual cages are indicated by the shape of mark representing the microbiome of each mouse. Genotypes are indicated by the colour (black=WT, red=*Adamdec1*$^{-/-}$). Sibling state (S) is indicated above each mark. Clustering of the samples according to the individual cages were observed. Clustering of the samples according to genotype and sibling state were also observed.
KO: *Adamdec1*$^{-/-}$, WT: Wild type

7.3.2.2.2 Effect of pooling of cage on the intestinal fungal composition

Relative abundances of fungi

Similar to the 16S rRNA gene analysis, the pooling of 6 individual cages into 2 cages to cohouse the WT and *Adamdec1*$^{-/-}$ mice of different sibling state overall homogenised the difference in the relative abundances of classified fungal taxonomic groups observed between the pre-pool samples of the WT and *Adamdec1*$^{-/-}$ mice (Figure 7.24). The relative abundances of the 4 fungal taxonomic groups which were observed to be significantly different in the pre-pool samples of the WT and *Adamdec1*$^{-/-}$ mice were no longer statistically different between the pre-DSS samples of the WT and *Adamdec1*$^{-/-}$ mice. In fact, there were no statistical differences in the relative abundances of any of the classified fungi between the pre-DSS samples of the WT and *Adamdec1*$^{-/-}$ mice assessed at 6 taxonomic levels.

Alpha diversity

Similar to the effect of pooling of cages on the 16S rRNA gene analysis, alpha diversity of the fungal composition of WT mice did not change significantly by the pooling of mice, but alpha diversity of the *Adamdec1*$^{-/-}$ mice decreased significantly by the pooling of mice assessed by Chao1 and Shannon indices (Figure 7.28).

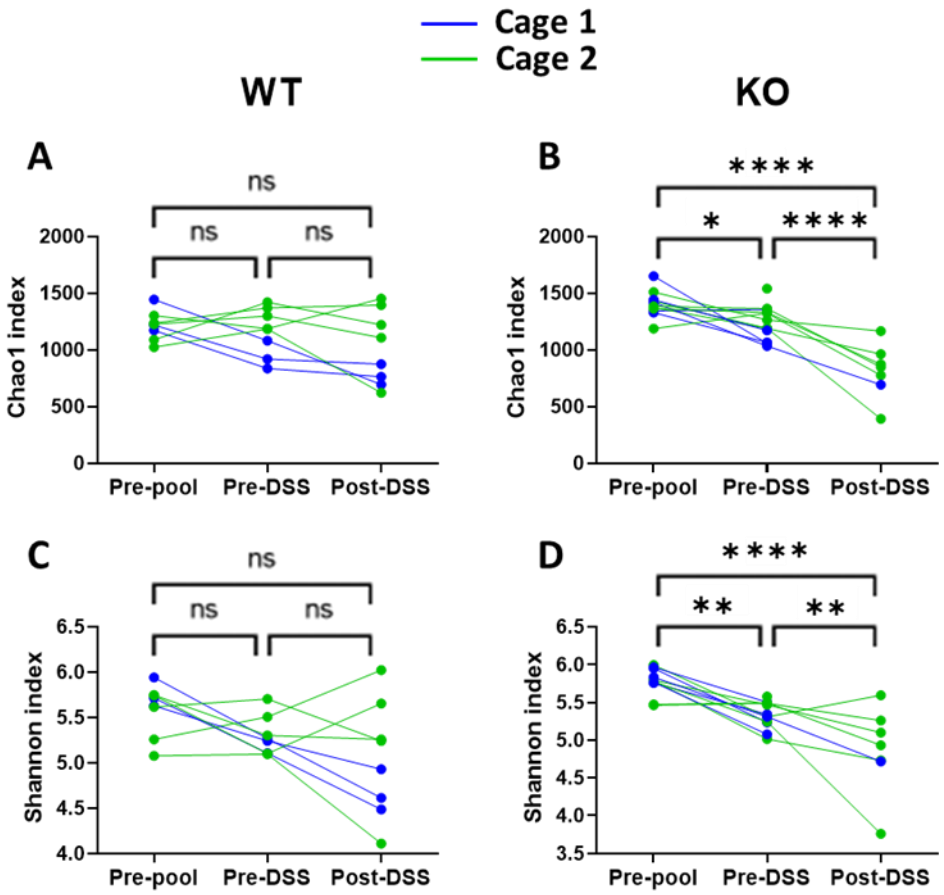

Figure 7.28 Change in the α diversity of WT and *Adamdec1*$^{-/-}$ mice fungal microbiome composition over pre-pool, pre-DSS and post-DSS timepoints assessed by Chao1 (A and B) and Shannon (C and D) indices. The mice in Cage 1 are indicated by blue dots and lines, and the mice in Cage 2 are indicated by green dots and lines. Alpha diversity of the WT mice, assessed by both Chao1 and Shannon indices, was not affected by the pooling of mice or by DSS-challenge. Alpha diversity of the *Adamdec1*$^{-/-}$ mice reduced significantly by the pooling of mice and by DSS-challenge, assessed by both Chao1 and Shannon indices. Kruskal-Wallis test was used.
KO: *Adamdec1*$^{-/-}$, WT: Wild type, *: $p < 0.05$, **: $p < 0.01$, ****: $p < 0.0001$, ns: Non-significant

Beta diversity

Once again, following the pooling of mice, a clear clustering of the samples according to the new cage was observed (Figure 7.29) which was statistically significant (PERNOVA p=0.001, ANOSIM p=0.002). Clustering of the samples according to the original cage was also observed to some degree (PERMANOVA p=0.003 ANOSIM p=0.005). However, when PERMANOVA was adjusted for the effect of pooling cage, the original cage effect was no longer statistically significant in shaping the fungal composition of the samples (p=0.266). Together with the findings from the β diversity of the ITS pre-pool samples, these findings suggested that the intestinal fungal microbiome composition was shaped by the individual cages that the mice were housed. Furthermore, similar to the bacterial microbiome analysis, this cage-specific composition was plastic and 8 weeks was long enough for the mouse fungal composition to lose the signature associated with the previous cage and acquired a new specific signature that was unique to the new cage. (See Appendix 10 for the detailed PERMANOVA and ANOSIM values.)

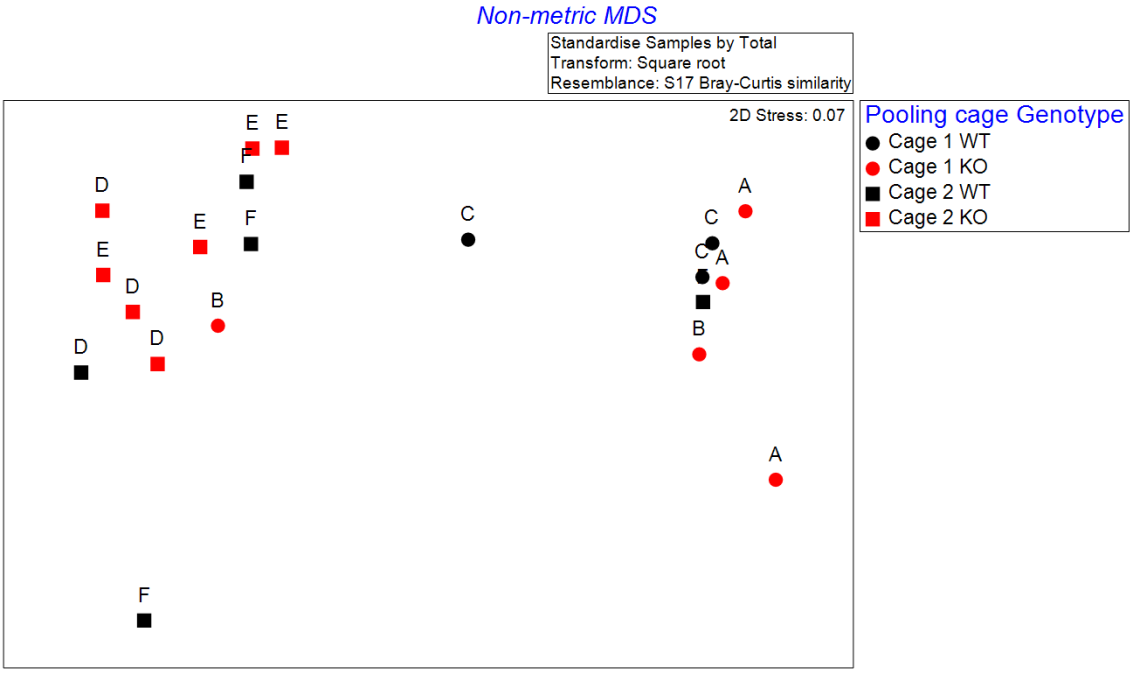

Figure 7.29 nMDS plot demonstrating β diversity of mycobiota composition in the pre-DSS samples of WT and *Adamdec1*$^{-/-}$ mice. Pooling cages are indicated by the shape of mark representing the mycobiome of each mouse (circle=Cage 1 and square=Cage 2). Genotypes are indicated by the colour (black=WT, red=*Adamdec1*$^{-/-}$). The original cages are indicated by the letters above each mark. Clear clustering of the samples according to the new pooling cage i.e. Cage 1 and Cage 2 were observed. The samples did not cluster according to the genotype.
KO: *Adamdec1*$^{-/-}$, WT: Wild type

7.3.2.2.3 Effect of DSS challenge on intestinal fungal composition

Relative abundances of fungi

The DSS challenge on the fungal composition of the WT and *Adamdec1*$^{-/-}$ mice was assessed using the post-DSS samples. The high proportion of the sequences being unclassified in the fungal microbiome analysis hindered a detailed evaluation of the effect of DSS challenge on the relative abundances of fungi.

Overall, at phylum level, DSS challenge resulted in an increase in the relative abundance of *Basidiomycota* and a decrease in the relative abundance of *Ascomycota* (Figure 7.24 A). An increase in the relative abundance of *Agaricomycetes* at class level (Figure 7.24 B), and an increase in the relative abundances of *Cantharellales* and *Agaricales* were observed at order level (Figure 7.24 C) as a result of the DSS challenge. At family, genus and species levels, the

effect of the DSS challenge was minimal on the relative abundances of the classified fungal taxonomic groups in the *Adamdec1*$^{-/-}$ mice (Figure 7.24 D, E and F). Whereas the relative abundance of *Symbiotaphrina* decreased in the WT mice by DSS challenge (Figure 7.24 E). There were no statistical differences in the relative abundances of any of the classified fungi between the WT and *Adamdec1*$^{-/-}$ mice assessed at 6 taxonomic levels.

Alpha diversity

Similar to the 16S rRNA gene analysis, the alpha diversity of fungal composition did not change by the DSS challenge in the WT mice. However the α diversity of the *Adamdec1*$^{-/-}$ mice decreased significantly by DSS challenge assessed by both Chao1 and Shannon indices (Figure 7.28).

Beta diversity

As anticipated, similar to the 16S rRNA gene analysis, β diversity of the pre and post-DSS samples showed a clear clustering of samples according to the DSS treatment state (Figure 7.30). This was confirmed to be statistically significant by both PERMANOVA (p=0.001) and ANOSIM (p=0.001). Additionally clustering of the pre- and post-DSS samples according to the pooling cage was also observed (Figure 7.30). This was confirmed to be statistically significant by both PERMANOVA (p=0.010) and ANOSIM (p=0.019). Even after adjusting PERMANOVA for the effect of DSS challenge, the effect of pooling cage remained statistically significant (p=0.012) indicating that the DSS treatment state and pooling cage independently shaped the fungal composition of the pre- and post-DSS samples that the change in the fungal composition by DSS challenge was unique in each pooled cage. Once again, clustering of the samples based on genotype was not observed which was confirmed by both PERMANOVA (p=0.566) and ANOSIM (p=0.648). (See Appendix 11 for the detailed PERMANOVA and ANOSIM values.)

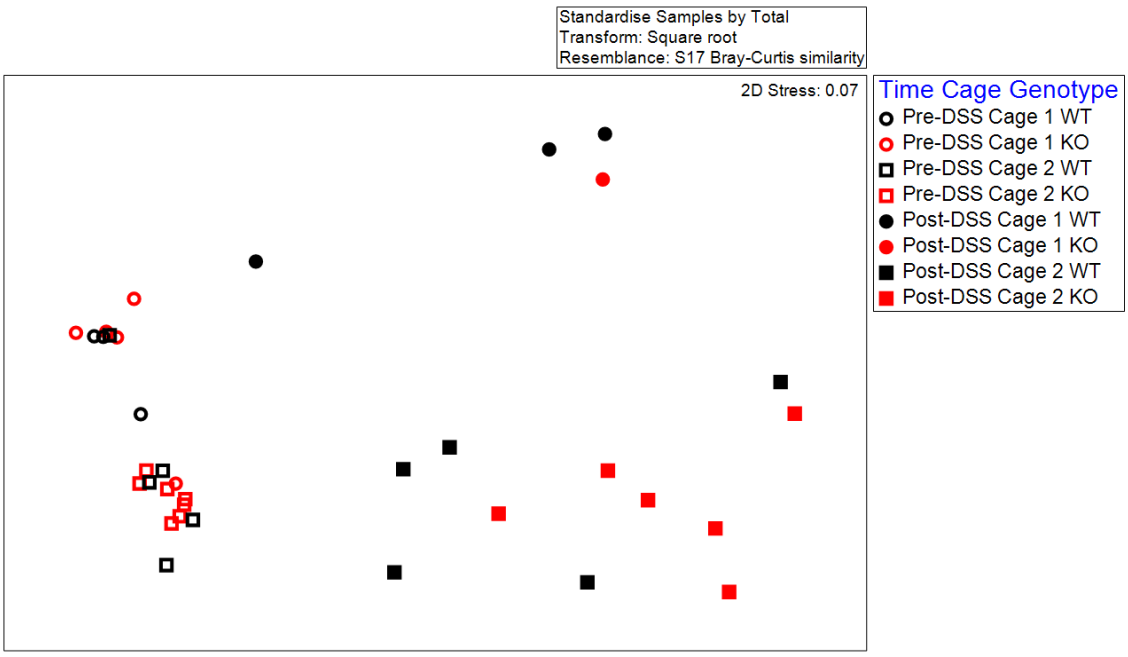

Figure 7.30 nMDS plot demonstrating the β diversity of mycobiome composition in the pre and post-DSS samples of WT and *Adamdec1*$^{-/-}$ mice. DSS challenge state is indicated by the open or close feature of the mark representing the microbiome of each mouse (open=pre-DSS, close=post-DSS). The pooling cage is indicated by the shape of mark (circle=Cage 1 and square=Cage 2). Genotype is indicated by the colour (black=WT, red=*Adamdec1*$^{-/-}$). Clustering of the samples according to the DSS challenge state and pooling cage were observed.
KO: *Adamdec1*$^{-/-}$, WT: Wild type

Beta diversity of the post-DSS samples alone once again showed clear clustering of the samples according to the pooling cage (Figure 7.31) which was statistically significant (PERMANOVA p=0.001, ANOSIM p=0.001). Additionally, clustering of the samples according to the original cage was also observed (PERMANOVA p=0.001 ANOSIM p=0.014). In contrast to the 16S rRNA gene analysis of the post-DSS samples for β diversity, when PERMANOVA was adjusted for the effect of pooling cage, the effect of original cage was no longer statistically significant in shaping the fungal composition of the samples. These findings indicated that the pooling cage was the factor that predominantly shaped the fungal composition in the post-DSS samples of WT and *Adamdec1*$^{-/-}$ mice. (See Appendix 12 for the detailed PERMANOVA and ANOSIM values.)

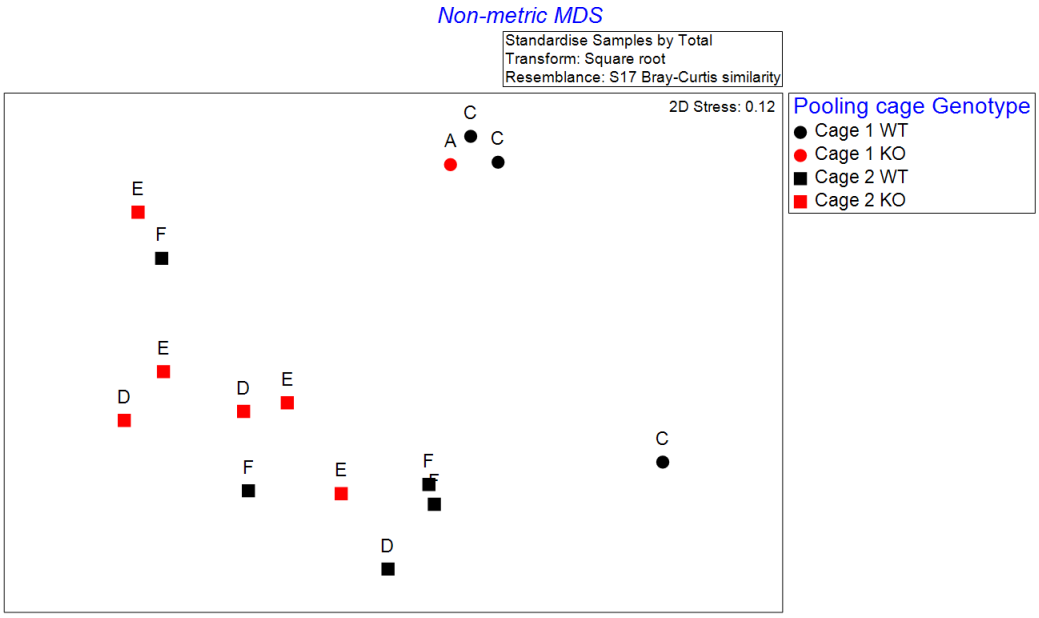

Figure 7.31 nMDS plot demonstrating the β diversity of mycobiome composition in the post-DSS samples of WT and *Adamdec1*$^{-/-}$ mice. The pooling cages are indicated by the shape of mark representing the mycobiome of each mouse (circle=Cage 1 and square=Cage 2). Genotypes are indicated by the colour (black=WT, red=*Adamdec1*$^{-/-}$). The original cages are indicated by the letters above each mark. Clustering of the samples according to the pooling cage was observed. KO: *Adamdec1*$^{-/-}$, WT: Wild type

7.3.2.3 Link between the bacterial and fungal compositions of the microbiome and the severity of systemic response to DSS challenge

To determine if there were bacterial and/or fungal compositions that were associated with the severity of response to DSS challenge, β diversity of both bacterial and fungal compositions in the pre-pool, pre-DSS and post-DSS samples were assessed for clustering of the samples according to the severity of weight loss using PERMANOVA and ANOSIM. However, no statistically significant clustering of the samples was seen according to the severity of the DSS-induced weight loss at all time points. (See Appendix 5 -12.)

Additionally, identification of the bacterial strains reported to influence the susceptibility to DSS-induced inflammation was attempted using the pre-DSS samples since current evidence suggested that the gut microbial composition prior to DSS challenge was likely to be linked to the severity of DSS-induced inflammation.[236,285,286] Sequences matched to *Duncaniella muricolitica* strain A60

and *Sangeribacter muris* strain A43 (100% identity) could be extracted in our samples. While sequences being highly similar to *Alistipes okayasuensis* strain A61 were retrieved, they presented only 99.73% identity. None or only a few single short sequences were matched to *Anaerostipes faecis* strain A14. Thus only the relative abundances of *Duncaniella muricolitica* strain A60, which is reported to exacerbate DSS-induced colitis, and *Sangeribacter muris* strain A43, which is reported to ameliorate DSS-induced colitis, were examined against the severity of weight loss in the mice. The mean relative abundance of *Duncaniella muricolitica* and *Sangeribacter muris* were 1.93% (SD=1.30) and 1.06% (SD=1.18) respectively in the mice used in Experiment 2 (Table 7.3). The mean relative abundance of *Duncaniella muricolitica* in the mice used in Experiment 2 was higher than the reported global mean abundance of 0.54%, which was analysed using mice faecal microbiome data collected from 31 institutes across 12 countries.[286] In contrast, the mean relative abundances of *Sangeribacter muris* in the mice used in Experiment 2 was lower than the reported global mean abundance of 6.2%.[286]

There were no differences in the relative abundances of *Duncaniella muricolitica* or *Sangeribacter muris* between the mice which exhibited no/mild weight loss and the mice which exhibited severe weight loss by the DSS-challenge (Figure 7.32). To support this, there were no significant correlations between the severity of weight loss by DSS challenge and the relative abundances of these two bacterial species (Figure 7.33).

Bacteria	Effect on DSS-colitis reported	Mean relative abundance (95% CI)	Ref
Duncaniella muricolitica	Exacerbation	1.93% (0.528 – 3.332)	286
Alistipes okayasuensis	Exacerbation	N/A	
Sangeribacter muris	Amelioration	1.06% (0.542 – 1.578)	
Anaerostipes faecis	Amelioration	N/A	

Table 7.33 Bacterial strains that have been reported to influence the severity of DSS-induced colitis and their relative abundances in the mice used in Experiment 2. The mean relative abundances of *Alistipes okayasuensis* and *Anaerostipes faecis* could not be assessed as their sequence matches were less than 100%.
CI: Confidence interval, N/A: Not applicable, Ref: Reference

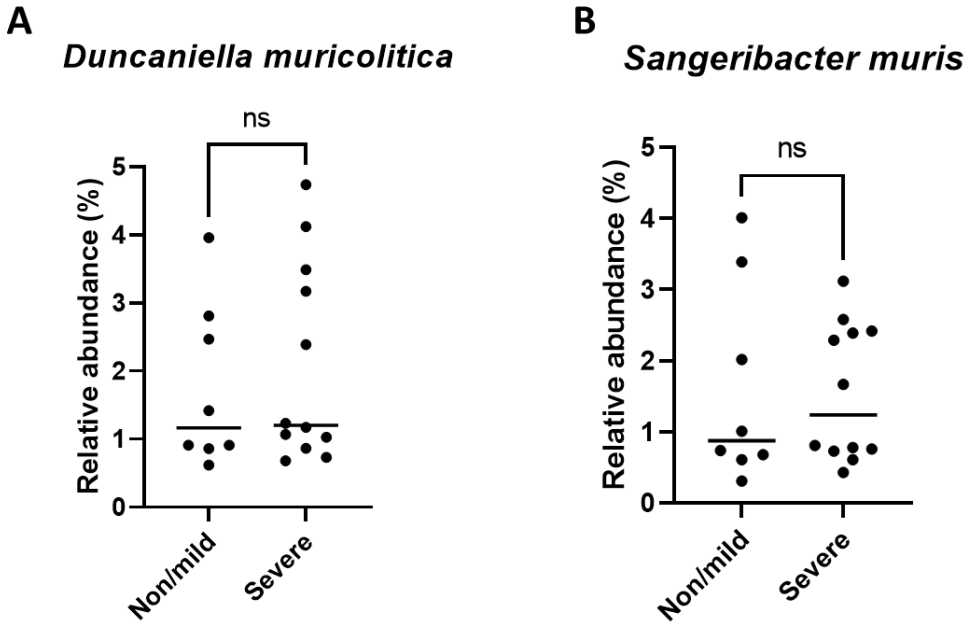

Figure 7.32 The relative abundances of *Duncaniella muricolitica* (A) and *Sangeribacter muris* (B) according to the severity of weight loss induced by DSS-challenge. Mann-Whitney test was used. Non/mild = weight loss < 10%, severe = weight loss ≥ 10%
ns: Non-significant

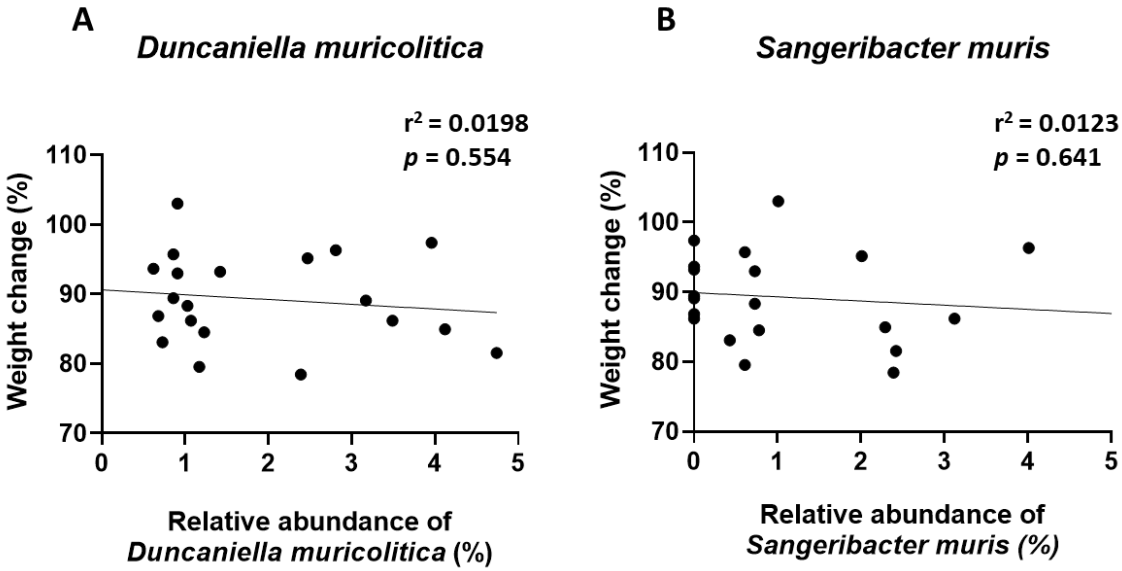

Figure 7.33 Correlation analysis between the DSS-induced severity of weight loss and relative abundance of *Duncaniella muricolitica* (A) and *Sangeribacter muris* (B). There was no significant correlation between the severity of weight loss and the relative abundance of *Duncaniella muricolitica* or *Sangeribacter muris*. Pearson correlation coefficient was used.
r^2: Coefficient determination

7.3.2.4 Difference in the microbiome between the *Adamdec1*$^{-/-}$ mice in pooling Cage 1 and Cage 2

The *Adamdec1*$^{-/-}$ mice in Cage 1 and Cage 2 exhibited a different response to the DSS challenge, where the *Adamdec1*$^{-/-}$ mice in Cage 1 lost significantly more weight in comparison to the *Adamdec1*$^{-/-}$ mice in Cage 2 (Figure 6.5). The expression of some of the immune and epithelial cell associated genes of the *Adamdec1*$^{-/-}$ mice in Cage 1 and Cage 2 also exhibited opposite trends (Table 6.7). Thus, the microbiome in the pre-DSS samples of the *Adamdec1*$^{-/-}$ mice in Cage 1 and Cage 2 were examined to determine if there were any differences between them which could potentially be linked to the difference in susceptibility to the DSS challenge.

7.3.2.4.1 Bacterial and fungal relative abundance

With regards to the relative abundance of bacteria, 8 different bacterial taxonomic groups, assessed at 4 taxonomic levels, were observed to be significantly different between the *Adamdec1*$^{-/-}$ mice in Cage 1 and Cage 2 (Figure 7.34).

At phylum level, the relative abundance of *Candida Saccharibacteria* and *Proteobacteria* were significantly lower in the *Adamdec1*$^{-/-}$ mice in Cage 1 in comparison to Cage 2 (*Candida Saccharibacteria* Cage 1 mean=0.002%, Cage 2 mean=0.01%; *Proteobacteria* Cage 1 mean=0.25%, Cage 2 mean=0.58%) (Figure 7.34 A and B). The relative abundance of *Tenericutes* was significantly higher in the *Adamdec1*$^{-/-}$ mice in Cage 1 in comparison to Cage 2 (Cage 1 mean=0.18%, Cage 2 mean=0.04%) (Figure 7.4 C).

At family level, the relative abundance of *Muribaculaceae* was significantly higher and the relative abundance of *Sutterellaceae* was significantly lower in the *Adamdec1*$^{-/-}$ mice in Cage 1 in comparison to Cage 2 (*Muribaculaceae* Cage 1 mean=64.90%, Cage 2 mean=56.86%; *Sutterellaceae* Cage 1 mean=0.05%, Cage 2 mean=2.04) (Figure 7.34 F and G).

At genus level, the relative abundance of *Bacteroides* was significantly higher and the relative abundance of *Paramuribaculum* was significantly lower in the in the *Adamdec1*$^{-/-}$ mice in Cage 1 in comparison to Cage 2 (*Bacteroides* Cage 1 mean=4.12%, Cage 2 mean=2.04%; *Paramuribaculum* Cage 1 mean=0.15%, Cage 2 mean=0.47%) (Figure 7.34 F and G).

At species level, the relative abundance of *Turicimonas muris* was significantly lower in the *Adamdec1*$^{-/-}$ mice in Cage 1 (mean=0.04%) in comparison to Cage 2 (mean=0.21%) (Figure 7.34 H).

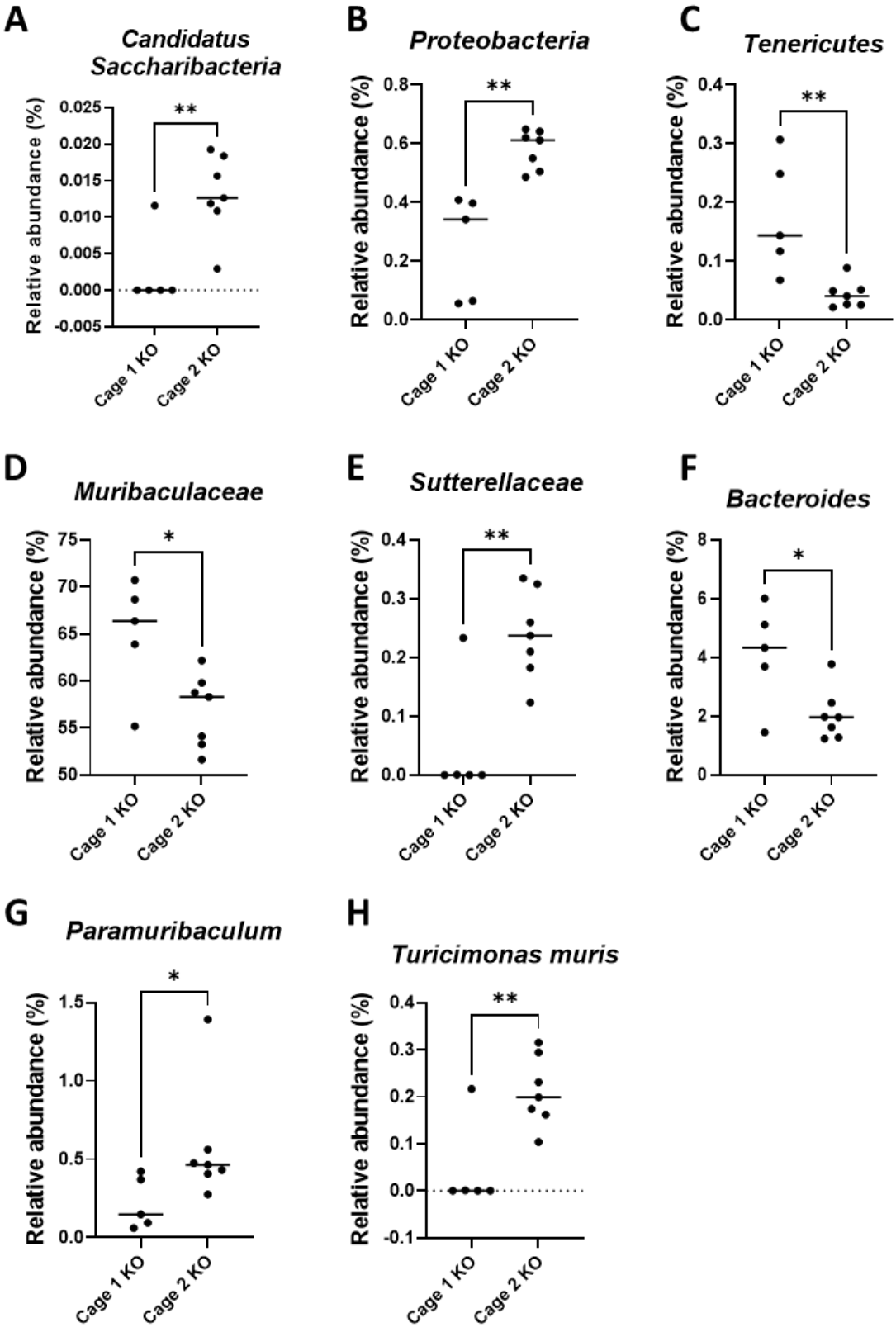

Figure 7.34 Relative abundances of the differentially abundant bacterial taxonomic groups compared between the pre-DSS microbiome of *Adamdec1*$^{-/-}$ mice in Cage 1 and Cage 2 assessed at phylum (A, B and C), family (D and E), genus (F and G) and species (H) levels. Mann-Whitney test was used.
KO: *Adamdec1*$^{-/-}$, *: $p < 0.05$, **: $p < 0.01$

Furthermore, the relative abundances of the 2 bacterial species reported to influence the susceptibility to DSS-induced colitis were examined between the *Adamdec1*$^{-/-}$ mice in Cage 1 and Cage 2. This revealed that the relative abundance of *Duncaniella muricolitica*, reported to exacerbate DSS-induced colitis, was significantly higher in the *Adamdec1*$^{-/-}$ mice in Cage 1 in comparison to Cage 2 (Cage 1 mean=3.12%, Cage 2 mean=0.91%) (Figure 7.35 A).[286] There was no significant difference in the relative abundance of *Sangeribacter muris*, reported to ameliorate DSS-induced colitis, between the *Adamdec1*$^{-/-}$ mice in Cage 1 (mean=2.30%) in comparison to Cage 2 (mean=0.73%) (Figure 7.35 B).[286]

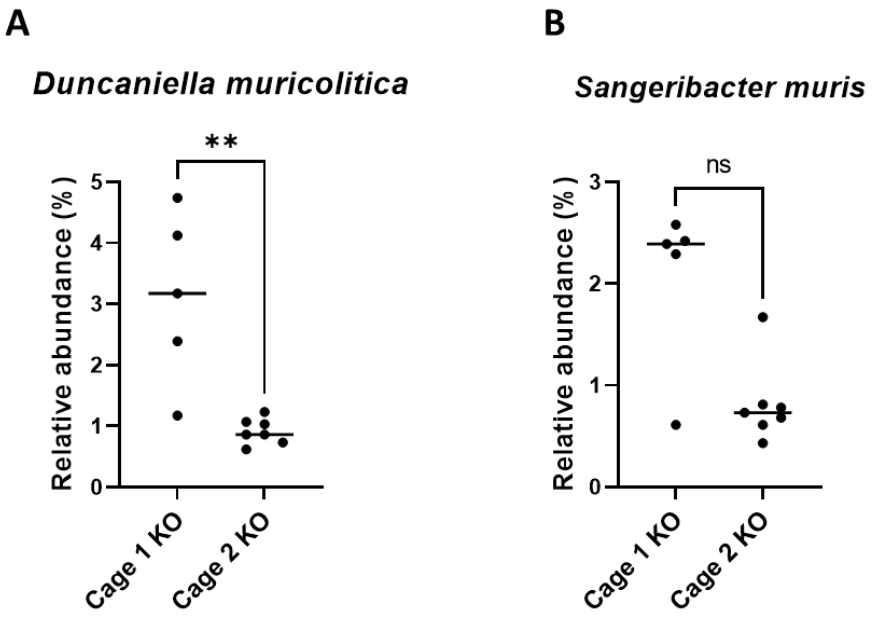

Figure 7.35 Relative abundances of *Duncaniella muricolitica* and *Sangerbacter muris* compared between the microbiome of *Adamdec1*$^{-/-}$ mice in Cage 1 and Cage 2. Mann-Whitney test was used.
KO: *Adamdec1*$^{-/-}$, **: $p < 0.01$, ns: Non-significant

Beta diversity of the pre-DSS samples from the mice (Chapter 7.3.2.1) indicated that the bacterial microbiome composition was shaped significantly by the pooling cage (Figure 7.16, Appendix 6). Thus, in order to determine whether the significantly different relative abundances of the 8 bacterial taxonomic groups observed between the *Adamdec1*$^{-/-}$ mice in Cage 1 and Cage 2 could be simply secondary to the cage effect irrespective of the genotype, the relative abundances of these 8 bacterial taxonomic groups were assessed between the

WT mice in Cage 1 and Cage 2. This revealed that only Bacteroides was significantly different (p = 0.003) in the WT mice in Cage 1 (mean=4.12%) in comparison to the WT mice in Cage 2 (mean=2.04%), the trend of which was the same as the observation in the *Adamdec1*$^{-/-}$ mice.

With regards to the relative abundance of fungi, the relative abundance of *Basidiomyota* was found to be significantly higher in the *Adamdec1*$^{-/-}$ mice in Cage 1 (mean=6.59%) in comparison to Cage 2 (mean=5.83%) (Figure 7.36). There were no differentially abundant fungal taxonomic groups assessed at 6 taxonomic levels between the WT in Cage 1 and Cage 2 (data not shown).

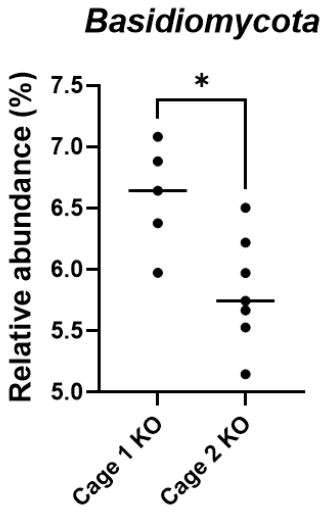

Figure 7.36 Relative abundance of Basidiomycota compared between the microbiome of *Adamdec1*$^{-/-}$ mice in Cage 1 and Cage 2. One-way ANOVA test was used.
KO: *Adamdec1*$^{-/-}$, *: $p < 0.05$,

These findings indicated that the 7 bacterial and 1 fungal taxonomic groups were differentially abundant between the microbiome of the *Adamdec1*$^{-/-}$ mice in Cage 1 and Cage 2, which were specific to the knockout mice. It is possible that the difference in the microbiome between the *Adamdec1*$^{-/-}$ mice in Cage 1 and Cage 2 attributed to the cage-dependant difference in the degree of DSS-induced inflammation in these mice.

Alpha diversity

Alpha diversity of bacterial and fungal microbiome in *Adamdec1*$^{-/-}$ mice in Cage 1 and Cage 2 were compared. There was no significant difference in the bacterial α diversity between the *Adamdec1*$^{-/-}$ mice in Cage 1 in comparison to Cage 2 by Chao1 index (Figure 7.37 A). However, the α diversity of the fungal microbiome was significantly lower in the *Adamdec1*$^{-/-}$ mice in Cage 1 in comparison to Cage 2 (Figure 7.37 B). There were no significant differences in bacterial or fungal α diversity between the *Adamdec1*$^{-/-}$ mice in Cage 1 and Cage 2 assessed by Shannon index (data not shown).

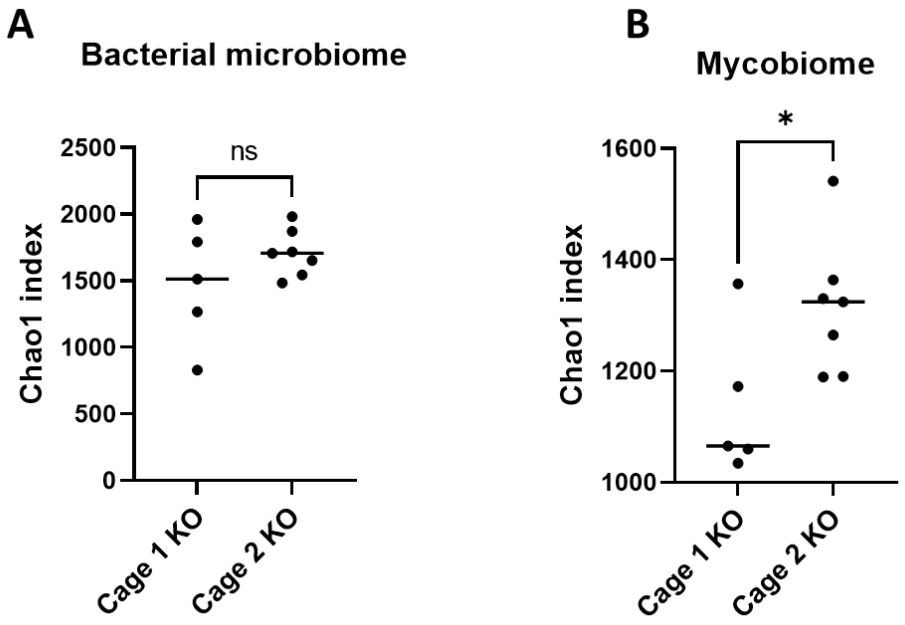

Figure 7.37 Bacterial (A) and fungal (B) α diversity by Chao1 index compared between the microbiome of *Adamdec1*$^{-/-}$ mice in Cage 1 and Cage 2. Mann-Whitney test was used.
KO: *Adamdec1*$^{-/-}$, *: $p < 0.05$, ns: Non-significant

Beta diversity

Within the cluster of Cage 1 samples, the dispersion value between the WT and *Adamdec1*$^{-/-}$ samples was 1.00 (Figure 7.38). In contrast, within the cluster of Cage 2 samples, the dispersion value between the WT and *Adamdec1*$^{-/-}$ samples was only 0.029 (Figure 7.38). This indicated that there was a greater dissimilarity between the WT and *Adamdec1*$^{-/-}$ samples within Cage 1 cluster than the WT and *Adamdec1*$^{-/-}$ samples within Cage 2 cluster. This mirrors the observation that the weight loss of the WT and *Adamdec1*$^{-/-}$ was significantly different in Cage 1 but not in Cage 2.

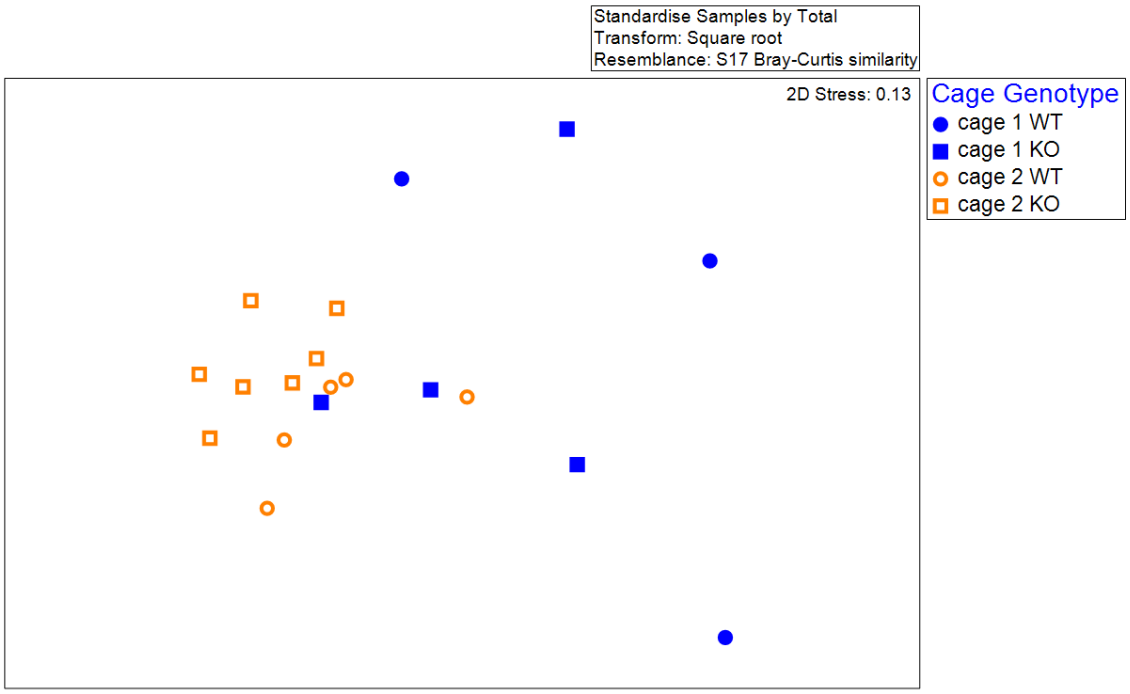

Figure 7.38 nMDS plot demonstrating the β diversity of bacterial microbiome composition in the pre-DSS samples of WT and *Adamdec1*$^{-/-}$ mice in Cage 1 and Cage 2. The bacterial microbiome composition of each mouse in cage 1 are indicated by blue marks and Cage 2 are indicated by orange marks. WT mice are indicated by circle and *Adamdec1*$^{-/-}$ mice are indicated by square marks.
KO: *Adamdec1*$^{-/-}$, WT: Wild type

7.4 Discussion

Experiment 1 examined the microbiome in faecal samples collected from young WT, heterozygous and *Adamdec1*$^{-/-}$ mice at the time of weaning. These mice were cohoused per litter since their birth with their parents. The findings revealed that both bacterial and fungal microbiome compositions were shaped by the cage and sibling state, assessed by β diversity using features observed. This was plausible given that mice are coprophagic and, therefore, are exposed to each other's microbiota within individual cages. By examining the relative abundances of the classified bacterial and fungal taxonomic groups in these samples, 3 bacterial taxonomic groups: *Lachnospiraceae*, *Duncaniella dubosii* and *Ligilactobicillus apodeme* were found to be differentially abundant between the WT and *Adamdec1*$^{-/-}$ mice. However, this required validation due to the low number of samples (WT n=2, *Adamdec1*$^{-/-}$ n=8). These findings, nevertheless, gave valuable knowledge for the planning of the experiment to characterise the immune response in the WT and *Adamdec1*$^{-/-}$ mice upon induction of DSS-induced colitis (Chapter 6). Based on the findings from Experiment 1 of this chapter, in an attempt to minimise the effect of the cage and sibling specific-microbiota composition, which may influence the severity of DSS-induced immune response, the mice were pooled into larger cages. By this, the mice from smaller individual cages were cohoused for 8 weeks mixing the sibling state and genotype prior to the DSS administration.

Experiment 2 examined the microbiome within the faecal samples collected from 20 sex-matched mice, which were caged per genotype in 6 individual cages, except one cage, for more than 10 weeks. This validated the finding from Experiment 1 that individual cages shaped both bacterial and fungal microbiome compositions. However, the effect of sibling state on the microbiome composition diminished, which suggested that the sibling-specific signature was transient and was likely to have been due to the effect of the parental microbiota via coprophagia. Although the statistical analysis of the β diversity using the features observed in these samples did not find the clustering of the samples according to the genotype to be significant, the assessment of the relative abundance of the classified individual bacteria and fungi revealed that 6 bacterial taxonomic groups: *Firmicutes, Lachnospiraceae*, *Erysipelotrichaceae*, *Bacteroides*, *Bacteroides acidifaciens* and *Turicibacter sanguinis*, and 4 fungal taxonomic groups: *Ascomycota*, *Cantharellales*, *Symbiotaphrina* and *Symbiotaphrina buchneri* were differentially

abundant between the microbiome of WT and *Adamdec1*$^{-/-}$ mice. These findings are consistent with numerous studies reporting a genotype-specific difference in the relative abundances of bacteria where mice were cohoused per genotype or housed individually.[290–293,302–304]

The pooling of the mice from 6 individual cages into 2 larger cages, thereby cohousing the WT and *Adamdec1*$^{-/-}$ mice for 8 weeks, completely homogenised the difference in the relative abundances of these 6 bacterial and 4 fungal taxonomic groups between the microbiome of WT and *Adamdec1*$^{-/-}$ mice observed in the pre-pooling samples. Though the relative abundance of another bacterial species, *Paramuribaculum intestinale*, was found to be significantly lower in the *Adamdec1*$^{-/-}$ mice in comparison to the WT mice following cohousing. *Paramuribaculum intestinale* is a relatively newly identified bacterial species in the murine gut microbiota whose characteristics remain largely unexplored. Thus, the significance of this finding is to be elucidated.[305] The homogenisation of the differentially abundant bacterial and fungal taxonomic groups following the pooling of mice was consistent with numerous studies where statistically significant differences in the microbiome according to genotype was no longer detected after cohousing of WT and mutant mice.[303,306,307] The duration of cohousing of mice was 4 weeks in these studies, whereas the duration of cohousing in one study, which reported persistence of the genotype-dependent difference in the microbiome of mice was 2 weeks.[304] Some of these studies have also reported that the degree of DSS-induced colitis in the WT and mutant mice became similar to each other following the cohousing of mice and normalisation of the genotype-specific difference in the microbiome.[303,306,307] In this project, the differentially abundant bacterial and fungal taxonomic groups observed between the WT and *Adamdec1*$^{-/-}$ mice microbiome before the pooling of mice were no longer detectable after 8 weeks of cohousing of the WT and *Adamdec1*$^{-/-}$ mice. The bacterial and fungal microbiome features assessed by β diversity also confirmed that there was no dissimilarity between the microbiome of WT and *Adamdec1*$^{-/-}$ mice. Furthermore, the DSS challenge altered the bacterial and fungal microbiome similarly in the WT and *Adamdec1*$^{-/-}$ assessed by both relative abundances of the classified bacteria and fungi, and β diversity using the features observed. Despite these, overall, the *Adamdec1*$^{-/-}$ mice demonstrated a significantly greater weight loss induced by the DSS challenge. This suggested that the exaggerated form of DSS-induced colitis in the absence of ADAMDEC1 was unlikely to be related to the gut microbiota.

Interestingly, the WT mice's bacterial and fungal α diversities were not affected by the pooling of mice and DSS challenge, but the bacterial and fungal α diversities of the *Adamdec1*$^{-/-}$ mice decreased significantly by the pooling of mice and DSS challenge. Previous studies have reported reductions in α diversity by DSS challenge in WT mice and lower α diversity in mutant mice in an association with a greater susceptibility to DSS-induced colitis in comparison to WT mice.[92,303,308,309] The finding from this project suggested that the α diversity in the *Adamdec1*$^{-/-}$ mice was possibly more susceptible to environmental changes, although the reason behind the reduction in α diversity in *Adamdec1*$^{-/-}$ mice by the pooling of mice is unknown.

Decidedly, excluding the DSS effect which was iatrogenic, throughout this analysis, the cage effect was the predominant and statistically significant driver for shaping the microbiome composition assessed by β diversity of the observed features. Furthermore, this cage-specific microbiome composition was plastic and 8 weeks was long enough for both bacterial and fungal microbiome composition to lose the signature associated with the previous cage and acquire a new specific signature unique to the new cage. The exception to this was the original cage effect regaining statistical significance in shaping the bacterial composition of the post-DSS samples. However, the number of samples used for the analysis of this timepoint was smaller (Table 7.2), with no samples available from the original cage B and only 1 sample available from the original cage A. PERMANOVA and ANOSIM tests are known to generate greater significance when the number of samples is small and exhibit great dispersion.[310] This observation, therefore, requires further validation. The finding of the cage effect being the predominant and statistically significant driver for shaping the microbiome composition was consistent with a previous study. The cage effect was shown to possess the strongest influence on the bacterial microbiome composition of mice, accounting for 31.7% of the observed variance in comparison to other factors such as genetic background and sex.[311] Considering that the cage environment is highly controlled and standardised in the setting of laboratory mice yet much more influential on the microbiome variability than the genotype, these findings highlight the minor influential role of the host's genetic background on the gut microbiome. This is also consistent with a study which examined the human gut microbiome, where only 1.9 – 8.1% of the inter-person microbiota variability was attributed by the host's genetic

background in comparison to environmental factors attributing for 22 – 36% of the variability in the gut microbiome.[264]

Additionally, in this chapter, potential bacterial and fungal compositions that may be associated with variability in response to DSS challenge were explored. However, using β diversity of the features observed, there was no evidence to suggest the presence of specific microbiome composition in association with variability in DSS-induced weight loss in the mice used in this project. In addition to this, 4 bacterial species that have recently been shown to influence the severity of DSS-induced colitis were searched in the sequences obtained to determine whether the relative abundances of these species were linked to the severity of DSS-induced weight loss. This resulted in the detection of only two of these bacterial species, *Duncaniella muricolitica* and *Sangeribacter muris*. However, there were no statistical differences in the relative abundances of these two bacterial species between the mice that exhibited no/mild weight loss and the mice that exhibited severe weight loss induced by the DSS challenge.

In order to gain more insight into the explanation behind the different degrees of DSS-induced weight loss observed in the *Adamdec1*$^{-/-}$ mice in Cage 1 and Cage 2, the microbiomes of the *Adamdec1*$^{-/-}$ mice in Cage 1 and Cage 2 were examined against each other. This revealed the relative abundances of 7 bacterial taxonomic groups: *Candidatus Saccharibacteria*, *Proteobacteria*, *Tenericutes*, *Muribaculaceae*, *Sutterellaceae*, *Paramuribaculum*, *Turicimonas muris* and *Duncaniella muricolitica*, and 1 fungal phylum, *Basidiomycota* were significantly different in the pre-DSS samples collected from the *Adamdec1*$^{-/-}$ mice in Cage 1 and Cage 2 that were specific to the knockout mice. Furthermore, the dispersion analysis using the β diversity of bacterial microbiome composition in the pre-DSS samples revealed that the difference in the microbiome composition of WT and *Adamdec1*$^{-/-}$ mice was greater within Cage 1 than the difference in microbiome composition between the WT and *Adamdec1*$^{-/-}$ mice within Cage 2. This mirrored the pattern of DSS-induced weight loss in which the difference in weight loss between the WT and *Adamdec1*$^{-/-}$ mice in Cage 1 was greater in comparison to cage 2. These findings raise the possibility that the difference in the degree of DSS-induced weight loss between the *Adamdec1*$^{-/-}$ mice in Cage 1 and Cage 2 may have been rendered by the difference in their microbiome, which influenced their immune response to the DSS-induced inflammation differently.

In summary, the findings suggest that the difference in the severity of DSS-induced response between the WT and *Adamdec1*$^{-/-}$ mice was unlikely to be mediated through the influence of ADAMDEC1 on the microbiota. However, the cage-dependent variability in response to the DSS challenge exhibited by the *Adamdec1*$^{-/-}$ mice could possibly be linked to the difference in their microbiota. The ameliorated degree of DSS-induced weight loss in the *Adamdec1*$^{-/-}$ mice in Cage 2 was consistent with previously reported homogenisation of both genotype-specific micriobiome and genotype-dependent difference in the severity of DSS-induced colitis by cohousing of WT and mutant mice.[303,306,307] It is likely that the effect of some unknown environmental factors had rendered the difference in the microbiome of the *Adamdec1*$^{-/-}$ mice in Cage 1 and Cage 2. However, the exact reason or mechanism behind the cage-dependent difference in the microbiome of *Adamdec1*$^{-/-}$ mice which was specific to the knockout mice is unknown.

The findings from this chapter suggested that in order to accurately assess any potential phenotypic difference of mice attributed by the difference in genotype, mice of different genotypes should be cohoused in order to ensure that any phenotypic differences observed are not mediated by their cage-specific difference in the microbiome. However, any potential genotype-specific microbiome signatures are likely to be diminished by cohousing. Thus, if the genotype-dependent phenotypic difference was mediated via genotype-dependent microbiome composition, the phenotypic difference may be more subtle and difficult to detect following cohousing. Furthermore, cohousing may achieve homogenisation of the microbiome of mice within a cage but this occurs concomitantly with an acquisition of a new cage-specific microbiome composition. This might lead to a cage-dependant variability in the phenotype of mice, as observed in the *Adamdec1*$^{-/-}$ mice in Cage 1 and Cage 2, which may affect the reproducibility of results. Overall, the findings from this chapter indicated, first of all, that the role of ADAMDEC1 in the immune response during DSS-induced inflammation was unlikely to be mediated by involving the gut microbiome. The findings also importantly highlighted the greater influential power of environmental factors on the gut microbiome in comparison to genotype, and the complex interplay between the host's genotype, environment and phenotype, as well as crucial challenges to be considered when designing experiments to investigate the relationship between these factors.

Chapter 8
General discussion

8.1 Summary of findings

Chapter 3:

- *ADAMDEC1* was induced in THP-1 cells via activations of TLR2, TLR4, NOD2, FcγR, PKC, TNFR1 and TNFR2, CSF1R, IL1R1, IL6R and IFNAR.
- Induction of *ADAMDEC1* correlated with monocyte-macrophage maturation in THP-1 cells irrespective of ligands used as a stimulant.
- Signalling pathways responsible for the induction of ADAMDEC1 in THP-1 cells were MAPK pathway via p38 and JNK.
- ADAMDEC1 was synthesised intracellularly as an immature form and secreted as a mature form constitutively from THP-1 cells and MDMs.

Chapter 4:

- The surface expression markers of the GMCSF Hoxb8-derived macrophages were consistent with macrophage surface markers.
- The surface expression markers of the GMCSF Hoxb8-derived macrophages and BMDMs were largely consistent with each other.
- There was inconsistency in the expression of ADAMDEC1 between the gifted and newly generated WT GMCSF Hoxb8-derived macrophages indicative of environment-dependent phenotypic alteration.
- BMDMs did not express ADAMDEC1 thus BMDMs and intestinal macrophages are likely to be phenotypically different.
- Murine bone marrow stem cells to macrophages differentiation in vitro was not affected by the absence of ADAMDEC1, assessed by surface expression markers.

Chapter 5:

- BEVS was effective in synthesising recombinant human and mouse ADAMDEC1 and E353A.

- Recombinant ADAMDEC1 and E353A were harvestable from the culture supernatant of the baculovirus infected ExpiSf 9 cells.
- Full length and secreted mature form of recombinant ADAMDEC1 and E353A could be synthesised and purified using the same protocol.
- A combination of diafiltration, IMAC and dialysis was effective in the purification of recombinant ADAMDEC1 and E353A.
- Human ADAMDEC1 synthesised by ExpiSf 9 cells was catalytically active.
- Human E353A synthesised by ExpiSf9 cells were catalytically inactive.
- The catalytical activity of the human ADAMDEC1 was stable during the purification process.
- ADAMDEC1 did not exhibit anti-microbial properties against *E.coli* and *Salmonella enterica*.

Chapter 6:

- *Adamdec1*$^{-/-}$ mice were more susceptible to DSS-induced inflammation in comparison to the WT mice.
- *Adamdec1*$^{-/-}$ mice exhibited cage-dependant variability in response to DSS-induced inflammation.
- Recruitment and proliferation of CD4+ helper T cells, CD8 cytotoxic T cells, dendritic cells, neutrophils and polarisation of naïve T cells to RORγt^{+} FOXP3^{+} cells did not differ between the WT and *Adamdec1*$^{-/-}$ mice during DSS-induced colitis.
- CD4 and CD8 expressed on the cell surface were digested by dispase.
- CD4 and CD8 were digested more readily by dispase in the absence of ADAMDEC1 upon induction of inflammation.
- Th17 polarisation at the early phase of acute inflammation was impaired and subsequent Th17 polarisation was prolonged in the absence of ADAMDEC1.
- A lower proportion of ILC3 was present in the early phase of acute inflammation in the absence of ADAMDEC1.
- The absence of ADAMDEC1 resulted in a higher ratio of SSC^{low} Ly6C^{high} monocytes to SSC$^{mid/high}$ Ly6C$^{low/mid}$ macrophages during acute inflammation.
- The absence of ADAMDEC1 reduced the cell surface expressions of CX3CR1 and Ly6C in the SSC^{low} Ly6C^{high} monocytes and SSC$^{mid/high}$ Ly6C$^{low/mid}$

macrophages, indicative of its influence on the phenotype of monocytes and macrophages during acute inflammation.

- The colonic gene expression of *Cd4*, *Cd8*, *Il1β* and *Cxcl1* increased significantly during DSS-induced inflammation irrespective of the genotype of mice.
- The colonic gene expression of *Lgr5* decreased significantly in the *Adamdec1*$^{-/-}$ mice but not in WT mice during DSS -induced inflammation.
- The colonic gene expressions of *Tnf-α*, *Ccl2*, *Ccr2*, *Ki67*, *Cdx2* and *Fgf2* were similar between the WT mice and *Adamdec1*$^{-/-}$ mice in Cage 2 but differed in the *Adamdec1*$^{-/-}$ mice in Cage 1.

Chapter 7

- The microbiome composition, assessed by β diversity, was shaped by cage and sibling state when young mice of mixed genotypes were cohoused per litter with their parents.
- Cage was the predominant driving factor for shaping the mouse gut microbiome composition, assessed by β diversity.
- The cage-specific microbiome composition, assessed by β diversity, was plastic, and a microbiome composition specific to the new cage was formed over 8 weeks following the pooling of mice.
- ADAMDEC1 genotype did not shape the microbiome composition assessed by β diversity.
- ADAMDEC1 genotype-specific difference in relative abundances of multiple bacterial and fungal taxonomic groups developed when sex-matched adult mice were housed per genotype for more than 10 weeks.
- ADAMDEC1 genotype-specific difference in the relative abundances of multiple bacterial and fungal taxonomic groups were homogenised by the pooling of mice and cohousing of WT and *Adamdec1*$^{-/-}$ mice for 8 weeks.
- DSS challenge caused marked changes in the microbiome composition, assessed by both β diversity and relative abundance, similarly in the WT and *Adamdec1*$^{-/-}$ mice.
- There were no microbiome composition or differentially abundant bacterial or fungal taxonomic groups which were associated with variability in the severity of DSS-induced weight loss.

- The relative abundances of some bacterial and fungal taxonomic groups were significantly different in the microbiome of *Adamdec1*$^{-/-}$ mice in Cage 1 and *Adamdec1*$^{-/-}$ in Cage 2.
- The relative abundance of *Duncaniella muricolitica* was significantly higher in the *Adamdec1*$^{-/-}$ mice in Cage 1 in comparison to *Adamdec1*$^{-/-}$ mice Cage 2.
- The pattern of change in the microbiome by the pooling of mice and DSS challenge, as well as the factors that shaped the composition it were similar in the bacterial and fungal microbiome.

8.2 Overall discussion

In Chapter 3, by utilising THP-1 cells, it was shown that more stimuli than previously reported (MDP, opsonised HkC, MCSF, TNF-α, IL-1β, IL-6, IFN-β) were able to induce ADAMDEC1 in THP-1 cells. Additionally, the induction of ADAMDEC1 correlated with upregulation of THP-1 derived macrophage markers, *CD14* and *CD80*. Recent studies have shown that ADAMDEC1 is expressed in macrophages of self-renewing origin as well as mesenchymal cells such as fibroblasts within the intestine.[50,53–56] These aspects were not explored specifically in this project since the evidence emerged towards the end of the project. Nevertheless, the result from this project was consistent with multiple other in vitro studies demonstrating induction of ADAMDEC1 during monocyte o macrophage differentiation.[25,34,42,312] The finding of this project, therefore, supported the hypothesis that the exclusively high physiological expression of ADAMDEC1 in the intestine is likely to be secondary to induction of ADAMDEC1 during monocyte to macrophage differentiation upon exposure to ligands and cytokines present in the lamina propria of the intestine. At the time of writing this final chapter, however, another intruding study was published.[313] This study showed that ADAMDEC1 was highly expressed in mucosal subepithelial platelet-derived growth factor receptor-alpha-positive (PDGFRα+) cells in a cell-specific manner within the murine and human colonic tissue. Mucosal PDGFRα+ cells are subepithelial fibroblast-like cells and are positioned in close proximity with epithelial cells, myofibroblast, capillary network and immune cells.[314] The study reported a minimal expression of ADAMDEC1 within the intestinal macrophages. The findings from this project and this newly published study added further knowledge to the controversy surrounding the

cellular origin of the expression of ADAMDEC1, which requires further studies to unravel.

The findings from both Chapter 3 and Chapter 4, utilising Hoxb8-cells suggested that preconditioning of monocytes in circulation might be indispensable for the differentiation of monocyte into macrophages that express ADAMDEC1, and that not macrophages of all phenotypes express ADAMDEC1. This highlighted the high plasticity of macrophages which is dependent on the environment, and the importance of selecting suitable in vitro macrophage models, as well as a limited applicability of in vitro macrophage models to study specific macrophages in *bona fide*. The findings from this project indicated that the murine model, in all, may not be an optimum model to study the property of ADAMDEC1 in monocytes and macrophages since murine BMDMs do not appear to express ADAMDEC1 and isolation of intestinal macrophages and peripheral blood monocytes from mice are either difficult or time consuming. Additionally, not limited to the studies involving ADAMDEC1, Hoxb8-derived macrophages and BMDMs may be unsuitable models to study functions of the intestinal macrophages in general since the phenotype of these macrophages are likely to be different from that of the intestinal macrophages.

The induction pathways responsible for ADAMDEC1 were found to be MAPK via activation of p38 and JNK in THP-1 cells. Reduced levels of ADAMDEC1 are observed in the tissue of intestinal diseases such as IBD and CRC. Thus these pathways could potentially be therapeutic targets to augment the expression of ADAMDEC1 in the future, if the reduced level of ADAMDEC1 is proven to play a mechanistic role in the pathogenesis of these intestinal diseases. Nevertheless, the mechanism behind this reduction in the normally high expression of ADAMDEC1 in association with these diseases is still to be elucidated. Likewise, p38 and JNK could potentially be therapeutic targets in extra-intestinal diseases, such as non-small cell lung cancer, rosacea and GBM, to inhibit ADAMDEC1 expression where increases in ADAMDEC1 expression levels are observed and may play a mechanistic role.[29,87,315] In fact, a hindrance of the disease progression of glioma has been demonstrated by the inhibition of the ADAMDEC1 expression in vitro.[315]

Since macrophages derived from the newly generated GMCSF WT Hoxb8 cells did not express ADAMDEC1, using these cells to study the role of ADAMDEC1 in

the function of macrophages was not possible. Thus, the project design was adjusted and recombinant human and mouse ADAMDEC1, as well as the protease dead mutant E353A, were produced using BEVS. These recombinant proteins were proposed to be utilised to characterise the biological and chemical properties of ADAMDEC1. The BEVS was found to be effective and efficient in producing both human and mouse ADAMDEC1 and E353A, although further optimisation is required to increase the yield of recombinant mouse proteins. Protein synthesis utilising insect cells has many benefits over prokaryotic cells. A particularly important characteristic of this system specifically for this project was that the insect cells are able to recognise and process signalling peptides allowing secretion of recombinant proteins since ADAMDEC1 is secreted as a mature protein. However, the post-translational modifications such as glycosylation in insect cells are not identical to that of mammalian cells which might affect the structure therefore the function of the protein. Thus, it was unknown whether the ADAMDEC1 produced in insect cells would impede its catalytic activity. The recombinant ADAMDEC1 synthesised and purified in this project indeed exhibited the catalytic activity similar to that of the recombinant ADAMDEC1 produced in mammalian cells by demonstrating a formation of ADAMDEC1-α2-macroglobulin complex.[14,16,28,316] At the time of conducting this experiment, there was no commercially available recombinant ADAMDEC1. Since then, some recombinant ADAMDEC1 have become commercially available. However, these recombinant ADAMDEC1 are costly and the majority of them are available as full immature inactive form requiring a cleavage of the prodomain prior to its usage in any functional studies. The protocol for synthesis and purification of mature ADAMDEC1 and E353A optimised in this project provides a powerful tool to generate functional recombinant ADAMDEC1, which could be used for various future experiments. Using the recombinant human ADAMDEC1, and E353A as a control, a potential anti-bacterial property of ADAMDEC1 was explored. There was no evidence to suggest that ADAMDEC1 inhibited growth of *E.coli* and *Salmonella enterica*. However, it is still possible for ADAMDEC1 to have anti-microbial properties against other microbial organisms. Examining ADAMDEC1's anti-microbial effect on *Lachnospiraceae* family and *Symbiotaphrina buchneri*, whose relative abundances were significantly higher in the pre-DSS samples of *Adamdec1*$^{-/-}$ mice in comparison to WT mice, would have been more logical.

However, the data from the microbiome analysis was not available at the time of conducting this pilot functional experiment.

The protective role of ADAMDEC1 during mucosal inflammation has been demonstrated previously by two individual studies using the mouse DSS-colitis model and *Adamdec1*$^{-/-}$ mice.[26,56] However, the mechanism through which such an effect is mediated was still very much undefined. The findings from Chapter 6, utilising DSS-colitis model in WT and *Adamdec1*$^{-/-}$ mice, first of all, confirmed the protective role of ADAMDEC1 during DSS-induced colitis. The findings also provided valuable knowledge into potential mechanisms through which ADAMDEC1 may be involved during mucosal inflammation. One of the findings was ADAMDEC1's potential inhibitory effect on dispase which raised the possibility of the protective role of ADAMDEC1 during mucosal inflammation by inhibition of bacterial enzymes. ADAMDEC1's role in the formation and functional stability of SMAC, which plays a vital role in the activation of CD4+ T cells and CD8+ cytotoxic T cells, was also a potential explanation for the observed loss in cell expression of these molecules in the tissue of the *Adamdec1*$^{-/-}$ mice after dispase treatment. Other components of mucosal defence and immune response where ADAMDEC1 may play a role during DSS-induced inflammation were: monocyte to macrophage differentiation, phenotype of monocytes and macrophages, polarisation of Th17 and Treg cells, susceptibility of epithelial cell to DSS-induced inflammation. These findings are all novel. The potential difference in susceptibility of the epithelial cells to DSS-induced inflammation identified by the reduction in the *Lgr5* expression in the absence of ADAMDEC1 is of particular interest. FGF2, which has been reported to be released by ADAMDEC1 from the ECM of GMB cancer stem cells in vitro, has a promoting effect on epithelial cell homeostasis as well as a protective role on the epithelial cells during mucosal inflammation.[29] This highlights the potential role of ADAMDEC1 as a sheddase of FGF2 in the intestine. It is, however, possible for ADAMDEC1 to play a role in other components of the immune system since the expression of only selected genes and cells could be examined by flow cytometry and qPCR, leaving an unexplored territory. The use of hypothesis-free methods such as RNA-seq or RNA microarray would provide a more comprehensive picture of the consequence of the loss of ADAMDEC1. Additionally, even though some components of the immune system and epithelial defence mechanisms were identified to be different in the presence and absence of ADAMDEC1, it cannot be inferred whether these differences observed were the

direct result of the absence of ADAMDEC1 or result of the exaggerated inflammation caused by the absence of ADAMDEC1. Furthermore, a particular difficulty associated with determining the role of ADAMDEC1 during mucosal inflammation is the fact that ADAMDEC1 is a secreted protein. It can, therefore, potentially act on any cell, extracellular substrate, antigen or even microbe within the intestine to mediate its protective role during mucosal inflammation. Further studies are clearly required to elucidate the exact role of ADAMDEC1 during mucosal inflammation. However, the findings from this project have narrowed down the components of the intestinal mucosal defence mechanism during inflammation which ADAMDEC1 might play a role in mediating its effect. The potential involvement of ADAMDEC1 in ECM remodelling during mucosal inflammation was not explored in this project since the evidence emerged at the very end of the project.[56]

Finally, the findings from Chapter 7 examining the microbiome of the WT mice and *Adamdec1*$^{-/-}$ mice before and after the DSS challenge suggested that the protective role of ADAMDEC1 during mucosal inflammation is unlikely to be mediated through a specific component of the microbiome. However, large proportions of the sequences, particularly in the ITS gene analysis, at lower taxonomic levels could not be classified. Thus, the analyses by relative abundance were limited and it is still possible for the relative abundances of some bacteria and/or fungi to differ between the microbiome of *Adamdec1*$^{-/-}$ mice and WT mice after a period of cohousing. The cage and not ADAMDEC1 genotype was the only significant factor which was shown to shape the microbiome composition of the mice consistently. This is in accordance with the currently available evidence that the host's genetic background plays a minor role in accounting for the variability in the microbiome.[264]

Furthermore, a cage-dependant difference in the relative abundances of some bacteria and fungi was observed at multiple taxonomic levels in *Adamdec1*$^{-/-}$ mice. This was in association with the cage-dependant difference in response to DSS-induced colitis observed in these *Adamdec1*$^{-/-}$ mice which was accompanied by the differences in expression of some immune-related genes during DSS-induced colitis. These findings suggested variability in expressivity of the genotype mediated by environment potentially by affecting microbiome. This is consistent with many human complex diseases, such as IBD, for which many disease-associated genetic variants have been identified mainly through genome-wide

association studies (GWAS). However, almost all of the disease-associated genetic variants exhibit incomplete penetrance and variability in the expressivity of genotype. Thus individuals with an identical disease-associated gene variant could each be free-from disease or develop the disease with a range of disease severity and phenotype. The factor that determines the degree of penetrance and expressivity of genotype is believed to be the environment. This is clearly evidenced by studies examining monozygotic twins. With regards to IBD, for example, twin studies have demonstrated concordance of 20 – 50% and 10% for Crohn's disease and ulcerative colitis respectively.[317–319] Additionally, the effect of environment on the penetrance of genotype is clearly seen in migration studies where increases in the incident of IBD were seen in individuals who migrated from developing to developed countries, indicating that certain environmental factors can trigger the penetrance of genotype thus the development of disease in a given genetic background.[320] The observations and findings from this project clearly demonstrated this phenomenon. The mice of the same genotype in 2 separate cages exhibited a difference in the phenotype, with respect to response to DSS-induced inflammation, which was specific to the knockout mice. This occurred despite the fact that their cage environment was highly controlled and standardised, highlighting the significant influential weight of the environment on the penetrance of susceptible genotype. Overall, the findings of this project and other available evidence emphasise the critical effect of environmental factor on penetrance and expressivity of genotype, thus the development of complex diseases. Yet, over the past two decades, in contrast to the profound advances made in genetic research of complex diseases, research into interrogating the link between the environment and gene has been relatively limited. Although the genetic studies may contribute to a better understanding of the disease pathogeneses by identification of specific genes that might be involved, the direct translational value of these genetic studies to therapies has been limited.[321] This is partly because these complex diseases are polygenetic disorders with variable genetic penetrance and expressivity, as well as the fact that a large proportion of the disease-associated loci are within non-coding regions of the genome.[321] Given the evidence that it is the environmental factors that ultimately influence the fate of transformation of risk-associated genotype into phenotype in complex diseases, research into the mechanism of the interaction between environment and gene deserves a greater emphasis. The findings from such research would have more direct, cost-effective

and safe therapeutic implications where complex diseases such as IBD can be prevented or treated by removing environmental factors that trigger penetrance or affect the expressivity of particular risk-associated genotype. This approach would have a huge implication in public health by disease prevention as well as management of individuals with complex diseases by offering personalised medical treatment in the future.

8.3 Proposed future works

- Confirm the expression of ADAMDEC1 in intestinal macrophages by isolating the intestinal macrophages from WT mice and determine the expression of ADAMDEC1 at the RNA messenger and protein level.
- Investigate the effect of ADAMDEC1 on epithelial cell integrity, proliferation and survival by incubation of epithelial cell line or intestinal organoids with recombinant ADAMDEC1 and measure epithelial integrity and gene expression.
- Investigate the potential inhibitory effect of ADAMDEC1 on dispase by incubation of dispase and its catalytical substrate e.g. collagen IV with recombinant ADAMDEC1.
- Investigate the effect of ADAMDEC1 on antigen presenting cell – T cell interaction by utilising OT-I and OT-II mice and recombinant ADAMDEC1.
- Investigate the effect of ADAMDEC1 on differentiation of naïve T cells to Th17 and Teg cell in vitro using recombinant ADAMDEC1.
- Investigate potential sheddase activity of ADAMDED1 on FGF2 in the intestine by quantifying soluble FGF2 in culture media after incubation colonic tissues of *Adamdec1*$^{-/-}$ mouse with recombinant ADAMDEC1.
- Isolate intestine macrophages from WT and *Adamdec1*$^{-/-}$ mice upon induction of DSS-colitis to perform a functional study on the WT and *Adamdec1*$^{-/-}$ macrophages such as bacterial killing and phagocytosis assay.
- Isolate intestine macrophages from WT and *Adamdec1*$^{-/-}$ mice upon induction of DSS-colitis to quantify and compare the expression of pro- and anti-inflammatory cytokines in these macrophages at the gene level.
- Investigate a potential effect of ADAMDEC1 in ECM remodelling during mucosal tissue repair by utilising the chronic DSS-colitis model in *Adamdec1*$^{-/-}$ mice and WT mice.

- Conduct degradomic analysis (protein substrate profiling) using recombinant ADAMDEC1 and E353A to identify the substrate sequence for the catalytical site of ADAMDEC1.
- Investigate the anti-microbial property of ADAMDEC1 on *Lachnospiraceae* family and *Symbiotaphrina buchnerit* using recombinant ADAMDEC1.

Appendix 1

Demographics and the DSS-induced weight loss in the mice used in Chapter 6 and Chapter 7

Animal No.	Original cage	Sibling	Animal ID	Genotype	Pooled cage	Age at pre-pool (weeks)	Age at pre-DSS (weeks)	Age at post-DSS (Weeks)	Weight change by DSS (%)
1	250667	S1	900594	KO	Cage 1	17.3	25.1	26.4	78.44
2			900595	KO					81.54
3			900596	KO					84.94
4	255830	S1	910236	KO		13.7	21.6	22.9	79.56
5			910237	KO					89.09
6	258099	S2	912963	WT		12.7	20.6	21.9	95.15
7			912964	WT					93.33
8			912965	WT					97.38
9	265433	S1	869819	KO	Cage 2	23.0	31.9	33.1	86.19
10			869820	KO					95.71
11			869821	KO					89.42
12		Charles River	921615	WT		21.1	30.0	31.3	92.98
13	250669	S1	900597	KO		17.3	25.1	28.7	93.64
14			900598	KO					84.51
15			900599	KO					83.08
16			900600	KO					88.31
17	258098	S2	912959	WT		12.7	21.6	22.9	86.86
18			912960	WT					103.00
19			912961	WT					93.22
20			912962	WT					86.17

Appendix 2

Change in MFI of CD4 (A) and CD8 (B) in the mice splenocytes by treatment with dispase

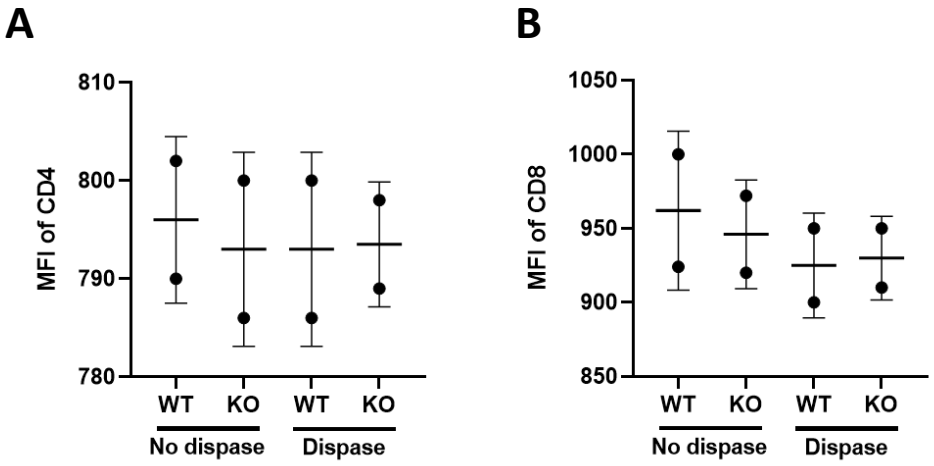

Appendix 3

PERMANOVA and ANOSIM values for Experiment 1 bacterial microbiome β diversity

PERMANOVA

	DF	Sum of Squares	Mean Squares	F Model	R^2	*p*-value
Genotype	2	0.9718	0.48589	1.003	0.13368	0.162
Cage	3	1.4781	0.49271	1.0209	0.20334	**0.001**
Gender	1	0.4838	0.48377	0.99812	0.06655	0.634
Sibling	2	0.9855	0.49274	1.0194	0.13557	**0.001**

PERMANOVA - Added sequentially, adjusted for factor

	DF	Sum of Squares	Mean Squares	F Model	R^2	*p*-value
Sibling	2	0.9855	0.49274	1.0210	0.13557	**0.001**
Cage	2	1.2926	0.19265	1.0208	0.18777	**0.001**

	DF	Sum of Squares	Mean Squares	F Model	R^2	*p*-value
Cage	2	1.4675	0.49274	1.0210	0.24456	**0.001**
Sibling	2	0.9584	0.23511	0.9563	0.16230	**0.001**

ANOSIM

	R-Statistic	*p*-value
Genotype	0.028	0.366
Cage	0.901	**0.001**
Gender	-0.08	0.780
Sibling	0.673	**0.001**

Appendix 4

PERMANOVA and ANOSIM values for Experiment 1 β diversity of mycobiome composition

PERMANOVA

	DF	Sum of Squares	Mean Squares	F Model	R^2	*p*-value
Genotype	2	0.14445	0.072223	1.2935	0.16598	0.194
Cage	3	0.51405	0.171349	5.7719	0.59067	**0.001**
Gender	1	0.06153	0.061532	1.0652	0.0707	0.362
Sibling	2	0.30680	0.153398	3.539	0.35252	**0.002**

PERMANOVA - Added sequentially, adjusted for factor on top

	DF	Sum of Squares	Mean Squares	F Model	R^2	*p*-value
Sibling	2	0.30680	0.153398	5.1673	0.35252	**0.001**
Cage	1	0.20725	0.207250	6.9813	0.23814	**0.001**

	DF	Sum of Squares	Mean Squares	F Model	R^2	*p*-value
Cage	1	0.51302	0.171350	5.1673	0.23654	**0.001**
Sibling	2	0.13259	0.123659	1.9856	0.19862	**0.001**

ANOSIM

	R-Statistic	*p*-value
Cage	0.861	**0.001**
Genotype	0.006	0.404
Gender	-0.017	0.486
Sibling	0.370	**0.019**

Appendix 5

PERMANOVA and ANOSIM values for Experiment 2, β diversity of the bacterial microbiome in pre-pool samples

PERMANOVA (Pre-pool)

	DF	Sum of Squares	Mean Squares	F Model	R^2	*p*-value
Genotype	1	0.4910	0.49103	1.0153	0.05636	0.057
Original cage	5	2.4528	0.49056	1.0188	0.28153	**0.001**
Siblings	2	0.9855	0.49277	1.0204	0.11312	**0.013**
Severity in weight loss	1	0.5698	0.34562	1.0023	0.05467	0.089
Pooling cage	1	0.4851	0.48507	1.0023	0.05568	0.28

PERMANOVA - Added sequentially, adjusted for factor on top (Pre-pool)

	DF	Sum of Squares	Mean Squares	F Model	R^2	*p*-value
Original cage	5	2.4528	0.49056	1.0193	0.28153	**0.001**
Siblings	1	0.8634	0.47563	1.0059	0.12364	0.215

	DF	Sum of Squares	Mean Squares	F Model	R^2	*p*-value
Original cage	5	2.4528	0.49056	1.0193	0.28153	**0.001**
Genotype	1	0.4841	0.48411	1.0059	0.05557	0.315

ANOSIM (Pre-pool)

	R-Statistic	*p*-value
Original cage	0.334	**0.001**
Genotype	0.091	0.090
Sibling	0.175	0.090
Severity in Weight loss	0.1123	0.080
Pooling cage	-0.011	0.484

Appendix 6

PERMANOVA and ANOSIM values for Experiment 2, β diversity of the bacterial microbiome in pre-DSS samples

PERMANOVA (Pre-DSS)

	DF	Sum of Squares	Mean Squares	F Model	R^2	*p*-value
Genotype	1	0.4913	0.49128	1.0053	0.0529	0.205
Pooling cage	1	0.5081	0.50809	1.0417	0.05471	**0.003**
Original cage	5	2.4674	0.49348	1.013	0.26567	**0.004**
Siblings	2	0.9774	0.48871	0.99976	0.10524	0.426
Age (<22 vs > 25 weeks)	1	0.4896	0.4896	1.0018	0.05272	0.295
Severity in weight loss	1	0.4893	0.48925	1.001	0.05236	0.720

PERMANOVA - Added sequentially, adjusted for factor on top (Pre-DSS)

	DF	Sum of Squares	Mean Squares	F Model	R^2	*p*-value
Pooling cage	1	0.5081	0.50809	1.0423	0.05471	**0.003**
Genotype	1	0.4921	0.49213	1.0095	0.05299	0.126

	DF	Sum of Squares	Mean Squares	F Model	R^2	*p*-value
Pooling cage	1	0.5081	0.50809	1.0430	0.05471	**0.003**
Original cage	4	1.9593	0.48982	1.0055	0.21096	0.139

ANOSIM (Pre-DSS)

	R-Statistic	*p*-value
Genotype	0.058	0.211
Pooling cage	0.369	**0.002**
Original cage	0.241	**0.006**
Sibling	0.059	0.287
Severity in weight loss	0.0246	0.316

Appendix 7

PERMANOVA and ANOSIM values for Experiment 2, β diversity of the bacterial microbiome in pre- and post-DSS samples

PERMANOVA (Pre-DSS and Post-DSS)

	DF	Sum of Squares	Mean Squares	F Model	R^2	*p*-value
DSS treatment	1	0.5645	0.56451	1.148	0.03362	**0.001**
Pooling cage	1	0.5111	0.51106	1.0358	0.03043	**0.005**
Genotype	1	0.4965	0.49645	1.0053	0.02956	0.208
Severity in Weight loss	1	0.4915	0.49149	0.99499	0.02927	0.672

PERMANOVA - Added sequentially, adjusted for factor on top (Pre-DSS and Post-DSS)

	DF	Sum of Squares	Mean Squares	F Model	R^2	*p*-value
DSS treatment	1	0.5656	0.56557	1.1516	0.03368	**0.001**
Pooling cage	1	0.5111	0.51106	1.0406	0.03043	**0.007**

ANOSIM (Pre-DSS + Post-DSS)

	R-Statistic	*p*-value
DSS treatment	0.637	**0.001**
Pooling cage	0.09	**0.016**
Genotype	-0.017	0.637
Severity in Weight loss	-0.07	0.706

Appendix 8

PERMANOVA and ANOSIM values for Experiment 2, β diversity of the bacterial microbiome in post-DSS samples

PERMANOVA (Post-DSS)

	DF	Sum of Squares	Mean Squares	F Model	R^2	*p*-value
Pooling cage	1	0.5058	0.50582	1.0202	0.07277	**0.004**
Original cage	4	2.0016	0.50039	1.0110	0.28795	**0.001**
Genotype	1	0.5017	0.50171	1.0113	0.07218	**0.019**
Siblings	2	0.9946	0.49731	1.0019	0.14309	0.281
Severity in weight loss	1	0.4963	0.49630	0.99954	0.07141	0.191

PERMANOVA - Added sequentially, adjusted for factor on top (Post-DSS)

	DF	Sum of Squares	Mean Squares	F Model	R^2	*p*-value
Pooling cage	1	0.5058	0.50582	1.0220	0.07277	**0.001**
Original cage	3	1.4957	0.49858	1.0073	0.21518	**0.018**

	DF	Sum of Squares	Mean Squares	F Model	R^2	*p*-value
Original cage	4	2.0016	0.50039	1.0105	0.28795	**0.001**
Genotype	1	0.4928	0.49277	0.9951	0.07089	0.858

ANOSIM (Post-DSS)

	R-Statistic	*p*-value
Pooling cage	0.642	**0.002**
Original cage	0.457	**0.001**
Genotype	0.186	**0.025**
Sibling	0.080	0.225
Severity in weight loss	0.067	0.143

Appendix 9

PERMANOVA and ANOSIM values for Experiment 2, β diversity of the mycobiome composition in pre-pool samples

PERMANOVA (Pre-pool)

	DF	Sum of Squares	Mean Squares	F Model	R^2	*p*-value
Original cage	5	0.8984	0.179680	4.2601	0.6210	**0.001**
Genotype	1	0.18317	0.183169	2.4644	0.12661	**0.025**
Sibling	2	0.34378	0.171891	2.4936	0.23763	**0.003**
Severity in weight loss	1	0.03713	0.037128	0.82719	0.0464	0.536

PERMANOVA - Added sequentially, adjusted for factor on top (Pre-pool)

	DF	Sum of Squares	Mean Squares	F Model	R^2	*p*-value
Original cage	5	0.89840	0.179680	4.1028	0.62100	**0.001**
Genotype	1	0.02276	0.022762	0.5198	0.01573	0.857

	DF	Sum of Squares	Mean Squares	F Model	R^2	*p*-value
Original cage	5	0.89840	0.179680	4.1028	0.62100	**0.001**
Siblings	1	0.02276	0.022762	0.5198	0.01573	0.874

B) ANOSIM (Pre-pool)

	R-Statistic	*p*-value
Original cage	0.765	**0.001**
Genotype	0.275	**0.004**
Sibling	0.384	**0.002**
Severity in weight loss	-0.028	0.494

Appendix 10

PERMANOVA and ANOSIM values for Experiment 2, β diversity of the mycobiome composition in pre-DSS samples

PERMANOVA (Pre-DSS)

	DF	Sum of Squares	Mean Squares	F Model	R^2	*p*-value
Pooling cage	1	0.34658	0.34658	6.2937	0.25907	**0.001**
Original cage	5	0.5953	0.119060	2.2449	0.44498	**0.003**
Genotype	1	0.06143	0.061435	0.86638	0.04592	0.469
Siblings	2	0.14803	0.074017	1.0576	0.11066	0.313
Severity in weight loss	1	0.0303	0.030305	0.4172	0.02265	0.956

PERMANOVA - Added sequentially, adjusted for factor on top (Pre-DSS)

	DF	Sum of Squares	Mean Squares	F Model	R^2	*p*-value
Pooling cage	1	0.34658	0.34658	6.5348	0.25907	**0.001**
Original cage	4	0.24872	0.06218	1.1724	0.18591	0.266

ANOSIM (Pre-DSS)

	R-Statistic	*p*-value
Pooling cage	0.534	**0.002**
Original cage	0.395	**0.005**
Genotype	-0.026	0.544
Siblings	0.013	0.348
Severity in weight loss	-0.080	0.894

Appendix 11

PERMANOVA and ANOSIM values for Experiment 2, β diversity of the fungal microbiome in pre- and post-DSS samples

PERMANOVA (Pre-DSS and Post-DSS)

	DF	Sum of Squares	Mean Squares	F Model	R^2	*p*-value
DSS treatment	1	3.5793	3.5793	26.317	0.44367	**0.001**
Pooling cage	1	0.8200	0.81996	3.7335	0.10164	**0.010**
Original cage	5	1.4714	0.29428	1.2938	0.18238	0.167
Genotype	1	0.1752	0.17520	0.73257	0.02172	0.566
Siblings	2	0.3966	0.19830	0.82724	0.04916	0.545
Severity in weight loss	1	0.1199	0.11987	0.49772	0.01486	0.810

PERMANOVA - Added sequentially, adjusted for factor on top (Pre-DSS and Post-DSS)

	DF	Sum of Squares	Mean Squares	F Model	R^2	*p*-value
DSS treatment	1	3.4658	3.5421	26.315	0.44367	**0.001**
Pooling cage	1	0.7032	0.8023	3.6235	0.10123	**0.012**

ANOSIM (Pre-DSS and Post-DSS)

	R-Statistic	Significance
DSS challenge	0.854	**0.001**
Pooling cage	0.193	**0.019**
Genotype	-0.013	0.548
Original cage	0.066	0.143
Siblings	-0.026	0.646
Severity in weight loss	-0.058	0.705

Appendix 12

PERMANOVA and ANOSIM values for Experiment 2, β diversity of the fungal microbiome in post-DSS samples

PERMANOVA (Post-DSS)

	DF	Sum of Squares	Mean Squares	F Model	R^2	*p*-value
Pooling cage	1	0.86304	0.86304	4.9049	0.27394	**0.001**
Original cage	4	1.4223	0.35556	2.0575	0.45145	**0.001**
Genotype	1	0.35188	0.35188	1.6346	0.11169	0.116
Siblings	2	0.64695	0.32347	1.5505	0.20535	0.064
Severity in weight loss	1	0.19789	0.19786	0.87118	0.06281	0.563

PERMANOVA - Added sequentially, adjusted for factor on top (Post-DSS)

	DF	Sum of Squares	Mean Squares	F Model	R^2	*p*-value
Pooling cage	1	0.86304	0.96304	4.9940	0.27394	**0.001**
Original cage	3	0.55922	0.18641	1.0786	0.17751	0.359

ANOSIM (Post-DSS)

	R-Statistic	*p*-value
Pooling cage	0.781	**0.001**
Original cage	0.392	**0.014**
Genotype	0.136	0.10
Siblings	0.163	0.085
Severity in weight loss	0.072	0.173

Appendix 13

List of publications and prize

- Gill, P. A., Inniss, S., Kumagai, T., Rahman, F. Z., & Smith, A. M. (2022). The Role of Diet and Gut Microbiota in Regulating Gastrointestinal and Inflammatory Disease. *Frontiers in Immunology, 13*, 866059. doi:10.3389/fimmu.2022.866059
- Kumagai, T., Fan, S., & Smith, A. M. (2020). ADAMDEC1 and Its Role in Inflammatory Disease and Cancer. *Metalloproteinases In Medicine, Volume 7*, 15-28. doi:10.2147/mnm.s263813
- Plyta, M., Patel, P. S., Fragkos, K. C., Kumagai, T., Mehta, S., Rahman, F., & Di Caro, S. (2020). Nutritional Status and Quality of Life in Hospitalised Cancer Patients Who Develop Intestinal Failure and Require Parenteral Nutrition: An Observational Study. *Nutrients, 12 (8)*. doi:10.3390/nu12082357
- Fragkos, K. C., Bouroncle, M. C. P., Kumar, S., Caselton, L., Menys, A., Bainbridge, A., Kumagai, T. . . Mehta, S. (2020). Serum scoring and quantitative magnetic resonance imaging in intestinal failure-associated liver disease: A feasibility study. *Nutrients, 12 (7)*, 1-21. doi:10.3390/nu12072151
- Vinayaga-Pavan, M., Kumagai, T., Parisi, I., Barragry, J., Sundramoorthi, R., Whitley, L., . . . Rahman, F. (2018). P592 Efficacy of vedolizumab for induction and maintenance of clinical remission in ulcerative colitis: The UCLH experience. *Journal of Crohn's and Colitis, 12 (supplement_1)*, S407-S408. doi:10.1093/ecco-jcc/jjx180.719
- Kumagai, T., Vinayaga-Pavan, M., Parisi, I., Barragry, J., Sundramoorthi, R., Whitley, L., . . . Rahman, F. (2018). P615 Efficacy of vedolizumab in patients with Crohn's disease may differ depending on the disease location: The UCLH experience. *Journal of Crohn's and Colitis, 12 (supplement_1)*, S420-S421. doi:10.1093/ecco-jcc/jjx180.742
- Kumagai, T., Rahman, F., & Smith, A. M. (2018). The Microbiome and Radiation Induced-Bowel Injury: Evidence for Potential Mechanistic Role in Disease Pathogenesis. *Nutrients, 10*, 10. doi:10.3390/nu10101405

1st Prize - 3 Minutes Thesis Presentation at Eastman Dental Institute Research Away Day

References

1. Wang, C. *et al.* Characterization of murine macrophages from bone marrow, spleen and peritoneum. *BMC Immunol* **14**, 1–10 (2013).

2. Mueller, C. G. *et al.* Polymerase chain reaction selects a novel disintegrin proteinase from CD40-activated germinal center dendritic cells. *J Exp Med* **186**, 655–63 (1997).

3. Wolfsberg, T. G. *et al.* ADAM, a Widely Distributed and Developmentally Regulated Gene Family Encoding Membrane Proteins with A_D_isintegrin A_nd M_etalloprotease Domain. *Dev Biol* (1995) doi:10.1006/dbio.1995.1152.

4. van Wart, H. E. & Birkedal-Hansen, H. The cysteine switch: a principle of regulation of metalloproteinase activity with potential applicability to the entire matrix metalloproteinase gene family. *Proc Natl Acad Sci U S A* **87**, 5578–82 (1990).

5. Seals, D. F. & Courtneidge, S. A. The ADAMs family of metalloproteases: multidomain proteins with multiple functions. *undefined* (2003).

6. Eto, K. *et al.* Functional classification of ADAMs based on a conserved motif for binding to integrin alpha 9beta 1: implications for sperm-egg binding and other cell interactions. *J Biol Chem* **277**, 17804–10 (2002).

7. Bridges, L. C. & Bowditch, R. D. ADAM-Integrin Interactions: potential integrin regulated ectodomain shedding activity. *Curr Pharm Des* **11**, 837–847 (2005).

8. Smith, K. M. *et al.* The cysteine-rich domain regulates ADAM protease function in vivo. *J Cell Biol* **159**, 893–902 (2002).

9. Reddy, P. *et al.* Functional analysis of the domain structure of tumor necrosis factor-alpha converting enzyme. *J Biol Chem* **275**, 14608–14 (2000).

10. Edwards, D., Handsley, M. & Penington, C. The ADAM metalloproteinases. *Mol Aspects Med* **29**, 258–289 (2008).

11. Black, R. A. *et al.* A metalloproteinase disintegrin that releases tumour-necrosis factor-α from cells. *Nature* **385**, 729–733 (1997).

12. Moss, M. L. & Minond, D. Recent Advances in ADAM17 Research: A Promising Target for Cancer and Inflammation. *Mediators Inflamm* **2017**, 1–21 (2017).

13. Chen, M. S. *et al.* Role of the integrin-associated protein CD9 in binding between sperm ADAM 2 and the egg integrin alpha6beta1: implications for murine fertilization. *Proc Natl Acad Sci U S A* **96**, 11830–5 (1999).

14. Lund, J. *et al.* ADAMDEC1 Is a Metzincin Metalloprotease with Dampened Proteolytic Activity. *Journal of Biological Chemistry* **288**, 21367–21375 (2013).

15. Mueller, C. G. F. *et al.* Mannose Receptor Ligand-Positive Cells Express the Metalloprotease Decysin in the B Cell Follicle. *The Journal of Immunology* **167**, 5052–5060 (2001).

16. Lund, J. *et al.* Monoclonal antibodies targeting the disintegrin-like domain of ADAMDEC1 modulates the proteolytic activity and enables quantification of ADAMDEC1 protein in human plasma. *MAbs* **10**, 118–128 (2018).

17. Lövgren, A., Zhang, M., Engström, A., Dalhammar, G. & Landén, R. Molecular characterization of immune inhibitor A, a secreted virulence protease from Bacillus thuringiensis. *Mol Microbiol* **4**, 2137–2146 (1990).

18. Ogierman, M. A. *et al.* Characterization of the Vibrio cholerae El Tor Lipase Operon lipAB and a Protease Gene Downstream of the hly Region. *J Bacteriol* **179**, 7072–7080 (1997).

19. Harada, S., Kinoshita, T., Kasai, N., Tsunasawa, S. & Sakiyama, F. Complete amino acid sequence of a zinc metalloendoprotease from Streptomyces caespitosus. *Eur J Biochem* **233**, 683–686 (1995).

20. Lund, J. *et al.* Evidence for restricted reactivity of ADAMDEC1 with protein substrates and endogenous inhibitors. *Journal of Biological Chemistry* **290**, 6620–6629 (2015).

21. Bates, E., Fridman, W. & Mueller, C. The ADAMDEC1 (decysin) gene structure: evolution by duplication in a metalloprotease gene cluster on Chromosome 8p12. *Immunogenetics* **54**, 96–105 (2002).

22. Bahudhanapati, H., Bhattacharya, S. & Wei, S. Evolution of vertebrate adam genes; Duplication of testicular adams from ancient Adam9/9-like Loci. *PLoS One* **10**, (2015).

23. Wei, S. *et al.* Conservation and divergence of ADAM family proteins in the Xenopus genome. *BMC Evol Biol* **10**, (2010).

24. Tissue expression of ADAMDEC1 - Summary - The Human Protein Atlas. https://www.proteinatlas.org/ENSG00000134028-ADAMDEC1/tissue.

25. Fritsche, J. *et al.* Inverse regulation of the ADAM-family members, decysin and MADDAM/ADAM19 during monocyte differentiation. *Immunology* **110**, 450–7 (2003).

26. O'Shea, N. R. *et al.* Critical Role of the Disintegrin Metalloprotease ADAM-like Decysin-1 [ADAMDEC1] for Intestinal Immunity and Inflammation. *J Crohns Colitis* **10**, 1417–1427 (2016).

27. ADAMDEC1 (ADAM like decysin 1) | Gene Report | BioGPS. http://biogps.org/#goto=genereport&id=100517917.

28. Yako, Y. *et al.* ADAM-like Decysin-1 (ADAMDEC1) is a positive regulator of Epithelial Defense Against Cancer (EDAC) that promotes apical extrusion of RasV12-transformed cells. *Sci Rep* **8**, 9639 (2018).

29. Jimenez-Pascual, A. *et al.* ADAMDEC1 maintains a growth factor signaling loop in cancer stem cells. *Cancer Discov* (2019) doi:10.1158/2159-8290.CD-18-1308.

30. Chen, R., Jin, G. & McIntyre, T. M. The soluble protease ADAMDEC1 released from activated platelets hydrolyzes platelet membrane pro-epidermal growth factor (EGF) to active high-molecular-weight EGF. *Journal of Biological Chemistry* **292**, 10112–10122 (2017).

31. Abud, H. E., Chan, W. H. & Jardé, T. Source and Impact of the EGF Family of Ligands on Intestinal Stem Cells. *Front Cell Dev Biol* **9**, (2021).

32. Akl, M. R. *et al.* Molecular and clinical significance of fibroblast growth factor 2 (FGF2/bFGF) in malignancies of solid and hematological cancers for personalized therapies. *Oncotarget* **7**, 44735–44762 (2016).

33. Danopoulos, S., Schlieve, C. R., Grikscheit, T. C. & al Alam, D. Fibroblast Growth Factors in the Gastrointestinal Tract: Twists and Turns. *Developmental Dynamics* **246**, 344–352 (2017).

34. Li, T. *et al.* SIRT1/2 orchestrate acquisition of DNA methylation and loss of histone H3 activating marks to prevent premature activation of inflammatory genes in macrophages. *Nucleic Acids Res* **48**, 665–681 (2020).

35. Bain, C. C. *et al.* Constant replenishment from circulating monocytes maintains the macrophage pool in the intestine of adult mice. *Nat Immunol* **15**, 929–937 (2014).

36. Ryan, G. R. *et al.* Rescue of the colony-stimulating factor 1 (CSF-1)-nullizygous mouse (Csf1(op)/Csf1(op)) phenotype with a CSF-1 transgene and identification of sites of local CSF-1 synthesis. *Blood* **98**, 74–84 (2001).

37. Brochériou, I. *et al.* Antagonistic regulation of macrophage phenotype by M-CSF and GM-CSF: Implication in atherosclerosis. *Atherosclerosis* **214**, 316–324 (2011).

38. Bazzi, S. *et al.* Defining genome-wide expression and phenotypic contextual cues in macrophages generated by granulocyte/macrophage colony-stimulating factor, macrophage colony-stimulating factor, and heat-killed mycobacteria. *Front Immunol* **8**, (2017).

39. Isidro, R. A. & Appleyard, C. B. Colonic macrophage polarization in homeostasis, inflammation, and cancer. *Am J Physiol Gastrointest Liver Physiol* **311**, G59 (2016).

40. Liang, S., Cai, J., Li, Y. & Yang, R. 1,25-Dihydroxy-Vitamin D3 induces macrophage polarization to M2 by upregulating T-cell Ig-mucin-3 expression. *Mol Med Rep* **49**, 3707–3713 (2019).

41. Rao Muvva, J., Parasa, V. R., Lerm, M., Svensson, M. & Brighenti, S. Polarization of Human Monocyte-Derived Cells With Vitamin D Promotes Control of Mycobacterium tuberculosis Infection. *Front Immunol* **10**, (2020).

42. Liu, T. *et al.* ADAMDEC1 promotes skin inflammation in rosacea via modulating the polarization of M1 macrophages. *Biochem Biophys Res Commun* **521**, 64–71 (2020).

43. Becker, M. *et al.* Integrated Transcriptomics Establish Macrophage Polarization Signatures and have Potential Applications for Clinical Health and Disease. *Sci Rep* **5**, (2015).

44. Derlindati, E. *et al.* Transcriptomic analysis of human polarized macrophages: More than one role of alternative activation? *PLoS One* **10**, (2015).

45. Gerrick, K. Y. *et al.* Transcriptional profiling identifies novel regulators of macrophage polarization. *PLoS One* **13**, (2018).

46. Mosser, D. M. & Edwards, J. P. Exploring the full spectrum of macrophage activation. *Nature Reviews Immunology 2008 8:12* **8**, 958–969 (2008).

47. Viola, M. F. & Boeckxstaens, G. Niche-specific functional heterogeneity of intestinal resident macrophages. *Gut* **70**, 1383–1395 (2021).

48. Fenton, T. M. *et al. Single-cell characterisation of mononuclear phagocytes in the human intestinal mucosa (Preprint)*. https://doi.org/10.1101/2021.03.28.437379 doi:10.1101/2021.03.28.437379.

49. Shaw, T. N. *et al.* Tissue-resident macrophages in the intestine are long lived and defined by Tim-4 and CD4 expression. *Journal of Experimental Medicine* **215**, 1507–1518 (2018).

50. de Schepper, S. *et al.* Self-Maintaining Gut Macrophages Are Essential for Intestinal Homeostasis. *Cell* **175**, 400-415.e13 (2018).

51. Baran, N., Kelly, P. A. & Binart, N. Decysin, a New Member of the Metalloproteinase Family, Is Regulated by Prolactin and Steroids During Mouse Pregnancy1. *Biol Reprod* **68**, 1787–1792 (2003).

52. Domanska, D. *et al.* Single-cell transcriptomic analysis of human colonic macrophages reveals niche-specific subsets. *J Exp Med* **219**, (2022).

53. Kinchen, J. *et al.* Structural Remodeling of the Human Colonic Mesenchyme in Inflammatory Bowel Disease. *Cell* **175**, 372–386 (2018).

54. Smillie, C. S. *et al.* Intra- and Inter-cellular Rewiring of the Human Colon during Ulcerative Colitis. *Cell* **178**, 714-730.e22 (2019).

55. Fawkner-Corbett, D. *et al.* Spatiotemporal analysis of human intestinal development at single-cell resolution. *Cell* **184**, 810-826.e23 (2021).

56. Jasso, G. J. *et al.* Colon stroma mediates an inflammation-driven fibroblastic response controlling matrix remodeling and healing. *PLoS Biol* **20**, e3001532 (2022).

57. Galamb, O. *et al.* Inflammation, adenoma and cancer: Objective classification of colon biopsy specimens with gene expression signature. *Dis Markers* **25**, 1–16 (2008).

58. de Bruyn, M. *et al.* Infliximab restores the dysfunctional matrix remodeling protein and growth factor gene expression in patients with inflammatory bowel disease. *Inflamm Bowel Dis* **20**, 339–352 (2014).

59. Smith, A. M. *et al.* Disruption of macrophage pro-inflammatory cytokine release in Crohn's disease is associated with reduced optineurin expression in a subset of patients. *Immunology* **144**, 45–55 (2015).

60. Segal, A. W. Studies on patients establish Crohn's disease as a manifestation of impaired innate immunity. *J Intern Med* **286**, 373–388 (2019).

61. Marks, D. J. B. *et al.* Defective acute inflammation in Crohn's disease: A clinical investigation. *Lancet* **367**, 668–678 (2006).

62. Smith, A. M. *et al.* Disordered macrophage cytokine secretion underlies impaired acute inflammation and bacterial clearance in Crohn's disease. *J Exp Med* **206**, 1883 (2009).

63. Hong, Y., Downey, T., Eu, K. W., Koh, P. K. & Cheah, P. Y. A 'metastasis-prone' signature for early-stage mismatch-repair proficient sporadic colorectal cancer patients and its implications for possible therapeutics. *Clin Exp Metastasis* **27**, 83–90 (2010).

64. GEO Accession viewer. https://www.ncbi.nlm.nih.gov/geo/query/acc.cgi?acc=GSE100179.

65. Sabates-Bellver, J. *et al.* Transcriptome profile of human colorectal adenomas. *Molecular Cancer Research* **5**, 1263–1275 (2007).

66. Lucafò, M., Curci, D., Franzin, M., Decorti, G. & Stocco, G. Inflammatory Bowel Disease and Risk of Colorectal Cancer: An Overview From Pathophysiology to Pharmacological Prevention. *Front Pharmacol* **12**, 2916 (2021).

67. Kelemen, P. R. *et al.* Loss of heterozygosity in 8p is associated with microinvasion in colorectal carcinoma. *Genes Chromosomes Cancer* **11**, 195–198 (1994).

68. Takanishi, D. M. *et al.* Chromosome 8 losses in colorectal carcinoma: Localization and correlation with invasive disease. *Molecular Diagnosis* **2**, 3–10 (1997).

69. Oh, B. Y. *et al.* Exome and transcriptome sequencing identifies loss of PDLIM2 in metastatic colorectal cancers. *Cancer Manag Res* **9**, 581–589 (2017).

70. Kajita, M. & Fujita, Y. EDAC: Epithelial defence against cancer—cell competition between normal and transformed epithelial cells in mammals. *The Journal of Biochemistry* **158**, 15–23 (2015).

71. Tanimura, N. & Fujita, Y. Epithelial defense against cancer (EDAC). *Semin Cancer Biol* **63**, 44–48 (2020).

72. Ohsawa, S., Vaughen, J. & Igaki, T. Developmental Cell Review Cell Extrusion: A Stress-Responsive Force for Good or Evil in Epithelial Homeostasis. *Dev Cell* **44**, 284–296 (2018).

73. Polakis, P. Wnt signaling in cancer. *Cold Spring Harb Perspect Biol* **4**, 9 (2012).

74. Zhan, T., Rindtorff, N. & Boutros, M. Wnt signaling in cancer. *Oncogene 2017 36:11* **36**, 1461–1473 (2016).

75. GEO Accession viewer. https://www.ncbi.nlm.nih.gov/geo/query/acc.cgi?acc=GSE79973.

76. Pasini, F. S. *et al.* A gene expression profile related to immune dampening in the tumor microenvironment is associated with poor prognosis in gastric adenocarcinoma. *J Gastroenterol* **49**, 1453 (2014).

77. Zhang, S. *et al.* Immune landscape of advanced gastric cancer tumor microenvironment identifies immunotherapeutic relevant gene signature. *BMC Cancer* **21**, 1324 (2021).

78. Liu, Y. *et al.* Immune Cell PD-L1 Colocalizes with Macrophages and Is Associated with Outcome in PD-1 Pathway Blockade Therapy. *Clinical Cancer Research* **26**, 970–977 (2020).

79. Gordon, S. R. *et al.* PD-1 expression by tumour-associated macrophages inhibits phagocytosis and tumour immunity. *Nature 2017 545:7655* **545**, 495–499 (2017).

80. Crouser, E. D. *et al.* Gene expression profiling identifies MMP-12 and ADAMDEC1 as potential pathogenic mediators of pulmonary sarcoidosis. *Am J Respir Crit Care Med* **179**, 929–938 (2009).

81. Galligan, C. L., Baig, E., Bykerk, V., Keystone, E. C. & Fish, E. N. Distinctive gene expression signatures in rheumatoid arthritis synovial tissue fibroblast cells: correlates with disease activity. *Genes Immun* **8**, 480–491 (2007).

82. Greenwell-Wild, T. *et al.* Chitinases in the salivary glands and circulation of patients with Sjögren's syndrome: Macrophage harbingers of disease severity. *Arthritis Rheum* **63**, 3103–3115 (2011).

83. Shi, L. *et al.* The SLE transcriptome exhibits evidence of chronic endotoxin exposure and has widespread dysregulation of non-coding and coding RNAs. *PLoS One* **9**, (2014).

84. Papaspyridonos, M. *et al.* Novel candidate genes in unstable areas of human atherosclerotic plaques. *Arterioscler Thromb Vasc Biol* **26**, 1837–1844 (2006).

85. Verdugo, R. A. *et al.* Graphical Modeling of Gene Expression in Monocytes Suggests Molecular Mechanisms Explaining Increased Atherosclerosis in Smokers. *PLoS One* **8**, (2013).

86. Reinholz, M. *et al.* Pathogenesis and clinical presentation of rosacea as a key for a symptom-oriented therapy. *JDDG: Journal der Deutschen Dermatologischen Gesellschaft* **14**, 4–15 (2016).

87. Zhu, W. *et al.* Upregulation of ADAMDEC1 correlates with tumor progression and predicts poor prognosis in non-small cell lung cancer (NSCLC) via the PI3K/AKT pathway. *Thorac Cancer* (2022) doi:10.1111/1759-7714.14354.

88. Liu, X. *et al.* Knockdown of adamdec1 inhibits the progression of glioma in vitro. *Histol Histopathol* **35**, 997–1005 (2020).

89. Kelly, J. J. P. *et al.* Proliferation of human glioblastoma stem cells occurs independently of exogenous mitogens. *Stem Cells* **27**, 1722–1733 (2009).

90. Haley, E. M. & Kim, Y. The role of basic fibroblast growth factor in glioblastoma multiforme and glioblastoma stem cells and in their in vitro culture. *Cancer Letters* vol. 346 1–5 Preprint at https://doi.org/10.1016/j.canlet.2013.12.003 (2014).

91. Melgar, S., Karlsson, A. & Michaëlsson, E. Acute colitis induced by dextran sulfate sodium progresses to chronicity in C57BL/6 but not in BALB/c mice: correlation between symptoms and inflammation. *Am J Physiol Gastrointest Liver Physiol* **288**, (2005).

92. Vidal-Lletjós, S. *et al.* Mucosal healing progression after acute colitis in mice. *World J Gastroenterol* **25**, 3572 (2019).

93. Xu, X. *et al.* Histological and ultrastructural changes of the colon in dextran sodium sulfate-induced mouse colitis. *Exp Ther Med* **20**, 1987–1994 (2020).

94. Song, X. *et al.* Growth Factor FGF2 Cooperates with Interleukin-17 to Repair Intestinal Epithelial Damage. *Immunity* **43**, 488–501 (2015).

95. Houchen, C. W., George, R. J., Sturmoski, M. A. & Cohn, S. M. FGF-2 enhances intestinal stem cell survival and its expression is induced after radiation injury. *Am J Physiol Gastrointest Liver Physiol* **276**, (1999).

96. Folkman, J. *et al.* Duodenal Ulcer Discovery ofa New Mechanism and Development ofAngiogenic Therapy That Accelerates Healing Address reprint requests to.

97. Plaza-Diáz, J. *et al.* Adamdec1, Ednrb and Ptgs1/Cox1, inflammation genes upregulated in the intestinal mucosa of obese rats, are downregulated by three probiotic strains. *Sci Rep* **7**, (2017).

98. Plaza-Diaz, J. *et al.* Effects of Lactobacillus paracasei CNCM I-4034, Bifidobacterium breve CNCM I-4035 and Lactobacillus rhamnosus CNCM I-4036 on hepatic steatosis in Zucker rats. *PLoS One* **9**, (2014).

99. Khan, S., Luck, H., Winer, S. & Winer, D. A. Emerging concepts in intestinal immune control of obesity-related metabolic disease. *Nature Communications 2021 12:1* **12**, 1–13 (2021).

100. de Bruyn, M. *et al.* Infliximab Restores the Dysfunctional Matrix Remodeling Protein and Growth Factor Gene Expression in Patients with Inflammatory Bowel Disease. *Inflamm Bowel Dis* **20**, 339–352 (2014).

101. Tsuchiya, S. *et al.* Establishment and characterization of a human acute monocytic leukemia cell line (THP-1). *Int J Cancer* **26**, 171–176 (1980).

102. Bosshart, H. & Heinzelmann, M. THP-1 cells as a model for human monocytes. *Ann Transl Med* **4**, (2016).

103. Chanput, W., Mes, J. J. & Wichers, H. J. THP-1 cell line: an in vitro cell model for immune modulation approach. *Int Immunopharmacol* **23**, 37–45 (2014).

104. Livak, K. J. & Schmittgen, T. D. Analysis of Relative Gene Expression Data Using Real-Time Quantitative PCR and the 2−ΔΔCT Method. *Methods* **25**, 402–408 (2001).

105. Yuan, J. S., Reed, A., Chen, F. & Stewart, C. N. Statistical analysis of real-time PCR data. *BMC Bioinformatics* **7**, 85 (2006).

106. Carpenter, S., Wochal, P., Dunne, A. & O'Neill, L. A. J. Toll-like Receptor 3 (TLR3) Signaling Requires TLR4 Interactor with Leucine-rich Repeats (TRIL). *J Biol Chem* **286**, 38795 (2011).

107. Pan, Z. K. *et al.* Bacterial LPS up-regulated TLR3 expression is critical for antiviral response in human monocytes: evidence for negative regulation by CYLD. *Int Immunol* **23**, 357 (2011).

108. Hornung, V. *et al.* Quantitative Expression of Toll-Like Receptor 1–10 mRNA in Cellular Subsets of Human Peripheral Blood Mononuclear Cells and Sensitivity to CpG Oligodeoxynucleotides. *The Journal of Immunology* **168**, 4531–4537 (2002).

109. Travassos, L. H. *et al.* Toll-like receptor 2-dependent bacterial sensing does not occur via peptidoglycan recognition. *EMBO Rep* **5**, 1000 (2004).

110. Eckmann, L. & Karin, M. NOD2 and Crohn's Disease: Loss or Gain of Function? *Immunity* **22**, 661–667 (2005).

111. Economou, M., Trikalinos, T. A., Loizou, K. T., Tsianos, E. v. & Ioannidis, J. P. A. Differential effects of NOD2 variants on Crohn's disease risk and phenotype in diverse populations: a metaanalysis. *Am J Gastroenterol* **99**, 2393–2404 (2004).

112. Forrester, M. A. *et al.* Similarities and differences in surface receptor expression by THP-1 monocytes and differentiated macrophages polarized using seven different conditioning regimens. *Cell Immunol* **332**, 58–76 (2018).

113. Taylor, P. R. *et al.* The β-Glucan Receptor, Dectin-1, Is Predominantly Expressed on the Surface of Cells of the Monocyte/Macrophage and Neutrophil Lineages. *The Journal of Immunology* **169**, 3876–3882 (2002).

114. Mollinedo, F., Gajate, C., Tugores, A., Flores, I. & Naranjot, J. R. Differences in expression of transcription factor AP-1 in human promyelocytic HL-60 cells during differentiation towards macrophages versus granulocytes. *Biochem. J* **294**, 137 (1993).

115. Kang, C. D. *et al.* Signaling mechanism of PMA-induced differentiation of K562 cells. *Biochem Biophys Res Commun* **221**, 95–100 (1996).

116. Holden, N. S. *et al.* Phorbol ester-stimulated NF-kappaB-dependent transcription: roles for isoforms of novel protein kinase C. *Cell Signal* **20**, 1338–1348 (2008).

117. Kawai, T. & Akira, S. TLR signaling. *Cell Death & Differentiation 2006 13:5* **13**, 816–825 (2006).

118. Saxena, M. & Yeretssian, G. NOD-like receptors: Master regulators of inflammation and cancer. *Front Immunol* **5**, 327 (2014).

119. Strober, W. & Watanabe, T. NOD2, an intracellular innate immune sensor involved in host defense and Crohn's disease. *Mucosal Immunology 2011 4:5* **4**, 484–495 (2011).

120. Mkaddem, S. ben, Benhamou, M. & Monteiro, R. C. Understanding Fc receptor involvement in inflammatory diseases: From mechanisms to new therapeutic tools. *Front Immunol* **10**, 811 (2019).

121. Wajant, H. & Siegmund, D. TNFR1 and TNFR2 in the control of the life and death balance of macrophages. *Front Cell Dev Biol* **7**, 91 (2019).

122. Stanley, E. R. & Chitu, V. CSF-1 Receptor Signaling in Myeloid Cells. *Cold Spring Harb Perspect Biol* **6**, (2014).

123. Martin, M. U. & Wesche, H. Summary and comparison of the signaling mechanisms of the Toll/interleukin-1 receptor family. *Biochimica et Biophysica Acta (BBA) - Molecular Cell Research* **1592**, 265–280 (2002).

124. Heinrich, P. C., Behrmann, I., Haan, S., Hermanns, H. M. & Schaper, F. Principles of interleukin (IL)-6-type cytokine signalling and its regulation 1. *Biochem. J* **374**, 1–20 (2003).

125. Hamza, T., Barnett, J. B. & Li, B. Interleukin 12 a Key Immunoregulatory Cytokine in Infection Applications. *International Journal of Molecular Sciences 2010, Vol. 11, Pages 789-806* **11**, 789–806 (2010).

126. Pastor-Fernández, G., Mariblanca, I. R. & Navarro, M. N. Decoding IL-23 Signaling Cascade for New Therapeutic Opportunities. *Cells* **9**, (2020).

127. Lurie, R. H. & Platanias, L. C. Mechanisms of type-I- and type-II-interferon-mediated signalling. *Nature Reviews Immunology 2005 5:5* **5**, 375–386 (2005).

128. Hoesel, B. & Schmid, J. A. The complexity of NF-κB signaling in inflammation and cancer. *Molecular Cancer 2013 12:1* **12**, 1–15 (2013).

129. Bennett, S., Por, S. B., Stanley, E. R. & Breit, S. N. Monocyte proliferation in a cytokine-freem serum-free system. *J Immunol Methods* **153**, 201–212 (1992).

130. Zhou, Y. Y., Li, Y., Jiang, W. Q. & Zhou, L. F. MAPK/JNK signalling: A potential autophagy regulation pathway. *Biosci Rep* **35**, 1–10 (2015).

131. Lu, C. *et al.* Serum starvation induces H2AX phosphorylation to regulate apoptosis via p38 MAPK pathway. *FEBS Lett* **582**, 2703–2708 (2008).

132. Wei, Y. *et al.* The stress-responsive kinases MAPKAPK2/MAPKAPK3 activate starvation-induced autophagy through Beclin 1 phosphorylation. *Elife* **4**, (2015).

133. Liu, S. Y. *et al.* Albumin prevents reactive oxygen species-induced mitochondrial damage, autophagy, and apoptosis during serum starvation. *Apoptosis* **17**, 1156–1169 (2012).

134. Mabbott, N. A., Donaldson, D. S., Ohno, H., Williams, I. R. & Mahajan, A. Microfold (M) cells: important immunosurveillance posts in the intestinal epithelium. *Mucosal Immunology 2013 6:4* **6**, 666–677 (2013).

135. Kotredes, K. P., Thomas, B. & Gamero, A. M. The protective role of Type I interferons in the gastrointestinal tract. *Front Immunol* **8**, 410 (2017).

136. Mahapatro, M., Erkert, L. & Becker, C. Cytokine-Mediated Crosstalk between Immune Cells and Epithelial Cells in the Gut. *Cells 2021, Vol. 10, Page 111* **10**, 111 (2021).

137. Freund, E. C. *et al.* Efficient gene knockout in primary human and murine myeloid cells by non-viral delivery of crispr-cas9. *Journal of Experimental Medicine* **217**, (2020).

138. Troegeler, A. *et al.* An efficient siRNA-mediated gene silencing in primary human monocytes, dendritic cells and macrophages. *Immunol Cell Biol* **92**, 699–708 (2014).

139. Zhang, X. H., Tee, L. Y., Wang, X. G., Huang, Q. S. & Yang, S. H. Off-target Effects in CRISPR/Cas9-mediated Genome Engineering. *Mol Ther Nucleic Acids* **4**, e264 (2015).

140. Fedorov, Y. *et al.* Off-target effects by siRNA can induce toxic phenotype. *RNA* **12**, 1188 (2006).

141. Tedesco, S. *et al.* Convenience versus biological significance: Are PMA-differentiated THP-1 cells a reliable substitute for blood-derived macrophages when studying in vitro polarization? *Front Pharmacol* **9**, 71 (2018).

142. Argiropoulos, B. & Humphries, R. K. Hox genes in hematopoiesis and leukemogenesis. *Oncogene 2007 26:47* **26**, 6766–6776 (2007).

143. Wang, G. G. *et al.* Quantitative production of macrophages or neutrophils ex vivo using conditional Hoxb8. *Nat Methods* **3**, 287–293 (2006).

144. Accarias, S. *et al.* Genetic engineering of Hoxb8-immortalized hematopoietic progenitors - a potent tool to study macrophage tissue migration. *J Cell Sci* **133**, (2020).

145. Rosas, M. *et al.* Hoxb8 conditionally immortalised macrophage lines model inflammatory monocytic cells with important similarity to dendritic cells. *Eur J Immunol* **41**, 356–365 (2011).

146. Retroviral packaging cell lines and systems. https://www.takarabio.com/products/gene-function/viral-transduction/retrovirus/packaging-systems-and-cells.

147. Auffray, C. *et al.* CX3CR1+ CD115+ CD135+ common macrophage/DC precursors and the role of CX3CR1 in their response to inflammation. *Journal of Experimental Medicine* **206**, 595–606 (2009).

148. Trento, C. *et al.* Bone marrow mesenchymal stromal cells induce nitric oxide synthase-dependent differentiation of CD11b+ cells that expedite hematopoietic recovery. *Haematologica* **102**, 818–825 (2017).

149. Rosmarin, A. *et al.* Differential Expression of CDllb/CD18 (Mol) and Myeloperoxidase Genes During Myeloid Differentiation. *Blood* **73**, 131–136 (1989).

150. Fleming, T. J., Fleming, M. L. & Malek, T. R. Selective expression of Ly-6G on myeloid lineage cells in mouse bone marrow. RB6-8C5 mAb to granulocyte-differentiation antigen (Gr-1) detects members of the Ly-6 family. *The Journal of Immunology* **151**, (1993).

151. Rose, S., Misharin, A. & Perlman, H. A novel Ly6C/Ly6G-based strategy to analyze the mouse splenic myeloid compartment. doi:10.1002/cyto.a.22012.

152. Ogawa, M. *et al.* Expression and function of c-kit in hemopoietic progenitor cells. *Journal of Experimental Medicine* **174**, 63–71 (1991).

153. Merad, M., Sathe, P., Helft, J., Miller, J. & Mortha, A. The Dendritic Cell Lineage: Ontogeny and Function of Dendritic Cells and Their Subsets in the Steady State and the Inflamed Setting. *Annu Rev Immunol* **31**, 563–604 (2013).

154. Panek, C. A. *et al.* Differential expression of the fractalkine chemokine receptor (CX3CR1) in human monocytes during differentiation. *Cellular & Molecular Immunology 2015 12:6* **12**, 669–680 (2014).

155. Aldo, P. B., Craveiro, V., Guller, S. & Mor, G. Effect of culture conditions on the phenotype of THP-1 monocyte cell line. *Am J Reprod Immunol* **70**, 80–86 (2013).

156. Stockholm, D. *et al.* The Origin of Phenotypic Heterogeneity in a Clonal Cell Population In Vitro. *PLoS One* **2**, e394 (2007).

157. Zajd, C. M. *et al.* Bone Marrow-Derived and Elicited Peritoneal Macrophages Are Not Created Equal: The Questions Asked Dictate the Cell Type Used. *Front Immunol* **11**, 269 (2020).

158. Jeske, R. *et al.* In Vitro Culture Expansion Shifts the Immune Phenotype of Human Adipose-Derived Mesenchymal Stem Cells. *Front Immunol* **12**, 46 (2021).

159. Sauter, A., Yi, D. H., Li, Y., Roersma, S. & Appel, S. The Culture Dish Surface Influences the Phenotype and Cytokine Production of Human Monocyte-Derived Dendritic Cells. *Front Immunol* **10**, 2352 (2019).

160. Mangum, L. H. *et al.* Tissue Source and Cell Expansion Condition Influence Phenotypic Changes of Adipose-Derived Stem Cells. *Stem Cells Int* **2017**, (2017).

161. Hughes, K. M. An annotated list and bibliography of insects reported to have virus diseases. *Hilgardia* **26**, 597–629 (1957).

162. Vlak, J. M. & Smith, G. E. Orientation of the Genome of Autographa californica Nuclear Polyhedrosis Virus: a Proposal. *J Virol* **41**, 1118–1121 (1982).

163. Martignoni, M. E. & Langston, R. L. Supplement to an annotated list and bibliography of insects reported to have virus diseases. *Hilgardia* **30**, 1–40 (1960).

164. Smith, G. E., Vlak, J. M. & Summers, M. D. Physical Analysis of Autographa californica Nuclear Polyhedrosis Virus Transcripts for Polyhedrin and 10,000-Molecular-Weight Protein. *J Virol* **45**, 215–25 (1983).

165. Smith, G. E., Summers, M. D. & Fraser, M. J. Production of human Beta interferon in insect cells infected with a Baculovirus expression vector. *Mol Cell Biol* **3**, 434–443 (1983).

166. Ailor, E. & Betenbaugh, M. J. Modifying secretion and post-translational processing in insect cells. *Curr Opin Biotechnol* **10**, 142–145 (1999).

167. ADAMDEC1 - ADAM DEC1 precursor - Homo sapiens (Human) - ADAMDEC1 gene & protein. https://www.uniprot.org/uniprot/O15204#structure.

168. Felberbaum, R. S. The baculovirus expression vector system: A commercial manufacturing platform for viral vaccines and gene therapy vectors. *Biotechnol J* **10**, 702–14 (2015).

169. Tomiya, N., Narang, S., Lee, Y. C. & Betenbaugh, M. J. Comparing N-glycan processing in mammalian cell lines to native and engineered lepidopteran insect cell lines. *Glycoconj J* **21**, 343–360 (2004).

170. Luckow, V. A., Lee, S. C., Barry, G. F. & Olins, P. O. Efficient generation of infectious recombinant baculoviruses by site-specific transposon-mediated insertion of foreign genes into a baculovirus genome propagated in Escherichia coli. *J Virol* **67**, 4566–79 (1993).

171. ExpiSf9™ Cells. https://www.thermofisher.com/order/catalog/product/A35243.

172. ExpiSf Baculovirus Expression System | Thermo Fisher Scientific - UK. https://www.thermofisher.com/uk/en/home/life-science/protein-biology/protein-expression/insect-protein-expression/expisf-expression-system.html.

173. Bornhorst, J. A. & Falke, J. J. Purification of Proteins Using Polyhistidine Affinity Tags. *Methods Enzymol* **326**, 245 (2000).

174. Garvey, J. S., Cremer, N. E. & Sussdorf, D. H. Methods in Enzymology - Guide to protein purification. *Academic Press* **463**, 535 (2009).

175. Biological Buffers Biological Buffers • AppliChem Introduction 2. (2008).

176. Potapov, V. & Ong, J. L. Examining Sources of Error in PCR by Single-Molecule Sequencing. *PLoS One* **12**, e0169774 (2017).

177. Fisher Scientific, T. ExpiFectamine™ Sf Transfection Reagent. https://assets.thermofisher.com/TFS-Assets/LSG/manuals/MAN0017502_ExpiFectamineSfReagent_UG.pdf.

178. Joeris, T., Müller-Luda, K., Agace, W. W. & Mowat, A. M. I. Diversity and functions of intestinal mononuclear phagocytes. *Mucosal Immunology 2017 10:4* **10**, 845–864 (2017).

179. Bain Allan McI Mowat, C. C., Calum Bain, address C., McI Mowat, A. & Mowat, A. Macrophages in intestinal homeostasis and inflammation. (2014).

180. Bain, C. C. & Schridde, A. Origin, differentiation, and function of intestinal macrophages. *Front Immunol* **9**, 2733 (2018).

181. Bain, C. C. & Mowat, A. M. I. The monocyte-macrophage axis in the intestine. *Cell Immunol* **291**, 41–48 (2014).

182. Kitajima, S., Takuma, S. & Morimoto, M. Histological Analysis of Murine Colitis Induced by Dextran Sulfate Sodium of Different Molecular Weights. *Exp Anim* **49**, 9–15 (2000).

183. Kiesler, P., Fuss, I. J. & Strober, W. Experimental Models of Inflammatory Bowel Diseases. *Cell Mol Gastroenterol Hepatol* **1**, 154–170 (2015).

184. Perše, M. & Cerar, A. Dextran sodium sulphate colitis mouse model: Traps and tricks. *J Biomed Biotechnol* **2012**, (2012).

185. Eichele, D. D. & Kharbanda, K. K. Dextran sodium sulfate colitis murine model: An indispensable tool for advancing our understanding of inflammatory bowel diseases pathogenesis. *World J Gastroenterol* **23**, 6016–6029 (2017).

186. Kim, Y. I. *et al.* Compensatory roles of CD8+ T cells and plasmacytoid dendritic cells in gut immune regulation for reduced function of CD4+ Tregs. *Oncotarget* **7**, 10947–10961 (2016).

187. Chunmei, M. *et al.* Gasdermin d in macrophages restrains colitis by controlling cgas-mediated inflammation. *Sci Adv* **6**, (2020).

188. Skordos, I., Demeyer, A. & Beyaert, R. Analysis of T cells in mouse lymphoid tissue and blood with flow cytometry. *STAR Protoc* **2**, 100351 (2021).

189. Haubruck, P. *et al.* Flow Cytometry Analysis of Immune Cell Subsets within the Murine Spleen, Bone Marrow, Lymph Nodes and Synovial Tissue in an Osteoarthritis Model. *JoVE (Journal of Visualized Experiments)* **2020**, e61008 (2020).

190. Autengruber, A., Gereke, M., Hansen, G., Hennig, C. & Bruder, D. Impact of enzymatic tissue disintegration on the level of surface molecule expression and immune cell function. *Eur J Microbiol Immunol (Bp)* **2**, 112–120 (2012).

191. Abuzakouk, M., Feighery, C. & O'Farrelly, C. Collagenase and Dispase enzymes disrupt lymphocyte surface molecules. *J Immunol Methods* **194**, 211–216 (1996).

192. Vignali, D. A. A., Collison, L. W. & Workman, C. J. How regulatory T cells work. *Nature Reviews Immunology 2008 8:7* **8**, 523–532 (2008).

193. Cosmi, L. *et al.* Human interleukin 17–producing cells originate from a CD161+CD4+ T cell precursor. *J Exp Med* **205**, 1903 (2008).

194. Gálvez, J. Role of Th17 Cells in the Pathogenesis of Human IBD. *ISRN Inflamm* **2014**, 1–14 (2014).

195. Zhou, L. *et al.* TGF-β-induced Foxp3 inhibits TH17 cell differentiation by antagonizing RORγt function. *Nature* **453**, 236–240 (2008).

196. Yang, B.-H. *et al.* Foxp3+ T cells expressing RORγt represent a stable regulatory T-cell effector lineage with enhanced suppressive capacity during intestinal inflammation. *Mucosal Immunol* **9**, 444–457 (2016).

197. Withers, D. R. & Hepworth, M. R. Group 3 Innate Lymphoid Cells: Communications Hubs of the Intestinal Immune System. *Front Immunol* **8**, (2017).

198. Yang, F. C., Chiu, P. Y., Chen, Y., Mak, T. W. & Chen, N. J. TREM-1-dependent M1 macrophage polarization restores intestinal epithelium damaged by DSS-induced colitis by activating IL-22-producing innate lymphoid cells. *J Biomed Sci* **26**, 1–14 (2019).

199. Lambert, C., Preijers, F. W. M. B., Yanikkaya Demirel, G. & Sack, U. Monocytes and macrophages in flow: an ESCCA initiative on advanced analyses of monocyte lineage using flow cytometry. *Cytometry B Clin Cytom* **92**, 180–188 (2017).

200. Jones, G. R. *et al.* Dynamics of colon monocyte and macrophage activation during colitis. *Front Immunol* **9**, 2764 (2018).

201. Zigmond, E. *et al.* Ly6Chi Monocytes in the Inflamed Colon Give Rise to Proinflammatory Effector Cells and Migratory Antigen-Presenting Cells. *Immunity* **37**, 1076–1090 (2012).

202. Becker, F. *et al.* A Critical Role for Monocytes/Macrophages During Intestinal Inflammation-associated Lymphangiogenesis. *Inflamm Bowel Dis* **22**, 1326–1345 (2016).

203. Weber, B., Saurer, L., Schenk, M., Dickgreber, N. & Mueller, C. CX3CR1 defines functionally distinct intestinal mononuclear phagocyte subsets which maintain their respective functions during homeostatic and inflammatory conditions. *Eur J Immunol* **41**, 773–779 (2011).

204. Geissmann, F., Jung, S. & Littman, D. R. Blood monocytes consist of two principal subsets with distinct migratory properties. *Immunity* **19**, 71–82 (2003).

205. Platt, A. M., Bain, C. C., Bordon, Y., Sester, D. P. & Mowat, A. McI. An Independent Subset of TLR Expressing CCR2-Dependent Macrophages Promotes Colonic Inflammation. *The Journal of Immunology* **184**, 6843–6854 (2010).

206. Parkos, C. A. Molecular events in neutrophil transepithelial migration. *BioEssays* **19**, 865–873 (1997).

207. Torres-Gomez, A., Cabañas, C. & Lafuente, E. M. Phagocytic Integrins: Activation and Signaling. *Front Immunol* **11**, 738 (2020).

208. Miller, L. J., Bainton, D. F., Borregaard, N. & Springer, T. A. Stimulated Mobilization of Monocyte Mac-1 and p150,95 Adhesion Proteins from an Intracellular Vesicular Compartment to the Cell Surface.

209. Hu, X. *et al.* Integrin CD11b attenuates colitis by strengthening Src-Akt pathway to polarize anti-inflammatory IL-10 expression. *Scientific Reports 2016 6:1* **6**, 1–11 (2016).

210. Bermudez, H. *et al.* P142 CONSTITUTIVELY ACTIVE MAC-1 (CD11B) AMELIORATES INFLAMMATION IN MOUSE DSS COLITIS MODEL. *Gastroenterology* **156**, S95 (2019).

211. Villegas, I., de La Lastra, C. A., Orjales, A. & la Casa, C. A new flavonoid derivative, dosmalfate, attenuates the development of dextran sulphate sodium-induced colitis in mice. *Int Immunopharmacol* **3**, 1731–1741 (2003).

212. Ki, H. K., Murakami, A., Hayashi, R. & Ohigashi, H. Interleukin-1β targets interleukin-6 in progressing dextran sulfate sodium-induced experimental colitis. *Biochem Biophys Res Commun* **337**, 647–654 (2005).

213. Alex, P. *et al.* Distinct Cytokine Patterns Identified from Multiplex Profiles of Murine DSS and TNBS-Induced Colitis. *Inflamm Bowel Dis* **15**, 341 (2009).

214. Wang, Z. *et al.* Tryptanthrin Protects Mice against Dextran Sulfate Sodium-Induced Colitis through Inhibition of TNF-α/NF-κB and IL-6/STAT3 Pathways. *Molecules : A Journal of Synthetic Chemistry and Natural Product Chemistry* **23**, (2018).

215. Reinecker, H. C. *et al.* Enhanced secretion of tumour necrosis factor-alpha, IL-6, and IL-1 beta by isolated lamina propria mononuclear cells from patients with ulcerative colitis and Crohn's disease. *Clin Exp Immunol* **94**, 174–181 (1993).

216. Carty, E., de Brabander, M., Feakins, R. M. & Rampton, D. S. Measurement of in vivo rectal mucosal cytokine and eicosanoid production in ulcerative colitis using filter paper. *Gut* **46**, 487 (2000).

217. Puleston, J. *et al.* A distinct subset of chemokines dominates the mucosal chemokine response in inflammatory bowel disease. *Aliment Pharmacol Ther* **21**, 109–120 (2005).

218. de Filippo, K. *et al.* Mast cell and macrophage chemokines CXCL1/CXCL2 control the early stage of neutrophil recruitment during tissue inflammation. *Blood* **121**, 4930–4937 (2013).

219. Boro, M. & Balaji, K. N. CXCL1 and CXCL2 Regulate NLRP3 Inflammasome Activation via G-Protein–Coupled Receptor CXCR2. *The Journal of Immunology* **199**, 1660–1671 (2017).

220. Shea-Donohue, T. *et al.* Mice Deficient in the CXCR2 Ligand, CXCL1 (KC/GRO-α), Exhibit Increased Susceptibility to Dextran Sodium Sulfate (DSS)-induced Colitis. *Innate Immun* **14**, 117 (2008).

221. Fujimura, N. *et al.* CCR2 inhibition sequesters multiple subsets of leukocytes in the bone marrow. *Scientific Reports 2015 5:1* **5**, 1–13 (2015).

222. Escaffit, F. *et al.* Cdx2 modulates proliferation in normal human intestinal epithelial crypt cells. *Biochem Biophys Res Commun* **342**, 66–72 (2006).

223. Song, X. *et al.* Growth Factor FGF2 Cooperates with Interleukin-17 to Repair Intestinal Epithelial Damage. *Immunity* **43**, 488–501 (2015).

224. Houchen, C. W., George, R. J., Sturmoski, M. A. & Cohn, S. M. FGF-2 enhances intestinal stem cell survival and its expression is induced after radiation injury. *Am J Physiol* **276**, (1999).

225. Chesler, E. J., Wilson, S. G., Lariviere, W. R., Rodriguez-Zas, S. L. & Mogil, J. S. Identification and ranking of genetic and laboratory environment factors influencing a behavioral trait, thermal nociception, via computational analysis of a large data archive. *Neurosci Biobehav Rev* **26**, 907–923 (2002).

226. Champy, M. F. *et al.* Mouse functional genomics requires standardization of mouse handling and housing conditions. *Mammalian Genome* **15**, 768–783 (2004).

227. Karp, N. A., Melvin, D. & Mott, R. F. Robust and Sensitive Analysis of Mouse Knockout Phenotypes. *PLoS One* **7**, 52410 (2012).

228. Richter, S. H., Garner, J. P. & Würbel, H. Environmental standardization: cure or cause of poor reproducibility in animal experiments? *Nat Methods* **6**, 257–261 (2009).

229. Festing, M. F. W. Reduction of animal use: experimental design and quality of experiments. *Lab Anim* **28**, 212–221 (1994).

230. Perel, P. *et al.* Comparison of treatment effects between animal experiments and clinical trials: systematic review. *BMJ* **334**, 197 (2007).

231. Horowitz, J. E. *et al.* Mutation spectrum of NOD2 reveals recessive inheritance as a main driver of Early Onset Crohn's Disease. *Scientific Reports 2021 11:1* **11**, 1–10 (2021).

232. Valdar, W. *et al.* Genetic and Environmental Effects on Complex Traits in Mice. doi:10.1534/genetics.106.060004.

233. Stenn, K. S., Link, R., Moellmann, G., Madri, J. & Kuklinska, E. Dispase, a Neutral Protease From Bacillus Polymyxa, Is a Powerful Fibronectinase and Type IV Collagenase. *Journal of Investigative Dermatology* **93**, 287–290 (1989).

234. Ogawa, A., Andoh, A., Araki, Y., Bamba, T. & Fujiyama, Y. Neutralization of interleukin-17 aggravates dextran sulfate sodium-induced colitis in mice. *Clin Immunol* **110**, 55–62 (2004).

235. Yang, X. O. *et al.* Regulation of inflammatory responses by IL-17F. *J Exp Med* **205**, 1063–1075 (2008).

236. Garrido-Mesa, N. *et al.* The association of minocycline and the probiotic Escherichia coli Nissle 1917 results in an additive beneficial effect in a DSS model of reactivated colitis in mice. *Biochem Pharmacol* **82**, 1891–1900 (2011).

237. Keir, M. E., Yi, T., Lu, T. T. & Ghilardi, N. The role of IL-22 in intestinal health and disease. *J Exp Med* **217**, (2020).

238. Brand, S. *et al.* IL-22 is increased in active Crohn's disease and promotes proinflammatory gene expression and intestinal epithelial cell migration. *Am J Physiol Gastrointest Liver Physiol* **290**, (2006).

239. Yan, J. *et al.* The Pathogenic Roles of IL-22 in Colitis: Its Transcription Regulation by Musculin in T Helper Subsets and Innate Lymphoid Cells. *Front Immunol* **12**, (2021).

240. Zenewicz, L. A. *et al.* Innate and adaptive interleukin-22 protects mice from inflammatory bowel disease. *Immunity* **29**, 947 (2008).

241. Mowat, A. M. I. & Bain, C. C. Mucosal macrophages in intestinal homeostasis and inflammation. *J Innate Immun* **3**, 550–564 (2011).

242. Bain, C. C. *et al.* Resident and pro-inflammatory macrophages in the colon represent alternative context-dependent fates of the same Ly6Chi monocyte precursors. *Mucosal Immunology 2013 6:3* **6**, 498–510 (2012).

243. Desalegn, G. & Pabst, O. Inflammation triggers immediate rather than progressive changes in monocyte differentiation in the small intestine. *Nat Commun* **10**, (2019).

244. Medina-Contreras, O. *et al.* CX3CR1 regulates intestinal macrophage homeostasis, bacterial translocation, and colitogenic Th17 responses in mice. *J Clin Invest* **121**, 4787–4795 (2011).

245. Marelli, G. *et al.* Heme-oxygenase-1 production by intestinal CX3CR1+ macrophages helps to resolve inflammation and prevents carcinogenesis. *Cancer Res* **77**, 4472–4485 (2017).

246. Paul, G. *et al.* Analysis of intestinal haem-oxygenase-1 (HO-1) in clinical and experimental colitis. *Clin Exp Immunol* **140**, 547 (2005).

247. Zhang, L. *et al.* Heme oxygenase-1 ameliorates dextran sulfate sodium-induced acute murine colitis by regulating Th17/Treg cell balance. *J Biol Chem* **289**, 26847–26858 (2014).

248. Hadis, U. *et al.* Intestinal tolerance requires gut homing and expansion of FoxP3+ regulatory T cells in the lamina propria. *Immunity* **34**, 237–246 (2011).

249. Kumar, A. H. S. *et al.* Bone marrow-derived CX3CR1 progenitors contribute to neointimal smooth muscle cells via fractalkine CX3CR1 interaction. *The FASEB Journal* **24**, 81–92 (2010).

250. Kumar, A. H. S. *et al.* Role of CX3CR1 Receptor in Monocyte/Macrophage Driven Neovascularization. *PLoS One* **8**, e57230 (2013).

251. Lee, M., Lee, Y., Song, J., Lee, J. & Chang, S. Y. Tissue-specific Role of CX3CR1 Expressing Immune Cells and Their Relationships with Human Disease. *Immune Netw* **18**, (2018).

252. Niess, J. H. *et al.* CX3CR1-mediated dendritic cell access to the intestinal lumen and bacterial clearance. *Science* **307**, 254–258 (2005).

253. Ryu, J. *et al.* Activation of fractalkine/CX3CR1 by vascular endothelial cells induces angiogenesis through VEGF-A/KDR and reverses hindlimb ischaemia. *Cardiovasc Res* **78**, 333–340 (2008).

254. Tumpara, S. *et al.* Polymerization of misfolded protein lowers CX3CR1 expression in human PBMCs. *bioRxiv* 2020.11.24.395640 (2020) doi:10.1101/2020.11.24.395640.

255. Bolós, M. *et al.* Absence of CX3CR1 impairs the internalization of Tau by microglia. *Mol Neurodegener* **12**, 1–14 (2017).

256. Muehlhoefer, A. *et al.* Fractalkine is an epithelial and endothelial cell-derived chemoattractant for intraepithelial lymphocytes in the small intestinal mucosa. *J Immunol* **164**, 3368–3376 (2000).

257. Kim, K. W. *et al.* In vivo structure/function and expression analysis of the CX3C chemokine fractalkine. *Blood* **118**, e156–e167 (2011).

258. Morimoto, J. *et al.* No Major Impact of Two Homologous Proteins Ly6C1 and Ly6C2 on Immune Homeostasis. *Immunohorizons* **6**, 202–210 (2022).

259. Naito, Y. *et al.* Enhanced intestinal inflammation induced by dextran sulfate sodium in tumor necrosis factor-alpha deficient mice. *J Gastroenterol Hepatol* **18**, 560–569 (2003).

260. Noti, M., Corazza, N., Mueller, C., Berger, B. & Brunner, T. TNF suppresses acute intestinal inflammation by inducing local glucocorticoid synthesis. *J Exp Med* **207**, 1057 (2010).

261. Kojouharoff, G. *et al.* Neutralization of tumour necrosis factor (TNF) but not of IL-1 reduces inflammation in chronic dextran sulphate sodium-induced colitis in mice. *Clin Exp Immunol* **107**, 353–358 (1997).

262. Sommer, F. & Bäckhed, F. The gut microbiota-masters of host development and physiology. *Nat Rev Microbiol* **11**, 227–238 (2013).

263. Thursby, E. & Juge, N. Introduction to the human gut microbiota. *Biochemical Journal* **474**, 1823 (2017).

264. Rothschild, D. *et al.* Environment dominates over host genetics in shaping human gut microbiota. *Nature* **555**, 210–215 (2018).

265. Durack, J. & Lynch, S. v. The gut microbiome: Relationships with disease and opportunities for therapy. *J Exp Med* **216**, 20 (2019).

266. Gevers, D. *et al.* The treatment-naive microbiome in new-onset Crohn's disease. *Cell Host Microbe* **15**, 382–392 (2014).

267. Joossens, M. *et al.* Dysbiosis of the faecal microbiota in patients with Crohn's disease and their unaffected relatives. *Gut* **60**, 631–637 (2011).

268. Walker, A. W. *et al.* High-throughput clone library analysis of the mucosa-associated microbiota reveals dysbiosis and differences between inflamed and non-inflamed regions of the intestine in inflammatory bowel disease. *BMC Microbiol* **11**, 1–12 (2011).

269. Favier, C. *et al.* Fecal β-D-Galactosidase Production and Bifidobacteria Are Decreased in Crohn's Disease. *Digestive Diseases and Sciences 1997 42:4* **42**, 817–822 (1997).

270. Martin, H. M. *et al.* Enhanced Escherichia coli adherence and invasion in Crohn's disease and colon cancer 1. *Gastroenterology* **127**, 80–93 (2004).

271. Verma, R., Verma, A. K., Ahuja, V. & Paul, J. Real-time analysis of mucosal flora in patients with inflammatory bowel disease in India. *J Clin Microbiol* **48**, 4279–4282 (2010).

272. Ott, S. J. *et al.* Reduction in diversity of the colonic mucosa associated bacterial microflora in patients with active inflammatory bowel disease. *Gut* **53**, 685–693 (2004).

273. Frank, D. N. *et al.* Molecular-phylogenetic characterization of microbial community imbalances in human inflammatory bowel diseases. (2007).

274. Fujimoto, T. *et al.* Decreased abundance of Faecalibacterium prausnitzii in the gut microbiota of Crohn's disease. *J Gastroenterol Hepatol* **28**, 613–619 (2013).

275. Pascal, V. *et al.* A microbial signature for Crohn's disease. *Gut* **66**, 813–822 (2017).

276. Sokol, H. *et al.* Fungal microbiota dysbiosis in IBD. *Gut* **66**, 1039–1048 (2017).

277. Chehoud, C. *et al.* Fungal Signature in the Gut Microbiota of Pediatric Patients With Inflammatory Bowel Disease. *Inflamm Bowel Dis* **21**, 1948–1956 (2015).

278. Round, J. L. & Mazmanian, S. K. The gut microbiome shapes intestinal immune responses during health and disease. *Nat Rev Immunol* **9**, 313–323 (2009).

279. Ding, S. *et al.* Lactobacillus brevis Alleviates DSS-Induced Colitis by Reprograming Intestinal Microbiota and Influencing Serum Metabolome in Murine Model. *Front Physiol* **10**, 1152 (2019).

280. Wang, Y. *et al.* Combination of probiotics with different functions alleviate DSS-induced colitis by regulating intestinal microbiota, IL-10, and barrier function. *Appl Microbiol Biotechnol* **104**, 335–349 (2020).

281. Zhu, W. *et al.* Precision editing of the gut microbiota ameliorates colitis. *Nature 2018 553:7687* **553**, 208–211 (2018).

282. Surana, N. K. & Kasper, D. L. Moving beyond microbiome-wide associations to causal microbe identification. *Nature 2017 552:7684* **552**, 244–247 (2017).

283. Sokol, H. *et al.* Faecalibacterium prausnitzii is an anti-inflammatory commensal bacterium identified by gut microbiota analysis of Crohn disease patients. *Proc Natl Acad Sci U S A* **105**, 16731–16736 (2008).

284. Quévrain, E. *et al.* Identification of an anti-inflammatory protein from Faecalibacterium prausnitzii, a commensal bacterium deficient in Crohn's disease. *Gut* **65**, 415–425 (2016).

285. Chang, C.-S. *et al.* Identification of a gut microbiota member that ameliorates DSS-induced colitis in intestinal barrier enhanced Dusp6-deficient mice. *CellReports* **37**, 110016 (2021).

286. Forster, S. C. *et al.* Identification of gut microbial species linked with disease variability in a widely used mouse model of colitis. *Nature Microbiology 2022 7:4* **7**, 590–599 (2022).

287. Kennedy, N. A. *et al.* The Impact of NOD2 Variants on Fecal Microbiota in Crohn's Disease and Controls Without Gastrointestinal Disease. *Inflamm Bowel Dis* **24**, 583–592 (2018).

288. Knights, D. *et al.* Complex host genetics influence the microbiome in inflammatory bowel disease. *Genome Med* **6**, 1–11 (2014).

289. Turpin, W. *et al.* Associations of NOD2 polymorphisms with Erysipelotrichaceae in stool of in healthy first degree relatives of Crohn's disease subjects. *BMC Med Genet* **21**, 1–8 (2020).

290. Ramanan, D., Tang, M. S., Bowcutt, R., Loke, P. & Cadwell, K. Bacterial sensor Nod2 prevents inflammation of the small intestine by restricting the expansion of the commensal bacteroides vulgatus. *Immunity* **41**, 311–324 (2014).

291. Petnicki-Ocwieja, T. *et al.* Nod2 is required for the regulation of commensal microbiota in the intestine. *Proc Natl Acad Sci U S A* **106**, 15813–15818 (2009).

292. Mondot, S. *et al.* Altered gut microbiota composition in immune-impaired Nod2−/− mice. *Gut* **61**, 634–635 (2012).

293. Couturier-Maillard, A. *et al.* NOD2-mediated dysbiosis predisposes mice to transmissible colitis and colorectal cancer. *J Clin Invest* **123**, 700–711 (2013).

294. Robertson, S. J. *et al.* Nod1 and Nod2 signaling does not alter the composition of intestinal bacterial communities at homeostasis. *Gut Microbes* **4**, 222–231 (2013).

295. Shanahan, M. T. *et al.* Mouse Paneth cell antimicrobial function is independent of Nod2. *Gut* **63**, 903–910 (2014).

296. Bharti, R. & Grimm, D. G. Current challenges and best-practice protocols for microbiome analysis. *Brief Bioinform* **22**, 178–193 (2021).

297. Stojanov, S., Berlec, A. & Štrukelj, B. microorganisms The Influence of Probiotics on the Firmicutes/Bacteroidetes Ratio in the Treatment of Obesity and Inflammatory Bowel disease. doi:10.3390/microorganisms8111715.

298. Dicksved, J. *et al.* Molecular analysis of the gut microbiota of identical twins with Crohn's disease. *The ISME Journal 2008 2:7* **2**, 716–727 (2008).

299. Willing, B. P. *et al.* A pyrosequencing study in twins shows that gastrointestinal microbial profiles vary with inflammatory bowel disease phenotypes. *Gastroenterology* **139**, 1844-1854.e1 (2010).

300. Liang, G. Altered gut bacterial and metabolic signatures and their interaction in inflammatory bowel disease. *Synth Syst Biotechnol* **6**, 377–383 (2021).

301. Elderman, M. *et al.* Sex and strain dependent differences in mucosal immunology and microbiota composition in mice. *Biol Sex Differ* **9**, 26 (2018).

302. Falcone, E. L. *et al.* Colitis susceptibility in p47phox-/- mice is mediated by the microbiome. *Microbiome* **4**, 1–16 (2016).

303. Nunberg, M. *et al.* Interleukin 1α-Deficient Mice Have an Altered Gut Microbiota Leading to Protection from Dextran Sodium Sulfate-Induced Colitis. *mSystems* **3**, (2018).

304. Brinkman, B. M. *et al.* Caspase deficiency alters the murine gut microbiome. *Cell Death Dis* **2**, (2011).

305. Lagkouvardos, I. *et al.* Sequence and cultivation study of Muribaculaceae reveals novel species, host preference, and functional potential of this yet undescribed family. *Microbiome* **7**, 1–15 (2019).

306. Elinav, E. *et al.* NLRP6 inflammasome regulates colonic microbial ecology and risk for colitis. *Cell* **145**, 745–757 (2011).

307. Brinkman, B. M. *et al.* Gut microbiota affects sensitivity to acute DSS-induced colitis independently of host genotype. *Inflamm Bowel Dis* **19**, 2560–2567 (2013).

308. Dong, F. *et al.* Pediococcus pentosaceus CECT 8330 protects DSS-induced colitis and regulates the intestinal microbiota and immune responses in mice. *J Transl Med* **20**, 1–16 (2022).

309. Zhao, B. *et al.* Lycopene Alleviates DSS-Induced Colitis and Behavioral Disorders via Mediating Microbes-Gut-Brain Axis Balance. *J Agric Food Chem* **68**, 3963–3975 (2020).

310. Anderson, M. J. & Walsh, D. C. I. PERMANOVA, ANOSIM, and the Mantel test in the face of heterogeneous dispersions: What null hypothesis are you testing? *Ecol Monogr* **83**, 557–574 (2013).

311. Hildebrand, F. *et al.* Inflammation-associated enterotypes, host genotype, cage and inter-individual effects drive gut microbiota variation in common laboratory mice. *Genome Biol* **14**, 1–15 (2013).

312. Shi, L. *et al.* Enhancer RNA and NFκB-dependent P300 regulation of ADAMDEC1. *Mol Immunol* **103**, 312–321 (2018).

313. Ha, S. E. *et al.* Metalloendopeptidase ADAM-like Decysin 1 (ADAMDEC1) in Colonic Subepithelial PDGFRα+ Cells Is a New Marker for Inflammatory Bowel Disease. *Int J Mol Sci* **23**, 5007 (2022).

314. Furuya, S. & Furuya, K. Subepithelial Fibroblasts in Intestinal Villi: Roles in Intercellular Communication. *Int Rev Cytol* **264**, 165–223 (2007).

315. Liu, X. *et al.* Knockdown of ADAMDEC1 inhibits the progression of glioma in vitro. *Histol Histopathol* **35**, 997–1005 (2020).

316. Lund, M. E., To, J., O'Brien, B. A. & Donnelly, S. The choice of phorbol 12-myristate 13-acetate differentiation protocol influences the response of THP-1 macrophages to a pro-inflammatory stimulus. *J Immunol Methods* **430**, 64–70 (2016).

317. Thompson, N. P., Driscoll, R., Pounder, R. E., Wakefield, A. J. & Bowel, I. Genetics versus environment in inflammatory bowel disease: results of a British twin study. *BMJ* **312**, 95–96 (1996).

318. Halfvarson, J., Bodin, L., Tysk, C., Lindberg, E. & Järnerot, G. Inflammatory bowel disease in a Swedish twin cohort: a long-term follow-up of concordance and clinical characteristics. *Gastroenterology* **124**, 1767–1773 (2003).

319. Orholm, M., Binder, V., Sorensen, T. I. A., Rasmussen, L. P. & Kyvik, K. O. Concordance of inflammatory bowel disease among Danish twins. Results of a nationwide study. *Scand J Gastroenterol* **35**, 1075–1081 (2000).

320. Ko, Y., Butcher, R. & Leong, R. W. Epidemiological studies of migration and environmental risk factors in the inflammatory bowel diseases. *World J Gastroenterol* **20**, 1238–1247 (2014).

321. Shu, L., Blencowe, M. & Yang, X. Translating GWAS Findings to Novel Therapeutic Targets for Coronary Artery Disease. *Front Cardiovasc Med* **5**, (2018).

322. The Human Protein Atlas. Single cell type - ADAMDEC1 - The Human Protein Atlas. https://www.proteinatlas.org/ENSG00000134028-ADAMDEC1/single+cell+type.

323. Klaver, E. J. *et al.* Trichuris suis soluble products induce Rab7b expression and limit TLR4 responses in human dendritic cells. *Genes Immun* **16**, 378–387 (2015).

324. Baculovirus Protein Expression Service | ProMab. https://www.promab.com/baculovirus-expression.

325. Thermo Fisher Scientific. Bac-to-Bac™ TOPO™ Cloning Kit USER GUIDE vers B.0. https://www.thermofisher.cn/document-connect/document-connect.html?url=https://assets.thermofisher.cn/TFS-Assets%2FLSG%2Fmanuals%2Fbactobac_topo_cloning_kit_man.pdf (2018).

326. Thermo Fisher Scientific. Bac-to-Bac™ TOPO™ Expression System USER GUIDE vers A.0. https://assets.thermofisher.com/TFS-Assets/LSG/manuals/MAN0000699_BactoBacTOPO_Expression_System_UG.pdf (2018).